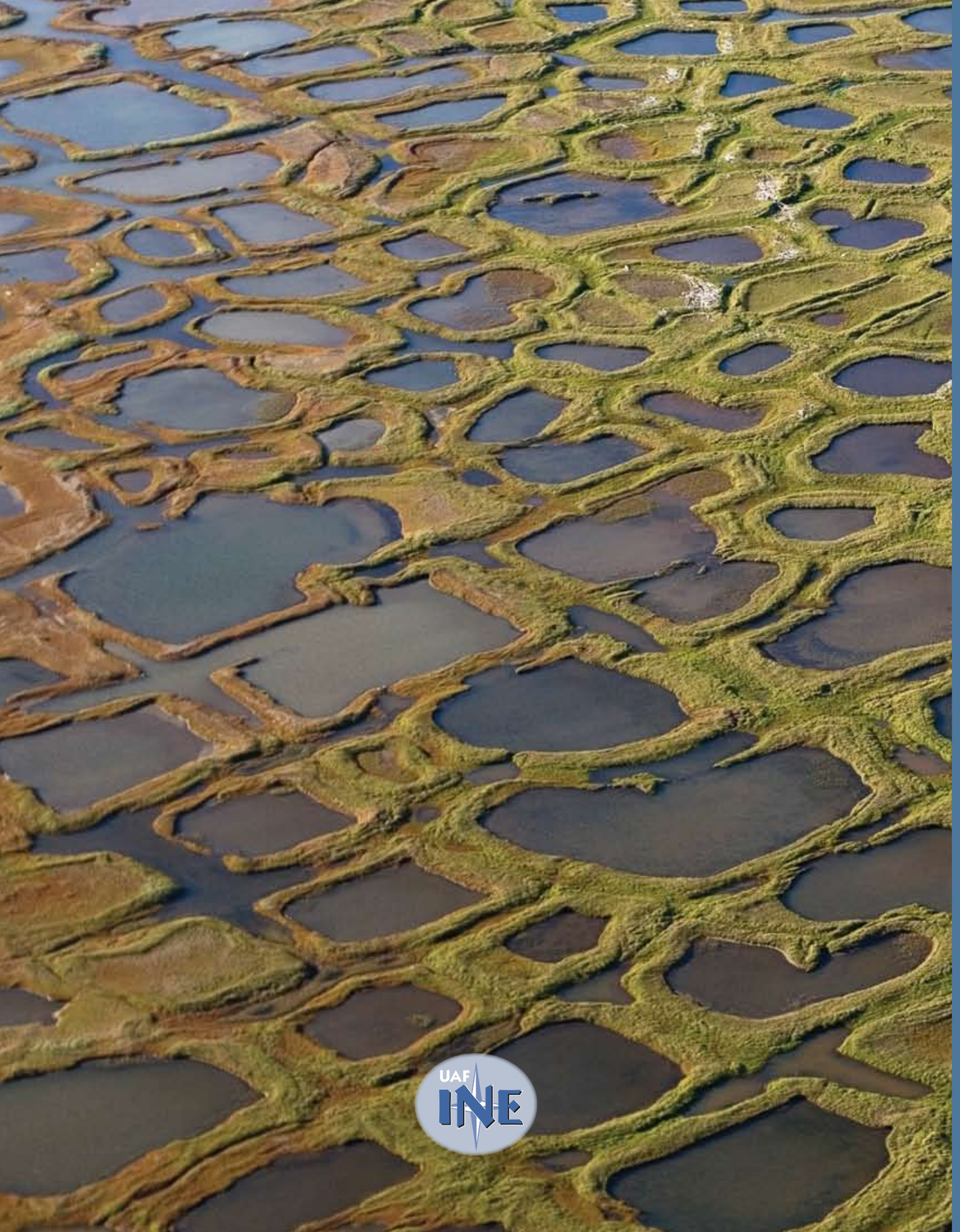

NICOP 2008 **Ninth International Conference on Permafrost** **Extended Abstracts** Kane and Hinkel, Editors

NICOP 2008

Ninth International Conference on Permafrost

Extended Abstracts

Edited by Douglas L. Kane and Kenneth M. Hinkel

Ninth International Conference on Permafrost

Ninth International Conference on Permafrost
University of Alaska Fairbanks
June 29–July 3, 2008

Ninth International Conference on Permafrost

Extended Abstracts

Edited by Douglas L. Kane and Kenneth M. Hinkel

Institute of Northern Engineering
University of Alaska Fairbanks
2008

Ninth International Conference on Permafrost
Extended Abstracts
Edited by Douglas L. Kane and Kenneth M. Hinkel

Printed in the United States of America

Cover Photo: Low-Centered Polygons, North Slope, Alaska

Production Editors: Thomas Alton and Fran Pedersen

Contents

Preface

One of the looming challenges in organizing an international conference on permafrost is determining the timetable. What should be the deadline for abstract and paper submittals? Early in the process we agreed that we wanted the proceedings published before the conference, and this challenge has become more taxing as the size of the conference has increased. We made a concerted effort to compress the timetable so that papers published in the proceedings were to be submitted only eight and one-half months before the conference. Still, there are those who want to report on their latest research at the permafrost conference. In the recent past, the International Permafrost Association (IPA) introduced the concept of extended abstracts (two pages in this case) that were published in a separate document. The idea was that the collection would represent the latest in permafrost research. It is clear that some researchers, finding the English language challenging, opted instead to submit the shorter extended abstract in lieu of the six-page manuscript. We have one hundred eighty-four extended abstracts that will be presented at the Ninth International Conference on Permafrost; this can be compared with the three hundred fifty-eight papers published in the proceedings. As in the past, the extended abstracts were not reviewed, and except for some minor changes (formatting, deletion of an abstract in the extended abstract, etc.), they are published as they were submitted. As with the proceedings and abstract volumes, we appreciate all the assistance we received from Thomas Alton and Fran Pedersen in producing this volume. We hope that you find these extended abstracts and accompanying poster presentations informative.

— Douglas L. Kane and Kenneth M. Hinkel

NICOP Sponsors

Universities
University of Alaska International Polar Year (Gold plus)
University of Alaska President's Fund (Gold)
Alaska University Transportation Center (Gold)
University of Alaska Fairbanks Institute of Northern Engineering (Silver)
University of Alaska Fairbanks International Arctic Research Center (Silver)
University of Alaska Fairbanks Experimental Program to Stimulate Competitive Research (EPSCoR) (Bronze)
University of Alaska Young Researchers' Network/UA IPY Outreach (Contributor plus)
University of Colorado-National Snow and Ice Data Center (Contributor)

Government Agencies
Alaska Division of Geological and Geophysical Surveys, Fairbanks (Gold)
U.S. National Science Foundation (Silver)
U.S. Geological Survey (Silver)
U.S. Army Cold Regions Research and Engineering Laboratory (Bronze)
U.S. Department of Energy (Bronze)
U.S. Arctic Research Commission (Brass)
U.S. Bureau of Land Management (Brass)
Denali Commission (Brass)
North Slope Science Initiative (Brass)
U.S. Minerals Management Service (Contributor plus)
Norwegian Thermal State of Permafrost IPY Project (Sustaining)

Corporate and Non-Governmental Organizations
Arctic Foundations, Inc., Anchorage (Gold)
Alyeska Pipeline Company, Anchorage (Silver)
International Permafrost Association (Bronze plus)
Arctic Slope Regional Corp. (Bronze plus)
BP Foundation (Bronze)
Geo-Watersheds Scientific, Fairbanks (Bronze)
Duane Miller & Associates, Anchorage (Bronze)
CH2MHILL Energy & Power, Anchorage (Brass)
ConocoPhillips Alaska (Brass)
EBA Engineering Consultants Ltd., Canada (Brass)
Golder Associates, Anchorage (Brass)
Michael Baker Jr, Inc., Anchorage (Brass)
Shannon & Wilson, Inc. Seattle (Brass)
PND Engineers, Inc, Anchorage (Contributor plus)
RA Kreig & Associates, Anchorage (Contributor plus)
BeadedStream, LLC, Anchorage (Contributor)
DOWL LLC, Anchorage (Contributor)
Kinross Fort Knox Gold Mine (Contributor)
Hawk Consultants, LLC, Anchorage (Contributor)
Houston Advanced Research Center (HARC) (Contributor)
Fairbanks Gold Mining, Inc., Fairbanks (Contributor)
Northern Engineering & Scientific, Anchorage (Contributor)
Northern Geotechnical Engineering, Inc., Anchorage (Contributor)
R&M Consultants, Inc., Anchorage (Contributor)
Tryck Nyman Hayes, Inc., Anchorage (Contributor)
Resource Data, Inc., Anchorage (Sustaining)
URS Corporation, Anchorage (Sustaining)
Usibelli Foundation (Sustaining)
Harley H. Hightower, FAIA, Anchorage (Sustaining)

ICOP Donor Circle (Contributor)
Jerry and Celia Brown
Edwin Clarke
Hugh M. French
Don W. Hayley
C.W. "Bill" Lovell
J. Ross Mackay (Honorary Member)
Michael C. Metz
Frederick E. Nelson
Jim and Florence Rooney
Ronald S. Sletten
Sarah M. Springman
Rupert "Bucky" Tart
Ted B. Trueblood
H. Jesse Walker
John Zarling

Individuals
Joe Malen

In-Kind Sponsors
Elsevier
Rite in the Rain
Fairbanks Convention and Visitors Bureau
American Water Resources Association
UAF Toolik Lake Field Research Station
Pogo Mine
U.S. Army CRREL
U.S. Geological Survey
Permafrost Young Researchers Network
Mountain Studies Institute
University of Cincinnati
University of Colorado at Boulder
Kinross Fort Knox Gold Mine
Institute of Arctic and Alpine Research
BP Exploration (Alaska), Inc.
University of Alaska Fairbanks
ABR, Inc.
U.S. National Park Service
Geo-Watersheds Scientific

UAF International Arctic Research Center
UAF Institute of Northern Engineering
University of Alaska IPY Office
Alaska Division of Geological & Geophysical Surveys
Barrow Arctic Science Consortium
Conoco Phillips Alaska

Deep Permafrost Studies at the Lupin Mine: Hydrogeological and Geochemical Information for Nuclear Waste Disposal

Lasse Ahonen
Geological Survey of Finland
Timo Ruskeeniemi
Geological Survey of Finland
Randy Stotler
University of Waterloo, Canada
Shaun Frape
University of Waterloo, Canada
Kimmo Lehto
Posiva Oy, Finland
Ignasi Puigdomenech
SKB (Swedish Nuclear Fuel and Waste Management Co), Sweden
Monique Hobbs
Nuclear Waste Management Organization, Canada
Paul Degnan
Nirex, UK (present position CSIRO Exploration & Mining, Australia)

Introduction

The deep geological disposal of high-level and long-lived nuclear waste requires a comprehensive understanding of the possible impacts of long-term future climate change on a repository environment and the surrounding rock mass. Despite the general scientific consensus that global warming is underway due to anthropogenic greenhouse gas emissions, future glaciation scenarios have to be taken into account and included in the long-term safety analyses of disposal systems, especially in Fennoscandian countries, Britain, and Canada.

The Lupin gold mine, situated in the territory of Nunavut, Canada, is located in a subarctic tundra environment, where continuous permafrost reaches depths of 400–600 m. The bedrock of the Lupin area consists of Archean metasedimentary crystalline rocks, which are considered to be good analogues for host rocks at potential repository sites in the Fennoscandian Shield. Consequently, several nuclear waste management organizations, together with the Geological Survey of Finland and the University of Waterloo, started a joint venture to study the hydrogeological and hydrogeochemical conditions below and within the permafrost at the Lupin mine (Ruskeeniemi et al. 2003).

Several important uncertainties relating to the potential effects of permafrost on the safety of nuclear waste disposal were identified as follows:

- *Depth range* and rate of formation of permafrost in crystalline rock and the controlling factors.
- *Hydrogeological conditions* in frozen rock, the importance of taliks as possible flow paths and the freezing of water in major fracture zones.
- *Hydrogeochemical effects* of permafrost, formation of saline segregations (cryopegs) in and/or below the frozen rock mass.
- *Methane hydrates, the* abundance and formation of methane in crystalline rock and the nature of any accumulations below the permafrost.

Research Activities

The research project at the Lupin mine was conducted in three phases. During the first phase, background data on geology and hydrology were compiled, potential fracture zones were identified by a seismic refraction study, and underground waters were sampled (Ruskeeniemi et al. 2002). Phase II activities included an electromagnetic survey (SAMPO), drilling of two research boreholes from inside the mine upwards through the bottom of the permafrost, water and gas sampling, crush and leach studies of the rock material, and freezing experiments of water samples (Ruskeeniemi et al. 2004, Frape et al. 2004).

Phase III (Stotler et al. 2008) focused on the collection of representative data concerning the chemistry and isotopic composition of waters and dissolved components from packed-off boreholes, the long-term monitoring of hydraulic heads in the boreholes, mineralogical studies of fractured rock, and a ground penetrating radar survey.

Hydrogeological Conditions

In the mine, the bedrock below the permafrost down to about 900 m appeared distinctly dry, as observed along the ramp roadway. Mine statistics indicate pumping rates of about 6 m^3/h (in 2003), of which a major proportion was identified to be fresh water supplied for various purposes in the mining process. Most of the water-producing boreholes situated at the level 1130 m were plugged. At higher levels the seepage of groundwater through frozen bedrock does not appear to take place at all. Measured effective porosities of

the Lupin rocks were less than 0.5%, which indicates that only major fracture systems are likely to serve as significant hydraulic conductors.

Lupin mine is situated near the large freshwater Lake Contwoyto, which—based on its size and elongated form—could potentially maintain a water-conducting talik beneath the surface. A ground penetrating radar study confirmed that there is only a narrow band of frozen ground along the shore of the lake.

Boreholes, most of them situated in the exploration drift at the 1130 m level were packered off with mechanical packers and equipped with valves for water and gas sampling and pressure gauges for monitoring of hydraulic heads. Hydraulic heads were monitored in 9 boreholes for 2 to 3 years, and the highest hydraulic head values measured in 2 of the boreholes correspond to the expected pressures arising from a hydrostatic column of water with its top at the base of the permafrost. Thus, there does not seem to be a clear hydraulic connection between the boreholes and the nearby lake through any non-frozen fracture zone. Lack of uniform hydraulic conductivity of the deep bedrock was also demonstrated by the large differences in hydraulic heads (up to 160 m_{H2O}) between monitored boreholes. On the other hand, traces of tritium in the deep saline waters indicate that a small portion of recent surficial water may be recharging to depth.

Drilling through the base of the permafrost indicated that the bedrock was not water-saturated, but a dry zone exists below the permafrost. A cone of depression generated by the mine drainage, together with the very limited recharge of surficial water, is the most likely explanation. However, it is also possible that given the limited potential for recharge, the piezometric surface below the permafrost may fall regionally over the very long time periods involved.

Hydrogeochemical Conditions and Gases

Permafrost waters sampled along the ramp down to the base of permafrost were typically very saline (TDS up to about 40 g/L). Geochemical and isotope studies indicate the contribution of drilling brine used for drilling in cold conditions, but the introduced salt has mixed with a natural salt source and subsequently been altered by the freezing process. Permafrost waters contained a high concentration of sulfate, which could not originate either from the salt used in drilling or from surficial fresh water, but rather indicates oxidation of the sulfide ore body.

The possible formation of saline water by segregation at the *base of the permafrost* was studied by drilling two boreholes at 570 m depth. With time, groundwater contamination by drilling water (labeled with a tracer) and other mine-induced contamination (e.g., nitrate) fade out, and representative water samples seeping from the bedrock were obtained in the upwards-directed borehole. The salinity of the basal permafrost water (TDS 3–5 g/L) was observed to be lower than in waters within the frozen bedrock. No distinct basal cryopeg was observed below the permafrost. Based on molar ratios and isotopic compositions, it is evident that the groundwater at the base of the permafrost is similar to deeper sub-permafrost waters, but more dilute.

Deep *sub-permafrost waters* sampled in one borehole at a depth of 890 m, and in several boreholes of the exploration drift at 1130 m were typically saline (TDS up to about 40 g/L). Interestingly, the salinity of the waters varied not only between different boreholes, but also in the same borehole at different times. Hydraulic connections between fractures are evidently very limited, and the water composition varies between different fracture systems.

Waters contain dissolved gases, mainly methane, in abundance (up to about 0.5L gas/L of water). Isotope compositions of methane samples plot within a relatively narrow range: δD = -330 – -350‰, δC-13 = -45 – -50‰. Isotope geochemical interpretation of the data suggests a thermogenic origin for the methane, but the contribution of bacterial methyl type fermentation cannot be ruled out. A carbon-14 model age of dissolved bicarbonate in deep sub-permafrost water was interpreted to be about 25 ky, while C-14 in methane was below the detection limit. Continuous monitoring of redox potential in a flow-through cell over several days indicated Eh-values around zero and dissolved oxygen concentrations were below detection limit (0.1 mg/L) in all measurements.

References

Frape, S.K., Stotler, R.L., Ruskeeniemi, T., Ahonen, L., Paananen, M. & Hobbs, M.Y. 2004. *Hydrogeo-Chemistry of Groundwaters at and Below the Base of the Permafrost at Lupin: Report of Phase II*. Ontario Power Generation. Report 06819-REP-01300-10047-R00. Toronto: Ontario Power Generation. 74 pp.

Ruskeeniemi, T., Paananen, M., Ahonen, L., Kaija, J., Kuivamäki, A., Frape, S., Morén, L. & Degnan, P. 2002. Permafrost at Lupin: Report of phase I. *Geological Survey of Finland* Report YST-112.

Ruskeeniemi, T., Ahonen, L., Paananen, M., Blomqvist, R., Degnan, P., Frape, S. K., Jensen, M., Lehto, K., Wikström, L., Morén, L., Puigdomenech, I. & Snellman, M. 2003. Groundwater under deep permafrost conditions. In: *8th International Conference on Permafrost, Zurich, Switzerland, July 20–25, 2003*. Extended abstracts reporting current reserch and new information. Zurich: University of Zurich, 141-142.

Ruskeeniemi, T., Ahonen, L., Paananen, M., Frape, S., Stotler, R., Hobbs, M., Kaija, J., Degnan, P., Blomqvist, R., Jensen, M., Lehto, K., Morén, L., Puigdomenech, I. & Snellman, M. 2004. Permafrost at Lupin: Report of phase II. *Geological Survey of Finland, Report* YST-119.

Stotler, R.L., Frape, S.K., Ruskeeniemi, T., Ahonen, L., Paananen, M., Hobbs, M.Y. & Zhang, M. 2008. *Hydrogeochemistry of Groundwaters at and Below the Base of the Permafrost at Lupin: Report of Phase III*. Ontario Power Generation Report (in print).

Effect of Fire on Pond Dynamics in Regions of Discontinuous Permafrost: A State of Change Following the Fires of 2004 and 2005?

Garrett Altmann
School of Natural Resources and Agricultural Sciences, University of Alaska Fairbanks
Dave Verbyla
School of Natural Resources and Agricultural Sciences, University of Alaska Fairbanks
Kenji Yoshikawa
Water and Environmental Research Center, Institute of Northern Engineering, University of Alaska Fairbanks
John Fox
School of Natural Resources and Agricultural Sciences, University of Alaska Fairbanks

Introduction

Climate change at high latitudes affects both the disturbance and hydrologic regimes of boreal forests. Throughout Interior Alaska, wildfire is the dominant disturbance regime regulating boreal forests associated with discontinuous permafrost. In recent years, fire activity has signaled a potential shift in this disturbance regime, as significant increases in total burned area and burn severity have occurred. The effects of a potential regime shift may have profound impacts on the permafrost and hydrologic features associated with it.

Previous studies have examined the effects of fire on permafrost and have attributed a deepening of the active layer, as well as increased soil moisture resulting from the removal of insulating vegetation during fire (Yoshikawa et al. 2002, Liljedahl et al. 2007, Burn 1998). Ishikawa et al. (2008) has further implicated fire severity as a significant source of variability among these effects. To examine the relationship between fire, burn severity, and pond dynamics, this study uses remote sensing and GIS to compare ponds affected by fire, to ponds not affected by fire.

Data and Methods

We use remote sensing and geographic information systems (GIS) to examine the effect of fire on pond sizes throughout four Interior Alaska basins: Tanana Valley, Yukon Flats, Innoko Flats, and Minchumina Basin (Fig. 1). Using Landsat TM/ETM+ imagery and historic fire parameters attained from the Alaska Fire Service, a multi-temporal analysis from 1980 to present is used to observe surface area changes in ponds following fires. To observe pond dynamics in fire-affected areas, historic burn parameters are overlaid on pre-fire and post-fire georeferenced Landsat scenes. All GIS layers are analyzed using the Alaska Alber's Equal Area projection to provide accurate representations of surface area. Pond dynamics within burn areas are then compared to ponds outside burn parameters. Ponds displaying variability are tagged and compared at varying time periods. To evaluate the influence of fire severity, we examine thermal IR (band 6) data within the burn area from imagery attained one year post-burn. As a test of our methodology, a pilot study was applied to the Yukon Flats portion of our study area. Despite the inability to assess pond depth from a remote sensing perspective, we feel confident our methodology will allow us to observe pond dynamics in relation to fire in the remaining study areas.

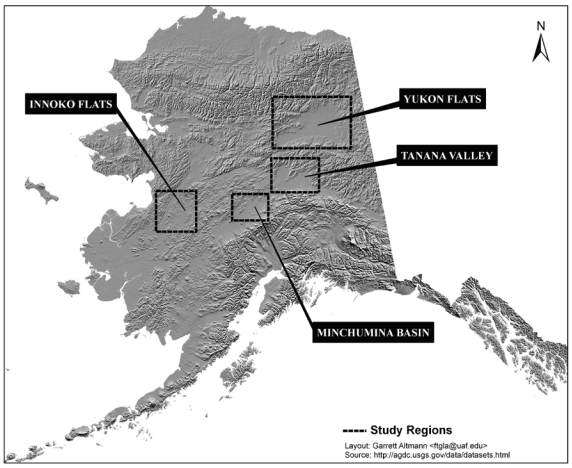

Figure 1. Study area locations.

Results

Initial results reveal a static state of pond sizes following fires prior to 2004. During the larger, more severe fires occurring in 2004 and 2005, ponds located in burn areas show greater variability in surface area than ponds located outside the burn area. Increased shrinkage was observed within burn areas during the years immediately following the fire. Short-term observations (1–3 years) in burn areas prior to 2004 do not reveal this effect. Periods 5–15 years following a fire show little/no variability in surface area, and fluctuations tend to be dominated by the regional water table. Long-term (15–25 years) reveal similar trends to those experienced during short-term observations associated with high fire severity.

Discussion

In our initial hypothesis, we expected pond sizes within burn parameters to increase as a result of the removal of a transpiring vegetation layer. Contrary to this hypothesis, we observe a decrease in surface area of ponds in areas

of high burn severity. This is attributed to either the loss and/or depletion of the insolating vegetation that provided protection from incoming solar radiation and prevented evaporation, or to an increase in the active layer thickness which results in more lateral and vertical drainage, and/or thermokarsting. The period 5–15 years following a fire showing little variability in surface area are likely attributed to seasonal refreezing of the active layer. Refreezing of the active layer prevents drainage and talik expansion, thus stabilizing ponds and minimizing changes attributed to fire disturbance. The mechanisms responsible for shrinking during long-term (15–25 years) periods is attributed to a more developed deciduous vegetation community with higher evapotranspiration (ET) flux and reduced levels of moisture availability.

Results from our pilot study in the Yukon Flats reveal evidence that our methodology is capable of attaining desired observations. Even though parameters such as lake depth and permafrost abundance are not quantifiable using this method, we are confident that examining our other study regions will allow us to anticipate changes as a result of fire. Further analysis will include remaining study areas, and results will be presented during the NICOP.

Acknowledgments

This project was funded through support from the Bonanza Creek LTER (Long-Term Ecological Research) program (funded jointly by NSF grant DEB-0423442 and USDA Forest Service, Pacific Northwest Research Station grant PNW01-JV11261952-231). The authors would like to thank the U.S. Fish & Wildlife service for their assistance in the acquisition of Landsat scenes, as well as the BLM and Alaska Fire Service for providing readily accessible fire history data.

References

Burn, C.R. 1998. The response (1958–1997) of permafrost and near-surface ground temperatures to forest fire, Takhini River Valley, southern Yukon Territory. *Canadian Journal of Earth Sciences* 35(2): 184-189.

Ishikawa, M. 2008. Heat and water processes of burned and unburned active layer. Presented at the *IARC-JAXA Collaborative Research Plan,* University of Alaska Fairbanks, 28 February 2008.

Liljedahl, A., Hinzman, L., Busey, R. & Yoshikawa, K. 2007. Physical short-term changes after a tussock tundra fire, Seward Peninsula, Alaska. *Journal of Geophysical Research* 112*:* F02S07.

Riordan, B., Verbyla, D. & McGuire, A.D. 2006. Shrinking ponds in subarctic Alaska based on 1950–2002 remotely sensed images. *Journal of Geophysical Research* 111: G04002.

Yoshikawa, K., Bolton W.R., Romanovsky V.E., Fukuda, M. & Hinzman, L.D. 2002. Impacts of wildfire on the permafrost in the boreal forests of Interior Alaska. *Journal of Geophysical Research* 107: 8148.

Cryological Status of Russian Soils: Cartographic Assessment

T.V. Ananko, D.E. Konyushkov, E.M. Naumov
V.V. Dokuchaev Soil Science Institute, Russian Academy of Agricultural Sciences, Moscow, Russia

Soil maps contain valuable information on the cryological conditions encoded in the names of soils and in knowledge of soil morphogenetic properties. In the new Russian soil classification system (Shishov et al. 2004), the presence and character of permafrost are not taken into account (except for an order of the cryoturbated nongley soils, *Cryozems*). A separate classification of soil cryological regimes is suggested (Sokolov et al. 2006). The following criteria are taken into account.

(I) The presence/absence of permafrost and seasonal freeze-thaw processes: (1) *seasonally thawing soils* (the depth of winter freezing exceeds the depth of summer thawing, the freezing layer merges with the permafrost table), (2) *seasonally freezing soils* (permafrost is absent or is below the depth of winter freezing), and (3) *nonfreezing soils* (cryogenic processes are absent).

(II) Duration of the thawed (group 1)/frozen (group 2) state of soils in the root zone (months): *long-term* (> 5), *medium-term* (3–5), *short-term* (1–3), and *very short-term* (< 1). The stability of soil freezing-thawing patterns in interannual cycles (stable, unstable, episodic) is considered as an additional criterion.

(III) The ice content in the transient layer of permafrost (group 1) or in the seasonally frozen soil layer (group 2): *ice-rich* (ice schlieren > 2 mm, the ice volume exceeds soil porosity in the thawed state); *medium-ice* (fine ice segregations, ice volume is approximately equal to soil porosity); *low-ice* (separate ice crystals; ice volume is less than soil porosity); and *dry frost* (no visible ice crystals; soil moisture after thawing is about maximum hygroscopy). For group 2, the ice content in the frozen state can be judged from the soil morphology and from the soil water content before freezing.

(IV) Depth of permafrost table (active layer thickness, seasonal thawing depth, cm) (group 1)/depth of seasonal freezing (group 2): *superficial* (< 25), *shallow* (25–50), *medium* (50–100), *medium deep* (100–150), *deep* (150–250), and *extremely deep* (> 250). The criterion of stability of the thawing/freezing depth may also be introduced (see II).

(V) The dynamics of phase transitions of soil water (freezing-thawing): *Arctic type* (in summer), *Boreal type* (in spring-early summer and in the late summer-fall), and *Subboreal type* (in winter). Additionally, the frequency of phase transitions in the root zone is to be taken into account.

A schematic pedocryological map of the FSU developed by us on a scale of 1:35 M (Fig. 1) contains information on the depth of soil seasonal thawing/freezing, mean annual temperature at the depth of zero seasonal temperature fluctuations, soil temperature characteristics at the depth of 20 cm, duration of the frozen state of soils, merging of permafrost table with the layer of seasonal freezing, the one-sided (from the top) or two-sided (from the top and from the bottom) character of soil freezing, etc. It is considered a part of the integral system of soil maps for the FSU (Ananko et al. 1998) developed for the cartographic assessment of the proper pedogenic, lithogenic, and regime (water and temperature) soil characteristics. The initial soil information was obtained from the *Soil Map of the Russian Federation* (1:2.5 M; 1988) and from the *State Soil Map* (1:1 M). In the presented variant, soil polygons are renamed according to the WRB system (2006) with due account for the earlier elaborated correlation tables (Goryachkin et al. 2002). Estimates of soil cryological characteristics are based on the *Geocryology of the USSR* (1988–1989), the monographs by Dimo (1972) and Romanovskii (1993), and numerous regional works. A fragment of the database to the map is shown in the table below; soil cryological characteristics for the polygons along meridian 120°E are included in it. The estimates are given for predominant soils. The real spatial and temporal variability of the cryological parameters within the polygons is much greater.

Information about cryogenic soil processes (cracking, ice-wedging, heaving, cryoturbation, dehydration, ice segregation, migration of solutes to freezing fronts, etc.) is included in a separate database. Their character and intensity depend on many factors—soil texture, water content, and freezing intensity being the most important.

Mean annual data reflected on the map were obtained from 1950–1980. Since the 1990s, a tendency for some warming of the climate (due to extremely warm winters or extremely warm summers) has been registered in many regions. Climate change results in a certain alteration of the soil cryological conditions (though its range is much less than the range of changes induced by anthropogenic impacts on soils and vegetation). Seasonally freezing soils beyond the permafrost zone become nonfreezing soils, and this phenomenon can be traced not only in the southern parts of European Russia but also in its northern regions (Mazhitova 2008).

In sharply continental regions with a shallow ice-rich and low-temperature permafrost, the buffer role of the latter in regulation of the soil temperature increases. At the same time, the upper layers of permafrost, being involved in seasonal freeze-thaw cycles, are subjected to degradation, which in enhanced by the development of thermokarst and thermal erosion in the case of ice-rich permafrost. A negative feedback in this system may occur due to the more active development of moss layers on the surface of waterlogged soils and a gradual increase in insulation properties of the moss and peat in the summer. In the areas of discontinuous permafrost, soils with a deep active layer merging with the permafrost table may lose their contact with permafrost. In general, the cryological response of soils to climate changes is as diverse and complicated as the diversity of different combinations of cryological parameters in the soil profiles.

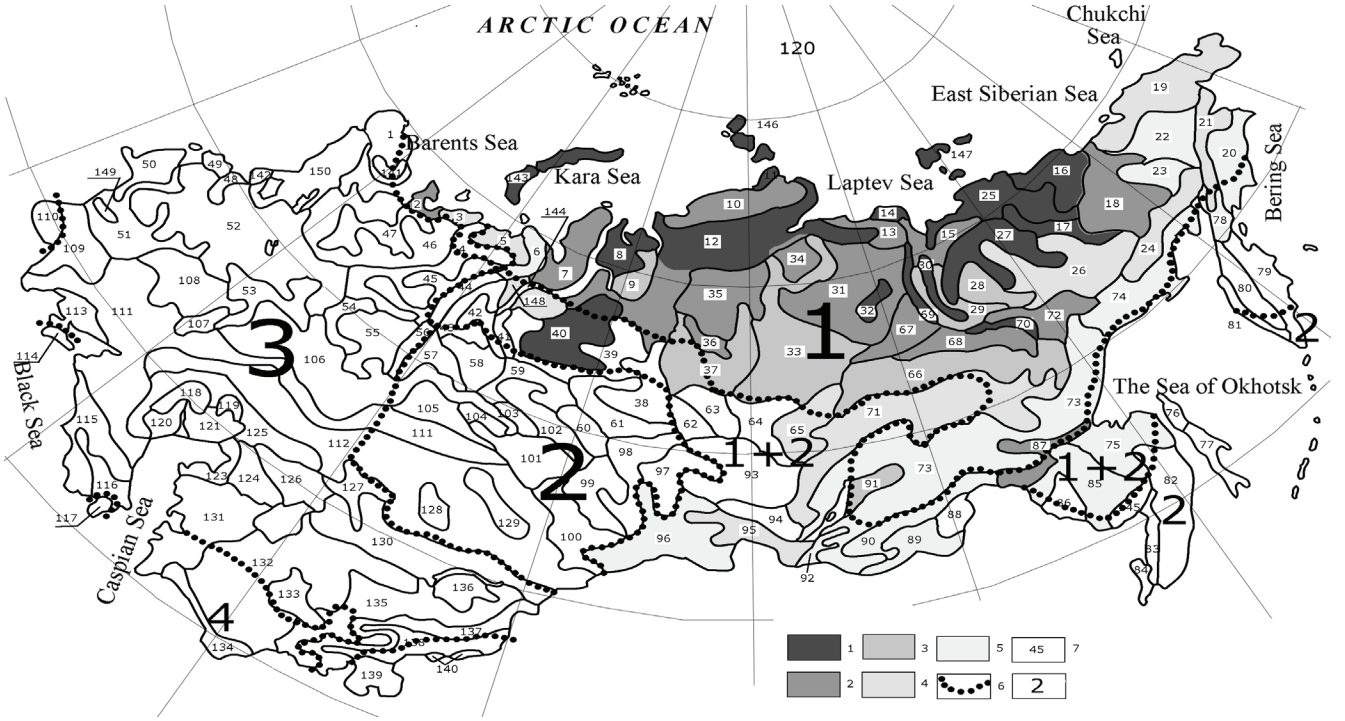

Figure 1. Cryological status of Russian soils. Thawing depths for permafrost-affected soils, cm: (1) < 50, (2) 50–100, (3) 100–150, (4) 150–200, (5) > 200; (6) boundaries of the zones of (**1**) seasonally thawing, (**1 + 2)** seasonally thawing and seasonally freezing, (**3)** seasonally freezing, and (**4**) nonfreezing soils; (7) soil polygon no. in the database; (8) pedocryological zones.

Note: Soil names are given according to the WRB (2006) codes. Soil texture (for predominant soil): S, sand; LS, loamy sand; L, loam; CL, clay loam; LC, loamy clay; Gr, gravelly; St, stony (bouldery). *Soil water content at the moment of freezing in the upper/lower parts of the profile: CR, capillary rupture; FC, field capacity; TC, total capacity; WP, wilting point. **FR, freezing regime: slow (↓) or fast (⇓) freezing from the top and slow (↕) or fast (⇕) freezing both from the top and from the bottom.

Table 1. Cryological parameters of soils along transect 120°E.

Poly-gon	Dominant soils (WRB)	Texture	Temp. at the depth of T_{ampl} = 0, °C	Annual T_{ampl}, °C	Water status*	FR**	Thawing depth, m	Freezing depth, m	Frozen state, months
13	CRoa,tu; CR	LS(Gr, St)	<-10	13-24	FC/TC	⇕↓	0.5-1.0	—	9-11
12	CRgl,tu; CRtu;	L	-5 to -10	11-21	FC/TC	⇕	<0.5(1.0)	—	9-11
31	CRoa,tu;	CL	-5 to -10/ -1 to-3	13-21	FC-TC	↓↕	0.5-1.0	—	9-11
32	HI; GLhi	Peat	-5 to -10	13-17	TC	↓↕	<0.5	—	9-11
67	CRca; CMca,ge	CL	-1 to -3	>24	FC-CR/TC	⇕	0.5-1.0	—	9-11
68	CMlv,ge; CMca,ge	CL	-1 to -3	>24	FC-CR/FC	⇕⇓	0.5-1.0	—	9-11
66	CMeu,ge; CMdy,ge	CL, SL	-2 to -5	21->24	CR-FC/FC	⇕	1.0-2.0	—	9-11
71	CMca; LPrz	CL,SL(Gr)	+2 to -2	13-24	FC/FC	⇓	1.5-2.5	1.5-2.5	7-9
73	PZet; ARab; CRet,sd	LS(Gr, St)	-1 to -3	11-21	FC/<FC	↓↕	2.5-3.5	2.5-3.5	7-9
90	CMdy	LS (Gr, St)	+2 to -2	21-24	<FC/<FC	⇓	—	> 3.0	4-7
88	PZha; PZet	LS (Gr, St)	+2 to -2	21-24	<FC/<FC	↓	—	> 3.0	>8
89	PHha; CH; PHab; KS	CL, LS	+2 to -2	17-24	FC-CR/FC	↓	—	> 3.0	5-8

References

Ananko, T.E. et al. 1998. A system of soil maps: experience in application of a polycomponent basic soil classification for mapping purposes. *Eurasian Soil Sci.* 31(5): 561-573.

Dimo, V.N. 1972. *The Heat Regime of Soils in the USSR*. Moscow: Kolos, 360 pp. (in Russian).

Goryachkin, S. et. al. 2002. Northern circumpolar soil database and derived soil maps in different classification systems. *17 World Congress of Soil Science. 14–21 August 2002,* Bangkok, Thailand. Transactions. CD-ROM, Vol. II., p. 838-1-9.

Mazhitova, G.G. 2008. Soil temperature regimes in the discontinuous permafrost zone in the East European Russian Arctic. *Eurasian Soil Sci.* 41(1): 48-62.

Romanovskii, N.N. 1993. *Basics of Cryogenesis in the Lithosphere.* Moscow: Mosk. Gos. Univ., 334 pp. (in Russian).

Shishov, L.L. et al. 2004. *Classification and Diagnostic System of Russian Soils*. Smolensk: Oikumena, Russia, 342 pp. (in Russian).

Sokolov, I.A. et al. 2006. Soil cryogenesis. In: *Soil-Forming Processes,* Moscow: Dokuchaev Soil Sci. Inst., 144-166 (in Russian).

Acoustical Surveys of Methane Plumes Using the Quantitative Echo Sounder in the Japan Sea

Chiharu Aoyama
Japan's Independent Institute Co., Ltd., Japan
Ryo Matsumoto
University of Tokyo, Japan
Mineo Hiromatsu
Chiba University, Japan
Glen Snyder
Rice University, USA

Introduction

Now methane hydrate is spotlighted as a next-generation energy resource to replace oil and natural gas. It is estimated that the methane hydrate deposits around Japan, a nation otherwise poor in energy resources, would be enough to last over 100 years, based on present levels of natural gas consumption (Matsumoto 1997, Sato 2001).

Many echo sounders have been effectively used for fisheries and surveys (McLennan & Simmons 1992). Echo sounders are classified into three types: depth measurement, including the detection of the sediments under sea floor; fisheries echo sounders; and quantitative echo sounders (Urick 1967). Figure 1 shows an echogram of a depth sounder. The horizontal line on the center part of this figure shows a sea floor. This echogram looks like no acoustic data under the water. On the other hand, Figure 2 shows an echogram of a fisheries echo sounder. This "candle-flame" phenomenon is likely due to density differences originated either by gas bubbles, abrupt water temperature anomalies, or the nucleation of gas hydrate crystals in the water column. Accordingly, we used a quantitative echo sounder on acoustical surveys of methane hydrate.

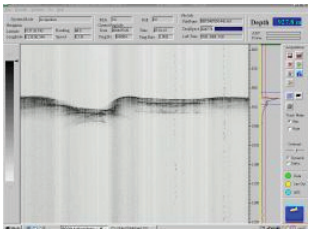

Figure 1. An echogram of a display of a depth sounder. It showed only a sea floor line.

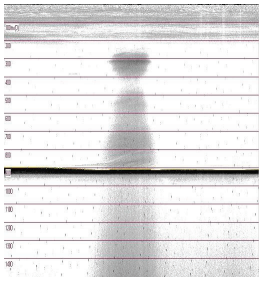

Figure 2. An echogram of a display of a fish echo sounder. It showed a sea floor line and a water column.

Echo sounder's principle

Acoustical observations were made using the quantitative echo sounder. The basic components of its hardware function are to transmit sound, receive, filter and amplify, record, and analyze the echoes. Fisheries hydro-acoustics uses sonar to detect fish.

Experimental Method

Figure 3 shows a schematic diagram of the quantitative echo sounder. As the sound pulse travels through water, it encounters objects that are of different density than the surrounding medium, such as fish that reflect sound back toward the sound source (Jitsuyoshi et al. 1990, Aoyama & Hamada 1997).

To change the ejection amount of methane hydrate bubbles, at the methane hydrate seep point, bubbles were captured with the funnel, whose volume is about 2000 ml (Aoyama et al. 2007), and the MT bottom sampler (inner diameter, 110 mm; length, 285 mm), fixed at the two manipulators of the vehicle that is called Hyper Dolphin (Fig. 3). With bubbles in the funnel and the MT bottom sampler, Hyper Dolphin was moved to 750 m depth underneath *Natsushima*, and then the funnel was turned upside down to release the methane hydrate bubbles from it. The MT bottom sampler was turned upside down to release the methane hydrate bubbles (second ejection). The upwelling of methane hydrate bubbles were observed with the quantitative echo sounder (transducer frequency, 38 kHz) to obtain acoustic data.

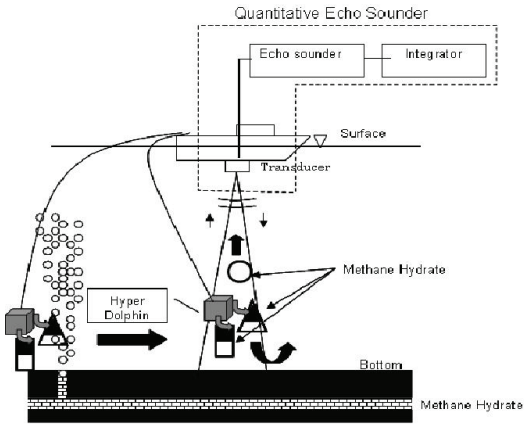

Figure 3. Schematic diagram of the method of the calibration.

Next, to change the depth for bubble release, bubbles were captured with the MT bottom sampler at the methane hydrate bubbles seep point, and Hyper Dolphin was moved to 400 m depth underneath *Natsushima*; then the methane hydrate bubbles were released. The upwelling of methane hydrate bubbles were observed with the quantitative echo sounder (transducer frequency, 38 kHz and 120 kHz) to obtain acoustic data.

Results

Figure 4 shows the echogram of the calibration experiment. The vertical axis represents depth. The grid lines were added at 250 m intervals. The seabed is at 930 m depth. The horizontal axis represents time; the right region shows the later state. The grid lines were added at 4-min intervals. The trapezoidal line that is in the center-left region of the figure represents the cruise line of Hyper Dolphin. It is obvious that Hyper Dolphin moved again from 750 m depth to 930 m depth. The two diagonal bands in the center region of the figure represent the reflection from released methane hydrates. These two "bands" are parallel, and so it can be understood that the bubbles ascend on the straight toward the ship at constant speed, without depending on the amount of methane hydrates. The left one shows the image of the reflection from the methane hydrates released from the funnel (whose volume is about 1000 ml). The right region shows the reflection from the methane hydrates ejected from the MT bottom sampler (whose volume is about 500 ml). This indicates that as the bubbles ascend, they diffuse while weakening its reflection.

With this, it is possible to study the previously obtained acoustic data of the methane hydrate plume in the past three years, and grasp the approximate state of the real methane hydrate plume.

In addition, the data is obtained with two kinds of transducers of 38 kHz and 120 kHz, concurrently, and then frequency characteristics are calculated.

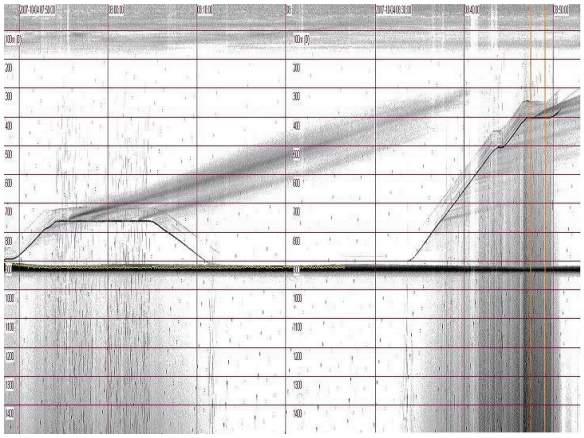

Figure 4. An echogram of the quantitative echo sounder

Acknowledgments

We would like to thank the many crew members of *Umitaka-maru* and *Natsushima* for their help with the surveys.

References

Aoyama, C. & Hamada, E. 1999. *Cruise Report of Tokyo Univ. of Fisheries*, May.

Aoyama, C., Matsumoto, R. Okuda, Y. et al. 2004. Acoustical surveys of methane plumes using the quantitative echo sounder in the eastern margin of the Sea of Japan. *2004 Fall Meeting, American Geophysical Union, San Francisco, California.*

Aoyama, C., Matsumoto, R. et al. 2007. Acoustical surveys using a multi narrow beam sonar and a quantitative echo sounder in gas hydrate area off Joetsu, Japan Sea. *Shinkai Symposium, May 2007*.

Jitsuyoshi, J. et al. 1990. *Acoustical Technical Handbook.* Tokyo: Japan Industry News, 18-19.

Matsumoto, R. 1997. Perspective of methane hydrate science. *Japan Energy Soc.* 76(5): 354-361.

McLennan, D.N. & Simmonds, E.J. 1992. *Fisheries Acoustics*. London: Chapman & Hall.

Sato, M. 2001. Distribution, amount of methane and resources of natural gas hydrates in the world and around Japan. *Aquabiology* 23(5): 460-464.

Urick, R.J. 1967. *Principles of Underwater Sound*. McGraw-Hill, 7-8.

Permafrost Delineation Near Fairbanks, Alaska, Using Geophysical Techniques

Beth N. Astley, Allan J. Delaney
Cold Regions Research and Engineering Laboratory, Fairbanks Alaska

Introduction

Surface geophysical methods can be used to accurately and rapidly map permafrost extent over limited areas and to measure changes in permafrost extent and thickness through time. We investigated discontinuous permafrost sites near Fairbanks, Alaska, using electrical resistivity tomography (ERT), ground-penetrating radar (GPR), and electromagnetic induction (EMI). Discontinuous permafrost in this region is present to depths as great as 60 m, and the active layer ranges from <1 to 3 m.

Between 2004 and 2007, three sites containing discontinuous permafrost were investigated: Fort Wainwright at the base of Birch Hill, Eielson Air Force Base near Mullins Pit, and the CRREL Permafrost Research Site at Farmers Loop Road (Fig. 1). The objectives were to determine permafrost extent and to test the ERT technique compared to more traditional techniques including GPR, EMI (using an EM-31), soil probe, and borehole data.

All three study locations contain relatively flat topography. The Birch Hill and Eielson sites are located on alluvial outwash sands and gravels that contain abandoned river channels. The Farmers Loop Research Site contains approximately 20 m of loess overlying gravels (Linell 1973a). Bedrock at all of these sites is below the depth of investigation. All three sites contain a combination of undisturbed areas and cleared areas.

Methods

Electrical resistivity has been used to define alpine permafrost (Hauck et al. 2003, Hauck & Kneisel 2006), and northern latitude permafrost (Osterkamp et al. 1980, Gilmore et al. 1995, Fortier et al. 1993). At temperatures less than 0°C, resistivity increases exponentially as ground temperature decreases, making it possible to interpret frozen boundaries. Generally, apparent resistivity values above 2000 Ω-m are considered permafrost in alluvial gravels in this region (Astley & Snyder 2005); however permafrost near 0°C in low-moisture silt can have significantly lower values, and apparent resistivity of clean, frozen alluvial gravels has been measured as high as 18,000 Ω-m.

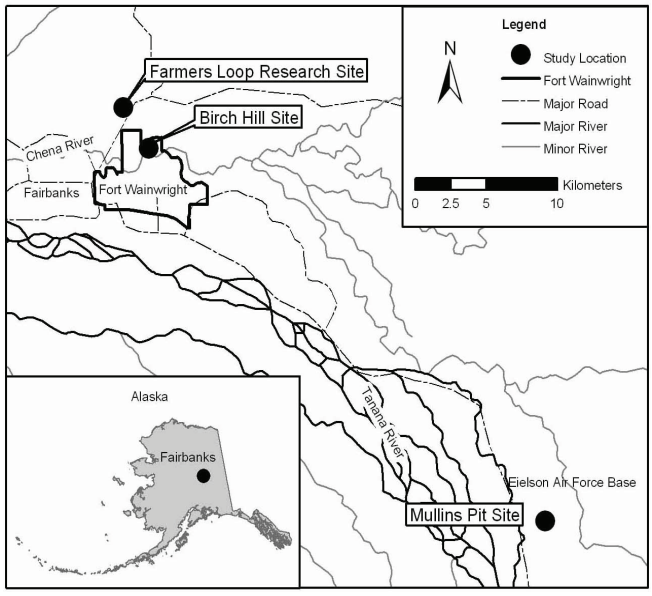

Figure 1. Study site locations near Fairbanks, Alaska.

ERT data were collected with an AGI Supersting R8/IP multi-channel switch resistivity meter and passive cables using Wenner and Dipole-Dipole arrays. Resistivity data were processed using Res2dinv (by Geomoto), a 2-dimensional resistivity inversion program. The inversion process uses forward modeling to produce a best-fit model to the apparent resistivity data (Loke & Barker 1996).

GPR has previously been used to characterize permafrost (Arcone et al. 1998, Lawson et al. 1998, Hinkel et al. 2001). GPR data were collected using GSSI 100- and 400-MHz antennas at the Mullins Pit Site and 50-MHz antennas at the Birch Hill Site. GPR was not attempted at the Farmers Loop Site due to expected signal attenuation in the thick silt there.

EMI methods have been used to map near-surface (<6m) permafrost for decades (Hoekstra & McNeill 1973, Arcone et al. 1979). The advantage to the EM-31 is a relatively fast survey speed compared to other methods. EM-31 data were only collected at the Birch Hill site.

Results

Birch Hill, Fort Wainwright

At the Birch Hill site, a disturbed area appears thawed to depths of 4–19 m. Adjacent, undisturbed areas contain permafrost within 1 m of the surface greater than 30 m thick according to ERT models. We compared the ERT models to EM-31 results and found high correlation for near-surface (<1.5 m) frozen ground. GPR (50-MHz) detected the top of permafrost consistently, but bottom of permafrost was only detected in a few profile segments at depths of 15 to 20 m.

Mullins Pit, Eielson Air Force Base

At the Mullins Pit site, we combined ERT with GPR and frost probing. The 400-MHz GPR detected the active layer depth and thaw zones and the 100-MHz detected thaw zones and the bottom of permafrost. A power line clearing that bisects the study area was found to be significantly thawed, with sporadic permafrost based on the ERT and GPR results.

Table 1. Depth to top and bottom of permafrost at three study locations near Fairbanks, Alaska based on ERT, GPR, EMI, soil probing, and borehole data.

Site	Top (m)	Bottom (m)
Birch Hill		
Undisturbed	<1	17– >30
Cleared	4–9	20–28 or NE
Mullins Pit		
Undisturbed	<1	18–22
Cleared	5–10 or NE	10–17 or NE
Farmers Loop Sections		
A. Undisturbed	<1	
B. Trees removed	<1–7	
C. Cleared	10	

NE = not encountered

Farmers Loop research site

ERT data were collected from two research plots that were created in 1946 by the U.S. Army Corps of Engineers to study the effects of vegetation cover and climate variability on permafrost (Linell 1973b). Section C (cleared plot) appeared thawed to 10 m, while Section B (trees were removed but not the moss layer) had varying depths of 1 to 7 m to permafrost (Table 1). The top of permafrost was detected within Section A (undisturbed) by probing.

Conclusion

Permafrost has thawed to depths as great as 9 m or more at Birch Hill, 10 m or more at Mullins Pit, and 10 m at the Farmers Loops site, where land was cleared and graded over 50 years ago and has remained clear of trees since that time.

The ERT technique was the most accurate compared to boreholes in areas where the permafrost boundaries were continuous and horizontal. Areas with sporadic permafrost containing thin (<1 m thick) frozen layers were not always apparent in the ERT model results. The dipole-dipole inversions were the most accurate for detecting shallow permafrost, while the Wenner inversions were most useful for deep permafrost. GPR interpretations of the top of permafrost matched the ERT data to within 0.5 m; however, the interpretations of the bottom of permafrost depth varied between the two methods. ERT data correlated with EMI data for detecting permafrost within 1 m of the surface. Soil probing and EMI are efficient methods for determining the presence of shallow permafrost (<1 m), while ERT and GPR are more useful for detecting deeper permafrost boundaries. For permafrost delineation, the capabilities and limitations of each geophysical technique should be considered in order to select the best methods for a particular location.

References

Arcone, S.A., Delaney, A.J. & Sellmann, P.V. 1979. Effects of seasonal changes in ground ice on electromagnetic surveys of permafrost. *CRREL Report* 79-23.

Arcone, S.A., Lawson, D.E., Delaney, A.J., Strasser, J.C. & Strasser, J.D. 1998. Ground-penetrating radar reflection profiling of groundwater and bedrock in an area of discontinuous permafrost. *Geophysics* 63(5): 1573-1584.

Astley, B.N. & Snyder, C. 2005. Operable Unit 3 permafrost resistivity investigation, Fort Wainwright, Alaska, *CRREL Letter Report* 05-10.

Gilmore, T.J. & Clayton, E.A. 1995. Mapping the top of the permafrost using surface direct current resistivity survey. *Environmental Geology* 30(1/2): 29-33.

Fortier, R., Allard, M. & Seguin, M.K. 1994. Effect of physical properties of frozen ground on electrical resistivity logging. *Cold Regions Science and Technology* 22: 361-384.

Hauck, C., Mühll, D.V. & Maurer, H. 2003. Using DC resistivity tomography to detect and characterize mountain permafrost. *Geophysical Prospecting* 51(4): 273-284.

Hauck, C. & Kneisel, C. 2006. Application of capacitively-coupled and DC electrical resistivity imaging for mountain permafrost studies. *Permafrost and Periglacial Processes* 17: 169-177.

Hinkel, K.M., Doolittle, J.A., Bockheim, J.G., Nelson, F.E., Paetzoid, R., Kimble, J.M. & Travis, R. 2001. Detection of subsurface permafrost features with ground-penetrating radar, Barrow, Alaska. *Permafrost and Periglacial Processes* 12(2): 179-190.

Hoekstra, P. & McNeill, J.D. 1973. Electomagnetic probing of permafrost. *Proceedings of the Second International Conference on Permafrost, Yakutsk, USSR, 1973*: 517-526.

Lawson, D.E., Arcone, S.A, Delaney, A.J., Strasser, J.D., Strasser, J.C., Williams, C.R & Hall, T.J. 1998. Geological and geophysical investigations of the hydrogeology of Fort Wainwright, Alaska. Part II: North-central cantonment. *CRREL Report* 98-6.

Linell, K.A. 1973a. Risk of uncontrolled flow from wells through permafrost. *Permafrost: North American Contributions Second International Conference, Yakutsk, USSR, July 1973*. National Academy of Sciences, 462-468.

Linell, K.A. 1973b. Long-term effects of vegetative cover on permafrost stability in an area of discontinuous permafrost. *Permafrost: North American Contributions Second International Conference, Yakutsk, USSR, July 1973*. National Academy of Sciences, 688-693.

Loke, M.H. & Barker, R.D. 1996. Rapid least-squares inversion of apparent resistivity pseudosections by a quasi-Newton method. *Geophysical Prospecting* 44(1): 131-152.

Osterkamp, T.E., Jurick, R.W., Gislason, G.A., & Akasofu, S.I. 1980. Electrical resistivity measurements in permafrost terrain at the Engineer Creek road cut, Fairbanks, Alaska. *Cold Regions Science and Technology* 3: 277-286.

Preparatory Work for a Permanent Geoelectrical Measurement Station for Permafrost Monitoring at the Hoher Sonnblick, Austria

Michael Avian
Institute of Remote Sensing and Photogrammetry, Graz University of Technology, Austria
Andreas Kellerer-Pirklbauer
Institute of Geography and Regional Science, University of Graz, Austria
Alexander Römer
Department of Geophysics, Geological Survey of Austria
Robert Supper
Department of Geophysics, Geological Survey of Austria

Introduction

The thermal and distributional state of permafrost in alpine environments is widely discussed in recent times due to hazardous geomorphic events threatening infrastructure, tourism, or residents. Subterrain processes in environments influenced by permafrost degradation might cause severe problems to alpine infrastructure (e.g., alpine huts, cable-cars). However, such processes are not fully understood so far.

The meteorological observatory at the top of the Hoher Sonnblick (3106 m a.s.l., 47°03′N, 12°57′E, Fig.1) has faced problems of permafrost degradation since the 1990s, leading to intense protection activities during the last years. This observatory has been operating continuously since 1886, presenting one of the longest records of meteorological data in the entire alpine arc. Data from this observatory indicate a rise of the mean annual air temperature (MAAT) by 1.6°C since 1886 (Auer et al. 2002), which is substantially above the global average of 0.74°C (IPCC 2007). The summit area of Hoher Sonnblick is stage of several investigations that focus on the relationship between recent climate change and alterations of a mountain permafrost body in a mountain top detritus environment. One of the most important projects investigates the thermal state of the uppermost 20 m of the summit area monitored at three boreholes—each equipped with 25 temperature sensors—aligned along a south-facing slope (Fig. 2). These three boreholes are the first permafrost boreholes installed within Austria and will therefore deliver important temperature data relevant for the mountain permafrost distribution of the Eastern Alps. However, no temperature data are published so far (Staudinger & Schöner 2008, pers. com.).

In order to get more information about the spatial distribution and temporal changes of the subsurface temperature conditions within shorter periods at Hoher Sonnblick, the installation of a permanent geoelectrical measurement profile is currently carried out. Logistical and technical information regarding the relevant preparatory work is presented here.

Methods

Geoelectrical investigations of areas underlain by permafrost have been carried out at numerous study areas in the Alps (e.g., Hauck et al. 2003, Kneisel 2004). Hilbich et al. (2008) report from repeated electrical resistivity tomography (ERT) measurements coupled with borehole temperature data at Schilthorn (Switzerland), thereby focusing on active layer dynamics. The application of ERT allows the determination of specific electrical resistivity within the subsurface structure. This parameter is mainly dependent on porosity, water saturation, conductivity of pore fluid and clay content. Minor influence is given by particle shape and pore geometry.

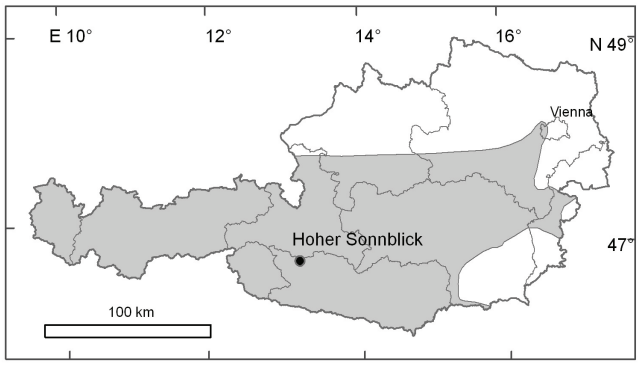

Figure 1. Location of the study area Hoher Sonnblick within Austria, as well as the Austrian part of the European Alps (grey).

Two measurements have been carried out manually so far (August 2006 and March 2007) but are planned to be remote controlled in the next project stage. So this test stage verifies the capability of the GEOMON4D for remote-controlled measurements of geoelectric pseudo-sections. Several requirements have to be considered: high-resolution measurements, possibility of snapshots of the underground, high reliability, and quick availability of data.

Preparatory Work and Outlook

The first ERT measurements, consisting of 16 electrodes at a spacing of 1 m, were carried out in August 2006 with a Sting RI (AGI) multi-electrode and the GEOMON4D system for comparison. Within the second campaign in March 2007, a permanent profile with 41 electrodes at 0.5 m spacing and 20 m length was installed near the profile of the first campaign. Three thousand measurements were carried out, each sampled for 1000 times. Furthermore, a lightning

protection system was developed in winter 2007/08 to consider the special location on this mountain top.

The ERT profiles were measured with different electrode configurations (Wenner/Schlumberger, Gradient). The results of the inversion for both periods are shown in Figure 3.

Figure 3 indicates an increase of electrical resistivity during winter time. In the measurements of March 2007, high electrical resistivities—representing bedrock or frozen ground—occur in shallow depths in comparison to the measurements of August 2006 (from 1.5–2 m). The overlying structure is characterized by a heterogeneous distribution of resistivity anomalies, ranging from a few hundred up to some thousands of Ohmm. This is addressed as the fragmented/broken rock with some silt fillings, and represents the active layer in such permafrost regions. Therefore, a change of the permafrost table can be interpreted of 1.5 m in 2006 and 0.5 m in 2007 (Fig. 3).

The accomplished test measurements for the installation of a permanent ERT station at the top of Hoher Sonnblick show that observed changes in resistivity allow a monitoring of seasonal changes of the thaw and freeze processes in the active layer. This should lead—in combination with other monitoring techniques—to a better understanding of the processes in the mountaintop detritus of Hoher Sonnblick. After field tests, the permafrost monitoring system will be installed at Hoher Sonnblick in May 2008. The system should then operate completely automatically and can be remote controlled from the Geological Survey of Austria in Vienna.

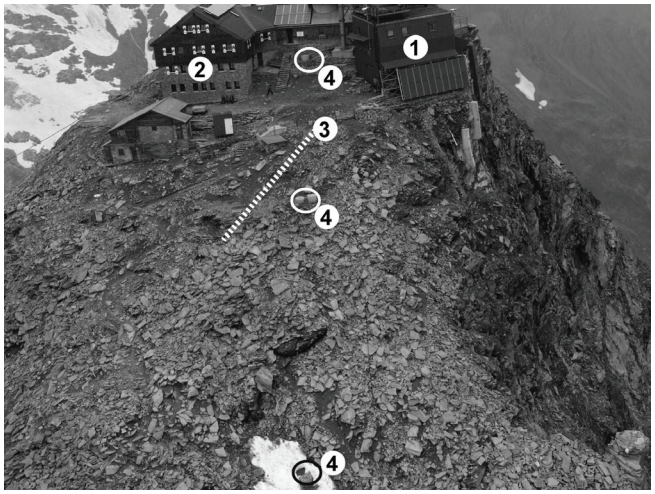

Figure 2. Location of the meteorological observatory (1), alpine hut (2), geoelectric profile (3), and the three boreholes (4). View towards the north. (Photograph kindly provided by M. Staudinger.)

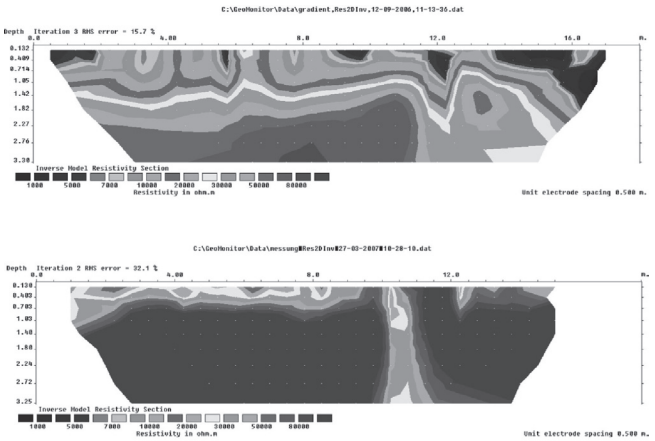

Figure 3. Electrical resistivity tomography (ERT) results from August 2006 and March 2007.

Acknowledgments

These activities were carried out mainly within the framework of the project ALPCHANGE (www.alpchange.at) funded by the Austrian Science Fund (FWF) through project no. FWF P18304-N10.

References

Auer, I., Böhm, R., Leymüller, M. & Schöner, W. 2002. Das Klima des Sonnblicks – Klimaatlas and Klimageographie der GAW-Station Sonnblick einschließlich der umgebenden Gebirgsregion. Österreichische Beiträge zur Meteorologie und Geophysik 28: 305 pp.

Hauck, C., Von der Mühll, D. & Maurer, H. 2003. Using DC resistivity tomography to detect and characterize mountain permafrost. *Geophys. Prospect.* 51: 273-284, doi:10.1046/j.1365-2478.2003.00375.x.

Hilbich, C., Hauck, C., Hoelzle, M., Scherler, L., Schudel, L., Völksch, I., Von der, Mühll, D. & Mäusbacher, R. 2008. Monitoring mountain permafrost evolution using electrical resistivity tomography: A 7-year study of seasonal, annual, and long-term variations at Schilthorn, Swiss Alps. *J. Geophys. Res.* 113: F01S90, doi:10.1029/2007JF000799.

IPCC. 2007. *Climate Change 2007: The Physical Science Basis*. Contribution of Working Group I to the Fourth Assessment Report of the Intergovernmental Panel on Climate Change, S. Solomon, D. Qin, M. Manning, Z. Chen, M. Marquis, K.B. Averyt, M. Tignor & H.L. Miller (eds.). Cambridge, U.K. & New York, NY, USA: Cambridge University Press.

A Provisional Soil Map of the Transantarctic Mountains, Antarctica

Megan R. Balks
Earth and Ocean Sciences, University of Waikato, Private Bag 3105, Hamilton, New Zealand
Malcolm McLeod
Landcare Research, Private Bag 3172, Hamilton, New Zealand
James G. Bockheim
Department of Soil Sciences, University of Wisconsin, 1525 Observatory Drive, Madison, WI 53706-1299, USA

Introduction

A provisional soil map has been prepared for the Transantarctic Mountain region of Antarctica in three wall-size (A0) sheets, each at a scale of 1:1,000,000. The maps contribute to the ANTPAS (Antarctic Permafrost and Soils) effort to develop a soil map of the Antarctic continent and pdf files of the maps will be made available on the ANTPAS website http://erth.waikato.ac.nz/antpas/.

The Transantarctic Mountains extend 3500 km across the Antarctic continent from 69°S in northern Victoria Land to 87°S in the upper Scott Glacier region. The Transantarctic Mountain region has an ice-free area of 21,000 km^2, which constitutes 42% of the total ice-free area (49,500 km^2) of Antarctica. The climate ranges from ultraxerous, with temperatures rarely exceeding 0°C, on the inland margins of the Transantarctic Mountains, to subxerous, with temperatures greater than 0°C for several weeks in summer and liquid water present for short periods, on coastal margins (Campbell & Claridge 1987). Soil parent materials are predominantly glacial tills with mixed lithologies, mainly dominated by sandstones, granites, and dolerites. Altitude ranges from sea level to peaks of over 2500 m with many steep valley sides. Topography has a strong influence on local microclimates. Soil surfaces range from Holocene to Pliocene in age. Over much of the area the influence of organisms on soil development is limited to microbial life. In warmer, moister, coastal sites small areas with extensive moss coverage occur and penguins have an impact on soil development, providing guano-rich soils, in small areas of nesting colonies.

While the general pattern and properties of Antarctic soils are well known (e.g., Tedrow & Ugolini 1966, Campbell & Claridge 1987, Bockheim 2002), little attention was paid to mapping the spatial distribution of Antarctic soils until recently, when soil maps of the Wright Valley (McLeod et al. 2008, this proceedings), the McMurdo Dry Valleys (Bockheim & Mcleod 2008), and the Seabee Hook (Hofstee et al. 2006) have been published. This paper is a "partner" to Bockheim et al. (2008, this proceedings), which describes permafrost maps of the Transantarctic Mountains.

Methods

The soil maps have been compiled from existing data, including published data and data archived by the National Snow & Ice Data Center (http://nsidc.org/cgi-bin/get_metadata.Pl?id-ggd221) and New Zealand Landcare Research (http://www.landcareresearch.co.nz). Scanned and geo-rectified 1:250,000 topographic maps prepared by the U.S. Geological Survey (http://usarc.usgs.gov) were joined in ArcGIS 9.2 and used as a base map. Aerial photograph and topographic map interpretation were used to extrapolate to areas where field data are limited. Because some parts of the region are more readily accessible, with more data available than others, a "confidence" rating was applied to each map unit as described in McLeod et al. (2007). Recent fieldwork was undertaken by the authors in the Darwin Glacier, Wright Valley, and Cape Hallet areas to add to existing data and corroborate our data, topographic map, and photo, interpretations.

Table 1 Provisional physiographic legend.*

Soils of the subxerous coastal regions
Formed on patterned ground
Typic Haploturbels + Typic Haplorthels
Formed on ice-core drift
Glacic Haploturbels + Glacic Haplorthels
Formed within penguin colonies
Ornithic Haplorthels
Formed on nunataks or rock outcrops
Lithic Haploturbels + Lithic Haplorthels
Formed in areas with patterned ground and rock outcrops
Lithic Haploturbels + Orthic Haploturbels + Lithic Haplorthels + Typic Haplorthels
Soils of the xerous and ultraxerous inland areas
Formed in areas with dry permafrost to > 70 cm depth and no patterned ground
Typic Anhyorthels
Formed on patterned ground with dry-permafrost to > 70 cm depth
Typic Anhyorthels + Typic Anhyturbels
Formed on patterned ground with ice-cement or seasonally moist soil at < 70 cm depth
Typic Haploturbels + Typic Haplorthels
Formed on patterned ground with ice-cement or seasonally moist soil at < 70 cm depth and rock outcrops
Typic Haploturbels + Typic Haplorthels + Lithic Haploturbels + Lithic Haplorthels
Formed on ice cored drift with dry-permafrost to > 70 cm depth
Glacic Anhyturbels + Glacic Anhyorthels
Formed on nunataks or rock outcrops including areas with dry permafrost to >70 cm depth
Lithic Anhyorthels + Typic Anhyorthels

* + denotes a soil association.

Soil Map Units

Soil classification

The soils were mapped to the Subgroup level following USDA Soil Taxonomy (Soil Survey Staff 2006). All of the soils key out within the Gelisol Soil Order. Typic Haplorthels, Typic Haploturbels, and Typic Anhyorthels predominate with Lithic, Salic, and Ornithic subgroups also recognised. The Ornithic subgroup has been included to informally distinguish guano-rich soils in penguin colonies.

Soil associations

At the small scale of this map, it is impossible to show all the detail of the soil landscape pattern. Where the pattern is predictable from interpretation of the surface topography, soil associations are mapped. The most common soil association occurs where there is patterned ground with Typic Haplorthels in the centre of the polygons and Typic Haploturbels in the strongly cryoturbated polygon margins. In areas where nunataks or rock outcrops occur, a soil association between Lithic and Typic Subgroups is recognised.

Map legend

The provisional physiographic legend (Table 1) provides a guide to the soils in relation to their landscape position.

Within the ultraxerous climate region of the dry valleys, seasonally moist soils (Haploturbels and Haplorthels) occur on lake margins and adjacent to ephemeral streams fed from glacial meltwaters. While calcic, salic, nitric, petrosalic, and petronitric soil Subgroups are described in the region they are not recognised on the small scale of these maps.

Concluding Statement

The maps presented here are an overview of the soils in the Transantarctic Mountains, and are intended to complement similar maps to be prepared by other ANTPAS workers to contribute to a soil map of the Antarctic continent. Work remains to develop a more detailed understanding of the diversity and distribution of Antarctic soils at larger scales (1:50,000 or larger). With over 30,000 tourists predicted to visit Antarctica in the 2008–2009 summer (*www.iaato.org*), one immediate application for a more detailed soil mapping effort is for identification and interpretation of the vulnerability of Antarctic soils to the effects of human activities. Detailed soil maps will also provide a benchmark against which effects of global change can be measured in the future.

Acknowledgments

The Landcare Research database contains the pioneering Antarctic soil work of Iain Campbell and Graeme Claridge. Thanks to Antarctica New Zealand for Logistic support.

References

Bockheim, J.G. 2002. Landform and soil development in the McMurdo Dry Valleys: A regional synthesis. *Arctic, Antarctic and Alpine Research* 34: 308-317.

Bockheim, J.G. & McLeod, M. 2008. Soil distribution in the McMurdo Dry Valleys, Antarctica. *Geoderma* 144: 43-49.

Bockheim, J.G., McLeod, M. & Balks M.R. 2008. A provisional permafrost map of the Transantarctic Mountains. *Proceeding of the Ninth International Conference on Permafrost, Fairbanks, Alaska, 29 June–3 July 2008*.

Campbell, I.B. & Claridge, G.G. C. 1987. *Antarctica, Soils, Weathering Processes and Environment. Developments in Soil Science 16.* Amsterdam: Elsevier, 368 pp.

Hofstee, E.H., Balks, M.R., Petchey, F. & Campbell, D.I. 2006. Soils of Seabee Hook, Cape Hallett, Antarctica. *Antarctic Science* 18: 473-486.

McLeod, M., Bockheim, J.G. & Balks, M.R. 2007. A fifth-order reconnaissance map of ice-free ares of the Transantarctic Mountains, Antarctica. *Proceedings of the 10th symposium on Antarctic Earth Sciences. U.S. Geological Survey and the National Academies; USGS F-2007-1047,* Extended Abstract 116.

McLeod, M., Bockheim, J.G. & Balks, M.R. 2008. Soil map of the Wright Valley, Antarctica. *Proceedings of the Ninth International Conference on Permafrost. Fairbanks, Alaska, 29 June–3 July 2008.*

Soil Survey Staff. 2006. *Keys to Soil Taxonomy*, 10th ed. U.S. Department of Agriculture, Natural Resources Conservation Service, 332 pp.

Tedrow, J.C.F. & Ugolini, F.C. 1966. Antarctic soils. In: J.F.C. Tedrow (ed.), *Antarctic Soils and Soil Forming Processes.* Antarctic Research Series. American Geophysical Union, Washington, DC, 8: 161-177.

Martian Permafrost Depths from Orbital Neutron and Temperature Measurements

Joshua L. Bandfield
Department of Earth and Space Sciences, University of Washington, Seattle
William C. Feldman
Planetary Science Institute, Tucson, Arizona

Introduction

The high abundance of hydrogen detected by the Mars Odyssey Neutron Spectrometer (MONS) and High Energy Neutron Detector measurements (e.g., Feldman et al. 2007, Mitrofanov et al. 2004) are consistent with a high concentration of water ice in the shallow subsurface on Mars. Martian high latitudes also have thermal properties consistent with an extensive high thermal inertia layer within a few centimeters of the surface. These results are in agreement with models of theoretical water-ice stability (e.g., Leighton & Murray 1966).

The purpose of this abstract is to show global and local thermally-derived permafrost depths and compare these results with neutron-derived water ice depths. We use the term "permafrost" to describe a buried high inertia surface detected using temperature measurements and "water ice" to describe the high latitude hydrogen concentrations detected using neutron measurements. Both models assume a relatively simple two-layered geometry of relatively dry soil cover on top of a semi-infinite water-rich layer that is assumed constant throughout the measurement field of view. More complicated systems are likely to be common on Mars, but the datasets do not have the leverage to converge on unique solutions with complex geometries.

Methods and Data

This study utilizes the surface kinetic temperature derived from the Mars Global Surveyor Thermal Emission Spectrometer (TES) and Mars Odyssey Thermal Emission Imaging System (THEMIS). TES data were averaged in bins of 2° latitude, 4° longitude and 4.5° L_s (1/80 year) to construct seasonal surface temperature profiles. THEMIS 100 m/pixel temperature images were acquired over a surface at two seasons to estimate the seasonal cooling rate. We use a thermal model (developed and provided by H.H. Kieffer) to predict surface temperatures. This model allows for customization of a wide variety of parameters such as changes in subsurface thermophysical properties and atmospheric aerosol properties.

The TES- and THEMIS-derived surface temperatures are fit using a non-linear least squares fitting routine. All modeling parameters were fixed except surface cover thermal inertia and depth of the permafrost layer. The seasons used for fitting were restricted to summer and early fall seasons. The model permafrost layer has fixed thermophysical properties, but was allowed to vary from 1.15 to 20.3 diurnal skin depths. As a result, the model and fitting routine is sensitive to permafrost at 0.3–6 and 12–220 cm depths for dusty and rocky surface covers, respectively. Water ice and solid rock have similar thermal inertias (primarily because of offsetting heat capacity and density values), and it is not possible to determine the concentration of water in the permafrost layer from the temperature data. Methods and uncertainties are discussed in detail in Bandfield & Feldman (in press).

The thermal and epithermal neutron currents derived from MONS are translated into the water equivalent hydrogen (WEH) abundance of a semi-infinite buried layer of soil. The top layer has the same composition as that of the bottom layer, but restricted to a WEH abundance of 1 wt. % (e.g., Feldman et al. 2007). The burial depth of the bottom layer is also determined from this model.

Results and Discussion

A qualitative comparison of Neutron Spectrometer hydrogen and TES permafrost depths displays remarkable agreement, considering the fundamental difference in the measurements (Fig. 1). In the Northern Hemisphere, water ice and permafrost depths are greater within lower latitude, higher surface cover thermal inertia, and low albedo regions. This shows that the water ice depth is generally following its predicted stability, as all three of these properties generally increase the depth of water ice stability. At higher latitudes, all surfaces are characterized by shallow water ice/permafrost depths.

In the Southern Hemisphere, water ice/permafrost depths are shallow at latitudes poleward of ~65°S. A relatively steep increase in depths appears between 60–65°S that, as in the North, coincides with an increase in surface cover thermal inertia and a decrease in latitude and albedo. This is relatively constant with longitude except between ~50–140°E, near the southern rim of Hellas Basin. In these regions, the surface cover thermal inertia remains low and the albedo is relatively high, which allows for water ice to remain stable at relatively shallow depths at lower latitudes.

Despite the similar spatial patterns present in the neutron- and temperature-derived water ice depths, temperature-derived depths are greater than neutron-derived depths at depths greater than ~10 cm. Part of this discrepancy may be explained by differences in the depths of sensitivity of the two techniques. There may also be a physical explanation as well. At greater burial depths, the neutron measurements may be more sensitive to layered hydrated minerals closer to the surface than more deeply buried deeper water ice. An additional explanation for the discrepancy may lie in the simplistic assumptions of a two-layered dry regolith/icy permafrost model. The general agreement of the neutron- and temperature-derived water ice depths adds robustness to the accuracy of both datasets and techniques. However, disagreements between the two sets of results may also lend

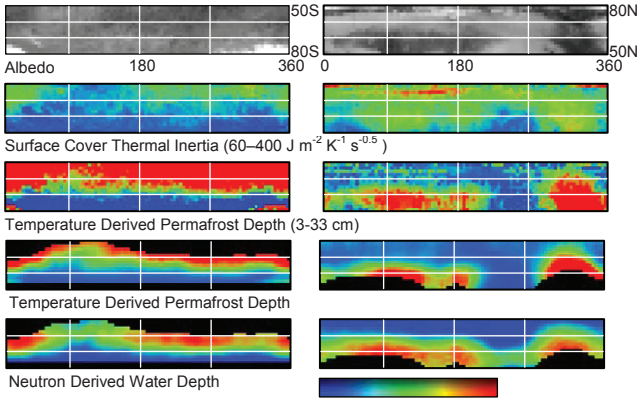

Figure 1. Albedo, surface cover thermal inertia, and permafrost/water depth maps. The temperature-derived depth map is shown twice: at full resolution (third from top) and spatially filtered and masked (fourth from top) to match the coverage and resolution of the neutron-derived water depth maps. The maps cover all longitudes and 50–80 N/S latitude.

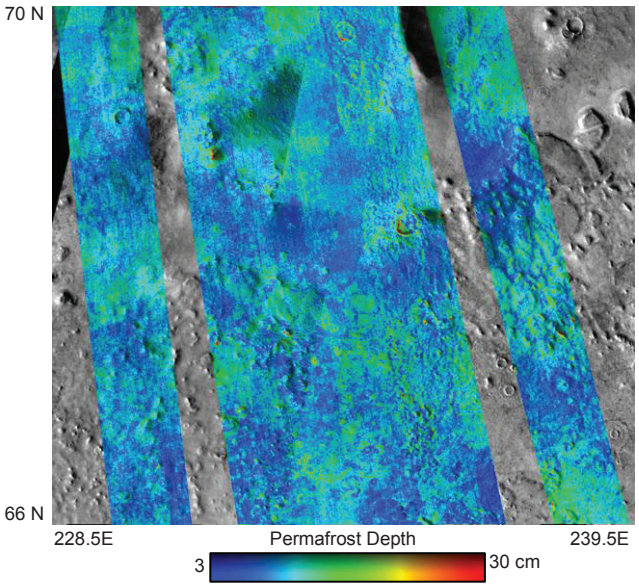

Figure 2. The permafrost depths derived from THEMIS seasonal temperature data are in reasonable agreement with the TES data from the same region. The area shown here includes the primary landing site for the Phoenix spacecraft. The region shown is approximately 250 km across.

insight into their inherent flaws as well as provide clues about the nature of the subsurface structure.

Although a general pattern of increased permafrost depth with decreasing latitude is present globally, the surface cover thermal inertia is also highly correlated with permafrost depth (Fig. 1). A surface with high thermal inertia conducts more energy into the subsurface and to a greater depth than a low thermal inertia surface cover. An exception to this correlation appears between 70–80°N and is concentrated near regions of permanent water ice exposures detached from the main polar cap from ~90–270°E. The most likely explanation for these high surface cover thermal inertia values is that the permafrost is shallow enough to influence the derived surface cover thermal inertia. These exposures are probably extensions of the exposed ice deposits covered by a lag of residual dust.

It is clear that there are regional variations in permafrost depth at the scale of the TES and Neutron Spectrometer measurements. Local slopes, surface cover thermal inertia, and albedo can all have significant effects on the depth of the permafrost. Permafrost depths have been shown to have this variability at the sub-km scale (Bandfield 2007). Figure 2 displays permafrost depths determined from THEMIS seasonal temperature data over the region of the 2007 Mars Scout Phoenix spacecraft landing site. The average permafrost depth retrieved from the TES data for the region is 4.5 cm. The THEMIS data has slightly higher values of 6.2 cm. This comparison shows that the low resolution measurements retain an overall accuracy, but are not able to resolve a large amount of detailed variability that is clearly present. Spatial variability in water ice/permafrost depths is present at all scales and the THEMIS data provide an important bridge between the tens to hundreds of km scales of the TES and Neutron Spectrometer measurements and the <1 m scales to be accessed by the Phoenix Lander.

Summary

It is possible, and indeed likely, that the current distribution of water ice is attributable to both recession of residual surface ice deposits as well as emplacement via vapor diffusion (Schorghofer 2007). Temperature and neutron measurements show water ice distributions largely consistent with the present stability limits. The subsurface distribution of the water ice may be more complicated than an icy/not-icy model that the simple nature of the datasets restrict us to, however. Climate cycles can be variable in both magnitude and duration, and these variations may leave their imprint on the subsurface water distributions.

Acknowledgments

We would like to thank Hugh Kieffer for providing guidance and use of the thermal model used in this work.

References

Bandfield, J.L. 2007. High-resolution subsurface water-ice distributions on Mars. *Nature* 447: 64-67.

Bandfield, J.L. & Feldman, W.C. 2008. Martian high latitude permafrost depth and surface cover thermal inertia distributions. *J. Geophys. Res.* (in press).

Feldman, W.C. et al. 2007. Vertical distribution of hydrogen at high northern latitudes on Mars: The Mars Odyssey Neutron Spectrometer. *Geophys. Res. Lett.* 34: 5201-5204.

Leighton, R.R. & Murray, B.C. 1966. Behavior of carbon dioxide and other volatiles on Mars. *Science* 153: 136-144.

Mitrofanov, I.G. et al. 2004. Soil water content on Mars as estimated from neutron measurements by the HEND instrument onboard the 2001 Mars Odyssey spacecraft. *Solar Sys. Res.* 38: 253-257.

Schorghofer, N. 2007. Dynamics of ice ages on Mars, *Nature* 449: 192-195.

Time Series Analyses of Active Microwave Satellite Data for Monitoring of Hydrology at High Latitudes

Annett Bartsch
Institute of Photogrammetry and Remote Sensing, Vienna University of Technology, Austria

Introduction

Microwaves can penetrate cloud cover and are independent from daylight conditions. Active systems onboard satellites provide coarse (scatterometer) to medium resolution data (ScanSAR and SAR). An increase of spatial resolution always goes along with reduced revisit intervals. In general, satellites with microwave sensors are polar-orbiting platforms. This means that data coverage increases at higher latitudes due to overlapping footprints and swaths, respectively. Scatterometer can provide here several measurements per day, and medium resolution ScanSAR, up to daily acquisitions.

The backscatter intensity depends on the used wavelength, polarization, incidence angle, and surface conditions (Henderson & Lewis 1998). The latter include dielectric properties and surface structure. Even surfaces such as lakes produce low backscatter compared to forests, where multiple scattering causes higher signal returns. Microwaves have a high application potential in hydrology, since dielectric properties are related to water content. Time series can be used to monitor soil moisture, snowmelt, and inundation. This extended abstract gives an overview of some available datasets and application examples in permafrost areas. Additional information can be found on http://www.ipf.tuwien.ac.at/radar/.

Near-Surface Soil Moisture

The ERS1 and ERS2 C-band scatterometer have been proven useful for derivation of relative soil moisture (Wagner et al. 1999, Wagner et al. 2007). Such data are available globally with 50km resolution since 1992. The long dataset allows the determination of deviations and thus anomalies. Continuation is ensured due to the launch of Metop in October 2006. The new ASCAT instrument on Metop provides even shorter revisit intervals and increased spatial resolution (25 km; Bartalis et al. 2007).

The near-surface soil moisture can be determined by time series analysis (Wagner et al. 2003). A dry and wet reference is identified for each grid point and each single measurement scaled between these limits. This results in a relative measure of near-surface soil moisture. By application of a simple infiltration model, profile soil moisture is derived (Wagner et al. 1999). The latter is referred to as Soil Water Index (SWI) and is available globally as 25 km grid cells in 10-day intervals (Wagner et al. 2007). The observed near-surface soil moisture variations are related to river discharge (Scipal et al. 2005). Although snowmelt is more important for the magnitude of discharge in high latitudes, a close relationship to soil moisture can be observed during the summer (Bartsch et al. 2007b).

The European satellite ENVISAT has a C-band SAR instrument onboard. This Advanced SAR (ASAR) provides higher resolution data (image mode) as well as medium resolution ScanSAR (Wide Swath and Global Mode). The latter has a wider swath (405 km) than high-resolution modes, which allows coverage of larger regions and provides shorter revisit intervals (with varying incidence angles). Therefore, a similar time series analysis, as developed for scatterometer data, can be applied to ScanSAR data for extraction of near-surface relative soil moisture. This has successfully been carried out for Southern Africa (Bartsch et al. 2007c) and Oklahoma (Pathe et al. 2007). It could be transferred to high latitudes where ENVISAT ASAR Gobal Mode (1km) data provide up to daily measurements (Bartsch et al. in press a). Such medium resolution ScanSAR data can also be used to derive spatial scaling properties, which allow an interpretation of coarse-resolution soil moisture from scatterometer (25 km) at local scale (1 km) (Wagner et al. 2008). Other new microwave sensors, such as the ALOS PALSAR (L-band, 12.5 m in fine beam mode), provide increased spatial and nevertheless low temporal resolution, but have potential for soil moisture retrieval (Bartsch et al. 2007d).

Snowmelt

C-Band (~5.6 cm) as well as K_u-band (~2.1 cm) radars are suitable for snowmelt detection. Changes in the snowpack, however, have a stronger impact on backscatter at shorter wavelengths. The SeaWinds Quikscat is a K_u-band scatterometer, which provides measurements with 25 km resolution since 1999. Re-gridded datasets are available with up to 5 km resolution (Long & Hicks 2005). The first entire snowmelt period on the Northern Hemisphere is covered in 2000. Large changes in backscatter between morning and evening acquisitions are characteristic for the snowmelt period, when freezing takes place overnight and thawing of the surface during the day. A change from volume to surface scattering occurs in case of melting. This may cause changes up to 6 dB (Kimball et al. 2004). When significant changes due to freeze/thaw cycling cease, closed snow cover also disappears (Bartsch et al. 2007a). For the identification of melt days over permanently snow- or ice-covered ground, only evening measurements are considered (Ashcraft & Long 2006). Diurnal differences (Bartsch et al. 2007a) on the other hand are calculated for the delimitation of the final spring snowmelt period. The exact day of year of beginning and end of freeze/thaw cycling can be clearly determined with consideration of long-term noise. Such an approach allows not only the monitoring of disappearance of snow. Areas which undergo thaw at a certain day can be identified

as well. The QuikScat-derived thaw patterns relate to spring river discharge in high latitudes (Bartsch et al. 2007b).

Lakes and Wetlands

Due to the backscatter properties of open water (even surface), lakes can be easily identified with active microwave data. Although wind may increase the surface roughness, lakes can be identified based on time series (Bartsch et al. 2007e, Bartsch et al. in press b). Due to the wider swath and thus increased spatial and temporal coverage of ScanSARs, large regions can be processed. For example, ENVISAT ASAR Wide Swath data with 150 m resolution provide considerably more detailed information in tundra regions than land cover products from MODIS (500 m; Bartsch et al. in press b). The spatial distribution of lakes larger than 2 ha can be used for the determination of tundra wetland extent and also estimation of methane emissions.

Peatlands are characterized by high soil moisture conditions. They can be identified due to the sensitivity of microwaves to moisture/dielectric properties (Bartsch et al. 2007e). ENVISAT ASAR Wide Swath (150 m) as well as Global Mode (1km) time series are suitable for mapping of large regions such as the West Siberian Lowlands (Bartsch et al. in press b).

Acknowledgments

The author is the recipient of a Hertha Firnberg research fellowship (Austrian Science Fund, T322-N10).

References

Ashcraft, I.S. & Long, D.G. 2006. Comparison of methods for melt detection over Greenland using active and passive microwave measurements. *International Journal of Remote Sensing* 27: 2469-2488.

Bartalis, Z., Wagner, W., Naeimi, V., Hasenauer, S., Scipal, K., Bonekamp, H., Figa, J. & Anderson, C. 2007. Initial soil moisture retrievals from the METOP-A Advanced Scatterometer (ASCAT). *Geophysical Research Letters* 34: L20401

Bartsch, A., Kidd, R.A., Wagner, W. & Bartalis, Z. 2007a. Temporal and spatial variability of the beginning and end of daily spring freeze/thaw cycles derived from scatterometer data. *Remote Sensing of Environment* 106: 360-374.

Bartsch, A., Wagner, W., Rupp, K. & Kidd, R.A. 2007b. Application of C and Ku-band scatterometer data for catchment hydrology in northern latitudes. In: *Proceedings of the 2007 IEEE International Geoscience and Remote Sensing Symposium, Barcelona, Spain 23–27 July 2007*: 3702-3705.

Bartsch, A., Pathe, C., Sabel, D., Wagner, W. & Doubkova, M. 2007c. Soil Moisture Time Series from Active Radar in Support of Runoff Monitoring on Local, Catchment and Regional Scale. *Proceedings of the Second ESA Space for Hydrology Workshop, Geneva, 12-14 November 2007*.

Bartsch, A., Pathe, C., Sabel, D. & Wagner, W. 2007d. Relative soil moisture from C- and L-band SAR time series. *Proceedings of the First Joint PI Symposium of ALOS Data Nodes, Kyoto, 19–23 November 2007*.

Bartsch, A., Kidd, R., Pathe, C., Wagner, W. & Scipal, K. 2007e. Satellite radar imagery for monitoring inland wetlands in boreal and sub-arctic environments. *Journal of Aquatic Conservation: Marine and Freshwater Ecosystems* 17: 305-317.

Bartsch, A., Wagner, W., Pathe, C., Scipal, K., Sabel, D. & Wolski, P. in press (a). Global monitoring of wetlands: The value of ENVISAT ASAR global mode. *Journal of Environmental Management*.

Bartsch, A., Pathe, C., Wagner, W. & Scipal, K. in press (b). Detection of permanent open water surfaces in central Siberia with ENVISAT ASAR wide swath data with special emphasis on the estimation of methane fluxes from tundra wetlands. *Hydrology Research*.

Kimball, J.S., McDonald, K.C., Frolking, S.E. & Running, S.W. 2004. Radar remote sensing of the spring thaw transition across a boreal landscape. *Remote Sensing of Environment* 89: 163-175.

Henderson, F.M. & Lewis, A.J. 1998. *Principles & Applications of Imaging Radar: Manual of Remote Sensing vol. II*. New York: John Wiley & Sons.

Long, D. & Hicks, B. 2005. *Standard BYU QuikSCAT/ SeaWinds Land/Ice Image Products*. Report Provo, Utah: Brigham Young University.

Pathe, C., Wagner, W., Sabel, D., Bartsch, A., Naemi, V., Doubkova, M. & Basara, J. 2007. Soil moisture information from multi-temporal ENVISAT ASAR ScanSAR data over Oklahoma, USA. *Proceedings of BioGeoSAR 2007, Bari.*

Scipal, K., Scheffler, C. & Wagner, W. 2005. Soil moisture-runoff relation at the catchment scale as observed with coarse resolution microwave remote sensing. *Hydrology and Earth System Sciences* 9: 173–183.

Wagner, W., Lemoine, G. & Rott, H. 1999. A method for estimating soil moisture from ERS scatterometer and soil data. *Remote Sensing of Env.* 70: 191–207.

Wagner, W., Scipal, K., Pathe, C., Gerten, D., Lucht, W. & Rudolf, B. 2003. Evaluation of the agreement between the first global remotely sensed soil moisture data with model and precipitation data. *Journal of Geophysical Research D: Atmospheres* 108 (19): ACL 9(1)-9(15).

Wagner, W., Naeimi, V., Scipal, K., de Jeu, R. & Martìnez-Fernàndez, J. 2007. Soil moisture from operational meteorological satellites. *Hydrology Journal* 15: 121-131.

Wagner, W., Pathe, C., Doubkova, M., Sabel, D., Bartsch, A., Hasenauer, S., Blöschl, G., Scipal, K., Martínez-Fernández, J. & Löw A. 2008. Temporal stability of soil moisture and radar backscatter observed by the Advanced Synthetic Aperture Radar (ASAR). *Sensors* 8: 1174-1197.

Impact of Permafrost Degradation on Carbon and Nitrogen Stocks Related to Pedogenesis and Ecosystem Functioning

Frank Baumann
Institute of Geography, University of Tuebingen, Tuebingen, Germany
Jin-Sheng He
Department of Ecology, College of Environmental Sciences, Peking University, Beijing, China
Peter Kühn
Institute of Geography, University of Tuebingen, Tuebingen, Germany
Thomas Scholten
Institute of Geography, University of Tuebingen, Tuebingen, Germany

Introduction

The Qinghai-Xizang (Tibetan) Plateau is a key area concerning the environmental evolution of the earth at regional as well as global scales and proves to be particularly sensitive to anthropogenic global change, especially in areas affected by permafrost. It is the youngest, largest, and highest plateau in the world, comprising an area of more than 2.4 million km² with an average altitude exceeding 4000 m a.s.l. and containing the largest high-altitude and low-latitude permafrost area on Earth with 54.3% of its total surface affected by permafrost (Cheng 2005). These areas are characterized by strong diurnal patterns, high radiation on the surface, as well as a distinct geothermal gradient (Wang & French 1994) that mainly control the permafrost distribution and, thus, soil temperature and soil moisture conditions. Further, the proposed decay of Tibetan permafrost will have a strong impact on soil hydrology. Global environmental change, largely caused by human activities, affects climate as well as soils, and consequently reassigns their role in ecosystem functioning (Vitoussek et al. 1997). The major parameters in this context are the organic carbon (C_{org}) stock of soils and the decomposition of organic matter, whereas the Qinghai-Xizang (Tibetan) Plateau stores the highest amount of C_{org} and total nitrogen (N_t) in Chinese soils (Wang & Zhou 1999). Therefore, periglacial environments of Central China play a major role in the global C and N cycles, especially due to the pronounced sensitivity of this region to climate changes.

During two expeditions in 2006 and 2007, in total 60 sites were investigated on the central-eastern Tibetan Plateau along a 1500 km long northeast–southwest transect. The research focused exclusively on alpine steppe and meadow grassland vegetation. Sites containing continuous or discontinuous permafrost as well as areas without or heavily degraded permafrost were studied for comparison of soil dynamics under changing environmental settings. The main objective was to figure out how carbon and nitrogen contents of the investigated soils on the Tibetan Plateau respond to other pedological parameters, such as texture, acidity and carbonate content, since the sites along the transect show a distinct variety of climate conditions, relief locations and geology. Another major goal was to assess impact of global change on permafrost and its implication concerning the carbon and nitrogen cycles related to the above-mentioned feedback paths. Permafrost, pedogenesis, and ecosystem functioning are, therefore, closely linked. Study of their detangled feedback processes and mechanisms allows a better understanding of the role of geological and anthropogenic factors controlling the development and the functioning of Tibetan Plateau ecosystems.

Methods

At each site a soil profile pit was established reaching the parent material of soil formation or permafrost, respectively. The detailed field investigations included soil profile description according to FAO (2006) and WRB IUSS Working Group (2007). Soil moisture was determined in the field by TDR-probes connected with a moisture meter type HH2 (Delta-T Devices Ltd, UK). Aboveground and belowground biomass as well as soil respiration and temperature were investigated. Moreover, on-site 1 M KCl extractions for the determination of mineralized N (N_{min}) were carried out.

The laboratory analysis included a combined sieving and pipette grain-size analysis. Electrical conductivity (EC) and acidity (pH) were determined potentiometrically. $CaCO_3$ was tested volumetrically with HCl treatment. N_t and C_{org} were measured by heat combustion (CNS-elemental analyzer VARIO EL III, Elementar, Germany). The KCl extractions were analyzed photometrically for N_{min} (Continuous Flow Analyzer SAN Plus, Skalar, Netherlands). Water content was determined gravimetrically.

Climate data for each site was calculated by Kriging out of a 50-year time series of 680 climatic stations in China (1951–2000) (He et al. 2006). The whole dataset was investigated by descriptive statistics, one-way ANOVA, as well as correlation and regression analysis (SPSS for Windows, R) for the relationships of variables.

Results and Discussion

Highest C and N contents occur in permafrost and groundwater-influenced soils. The lower amount in soils not influenced by permafrost can be explained by shorter duration of pedogenesis and different temperature-moisture regimes. Pedogenesis is described here by acidity, carbonates, grain size distribution, and other soil parameters. Particularly at sites with initial soil formation, frequently influenced by

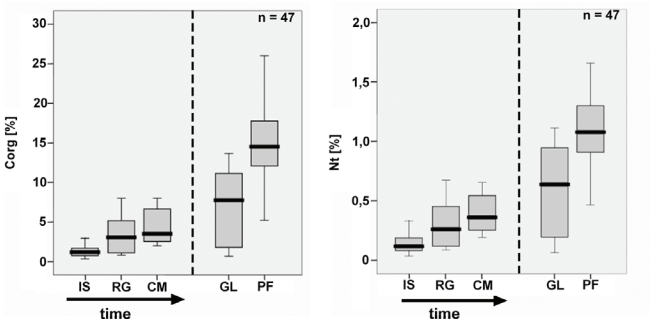

Figure 1. C_{org} and N_t stocks related to the stage of pedogenesis: IS = initially formed soils; RG = Regosols; CM = Cambisols; GL = groundwater influenced; PF = permafrost influenced.

aeolian sedimentation, extremely low contents of C and N combined with a high spatial variability were observed. These layers are composed of sandy and coarse-silty proximal generated material, mostly linked to direct (e.g., overgrazing, construction) and indirect (climate change) human impact. Therefore, the stage of soil development is an important co-variable in explaining the nutrient fluxes in grassland ecosystems on the Tibetan Plateau (Fig. 1). Highly fluctuating C and N contents of topsoils are evident on small spatial scales, mainly controlled by relief position and, in particular, by permafrost distribution in discontinuous permafrost areas. Semi-natural systems like alpine grasslands are generally limited in available plant nutrients. Thus, the productivity of alpine grassland ecosystems is determined by the available nitrogen pool, the amount of nitrogen input, as well as by nitrogen fixation, modified by water availability to plants over the year. Consequently, the degradation processes have severe impact on nutrient supply of plant species and accordingly alter biodiversity patterns.

Botanical and ecological studies on the Qinghai-Xizang (Tibetan) Plateau lead to the assumption that temperature changes alter biodiversity and biomass production in grassland ecosystems and are the main driving parameter for C and N turnover (e.g., He et al. 2006). Moreover, recent research has shown that changes in temperature and moisture conditions will also have serious impact on nitrogen and carbon cycling of soils (e.g., Shaver et al. 2006). Due to the high number of samples and the large-scale transect concept, sophisticated statistical analysis showing significant relationships between pedological parameters as well as carbon and nitrogen contents could be conducted. The results indicate that, in high altitude grassland ecosystems, soil moisture conditions can be determined as the main influencing parameter of C and N stocks, which are in turn closely linked to temperature. Furthermore, similar results are evident for annual precipitation, whereas no significant correlations were found concerning the mean annual temperature or soil temperature (Table 1). Comparable relationships can be shown for the soil respiration measurements. These linkages are in close connection to feedback mechanisms with temperature, which is predominantly affected by permafrost, aeolian sedimentation, and the stage of soil development. Permafrost and aeolian sedimentation are again a function of relief

Table 1. Correlations: C/N stock and selected control parameters.

	MAT (°C)	MAP (mm/a)	Soil Moisture (%)	Sand (%)
N_t (%)	n.s.	0.54 (**)	0.57 (**)	-0.38 (**)
C_{org} (%)	n s.	0.53 (**)	0.55 (**)	-0.37 (**)
NO_3^- (mg/l)	0.28 (**)	n.s.	n.s.	n.s.
NH_4^+ (mg/l)	n.s.	0.30 (**)	0.30 (**)	n.s.

(**) correlation is significant (0.01 two-sided).
(*) correlation is significant (0.05 two-sided).
(n.s.) correlation is not significant.

position, parent material, and seasonal climatic fluctuations, with an overall impact of climatically and human-induced degradation processes.

An evident trend of climate parameters in the above-mentioned direction to warmer conditions was observed during the past decades on the Qinghai-Tibetan Plateau (Yang et al. 2004), obviously leading to permafrost degradation (Cheng 2005). A relatively quick turnover rate of organic matter is expected for the turf-like upper layers in only some tens of years (Hirota et al. 2006). This process will be amplified if warming is accompanied by drier conditions.

References

Cheng, G. 2005. Permafrost Studies in the Qinghai-Tibet Plateau for Road Construction. *Journal of Cold Regions Engineering* 19(1): 19-29.

He, J.-S., Wang, Z., Wang, X., Schmid, B., Zuo, W., Zhou, M., Zheng, C., Wang, M. & Fang, J. 2006. A test of generality of leaf trait relationships on the Tibetan Plateau. *New Phytologist* 170: 835-848.

Hirota, M., Tang, Y., Hu, Q., Hirata, S., Kato, T., Mo, W., Cao, G. & Mariko, S. 2006. Carbon Dioxide Dynamics and Controls in a Deep-water Wetland on the Qinghai-Tibetan Plateau. *Ecosystems* 9: 673-688.

Shaver, G.R., Giblin, A.E., Nadelhoffer, K.J., Thieler, K.K., Downs, M.R., Laundre, J.A. & Rastetter, E.B. 2006. Carbon turnover in Alaskan tundra soils: effects of organic matter quality, temperature, moisture and fertilizer. *Journal of Ecology* 94: 740-753.

Vitousek, P.M., Mooney, H.A., Lubchenco, J. & Melillo, J.M. 1997. Human domination of earth's ecosystems. *Science* 277: 494-499.

Wang, B. & French, H.M. 1994. Climate Controls and High-Altitude Permafrost, Qinghai-Xizang (Tibet) Plateau, China. *Permafrost and Periglacial Processes* 5: 87-100.

Wang, S. & Zhou, C. 1999. Estimating soil carbon reservoir of terrestrial ecosystem in China. *Geogr. Res.* 18: 349-356.

Yang, M., Wang, S., Yao, T., Gou, X., Lu, A. & Guo, X. 2004. Desertification and its relationship with permafrost degradation in Qinghai-Xizang (Tibet) plateau. *Cold Regions Science and Technology* 39: 47-53.

DC Resistivity Soundings Across a Pebbly Rock Glacier, Kapp Linné, Svalbard

Ivar Berthling
Norwegian University of Science and Technology, Trondheim, Norway
Håvard Juliussen
UNIS – The University Centre in Svalbard, Longyearbyen, Norway

Introduction

Recently, Ikeda and Matsuoka (2006) have drawn attention towards what they call "pebbly" rock glaciers that differ from "bouldery" rock glaciers both with respect to lithological content, mean size of clasts, and rock glacier dimensions. The present paper reports on pebbly rock glaciers close to Isfjord Radio on Kapp Linné, Svalbard, and their internal structure based on a detailed DC resistivity profiling campaign. A working hypothesis is proposed for their development.

Setting

Kapp Linné is located on the northern part of the coast of Nordenskiølds land, western Svalbard (Fig. 1). The pebbly rock glaciers have developed along Griegaksla at the transition between talus slopes and the strandflat area, a topographical position similar to that of the rock glaciers on Prins Karls Forland (Berthling et al. 1998, 2007) and rock glaciers further south on the coast of Nordenskiølds land (Kääb et al 2002, Farbrot et al. 2005).

The western flank of Griegaksla is composed of phyllitic bedrock that weathers to matrix-supported highly frost-susceptible debris. The lower part of the mountain wall is covered by talus deposits that in some cases have developed into small rock glaciers.

Fieldwork and Methods

The DC resistivity measurements where carried out in July 2007 on the largest of these rock glaciers (Fig. 1), as part of the IPY project "Permafrost Observatory Project: A Contribution to the Thermal State of Permafrost in Norway and Svalbard (TSP Norway)." The investigated rock glacier is from 50 to 100 m long and has a frontal slope with a height of about 30 m.

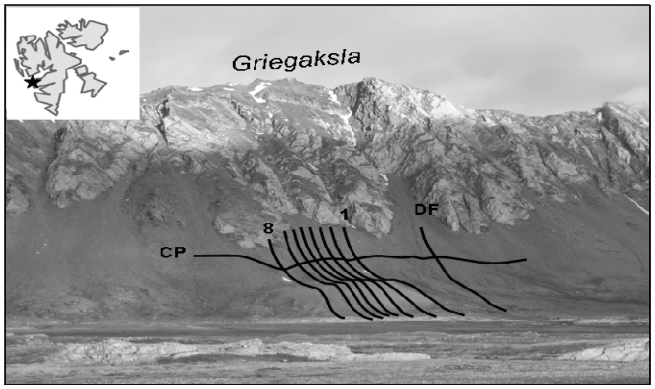

Figure 1. The study site at Griegaksla, Kapp Linné (arrow on Svalbard map). 1–8 are the resistivity lines along the talus slope–rock glacier system. CP is the cross profile and DF is a resistivity profile along a talus slope with debris-flow tracks.

We used ABEM equipment, with an along-slope electrode spacing of 10 m. Spacing between resistivity lines were 10 m (profiles 1–7) and 20 m (profile 7–8). We also collected a resistivity profile along a neighboring talus slope and a profile across the talus (Fig. 1). The topography of all profiles was established using differential GPS.

Results

The resistivities are highest in the talus cone, while on the rock glacier itself, resistivity decreases (Fig. 2). On the northern part of the rock glacier (profile 7–8), higher resistivity reaches further down into the rock glaciers. The northern part of the rock glacier is longer, lacks an inner depression, and does not display a very sharp transition between rock glacier surface and front. Resistivities in talus areas outside of the rock glacier system are lower, but comparable to that of the rock glacier itself.

Discussion and Conclusions

The results obtained underline the importance of processes operating in talus slopes for the development of rock glaciers. The environmental conditions along Griegaksla are fairly similar, and it is a question why rock glaciers have only developed along parts of the more or less continuous talus sheet found here. However, it seems to be a pattern that these rock glaciers are developed beneath areas where the talus slope is shorter than elsewhere. One possible explanation is that a larger and more active talus slope, including snow avalanche and debris flow processes, will tend to erode the upper part of the talus cone and transport debris to its lower part. This will set up a tendency for melting at the bottom of the active layer, inhibiting accumulations of segregation ice beneath the active layer, while at the same time lowering shear stresses within the talus cone. On a less active talus, especially one composed of frost-susceptible debris, the potential for water migration into the permafrost, segregation ice development, and aggradation of permafrost will be higher.

Acknowledgments

The "Permafrost Observatory Project: A Contribution to the Thermal State of Permafrost in Norway and Svalbard (TSP Norway)" is led by Hanne H. Christiansen, UNIS, who was in charge of the field campaign at Kapp Linné. Andreas Kääb, University of Oslo, calculated the DGPS data. The assistance provided in the field by Jaran Wasrud is greatly appreciated.

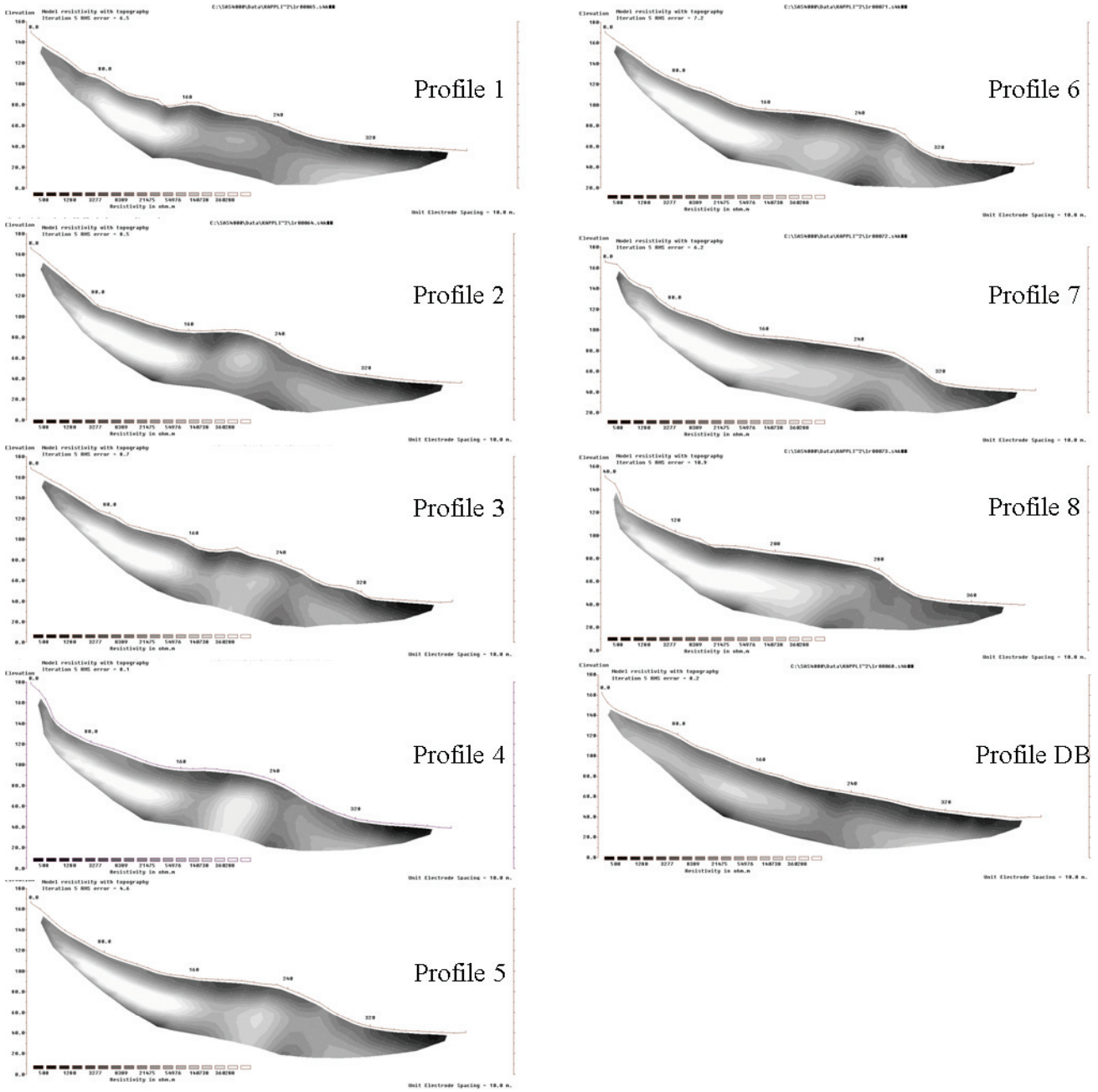

Figure 2. Results from the resistivity profiling. Light tones indicate high resistivities (around 400 KΩm). For position of profiles, see Figure 1. The cross profile is not shown.

References

Berthling, I., Etzelmuller, B., Eiken, T. & Sollid, J.L. 1998. Rock glaciers on Prins Karls Forland, Svalbard. I: Internal structure, flow velocity and morphology. *Permafrost and Periglacial Processes* 9: 135-145.

Berthling, I., & Etzelmuller, B. 2007. Holocene rockwall retreat and the estimation of rock glacier age, Prins Karls Forland, Svalbard. *Geogafiska Annaler* 89A: 83-93.

Kääb, A., Isaksen, K., Eiken, T. & Farbrot, H. 2002. Geometry and dynamics of two lobe-shaped rock glaciers in the permafrost of Svalbard. *Norsk Geografisk Tidsskrift – Norwegian Journal of Geography* 56: 152-160.

Farbrot, H., Isaksen, K., Eiken, T., Kääb, A. & Sollid, J.L. 2005. Composition and internal structures of a rock glacier on the strandflat of western Spitsbergen, Svalbard. *Norsk Geografisk Tidsskrift - Norwegian Journal of Geography* 59: 139-148.

Ikeda, A. & Matsuoka, N. 2006. Pebbly versus bouldery rock glaciers: morphology, structure and processes. *Geomorphology* 73: 279-296.

Modeling Thermal and Moisture Regimes of Permafrost with New Deep Soil Configuration in CLASS

Jean-Philippe Blanchette, Laxmi Sushama, René Laprise
Centre pour l'étude et la simulation à l'échelle régionale, Université du Québec à Montréal, Montréal, Canada
Canadian Regional Climate Modelling and Diagnostics Network, Montréal, Canada
Consortium Ouranos on Regional Climate and Adaptation to Climate Changes, Montréal Canada

Introduction

Most of the climate models, including Regional Climate Models (RCMs), employ land-surface schemes that vary in depth between 3 and 10 m; for example, the current version of the Canadian Regional Climate Model (CRCM) has a physically-based land surface scheme, CLASS (Canadian Land Surface Scheme; Verseghy et al. 1991, Verseghy 1993), which is 4.1 m deep, with three soil layers that are 0.1, 0.25, and 3.75 m thick, respectively. As shown by many recent studies (Smerdon & Stieglitz 2006, Alexeev et al. 2007, Nicolsky et al. 2007, Stevens et al. 2007), such shallow-soil models, though coupled, cannot simulate active-layer and near-surface permafrost realistically. To simulate realistic soil thermal and moisture regimes in the CRCM, it is intended to use the latest version (v. 3.3) of CLASS, which is particularly suitable for permafrost studies due to its more flexible layering scheme and bottom boundary conditions. Sensitivity of the soil thermal and moisture regimes to the soil model depth/configuration is assessed using offline simulations with this latest version of CLASS, which is presented in this paper.

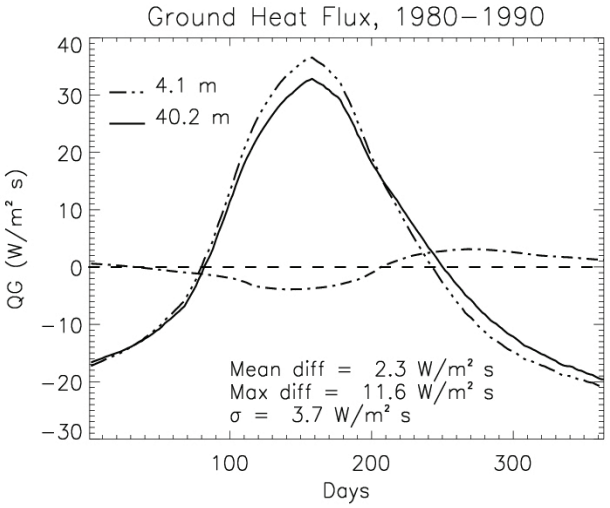

Figure 1. Average ground heat flux for the 1980–1990 period, for 6 (dash-multidotted line) and 10-layer (solid line) configurations, and their differences (dash-dotted line). The annual maximum difference, the annual mean difference, and the standard deviation are also indicated in the Figures.

Experiments and Model Configuration

The offline simulations were performed with CLASS for a location in northern Québec with continuous permafrost, for the 1961–1999 period. The input variables (downward visible and infrared radiation, precipitation, atmospheric pressure, surface air temperature, specific humidity, and wind) required to drive the soil model were specified using the European Re-analysis datasets (ERA-40, Uppala et al. 2005). The soil properties were specified using the land surface datasets developed by Wilson and Henderson-Sellers (1985), according to which the bedrock is at 0.1 m below surface for the chosen location. Three experiments were performed, with the lower boundary at 4.1, 40.2, and 133.7 m below surface, respectively. The layer thickness varies exponentially from top to bottom (0.10, 0.17, 0.31, 0.57, 1.04, and 1.91 m for the first six layers and so on), and accordingly the number of layers for the three cases is 6, 10, and 12, respectively. The initial profile is determined by iteratively running the soil model from chosen conditions using 1961 data, until equilibrium is reached.

Results

Preliminary results confirm that adding deeper layers to CLASS, and in doing so, lowering the bottom boundary with zero soil heat conduction flux, changes the thermal regime, as shown in Figures 1, 2, and 3, comparing the six and ten-layer configuration. The thermal inertia brought by new deeper

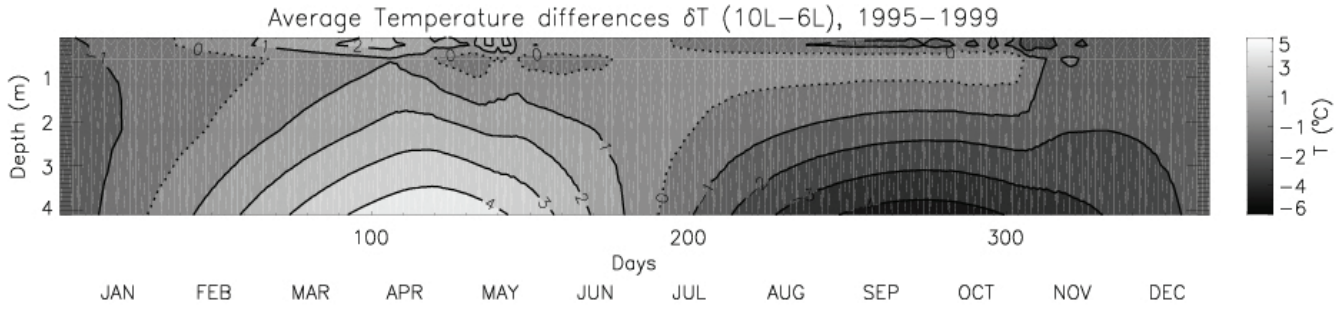

Figure 2. Average temperature differences between the 10- and 6-layer configuration for the 1995–1999 period.

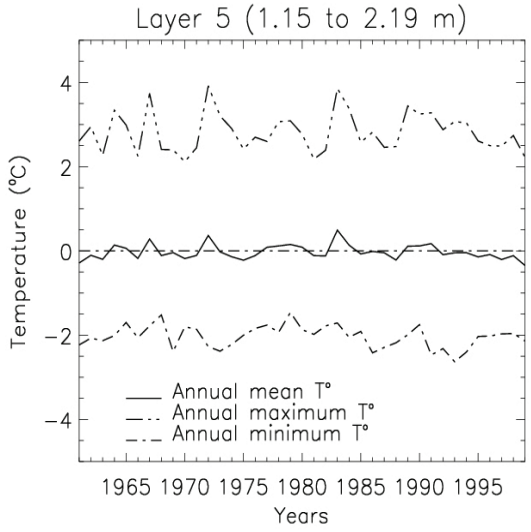

Figure 3. Evolution of the differences in the annual minimum (upper dash-multidotted line), average annual (solid line), and annual maximum (bottom dash-dotted line) temperatures of layer 5, for the period 1961–1999, between the 6- and 10-layer configuration. The annual minimum (maximum) temperature is warmer (colder) in the deeper version compared to the shallow one. The mean annual temperature of both models, however, is very similar.

layers modifies the heat fluxes and, thus, the heat storage of the soil. With deeper soil, the top 4 m soil temperature is colder in summer and fall, and warmer during winter and spring. Figure 2 suggests differences of 5°C at 4 m during March to May. The influence of these changes on the surface fluxes and on other fields (albedo, latent heat flux, runoff, etc., not shown here) need to be further explored. However, it appears that the impact is significant during the snowmelt period or during the beginning of the snow accumulation. For example, the snow cover accumulation starts earlier in the deeper model, because of the colder soil temperature present in early fall, which is reflected by higher accumulation in the 10-layer model. However, the higher soil temperature in spring for the 10-layer model compared to the 6-layer one causes early snowmelt. This is also reflected in the liquid and solid water content of the first layer. The ratio of solid to liquid soil water content is higher at the beginning of the freezing period for the 10-layer configuration, and inversely, the ratio is lower at the beginning of the snowmelt.

Further tests need to be conducted with deeper bedrock, organic matter, etc., which will be followed by coupled simulations to understand the importance of the deeper soil on surface fluxes.

Acknowledgments

Jean-Philippe Blanchette is supported by the Réal-Décoste/ Ouranos Scholarships, the Canada Graduate Scholarship (CGS M) from NSERC, and by the partial GEC3 Graduate Student Stipend.

References

Alexeev, V.A., Nicolsky, D.J., Romanovsky, V.E. & Lawrence, D.M. 2007. An evaluation of deep soil configurations in the CLM3 for improved representation of permafrost. *Geophys. Res. Lett*. (34): L09502.

Nicolsky, D.J., Romanovsky, V.E., Alexeev, V.A. & Lawrence, D.M. 2007. Improved modeling of permafrost dynamics in a GCM land-surface scheme. *Geophysical Research Letter* (34): L08501.

Stevens, M.B., Smerdon, J.E., Gonzalez-Rouco, J.F. & Stieglitz, M. 2007. Effects of bottom boundary placement on subsurface heat storage: Implications for climate model simulations. *Geophys. Res. Lett*. (34): L02702.

Uppala, S.M. et al. 2005. The ERA-40 re-analysis. *Q.J.R.Meteorol. Soc* (131): 2961-3012.

Verseghy, D.L. 1991. CLASS – A Canadian land surface scheme for GCMs, I. Soil model and coupled runs. *International Journal of Climatology* (11): 111-133.

Verseghy, D.L., McFarlane, N.A. & Lazare, M. 1993. CLASS – A Canadian land surface scheme for GCMs, II. Vegetation model and coupled runs. *International Journal of Climatology* (13): 347-370.

Wilson, M.F. & Henderson-Sellers, A. 1985. A global archive of land cover and soil data for use in general circulation climate models. *Journal of Climatology* (5): 119-143.

A Provisional Permafrost Map of the Transantarctic Mountains

J.G. Bockheim
Department of Soil Science, University of Wisconsin, 1525 Observatory Drive, Madison, WI 53706-1299, USA
M. McLeod
Landcare Research, Private Bag 3127, Hamilton, New Zealand
M.R. Balks
Department of Earth and Ocean Sciences, University of Waikato, Private Bag 3105, Hamilton, New Zealand

Introduction

The Transantarctic Mountains (TAM) extend 3,500 km across the Antarctic continent from 69°S in northern Victoria Land to 87°30′S in the upper Scott Glacier region. The TAM form a natural barrier between ice in East and West Antarctica and record the history of Cenozoic glaciations of Antarctica (Lyons & Elliot 2006). The TAM have an ice-free area of 20,910 km^2, which constitutes 42% of the total ice-free area (49,500 km^2) of Antarctica.

Bockheim (1995) prepared the first permafrost map of Antarctica. He showed that permafrost was limited to ice-free areas and that all of East Antarctica and most of West Antarctica contain continuous permafrost. More recently, Bockheim and others (2007) prepared a provisional permafrost map of the McMurdo Dry Valleys portion of the TAM (6,700 km^2), reporting that buried ice, ice-cemented permafrost, and dry-frozen permafrost comprised 2, 55, and 43% of the area, respectively. A task force under the auspices of the IPA and Scientific Committee on Antarctic Research (SCAR), identified as the Antarctic Permafrost and Soils (ANTPAS) Group (http://erth.waikato.ac.nz/antpas/), is preparing a series of permafrost and ground-ice maps of Antarctica. The text that will accompany these maps is included in this volume (Bockheim et al. 2008). The poster accompanying the present abstract displays permafrost distribution in the TAM on three maps at scales of 1:1 million.

Methods

To prepare a permafrost map of the TAM, we used 62 scanned and geo-rectified 1:250K topographic maps prepared by the US Geological Survey (http://usarc.usgs.gov/drg_dload.shtml). We joined these seamless maps in ArcGIS 9.2 and used the composite map as a base map. To display the entire TAM, we divided the mountains into three regions: northern Victoria Land (69°30′–75°S), central Victoria Land (75–80°30′S), and southern Victoria Land (80°30′–86°30′S). Each map could be displayed as a standard A0 wall size (841 x 1188 mm) at a scale of 1:1 million.

Expert permafrost scientists working in Antarctica prepared a legend that includes the following map units: (i) buried or ground ice within the upper 100 cm, (ii) ice-cemented permafrost with a surface within 70 cm, (iii) ice-cemented permafrost with a surface below 70 cm (excluding dry-frozen permafrost), and (iv) dry-frozen permafrost with an ice-cemented surface below 70 cm. To determine the distribution of these permafrost forms throughout the TAM, we used published data and data archived by the National Snow & Ice Data Center (http://nsidc.org/cgi-bin/get_metadata.Pl?id-ggd221) and New Zealand Landcare Research (http://www.landcareresearch.co.nz). In northern Victoria Land, we used data from Denton and others (1986) and Guglielmin and French (2004). In central Victoria Land, we used data collected by Bockheim and others (1989, 2007). For southern Victoria Land, data were used from Claridge and Campbell (1968) and Bockheim and others (1990). For unmapped areas we extrapolated the database using the following criteria: ice-cored drift was identified from a stippled pattern on topographic maps; ice-cemented permafrost was identified from patterned ground on remotely sensed images and proximity to streams, lakes, and ponds; and dry-frozen permafrost comprised the remaining areas, particularly in interior mountains and broad central valleys.

Polygons were drawn on the base maps, numbered, and identified in the accompanying attribute table by permafrost form. The maps were prepared using an agreed upon colour scheme for continuous permafrost that included: dark brown = buried or ground ice; dark green = ice-cemented permafrost <70 cm; dark purple = ice-cemented permafrost >70 cm (excluding dry-frozen permafrost); dark red = dry-frozen permafrost with an ice-cemented surface below 70 cm. The areal distribution of permafrost by form was determined using a GIS.

Results

Buried ice comprised 12% of the total permafrost in the TAM and was most abundant in northern Victoria Land. Ice-cemented permafrost, with the surface at <70 cm, comprised 44% of the area and was most abundant in the McMurdo Dry Valleys. Few sites (2%) had the surface of ice-cemented permafrost deeper than 70 cm. These sites were primarily in coastal areas of central Victoria Land. Dry-frozen permafrost occurred in the upper 70 cm in 44% of the TAM. Dry-frozen permafrost is particularly abundant in the Beardmore Glacier region.

Discussion

The distinction between soils with ice-cemented permafrost <70 cm and dry-frozen permafrost with an ice-cemented surface below 70 cm is based on both direct observation during field work and insights gained during fieldwork. Where there are large areas with no observations we have

used a distance from coast rule to determine the nature of the permafrost, reasoning that soils closer to the coast are likely to have greater moisture recharge and thus ice-cemented permafrost at <70 cm. However, our field observations suggest that ice-cemented permafrost at <70 cm can occur at other locations where soil moisture is being recharged. Examples of recharge areas include land where snow has accumulated in discrete patches in predominantly snow-free regions or land below snow or ice patches which melt producing downslope subsurface flow. Unfortunately, such areas as these are not readily identifiable on the 1:250,000 scale topographic maps. Inland nunataks have generally been allocated dry permafrost form using the a priori reason that they predominantly have very shallow soils over rock or are comprised of rock only.

Because of the large area and relatively sparse density of observations in many locations, the permafrost map is a dynamic document with further contributions welcome following individuals review or field observation in the future.

Acknowledgments

This work was largely unfunded and conducted by the authors on their own time. One author (MM) received a capability development travel grant from Landcare Research to initiate the work. Anne Sutherland and Craig Briggs are thanked for tireless GIS assistance. We gratefully acknowledge the support of ANTPAS personnel.

References

Bockheim, J.G. 1995. Permafrost distribution in the Southern Circumpolar Region and its relation to the environment: a review and recommendations for further research. *Permafrost and Periglacial Processes* 6: 27-45.

Bockheim, J.G., Wilson, S.C., Denton, G.H., Andersen, B.G. & Stuiver, M. 1989. Late Quaternary ice-surface fluctuations of Hatherton Glacier, Transantarctic Mountains. *Quaternary Research* 31: 229-254.

Bockheim, J.G., Wilson, S.C., & Leide, J.E. 1990. Soil development in the Beardmore Glacier region, Antarctica. *Soil Science* 149: 144-157.

Bockheim, J.G., Campbell, I.B. & McLeod, M. 2007. Permafrost distribution and active layer depths in the McMurdo Dry Valleys, Antarctica. *Permafrost and Periglacial Processes* 18: 217-227.

Bockheim, J.G. & McLeod, M. 2007. Soil distribution in the McMurdo Dry Valleys, Antarctica. *Geoderma*, doi: 10:10.16/j.geoderma.2007.10.015.

Bockheim, J.G., Campbell, I.B., Guglielmin, M. & López-Martínez, J. 2008. Distribution of types of permafrost and buried ice in ice-free areas of Antarctica.

Claridge, G.G.C. & Campbell, I.B. 1968. Soils of the Shackleton Glacier region, Queen Maud Range, Antarctica. *New Zealand Journal of Science* 11: 171-218.

Denton, G.H., Bockheim, J.G., Wilson, S.C. & Schlűchter, C. 1986. Late Cenozoic history of Rennick Glacier and Talos Dome, northern Victoria Land, Antarctica. In: E. Stump (ed.), *Geological Investigations of Northern Victoria Land*. American Geophysical Union, Antarctic Research Series 46: 339-375.

Guglielmin, M. & French, H.M. 2004. Ground ice in the Northern Foothills, northern Victoria Land, Antarctica. *Annals of Glaciology* 39: 495-500.

Lyons, W.B. & Elliot, D.H. 2006. Transantarctic Mountains Transition Zone Project. *Proceedings of a Workshop on Multi-disciplinary Research in the Central and Southern Transantarctic Mountains.* http://www-bpre.mps.ohio-state.edu/workshops/tam_2006.php.

Alpine Permafrost Distribution at Massif Scale: Assessment of Mean Surface Temperatures During Winter Equilibrium Period Thanks to Topoclimatic and Geomorphological Data (Combeynot Massif, French Alps)

Xavier Bodin
University Paris Diderot-Paris 7/Institute of Alpine Geography, Joseph Fourier University, Grenoble, France
Philippe Schoeneich
Institute of Alpine Geography, Joseph Fourier University, Grenoble, France
Monique Fort
UMR 8586 PRODIG, University Paris Diderot-Paris 7

Introduction

Statistical modeling using BTS (Bottom Temperature of the Snow cover; Haeberli 1985) have been attempted by authors (e.g., Hoelzle 1992, Gruber & Hoelzle 2001, Lewkovicz & Ednie 2004) to model mountain permafrost distribution. Field validations generally show good agreement with rock glaciers, which are the most common geomorphological evidences of the permafrost. The main limit of this approach is the necessity of well-distributed BTS data over the studied area.

In the Combeynot massif (Hautes Alpes, France – around 45.0°N, 6.4°E), numerous rock glaciers may be observed on various topoclimatic contexts, whereas BTS datasets are available on some limited areas (Bodin 2007). In order to get a spatialized overview of the surface temperature, and hence of the permafrost presence, a linear relationship between the main topoclimatic parameters (air temperature and solar radiation) and the WEqT is proposed.

A Spatial Model of the WEqT

Starting hypothesis

In order to quantify respective influences of the main parameters, the following hypotheses are made:

- The WEqT is equal to the mean annual air temperature (MAAT), to which is added, or subtracted, the influences of the solar radiation and the debris cover.
- The thermal influence of the solar radiation (α), positive, is linearly related to the potential solar incoming radiation (PSIR) during summer (June–July–August) and proportional to the PSIR/PSIRmax ratio.
- The thermal influence of the openwork debris mantles (β) is negative and, on yearly average, homogeneous independently of other factors.
- For similar topoclimatic conditions, WEqT is equal from one place to the other.

Parameterization of the linear model

Within the linear model of WEqT, the α and β parameters were parameterized by minimizing the sum of residuals in two steps:

1. First, for rock glaciers with topoclimatic conditions close to those of the root of the Laurichard rock glacier, where BTS in 2004 shows a mean WEqT of -3.44°C. Due to very low PSIR, α was minimal, and the adjustment led to β = -3.9°C.

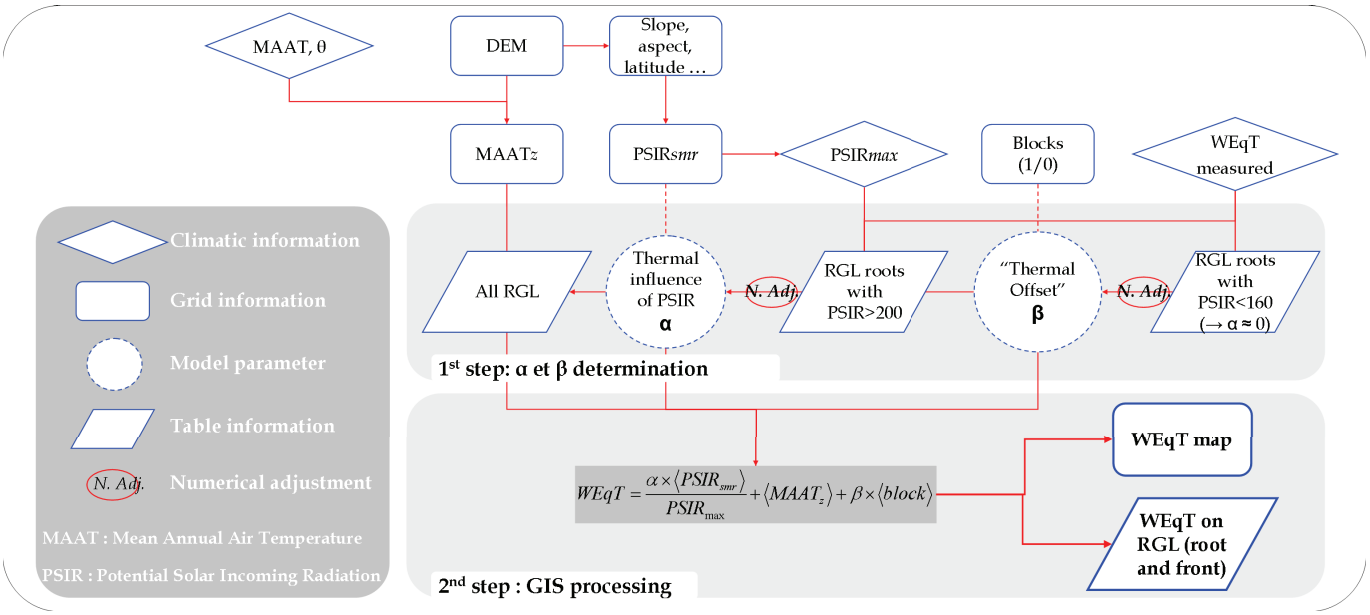

Figure 1. Processing steps (1 = calibration of α and β by numerical adjustment; 2 = GIS processing) to model WeqT.

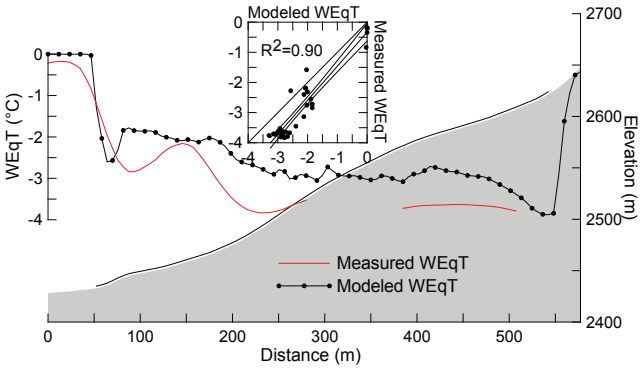

Figure 2. Comparison between modeled WEqT and measured BTS on the Laurichard rock glacier (Combeynot Massif, Hautes Alpes, France).

2. Second, for locations with high PSIR and using the previously defined β, the BTS values of the Pradieu Valley give α = 2.9°C.

The flow chart of the model describes the different datasets used and the main steps of the process (Fig. 1).

Results at Different Spatial Scales

The Laurichard rock glacier case

A first validation of the model is given by comparing the extrapolated WEqT to the measured BTS on the whole surface of the Laurichard rock glacier.

The model correctly reproduces the measured BTS on the rock glacier (Fig. 2), and suggests that the general trend of the WEqT is, at this scale, visibly driven by the solar radiation received during summer.

The WEqT on the rock glaciers of the Combeynot Massif

The mean modeled WEqT at the rooting zone of the rock glaciers of the Combeynot massif amounts to -3.4°C, whereas it reaches -2.9°C at the front of the landforms. Some fronts, nevertheless, are located on warmer conditions, mainly when glacier is or has been, historically, present on the rooting area.

Conclusion

A statistical model of the WEqT has been presented in which the influences of solar radiation and coarse debris presence have been adjusted thanks to BTS measurements. Though local processes (e.g., permafrost creeping) or influences of other parameters (e.g., snow) are not taken into account, the validation of the model on the Laurichard rock glacier encourages the use of this kind of topoclimatic approach for permafrost study at massif scale.

Acknowledgments

This work was funded by the French Ministry of Education and Research. S. Gruber (Univ. of Zürich) is greatly acknowledged for running the TEBAL model to get the PSIR map of the Combeynot massif, as well as for his advice concerning the presented model.

References

Bodin, X. 2007. *Géodynamique du pergélisol de montagne : fonctionnement, distribution spatiale et évolution récente. L'exemple du massif du Combeynot (Hautes Alpes)*. PhD, University of Paris-Diderot Paris 7, 274 pp.

Gruber, S. & Hoelzle, M. 2001. Statistical modeling of mountain permafrost distribution: local calibration and incorporation of remotely sensed data. *Permafrost and Periglacial Processes* 12(1): 69-77.

Haeberli, W. 1973. Die Basis-Temperature der winterlichen Schneedecke als möglicher Indikator für die Verbreitung von Permafrost in den Alpen. *Zeitschrift für Gletscherkunde und Glazialgeologie* 9: 221-227.

Hoelzle, M. 1992. Permafrost occurrence from BTS measurements and climatic parameters in the Eastern Swiss Alps. *Permafrost and Periglacial Processes* 3: 143-147.

Lewkovicz, A.G. & Ednie, M. 2004. Probability mapping of mountain permafrost using the BTS method, Wolf Creek, Yukon Territory, Canada. *Permafrost and Periglacial Processes* 15: 67-80.

Cryogenic Formations of the Caucasus and the Significance of Their Impact on the Natural Phenomena of the Region

Igor V. Bondyrev
Vakhushti Bagrationi Institute of Geography, Ministry of Education and Sciences of Georgia, Tbilisi

Cryogenic or periglacial phenomena are widespread within the high mountain Caucasian region. The modern area of spreading cryogenic processes on the south slope of the Central Caucasus (Georgia) forms 3300 km^2 and within the Republic of North Osetia-Alanya, 5400 km^2, but in Kabardino-Balkaria, 4600 km^2 (1, 2). These processes are widely spread as well on the territory of the Pontides Mountains and the Iranian upland, covering 14,200 km^2. The set of factors defining the genesis and morphology of the forms of periglacial relief changes depending on the height of the area. Three hypsometric levels are singled out:

1. The upper belt occupies the whole area of the nival zone and is limited from underneath by snow line lying at the height of 3000–3200 m a.s.l. Frost weathering and gravitational talus processes, which play the leading role in formation of present-day relief forms, take place here.

2. The middle belt is situated below snow line and practically coincides with the alpine and sub-alpine landscape zones (1750–2300 m). Here prevail slope (solifluction, rock-streams, stone and snow avalanches, talus trains, mud flows, etc.) and plane (polygonal-structural groundboulder pavement, thufurs).

3. Relict cryogenic formations (fluvioglacial deposits, cryoturbation, etc.) are spread in the lower belt down to 1400–1600 m a.s.l.

The given formations are characterized by the following regularities of their spatial distribution:

1. Formations related to rocky ground occupy the belt of tops, ridges of watersheds, and steep slopes of high mountains.

2. Formations related to rudaceous ground and pebbles are mainly placed on gentle slopes and at the foot of mountain ridges and massifs within 2700–1900 m a.s.l.

3. Formations related to fine detrital and rock debris are well observed on the high mountain plateaus in the zone of Neocene-quaternary volcanism.

4. Formations related to loamy and turf/soddy surfaces cover quite a large area, mostly alpine and sub-alpine meadows and alluvial soils of high mountain zones (see the scheme of classification of periglacial formations of the Caucasus).

Widespread morainic mantles and sheets and gravitational talus processes define the existence of numerous "fossil" glaciers (dead ice), on their part testifying to the regression of the glaciation process. The value of seasonal freezing of ground soil is an important feature for determining main relief-forming processes in high mountains. Information on these parameters helps with decisions about engineering-geological, building, agro-biological, and other problems. We offered theoretical determination for the values of seasonal freezing depth for different points in periglacial areas in Georgia, having minimum information on those areas. For this purpose, the formula of Budnikov was used with some amendments of ours on the high-mountainous relief character, the height of snow cover, and influence of wind (2, 3, 6, 8). Comparison of meteorological yearbook records of the Hydrometeorological Institute of Georgia with ours on the depth of seasonal freezing showed little discrepancy (not more than 3–6 cm). The gained records are well founded only for subhorizontal surfaces deprived of mantle and vegetative cover, with similar mechanical composition and equal humidity value. Calculations were carried out per formula:

$$h_{np} = 5k\left[\sqrt{Tn - \frac{50_{\ell}\left(n_1 + L\right)}{t\sqrt{H \cdot V}}}\right] \qquad (1)$$

Table 1. Experimental evaluation of the rate of frosty weathering of mountain rocks (5).

Number of version	Mean amplitude of temperature fluctuation during the experiment	Area of frozen surface (sm^2)	Initial weight of sample (r)	Weight of frozen sample	Number of "freezing-thawing" cycle	Weight of disintegrated particles	Velocity of disintegration of frozen surface a day/gr/m^2.a day/	Velocity of disintegration/ mm/year/
1 – over-moistured	28.2°C	22.56	31.70	31.74	80	0.73	4.0514	0.288
2 – dry		31.34	41.10	41.47	80	0.07	0.2819	0.040
3 – over-moistured		34.23	41.94	42.03	70	0.53	2.2079	0.672
4 – dry		37.84	25.19	25.45	70	0.10	0.3790	0.047

where $\sqrt{Tn}$ = Budnikov formula, k = lithological coefficient, provisionally equal to unity, T = mean air temperature during winter, t = mean ground surface temperature during winter, n = longness of the period with temperature below zero, n_1 = the same with temperature above zero during winter, H = area altitude above sea level, V = winter wind mean velocity (m/sec), L = thickness of snow cover /average for winter (3).

Therefore, we have conducted a number of experiments studying the rate of frosty weathering in different types of rock. With this purpose different types of rock were taken. Core sample No. 1 was taken from the well on Tbilisi site and represents carbonate fine-grained rock of Eocene age (marl), taken at a 2574–2580 m depth. The other sample was a monolith of andezite-dacitic lava (SiO2-50%) from the top of Emlikli massif (2750–2800 m a.s.l., Southern Georgia).

The conditions similar to those of high mountain natural conditions were specially created. Experiments went on for 31 days.

About 315 regimes of "freezing-thawing" changed one after another. As a result, it became possible to find the decisions of such issues as estimation of the rate of disintegration of mountain rocks under frosty weathering. Data are given in Table 1, estimating the rate of frosty weathering of separate units depending on the lithology of mountain rocks and extent of their moistening.

References

Bondyrev, I.V. & Maisuredze, G.M. 1978. Some particularities of dynamics, morphogenesis and spatial distribution of frozen ground in the Caucasus. In: *Cryogenic Phenomena in High Mountains*. Novosibirsk: Nauka, 43-59

Bondyrev, I.V. 1987. Main problems of study and development of high mountain regions in Georgia, Tbilisi: GruzNIINTI, 72 pp.

Bondyrev, I.V., Tatashidze, Z.K., Singh, V.P., Tsereteli E.D. & Yilmaz, A. 2004. Impediments to the sustainable development of the Caucasus-Pontdes region: New global development. *Journal of International & Comparative Social Welfare* Twentieth Anniversary Special 20(1): 33-48

Bondyrev, I.V., Tatashidze, Z.K. & Tsereteli, E.D. 2004. Actual ecological situations in the territory of mountain regions and biodiversity problems (the case of Georgia). *NATO ARW Seminar: Environmental Security and Sustainable Land Use of Mountain and Steppe Territories of Mongolia and Altay, Barnaul, Russia, October 25–27, 2004*: 89-98.

Modeling Potential Climatic Change Impacts on Mountain Permafrost Distribution, Wolf Creek, Yukon, Canada

Philip P. Bonnaventure, Antoni G. Lewkowicz
Department of Geography, University of Ottawa, Ottawa, Canada

Introduction

Differences in air temperature, precipitation, and vegetation cover that develop across hundreds of kilometres in lowland areas can be generated by a few hundred metres of elevation change in mountainous regions. Consequently, a mountain basin located in the discontinuous permafrost zone may span the entire range of permafrost conditions, from isolated patches at low elevations on north-facing slopes to continuous permafrost on summits (Lewkowicz & Ednie 2004). It is reasonable to infer that within such a basin there will be terrain present at temperatures close to 0°C that can be affected by changes in climate. If unfrozen, this terrain may become permafrost during sustained climate cooling, or if permafrost, it may thaw during sustained warming or long-term increases in snow depths. Consequently, mountain basins with permafrost may be particularly sensitive to climate change. However, the complexity of permafrost distribution within them means that there have been relatively few attempts to model climate change impacts (e.g., Janke 2005). Our goal here is to present a method that can be used to explore the potential effects of past and future climate change on mountain basins with permafrost.

Study Area

Wolf Creek Basin (60°30′N, 135°10′W) is a mountainous watershed of approximately 190 km^2, with elevations ranging from 700–2080 m a.s.l. and located 20–30 km south of Whitehorse in the Yukon Territory. The climate is continental with dry, cold conditions (Wahl et al. 1987), and the basin falls within the zone of sporadic, discontinuous permafrost zone according to the Permafrost Map of Canada (Heginbottom et al. 1995). Basin vegetation comprises boreal forest, with sub-alpine forest, a shrub zone, and an alpine tundra zone at progressively higher elevations. Under current conditions, permafrost probability models in Wolf Creek indicate that 38 to 43% of the area is underlain by permafrost (Lewkowicz & Ednie 2004, Lewkowicz & Bonnaventure 2008).

Methodology

BTS measurements were collected in Wolf Creek during the winters of 2001 and 2002 (Lewkowicz & Ednie 2004). The spatial field of BTS was modeled in a GIS using elevation and Potential Incoming Solar Radiation (PISR) as independent variables. Logistic regression was used to relate the modeled BTS temperatures to the presence or absence of permafrost at numerous sites within the basin in late-summer. The end result of this procedure is a map of permafrost probability at a grid cell resolution of 30 x 30 m.

The effects on permafrost distribution of climate cooling or warming scenarios can be simulated by respectively increasing or decreasing the values of the elevation throughout the study area (Janke 2005). This alters the modeled BTS field which in turn affects the predicted permafrost probabilities. We used a standard environmental lapse rate of 6.5°C/1000 m to calculate the necessary change of elevations, a value which is less than the BTS lapse rate (8.2°C/1000 m) (Lewkowicz & Bonnaventure 2008). Temperature changes of -2 to +5°C were used in order to examine how permafrost distributions might have appeared under equilibrium conditions similar to those of the Little Ice Age, when temperatures in the basin were lower (e.g., Farnell et al. 2004), and for future changes through to the most aggressive temperature warming scenarios proposed by the Intergovernmental Panel on Climate Change (IPCC 2007). As in previous work, we assume that permafrost probability can be equated over many grid cells to permafrost extent.

Results and Discussion

It should be emphasized that model predictions are for equilibrium states; the model does not account for lag times associated with permafrost formation and degradation. Given these lag effects, the model outputs are best thought of as referring to the upper few metres of permafrost only.

Under cooler-than-present conditions, permafrost area within the basin expands, doubling to about 75% for a temperature reduction of 2°C. The form of the change is approximately linear within this range (Fig. 1). Spatially, permafrost zones become more extensive at intermediate elevations and the boundary between continuous and extensive discontinuous permafrost (90% probability) descends from about 1600 m to 1250 m, while that between extensive and sporadic permafrost (50% probability) changes from 1400 to 1100 m.

Under warming conditions, such as those expected under IPCC projections, permafrost extent is substantially reduced in a nonlinear fashion. An increase of only 1°C halves the permafrost extent in the basin, and a further 1°C change reduces it to less than 10% of the basin area (Fig. 1). Boundaries of permafrost zones within the basin move upwards so that a 1°C change causes the continuous permafrost boundary to rise to 1700 m. At an increase of 2°C, permafrost is present only on high elevation mountain tops and upper elevation north-facing slopes. A 4°C increase reduces permafrost extent to less than 1% of the basin area, and probabilities exceed 10% only on the highest mountain peaks above 1850 m.

The changing slope of the line in Figure 1 relates to the hypsometry of the basin (Fig. 2). The elevation zones with the most area occur from 1200–1500 m a.s.l., and these have intermediate permafrost probabilities under the current climate. Cooling enhances permafrost probability in these extensive zones, and permafrost also moves downwards into lower terrain. Even a warming of 1°C reduces probability substantially in these extensive areas. For large increases in temperature, permafrost is confined to the highest peaks which occupy only a small part of the basin, so there is little further loss as warming continues.

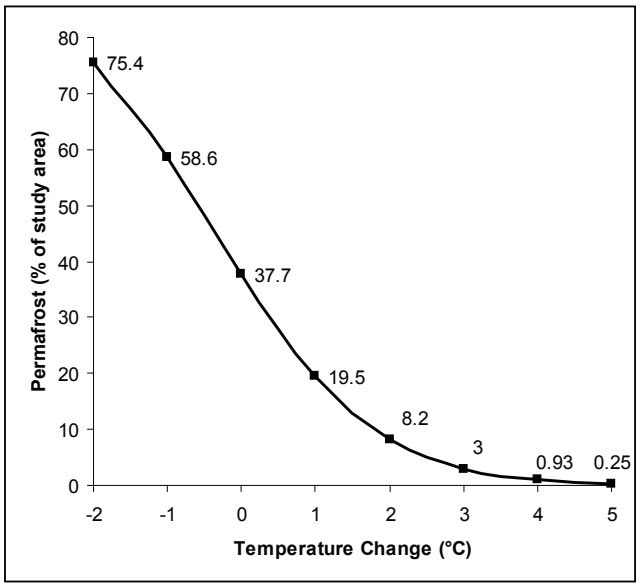

Figure 1. Predicted percent of Wolf Creek basin underlain by permafrost for climate change scenarios of -2 to +5°C.

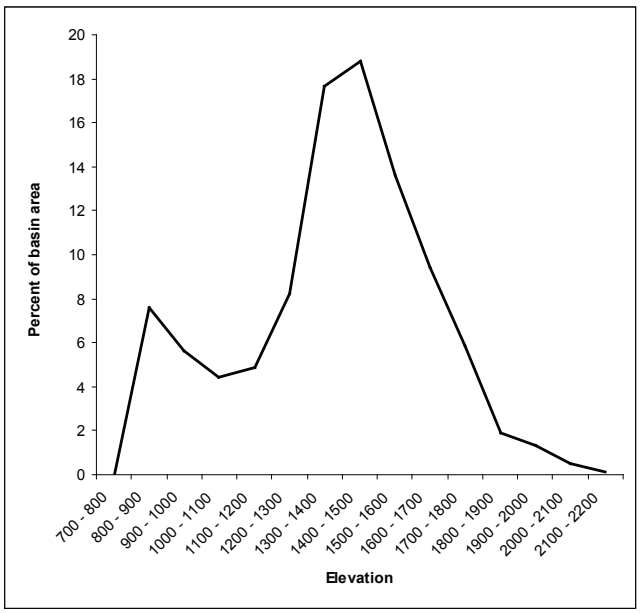

Figure 2. Hypsometric curves illustrating the percent area of Wolf Creek basin in each elevation band.

Conclusions

This simple equilibrium modeling indicates that substantial change in permafrost extent has probably occurred in Wolf Creek since the Little Ice Age, and loss of permafrost can be expected as the climate warms. Mountain permafrost is highly sensitive to climatic change as ground thermal conditions vary spatially, and thus there is always permafrost on the point of thaw (warming scenarios) or nonpermafrost areas ready to become perennially frozen (cooling scenarios). Although not shown here, the modeling produces a spatial field of permafrost probabilities that may be useful for purposes such as distributed hydrological modeling or hazard mapping.

Acknowledgments

Funding was provided by NSERC, the Canadian Foundation for Climate and Atmospheric Sciences, the Yukon Geological Survey, the Geological Survey of Canada and the University of Ottawa.

References

Bonnaventure, P.P. & Lewkowicz, A.G. Mountain permafrost probability mapping using the BTS method in two climatically dissimilar locations, northwest Canada. *Canadian Journal of Earth Sciences* (in press).

Farnell, R., Hare, P.G., Blake, E., Bowyer, V., Schweger, C., Greer, S. & Gotthardt, R. 2004. Multidisciplinary investigations of alpine snow patches in southwest Yukon. *Arctic* 57: 247-259.

Heginbottom, J.R., Dubreuil, M.A. & Harker, P.T. 1995. Canada Permafrost. (1:7,500,000 scale). In: *The National Atlas of Canada*, 5th ed., sheet MCR 4177. Ottawa: National Resources Canada.

Janke, J.R. 2005. Modeling past and future alpine permafrost distribution in the Colorado Front Range. *Earth Surface Processes and Landforms* 30: 1495-1508.

IPCC. 2007. http://www.ipcc.ch/ipccreports/assessments-reports.htm.

Lewkowicz, A.G. & Bonnaventure, P.P. 2008. Interchangeability of mountain permafrost probability models, Northwestern Canada. *Permafrost and Periglacial Processes* 19 (in press).

Lewkowicz, A.G. & Ednie, M. 2004. Probability mapping of mountain permafrost using the BTS method, Wolf Creek, Yukon Territory, Canada. *Permafrost and Periglacial Processes* 15: 67-80.

Wahl, H.E., Fraser, D.B., Harvey, R.C. & Maxwell, J.B. 1987. *Climate of Yukon.* Canadian Government Publishing Centre.

A Hypothesis: A Condition of Growth of Thick Ice Wedges

Anatoli Brouchkov
Tyumen State Oil and Gas University

So-called Ice Complex or "edoma" in Siberia, which represents extremely ice-rich and perennially-frozen sediments with thick polygonal ice wedges, is formed in territories acting as terrestrial accumulation basins during the Pleistocene. It sometimes consists of more than 90% ice by volume. Simplifying, a decrease of temperature causes soil to shrink and cracks to form; then water seeps into the cracks in spring. It freezes and expands when it is chilled by permafrost. This cycle continues to enlarge the wedges year by year until the soil above the wedges is pushed up and finally almost disappears around. However, details of the mechanism of thermal contraction cracking and ice wedge formation still remain unclear (French 1996). Ice is known to be able to flow under loads, and it probably could be easier for ice to be pressed up than for soil. Why do we observe the result of soil pushing up only, not ice, and what is the mechanical condition of the process?

Water freezing and expanding when it is chilled by permafrost can be expressed by the Clapeyron equation. Stresses can be estimated approximately as 13.4 MPa per a decrease in negative temperature by 1°C. In the case of mechanical equilibrium, if horizontal stresses σ_z are equal in soil and ice, the heaving strain of about 9% of volume of freezing water ε_f is connected to mechanical compression of frozen soil ($d\sigma_z * l_{fr}/E_{fr}$) and ice ($d\sigma_z * l_{ice}/E_{ice}$), being of l_{fr} and l_{ice} in size and having the strain modulus E_{fr} and E_{ice}, respectively:

$$d\sigma_z = \frac{d\varepsilon_f}{\frac{l_{fr}}{E_{fr}} + \frac{l_{ice}}{E_{ice}}} \quad (1)$$

If, for example, ε_f is 0.0045 m as a result of freezing of 0.05 m of water, l_{fr} = 5 m and l_{ice} = 0.5 m, and the long-temp compression modulus E_{fr} = 20 MPa and E_{ice} = 50 MPa, then stress σ_z = 0.017 MPa. In many cases, the value of ε_f is even less then 0.05 m; for example 0.001–0.003 m only in Barrow (Black 1951), and 0.002–0.01 m in Kolyma plain (Berman 1965). Due to higher modulus values, compression of soil reaches 4.33 and ice 0.17 mm consequently. The size of the deformed soil area varies, for example, near Fairbanks in the range of 0.3–3 m (Pewe 1962). The lateral strains depending on Poisson's ratio will be less than compression, but probably they will be more for soil than for ice. Stresses are small and perhaps unable to make considerable structural changes of soil mass. Repeating a thousand times, it results in ice wedge thickness of about 4 m. This is generally in agreement with the point that soil is pushed up during ice wedge formation. However, it was found that soil layers at a certain distance from the ice wedge are almost not affected (Popov 1965).

An area of high density of deformed soil should be created on contact with an ice wedge to give space to ice, and that area should be gradually increased in size in accordance with an increase of wedge thickness. One reason for the deformed area to remain small is the stress distribution in soil mass. The stresses are basically not equal and become smaller with distance from an ice wedge. Using q/unit length on the surface of a semi infinite soil mass, or if the excess stress is according to the Boussinesq equation (Ahlvin & Smoots 1988), the stress can be found approximately:

$$\Delta\sigma_z \sim \frac{\sigma_z}{z^n} I \quad (2)$$

where n changes from about 1 to 2, I = influence factor for the load, and z = distance from the ice wedge. Formula (1) should be adjusted then according (2). If horizontal stress σ_z = 0.017 MPa near an ice wedge, it is about σ_z = 0.004 MPa only on distance of 2 m. Thus, stresses might be too small to cause deformations far from the ice wedge, but they are big enough to move soil particles and pore ice near the ice wedge. Another reason for the deformed area to be small is perhaps because of gradual movement of attached ice soil towards the surface together with ice caused by pressure and buoyancy.

Signs of diapirism and soil circulation are widespread in periglacial areas (Hallet & Waddington 1991). Buoyancy can be an effective driving force in the case of ice wedges due to different densities of frozen soil (1.5–1.7 and more cm^3/g) and ice (0.9–1 cm^3/g). If the size of polygons are more than or equal to the height of an ice wedge h, and the viscosity of ice η_i is much less than the viscosity of the surrounding soil η_s, the rate of vertical movement of an ice wedge wall υ will be (Artyushkov 1969):

$$\upsilon \sim \frac{\Delta\rho g h^2}{\eta_s} \quad (3)$$

where $\Delta\rho$ = difference of densities of soil and ice; g = gravity acceleration, 9.81 m/sec; η_s = viscosity of surrounding soil, Pa*s. However, the assumption that the viscosity of ice is less than the viscosity of the surrounding soil is far from being acceptable: relationship is opposite. The ice viscosity can be assumed as 10^{12}–10^{13} Pa*s, and frozen soil viscosity as 10^{10}–10^{11} Pa*s. The buoyancy of an ice wedge and its vertical movement z can still be found from the similar Navier-Stoks equation:

$$z \sim vt \sim \frac{\Delta\rho g l^2}{18\eta_s} t \quad (4)$$

where t = time; l = width of ice wedge. If the width of the ice wedge l = 1 m, and time t is 1000 years, then resurfacing of ice can reach about 1.5 m. That value of vertical movement may change the shape of ice wedges drastically, especially in saline or high-temperature permafrost. Vertical orientation of

rod-shaped air bubbles (Kurdyakov 1965), "echelon breaks" (Pewe 1962), and the foliated structure of ice can serve as indirect evidence of it. Sometimes soil layers near an ice wedge look like they are "drawing in ice" (Pewe 1962). Flexures of soil layers near ice wedges are mostly directed up (Popov 1965) probably because of vertical ice flow. Unusual deformations of soil layers under an ice wedge, described by Kostyaev (1965) in the Yana River terrace, can also be a result of buoyancy. Ice wedges flowing upward 1–3 m, like diapers, were described by Black (1983).

Therefore, the thick ice wedges can be formed easier in conditions of low values of the soil creep threshold σ_0 and their higher deformability; it is a condition of their growth by the cracking-fullfiling-freezing mechanism. Stresses induced by freezing are small and perhaps unable to make considerable structural changes of soil mass. However, creep threshold σ_0 values of frozen saline soil are low, and that gives a vital reason for wide distribution of thick ice wedges in regions of saline permafrost. Ice is able to flow at any stress, and should be flowing up during ice wedge formation. A number of features appears to be created during the evolution of ice wedge shape due to the flow; among them irregular shapes of underground ice are common. Buoyancy can be another effective driving force in the case of ice wedges due to the difference of densities of frozen soil and ice. An estimation shows the buoyancy of ice can reach substantial values.

References

Ahlvin, R.G. & Smoots, A.V. 1988. Construction *Guide for Soils and Foundation*. New York: John Wiley & Sons.

Artyushkov, E.V. 1969. About pressing of ice-wedges by surrounded deposits. In: *Problems of Cryolithology*, Issue 1. Moscow University Press, 34-37 (in Russian).

Berman, L.L. 1965. Underground ice in northern part of Kolyma plain. In: *Underground Ice,* Issue 1. For the 7th International Congress on Quarternary (INQUA), USA. Moscow University Press, 112-119 (in Russian).

Black, R.F. 1951. Structure in ice wedges of Northern Alaska. *Geol. Soc. Am. Bull*. 62, Pt. 2.

Black, R.F. 1983. Three superposed systems of ice wedges at McLeod Point, northern Alaska, may span most of the Wisconsian stage and Holocene. *Proceedings of the Fourth International Conference on Permafrost, July 17–22, 1983.* Washington, DC: National Academy Press, 68-73.

French, H.M. 1996. *The Periglacial Environment,* 2nd ed. Longman, Harlow, 1-341.

Hallet, B. & Waddington, E.D. 1991. Buoyancy forces induced by freeze-thaw in the active layer: Implications for diapirism and soil circulation. In: J.C. Dixon & A.D. Abrahams (eds.), *Periglacial Geomorphology*. John Wiley and Sons Ltd., 251-279.

Kostyaev, A.G. 1965. Ice wedges and convective instability of soils. In: *Underground Ice*, Issue 1. For the 7th International Congress on Quarternary (INQUA), USA. Moscow University Press, 133-140 (in Russian).

Kurdyakov, V.S. 1965. Polygonal ice-wedges in Amguema river basin. In: *Underground Ice,* Issue 1. For the 7th International Congress on Quarternary (INQUA), USA. Moscow University Press, 87-103 (in Russian).

Pewe, T.L. 1962. Ice wedges in permafrost, Lower Yukon river near Galena Alaska. *Biuletyn Peryglacjalny* 11. Lodz.

Pewe, T.L. 1966. Ice wedges in Alaska: Classification, distribution and climatic significance. *Proceedings of the First International Conference on Permafrost.* National Academy of Science: National Research Council of Canada, Publication 1287, 76-81.

Popov, A.I. 1965. Underground ice. In: *Underground Ice*, Issue 1. For the 7th International Congress on Quarternary (INQUA), USA. Moscow University Press, 7-39 (in Russian).

Modeled Continual Surface Water Storage Change of the Yukon River Basin

Rena Bryan
Larry D. Hinzman
Robert C. Busey
International Arctic Research Center, University of Alaska Fairbanks, Fairbanks, Alaska, USA

Introduction

Climate change in high latitudes, occurring at an observable pace, provides a window into changes the rest of the earth may experience over a longer time scale (Shaver et al. 1992). Large-scale datasets of surface water, groundwater, and permafrost dynamics serve as prerequisites in a variety of other analyses and applications (Lehner et al. 2008). This study models continual surface water storage change in the Yukon River Basin. The project is the underpinning for carbon dioxide and methane flux; taiga-tundra shift; regional surface energy balance; regional weather pattern; migratory waterfowl habitat availability; and infrastructure, building, and community stability studies.

The purpose of this study is to determine how the future surface water storage of the Yukon Basin will compare to present. The project considers the changes to surface water storage as affected by warming climate, permafrost degradation, and the vertical flux of water, but ignores changes induced by altered evapotranspiration or lateral flow. Transition from birch forests to fens and bogs has been documented over the last twenty years in the Tanana Flats (Jorgenson et. al. 2001). Also in the last twenty years, thermokarst lakes developed and initiated large taliks that completely penetrated the permafrost near Council, Alaska. As a result, drier environments than before exist near Council (Yoshikawa & Hinzman 2003). In areas of discontinuous permafrost, where projected permafrost will be warm enough to degrade, (1) if the local hydraulic gradient is upwards, the surface will be inundated with water and (2) if the hydraulic gradient is downwards, existing surface water will drain. In areas of continuous permafrost, where projected permafrost will be warm enough to degrade, the surface will subside and surface ponds may increase. To investigate this hypothesis, we utilize synoptic meteorology, permafrost thermal composition, and potentiometric surface algorithms.

Background

According to the International Permafrost Association *Circum-Arctic Map of Permafrost and Ground-Ice Conditions* (Brown et al. 1998), discontinuous permafrost dominates the interior of the basin. Continuous permafrost is second most prominent and present in the northern rim of the basin and at Yukon-Kuskokwim Delta. Sporadic permafrost exists in southern Yukon Territory. Isolated permafrost can be found sparsely in the glaciated region at the river's source. Closer examination of local variation in vegetation, soil moisture and thermal properties, and snow cover produces finer resolution permafrost thermal composition (Smith & Riseborogh 1996). Continuous permafrost, frozen ground (0°C and below) in spatial continuity, provides an impervious barrier to groundwater movement. Because of overall permafrost stability, much of the Arctic is spotted by ponds perched above the permafrost. Most groundwater-surface water interactions occur in areas of discontinuous permafrost. In areas where the hydraulic gradient is downwards, as the confining layer of permafrost degrades and an open talik forms, surface water formerly underlain by permafrost can drain into the subpermafrost groundwater. In contrast, where the local hydraulic gradient is upwards, subpermafrost groundwater may discharge at the surface.

Methods

Referencing topographic features, the weather forecast model, National Weather Service Global Forecast System, is synoptically represented and accounts for topographically driven processes. TopoClimate is developed at the International Arctic Research Center, University of Alaska Fairbanks by Atkinson and Gourand. Driven by high-resolution surface air temperatures available from TopoClimate, the TTOP model is a numerical model using surface n-factors, bulk thermal conductivities, and freezing and thawing indices. TTOP was originally developed by Smith & Riseborough (1996) (Busey et al. 2008). The model is applied to estimating the permafrost thermal composition in the Yukon Basin. Extracting steepness and relative elevations from the digital elevation model, modeled potentiometric surfaces generate a hydraulic gradient map. (1) The surface air temperature, (2) permafrost thermal composition, and (3) hydraulic gradient maps in concert assess surface water storage change. This study reviews existing observations of spring, aufeis, and lake size and distribution change locations in order to calibrate the model. Remote sensed imagery analysis has defined some areas of lake change. Thermal conductivity, thermokarst, and $\delta\ ^{18}O$ field observations validate the model. Thermal conductivity measurements and thermokarst documentation validate permafrost thermal composition modeled by TTOP and permafrost destabilization. The $\delta\ ^{18}O$ values from lakes with a deep groundwater component are distinct from those lacking connection to the groundwater. Lakes possessing a deep groundwater component as revealed by isotope analysis validate the hydraulic gradient model. Model validation data will be collected in Innoko National Wildlife Refuge, Yukon Flats National Wildlife Refuge, and locations throughout the road system of Alaska and the Yukon Territory.

Implications to surface water storage change

Projecting ecosystem dynamics will moderate concerns and help us plan for a warming Arctic and its effects on

the rest of the globe. Drying of soils allows increased O_2 levels to penetrate the soil deeper and may therefore increase the release of CO_2 to the atmosphere (Oechel et al. 2000). Expansion of thaw lakes due to thawing of permafrost, increasing the expanse of waterlogged soils, may increase the release of CH_4 into the atmosphere (Walter et al. 2006). Closer examination of the taiga-tundra ecotone reveals a more complex situation than the simple northward migration of trees in response to warming (Skre et al. 2002). Permafrost thawing, surface water drainage, and drying of soils in areas of low precipitation are likely to lead to a shift to grassy tundra vegetation (Callaghan et al. 2004). Wet systems of relatively continental climates, for example wet sedge tundra, experience high evapotranspiration, cool surface, and, therefore, a high latent heat flux. Dry systems, for example dry heath, have a warm surface and experience high sensible heat flux (McFadden 1998). The regional surface energy balance forces regional weather patterns. Global climate change is made up of long-lasting regional weather changes. Habitat for migratory waterfowl, affected by the availability of surface water, is an issue of concern to wildlife managers. This is also a region where societal impacts are acute. Town and village infrastructure will likely experience a variety of changes due to permafrost and surface water changes. Changes in permafrost cause the pavement to heave and slump on Farmers Loop Road in Fairbanks, and uncontrolled flow from wells damaged houses in the same area. This area of upwelling holds potential danger. Traditional travel routes, berry picking, and hunting places are likely to be affected.

Acknowledgments

Support for this research is provided by the U.S. National Science Foundation (Grant No. 0327664).

References

Brown, J., Ferrians Jr., O.J., Heginbottom, J.A. & Melnikov, E.S. 1998. Revised February 2001. *Circum-Arctic map of permafrost and ground-ice conditions.* Boulder, CO: National Snow and Ice Data Center/World Data Center for Glaciology. Digital Media.

Busey R.C., Hinzman, L.D., Cassano, J.J. & Cassano, E. 2008. Permafrost distributions on the Seward Peninsula: Past, present, and future. *Proceedings of the Ninth International Conference on Permafrost, Fairbanks, Alaska, June 29–July 3, 2008.*

Callaghan, T.V., Björn, L.O., Chernov, Y., Chapin, T., Christensen, T.R., Huntley, B., Ims, R.A., Johansson, M., Jolly, D., Jonasson, S., Matveyeva, N., Panikov, N., Oechel, W., Shaver, G., Schaphoff, S. & Sitch, S. 2004. Effects of changes in climate on landscape and regional processes, and feedbacks to the climate system. *Royal Swedish Academy of Sciences Ambio* 33(7): 459-468.

Jorgenson, M.T., Racine, C.H., Walters, J.C. & Osterkamp, T.E. 2001. Permafrost degradation and ecological changes associated with a warming climate in central Alaska. *Climatic Change* 48: 551-579.

Lehner, B., Verdin, K. & Jarvis, A. 2008. New Global Hydrography Derived from Spaceborne Elevation Data. *EOS* 89(10): 93-94.

McFadden, J.P., Chapin III, F.S. & Hollinger, D.Y. 1998. Subgrid-scale variability in the surface energy balance of arctic tundra. *Journal of Geophysical Research* 103: 28,947-28,961.

Oechel, W.C., Vourlitis, G.L., Hastings S.J., Zulueta R.C., Hinzman, L.D. & Kane, D.L. 2000. Acclimation of ecosystem CO_2 exchange in the Alaskan Arctic in response to decadal climate warming. *Nature* 406: 978-981.

Shaver, G.R., Billings, W.D., Chapin III, F.S, Giblin, A.E., Nadelhoffer, K.J., Oechel, W.C. & Rastetter E.B. 1992. Global Change and the Carbon Balance of Arctic Ecosystems. *BioScience* 42(6): 433-441.

Skre, O., Baxter, R., Crawford, R.M.M., Callaghan, T.V. & Fedorkov, A. 2002. How will the tundra-taiga interface respond to climate change? *Swedish Royal Academy of Sciences, Ambio Special Report* 12: 37-46.

Smith, M.W. & Riseborough, D.W. 1996. Permafrost monitoring and detection of climate change. *Permafrost and Periglacial Processes* 7: 301-310.

Walter, K.M., Zimov, S.A., Chanton, J.P., Verbyla, D. & Chapin III, F.S. 2006. Methane bubbling from Siberian thaw lakes as a positive feedback to climate warming. *Nature* 443(7107): 71-75.

Yoshikawa, K. & Hinzman, L.D. 2003. Shrinking thermokarst ponds and groundwater dynamics in discontinuous permafrost near Council, Alaska. *Permafrost and Periglacial Processes* 14: 151-160.

Freeze/Thaw Properties of Tundra Soils, with Applications to Trafficability on the North Slope, Alaska

Christina F. Bryant
Geo-Watersheds Scientific, College Station, USA
Ron F. Paetzold
Geo-Watersheds Scientific, College Station, USA
Michael R. Lilly
Geo-Watersheds Scientific, Fairbanks, USA

Introduction

This abstract focuses on the application of soil temperature profile data and its relationship to tundra-travel management on the North Slope of Alaska, with particular attention to winter travel. Current standards regulate tundra-travel on the North Slope of Alaska to conditions at or below -5°C at a depth of 30 cm in the soil profile (Bader 2005). These regulations are meant to ensure adequate soil strength for such activities. Additionally, six inches of snow cover is needed in the Coastal Plain region for tundra-travel to be open.

Frozen water affects tundra soils through added strength from the addition of solids (ice) in soil pore spaces, which decreases slipping between soil particles. Soil cohesive properties are also augmented by frozen water, which "cements" soil particles to one another (Lilly et al. 2008). Thus, in areas where soil water content is high, soil strength increases during winter freezes, and conversely decreases in conjunction with summer thaws.

Little or no data are available to assess travel limitations resulting from seasonal freeze/thaw cycles of tundra soils on the North Slope, especially in areas of interest to those involved in the oil and gas exploration and field operations.

Although this abstract makes no suggestions pertaining to revisions or alterations to current management standards, the knowledge gained in respect to freeze/thaw time constraints and conditions on tundra-travel will aid others when making such decisions. Data analysis is specifically useful when assessing seasonal time limits on ice-road construction and use as a basis of frozen soil freeze/thaw properties.

Methods

A system of twelve weather stations was set up in northern Alaska in fall of 2006 and has since been collecting soil moisture data by TDR, and soil temperature data from Thermisters each hour at 0, 5, 10, 15, 20, 40, 60, 80, 100, 120, 135, and 150 cm depths (Fig. 1). These depths may vary for some sites due to local soil conditions and the depth of the active layer during sensor installations. Relative humidity, dew point, wind speed and direction, wind chill, snow depth, solar radiation, net radiation, and snow and rain precipitation data are also available from the data network. Station dataloggers are connected to radios, allowing for near real-time measurement, which is specifically applicable when analyzing current conditions for tundra-travel.

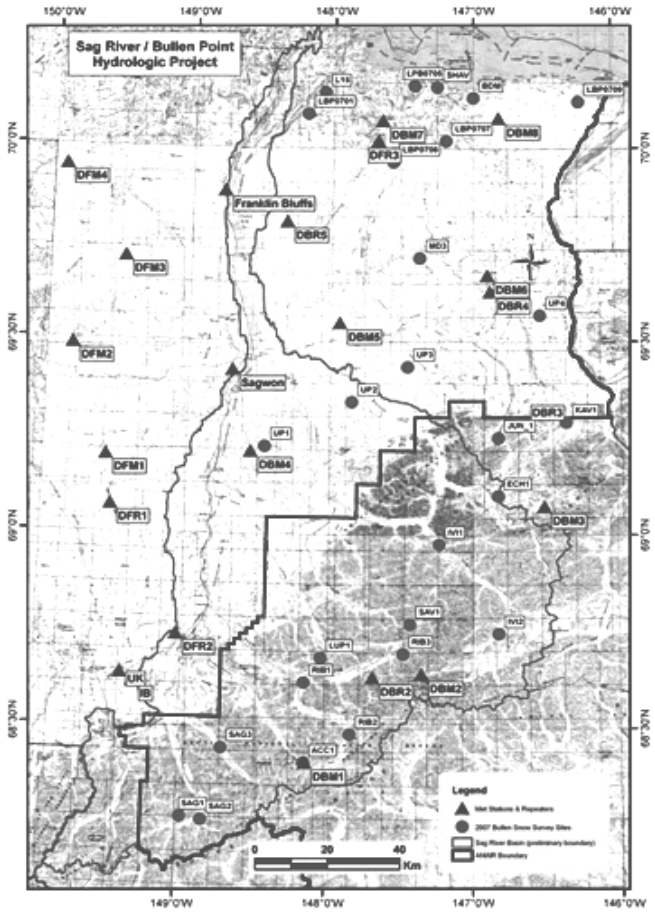

Figure 1. Map of meteorological station locations along the North Slope, Alaska.

Soil temperature data were analyzed to show temporal variation in one-degree incremental temperature conditions in the freezing soils. Analyzing the differences in dates that soils reach these one-degree temperatures helps illustrate the potential differences in timing of tundra-travel openings when using different soil temperatures**.** Soil temperature data were also spatially examined to display the effects of relative location on timing of one-degree changes during the annual freeze/thaw cycle in the active layer.

Results and Discussion

Current data analyses include plotted freeze/thaw cycles from winter 2006 to summer 2007 for stations DMB2,

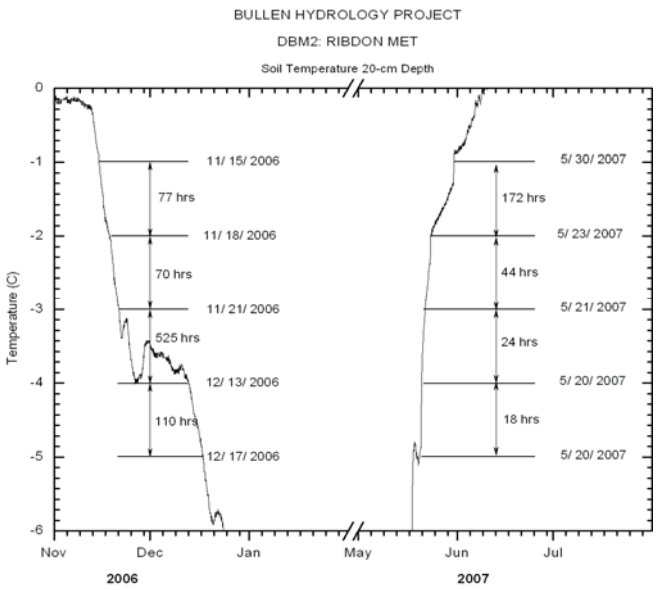

Figure 2. Soil temperature and water content for the 20 cm depth at DBM2 Ribdon met.

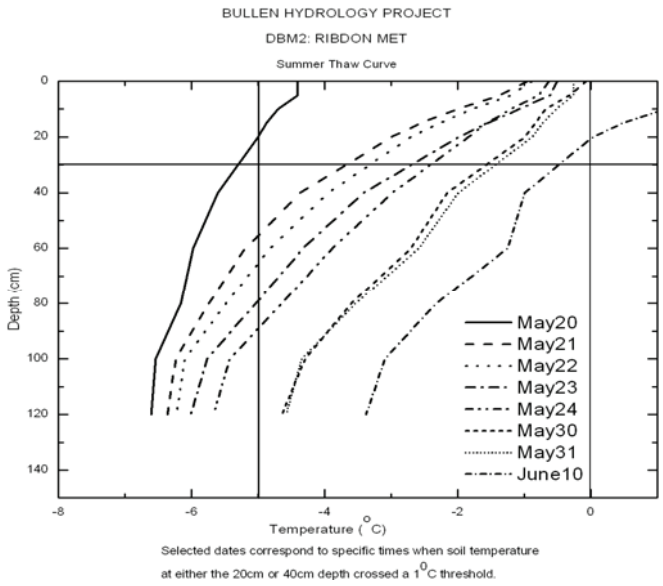

Figure 3. Soil temperature profile for the 2007 summer at DBM2 Ribdon met.

DMB4, DMB5, and DMB6, respectively. Note that data are not available at the regulated 30 cm depth, and so must be interpolated by averaging data from the 20 and 40 cm depths. (See Figure 2 for an example of the 2006/2007 freeze/thaw curve at the 20 cm depth for DBM2 Ribdon met.) Relaxing tundra-travel regulations from -5°C to -2°C would add approximately 34 days of travel time at station DBM2, approximately 28 days of travel time at station DBM4, approximately 30 days of travel time at station DBM5, and approximately 29 days of travel time at station DBM6. In all four cases, the majority of additional travel time would occur during the winter freeze, as tundra soils freeze slower than they thaw. At each of the aforementioned sites, the ratio of additional winter travel time to additional summer travel time was at least 1:1.4, with the mean ratio being 1:2.8, and the maximum ratio being 1:4.9.

Profile curves showing temperature changes based on soil depth were also created for stations DBM2, DBM4, and DBM6. The dates selected on these plots correspond to specific times when soil temperature at either the 20 or 40 cm depth crossed a 1°C incremental threshold. (See Figure 3 for an example of a temperature profile curve for DBM2 Ribdon met for the 2007 summer period.) Of the analyzed stations, DBM2 had both the earliest freeze and earliest thaw dates. In respect to DBM4 and DBM6, DBM2 is the furthest station from the coastline. Soils at DBM4, the westernmost station analyzed, began both the freeze cycle and thaw cycle on the latest dates.

Summary

Soil temperature data were collected and analyzed from a system of 12 weather stations. This data can be used to help evaluate tundra-travel management policy along the North Slope of Alaska. Variation in incremental one-degree conditions in the freezing soils was used to illustrate the potential differences in timing of tundra-travel openings. Relaxing tundra-travel regulations from -5°C to -2°C would add an average of 30 days of travel time throughout the analyzed stations, with the majority of additional time occurring during winter freeze-up. Freeze/thaw curves had the earlier start times at the inland locations, as compared to those locations closer to the coastline.

To better assess freeze/thaw tundra soil conditions, a larger quantity of data must be analyzed. Other station locations as well as current winter freeze data should be plotted to broaden the depth of analyzed trends. Spatial analyses of data will also be performed. Soil parameters associated with freeze/thaw cycles will be compared between coastal and foothill sites, as well as resulting variations from east/west locations. Current data for the 2007/2008 freeze curve will also be compared to data from the previous winter. Soil-strength measurements on a variety of soils as a function of temperature and water content are also needed to better relate travel conditions to soil parameters.

References

Bader, H.R. 2005. *Tundra Travel Research Project: Validation Study and Management Recommendations*. Alaska Department of Natural Resources, 20 pp. http://www.dnr.state.ak.us/mlw/tundra/validation2005final_with_figures.pdf.

Lilly, M.R., Paetzold, R.F. & Kane, D.L. 2008. Tundra soil-water content and temperature data in support of winter tundra travel. *Proceedings of the Ninth International Conference on Permafrost, Fairbanks, Alaska, June 29–July 3, 2008.*

Discontinuous Permafrost Distribution and Groundwater Flow at a Contaminated Site in Fairbanks, Alaska

Andrea E. Carlson
Shannon & Wilson, Inc., Fairbanks, Alaska, USA
David L. Barnes
Civil & Environmental Engineering, Water and Environmental Research Center, University of Alaska Fairbanks (UAF), Fairbanks, Alaska, USA

Introduction

Permafrost distribution substantially influences groundwater hydrology. Permafrost can affect hydrologic processes of water distribution, movement, and storage capacity, controlling zones of recharge and groundwater flow pathways (Anderson 1970, Prowse & Ommanney, 1990, Hinzman et al. 2005). These effects are noticeable in discontinuous permafrost regions because of lateral and vertical variability in frozen and unfrozen soil distribution.

Borehole and monitoring well installations revealed the variable nature and distribution of discontinuous permafrost during a site investigation to characterize and delineate the extent of groundwater contamination at a site in Fairbanks, Alaska.

We compiled borelogs and field observations and used ArcGIS to create thematic maps of groundwater elevations and the top of the permafrost surface below the ground. The groundwater elevation maps were overlain on the permafrost distribution map to investigate if changes in groundwater flow direction and gradient could be correlated to or were associated with areas of frozen soil. We measured water levels in nested wells to determine if vertical gradients due to frozen soils were affecting the groundwater flow regime.

Site Environment

The site is in the Alaskan subarctic, located in the zone of discontinuous permafrost. Environmental consulting reports (Shannon & Wilson 2002–2007) documented that several contaminants, including trichloroethylene and benzene, are present in the area's soil and groundwater. In an effort to characterize and delineate site contamination, monitoring wells and soil borings were installed and sampled over the past 16 years.

Soils at the site consist of 2 feet to 20 feet of surficial silt and organics underlain by sand and gravel deposits. Swale and slough channels cut through the area and are filled with finer grained silt and sand. Soil borings encountered seasonal frost to a thickness of 20 feet, and discontinuous permafrost was encountered from the surface to greater than 65 feet at some locations. The majority of frozen soils were bonded with no excess visible ice.

Methods

We compiled consultant reports (Shannon & Wilson 2002–2007), field data, borelogs, and analytical geochemical data for geostatistical analysis. Northing and easting data are in Alaska State Plane North America Datum 1983, Zone 3 (NAD '83); elevation data are in National Geodetic Vertical Datum of 1929 (NGVD '29). Using Environmental Systems Research Institute (ESRI), ArcGIS Desktop software, version 9.2 released in 2006, we created interpolated surfaces and contour maps of the top of the permafrost below ground surface and groundwater elevations. ArcGIS Desktop Extension, including Spatial Analyst and 3-D Analyst, were the primary geostatistical analysis tools.

To determine if vertical gradients could be affecting groundwater movement, groundwater elevation data was collected once a week over a two-month period in three sets of nested wells where permafrost was not encountered during well installation. The depth to groundwater below the top of the well casing was measured using a handheld water level indicator, and the elevation was calculated based on the top of casing elevation.

Results

The permafrost distribution map (Fig. 1) shows the elevation of the top of the permafrost relative to NGVD '29; the approximate ground surface elevation at the site is 435 feet above mean sea level. The permafrost map was created using data from 54 locations, including 38 monitoring well borings, 13 well point installations, and 3 geotechnical-investigation borings in the vicinity. The depth to permafrost varies across the site, from the ground surface to greater than 60 feet; the elevation of the top of permafrost ranges from less than 370 feet to the ground surface (435 feet). Groundwater elevation maps were created for two 24-hour periods for each data collection event (six total maps). The groundwater elevations ranged from 421.59 feet to 423.52 feet during October 2004; from 419.87 feet to 422.08 feet in April 2006; and from 421.38 feet to 424.94 feet in October 2007. The mapped configurations of the elevations illustrate localized variations in groundwater flow direction and velocity.

Groundwater elevations, recorded for two sets of the nested wells, did not show significant differences in elevations between the deep (50 feet) and shallow (20 feet) wells. However, measurements taken at one location did have significant differences in head between the deep and shallow wells, ranging from 0.07 feet to 0.19 feet, with an average difference of 0.10 feet during the period of measurement.

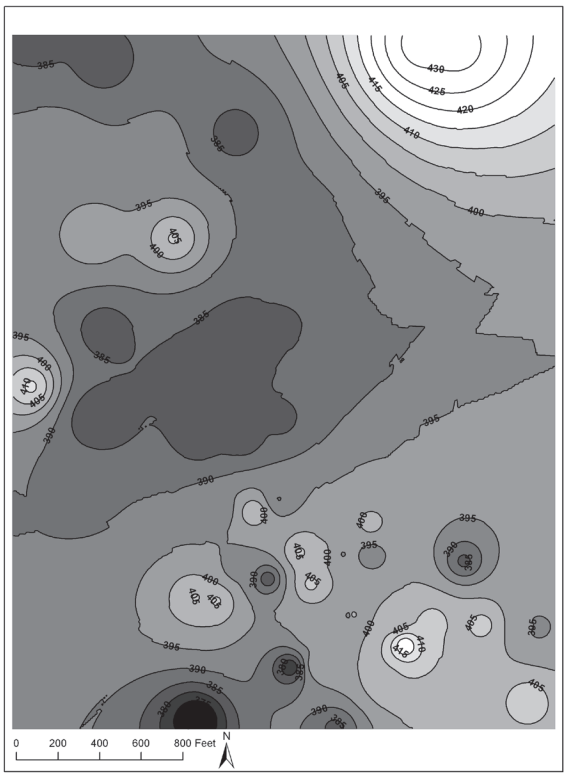

Figure 1. Permafrost distribution map showing contours of the elevation of the top of permafrost below the ground surface; the permafrost contour interval is 5 feet. The dark areas represent areas where the top of permafrost is at a greater depth below the ground surface; light areas represent where the top of permafrost is closer to the ground surface.

Discussion

Permafrost distribution

The permafrost distribution map illustrates that the top of the permafrost is highly variable within short horizontal distances across the study site. The southeastern portion of the map has a larger number of sample points, and discontinuities are better represented. The central area of the site shows an area where permafrost was not encountered during the well installations. The wells were installed to 50 feet in this location, which represents a "hole" in the permafrost. In the northwestern area of the site, shallow permafrost was encountered at 20 feet to 25 feet below the ground surface. The thickness of the permafrost masses is unknown; and none of the wells in the area extend through permafrost. There are very few sample points in the northeast section of the map, as this area is outside the delineated contaminant plume boundary; it is likely discontinuities exist on the same scale as in the other portions of the site.

Groundwater elevations

A general groundwater trend towards the northwest is evident in the groundwater elevation maps (not shown). In addition to the regional trends, each of the groundwater elevation configurations exhibit patterns with varying gradients that show changing groundwater directions and velocities. Several regions of the project site have similar groundwater contours during each sampling event. By comparing the permafrost distribution with the converging and diverging groundwater flow-paths, the variances in groundwater flow can be attributed to areas of discontinuous permafrost.

Vertical gradient measurements in the nested wells also indicate that masses of discontinuous permafrost likely affect the hydraulic gradient in those areas.

Conclusions

The permafrost distribution map shows a high degree of lateral and vertical variability between frozen and unfrozen soils at the site. The groundwater elevation maps demonstrate that the heterogeneity of subsurface hydraulic conductivities, attributable to areas of discontinuous permafrost, affect lateral and vertical groundwater flow. Vertical gradients were measured in the aquifer and are likely a result of the distribution of frozen soils.

Further Work

The permafrost distribution and groundwater elevation maps served as a starting point for further research to investigate the relationship between contaminant movement and areas of discontinuous permafrost. Thematic maps of contaminant concentrations were also created and overlain on the permafrost distribution and groundwater gradient maps to assess spatial and temporal trends in the concentration data that may be correlated to areas of discontinuous permafrost.

Acknowledgments

The authors would like to acknowledge input and support provided by project managers at Shannon & Wilson Inc, and the Alaska Department of Environmental Conservation.

References

Anderson, G.S. 1970. Hydrological Reconnaissance of the Tanana Basin, Central Alaska: *U.S. Geological Survey Hydrologic Investigations Atlas* HA-319.

Hinzman, L.D., Kane, D.L. & Woo, M.K. 2005. Permafrost hydrology. In: M.G. Anderson (ed.), *Encyclopedia of Hydrological Sciences*. John Wiley & Sons, Ltd., 2679-2693.

Prowse, T.D. & Ommanney, C.S.L. 1990. *Northern Hydrology: Canadian Perspectives. National Hydrology Research Institute*. Science Report No. 1, 308 pp.

Shannon & Wilson, Inc. 2002–2007. *Groundwater Quality Assessments ADOT & PF Peger Road Operations and Maintenance Facility, Fairbanks, Alaska*.

Thermal Regime Within an Arctic Waste Rock Pile: Observations and Implications

Jim W. Cassie
BGC AVOT Ingenieria Ltda., Santiago, Chile
Lukas U. Arenson
BGC Engineering Inc., Vancouver, BC, Canada

Introduction

As part of the advanced exploration for diamond mining projects in Canada's north, a small waste rock pile of run of mine materials was constructed at the Snap Lake Diamond Project to investigate its long-term thermal behavior. The site is located approximately 220 km northeast of Yellowknife (Fig. 1), and it is in continuous permafrost with a mean annual air temperature (MAAT) of -8.3°C (Fig. 2). The maximum active layer thicknesses at the location of TH 12 (Fig. 3) varied between 5.93 m (9/29/2001) and 5.21 m (9/28/2004).

Test cell configuration and materials

The 8 m high "test cell" (Fig. 4) was instrumented with two horizontal thermistor cables at the base of the rock pile: one cable from west to east (TH 9) and one from south to north (TH 10). The cables were installed to confirm the expected subzero nature of the rock pile, along with measurements of active layer depths within the rockfill material. The test cell consists of clean to sandy gravel. Temperature measures from the base of the rock pile are available for a period of five years. Unfortunately, the rockfill material from the test cell was later excavated to make room for the full-scale mine.

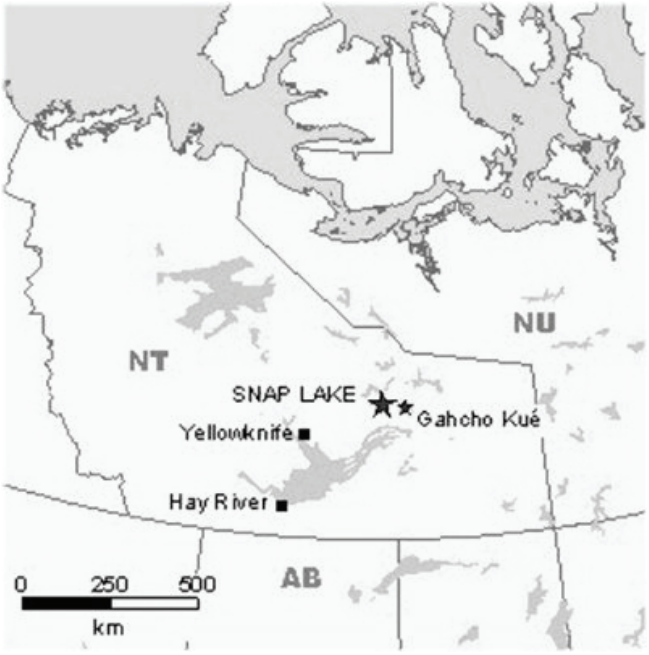

Figure 1. Location of Snap Lake (De Beers Canada).

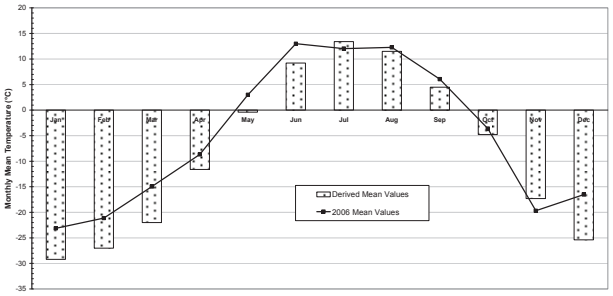

Figure 2. Mean monthly air temperatures for Snap Lake (1998–2006).

Thermal Monitoring

Temperature trends from the south-to-north thermistor are presented in Figure 6 as one-year moving averages. There is a clear cooling trend for all locations as well as a dampening of the seasonal variations close to the boundaries of the test cell. The cooling rates change with distance from the edge and are highest (~0.7–0.8°C/year) at the edge and the centre of the pile and lowest (~0.3°C/year) half way into the

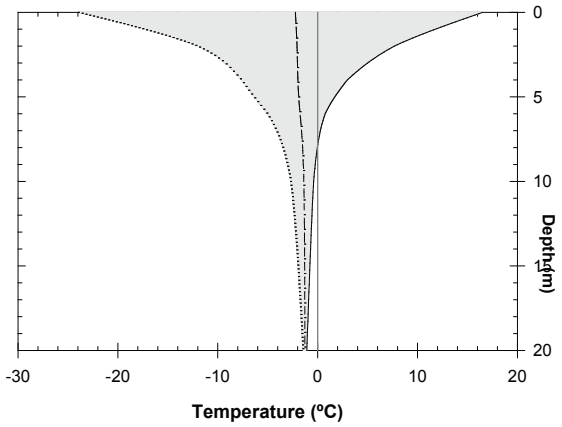

Figure 3. Temperature trumpet (2000–2005). The borehole (TH 12) is located approximately 100 m from the shoreline of Snap Lake.

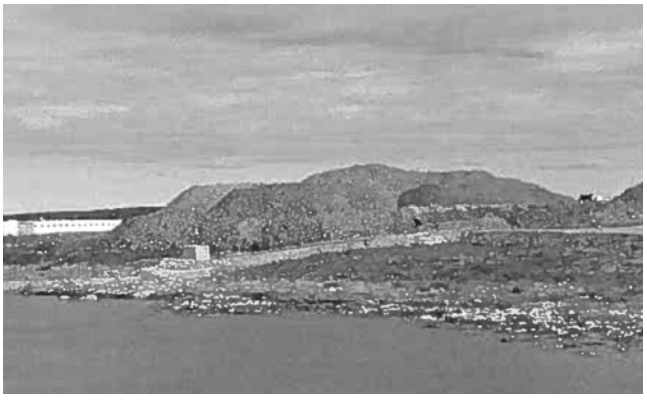

Figure 4. View of the test cell form the southeast (Photo: J.W. Cassie, 2003).

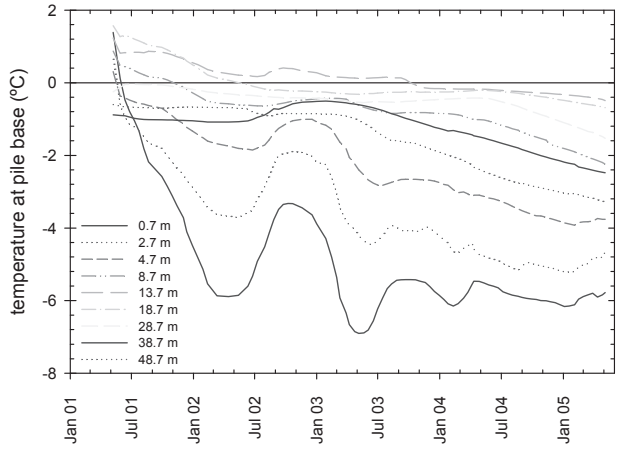

Figure 5. One-year moving average temperature trends for TH 10.

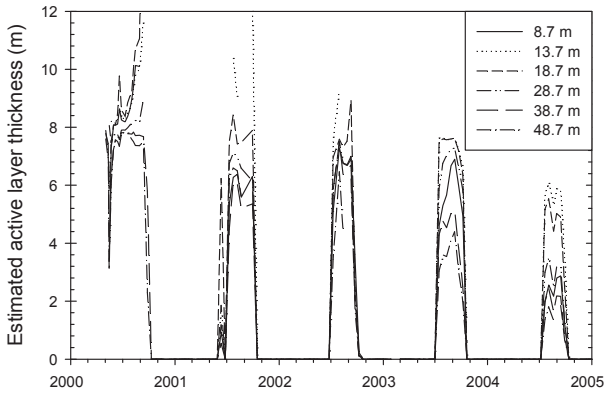

Figure 6. Estimated active layer thickness at different distances from the edge in the waste rock test cell calculated from the temperatures at the base.

pile. This difference can be explained by the formation of convective cells within the pile that force cold air to funnel down the centre of the pile, therefore, generating increased cooling.

Active Layer Depths/Permafrost Aggradation

Changes in the active layer depth underneath the test cell had to be estimated from the horizontal temperature readings at the base of the waste rock. At a distance of 2.7 m from the edge, the temperatures stayed below 0° during the whole summer after construction. TH 9 showed subzero temperatures even at a distance of only 0.7 m from the edge, whereas TH 10 seemed to stay at a zero curtain. No positive ground temperatures, however, were recorded on this side. These readings show that, at the edge of the waste rock pile, the active layer thickness is in the order of 2 m, assuming a slope angle of 37°, which is the angle of repose for the rockfill material.

In order to estimate the active layer of the waste rock test cell, temperatures at the edge and the base were compared. It was assumed that the ground surface temperature at the top of an 8 m pile is similar to the temperatures measured at the edge of the test cell. By linearly comparing this temperature with the temperature at the base, an active layer thickness can be calculated. The cooling, hence permafrost aggradation in the waste pile, can be followed by the thinning active layer thickness (Fig. 6). It can be noted that the active layer thickness also decreases with distance from the edge. In the centre of the test cell (i.e., 28.7–48.7 m), the active layer thickness is reduced from 8 m to 2–3 m during this 5-year period. A thicker active layer was noted closer to the edge. However, the active layer thickness was still reduced by 2 m.

Test cell excavation observations

In summer 2005, the test cell had to be excavated. Observations made during this excavation confirmed the temperature readings, in that the core of the test cell was frozen in only 5 years.

Conclusions

The thermal regime within coarse-grained mine waste rock piles is of particular importance when designing short- and long-term mine facilities in cold regions. To investigate the temperatures at the base of a gravelly rock pile, thermistors were placed at the base of a test cell at Snap Lake, and temperatures were recorded between 2000 and 2005 before the pile had to be excavated to make room for the full-scale mine. The pile temperatures cooled rapidly, and permafrost under the pile was reestablished within 5 years of operation. The active layer completely remained within the pile. The cooling rates differ spatially within the pile confirming the development of convective circles during winter. Cold surface air penetrates down the center of the waste rock pile. The pile excavation further confirmed that ice built; that is, permafrost aggradation occurred at the location of the test cell.

These measurements confirm predictions from various numerical simulations recently published that suggest accelerated cooling within coarse-grained waste rock piles in the Arctic.

The composition and internal thermal behavior has to be considered in the design of waste rock piles, in particular for permafrost aggradation/degradation under warming climate conditions. These results provide further evidence as to the water balance of waste rock piles in cold regions.

Acknowledgments

The authors would like to thank De Beers Canada for their support and for allowing the publication of these results.

Seasonal and Interannual Variability of Active Layer Development in Permafrost Wetland Systems

C.M. Chiu
Department of Agronomy, Purdue University, West Lafayette, IN, USA
L.C. Bowling
Department of Agronomy, Purdue University, West Lafayette, IN, USA

Introduction

Over the last decades, the arctic region has been warming at an accelerated rate with sometimes puzzling effects on lakes and wetlands. Wetlands are common landscape characteristics in the northern high latitudes. Permafrost and seasonal frost can be a powerful factor affecting wetland hydrology. The interaction of soil thermal and moisture regimes controls the structure of the seasonally thawed active layer and hydrological response in permafrost regions. Soil thermal and moisture properties regulate the transfer of heat though the active layer, thus affecting the annual thaw and frost depth. The maximum active layer thickness can vary substantially with annual soil temperature change, given similar moisture conditions (Brown & Hinkel 2000). Spatially, the active layer thickness can vary over short lateral distances due to differences in heat transfer under different soil moisture conditions subject to freezing and thawing (Outcalt et al. 1990). For example, Woo and Xia (1996) found that a wetland site had shallower maximum thaw depth than a drier site due to the buffering effect of the large ice content. The spatial variation may also reflect the interaction of a large number of highly localized factors, including vegetation type, snow cover, organic layer thickness, soil thermal properties, microtopography, and the operation of nonconductive heat transfer processes (Outcalt et al. 1990). This study will examine the spatial and temporal variation of soil temperature and soil moisture content in a continuous permafrost environment and how they relate to the duration and thickness of seasonal active layer in upland and wetland systems. In particular, the ability of the Variable Infiltration Capacity (VIC) land surface model to reproduce the observed relationship between moisture condition and maximum annual thaw depth will be evaluated

Study Area

The study area is the 471 km^2 Putuligayuk River watershed located on the coastal plain south of Prudhoe Bay on the Alaskan North Slope. Observations of soil temperatures and weather are taken from the Betty Pingo weather station (70°16′46.3″N, 148°53′44.5″W) operated by the University of Alaska Fairbanks. The watershed is dominated by drained lakes and numerous permafrost features such as high- and low-centered polygons, pingos, hummocky terrain, frost boils, and strangemoor ridges (Kane et al. 2000). The poor drainage results in extensive wetlands, ponds, and lakes. The maximum thickness of the permafrost along the arctic coast is about 600 m, whereas the maximum depth of thaw of the active layer was about 53 cm between 1993 to 2002 (Brown & Hinkel 2000). The vegetation in this area is dominated by sedge tundra, with shrubs in wetter areas and tussock tundra in higher and drier areas. Observed meteorological and soil temperature data for the period 1994–2004 was obtained through the National Snow and Ice Data Center (Kane & Hinzman 1997).

Model Description

The Variable Infiltration Capacity (VIC) model is a macroscale hydrologic model which has been applied to many environmental studies associated with global climate and land use change prediction (Liang et al., 1994). VIC model features relevant to this application include (1) a finite difference soil thermal solution (Cherkauer & Lettenmaier 1999, Cherkauer & Lettenmaier 2003) and (2) representation of the surface storage and energy dynamic of sub-grid lakes and wetlands (Bowling 2003, Cherkauer & Lettenmaier 2003). In this study, we will examine the ability of the VIC model to simulate upland and wetland soil temperature, soil moisture, and active layer depth. The VIC model is run as a single point centered on the two sites. A constant temperature bottom boundary condition is used with a fixed temperature of -10°C at 4 m damping depth. Two scenarios are run with contrasting initial moisture conditions, bulk density and base flow parameters to simulate the contrasting moisture conditions of the site.

Preliminary Result

Adjacent upland and wetland sites were instrumented by UAF beginning in 1994. The upland site was instrumented with 12 temperature probes vertically arranged at depths of 0, 1, 2, 3, 4, 5, 6, 7, 8, 15, 35, and 60 cm. The adjacent wetland site was also instrumented with 12 temperature probes vertically arranged at depths of 0, 0.5, 1, 2, 3, 4, 5, 6, 15, 30, 50, and 75 cm. Mean annual soil temperatures for the upland and wetland sites derived from hourly observations between 1996–2001 are shown in Figure 1. The patterns at both sites are very similar, although observed annual average temperatures are 0.27 to 0.74°C warmer for the wetter soils. The simulated temperatures are 0.35 to 0.6°C warmer for the wetter soil. In the wetter soil, water or ice displaces air in soil pores, increasing the bulk conductivity as well as the soil heat capacity. Thus, more energy may be required to change the temperature within the same depth resulting in a shallower active layer depth and shorter thawed period in the wetter soil (Figs. 2, 3).

As shown in Figure 2, simulated annual average active layer depth is slightly underestimated for the wetland site (58.78 cm). Since the 60 cm temperature sensor at the upland site exceeds 0°C in most years, the annual active layer depth is unknown, but still deeper than wetland. Figure 3 illustrates that both the observed and simulated frost-free period is longer in the upland than in the wetland site.

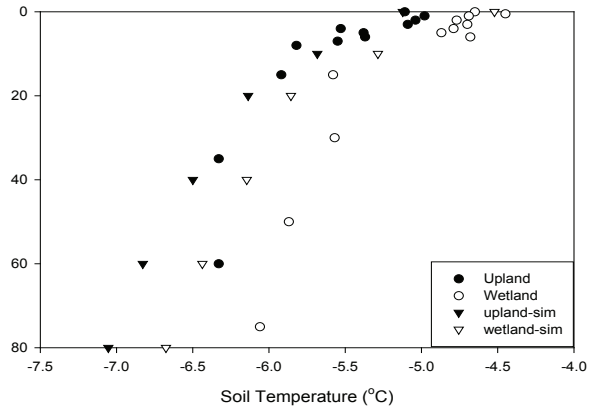

Figure 1. Mean annual soil temperature at 12 probe levels from 1996 to 2001 at upland and wetland site at Betty Pingo, Alaska.

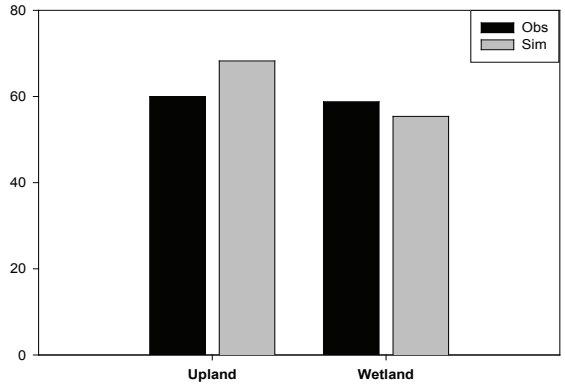

Figure 2. Observed and simulated maximum active layer depths (depth to the 0° isotherm) from 1996 to 2001 at upland and wetland site at Betty Pingo, Alaska. (The maximum temperature sensor in upland site is located at 60 cm.)

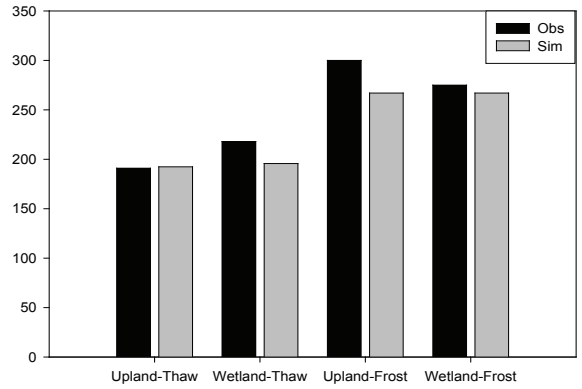

Figure 3. Observed and simulated mean Julian day that soil thaw reaches 50 cm (Thaw) and Julian day that soil freezes to within 1 cm (Frost) from 1996 to 2001 at upland and wetland site at Betty Pingo, Alaska.

Summary

The wetter wetland site is observed to have higher average soil temperature than the dryer upland site. The higher water or ice content in the soil retards the development of the active layer and results in a shallower active layer and shorter thawed period than the upland site. The VIC soil temperature predictions appear to be less sensitive to the soil moisture differences due to heat capacity and bulk conductivity, although the actual difference in moisture content between the sites is unknown. Future work will focus on the active layer seasonal dynamic and hydrology response above continuous permafrost at the watershed scale.

Acknowledgments

This research has been supported and funded by NASA through the Northern Eurasia Earth Science Partnership Initiative (NEESPI). The observed data was collected by Water and Environmental Research Center, University of Alaska Fairbanks.

Reference

Brown, J. & Hinkel, K. 2000. Circumpolar Active Layer Monitoring (CALM) Network. Available online: http://www.geography.uc.edu/~kenhinke/CALM/sites.html.

Bowling, L.C. 2002. *Estimating the freshwater budget of high-latitude land areas.* Ph.D. dissertation. Univ. of Washington, Seattle.

Cherkauer, K.A. & Lettenmaier, D.P. 1999. Hydrological effects of frozen soils in the upper Mississippi River basin. *J. of Geophysical Research* 104: 19559-19610.

Cherkauer, K.A., Bowling, L.C. & Lettenmaier, D.P. 2003. Variable infiltration capacity cold land process model updates. *Global and Planetary Changes* 38: 151-159.

Kane, D.L. & Hinzman, L.D. 1997. updated 2003. *Meteorological and hydrographic data, Kuparuk River Watershed*. Boulder, CO: National Snow and Ice Data Center, World Data Center for Glaciology. Digital media.

Kane, D.L., Hinzman, L.D., McNamara, J.P., Zhang, Z. & Benson, C.S. 2000. An overview of a nested watershed study in Arctic Alaska. *Nordic Hydrology* 31(4/5): 245-266.

Liang, X., Lettenmaier, D.P., Wood, E.F. & Burges, S.J. 1994. A simple hydrogically based model of land surface water and energy fluxes for GSMs. *J. Geophys. Res.* 99(D7): 14415-14428.

Nixon, J.F. 1975. The role of convective heat transport in the thawing of frozen soil. *Canadian Geotechnic Journal*. 12: 425-429.

Outcalt, S.I., Nelson, F.E. & Hinkel, K.M. 1990. The zero curtain effect: heat and mass transfer across and isothermal region in freezing soil. *Water Resour. Res.* 26: 1509-1516.

Woo, M.K. & Xia, Z.J. 1996. Effects of hydrology on the thermal conditions of the active layer. *Nordic Hydrology*. 27: 129-142.

Twelve-Year Thaw Progression Data from Zackenberg, Northeast Greenland

Hanne H. Christiansen
The University Centre in Svalbard, UNIS
Charlotte Sigsgård
Institute of Geography and Geology, University of Copenhagen

Introduction

In Greenland, it is only in the northeast part, at 74°30′N in Zackenberg, that a continuous CALM data series exists since 1996 (Christiansen et al., in press). Circumpolar Active Layer Monitoring (CALM) data are collected as part of the Zackenberg Ecological Research Operations (ZERO) monitoring programme GeoBasis, which is maintained by the National Environmental Research Institute and the University of Copenhagen. As this programme has been manned during entire summer seasons since 1996, progressive summer thaw data have been collected to allow full season annual thaw progression data collection.

The CALM monitoring at Zackenberg was designed to investigate, at site scales, the effects of interannual temporal and spatial changes in snow cover, as determined by air temperature, wind speed, dominant wind direction and snow precipitation on thaw progression and active layer thickness. This is done by operating two different so-called ZEROCALM sites. The ZEROCALM-1 (ZC1) site consists of 121 grid points, covering a 100 m x 100 m area, with 10 m grid size. It is located on a flat marine abraded ground moraine (Christiansen 2004). The ZEROCALM-2 (ZC2) site has 208 grid points, covering 120 m x 150 m and also has a 10 m grid size. ZC2 is located in and around a natural snowdrift site (Christiansen 2004). The two sites are located 750 m apart in the Zackenberg lowlands, and are located between 20 and 37 m a.s.l. They are numbered G1 and G2, respectively, in the CALM database (Brown et al. 2000).

Thaw Progression

Probing of ZC1 and ZC2 from early June to the end of August for the last 12 years, including from 6 to 11 sets of measurements in ZC1 and from 6 to 13 sets in ZC2, has enabled continuous summer thaw progression curves (Fig. 1). In the ZC1 grid, thawing was quick down to around 50 cm, and below was significantly slower. In the end of the summer, the curves show very little to no increase in thaw thickness, which is when the active layer was established, typically in mid to late August. Some refreezing was registered when measurements were done in September.

In the ZC2 site, the thaw rate was relatively homogeneous for most of the summer, with average rates below ZC1. In the end of summer, only little or no additional thawing happened, like in ZC1, when the active layer was reached. Also in the ZC2 site, some refreezing was registered in years when measurement proceeded into early September.

The difference in thaw progression between the ZC1 and ZC2 sites is mainly controlled by the different rate of annual

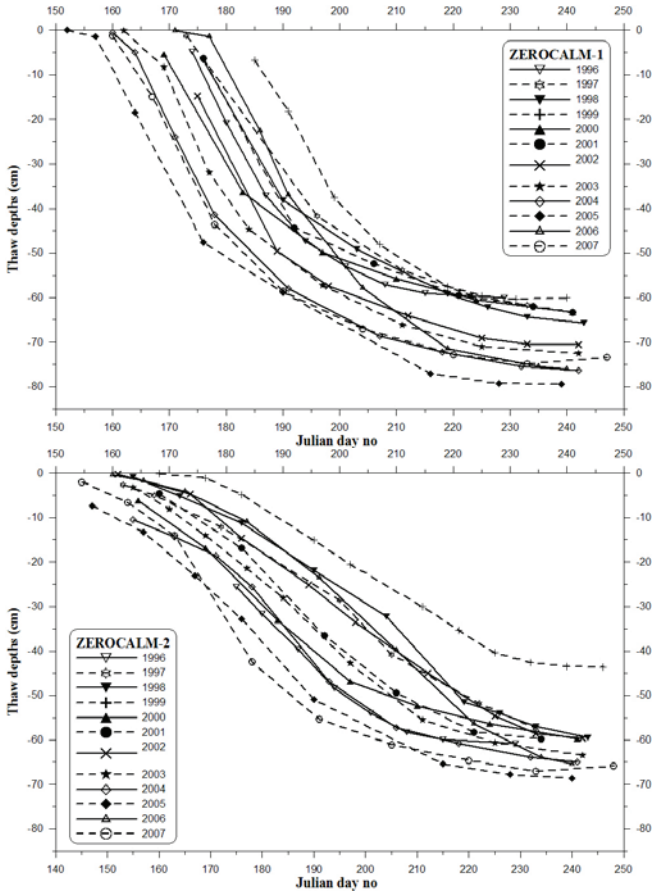

Figure 1. Thaw progression calculated as the mean of 121 points in ZEROCALM-1 site and as the mean of 208 points in the ZEROCALM-2 site.

snow depletion in the two sites (Christiansen 2004, Fig. 4). Ground thawing only starts when the snow has melted. As the ZC2 site is completely containing the snowpatch, its gradual backmelting during summer allows still more grid points to start thawing, and, therefore, a less steep thawing curve is established for the entire grid. The year 1999 was special in that the snowpatch stayed through the summer, which caused a much-reduced active layer of only 44 cm in ZC2, as several grid points did not melt at all.

Active Layer Thickness

The active layer thickness (ALT) in the ZC1 and ZC2 sites varied, respectively, 20 cm and 26 cm in the 12-year period, with the deepest thaw in 2005 (ZC1 80 cm, ZC2 70 cm) and the thinnest in 1999 (ZC1 60 cm, ZC2 44 cm) for both sites (Fig. 1). Generally, the interannual ALT

variation was 20 cm in ZC1, but only 10 cm in ZC2, when excluding the 1999 snowdrift-affected year. This shows that the influence of the snowdrift seems to be larger than any other meteorological factor in this type of landscape setting, where the combination of topography and meteorology lead to snowpatch accumulation. The snowdrift size is controlled by the amount of winter snow, but mainly by the late winter wind activity causing snowdrifting (Christiansen 2004).

Comparing the ZEROCALM sites with the UNISCALM site in Svalbard, the nearest CALM site on the opposite site of the Greenland Sea is interesting. There is no simple correlation of ALT between the two CALM sites. The deepest thaw in Svalbard occurred in 2007 (Christiansen & Humlum 2008), while this was in 2005 for both sites in northeast Greenland (Fig. 1). In 2005, Svalbard actually experienced the shallowest active layer since measurements started in 2000.

Air Temperature Control on Active Layer Thicknesses

Traditionally, the relationship between ALT and TDD of the thaw period is established using the Stefan solution to investigate the influence of air temperature forcing or other factors on ground thawing (Hinkel & Nelson 2003). Just 10 m south of the ZC1 site, the ZEROCALM official meteorological station is located. Air temperature is a standard parameter measured at this station, enabling calculations of thawing degree-days (TDD) of the thaw period.

The correlations between ALT and the square root of the TDD are shown for the entire 12-year period for both ZC1 and ZC2 in Figure 2. Clearly, ZC1 has a relatively high correlation to positive air temperatures in the thawing season, but also ZC2 has some correlation. Interestingly, both sites have a significantly better correlation than what has been found for a flat site in neighboring Svalbard based on 8 years of data ($r^2 = 0.004$) (Christiansen & Humlum 2008). Previously, based on the 7 first years of observations in the ZC1 and ZC2 sites, reduced correlations (ZC1: $r^2 = 0.53$ and ZC2: $r^2 = 0.00$) were also found for these sites (Christiansen 2004). This indicates that longer data series, such as the 12-year record from Zackenberg, must be collected to analyze with confidence the air temperature influence on ground thawing.

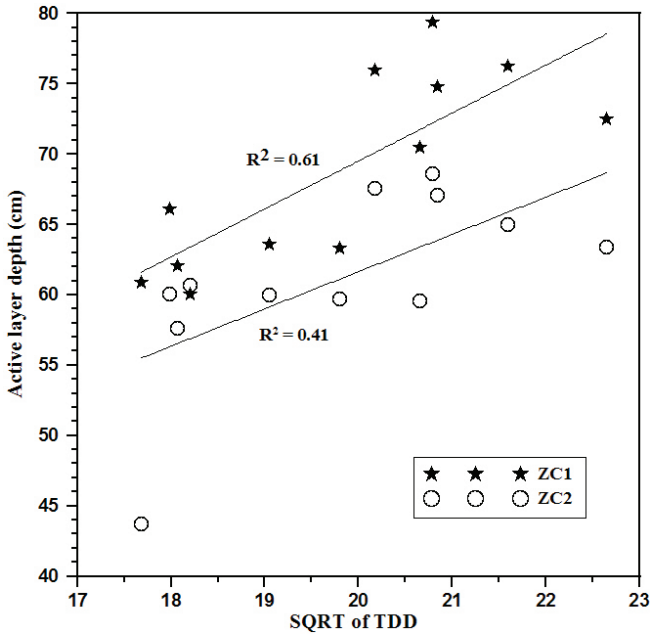

Figure 2. ZEROCALM-1 and ZEROCALM-2 active layer thickness correlated to the square root of the thawing degree-days until the time of the active layer measurement in the 1996–2007 period.

Acknowledgments

The data collection of thaw depths is the responsibility of the Zackenberg Ecological Research Operations monitoring programme GeoBasis, to which we extend our sincere thanks for keeping this basic monitoring running and thus providing a rather unique CALM data series from Greenland.

References

Brown, J., Hinkel, K.M. & Nelson, F.E. 2000. The Circumpolar Active Layer Monitoring (CALM) Program: Research designs and initial results. *Polar Geography* 24: 165-258.

Christiansen, H.H. 2004. Meteorological control on interannual spatial and temporal variations in snow cover and ground thawing in two northeast Greenlandic Circumpolar-Active-Layer-Monitoring (CALM) sites. *Permafrost and Periglacial Processes* 15: 155-169.

Christiansen, H.H., Sigsgaard, C., Humlum, O., Rasch, M. & Hansen, B.U. In press. Permafrost and periglacial geomorphology at Zackenberg. *Advances in Ecological Research* 40.

Christiansen, H.H. & Humlum, O. 2008. Interannual variations in active layer thickness in Svalbard. *Proceedings of the Ninth International Conference on Permafrost, Fairbanks, Alaska, June29–July 3, 2008*.

Hinkel, K.M. & Nelson, F.E. 2003. Spatial and temporal patterns of active layer thickness at Circumpolar Active Layer Monitoring (CALM) sites in northern Alaska, 1995–2000. *Journal of Geophysical Research* 108: D2: ALT 9, 1-13.

Continued Permafrost Warming in Northwest Alaska as Detected by the DOI/ GTN-P Borehole Array

Gary D. Clow
U.S. Geological Survey, Lakewood CO 80225, USA

The U.S. Department of the Interior contributes to the Global Terrestrial Network for Permafrost (GTN-P) with a 21-element deep borehole array located in northwest Alaska. The majority of the holes are located on the Arctic Coastal Plain (ACP) with the remainder being in the northern foothills of the Brooks Range (Fig. 1). All but two of the boreholes penetrate the base of permafrost which is situated between 210 and 410 m in this region.

The U.S. Geological Survey began monitoring temperatures in the DOI/GTN-P boreholes in the late 1970s, soon after the holes were drilled. This was done by periodically relogging the wells with a portable temperature logging system (PTLS) developed especially for this purpose at USGS. While the original PTLS was limited to an incremental or "stop-and-go" logging mode, improvements allowed the PTLS to acquire "continuous" temperature logs by the mid-1980s. Further refinements have reduced the standard uncertainty of the ITS-90 temperature measurements obtained with this system to less than 3.3 milliKelvin. Early results which focused on interpretation of the curvature of the borehole temperature profiles for past climatic changes were reported by Lachenbruch and Marshall (1986) and Lachenbruch et al. (1988).

Monitoring the thermal response of permafrost to contemporary climate change has been the primary research focus of the DOI/GTN-P monitoring network for the last decade. Due to logistical constraints, our current protocol is to relog the entire borehole array every five years with a few key wells being relogged annually. Measurements in the wells show that near-surface temperature fluctuations in NW Alaska were generally small during the late 1970s and most of the 1980s, except for a short cold period during 1983–84. Permafrost temperatures began warming dramatically in 1989. By 2002–03, near-surface permafrost temperatures had warmed 3 K on average across the array relative to 1989. The coastal plain portion of the borehole array was relogged again during 2007 in support of the international Thermal State of Permafrost (IPY/TSP) project. These new measurements show that shallow permafrost temperatures have continued to warm on the ACP since 2002–03; the magnitude of the warming since 2002–03 ranges 0.0 to 1.0 K (mean = 0.4 K), depending on local site conditions. The total average (shallow) permafrost warming in this region since 1989 is now ~ 3.5 K (Fig. 1).

Data from the co-located DOI/GTN-P active layer/ meteorological network show that the 2002–03 borehole measurements coincided with a peak in mean annual air temperatures in NW Alaska. Mean annual air temperatures cooled substantially during 2004, but have been rising since and are now warmer than those experienced during 2002–03. Permafrost temperatures have not tracked the post-2004 air temperature warming due to the effects of changing snow cover.

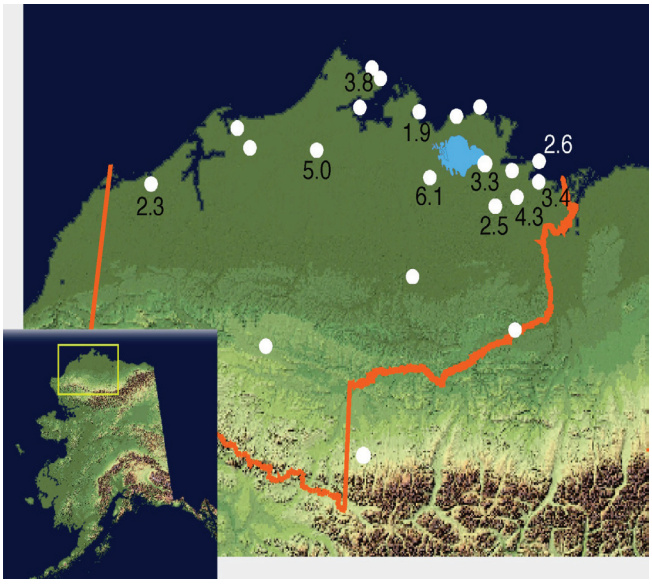

Figure 1. Location of the DOI/GTN-P boreholes in northwest Alaska. Also shown is the magnitude (degrees Kelvin) of shallow permafrost warming at various well sites on the coastal plain between 1989 and 2007.

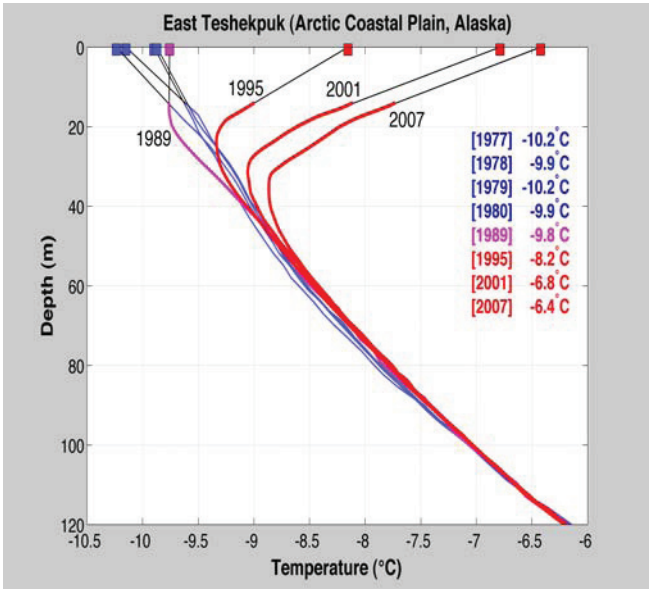

Figure 2. Sample permafrost temperatures measured in one of the coastal plain DOI/GTN-P boreholes (East Teshekpuk) since 1977. Extrapolated mean annual surface temperatures have increased about 3.6 K at this site since the late 1970s, close to the average for the entire array.

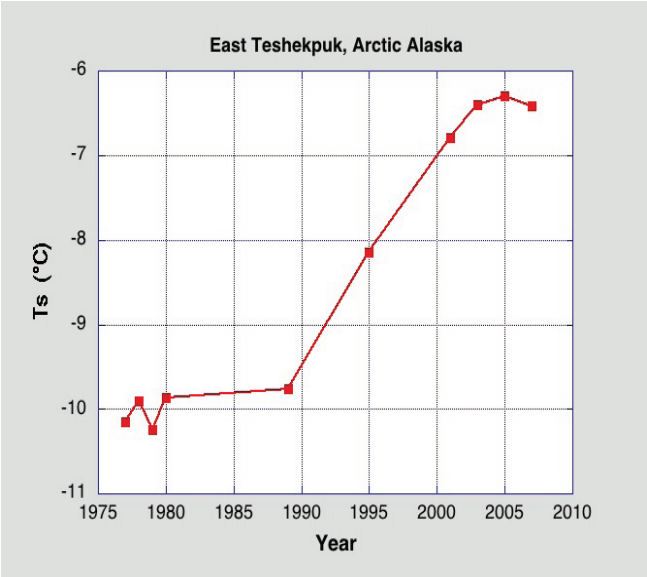

Figure 3. Time series of extrapolated mean annual surface temperatures derived from the borehole temperature measurements at the East Teshekpuk well site.

References

Lachenbruch, A.H. & Marshall, B.V. 1986. Changing climate: geothermal evidence from permafrost in Alaska. *Science* 234: 689-696.

Lachenbruch, A.H., Cladouhos, T.T. & Saltus, R.W. 1988. Permafrost temperature and the changing climate. *Proceedings of the Fifth International Conference on Permafrost, 1988*: 9-17.

Landsliding Following Forest Fire on Permafrost Slopes, Klondike Area, Yukon, Canada

Jim Coates, Antoni G. Lewkowicz
Department of Geography, University of Ottawa, Ottawa, Ontario

Introduction

In the boreal forest, fire is often followed by widespread active layer detachment sliding (McRoberts & Morgenstern 1974a, 1974b, Lewkowicz & Harris 2005a, 2005b). Forest fire, with a recurrence interval of 25–300 years, kills adult trees, destroys much of the insulating mossy organic layer, and blackens the ground surface (Dyrness et al. 1986).

Seasonal thaw depths (active layer thickness) generally increase in the years following forest fire (Yoshikawa et al. 2003), although this can vary according to the slope aspect and state of vegetation (Swanson 1996, Lewkowicz & Harris 2005b). When the heat reaches the permafrost, it may thaw the ice-rich transient layer, which lies just below the average maximum depth of thaw (Shur et al. 2005). Water released by this process may raise soil porewater pressures sufficiently to destabilize slopes and cause active layer detachment sliding (McRoberts & Morgenstern 1974a).

Active layer detachment failures occur when all or a portion of the active layer separates from the permafrost beneath and moves as a semi-competent, unsaturated mass downhill over the lubricated slip surface of the thaw plane. Failures occur within the active layer or the transient layer and are triggered by high porewater pressures over frozen ground (Lewkowicz & Harris 2005b). The depth of the initial failure plane is limited by the position of the permafrost table (Harris & Lewkowicz 2000).

Klondike Detachment Failures

Numerous forest fires occurred during the summer of 2004 in the Klondike Goldfields region of the Yukon Territory, an area of extensive discontinuous permafrost. Significant detachment failure landslide activity developed in subsequent weeks in Steele Creek, a small drainage basin located about 60 km south of Dawson City at approximately 63°35′N and 138°59′W.

Preliminary observations of the failures and near-surface thermal regime were made through freeze-up of 2004 and continued in the summers of 2005 and 2006. Detachment failures were mapped, and individual sites were surveyed. Two-dimensional DC resistivity transects were used to examine subsurface conditions in the area.

Thirty-five detachment failures occurred in 2004 along a 3.7 km section of the main Steele Creek Valley and on slopes within its tributaries. Five new failures developed by mid-August 2005, and several failures from 2004 reactivated. No more failures developed in the summer of 2006.

Table 1. Failure characteristics (n = 37).

	Mean	Max	Min
Failure Angle	23	32.0	12.0
Length (m)	32	105.5	5.0
Width (m)	7	23.0	1.6
Depth (cm)	48	160.0	17.0
Scar (m)	23	88.5	2.0
Length/Width ratio	4	10.6	1.2

Form

The failures in the Steele Creek Valley varied in length from 5–105 m, in width from 7–23 m, and in depth from 17–160 cm (Table 1). Only elongate detachment failures were observed (length-to-width ratio >1; e.g., Lewkowicz & Harris 2005a). The majority of these took place in coarse-grained soils with high pore-water pressures at the time of failure. Headscarps were coincident or proximal to convex breaks-of-slope. At the headscarps of nearly all the failures, tension cracks were observed with roots stretched across them. These tension cracks were more common on convex breaks-of-slope which are concentrations of stress. Near many of the failures, the organic mat was thinner near the headscarp but thicker downslope as a result of burning or pre-fire vegetation conditions.

Failure surfaces were generally higher than the inferred frost plane and dipped towards the centre of the failure scar. Displaced soil and organic material in most debris piles was highly disturbed. Trees were left standing in debris piles, indicating that the organic layer moved without overturning until it lost momentum or reached material that would not detach. It then piled up with liquefied mineral soil sandwiched between folded layers of the original surface organics. At some of the larger failures, the moving mass acquired sufficient weight and momentum to scour down to the permafrost table. Failure angles were all moderate (Fig. 1), with none below 10°.

Mechanism

Forest fire contributed to detachment failure activity on permafrost slopes by destroying the surface organic mat, causing burned surface temperatures to rise, thawing active layers by up to 20 cm (+30%) deeper than adjacent unburned slopes and weakening the surface root structures. Deeper thaw melted transient layer ground ice, raising soil pore-water pressures.

These landslides appeared to have behaved as flows within unfrozen soils. The permafrost affected the failures by providing an aquiclude, which raised pore-water pressures, and by supplying water released from the transient layer due to thermal disequilibrium caused by the forest fire.

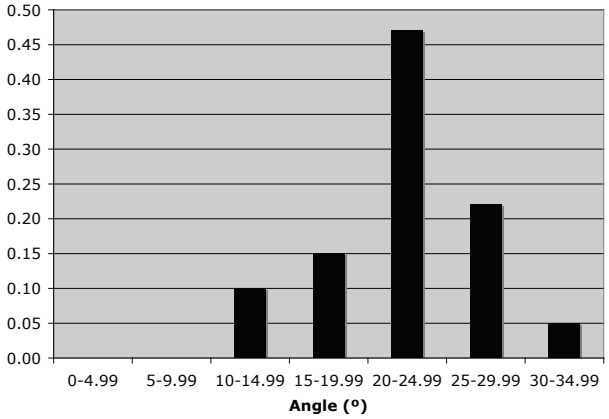

Figure 1. Histogram of landslide failure angles (n = 37).

Failures in Steele Creek occurred where the subsurface mineral soil consisted of completely saturated coarse-grained material with low cohesion, the organic mat was weak on the break of slope but strong below, and there was significant downslope stress. The saturated soil mass liquefied and began to flow below the organic mat, which was elevated above, and detached from, the mineral soil. Tree roots that were still anchored in the mineral soil supported the suspended organic mat.

Significance

The failures are similar in planar dimensions to those described previously in other permafrost regions (e.g., Lewkowicz & Harris 2005a, 2005b, McRoberts & Morgenstern 1974b). However, they are towards the upper end of the range of slope angles observed, and no low-angled forms were present. Moreover, in contrast to most other shallow failures over permafrost, the frost table did not act as a failure plane, and soil materials were cohesionless and coarse-grained. The critical role of permafrost in Steele Creek was to release water from upslope as the transient layer thawed, and by acting as an aquiclude, to generate high pore-water pressures near the base of the slope.

Fossil failures in the Steele Creek Valley and other Yukon locations (e.g., Lipovsky et al. 2006) indicate that detachment failure is an episodic process controlled by fire. In unglaciated areas such as Steele Creek, given a fire recurrence interval in the order of 100 years, this process has likely occurred thousands of times during the Pleistocene and may be responsible for elements of the form of the region's slopes. These include permafrost slopes having a generally gentler gradient and more defined mid-slope break of slope than nonpermafrost slopes.

The potential for climate change-induced thaw of permafrost as well as larger and hotter forest fires raise the possibility of greater active layer detachment failure activity in the future (McCoy & Burn 2005, Lipovsky et al. 2006).

Acknowledgments

Financial Support came from NSERC through its Northern Internship Program and Discovery Grant (to A. Lewkowicz), the Yukon Geological Survey, Northern Scientific Training Program (Indian and Northern Affairs Canada), University of Ottawa (to A. Lewkowicz). We are also grateful for support from Klondike Star, Indian River Farm, EBA Engineering Consultants Ltd., Cam Arkinstal, Yukon Client Services and Inspections, Gimlex Mining, Mike Schultz, Geoff Hodgeson, Martina Knopp, Yukon Geological Survey, Dr Bernd Etzelmüller, Phil Bonaventure, and Emily Schultz.

References

Dyrness, C.T., Viereck, L.A. & Van Cleve, K. 1986. Fire in taiga communities of interior Alaska. In: K. Van Cleve, F.S. Chapin III, P.W. Flanagan, L.A. Viereck & C.T. Dyrness (eds.), *Ecological Series* 57: *Forest Ecosystems in the Alaskan Taiga.* New York: Springer-Verlag, 74-86.

Harris, C. & Lewkowicz, A.G. 2000. An analysis of the stability of thawing slopes, Ellesmere Island, Nunavut, Canada. *Canadian Geotechnical Journal.* 37: 449-462.

Lewkowicz, A.G. 1988. Slope processes. In: M.J. Clarck (ed.), *Advances in Periglacial Geomorphology.* Chichester: Wiley, 325-368.

Lewkowicz, A.G. & Harris, C. 2005a. Morphology and geotechnique of active-layer detachment failures in discontinuous and continuous permafrost, northern Canada. *Geomorphology* 69: 275-297.

Lewkowicz, A.G. & Harris C. 2005b. Frequency and magnitude of active-layer detachment failures in discontinuous and continuous permafrost, northern Canada. *Permafrost and Periglacial Processes* 16: 115-130.

Lipovsky, P.S., Coates J, Lewkowicz, A.G. & Trochim, E. 2006. Active layer detachments following the summer 2004 forest fires near Dawson City, Yukon. In: D.S. Edmond, G.D. Bradshaw, L.L. Lewis & L.H. Weston (eds.), *Yukon Exploration and Geology 2005*. Yukon Geological Survey, 175-194.

McCoy, V.M. & Burn, C.R. 2005. Potential alteration by climate change of the forest-fire regime in the boreal forest of central Yukon Territory. *Arctic* 58: 276-285.

McRoberts, E.C. & Morgenstern, N.R. 1974a. The stability of thawing slopes. *Canadian Geotechnical Journal* 11: 447-469.

McRoberts, E.C. & Morgenstern, N.R. 1974b. Stability of slopes in frozen soil, Mackenzie Valley, N.W.T. *Canadian Geotechnical Journal* 11: 554-573.

Shur, Y., Hinkel, K. & Nelson, F. 2005. The Transient Layer: Implications for Geocryology and Climate-Change Science. *Permafrost and Periglacial Processes* 16: 5-17.

Swanson, D.K. 1996. Susceptibility of permafrost soils to deep thaw after forest fires in interior Alaska, USA, and some ecologic implications. *Arctic and Alpine Research* 28: 217-227.

Yoshikawa, K., Bolton, W.R., Romanovsky, V.E., Fukuda, M. & Hinzman, L.D. 2003. Impacts of wildfire on the permafrost in the boreal forests of Interior Alaska. *Journal of Geophysical Research* 107: 8148.

A Permafrost Model Incorporating Dynamic Variable Soil Depth and Properties

Richard Coppell
School of Geography, University of Leeds, Leeds, UK
Met Office – Hadley Centre for Climate Prediction and Research, Exeter, UK
Sergey Venevsky
School of Geography, University of Leeds, Leeds, UK
Met Office – Hadley Centre for Climate Prediction and Research, Exeter, UK

Introduction

Recent dynamic global vegetation models, for example, LPG, SEVER (Sitch et al. 2003, Venevsky & Maksyutov 2007), and land surface schemes, for example, IMOGEN, MOSES (Cox et al. 1999), have deficiencies in their representations of thermal and hydrological dynamics in the permafrost zone. These deficiencies are related to the following:

(a) Inadequate representation of thaw/freeze processes (absence of frozen soil water fraction). This relates to differing thermal conduction regimes between frozen (high conduction) and unfrozen (lower conduction) surface layers that experience thawing and freezing, particularly seasonally (see French 2007).

(b) Absence of the upper soil organic layer (moss/lichen). Distinctions may be made between thermal and hydrological properties of moss-dominated and lichen-dominated soils (Beringer et al. 2001), also modified by the influence of sedges (Usowicza et al. 2006).

(c) Inadequate parameterisation of soil properties. The number of types of soils represented within models may be expanded to test if this is also a sensitive parameter.

Methods

Permafrost data (Brown 1998, International Permafrost Association Standing Committee on Data Information and Communication [comp.] 1998, 2003) is being compared with representations in SEVER, considering active layer depth, seasonal variation, time precision, temperature profile, soil moisture profile, and physical and biological soil constituents.

Peatland soil profiles and vegetation cover develop over periods of thousands of years, and a MATLAB model reproducing this based on Frolking et al. (2001) is also being assessed.

This will provide the opportunity to create a dynamic soil and vegetation representation within SEVER in place of more static representations of peatland and soil types.

Acknowledgments

Richard Coppell is in receipt of UK NERC scholarship NE/F008341/1 with CASE funding from the Hadley Centre.

References

Beringer, J., Lynch, A.H., Chapin, F.S., Mack, M. & Bonan, G.B. 2001. The representation of Arctic soils in the land surface model: The importance of mosses. *J. Climate* 14(15): 3324-3335.

Brown, J. 1998. Circumpolar Active-Layer Monitoring (CALM) Program: Description and data. In: M. Parsons & T. Zhang (eds.), *Circumpolar Active-Layer Permafrost System, version 2.0.* International Permafrost Association Standing Committee on Data Information and Communication. Boulder, CO: National Snow and Ice Data Center/World Data Center for Glaciology.

Cox, P.M., Betts, R.A., Bunton, C.B., Essery, R.L.H., Rowntree, P.R. & Smith, J. 1999. The impact of new land surface physics on the GCM simulation of climate and climate sensitivity. *Climate Dynamics* 15(3): 183-203.

French, H.M. 2007. *The Periglacial Environment*. Chichester, UK: Wiley, 478 pp.

Frolking, S., Roulet, N.T., Moore, T.R., Richard, P.J.H., Lavoie, M. & Muller, S.D. 2001. Modeling northern peatland decomposition and peat accumulation. *Ecosystems* 4(5): 479-498.

International Permafrost Association Standing Committee on Data Information and Communication (comp.). 1998. *Circumpolar Active-Layer Permafrost System, Version 1.0*. Edited by J. Branson, J. Brown & M.O. Leibman. Boulder, CO: National Snow and Ice Data Center/World Data Center for Glaciology. CD-ROM.

International Permafrost Association Standing Committee on Data Information and Communication (comp.). 2003. *Circumpolar Active-Layer Permafrost System, Version 2.0*. Edited by M. Parsons & T. Zhang. Boulder, CO: National Snow and Ice Data Center/World Data Center for Glaciology. CD-ROM.

MacDonald, G.M., Beilman, D.W., Kremenetski, K.V., Sheng, Y., Smith, L.C. & Velichko, A.A. 2006. Rapid early development of circumarctic peatlands and atmospheric CH_4 and CO_2 Variations. *Science* 314(5797): 285-288.

Sitch, S., Smith, B., Prentice, I.C., Arneth, A., Bondeau, A., Cramer, W., Kaplan, J.O., Levis, S., Lucht, W., Sykes, M.T., Thonicke, K. & Venevsky, S. 2003. Evaluation of ecosystem dynamics, plant geography and terrestrial carbon cycling in the LPJ dynamic global vegetation mode. *Global Change Biology* 9: 161-185.

Usowicza, B., Lipieca, J., Marczewskib, W. & Ferreroc, A. 2006. Thermal conductivity modelling of terrestrial soil media: A comparative study. *Planetary and Space Science* 54: 1086-1095.

Venevsky, S. & Maksyutov, S. 2007. SEVER: A modification of the LPJ global dynamic vegetation model for daily time step and parallel computation. *Environmental Modelling and Software* 22: 104-109.

Seasonal Sources of Soil Respiration from High Arctic Landscapes Dominated by Polar Stripes

Claudia I. Czimczik
Department of Earth System Science, University of California, Irvine, CA 92614, USA
Susan E. Trumbore
Department of Earth System Science, University of California, Irvine, CA 92614, USA
Jeffrey Welker
Environment and Natural Resources Institute and Biology Department, University of Alaska Anchorage

Introduction

Carbon (C) cycling studies in the Arctic have largely focused on Low Arctic wet sedge and tussock tundra ecosystems, with studies in the High Arctic only recently contributing to our understanding of the complete Pan Arctic C biogeochemistry. It is becoming increasingly clear that High Arctic soils contain significant amounts of soil C that previously have been underestimated by up to an order of magnitude (Horwath 2007). In addition, we now recognize that soil C pools in portions of the High Arctic landscape may be spatially heterogeneous (horizontally and vertically), especially in areas where pattern ground is extensive such as landscapes, where polar strips result in vegetated troughs and barren ridges. In addition, because this region is warming at some of the highest rates across the entire biome, increasing levels of microbial decomposition and soil respiration may provide an important positive feedback to global warming that warrants quantification.

We studied the seasonal pattern of CO_2 evolved from the soil surface (soil respiration) and its production within the mineral soil to 60 cm depth from a High Arctic prostrate dwarf shrub tundra (polar semi-desert) ecosystem in northwest Greenland as part of a NSF Biocomplexity project on C cycling in cold, dry ecosystems. We used radiocarbon to (1) partition the net flux of soil respiration into plant-derived C sources (C cycling on a time scale of days to a few years) and microbial-derived sources (slower cycling C) and (2) to investigate whether microorganisms are currently accessing very old C pools that used to be unavailable under previous climatic conditions.

Material and Methods

Study site

Samples were taken at two locations near Thule Air Base, northwest Greenland (76°32′N, 68°50′W) throughout the growing season from June to August 2007. The landscapes were dominated by classic polar stripes formed from frost cracking, aeolian in-filling, colonization by higher plants, and freeze thaw dynamics resulting in troughs dominated by *Dryas integrifolia* and *Salix arctica* and ridges that were non-vegetated. This landscape type represents about one-third of the entire High Arctic terrestrial land cover.

Sampling

Soil respiration rates were measured with paired, dynamic chambers (n = 3) in troughs and ridges, together with measurements of air and soil temperature. In addition, we monitored the concentration and isotopic signature ($\delta^{13}C$, $\Delta^{14}C$) of CO_2 within the soil profile to 60 cm depth as well as the isotopic signature of CO_2 in ambient air. Gas fluxes and concentrations were monitored approximately weekly. The isotopic signature of CO_2 was measured monthly. CO_2 was sampled with evacuated canisters.

At UC Irvine, CO_2 was cryogenically purified, reduced to graphite, and analyzed for its stable isotope signature (IRMS) and radiocarbon content (AMS) (Xu et al. 2007). The isotopic signature of the main soil respiration sources (roots and microorganisms) were investigated using laboratory incubations or freshly-cut roots and intact soil cores. In addition, we measured the content and isotopic composition of C and nitrogen in each core.

Results and Discussion

In vegetated troughs, soil respiration rates peaked in the summer, when temperatures were highest (Fig. 1). CO_2 concentrations in the soil pore space reached a plateau in the summer. Respiration rates from ridges were low throughout

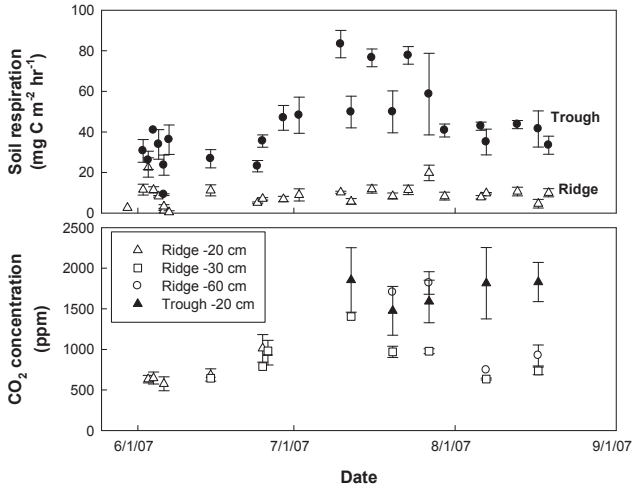

Figure 1. Flux of CO_2 from the soil surface (top panel) and concentration of CO_2 in the soil pore space (bottom panel) throughout the growing season.

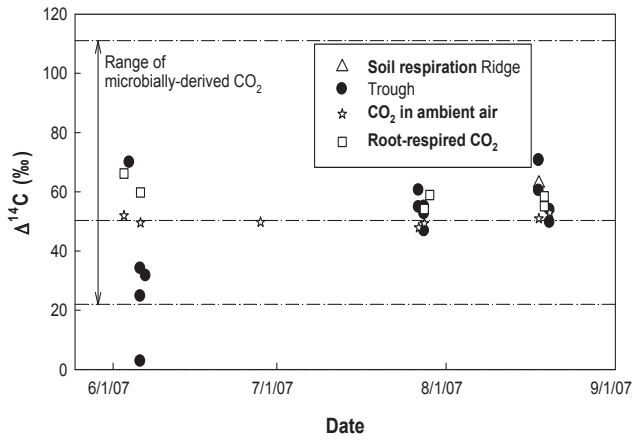

Figure 2. Radiocarbon signature of soil respiration, root- and microbially-respired CO_2 (from incubations), and of CO_2 in ambient air throughout the growing season.

the growing season. Pore space CO_2 concentrations were also lower, and peaked during the summer.

Although soil C pools had mean ages of up to 5000 years, the ^{14}C signature of all CO_2 respired from the soil surface, roots, and soil cores, as well as the CO_2 in the soil pore space, was modern (fixed by photosynthesis post-1950) (Fig. 2). Throughout the growing season, soil respiration had ^{14}C signatures higher than the current atmospheric CO_2, indicating that the source is C cycling on decadal time scales. At the end of winter, the source of soil respiration was a mixture of older and modern C, indicated by modern signature lower than that of current atmospheric CO_2. A clear source portioning into plant- and microbial-derived sources was complicated by a very high spatial variability of the ^{14}C signature of microbial-derived CO_2.

High Arctic soils contain considerable amounts of old C currently protected from microbial decomposition by cold temperatures. The mobilization of these pools could act as a positive feedback to global climate change. However, during the growing season, CO_2 fluxes from High Arctic soils were dominated by modern (post-1950) C. Erosion of older C sources was observed at the end of winter when plants were largely dormant, but measurements were complicated by low flux rates and very high 3D-spatial variability of potential C sources.

Acknowledgments

We thank M. Rogers, H. Kristenson, and K. Nagel for their assistance in the field, and Thule Air Base for logistical support. This work was funded by the U.S. NSF Biocomplexity Program.

References

Horwath, J.L. 2007. *Quantification and Spatial Assessment of High Arctic Soil Organic Carbon Storage in Northwest Greenland*. PhD Thesis. Seattle, WA, USA: Department of Earth and Space Sciences, University of Washington.

Xiaomei, X. Trumbore, S.E., Zheng, S., Southon, J.R., McDuffee, K.E., Luttgen, M. & Liu, J.C. 2007. Modifying a sealed tube zinc reduction method for preparation of AMS graphite targets: Reducing background and attaining high precision. *Nuclear Instruments and Methods in Physics Research* B 259: 320–329, doi:10.1016/j.nimb.2007.01.175.

Greenland Permafrost Temperature Simulations

R.P. Daanen
Geophysical Institute, University of Alaska Fairbanks, Fairbanks, Alaska
V.E. Romanovsky
Geophysical Institute, University of Alaska Fairbanks, Fairbanks, Alaska
S.S. Marchenko
Geophysical Institute, University of Alaska Fairbanks, Fairbanks, Alaska
J.H. Christensen
Danish Meteorological Institute, Copenhagen, Denmark
M. Stendel
Danish Meteorological Institute, Copenhagen, Denmark
T. Ingeman-Nielsen
Technical University of Denmark, Copenhagen, Denmark

Introduction

Tourism in Greenland has increased in recent years and has put more stress on infrastructure. Expansion of airstrips and roads to accommodate increased travel in conjunction with climate warming (IPCC 2001, ACIA 2004) requires an assessment of permafrost in the area. Complex topography and coastal configurations are key characteristics of the Alaskan and Greenland regions on which this study will focus. This requires high-resolution simulation of climate as well as permafrost distribution. We used a numerical simulation model called GIPL 2.1 (Tipenko & Romanovsky 2001, Sergeev et al. 2003) for simulating spatially distributed ground temperatures over Greenland.

Results

The permafrost in this country is dominated by areas of frozen bedrock with pockets of sediments and organic matter. For this study, we split the simulation in two categories: bedrock simulations and sediment simulations. Snow is treated the same for sediment areas and bedrock areas, and taken from HIRHAM snow water equivalent predictions. It was corrected for a constant density (0.15 gr/cm^3) and shows a fairly close fit for some of the observed years in the dataset from Illulisat (Fig. 1).

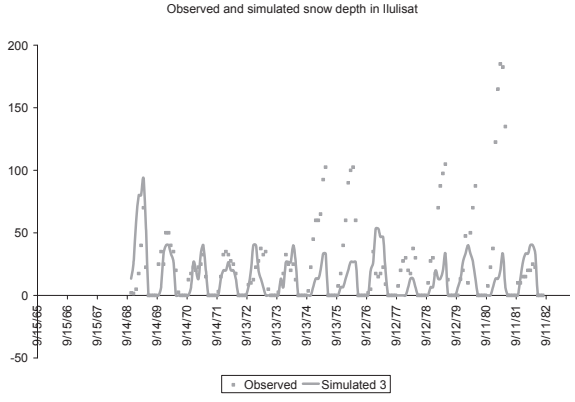

Figure 1. Observed and simulated snow depth for the Illulisat region.

Figure 2 shows the temperature distribution in bedrock material over entire Greenland at a 25 km resolution. The first image is the result of a ten-year-average ground temperature from 1955 till 1965 for a depth of 2 m; the second image is for the same depth at the end of the simulation period from 2065 till 2075.

The simulation data does not show a large difference over the simulation period. In bedrock, the temperature fluctuation between summer and winter are larger then in the sediment, due to a lack of ice or liquid water that buffers the temperature fluctuation. Figure 3 shows the active layer depth for the beginning of the simulation period and the end of the simulation period.

For sediment we find cooler average temperatures due to the thermal offset in the organic materials in the upper soil layers. In addition, there is a larger quantity of liquid water present and a larger amount of ice in the winter. The results for the sediment simulations are given in Figure 4 for the 2 m temperature and in Figure 5 for the active layer depth.

Discussion

The data provided in this abstract are average data over ten years and show little change over the simulation period from 1950 till 2075. Even the higher spatial resolution simulated in this study is relatively coarse when comparing it with the heterogeneity of the landscape.

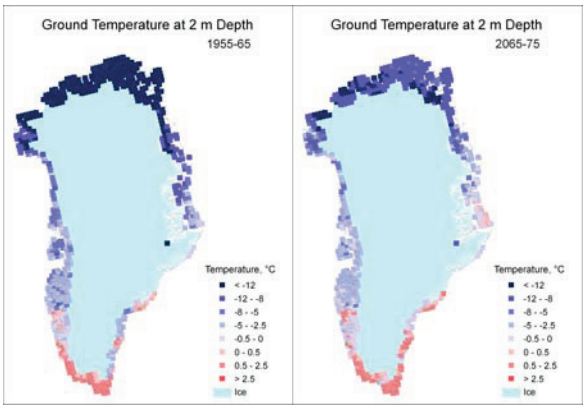

Figure 2. Bedrock temperature distribution at 2 m depth.

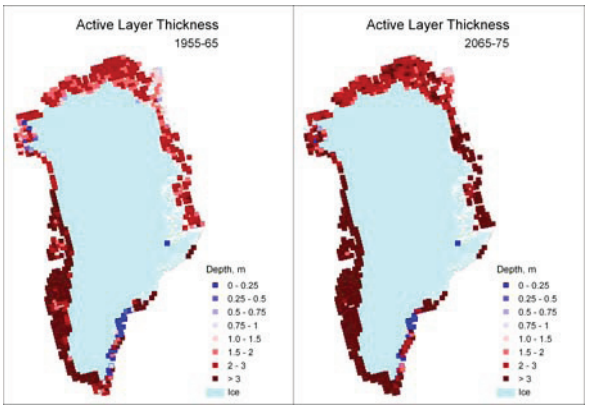

Figure 3. Active layer depth distribution in bedrock.

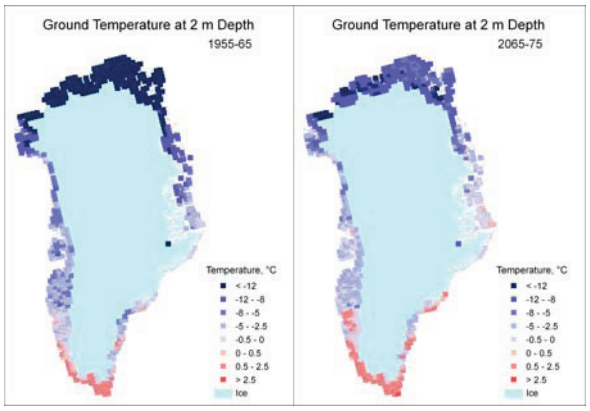

Figure 4. Annual average ground temperature distribution at 2 m depth in sediment with organic layer.

Temperatures in the northern part of Greenland seem to be most affected by the warming climate for bedrock and for the sediment simulation.

The active layer seems to be sensitive to the warming trend over the simulation period. Active layer depth increases at some locations in bedrock from 2 to 3 m. The eastern portion of Greenland shows soil warming, but the southwestern portion shows active layer depths in bedrock greater then 3 m as well. For sediment areas, which are important for infrastructure, the active layer deepens in the western portion of the country.

Conclusion

Permafrost temperatures are simulated for Greenland, and it was found that most areas are warming as the climate warms over the period from 1950 till 2075.

Permafrost temperatures in the northern portion of the country are strongly affected by warming winter temperatures, whereas the temperatures in the south are buffered by disappearing ground ice.

The active layer depths are increasing with time for bedrock and sedimentary substrates. Increases of the active layer with 1 m are commonly seen in the southern portion of the country.

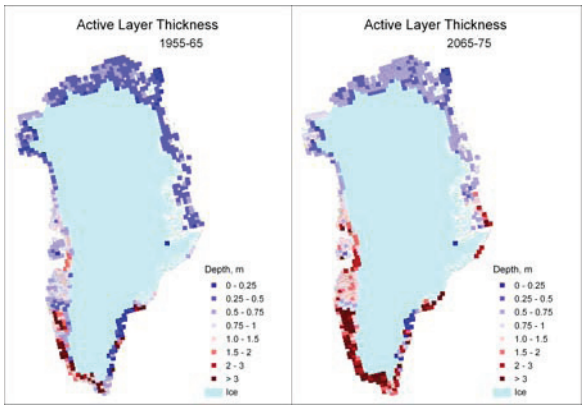

Figure 5. Active layer depth distributions for areas with sediments and organic matter.

Acknowledgments

Funding for this project was provided by the National Science Foundation under grant no. ARC-0612533.

We would also like to thank our collaborators from ASIAQ, the DMI, DTU, and ARSC.

References

ACIA. 2004: *Impacts of a Warming Arctic*. *Arctic Climate Impact Assessment (Highlights)*. Cambridge, UK: Cambridge University Press, 110 pp.

IPCC. 2001: *Summary for Policy Makers: Climate Change 2001: The Scientific Basis*. Contribution of Working Group I to the Third Assessment Report of the Intergovernment Pannel on Climate Change. J.T. Houghton, Y. Ding, D.J. Griggs, M. Noguer, P.J. van de Linden, X. Dai, K. Mashell, & C.A. Johnson (eds.). Cambridge, UK & New York, NY, USA: Cambridge University Press, 1-20.

Sergeev, D.O., Tipenko, G.S. & Romanovsky, V.E. 2003. Mountain permafrost evolution under long term climate fluctuations (results of numerical simulation). *Proceedings of the Eighth International Conference on Permafrost, Balkema, Zurich*: 1017-1021.

Tipenko, G.S. & Romanovsky, V.E. 2001. Simulation of soil freezing and thawing: Direct and inverse problems. *EOS*, *Trans. AGU* 82(47), Fall Meet. Suppl., Abstract, F551.

The Importance of Snow Cover Evolution in Rock Glacier Temperature Modeling

Matteo DallAmico
Department of Civil and Environmental Engineering, University of Trento, Italy
Stefano Endrizzi
Department of Civil and Environmental Engineering, University of Trento, Italy
Riccardo Rigon
Department of Civil and Environmental Engineering, University of Trento, Italy
Stephan Gruber
Department of Physical Geography, University of Zurich, Switzerland

Introduction

The snow cover evolution is one of the crucial factors affecting the thermal and hydraulic regime of rock glaciers (Mittaz et al. 2000), as snow strongly controls soil energy balance through its high albedo and insulating properties. Therefore, accurate modeling of the snowpack is absolutely necessary to reliably describe soil temperatures. The importance of accurate snow modeling entails the use of sophisticated models based on the solution of the snow energy balance and, consequently, on a good parameterization of radiation and turbulent fluxes (e.g., Jordan 1991). An advance or delay in estimating the time of snow disappearance would cause a strong error in the calculation of the energy balance at the soil surface, altering the ground heating or freezing and, therefore, affecting the soil temperature profile for the whole summer.

The goal of this work is to simulate and discuss the rock glacier snow evolution in order to analyze the influence of the snow cover and accumulation/melting time on the temperature regime of the active layer of a rock glacier.

Modeling Features and Case Study

The model used in the simulation is GEOtop (Rigon et al. 2006), a distributed physically-based model which jointly solves the energy and water balance of soil (Bertoldi et al. 2006) and snow (Zanotti et al. 2004), and accounts for the geotechnical parameters of unsaturated soils affecting slope stability (Simoni et al. 2007). The model has been improved recently to include a correct treatment of frozen soil (Endrizzi et al. 2008) and to model snow with a multilayer scheme capable of describing snow metamorphism and water circulation and refreezing in the snowpack (Endrizzi 2007).

Commonly, in alpine climates the soil exchanges heat directly with the atmosphere only in a short time window, roughly spanning from June to October, whereas during winter and early spring, heat transfer between soil and atmosphere is mediated by the snowpack. Consequently, the heat flux reaching the soil surface is strongly reduced due to high snow albedo, which reduces net energy input, and to snow insulating properties, which cause heat conduction to be very small below the upper snow layers. In fact, the snow energy balance equation can be written as follows (Oke 1990):

$$\Delta Q_S + \Delta Q_M = R_n + P - H - L - G \qquad [\mathrm{W/m^2}] \qquad (1)$$

where the terms in the left-hand side (LHS) represent the heat storage rate in the snowpack due to sensible heat (ΔSQ_S) and to latent heat (ΔQ_M, melting/refreezing and rain on snow). In the right-hand side (RHS), R_n is the net all-wave radiation, P is the sensible heat flux supplied by precipitation, H and L are, respectively, the sensible and latent heat fluxes exchanged between the surface (be it snow or soil) and the atmosphere, and G is the heat flux reaching the soil surface acting as soil energy input. When the ground is snow-free, the LHS in equation (1) is null, and G is equal to the net energy flux exchanged with the atmosphere. On the other hand, for snow covered ground, G is proportional to the temperature gradient at the snow-soil interface, namely:

$$G_{sn} = -K \frac{T_{sn} - T_S}{\frac{1}{2}(D_{sn} + D_S)} \qquad [\mathrm{W/m^2}] \qquad (2)$$

where K is the snow-soil averaged thermal conductivity calculated as a harmonic mean, T_{sn} is snow temperature in the layer close to the soil surface, T_S is the soil surface temperature, and D_{sn} and D_S are the depths of the snow and surface layer, respectively.

Investigated site

Simulations have been carried out on the active rock glacier Murtèl (Upper Engadin, Swiss Alps: 46°26′N, 9°49.5′E, 2670 m a.s.l., 15° slope with NW aspect) in which the oldest temperature time series of Alpine Permafrost has been measured (Vonder Mühll & Haeberli 1990, Hoelzle et al. 1999). Input data include incoming shortwave radiation (both direct and diffuse), incoming longwave radiation, air temperature, wind speed and direction, air pressure, and precipitation.

Simulations and Results

The simulation spans a period of two hydrological years beginning from October 1997. As the first snowfall normally occurs in November, this choice allows the avoidance of the problem of determining the initial condition of snow on the surface. Most of the parameters used by the snow model of GEOtop were simply taken from literature, for example, snow reflectance and snow thermal and hydraulic properties. As only total precipitation was available, the calibration was reduced to the definition of the threshold air temperatures above (below), where precipitation is considered to occur as rain (snow).

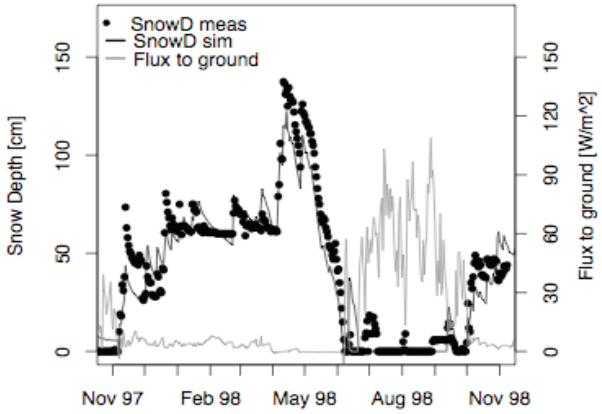

Figure 1. Simulated vs. measured snow depth and energy flux input to the ground in the Murtèl rock glacier.

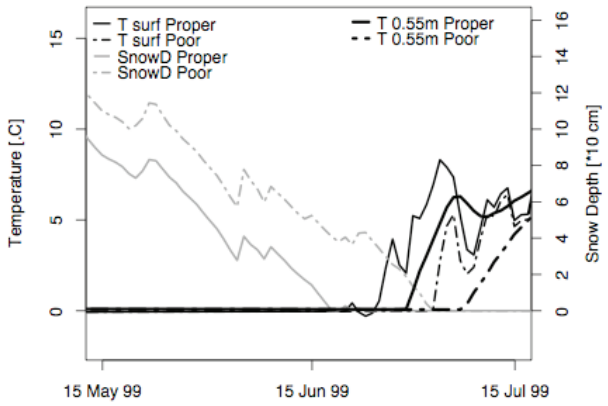

Figure 2. The error in temperature profile depends on snow modeling and becomes bigger the deeper in the ground. "Proper" and "Poor" refer to real measures and delayed modeling, respectively

As can be seen in Figure 1, the model proves to simulate well both the snow depth and the time when snow is completely ablated. The heat flux reaching the soil surface clearly depends on snow presence. When soil is snow free, the flux is of the order of 50 W/m^2, but it can drop by an order of magnitude or more when snow is present.

A delay (anticipation) in the estimation of the snow cover complete ablation date may lead to an underestimation (overestimation) of the ground surface temperature and of the temperature profile of the layers below. For example, in Figure 2 the temperature behavior at the soil surface and at 55 cm depth during the snow melting period is reported, considering a "proper" snow simulation (full grey line) and a "poor" delayed snow simulation (dotted grey line). The surface temperature increases as the snow is melted, and the delay between the two scenarios is disappear after few days. At 55 cm depth, instead, the delay in the temperature evolution is still visible after one month, indicating that the error in snow model will propagate and increase as we go deeper in the soil.

Conclusions

The work shows that the model is capable of reproducing the evolution of the snow cover and the temperatures in the active layer of the rock glacier. Snow evolution, together with the thermal and hydraulic parameters (DallAmico et al. submitted), is a crucial process to take into consideration when the thermal regime of an active layer is to be modeled. A proper representation of the snow evolution can provide the right time window of direct soil exposure to solar radiation and, in turn, a reliable quantification of the soil energy fluxes. Conversely, a poor representation may lead to significant errors that propagate and increase the deeper we go in the ground.

References

Bertoldi, G., Rigon, R. & Over, T.M. 2006. Impact of watershed geomorphic characteristics on the energy and water budgets. *J. Hydrometeorology* 7: 389-403.

DallAmico, M., Endrizzi, S., Rigon, R. & Gruber, S. Submitted. Modelling the thermal regime of a rock glacier active layer using GEOtop. *Proceedings of the Ninth International Conference on Permafrost, Fairbanks, Alaska, June 29–July 3, 2008.*

Endrizzi, S. 2007. *Snow cover modeling at local and distributed scale over complex terrain.* Ph.D. dissertation. Dept. of Civil and Environmental Engineering, University of Trento, Italy.

Endrizzi, S., Rigon, R. & DallAmico, M. 2008. A soil freeze/thaw model through the soil water characteristic curve. *Extended Abstracts, Ninth International Conference on Permafrost, Fairbanks, Alaska, June 29–July 3, 2008.*

Hoelzle, M., Wegman, M. & Krummenacher, B. 1999. Miniature temperature dataloggers for mapping and monitoring of permafrost in high mountain areas: first experience from the Swiss Alps. *Permafrost and Periglacial Processes* 10: 113-124

Jordan R. 1991 A one-dimensional temperature model for a snow cover. *Technical documentation for SNTHERM 89*. CRREL, Hanover, NH, USA.

Mittaz, C., Hoelzle, M. & Haeberli, W. 2000. First results and interpretation of energy-flux measurements of Alpine permafrost. *Annals of Glaciology* 31: 275-280.

Oke, T.R. 1990. *Boundary Layer Climates*. Routledge.

Rigon, R., Bertoldi, G. & Over, T.M. 2006. GEOtop: A distributed hydrological model with coupled water and energy budgets. *J. of Hydromet.* 7: 371-388.

Simoni, S., Zanotti, F., Bertoldi, G. & Rigon, R. 2007. Modelling the probability of occurrence of shallow landslides and channelized debris flows using GEOtop-FS. *Hydrological. Processes.*

Vonder Mühll, D. & Haeberli, W. 1990. Thermal characteristics of the permafrost within an active rock glacier (Murtèl/Corvatsch, Grisons, Swiss Alps). *Journal of Glaciology* 36(123): 151-158.

Zanotti F., Endrizzi, S., Bertoldi, G. & Rigon, R. 2004. The GEOTOP snow module. *Hydrological. Processes* 18: 3667-3679. doi:10.1002/hyp.5794.

The Account of Long-Term Air Temperature Changes for Building Design in Permafrost

I.V. Davidova
The Moscow State University, The Faculty of Geology, 119992, GSP-2, Moscow, Lenin Mountains, Russia
L.N. Khroustalev
The Moscow State University, The Faculty of Geology, 119992, GSP-2, Moscow, Lenin Mountains, Russia

Introduction

One of the main parameters defining permafrost-bearing capacity as a base of buildings is their temperature depending on air temperature. According to meteorological supervision, it is established that air temperature increase became practically appreciable since 1970, and it is expected that, to the middle of the 21st century, increase of mean annual air temperature will reach from 1.5 to 7.0°C.

A rise in soil and air temperature leads to an increase of rated building base temperature, which defines rated resistance of frozen ground. Knowing rated resistance decrease during the time, it is possible to plan engineering actions which will provide necessary bearing capacity of the building under condition of climate warming. On a design stage the main action is the increase of supporting structure of foundation, that is, increase of reliability factor. Thus the problem is divided into three interconnected problems: the forecast of mean annual air temperature, the forecast of ground temperature, and the definition of reliability factor.

The Forecast of Mean Annual Air and Permafrost Temperature

Laws of long-term changes of mean annual air temperature were established by the method of autoretrospective analysis of meteorological supervision series. The method is based on harmonious decomposition of time series and considers cyclic, trend, and casual changes in meteorological series. In detail the method is described in the work of Khroustalev et al. (2000).

Received forecast air temperatures were used for modeling of temperature ground conditions. For the forecast of permafrost temperature, a numerical method—the final difference method—was used. The mathematical model of permafrost evolution was the Stefan problem. Calculations were carried out in the program "Warm," developed on the Geocryological Faculty of the Geological Department of the Moscow State University (Khruostalev et al. 1994). The mathematical model has been realized by us for 10 settlements located in Sakha-Yakutia Republic (6 items) and in Western Siberia (4 items).

Obtained data have been estimated by us from a position of the reliability theory.

Reliability Estimation of the Building Foundations in Permafrost

At first we defined a cost optimum reliability of the bases without taking into account climatic changes, taking as the base data from the boundary year (standard reliability).

The analytical calculation method for optimum reliability of the building foundations when construction is built with principle I (we consider only this case in the report) has been developed by Pustovoit (Khrustalev & Pustovoit 1988). Its basis is minimization of the total expenses consisting of the building initial cost (C_0) and expenses connected with possible damage before the termination of the operation life (C_R).

Except for optimum reliability, another important parameter is the optimum factor of reliability ($K_{H,0}$), which corresponds to optimum reliability.

The factor of reliability allows the connection of two determined approaches which are put in a basis of normative documents and developed by us as probability-statistical. This factor depends on many parameters: climatic, geological, constructive, and economic. Therefore, it cannot be appointed directly, but should be calculated separately for each area.

The calculated result of optimum reliability and reliability factors for the residential building bases in 10 areas allow the following conclusions to be drawn:

Optimum reliability increases, and optimum reliability factor decreases when air temperature decreases and foundation depth increases. These changes occur in interval $P(te) = 0.747 - 0.998$ and $K_{H,0} = 1.1 - 2.5$.

Casual fluctuations of mean annual air temperature influence the optimum reliability and optimum reliability factor. When air temperature fluctuation increases, the optimum reliability decreases and the optimum reliability factor increases. For example, at practically identical air temperature in areas of Chekurdah ($\sigma = 1.3$) and Tiksi ($\sigma = 1.86$), in the first case optimum reliability is above, and optimum reliability factor is below, than in the second.

Greater building cost (smaller value of economic factor) should correspond to greater base reliability and greater optimum reliability factor. Unfortunately, this trivial conclusion does not find reflection in operating normative documents.

After definition of optimum values of reliability and reliability factor, the forecast of the base reliability for a residential building on the pile foundation for the nearest 50 years has been executed, considering variability of air and ground temperatures and depth of seasonal thawing during the time.

For Nadym city, the optimum value of reliability factor is 1.697, if long-term changes of air temperature do not occur (a modeling problem), function of reliability changes a little,

Table 1. Recommended values of reliability and reliability factor for residential buildings during the period 2000–2050.

Area	T_{air}, °C	g, °C/year	l=6m		l=8m		l=12m	
			$P(t_e)$	K_H	$P(t_e)$	K_H	$P(t_e)$	K_H
					Yakutia			
Chekurdah	-11.1	0.01	0.992	1.214	0.996	1.16	0.998	1.104
Tiksi	-10.7	0.02	0.984	1.411	0.990	1.301	0.995	1.190
Verhoyansk	-7.3	0.033	0.986	1.263	0.991	1.198	0.996	1.129
Ust-Maya	-4.0	0.042	0.913	1.403	0.923	1.316	0.943	1.214
Mirniy	-3.4	0.031	0.746	1.183	0.773	1.646	0.804	1.436
Tuoy-Haya	-2.8	0.032	0.949	1.549	0.958	1.451	0.966	1.319
					Western Siberia			
Beliy island	-8.6	0.006	0.983	1.344	0.989	1.255	0.995	1.165
Salehard	-2.02	0.02	0.727	2.222	0.777	1.892	0.824	1.581
Nadim	-1.64	0.017	0.73	2.62	0.79	2.21	0.849	1.823
Poluy	-0.56	0.013	0.63	3.96	0.767	2.99	0.878	2.21

and reliability remains high enough. In a real case, reliability intensively tends to zero, reaching value 0.08 at the end of operation. This means that the building will be destroyed before the termination of operation period with probability of 92%. At reliability factor $K_H = 2.62$, the reliability at the initial stage surpasses reliability of the modeling problem, and then decreases to 0.73. Thus the material damage caused by reliability decrease remains the same as in case of the modeling problem.

Values of reliability $P(t_e)$ and the factor of reliability K_H for all 10 considered areas have similarly been calculated (Table 1).

References

Khroustalev, L.N., Emeljanov, N.V., Pustovojt, G.P. & Jakovlev, S.V. 1994. *The Calculation Program of Thermal Interaction of Engineering Constructions with Permafrost*. The Certificate 940281. RosAPO.

Khroustalev, L.N. & Pustovoit, G.P. 1988. Calculations of the building bases in permafrost. *Novosibirsk: the Science*. 253 pp.

Khroustalev, L.N., Medvedev, A.V. & Pustovoit, G.P. 2000. Long-term change of air temperature and construction stability projected in permafrost area. *Cryosphere of the Earth* IV(3): 35-41.

Pavlov, A.V., Ananev, G.V & Drozdov, D.S. 2002. Monitoring of seasonal thawing layer and temperature of frozen ground in the north of Russia. *Cryosphere of the Earth* VI(4): 30-39.

Pavlov, A.V. 2003. Permafrost and climatic change in the north of Russia: supervision, forecast. *Proceedings of the Russian Academy of Sciences* 6: 39-50.

Pustovoit, G.P. 1997. The account of climate variability at maintenance of construction base reliability in permafrost area. *Cryosphere of the Earth* I(4) :50-53.

SNiP 2.02.04-88. 1990 *The Bases and the Foundations in Permafrost*. Moscow: Stroyizdat, 53 pp.

The Combined Isotopic Analysis of Late Quaternary Ice Wedges and Texture Ice at the Lena-Anabar Lowland, Northern Siberia

Alexander Dereviagin
Moscow State University, Faculty of Geology, Vorobievy Gory, 119899, Moscow, Russia
Hanno Meyer
Alfred Wegener Institute for Polar and Marine Research, Research Unit Potsdam, Telegrafenberg A43, 14473 Potsdam, Germany
Alexander Chizhov
Moscow State University, Faculty of Geology, Vorobievy Gory, 119899, Moscow, Russia
Diana Magens
Alfred Wegener Institute for Polar and Marine Research, Am Alten Hafen 26, 27568 Bremerhaven, Germany

Introduction

Different types of ground ice are fed by meteoric water sources and are considered to be a unique archive of paleoenvironmental and paleoclimatic information (Mackay 1983, Meyer et al. 2002). The isotopic signal of an ice wedge is indicative for winter temperatures. Texture ice (both segregated and pore ice) may be assumed as a mixture of summer and winter precipitation. Isotope variations within sediment columns are difficult to interpret in paleotemperature terms, because of various processes involved such as seasonality of precipitation, amount of rain and snow feeding the active layer, fractionation during evaporation, melting and freezing may influence its isotopic composition. This study focuses on the combined isotopic analysis of Late Quaternary ice wedges and texture ice in an ice-rich sedimentary complex named Ice Complex. The isotopic composition ($\delta^{18}O$, δD) of ground ice dating to ca. 60 ka was studied in the framework of Russian-German multidisciplinary research expeditions at the Laptev Sea coast.

Study Sites and Methods

The investigations were carried out at two sites located in the Lena-Anabar lowland at the Laptev Sea coast at Bykovsky Peninsula (eastern part of Lena Delta): at Mamontovy Khayata outcrop, 71°60′N, 129°20′E (site 1) and at Cape Mamontov Klyk, 73°36′N, 117°10′E (site 2).

The region is characterized by a continental Arctic climate. Mean annual air temperatures (MAAT) at site 1 are about -14°C, mean January temperatures (T_J) are about -34°C and mean winter temperatures (T_w) are about -22°C (data of Tiksi). MAAT at site 2 are about -15°C, T_J are about -33°C, and T_w are about -23°C (data of Cape Terpey-Tumasa). Annual precipitation reaches 300 mm, with a maximum (about 75%) in summer. The region belongs to the zone of continuous permafrost with a thickness of about 300–500 m and mean annual ground temperature around -12°C. The coastal lowland is characterized by widespread Ice Complex remains, composed of ice-rich silty fine-grained sand with peaty paleosol horizons and huge syngenetic polygonal ice wedges (heights of 20–40 m and widths of 2–6 m) and columns of frozen sediments (width of 2–4 m) with belt-like cryostructure.

The formation of Late Pleistocene Ice Complex is usually associated with Karginsky and Sartansky periods of the Russian stratigraphy, which correspond to MIS-3 and MIS-2 of the global classification. According to AMS dates, Ice Complex formation at Bykovsky Peninsula was between 58.4 ka (at sea level) and 12.2 ka BP (Schirrmeister et al. 2002). At Cape Mamontov Klyk, Ice Complex formation took place between 31–28 ka and 10.7 ka BP (Schirrmeister et al. 2008). At both sites, Ice Complex is partly covered by a 2 m thick horizon of peat-rich, silty sediments with Holocene ice wedges. Holocene ground ice was also studied in alases, thermo-erosional and river valleys.

The investigations are based on the combined application of stable isotopes to both ice wedges and texture ice sampled in parallel. Measurements of isotope composition ($\delta^{18}O$, δD) were carried out at the Alfred Wegener Institute in Potsdam. The stable isotopic composition is given in ‰ vs. V-SMOW standard. The 1σ errors for H and O isotopes are better than 0.8‰ and 0.10‰, respectively.

Results and Discussion

The available data of isotope analyses are presented in Table 1. Both wedge and texture ice differs considerably in their isotopic composition between Holocene and Pleistocene, with 3–8‰ lower $\delta^{18}O$ in Pleistocene ice following the global warming trend. The isotopic composition of both Late Pleistocene wedge and texture ice is very close at site 1 and site 2. This can be evidence both of the similarity of ice complex formation and climatic conditions in the region.

The mean $\delta^{18}O$ of ice wedges differs by 0.1‰ in Sartansky (MIS-2) time, and by 1.6‰ in Karginsky (MIS-3) time between both sites. For texture ice, the differences are about 0.1‰ in Karginsky time. In Holocene, differences in mean $\delta^{18}O$ reach about 3‰ for ice wedges and 0.7‰ for texture ice between both sites. The observed differences of Holocene ice wedges are likely the result of different ages of the sampled ice wedges at sites 1 and 2. At site 1, many Early Holocene ice wedge samples were taken at the top of the Ice Complex.

The ice wedge isotopic composition is similar in Karginsky and Sartansky with more negative minimum values (of -33.9 to -34.9‰) in Karginsky time. This leads to the assumption

Table 1. Isotopic composition (‰) of ice wedges and texture ice: mean (in bold)/min./max. values). *N* = number of samples.

Ice wedges				Texture ice			
N	$\delta^{18}O$	δD	d_{ex}	N	$\delta^{18}O$	δD	d_{ex}
Site 1 (Bykovsky Peninsula)							
Holocene (MIS-1)							
184	**-27.5**	**-203.5**	**13.5**	14	**-20.8**	**-155.5**	**11.2**
	-30.2	-224.3	8.5		-23.3	-173.1	7.0
	-22.5	-168.5	17.8		-17.7	-134.8	15.1
Sartansky (MIS-2)							
178	**-29.7**	**-231.2**	**6.1**	no data			
	-32.1	-253.5	1.9				
	-23.1	-174.5	13.3				
Karginsky (MIS-3)							
158	**-30.6**	**-241.3**	**3.7**	40	**-23.8**	**-193.1**	**-2.5**
	-33.9	-267.5	-3.9		-29.5	-231.7	-11.7
	-25.6	-208.3	7.9		-18.9	-158.5	14.0
Site 2 (Cape Mamontov Klyk)							
Holocene (MIS-1)							
54	**-24.1**	**-182.9**	**10.0**	13	**-20.1**	**-150.8**	**9.7**
	-27.3	-212.6	6.1		-28.2	-204.5	5.2
	-20.4	-155.5	14.3		-17.2	-130.6	21.4
Sartansky (MIS-2)							
120	**-29.8**	**-234.3**	**4.5**	51	**-27.6**	**-210.3**	**10.4**
	-31.9	-253.4	0.4		-31.6	-242.1	-7.3
	-26.1	-199.6	9.4		-19.5	-147.0	24.2
Karginsky (MIS-3)							
62	**-29.0**	**-227.5**	**4.4**	20	**-23.7**	**-186.3**	**3.6**
	-34.9	-272.2	-0.6		-27.7	-215.3	-16.8
	-24.0	-180.6	14.6		-16.7	-150.4	19.2

that winter conditions in Sartansky were slightly less severe than in Karginsky time.

The isotopic composition of texture ice is always less negative than the isotopic composition of ice wedges (Table 1), because of the influence of summer precipitation (as well as fractionation effects). Texture ice from Karginsky time is about -23.7‰ for both sites, whereas Holocene texture ice is much heavier ($\delta^{18}O$ around -20‰), again showing the similarity between both sites and the relatively warmer Holocene. In contrast, texture ice from Sartansky time is characterized by very light isotopic composition (-27.6‰) close to that of ice wedges (-29.8‰). This may correspond to extremely cold summer temperatures and/or a relatively smaller amount of summer precipitation taking part in texture ice formation at that time. The late glacial maximum (LGM) apparently is visible only in summer.

The higher differences between isotopic composition of ice wedges and texture ice (as well as the heavier $\delta^{18}O$ of texture ice) in Karginsky time may reflect relatively warm summer conditions. Additionally, the negative $\delta^{18}O$ values of ice wedges point to severe winter conditions at that time.

$\delta^{18}O$ and δD of ice wedges at both sites are aligned parallel to GMWL with slopes close to 8. This indicates that the isotopic composition of initial meteoric water-formed ice wedges was not subject to pronounced fractionation processes. In contrast, isotopic composition of texture ice crosses the GMWL with slopes of 6.8 (site 1) and 7.2 (site 2). This is a result of fractionation processes during evaporation and freezing as well as mixing of both snowmelt and rainwater, also reflected in *d* excess. In general, low *d*-excess values of texture ice point to fractionation during evaporation and reflect the influence of rainwater enriched in heavy isotopes. High *d*-excess values can be considered a result of fractionation during freezing.

Conclusions

The isotopic records of ground ice correlate well with the global climatic trend, and show progressive warming from MIS-3 to MIS-1. Ice wedge isotopic composition is indicative for T_w. $\delta^{18}O$ values of texture ice allow estimating summer climatic conditions (by comparing with ice wedges). The *d* excess, well known as an indicator of precipitation sources, also reflects fractionation processes during ground ice formation.

Negative $\delta^{18}O$ of ice wedges reflect (stable) cold winter conditions during Karginsky (MIS-3) and Sartansky (MIS-2) time with minimum in Karginsky time. Differences of $\delta^{18}O$ values between ice wedges and texture ice point to relatively warmer summers in Karginsky time and colder summer periods in Sartansky time. This let us believe that the LGM in the region is visible only in summer indicators.

The combined isotopic analysis of both ice wedges and texture ice extends considerably the quantitative and qualitative capabilities of paleoenvironmental interpretation.

References

Mackay, J.R. 1983. Oxygen isotope variations in permafrost, Tuktoyaktuk Peninsula area, Northwest Territories. *Current Research, Part B, Geological. Survey of Canada* Paper 83-1B: 67-74.

Meyer, H., Dereviagin, A., Siegert, C. & Hubberten, H.-W. 2002a. Paleoclimate studies on Bykovsky Peninsula, North Siberia. Hydrogen and oxygen isotopes in ground ice. *Polarforschung* 70: 37-52.

Schirrmeister, L., Grosse, G., Kunitsky, V., Magens, D., Meyer, H., Dereviagin, A., Kuznetsova, T., Andreev, A., Babiy, O., Kienast, F., Grigoriev, M. & Preusser, F. 2008. Periglacial landscape evolution and environmental changes of Arctic lowland areas during the Late Quaternary (Western Laptev Sea coast, Cape Mamontov Klyk). *Polar Research* (accepted).

Schirrmeister, L., Siegert, C., Kuznetsova, T., Kuzmina, S., Andreev, A.A., Kienast, F., Meyer, H. & Bobrov, A.A. 2002. Palaeoenvironmental and palaeoclimatic records from permafrost deposits in the Arctic region of Northern Siberia. *Quaternary International* 89: 97-118.

Adaptating and Managing Nunavik's Transportation Infrastructure

Guy Doré
Laval University
Anick Guimond
Quebec Ministry of Transportation
Gilles Grondin
Quebec Ministry of Transportation

Introduction

In Nunavik (Quebec, Canada), an important increase in mean annual temperatures has occurred over the last 15 years. As a result, permafrost is degrading and is threatening the integrity of roads and airfields in 13 Inuit communities. This study was initiated by the Quebec Ministry of Transportation in order to adapt transportation embankments to the new climatic reality. The purpose of this study is to identify the consequence of global warming on the transportation infrastructure, to carry out a performance assessment of the Nunavik runways and access roads since their construction, and to develop a management strategy in order to effectively maintain a safe airport and access road network in Nunavik.

Problem Statement

Damages observed on Nunavik's airstrips and access roads caused by degrading permafrost have led the Quebec Ministry of Transportation to take action. Research has been undertaken to assess current and foreseeable impacts on northern infrastructures, recommend adaptation strategy and propose a management plan for these transportation infrastructure networks.

Condition of Nunavik's Airports and Access Roads

The study led to the identification of six unstable runways and two unstable access roads. Depressions along airstrip edges and roadsides and water ponding in drainage ditches are the most frequent problems observed in Nunavik. These problems are mainly caused by snow accumulation on the side-slopes and by climate warming. As a result, the ground temperature under the embankments and more specifically under side-slopes tends to increase, causing permafrost degradation and loss of support if the permafrost is ice-rich.

Experimentation of Protection Techniques

Three protection techniques that have the potential for large-scale application in Nunavik have been chosen to mitigate permafrost degradation under transportation infrastructures in Nunavik. Air convective embankment, heat drain, and reflective surfaces have been selected for their operational and economical feasibility. The intent is to use these techniques in cases of severe degradation on recently paved access roads and on airstrips. The use of protection technique should extend the service life or reduce the maintenance requirements of Nunavik's transportation infrastructure. The heat drain was developed at Laval University (Beaulac & Doré 2006). This technique allows heat extraction from the embankment during winter through a highly permeable geocomposite placed in the embankment shoulder. The air convection embankment, developed in Alaska (Goering 2003), uses convective flow in large pores of a uniform-size stone material to activate heat loss in embankments during winter. Use of reflective surfaces can reduce the *n*-factor and has proven to be effective in reduction of the depth of thaw penetration in permafrost regions. Reflective surfaces, based on the use of white paint applied on pavement surfaces, have been tested in several experimental projects in Alaska (Reckard 1985).

The solutions based on heat extraction (heat drain and convection embankment) have been tested in a laboratory on small-scale embankments built in a cold room. Laboratory testing has demonstrated the effectiveness of the heat drain and of the air convection embankment. The results showed that it is possible to lower ground temperature significantly during winter when these techniques are used in the embankment. Temperature differences reaching 7°C have been observed between the two protection techniques and the reference embankment. The testing program will continue to support thermal modeling and development of design parameters for these techniques.

The reflective surface has been tested at the Laval University Road Experimental Site (SERUL) and the results of the experiment are discussed in (Stuhr-Jorgensen & Doré 2007). All these techniques are also being tested in the field on the Salluit airport access road and on the embankment of the Tasiujaq airstrip. The objective of the experimental program is to assess the technical, operational, and economical feasibility of these techniques and to identify those having the best potential for large-scale application. The Salluit test site, including six test sections, was constructed in summer 2006 to determine the operational and economical feasibility of the techniques (initial construction cost, maintenance cost, labour and materials cost, heavy equipment location cost, and shipping cost). The three protection techniques described above have been used alone (3 sections) and by combining the reflective surface with both heat extraction techniques (2 sections). An additional section is used as a reference to assess the relative effectiveness of the protection techniques.

The Tasiujaq airstrip project involves the experimentation of the air convection embankment and the heat drain in the shoulder of the embankment. The project also includes a

Figure 1. Installation of the heat drain in the shoulder of the Tasiujaq airstrip embankment.

gentle slope section to measure the benefit of modifying the embankment geometry in order to reduce problems caused by snow accumulation along the embankment. Figure 1 illustrates the installation of the heat drain section besides the air convection section in Tasiujaq, Nunavik. Thermistor strings have been installed in the test sections. Data is recorded by automatic data acquisition systems every four hours for the duration of the project (3 years). Thermal regimes in the test sections will be the basic information used to quantify the performance of each technique used. Despite numerous operational problems, some encouraging data trends were observed during the first months of operation.

It is expected that the use of protection techniques will increase the service life of the Nunavik transportation infrastructure.

Management Strategy

The last step of the research project was to develop the framework of a management strategy for the transportation infrastructure of Nunavik. The strategy is based on four coordinated groups of activities:

1. Data collection
   a. Identification of thaw sensitive areas along airstrips and access roads
   b. Characterization of thaw sensitive areas including thaw and settlement rates as well as characteristics of soils in the top part of the permafrost
2. Identification of applicable solutions, and assessment of their effectiveness and economical benefit
3. Implementation of the selected solution
4. Long term monitoring of the performance of the selected solution

Conclusion

The study led to the identification of six unstable runways and two unstable access roads. Three mitigation methods and a management plan are proposed to reduce permafrost degradation at Nunavik transportation infrastructures. The protection techniques include heat drains, air convective embankments, and reflective surfaces. These techniques have been experimented with in controlled conditions in order to assess their relative effectiveness and to determine design parameters in view of their application on road and airfield embankments. They are also being tested in a full-scale test embankment on the Salluit access road and the Tasiujaq airstrip in Nunavik. The management plan involves the identification of thaw-sensitive areas in the Nunavik airport and access roads network. It also involves monitoring the rate of evolution of these problem areas and investigation of permafrost conditions beneath the embankments. Finally, the management plan involves the development of a series of maintenance and construction actions in order to maintain the transportation network in safe and good condition.

References

Beaulac, I. & Doré, G. 2006. Development of a new heat extraction method to reduce permafrost degradation under highway and airfield embankments, *Compte Rendu de 13th Int. Conf. on Cold Region Engineering Orono, ME, 2006*: CDROM.

Goering, D.J. 2003. Thermal response of air convective embankments to ambient temperature fluctuations. *Proceedings of the Eighth International Conference on Permafrost, Zurich, Switzerland, 20–25 July 2003*: 291-296.

Reckard, M.K. 1985. *White Paint for Highway Thaw Settlement Control*. Fairbanks, Alaska, USA: Alaska Department of Transportation and Public Facilities. Report no. FHWA-AK-RD-85-16: 1-7.

Stuhr-Jorgensen, A. & Doré, G. 2007. *Use of Reflective Surfaces on Roadway Embankment*. Tempere, Finland: ISCORD.

Human Experience of Cryospheric Change in Nunavut, Canada: Preliminary Findings

Nancy Doubleday
Carleton University, Ottawa, Canada
Shawn Donaldson
Carleton University, Ottawa, Canada
Tatiana Vlasova
Russian Academy of Sciences, Moscow, Russia
Anita Kushwaha
Carleton University, Ottawa, Canada
Morgan Ip
Carleton University, Ottawa, Canada

There is a significant consensus within both scientific and northern communities: dramatic change is occurring in the Arctic (e.g., ACIA 2005, Hinzman 2005, Duerden 2004) and the transformation of the cryosphere itself provides a critical focal point for research contributing to our understanding of health and well-being. Despite debates about the relative importance of drivers of change (e.g., Zalasiewicz et al. 2008), the occurrence of environmental change, both gradual and rapid, is not at issue (although many elements of landscape processes and impacts still require further study). The necessity of adaptation at all scales of both human organization and landscape dynamics is not in dispute either. However, in moving forward from identification of processes of environmental change to definition of impacts, then to development of strategies for mitigation and adaptation, we enter stormy and contested regions. Why? Because integration of physical and social science perspectives, along with those of actors who engage locally, regionally, nationally, and internationally with realities of a changing cryosphere, is necessary in order to build effective policy and to set priorities for mitigation and for adaptation. In reaching for multiparty consensus on actions, we face limitations of knowledge, of knowledge interoperability, and of decision-making processes; as well as potentially conflicting goals and objectives, priorities, and visions. Lack of agreement and cooperation can affect both capacities for communication and adaptation as well as resources available for mitigation. Standard approaches to decision-making in the south and the north see government agencies consulting with stakeholder representatives, usually at a point after an issue has been defined and after measures available to address it have already been scoped, but before a final decision is taken. This process is also a reflection of past practice with respect to knowledge creation, and assumes that community and other "local" interests are farther removed from expert knowledge. Here, by positioning local or traditional knowledge as complementary source, in conjunction with social and physical sciences in current research, we are building transdisciplinary knowledge (Wilcox 2008) as a starting point for multiparty consensus around environmental change in Nunavut, Canada, and for inclusive strategies for mitigation and adaptation, emphasizing local communities and their concerns.

Preliminary findings

Practically, we integrate physical and social science of northern environmental change by situating our research at the nexus of environment, health, and well-being, as framed by northerners themselves, in a series of specific studies constructed to include both research and design elements in methods of enquiry. We report briefly on five related studies currently under investigation: (1) food choice among women and men, and thus impacting health and well-being; (2) local perceptions and understanding of ecological changes linked to a changing cryosphere through investigation of spatial and temporal variation in observations of plants and as interpreted from photographs; (3) design choices in arctic architecture as represented by a healing centre, directly contributing to health and well-being; (4) integration of data from these substudies, and refinement of mixed methods for advancing transdisciplinary work, as steps in the iterative research process; and (5) development of protocols modeled on Canadian standards for ethical and just research involving humans that yield both point-in-time images ("snapshots") of social, environmental, and economic conditions, as well as in-depth profiles at selected sites. The purpose of this research is to understand adaptation, mitigation, and community resilience, in the face of cryospheric environmental change, using mixed methods to achieve social-ecological systems integration.

In Nunavut, Canada, we are documenting food choice among women and men. Previously, Donaldson investigated factors influencing food choice, and Kushwaha documented Inuit traditional knowledge of the effects of environmental change on sea ice and ringed seal. Results here indicated that multiple factors are involved both in food choices and in traveling and hunting decisions. We note that uncertainty plays a larger role: for example, the thickness, extent, and stability of sea ice in the Cape Dorset area have changed in recent years, making it increasingly difficult to travel and hunt; and weather patterns have also changed. While hunters report ringed seals in the surrounding area to be

physically healthy, they have become increasingly difficult to hunt, as the occurrence of sinking seals has become more common. Local residents have been responding and coping to environmental changes primarily by adapting their subsistence hunting practices. These findings are consistent with Reidlinger and Berkes' (2001) earlier work in the Western Arctic, and suggest that adaptation to rapid cryological change is occurring in the Foxe Basin, off Baffin Island, as well.

During preliminary site visits to Sanikiluaq, Rankin Inlet, and Baker Lake in 2007, other community observations and reports of impacts confirmed the regional nature of change. While the form of environmental expression varied (i.e., skinny seals in marine environments and thicker willows inland), the reports all pointed to systemic change.

We find these "social observations" (Vlasova 2006) to be an extremely sensitive detector of environmental change. The challenge is then to communicate these findings so that they can be integrated with studies that model change on global or regional scales. If synergies among multiple factors across scales are in fact the case, as the regional variability of the warming trends suggest, then strategies for adaption and mitigation must be capable of recognizing and addressing local and regional factors implicated in these changes. Additionally, linking the data generated by physical environmental studies with social impacts requires social data. The fine-grained "social observations" approach may contribute most significantly here. We anticipate additional data on this question from the second project "plants and photographs through time," which provides a direct link to daily life, focusing spatial and temporal observations of plants, and using photographs to derive anecdotal information.

In terms of proactive adaptation through design, the third study, investigating appropriate architecture, offers a critical view of past practice and resulting increases in risk associated with cryospheric change. Next steps will address incorporation of community values in design of a healing centre. The fourth project is iterative, and will integrate results from the other studies as they become available. The fifth project to develop protocols for social, environmental, and economic observations is well underway, with a consultation meeting scheduled in April 2008.

These projects are contributions to PPS Arctic, an international study of the impacts of a changing tree line, led by Annika Hofgaard of Norway. We will conduct a second season of fieldwork on all five studies in 2008–09. In the longer term, we plan to continue transdisciplinary work and welcome connections with other researchers who are similarly engaged.

Acknowledgments

We thank the people of the communities of Nunavut, the Nunavut Research Institute, the International Polar Year Office of the Government of Canada, Carleton University, and the Russian Academy of Science, Institute of Geography. We also thank the organizers of NICOP 2008.

References

ACIA 2005. *Arctic Climate Impact Assessment*. Cambridge University Press, 1042 pp. Web site: http://www.acia.uaf.edu (accessed 10 March 2007).

Duerden., F. 2004. Translating climate change impacts at the community level. *Arctic* 57(2): 204-212.

Furgal, C. & Seguin, J. 2006. Climate change, health, and vulnerability in Canadian northern aboriginal communities. *Environmental Health Perspectives* 114(12): 1964-1970.

Hinzman, L.D., Bettez., N.D., Bolton, W.R., Chapin, F.S., Dyurgerov, M.B., Fastie, C.L., Griffith, B., Hollister, R.D., Hope, A., Huntington, H.P., Jensen, A.M. Jia, G.J., Jorgenson, T., Kane, D.L., Klein, D.R., Kofinas, G., Lynch, A.H., Lloyd, A.H., Mcguire, A.D., Nelson, F.E., Oechel, W.C., Osterkamp, T.E., Racine, C.H., Romanovsky, V.E., Stone, R.S., Stow, D.A., Sturm, M., Tweedie, C.E. Vourlitis, G.L., Walker, M.D., Walker, D.A., Webber, P.J., Welker, J.M. 2005. Evidence and implications of recent climate change in northern Alaska and other Arctic regions. *Climatic Change* 72: 251-298.

Reidlinger D, & Berkes F. 2001. Responding to climate change in northern communities: Impacts and adaptations. *Arctic* 54(1): 96-98.

Vlasova, T. 2006. Arctic residents' observations and human impact assessments in understanding environmental changes in boreal forests: Russian experience and circumpolar perspectives. *Mitigation and Adaptation Strategies for Global Change* 11: 897-909.

Wilcox, B. & Kueffer, C. 2008. Transdisciplinarity in EcoHealth: Status and future prospects. *EcoHealth* doi:10.1007/s10393-008-0161-5 (accessed 21 March 2008).

Zalasiewicz, J., Williams, M., Smith, A., Barry, T.L., Coe, A.L., Bown, P.R., Brenchley, P., Cantrill, D., Gale, A., Gibbard, P., Gregory, F.J., Hounslow, M.W., Kerr, A.C., Pearson, P., Knox, R., Powell, J., Waters, C., Marshall, J., Oates, M., Rawson, P. & Stone, P. 2008. Are we now living in the Anthropocene? *GSA Today* 18(2): 4-8.

HiRISE Observations of Fractured Mounds in the Martian Mid-Latitudes

Colin M. Dundas
The University of Arizona, Department of Planetary Sciences, Tucson, AZ, USA
Alfred S. McEwen
The University of Arizona, Department of Planetary Sciences, Tucson, AZ, USA

Introduction

The planet Mars has widespread permafrost, much of it ice-rich. Some ground ice features such as thermal contraction cracks have been confidently identified based on orbital imagery (e.g., Mellon 1997). The possibility of other periglacial features has been considered; in particular, a number of authors have suggested various Martian features as pingos (Judson & Rossbacher 1979, Parker et al. 1993, Cabrol et al. 2000, Soare et al. 2005, Burr et al. 2005, Page & Murray 2006). However, low resolution of orbital imagery made it difficult to assess detailed morphologies of such features, and in several cases, later work has indicated different formation mechanisms (Farrand et al. 2005, Martinez-Alonso et al. 2005, Jaeger et al. 2007). This has left the possibility of pingos on Mars an open question. The issue is of particular importance, since pingos would provide information about the state and history of water on Mars, with implications for the origins of other water-related features such as young gullies (Malin et al. 2000).

The High Resolution Imaging Science Experiment (HiRISE) camera on the Mars Reconnaissance Orbiter (MRO) spacecraft has returned several thousand images of the Martian surface with scale as small as 26 cm/pixel. This resolution allows assessment of fine-scale morphologies in much more detail than previously possible. Early images revealed fractured mounds, similar to pingos on Earth in some respects, in both northern and southern mid-latitudes (Dundas et al. 2008). Dundas et al. (2008) also used lower-resolution images to examine the distribution of flat-topped mounds (matching the approximate shape of some of the observed features) and found that in the northern plains region of Utopia Planitia, the mounds occurred in the latitudinal band where gullies are most common. This study uses HiRISE images to examine the planet-wide distribution and range of morphologies in order to better compare these mounds with pingos on Earth.

HiRISE Observations

HiRISE survey

HiRISE images from across Mars were examined in order to assess the distribution of fractured mounds. This is a non-genetic definition that could encompass a range of morphologies and origins, used here in order to ensure a comprehensive survey of possible pingos. We search for features where fracturing occurs only on the mound or is distinctly enhanced there, since much of the Martian surface has fractures of various origins. We specifically exclude outcrops of jointed rock and knobs with superposed polygonal cracks occurring as part of a widespread network (e.g., thermal contraction cracks).

To date, 1350 HiRISE images have been incorporated into this survey. All images obtained through orbit 2150 were used; among images from subsequent orbits, only those from latitudes 20°–60° of each hemisphere were examined.

Fractured mound morphologies

A wide range of morphologies fitting the loose definition of fractured mound have been observed. Some are isolated, while others, typically smaller, are clustered. In several instances, roughly radial fracture patterns are observed, but in other cases the fractures are irregular. Mounds are found in pits or small impact craters at several sites, often in association with other fractured features. The breadth of the definition also includes some anomalous forms, such as irregular, few-hundred-meter scale raised plateaus with distinct fracturing.

This breadth prevents any feature from being truly typical, but several broad categories are observed. Fractured mounds in the Southern Hemisphere are generally found on the floors of multi-kilometer diameter impact craters, often with gullied walls. This group includes both isolated mounds (e.g., Fig. 1) and clusters of fractured features. A group of flat-topped mounds in Utopia Planitia displays distinct summit fracturing, often radially oriented, and is often found

Figure 1. Fractured mound in HiRISE image PSP_007522_1480. The mound is approximately 100 m across and lies on the floor of an impact crater with gullied walls. Illumination is from the right and north down in this non-map-projected image.

in conjunction with irregular mounds in small craters. A third major class encompasses those mounds found on lineated valley fill. These are often irregular or degraded and, in some cases, may include remnants of a mantling deposit.

Fractured mound distribution

Despite the scope of the definition, the mounds exhibit notable latitudinal control. They are generally found between 30°–45° in each hemisphere. The distribution also exhibits some longitudinal variation; fractured mounds are generally absent from the volcanic provinces of Tharsis and Elysium, although some portion of this variation may be due to biases in HiRISE image coverage, which is concentrated over certain areas.

Discussion

Fractured mounds are a broad category, which may include features of multiple origins. The apparent latitudinal control suggests that these features have origins related to water or ice activity, particularly since the latitude bands of the mounds are also the locations of other water- or ice-related features (e.g., Milliken et al. 2003).

Several of the fractured mounds appear to be very good morphological analogues for terrestrial pingos, particularly the isolated examples near the base of gullied slopes. Since gullies may indicate shallow groundwater outflow (Mellon & Phillips 2001), these could be similar to hydraulic pingos. In other cases, a pingo-like origin is less likely: at least some of the mounds on lineated valley fill may be degraded impact craters with inverted relief (Mangold 2003) or eroding mantling material. The mounds in Utopia Planitia are morphologically similar to pingos in several ways, including scale and (frequently) distinct radial fractures, but often have distinctly trapezoidal profiles and are found in level terrain rather than in depressions or at the base of slopes.

The possible effects of different Martian conditions on morphology complicate interpretation. Different processes could produce similar resulting landforms, and Mars may have a different range of ground ice processes than Earth. However, the mounds discussed here include the best morphological analogues for pingos yet observed on Mars. Further coverage from HiRISE will clarify the range of morphologies and settings and allow more detailed analysis of formation mechanisms.

Acknowledgments

We thank the HiRISE science and operations teams for their work in producing outstanding images and the MRO project for support.

References

Burr, D.M., Soare, R.J., Wan Bun Tseung, J.-M. & Emery, J.P. 2005. Young (late Amazonian), near-surface, ground ice features near the equator, Athabasca Valles, Mars. *Icarus* 178(1): 56-73.

Cabrol, N.A., Grin, E.A. & Pollard, W.H. 2000. Possible frost mounds in an ancient Martian lake bed. *Icarus* 145: 91-107.

Dundas, C.M., Mellon, M.T., McEwen, A.S., Lefort, A., Keszthelyi, L.P. & Thomas, N. 2008. HiRISE Observations of fractured mounds: Possible Martian pingos. *Geophysical Research Letters* 35(4): L04201.

Farrand, W.H., Gaddis, L.R. & Keszthelyi, L. 2005. Pitted cones and domes on Mars: Observations in Acidalia Planitia and Cydonia Mensae using MOC, THEMIS and TES data. *Journal of Geophysical Research (Planets)* 110(E5): E05005.

Jaeger, W.L., Keszthelyi, L.P., McEwen, A.S., Dundas, C.M. & Russell, P.S. 2007. Athabasca Valles, Mars: A lava-draped channel system. *Science* 317(5845): 1709-1711.

Judson, S. & Rossbacher, L. 1979. Geomorphic role of ground ice on Mars. *NASA Technical Memo 80339*: 229-231.

Malin M.C. & Edgett, K.S. 2000. Evidence for recent groundwater seepage and surface runoff on Mars. *Science* 288(5475): 2330-2335.

Mangold, N. 2003. Geomorphic analysis of lobate debris aprons on Mars at Mars Orbiter Camera scale: Evidence for sublimation initiated by fractures. *Journal of Geophysical Research (Planets)* 108(E4): CiteID 8021.

Martinez-Alonso, S., Jakosky, B.M., Mellon, M.T. & Putzig, N.E. 2005. A volcanic interpretation of Gusev Crater surface materials from thermophysical, spectral and morphological evidence. *Journal of Geophysical Research (Planets)* 110(E1): CiteID E01003.

Mellon, M.T. 1997. Small-scale polygonal features on Mars: Seasonal thermal contraction cracks in permafrost. *Journal of Geophysical Research* 102(E11): 25,617-25,628.

Mellon, M.T. & Phillips, R.J. 2001. Recent gullies on Mars and the source of liquid water. *Journal of Geophysical Research* 106(E10): 23,165-23,180.

Milliken, R., Mustard, J.F. & Goldsby, D.L. 2003. Viscous flow features on the surface of Mars: Observations from high-resolution Mars Orbiter Camera (MOC) images. *Journal of Geophysical Research (Planets)* 108(E6): CiteID 5057.

Page, D.P. & Murray, J.B. 2006. Stratigraphical and morphological evidence for pingo genesis in the Cerberus plains. *Icarus* 183(1): 46-54.

Parker, T.J., Gorsline, D.S., Saunders, R.S., Pieri, D.C. & Schneeberger, D.M. 1993. Coastal geomorphology of the Martian northern plains. *Journal of Geophysical Research* 98(E6): 11,061-11,078.

Soare, R.J., Burr, D.M. & Wan Bun Tseung, J.-M. 2005. Possible pingos and a periglacial landscape in northwest Utopia Planitia. *Icarus* 174(2): 373-382.

A Soil Freeze-Thaw Model Through the Soil Water Characteristic Curve

Stefano Endrizzi
Department of Civil and Environmental Engineering, University of Trento, Italy
Riccardo Rigon
Department of Civil and Environmental Engineering, University of Trento, Italy
Matteo DallAmico
Department of Civil and Environmental Engineering, University of Trento, Italy

Introduction

The mathematical description of the freeze-thaw behavior of soil mainly depends on its texture. Usually coarse-grained soils follow a moving boundary with phase change, commonly referred to as the *Stefan problem*, whereas fine-grained soils show the existence of a "frozen-fringe" (Fowler & Krantz 1994) of partially frozen soil between frozen and unfrozen regions. Therefore, the possibility of including the freezing characteristic of soil in a model (Hansson et al. 2004) appears promising, as it allows the description of the freezing/thawing cycles of natural soils.

The goal of this work is to propose a freezing soil scheme based on soil freezing characteristic curves and to test it against the analytical solution of the Neumann problem.

The Freeze-Thaw Model

The freezing soil model can be explained by the following equations:

$$\begin{cases} C_T \dfrac{\partial T}{\partial t} + L_f \dfrac{\partial W}{\partial t} = \dfrac{\partial}{\partial z}\left(\lambda_T \dfrac{\partial T}{\partial z} \right) \\ \rho_w \dfrac{\partial \theta_w}{\partial t} = -\rho_i \dfrac{\partial \theta_i}{\partial t} = \dfrac{\partial W}{\partial t} \end{cases} \tag{1}$$

The first term represents the energy budget equation where θ_w and θ_i (-) are the volumetric content of water and ice, respectively; n is the porosity, ρ_w and ρ_i (Kg/m^3) are the density of water and ice, respectively; W (Kg/m^3) is the quantity of water in the control volume subject to phase change; L_f (J/Kg) is the latent heat of fusion; T (°C) is the temperature; and z (m) is the soil depth coordinate. $C_T=C_s(1-n)+c_w\theta_w\rho_w+c_i\theta_i\rho_i$ (J m^{-3} K^{-1}) is the total thermal capacity of the soil, where C_s is the volumetric heat capacity of the soil, and c_w and c_i, the mass heat capacity of liquid and ice, respectively. $\lambda_T=K_e(\lambda_s^{(1-n)}\lambda_w^{\theta w}\lambda_i^{\theta i})+(1-K_e)\lambda_{dry}$ (W m^{-1} K^{-1}) represents the thermal conductivity of the soil matrix and follows the formulation of Farouki (1981), where λ_s, λ_w, and λ_i are the thermal conductivities of soil, water, and ice, respectively; λ_{dry} is the thermal conductivity of the dry soil (Johansen 1975); and K_e is the Kersten number.

The second equation in (1) is a closure relation and is usually known as the "no flow condition"; that is, the water flux during phase change may be neglected (Fuchs et al. 1978). The left-hand side (LHS) of the second equation represents the freezing/thawing rate and may be described by proper equilibrium and closure relations as follows:

$$\begin{cases} \dfrac{1}{g} \cdot \dfrac{p_w}{\rho_w} = \dfrac{L_f \cdot T}{g \cdot 273.15} = \psi_{eq}(T) \\ \dfrac{\theta_w - \theta_r}{(n - \theta_r)} = \left[1 + \left(-\alpha \cdot \psi_{eq} \right)^{\beta} \right]^{\left(1-\frac{1}{\beta}\right)} \end{cases} \tag{2}$$

The first equation represents the thermodynamic equilibrium during phase change, when pressure head ψ (m) and T (°C) satisfy the Clapeyron equation (Christoffersen & Tulazczyk 2003). The second equation represents the unsaturated soil condition by using the soil water characteristic curve (SWCC) according to the Van Genuchten (1980) model, where α (m^{-1}) and β (-) are Van Genuchten parameters and θ_r is the residual water content.

Eventually, the allowed unfrozen water content can be plotted against the temperature, and becomes the soil freezing characteristic curve (SFCC) (see Fig. 1). Applying the chain rule to $\partial\theta_w/\partial t=\partial\theta_w/\partial\psi \bullet \partial\psi/\partial T \bullet \partial T/\partial t$ the first equation in (1) may be rewritten as:

$$\left[C_T + \rho_w C_H \frac{L^2 f}{g \cdot 273.15} \right] \frac{\partial T}{\partial t} = \frac{\partial}{\partial z}\left(\lambda_T \frac{\partial T}{\partial z} \right) \tag{3}$$

where $C_H=\partial\theta_w/\partial\psi$ (m^{-1}) is the hydraulic capacity of the soil. The term in squared brackets is often referred to as the *apparent heat capacity* (Williams & Smith 1989) and accounts for both sensible and latent heat capacity of soils.

The numerical scheme

The numerical model follows a finite difference discretization with a Crank Nicholson scheme. At the first iteration, the system is solved neglecting phase change in order to calculate the temperature at the time step $k+1$ (T^{k+1}): if $T^{k+1}<0$ or $\theta_i>0$, then the freezing soil module is activated. Given the unfrozen water content θ_u^{eq} at the equilibrium, four alternatives may occur: (a) $T^{k+1}<T^k$ and $\theta_u>\theta_u^{eq}$: cooling soil and excess water content; (b) $T^{k+1}>T^k$ and $\theta_w>\theta_w^{eq}$: warming soil and excess water content; (c) $T^{k+1}<T^k$ and $\theta_u<\theta_u^{eq}$: cooling soil and defect water content; and (d) $T^{k+1}>T^k$ and $\theta_u<\theta_u^{eq}$: heating soil and defect water content. If the current point does not lay on the curve, it has to be moved to equilibrium curve. Under the alternatives (a) and (d) a vertical path at constant temperature is followed, where the unknown in the energy budget equation becomes W, that is, the water to be frozen/thawed to reach equilibrium. Under the alternatives (b) and (c), a horizontal path at constant θ_u is followed, and

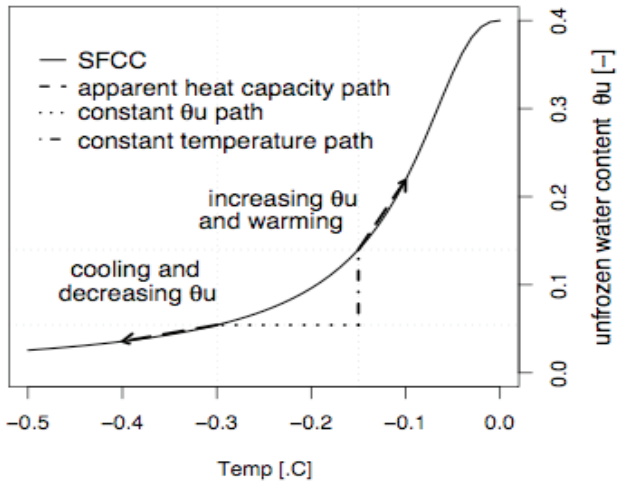

Figure 1. Soil freezing characteristic curve (SFCC) and paths for freezing and thawing calculations.

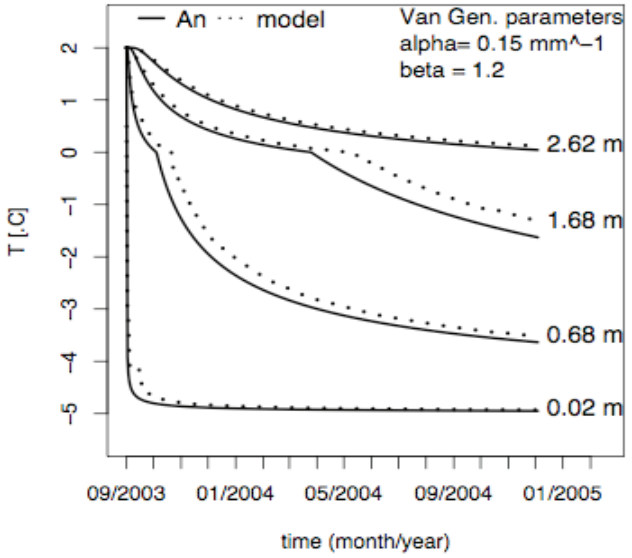

Figure 2. A comparison between the model and the analytical solution at various depths.

the unknown is the temperature T_{eq} at the equilibrium. When the equilibrium curve is reached, the model follows the curve with linearized paths using the apparent heat capacity formulation.

Application

The model has been tested against the Neumann problem, a simple case of a moving boundary. Nakano and Brown (1971), following the approach described by Carslaw and Jaeger (1959) for a homogeneous substance, give the analytical solution of an initially frozen soil bound to a constant Dirichlet boundary condition at the top. We applied the same formulation to a saturated soil initially thawed at an initial temperature T_i=2°C, and later forced to a freezing boundary condition T_s=-5°C at the surface.

The results in Figure 2 show that the model follows the analytical solution at the surface, whereas at depths, a little delay is maintained in the frozen part of the curve, progressively increasing with depth. As the same thermal parameters (conductivity and capacity) are given both to the analytical solution and to the model, it seems that the uncertainty relies on the choice of the Van Genuchten parameters, upon which depends the unfrozen water content and the apparent heat capacity. Further investigations are being taken at present to evaluate the influence of these parameters through a sensitivity analysis.

Conclusions

This work describes a new freezing soil paradigm based on the soil freezing characteristic curves. The model, tested against the analytical solution of the Neumann problem with a moving boundary, seems to be very sensitive to the Van Genucthen parameters and therefore to the shape of the SFCC.

References

Carslaw, H.S. & Jaeger, J.C. 1959. *Conduction of Heat in Solids*. Oxford: Clarendon Press.

Christoffersen, P. & Tulaczyk, S. 2003. Response of subglacial sediments to basal freeze-on: 1. Theory and comparison to observations from beneath the West Antarctica Ice Sheet. *J. Geophys. Res.* 108: 2222.

Farouki, O.T. 1981. The thermal properties of soils in cold regions. *Cold Regions Sci. and Tech.* 5: 67-75.

Fowler, A.C. & Krantz W.B. 1994. A generalized secondary frost heave model. *SIAM Journal on Applied Mathematics* 54(6): 1650-1675

Fuchs, M., Campbell, G.S. & Papendick, R.I. 1978. An analysis of sensible and latent heat flow in a partially frozen unsaturated soil. *Soil Sci. Soc. Am. J.* 42(3): 379-385.

Hansson, K. et al 2004. Water flow and heat transport in frozen soil: Numerical solution and freeze-thaw applications. *Vadose Zone Journal* 3(2): 693-704.

Johansen, O. 1975. *Thermal Conductivity of Soils.* Ph.D. dissertation. Trondheim: Norwegian Technical Univ.

Nakano, Y. & Brown, J. 1971. Effect of a freezing zone of finite width on the thermal regime of soils. *Water Resources Research* 5: 1226-1233.

Van Genuchten, M.Th. 1980. A closed-form equation for predicting the hydraulic conductivity of unsaturated soils. *Soil Sci. Soc. Am. J.* 44: 892-898.

Williams, P.J. & Smith, M.W. 1989. *The Frozen Earth: Fundamentals of Geocryology*. Cambridge: Cambridge University Press.

Mapping and Modeling the Distribution of Permafrost in the Nordic Countries

Bernd Etzelmüller, Herman Farbrot, Ole Humlum
University of Oslo, Norway
Hanne Christiansen, Håvard Juliussen
The University Centre in Svalbard, Norway
Ketil Isaksen
Norwegian Meteorological Institute, Norway
Thomas V. Schuler
Norwegian Water and Energy Directorate and University of Oslo, Norway
Rune S. Ødegård
University College of Gjøvik, Norway
Hanne Ridefelt
University of Uppsala, Sweden

Introduction

In the Nordic countries (Norway including Svalbard, Sweden, Finland, and Iceland) permafrost is widespread and ranges from continuous permafrost in Svalbard, to widespread discontinuous permafrost in high-mountain regions of Iceland and the Scandes, to isolated patches related to palsas, especially in Iceland and northern Scandinavia. Numerous studies exist, especially in Norway and Svalbard, addressing the distribution and thermal regime of permafrost. Here we present the status of permafrost mapping for the Nordic countries, present a map including new borehole information, and draw lines to actual monitoring programmes (TSP NORWAY – Thermal state of permafrost IPY project) and numerical modeling projects (CRYOLINK).

The Regional Nordic Permafrost Map

As a basis, a simple climate-permafrost relationship has been used to generate a permafrost map of the Nordic countries (Fig. 1). The approach used the relation of gridded mean annual air temperature (1961–90, MAAT) values to permafrost existence, not considering snow conditions and topographic heterogeneity (Etzelmüller et al. 2007). The resulting permafrost distribution was compared with observations in the different regions in Norway, Sweden, and Iceland (e.g., Isaksen et al. 2002, Heggem et al. 2005, Farbrot et al. 2008, Ridefelt et al. in press, Etzelmüller et al. 2007). All validation showed that the general permafrost pattern is well reproduced, indicating a decrease in the lower permafrost limit from west to east in Scandinavia. In Iceland, a southwards increase in altitude of the permafrost limit is due to more maritime and snow-rich conditions in southeastern Iceland.

Borehole Information – The TSP NORWAY Project

Boreholes for ground thermal monitoring exist especially in Norway and Iceland. The deepest boreholes down to 130 m

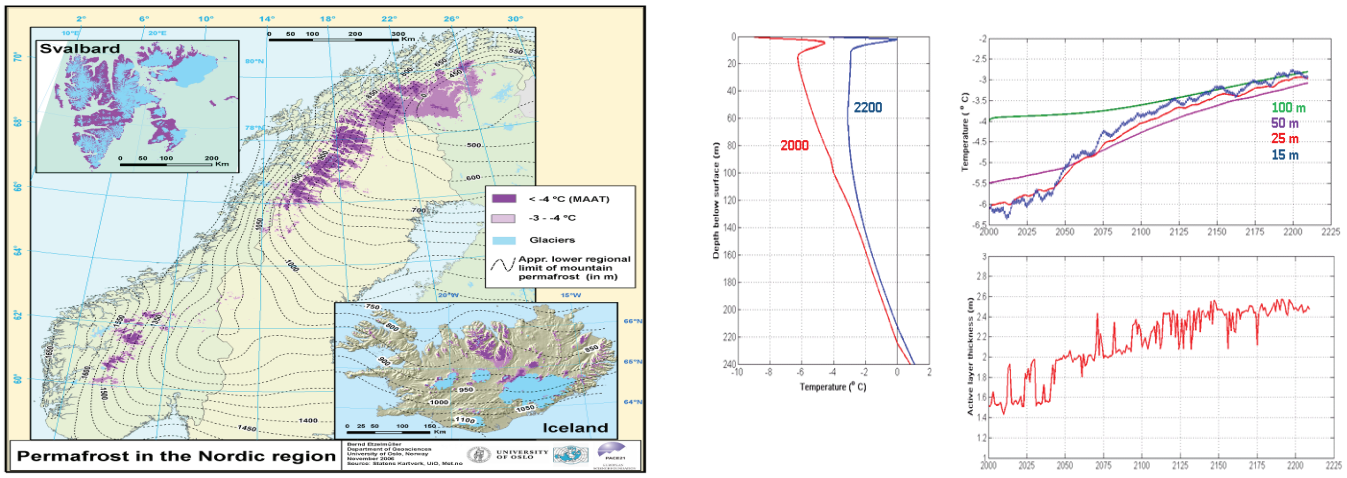

Figure 1. Left: Map of mean annual air temperatures, indicating permafrost distribution in the Nordic countries. This study uses this map as a basis. Information about local permafrost mapping and ground temperature recordings will be added. Right: Projected ground temperatures and active layer depth on Jansonhaugen, Svalbard. A 1D heat-flow model was calibrated based on borehole temperatures, and forced by monthly air temperatures generated from the Hadley Center 1B scenario, down-scaled to Longyearbyen (REGCLIM, e.g., Hanssen-Bauer et al. 2005).The initialization and calibration was based on ground temperature measurements in a borehole (100 m) and extrapolation with depth. Left inlet: Start condition and simulated temperature at end of simulation run. Upper right: Temperature development in various depths. Lower left: Modeled active layer thickness development.

are related to the European PACE project, which commenced in 1997 (Harris et al. 2001). Several shallow boreholes are drilled using nationally funded projects, such as the ongoing IPY project TSP NORWAY (Permafrost Observatory Project: A Contribution to the Thermal State of Permafrost in Norway and Svalbard) (Christiansen et al. NICOP extended abstract), the long-term monitoring programme on Dovrefjell, southern Norway (Sollid et al. 2003), and the currently finished project "Mountain permafrost in Iceland" (Farbrot et al. 2007). All boreholes will be shown on the map, and key parameters will be indicated (average active layer depth, TTOP temperature, ground and surface air temperatures). Furthermore, selected ground temperature profiles will be given as inlets.

Inlet Maps of Local Permafrost Studies

In addition to the regional map, inlet maps are provided to display permafrost distribution in local settings. These maps comprise the areas of Jotunheimen, Dovrefjell (Isaksen et al. 2001, 2002) and Sølen-Elgå (Heggem et al. 2005) in southern Norway, the Gaissane Mountains in northern Norway (Farbrot et al. 2008), and the Abisko area in Sweden (Ridefelt et al. in press). These larger scaled maps are compiled from multiple logistic regressions of BTS measurements or GIS-based multi-criteria analysis (MCA).

Future Permafrost Modeling – The CRYOLINK Project

Regional spatial modeling in mountains until now mainly used empirical or statistical modeling approaches (Riseborough et al. 2008). A newly started project funded by the Norwegian Research Council aims to apply existing and develop new numerical modeling tools to address the near-surface heat transfer processes, the spatial distribution of surface and ground temperatures, and the seasonal ground thaw and freeze. As a first step we use a 1D heat flow model on the PACE borehole located at Janssonhaugen, Svalbard (Isaksen et al. 2001) to address thermal responses in the ground to atmospheric forcing. An example is given in Figure 1. Furthermore, the project aims to establish appropriate relations, describing the influence of snow and vegetation (surface offset) and ground type (thermal offset) for the near-surface energy exchange processes as a basis for further spatial modeling of permafrost and seasonal frost. The Norwegian Water and Energy Directorate and the Norwegian Meteorological Institute have developed gridded air temperature and snow data (daily, ground resolution 1 km), enabling the calculation of *N*-factors, GST, TTOP, and permafrost thickness in space. The project's ultimate aim is to develop a spatially distributed model which yields spatial information of ground surface temperatures, ground temperatures, active layer thickness and timing, and seasonal ground freezing depth and duration, as a response to past and future climate changes.

References

Etzelmüller, B., Farbrot, H., Guðmundsson, Á., Humlum, O., Tveito, O.E. & Björnsson, H. 2007. The regional distribution of mountain permafrost in Iceland, *Permafrost and Periglacial Processes* 18: 185-199.

Farbrot, H., Etzelmüller, B., Gudmundsson, A., Schuler, T.V., Eiken, T., Humlum, O. & Björnsson, H. 2007. Thermal characteristics and impact of climate change on mountain permafrost in Iceland. *Journal of Geophysical Research* 112: F03S90, doi:10.1029/2006JF000541.

Farbrot, H., Etzelmüller, B. & Isaksen, K. 2008. Present and Past Distribution of Mountain Permafrost in Gaissane Mountains, Northern Norway. *Proceedings of the Ninth International Conference on Permafrost, Fairbanks, Alaska, 29 June–3 July 2008.*

Hanssen-Bauer, I., Achberger, C., Benestad, R.E., Chen, D. & Forland, E.J. 2005. Statistical downscaling of climate scenarios over Scandinavia. *Climate Research* 29: 255-268.

Harris, C., Haeberli, W., Vonder Mühll, D. & King, L. 2001. Permfrost monitoring in the high-mountains of Europe: the PACE project in its global context. *Permafrost and Periglacial Processes* 12: 3-12.

Heggem, E.S.F., Juliussen, H. & Etzelmüller, B. 2005. The permafrost distribution in central-eastern Norway. *Norsk Geografisk Tidskrift* 59: 94-108.

Isaksen, K., Hauck, C., Gudevang, E., Ødegård, R.S. & Sollid, J.L. 2002. Mountain permafrost distribution on Dovrefjell and Jotunheimen, southern Norway, based on BTS and DC resistivity tomography data. *Norsk Geografisk Tidsskrift* 56: 122-136.

Isaksen, K., Holmlund, P., Sollid, J.L. & Harris, C. 2001. Three deep alpine permafrost boreholes in Svalbard and Scandinavia. *Permafrost and Periglacial Processes* 12: 13-26.

Ridefelt, H., Etzelmuller, B., Boelhouwers, J. & Jonasson, C. in press. Mountain permafrost distribution in the Abisko region, sub-Arctic northern Sweden. *Arctic. Antarctic and Alpine Research.* Submitted.

Riseborough, D., Etzelmuller, B., Gruber, S., Marchenko, S. & Shiklomanov, N.I. 2008. Space, time, and permafrost: Recent advances in permafrost modeling. *Permafrost and Periglacial Processes.* Submitted.

Sollid, J.L., Isaksen, K., Eiken, T. & Ødegård, R.S. 2003. The transition zone of mountain permafrost on Dovrefjell, southern Norway. *Proceedings of the Eighth International Conference on Permafrost, Zurich, Switzerland*: 1085-1090.

First Results of Ground Surface Temperature Modeling in Finnmark, Northern Norway

Herman Farbrot
Department of Geosciences, University of Oslo, Norway and Norwegian Meteorological Institute, Oslo, Norway
Bernd Etzelmüller
Department of Geosciences, University of Oslo, Norway
Ketil Isaksen
Norwegian Meteorological Institute, Oslo, Norway
Thomas V. Schuler
Norwegian Water Resources and Energy Directorate, Oslo, Norway
Ole Einar Tveito
Norwegian Meteorological Institute, Oslo, Norway
Hanne H. Christiansen
The University Centre in Svalbard, Longyearbyen, Norway

Introduction

The main objective of the Norwegian IPY project "Permafrost Observatory Project: A Contribution to the Thermal State of Permafrost in Norway and Svalbard" (TSP NORWAY) (http://www.tspnorway.com) is to measure and model the distribution of permafrost in northern Norway and Svalbard, as well as to assess its thermal state, thickness, and influence on periglacial landscape-forming processes.

The inner part of Finnmark (Fig. 1), the northernmost county of mainland Norway, is a plain, having strong

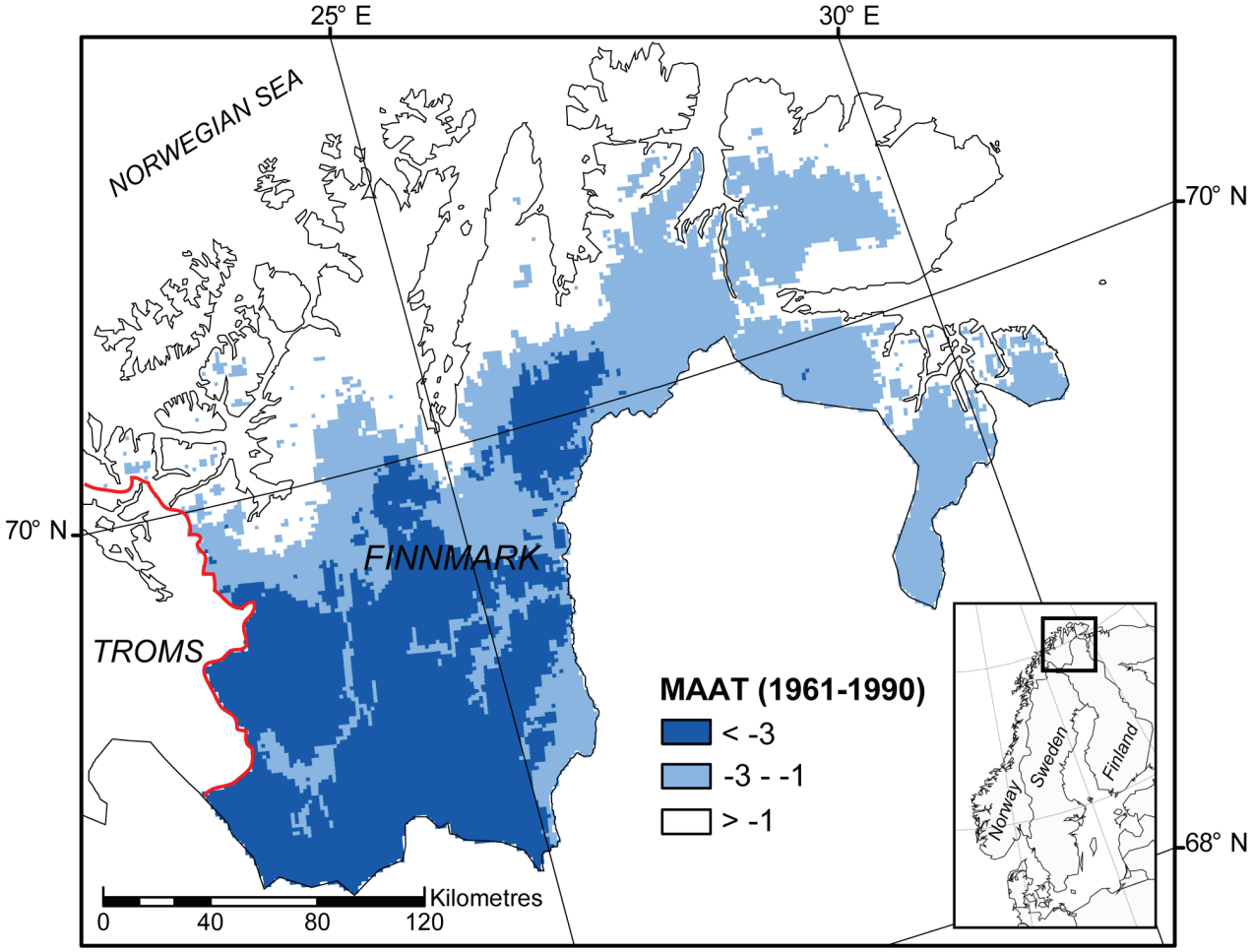

Figure 1. Location map showing three classes of mean annual air temperature (MAAT, 1961–1990) in Finnmark (based on Tveito et al. 2000). The dark grey shows areas where MAAT is lower than -3°C, light grey shows areas where MAAT is between -3°C, and -1°C, and white is MAAT higher than -1°C.

continentality and the lowest MAAT when reduced to sea level in Norway. Typically in this area MAAT is -2.5°C to -4°C, with mean summer temperature of 8°C to 10°C and mean winter temperature -15°C to -20°C. In winter, mean maximum snow depth is 25–75 cm. The current knowledge on the extent and the thermal conditions of permafrost is scarce (Isaksen et al. 2008). Thawing of permafrost in this area may lead to subsidence of the ground surface, having a substantial impact on, for example, the stability of mountain slopes and infrastructure. It is important, therefore, to delineate the distribution of permafrost.

Modeling the Distribution of Mountain Permafrost

Regional permafrost modeling in southern Norway has so far been based on maps of gridded mean annual air temperature (MAAT), indicating permafrost as probable in non-glaciated mountain areas where MAAT is below -3°C (Etzelmüller et al. 1998, 2003). This crude approach does not take into consideration the effects of the uneven thickness and timing of the winter snow cover as well as the vegetation cover. In Finnmark, permafrost is presumably absent in large forested areas although MAAT < -3°C (Isaksen et al. 2008). The reason is the influence of the forest, where more snow is accumulated than at wind-exposed locations. The low thermal conductivity of snow efficiently insulates the ground surface from the atmosphere at locations having considerable snow cover. Aiming for a better spatial representation of ground temperature and, thus, permafrost conditions in Finnmark, ongoing work elaborates on the connection between MAAT and mean annual ground surface temperature (MAGST) through the Canadian "temperature at the top of permafrost" (TTOP) model. The TTOP model uses seasonal *n*-factors and air temperatures to model MAGST, and a ratio of thawed-to-frozen conductivity of the ground to model the average TTOP (Smith & Riseborough 2002). In a first step, we derive seasonal *n*-factors based on records of air and ground surface temperatures for different land cover and of snow parameters. As input to a regional MAGST model, we use a land-cover map of Finnmark and gridded data of snow thickness and freezing and thawing degree-days sum of air at a resolution of 1 × 1 km. This poster presents first results of this ground surface temperature modeling.

References

Etzelmüller, B., Berthling, I. & Sollid, J.L. 1998. The distribution of permafrost in Southern Norway; a GIS approach. *Proceedings of the Seventh International Conference on Permafrost, Quebec, PQ, Canada*, Centre d'Etudes Nordiques, Universite Laval, Collection Nordicana 57: 251-257.

Etzelmüller, B., Berthling, I. & Sollid, J.L. 2003. Aspects and concepts on the geomorphological significance of Holocene permafrost in southern Norway. *Geomorphology* 52: 87-104.

Isaksen, K., Farbrot, H., Blikra, L.H. & Sollid, J.L. 2008. Five year ground surface temperature measurements in Finnmark, Northern Norway. *Proceedings of the Ninth International Conference on Permafrost, Fairbanks, Alaska, 29 June–3 July 2008*.

Smith, M.W. & Riseborough, D.W. 2002. Climate and the limits of permafrost: A zonal analysis. *Permafrost and Periglacial Processes* 13: 1-15.

Tveito, O.E., Førland E.J., Heino, R., Hanssen-Bauer, I., Alexandersson, H., Dahlström, B., Drebs, A., Kern-Hansen, C., Jónsson, T., Vaarby-Laursen, E. & Westman, Y. 2000. Nordic Temperature Maps. *DNMI Klima 9/00 KLIMA*, 54 pp.

Historical Changes in the Seasonally Frozen Ground Regions of the Russian Arctic

Oliver W. Frauenfeld, Tingjun Zhang, Andrew J. Etringer, Roger G. Barry
CIRES National Snow and Ice Data Center, University of Colorado, Boulder, Colorado, USA
David Gilichinsky
Soil Cryology Laboratory, Institute of Physico-Chemical and Biological Problems in Soil Sciences, Russian Academy of Sciences, Pushchino, Moscow Region, Russia

Introduction

Seasonal freezing and thawing processes in cold regions play an important role in ecosystem diversity, productivity, and the Arctic hydrological system (Hinzman et al. 1991, Kane et al. 1991, Woo 1992, Osterkamp et al. 2000, Nelson 2003). Long-term changes in seasonal freeze and thaw depths are also useful indicators of climate change (Frauenfeld et al. 2004). However, only sparse historical measurements of seasonal freeze and thaw depths are available for permafrost and seasonally frozen ground regions. In previous work, we applied mean monthly soil temperature data for 1930–1990 at 242 sites located throughout Russia, and employed a simple interpolation scheme to determine the depth of the 0°C isotherm based on soil temperature data measured at 13 depths between 0.2 m and 3.2 m. The relationship between available observed annual maximum freeze and thaw depths and our interpolated values indicates a perfect correlation, and thereby verifies our methodology (Frauenfeld et al. 2004).

In this analysis, we improve on our previous work by employing a greatly expanded station database with soil temperatures for 423 sites with updated observations through the year 2000. These 423 stations are located throughout Russia (Fig. 1) and can be obtained from the Frozen Ground Data Center (http://nsidc.org/fgdc/). The addition of 181 sites throughout the Russian Arctic combined with 10 more years of observations allows for a significantly more comprehensive evaluation. Furthermore, the addition of 1991–2000 allows us to quantify changes in the soil thermal regime during a decade when accelerated climate warming has potentially occurred.

Data and Methods

Detailed descriptions of soil temperature measurements in the former Soviet Union were provided by Gilichinsky et al. (1998), by Zhang et al. (2001), and in the instruction manuals of the State Committee of the U.S.S.R. for Hydrometeorology and Environmental Control (1985). Observations are available for the 0.2 m, 0.4 m, 0.6 m, 0.8 m, 1.2 m, 1.6 m, 2.0 m, 2.4 m, and 3.2 m depths. We linearly interpolated the depth of the 0ºC isotherm throughout the 0.2 m–3.2 m temperature profile (recognizing that this is not necessarily the same as the "true" freeze/thaw depth). The 423 stations were first classified as either permafrost or seasonally frozen ground, depending on soil temperature at the 3.2 m depth. If, for the entire record, a station's soil temperature at 3.2 m was positive, that station was classified as a seasonally frozen ground station; 387 of the 423 stations qualified. We also employ kriging to improve data quality and in-fill missing observations, and produce nearly continuous station time series for 1930–2000. For the seasonally frozen ground stations, the freeze depth was interpolated between those layers where the temperature switched from negative to positive. The maximum depth of freezing was selected from the months of March, April, and May only. An average time series was generated by averaging all available stations' maximum annual freezing depth departures (with respect to each station's long-term mean) in the seasonally frozen ground region of the Russian Arctic. Linear least-squares regression was then applied to the time series to quantify its long-term changes.

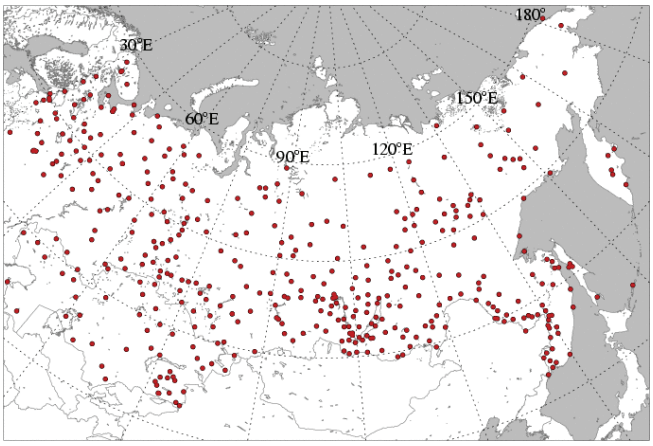

Figure 1. Location of the 428 soil temperature observing sites in Russia.

Results and Discussion

In our previous work the long-term trend for the 1930–1990 period based on 211 seasonally frozen ground stations indicated a decrease in seasonal freeze depths of approximately 4.4 cm decade^{-1}, or 27 cm overall (Fig. 2). This trend is statistically significant (95%-level). However, because prior to the mid-1950s there were too few stations to produce a robust trend (Fig. 2), this 27 cm change had to be interpreted cautiously. Based on the 1956–1990 period, when 100 or more stations contribute to each year's mean value, the overall change is approximately -34 cm (not shown). Note that while a total of 211 stations were available to generate the time series, a maximum of 158 stations contribute at any given year, as most individual station time series are incomplete and have gaps due to missing data.

With the addition of 176 new sites in seasonally frozen ground regions, more data for the original 211 sites, and

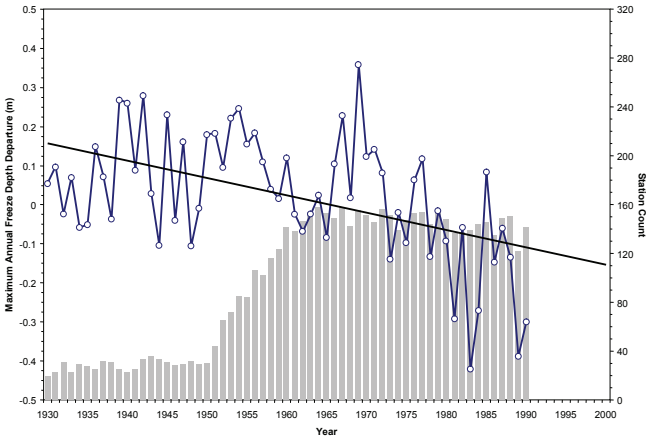

Figure 2. Mean 1930–1990 time series, based on a total of 211 stations, of the maximum annual freeze depth departures. Included also is the linear trend (-4.4 cm decade^{-1}). The number of stations contributing to each year's mean value is indicated by the grey bars.

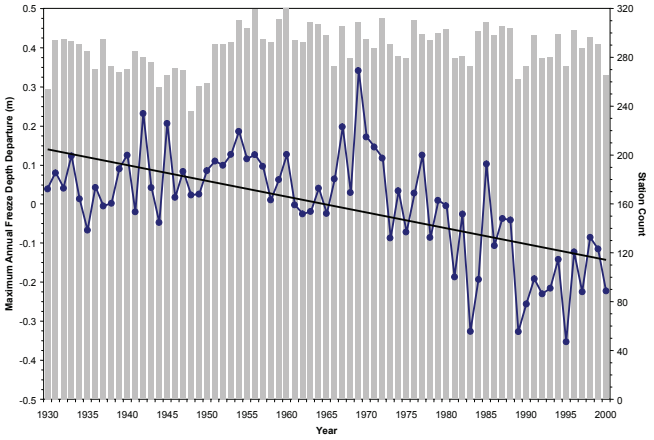

Figure 3. Mean 1930–2000 time series, based on a total of 387 stations, of the maximum annual freeze depth departures. Included also is the linear trend (-4.0 cm decade^{-1}). The number of stations contributing to each year's mean value is indicated by the grey bars.

our kriging efforts, we are now able to provide much more robust trend estimates. As shown in Figure 3, up to 320 (of the total 387) stations now contribute to each year's mean freeze depth departure. For the same period as shown in Figure 2, 1930–1990, the trend indicates a decrease of only 17 cm in seasonal freeze depth (not shown). It appears as if the early period prior to 1956 indeed biased our long-term trend estimation in our earlier work. However, the 1956–1990 trend, based on these more complete data, shows an overall decrease of 48 cm. This change is 30% greater than previously reported in Frauenfeld et al. (2004).

The overall change for the 71-year period from 1930–2000 is a statistically significant (95%-level) -4.0 cm decade^{-1}, or an overall decrease of 29 cm (Fig. 3). Interestingly, this time series also indicates some patterns of interdecadal variability (and we need to exercise caution, therefore, in applying linear regression). Freeze depths actually increased slightly until ~1970, followed by a sharp decrease until ~1990. From 1990 on, freeze depths may actually be increasing again. In our ongoing efforts, we are trying to establish the degree to which these interdecadal patterns are real or potentially caused by changes in the amount and quality of available data.

Acknowledgments

This work was funded by the U.S. National Science Foundation under grants ARC-0612431, OPP-0229766, and OPP-0352910, and the International Arctic Research Center, University of Alaska Fairbanks, under the auspices of the NSF cooperative agreement number OPP-0327664.

References

Frauenfeld O.W., Zhang, T., Barry, R.G. & Gilichinsky. D. 2004. Interdecadal changes in seasonal freeze and thaw depths in Russia. *J. Geophys. Res.* 109: D05101, doi:10.1029/2003JD004245.

Gilichinsky, D.A. et al. 1998. A century of temperature observations of soil climate: Methods of analysis and long-term trends. In: A.G. Lewkowicz & M. Allard (eds.), *Proceedings of the 7th International Conference on Permafrost*, Ste.-Foy, Canada: Centre d'Études Nordiques, Université Laval, 313-317.

Hinzman, L.D., Kane, D.L, Gieck, R.E. & Everett, K.R. 1991. Hydrologic and thermal properties of the active layer in the Alaskan Arctic. *Cold Reg. Sci. Technol.* 19: 95-110.

Kane, D.L., Hinzman, L.D. & Zarling, J.P. 2003. Thermal response of the active layer to climatic warming in a permafrost environment. *Cold Regions Sci. Technol.* 19: 111-122.

Nelson, F.E. 2003. (Un)frozen in time. *Science* 299: 1673-1675.

Osterkamp T.E., Viereck, L., Shur, Y., Jorgenson, M.T. Racine, C., Falcon, L., Doyle, A. & Boone, R.D. 2000. Observations of Thermokarst and its Impact on Boreal Forests in Alaska, U.S.A. *Arct. Antart. Alp. Res.* 32: 303-315.

State Committee of the U.S.S.R. for Hydrometeorology and Environmental Control. 1985. *Instructions for Meteorological Stations and Posts* Vol. 3, Part 1 in Meteorological Observations at Stations, Gidrometeoizdat, Leningrad.

Woo, M.-K. 1992. Impacts of Climatic Variability and Change on Canadian Wetlands. *Can. Water Resour. J.* 17: 63-69.

Zhang, T., Barry, R.G., Gilichinsky, D., Bykhovets, S.S., Sorokovikov, V.A. & Ye. J. 2001. An amplified signal of climatic change in soil temperatures during the last century at Irkutsk, Russia. *Clim. Change* 49: 41-76.

Rock Glaciers in the Kåfjord Area, Troms, Northern Norway

Regula Frauenfelder
Department of Geosciences, University of Oslo, Norway,
currently at Norwegian Geotechnical Institute, Oslo, Norway
Jon Tolgensbakk
Department of Geosciences, University of Oslo, Norway
Herman Farbrot
Department of Geosciences, University of Oslo, Norway
Tom Rune Lauknes
NORUT AS, Forskningsparken, Tromsø, Norway

Introduction

Rock glacier distribution in mainland Norway was inventoried on a macro scale by Sollid & Sørbel (1992). They found that active rock glaciers exist in the high mountain areas of southern and northern Norway, while relict rock glaciers can be found in low-lying areas near the coast of northern Norway and in higher inland areas.

Detailed geomorphological mapping in Troms by Tolgensbakk & Sollid (1988) revealed the existence of more than 100 rock glaciers in the Kåfjord area on the eastern side of Lyngenfjorden. Most of the area lies inside the glacial limit of the Younger Dryas (YD) ice sheet (Andersen et al. 1995), with the youngest YD moraines situated at the valley entrances. Compared to surrounding areas with similar relief and geology, the high frequency of rock glaciers in this region is quite striking. The mapped rock glaciers are mostly of talus-derived origin and are found between the present coastline and the highest mountains in the area (c. 1360 m a.s.l.). Most of the rock glaciers seem to be associated with rockslides caused by neotectonic activity, which was very pronounced in the region during the early Holocene (Tolgensbakk & Kverndal 1995, 1996, Dehls et al. 2000). Due to the general orientation of the main fault (NW–SE trending normal fault, cf. Dehls et al. 2000), the majority of the rock glaciers is concentrated in the sectors SW-W-NW (Fig. 1).

While most of these rock glaciers seem to be relict today, exceptions can be found. Velocity measurements carried out in the early 1990s on one of the rock glaciers showed surface movement in the order of less than 1 cm a^{-1} (Tolgensbakk & Kverndal 1995, 1996). Measurements on this rock glacier, hereafter called Sannjarriep'pi rock glacier, were continued during summer 2006, and the findings are reported in the following.

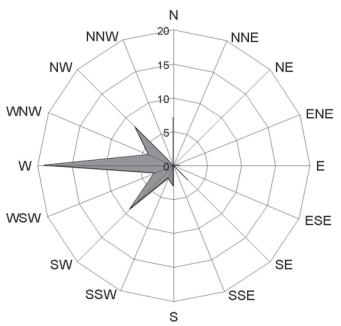

Figure 1. Main aspect of talus-derived rock glaciers in the Kåfjord area (n = 59).

The Sannjarriep'pi rock glacier is situated on the orographic right side of Nordmannvikdalen, a tributary valley to the Lyngenfjord. The rock glacier lies on the western slope of a 1207 m high peak, is approximately 700 m long and 700 m wide, and is situated between 580 and 780 m a.s.l.

Methods

The deformation of Sannjarriep'pi rock glacier was tracked by two different methods: (a) by polar survey using an electronic theodolite (Wild DI 3000 Distomat), and (b) by space-borne Differential SAR interferometry (DInSAR) using ERS SAR imagery covering the period 1992–1999 (e.g., Bamler & Hartl 1999).

For two-dimensional resistivity tomography (ERT) over one of the lobes of the rock glacier, an ABEM Lund multi-electrode, high-resolution 2D resistivity system was used, applying the Wenner configuration (Reynolds 1997).

Miniature temperature data logger devices have been installed at three locations on the rock glacier in summer 2006. These loggers record the ground surface temperature (GST) at shallow depths in a 2 h interval.

Measurements of Schmidt-hammer rebound values—a proxy for rock hardness, that is, the rock weathering degree—were performed on three different transects perpendicular to the central flow line of the rock glacier. Samples for cosmogenic nuclide exposure dating have been taken on two conspicuous ridges and at the front of the rock glacier (see Fig. 2a for location of measurements).

Results

The velocity measurements from summer 2006 show that the lower northern lobe of the Sannjarriep'pi rock glacier has been stagnant during the last 17 years (1989–2006), while the upper southern lobe has been steadily moving with c. 1 to 6 mm a^{-1}; maximum movement is in the order of 10 cm in 17 years. The DInSAR survey confirms these measurements, with maximum displacement values of -4.9 mm a^{-1} for the southern lobe (Fig. 2b).

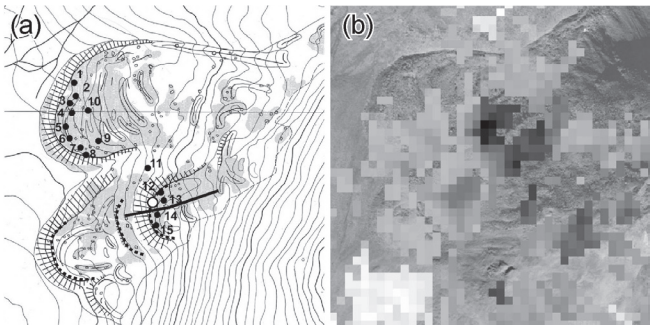

Figure 2. (a) Location of measurements on the Sannjarriep'pi rock glacier: black dots = bolts for terrestrial survey, white dot = location of miniature temperature data loggers, stippled lines = Schmidt-hammer rebound measurement transects, black line = electrical resistivity tomography (ERT) profile. (b) Results of DInSAR measurements: black = -4.9 mm a^{-1}, white = stagnant.

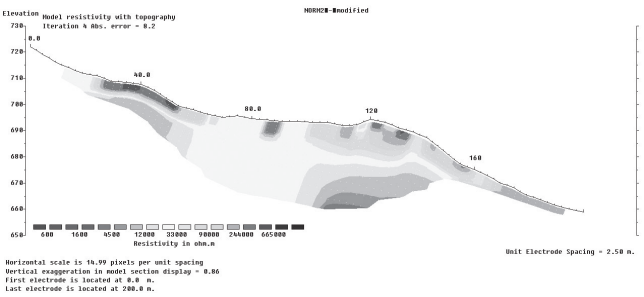

Figure 3. Result of the Electrical resistivity tomography (ERT) measurements. The active layer is highly heterogeneous, characterized by large air voids in the very coarse blocky surface layer. Below the active layer, maximum resistivity values are in the order of 30 to 100 kOhm.m, being indicative for ice.

Mean air temperature at Sørkjosen lufthavn during 2006–2007 was +3.2°C. Applying a lapse rate of -0.005°C/m yields a mean air temperature at the front of the rock glacier (580 m a.s.l.) of c. +0.3°C for the same period. During this period, mean ground surface temperature (GST) on the rock glacier was between +1.0°C (at 10 cm depths, within fine debris) and +1.6°C (below 7 cm thick moss cover on top of large boulder). Mean air temperature measured in an air void of the coarse blocky layer was 1°C (Fig. 4).

The results of the Schmidt-hammer rebound measurements show that the rock glacier is, indeed, a continuous landform with increasing surface age from its source zone (close to the foot of the rock-free face behind it) to its tongue. This result is a prerequisite for the correct interpretation of cosmogenic nuclide exposure dating.

Acknowledgments

Fieldwork has been financially supported by the Department of Geosciences, University of Oslo and the Swiss Academy of Sciences (Reisestipendien in Botanik, Zoologie und Erdwissenschaften). The ERS-1/2 data set is provided by the European Space Agency (ESA) under the project AOALO.3668. Further thanks go to Christian Hauck for his help with the interpretation of the geophysical results and to Trond Eiken for the post-processing of the distance measurements.

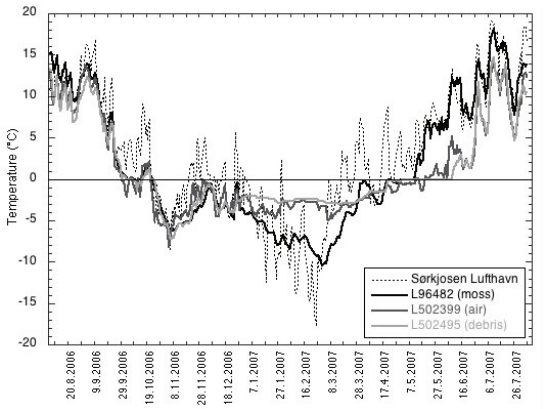

Figure 4. Ground surface temperatures (GST) and air void temperature in the blocky surface layer of the Sannjarriep'pi rock glacier during the period 2006–2007. Air temperature at Sørkjosen Lufthavn, 20 km northeast of Sannjarriep'pi rock glacier is given for comparison.

References

Andersen, B.G., Mangerud, J., Sørensen, R., Reite, A., Sveian, H., Thoresen, M. & Bergstrøm, B. 1995. Younger Dryas ice-marginal deposits in Norway. *Quaternary International* 28: 147-169

Bamler, R. & Hartl, P. 1998. Synthetic aperture radar interferometry. *Inverse Problems* 14: R1.

Dehls, J., Olesen, O., Olsen, L. & Blikra, L.H. 2000. Neotectonic faulting in northern Norway; the Stuoragurra and Nordmannvikdalen postglacial faults. *Quaternary Science Reviews* 19: 1447-1460

Reynolds, J.M. 1997. *An Introduction to Applied and Environmental Geophysics*. Chichester: John Wiley & Sons, 796 pp.

Sollid, J.L. & Sørbel, L. 1992. Rock glaciers in Svalbard and Norway. *Permafrost and Periglacial Processes* 3: 215–220.

Tolgensbakk, J. & Sollid, J.L. 1988. *Kåfjord, kvartærgeologi og geomorfologi,* 1:50,000, 1634 II. Geographical Institute, University of Oslo (map).

Tolgensbakk. J. & Kverndal A.-I. 1995. Fjellskred og steinbreer I Kåfjordområdet, Troms. *Geonytt* 22: 70.

Tolgensbakk. J. & Kverndal A.-I. 1996. Rock glaciers and Neotectonics in the Kåfjord area, North Norway. *Abstracts of the 28th International Geographical Congress*: 471–472.

Snowpack Evolution on Permafrost, Non-Permafrost Soils, and Glaciers in the Monte Rosa Massif (Northwest Alps, Italy)

M. Freppaz
Di.Va.P.R.A. - LNSA, Università di Torino, Grugliasco (TO), Italy
M. Maggioni
Di.Va.P.R.A. - LNSA, Università di Torino, Grugliasco (TO), Italy
S. Gandino
Comando Truppe Alpine - Servizio Meteomont, Bolzano, Italy
E. Zanini
Di.Va.P.R.A. - LNSA, Università di Torino, Grugliasco (TO), Italy

Introduction

Snow cover evolution is governed by several variables, such as meteorological factors, local topography, and snow characteristics. Different types of substrata might present different surface temperatures, influencing therefore the temperature gradient within the snowpack and its evolution.

In non-permafrost soils, a thick early winter snow cover maintains soil temperature close to 0°C, independently from air temperature (Edwards et al. 2007). In permafrost soils, beneath at least a 1 m cover of snow, the ground temperature during February and March is below -2 to -3°C (Haeberli 1973, Hoelzle 1992). For glaciers, less literature exists. Kuhn et al. (1998) found an interface temperature between snow and ice of about -5°C.

The aim of this study is to follow the evolution of the snow cover on three different substrata (permafrost, non-permafrost soils, and glacier) in the Monte Rosa Massif on the Italian Northwest Alps.

Materials and Methods

Study area

The three study sites are located in the area of the Monte Rosa Massif in the northwestern Italian Alps. The permafrost site is at an elevation of 2910 m a.s.l. on a northwest-oriented slope of about 10° of inclination; the non-permafrost site is placed at an elevation of 2900 m a.s.l., on horizontal terrain; and the glacier site is located on Indren Glacier at an elevation of 3400 m a.s.l., with a southwest aspect and about 10° of inclination.

Nivometeorological data

Snow pits were dug periodically, according to the accessibility of the sites, from December 2006 to July 2007: 9 surveys at the permafrost site, 8 surveys at the non-permafrost site, and 6 surveys at the glacier site. Snow temperature was measured every 10 cm with 10 cm long dial stem thermometers. Snow density measurements were made using a 0.5 L stainless steel core in each layer of the snowpack, where also grain type and dimension were recorded. Continuous measurements of the temperature at the interface between snow and the three different substrata have been made through dataloggers (UTL-1).

Meteorological data in the area, such as wind speed and direction, air temperature, and humidity, were registered by an automatic station of the Italian Army (Comando Truppe Alpine-Servizio Meteomont) located at 2901 m a.s.l. near the three sites.

Results and Discussion

In the study area, winter 2006–2007 was characterized by a lack of snow cover in the early winter and relatively high air temperature, with a minimum of -17.9°C recorded on January 26. As in Phillips & Schweizer (2006), the characteristics of the snow cover above the three different substrata are summarized in Table 1 and described briefly in the following sections.

Non-permafrost site

In the non-permafrost site, the maximum snow depth was recorded on April 4 (180 cm), while until the end of February, the amount of snow was less than 80 cm. Seventy-five percent of the snow profiles were weak-based, with a bottom layer of faceted and depth hoar crystals due to the medium-high temperature gradient recorded mainly in the early winter season. The average snow/soil interface temperature was greater than -1°C.

Permafrost site

In the permafrost site, the maximum snow depth was recorded on May 7, greater than in the other two sites. Fifty-six percent of the snow profiles were characterized by faceted and depth hoar crystals, due to the high temperature gradient (recorded especially during March) closely related to the low air temperature, as this site is on a northwest-oriented slope. But 22% of the snow profiles were also characterized by small rounded crystals, typical of an equi-temperature gradient, revealing how the lower ground temperature may induce a lower temperature gradient (Keller & Gubler 1993). The average snow/permafrost interface temperature was -5.1°C, 4.2° colder than the interface temperature between snow and non-permafrost soil.

Glacier site

In the glacier site, the maximum snow depth was recorded on May 16. Except for the last snow profile, the snow cover was characterized by a bottom layer of faceted crystals,

Table 1. Snow cover characteristics for the three sites. Except for snow depth and the snow/substratum interface temperature, the other parameters are average values computed on data from manual snow profiles (N = 8 at non-permafrost site, N = 9 at permafrost site, N = 6 at glacier site).

Parameter	Non-permafrost	Permafrost	Glacier
max snow depth (cm)	180	230	125
grain type in bottom layer of snowpack	5a, 4a	5a, 4a, 3a	4c
maximum grain size in bottom layer (mm)	2.4	1.8	1.7
hand hardness index in bottom layer	1.8	2.2	5.0
snow/substratum interface temperature* (°C)	-0.9	-5.1	-4.8
temperature gradient within the snowpack (°C/m)	-6.5	-7.4	-2.1
density (Mg/m^3)	0.305	0.273	0.389
Effective heat conductivity (W/mK)	0.131	0.116	0.257

* average values computed on data recorded by dataloggers (12/29/2006–04/20/2007).

often well bonded together. The snow hardness was very high (level 5), higher than in the other sites. The average snow/glacier interface temperature was -4.8 °C.

The main differences between the three sites can be summarized in the following points:

• A very hard bottom layer was present on the glacier in respect to a snow hardness of 2 for the other two sites; the assumption is that the cold temperature of the glacier surface together with the high density and low gradient might create good conditions for the snow crystals to bond well together.

• The permafrost and glacier sites presented similar interface temperatures, close to -5°C, before reaching isothermal conditions.

• The average temperature gradient at the glacier site was lower than in the other two sites. The possible reason is that the air temperature was higher, as this site is southwest exposed, resulting then in a lower temperature gradient.

In all the sites, the interface temperature remained constant around a certain value (non-permafrost soil -0.9°C, permafrost -5.1°C, glacier -4.8°C) without great oscillations when the snow cover was deep enough to insulate the substrata.

Conclusions

The main purpose of this work was to analyze the evolution of the snow cover on different substrata to understand if they might generate appreciable differences in the snow cover characteristics.

Our results shows that the main differences in the evolution of the snow cover on permafrost, non-permafrost, and glacier substrata are related to hand hardness in the bottom layer (higher on glacier), snow/substrata interface temperature (higher on non-permafrost soil), and temperature gradient (lower on glacier).

Moreover, an important outcome of this work is that the temperature at the snow/substrata interface remains constant around certain values, without oscillating in relation to air temperature, when enough snow covers the substrata, showing the important insulating effect of the snow.

Acknowledgments

Fot the technical support we thank MonterosaSki, Roberto Cilenti, Corpo Guide Alpine di Alagna Valsesia, Regione Autonoma Valle d'Aosta-Ufficio Neve e Valanghe, Hervè Jaccond, Emil Squinobal, and Antoine Brulport.

References

Edwards, A.C., Scalenghe, R. & Freppaz, M. 2007. Changes in the seasonal snow cover of alpine regions and its effect on soil processes: A review. *Quaternary International* 162-163: 172-181.

Haeberli, W. 1973. Die Basis-Temperatur der winterlichen Schneedecke als morfologischer Indikator fuer die Verbreitung von Permafrost in den Alpen. *Zeitschrift fuer Gletscherkunde und Glazialgeologie* 9: 221–227.

Hoelzle, M. 1992. Permafrost occurrence from BTS measurements and climatic parameters in the Eastern Swiss Alps. *Permafrost and Periglacial Processes* 3: 143-147.

Keller, F. & Gubler, H. 1993. Interaction between snow cover and high mountain permafrost; Murtèl/Corvatsch, Swiss Alps. *Proceedings of the Sixth International Conference on Permafrost, Beijing, China, 5-9 July 1993. Proceedings*. Guangzhou, China: South China University of Technology Press, 1: 332-337.

Kuhn, M., Haslhofer, J., Nickus, U. & Schellander, H. 1998. Seasonal development of ion concentration in a high alpine snow pack. *Atmospheric Environment* 32(23): 4041-4051.

Phillips, M. & Schweizer, J. 2007. Effect of mountain permafrost on snowpack stability. *Cold Regions Science and Technology* 47: 43-49.

Climate Change in Permafrost Regions in North America

Maria K.Gavrilova
Melnikov Permafrost Institute SB RAS, Yakutsk, Russia

Introduction

In North America, permafrost occurs in three-fourths of Alaska, half of Canada, and along the coasts and below ice sheets in Greenland.

Method

Weather station records have been used to analyze climate variations during the last centuries. The method of 10-year moving averages has been used in the analysis, which excludes casual errors.

Results and Discussion

For the Barrow station (the northern coast of Alaska*)* which has a relatively long record spanning from the 1910s to 2000s, the change of air temperature in winter was within the limits of similar values of mean annual temperature for January (-25.8°C) from the 1920s to 1970s. Significant cooling occurred in the 1910s (up to-29°C). Then, intensive warming was observed in the 1970s. The winter air temperature lowered nearly to the long-term average in the 1990s and began to increase again in the 2000s.

Summer temperatures changed less, within the limits of ±1–1.5°C. Warming was observed in the 1920s, cooling in the 1950s, and warming in the 1990s. The mean annual temperature which dictates whether the ground is frozen or unfrozen varied within ±1–1.5°C. Significant warming occurred in the 1930s, cooling was observed from the 1940s through the 1970s, and rapid warming has occurred since the 1990s to the end of the century. The latter warming was due to increases in both winter and summer temperatures observed in the last decades.

For Fairbanks (central Alaska), the length of the record is 20 years shorter than at Barrow. Significant cooling of winter temperatures of up to -30° (the long-term average is -23.2°) in the 1960s–1970s and significant warming in the late 1970s–1980s (up to -19°) are evident. In the 1990s and 2000s, temperatures decreased to the long-term average.

Summer temperatures were lower than the average from the 1930s to 1960s, and have been persistently higher than the average since the 1970s. Mean annual temperatures were below the long-term average of -2.9° prior to the mid 1970s (up to -4°C), and have been higher since the mid 1970s (up to -2°).

St. Bethel (southwestern Alaska) shows nearly the same variations as Fairbanks, but only with a smaller range.

Mt. Washington is situated in southern Alaska, and records are available since 1940. A significant increase in winter temperatures was observed from the mid 1940s to mid 1960s, when temperatures reached -12.5°C, while the long-term mean is -15°. Then, cooling occurred in the 1960s–1980s (up to -17°). This cooling was followed by warming from the mid 1980s to mid 2000s. The last warming, however, was less in magnitude than the warming of the 1950s. Then, temperatures began decreasing again.

Summer temperatures are surprisingly stable, varying within the limits of ±0.5°C. The mean annual temperature also varied more or less stable. Slight warming occurred in the mid 1950s, extended cooling from the mid 1950s–1980s and a steady temperature increase in the 1990s. All these variations were within the range of ±0.5°C.

Unfortunately, in northern *Canada,* meteorological observations were begun later, and recent data, probably, are not published.

At the Alert station located on the most northern extremity of the Canadian Archipelago, observations were apparently begun in the 1950s and ended in the 1990s. During this period, there were two peaks in winter temperatures: a smaller one in the 1950s and a larger one in the 1970s (-29° at the mean of -32°). Then temperatures began to decrease.

Summer temperatures were above the long-term average in the 1950s–1960s and have been below the average since the latter half of the 1980s. There has been a slight increasing trend in recent years. The mean annual temperature varied ±0.5°C.

Along the northern coast of the continent (Aklavik station) there were alternating cold and warm winters within the range of typical variation. Unfortunately, only the data prior to the mid 1960s are available for us.

For the Frobisher Bay station (Baffin Island) data are available from the 1940s to 2000s. Winter warming was observed in the 1960s and the 1980s, similar in magnitude (-24°, while the long-term mean is -26.5°). In the mid 1940s, late 1980s and 1990s, winter temperatures lowered to -29°C.

After significant cooling in the mid 1980s and in the 1990s, summer and mean annual temperatures have increased by 1–1.5°C in the early 2000s.

The longest record for the permafrost region at our disposal is from the Churchill station, where observations began in the 1890s. January temperatures increased significantly in the 1940s and, in similar magnitude, in the 1980s and the 1990s. During these warmer periods, temperatures were -25° to -25.5°, while the long-term average is -27.2°C.

Increases in summer temperature were observed in the second half of the 1930s and in the 1990s. The mean annual temperature increased noticeably during the last decades of the 20th century, having reached -5.5° (the long-term normal is -7°C).

Greenland stations, for which records are available, are situated on the western coast. The longest record is from the

station where observations were started in the 1870s. At the Upernavik station (central coast), significant warming began in the 1920s which reached -13° in 1940 (the long-term average is -19°C). This warming apparently is related to the proximity to the warm Gulf Stream, which had the greatest influence on the stations of Western Europe.

Summer temperature variations are within the range of ±1–1.5°C. Mean annual temperatures varied within ±2°C.

Jodhab station records show variations similar to Upernavik, with significant cooling from the 1970s to the early 20th century, and significant warming from the 1920s to the end of the 20th century.

Summer temperatures were highest in the 1930s and in the 1960s (-6° to -5.5°, the long-term average = -8.6°C). Warmer winter and summer temperatures resulted in higher mean annual temperatures. In the 1930s and 1960s, they exceeded the "norm" (-1.4°C) by 1–1.5°C and frequently approached 0°C; that is, unstable permafrost conditions occurred now and then.

Conclusions

The coldest years in North America during the period of instrumental observations occurred from the late 19th century to the 1910s–1920s. Arctic warming was not reflected in Alaska and Canada records, and some locations experienced cooling. But the stations in Greenland responded well to the Arctic warming. Recent climate warming occurred in Alaska in the 1980s, in Canada in the 1970s and in Greenland in the 1960s. In the end of the 20th century, mean annual temperatures at many stations increased by 1–1.5°C compared to the long-term average (Gavrilova 1998, 2003).

Acknowledgments

The author thanks her assistant, Tamara Sofroneeva, for helping.

References

Gavrilova, M.K. 1998, 2003. *Climates of Earth's Cold Regions*. Yakutsk: 2008 pp.

Maximizing Construction Season in a Subarctic Environment, Fort Wainwright, Alaska

Quentin Gehring
Shannon & Wilson, Inc.
Frank J. Wuttig
Shannon & Wilson, Inc.

Introduction

The Denali Village housing project involves the construction of approximately 200 housing units (50 buildings) on a partially-developed site along the banks of the Chena River, encompassing approximately 150 acres on Fort Wainwright near Fairbanks, Alaska. Common construction practice on Fort Wainwright has been to replace frost-susceptible foundation soils with nonfrost-susceptible fills, mitigating the risk of undesirable frost-related movements. However, the design build team proposed founding the housing units on frost-protected shallow foundations to reduce both construction and costs.

Construction of the project provided several design challenges from a frozen-ground standpoint. This presentation describes the design of frost-protected shallow foundations outside standard design criteria, and lists strategies we considered to provide temporary frost protection for overwintered unfinished buildings and building pads. The desired outcome of temporary frost protection was to lengthen the construction season and accelerate the construction schedule.

Climate

ASCE 32-01 has developed a standard for the design and construction of frost-protected shallow foundations. The standard applies to areas free of permafrost, to areas where the mean annual air temperature is greater than 0°C, and to areas where the design air-freezing index is less than 2,500°C-days.

Interior Alaska, including Fort Wainwright, has a continental climate characterized by large daily and annual temperature ranges. Mean annual temperatures are slightly below freezing. The mean annual air freezing index exceeds 3,000°C-days. The recorded freezing index for Fairbanks is plotted in Figure 1. The 100-year mean return period design freezing index developed by the U.S. National Oceanic and Atmospheric Administration (NOAA) is 3,900°C-days.

The mean daily temperatures typically rise above freezing in mid-April and fall below freezing in mid-October, providing about a six-month construction season. Foundation construction in frost-susceptible soils generally begins after the seasonal frost has thawed, delaying the start of construction until late spring. Seasonal frost depths can extend several meters into the ground in cold, low-snow years. In areas kept clear of insulating snow cover, frost depths can exceed 4 m.

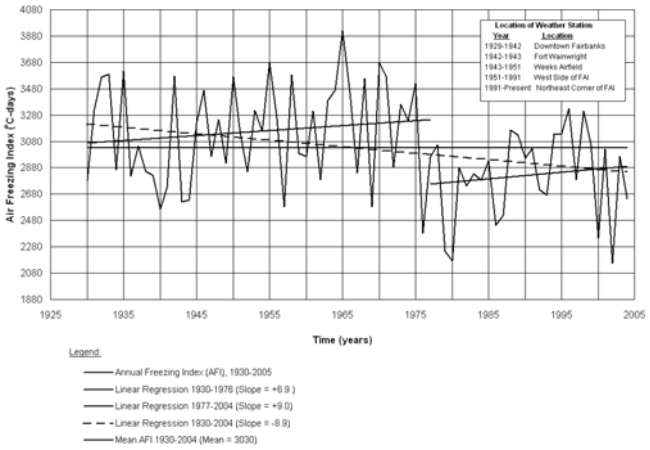

Figure 1. Climate information.

Site Conditions

The site is on the Chena River floodplain. Prior to construction, the site was primarily wooded with birch and spruce with an under-story of alder and willow. A portion of the site was developed as a campground, including gravel roads, parking areas, and trails.

Exploratory drilling by the U.S. Army Corp of Engineers and follow-up drilling by our firm showed that the site is underlain by a surficial layer of silty frost-susceptible soils overlying generally nonfrost-susceptible (NFS) sands and gravels. Localized areas of both shallow and deep permafrost were encountered across the site, which affected the foundation design. Groundwater levels were 3 m or more below the planned finished floor elevation, but past experience in the area indicates the water table can fluctuate seasonally 1 m to 2 m.

Foundation Design

The housing units are being founded on shallow, thickened-slab foundations with in-slab radiant floor heat bearing on controlled nonfrost-susceptible fills. A typical section of a frost-protected shallow foundation is shown in Figure 2. Frost protection is provided with either perimeter insulation designed to keep the soils below the foundations in a permanently thawed state, or by excavating and replacing frost-susceptible soils beneath the foundation system with a NFS fill. For this project, given the variation in subsurface conditions, four distinct foundation design solutions were proposed to address permafrost and frost-susceptibility issues.

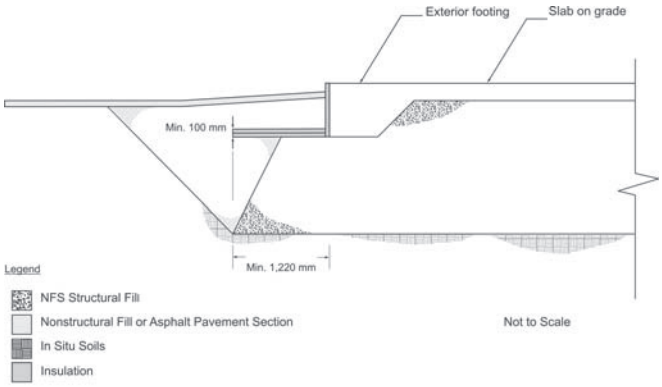

Figure 2. Typical frost-protected shallow foundation section.

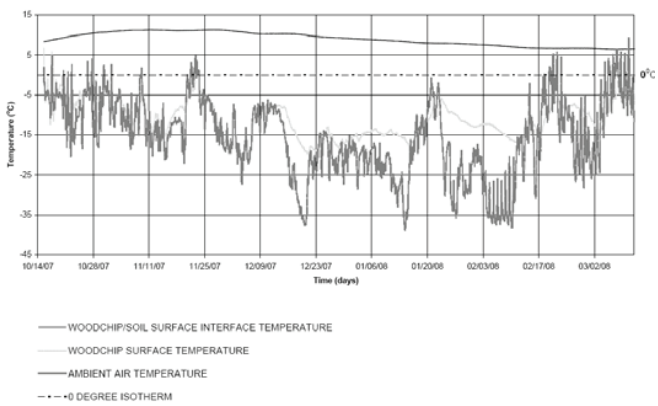

Figure 3. Foundation monitoring temperature data.

The climate parameters for Fort Wainwright are outside the ASCE design standard for the design and construction of frost-protected shallow foundations. In addition, discontinuous permafrost underlies portions of the site. To determine the insulation requirements for a frost-protected foundation design in areas without permafrost, thermal analyses were conducted using Temp/W, a finite element simulation package developed by Geoslope International, Inc., in Calgary, Alberta. Based on the results of the analyses, we recommended a 100-mm-thick wing of insulation, 1.22 m wide, extending out horizontally from the base of the foundation around the entire perimeter of the frost-protected slab foundations.

Complete excavation of frost-susceptible soils was recommended in permafrost areas.

Temporary Frost Protection Strategies

The short construction season placed limitations on the schedule for such a large construction project. Foundations that had been started had to be heated by the end of the construction season to prevent frost-susceptible foundation soils from freezing. Furthermore, deep seasonal frost would delay foundation construction in the spring. The following strategies were considered to reduce the affects of seasonal frost on the construction schedule:

1. Complete removal of frost-susceptible soils below planned foundations.
2. Use of board insulation, laid horizontally across pads and recycled the following spring for use as slab and foundation insulation.
3. Use of on-site soils or chipped organics as insulation over building pads designed for frost-protected foundations.
4. Continuous heating of pads and foundations throughout winter with glycol heating loops.

Using a combination of these strategies, the majority of the foundations were prepared in the first construction season. The following spring, construction began without the need to wait until the seasonal frost had thawed, effectively and efficiently achieving the desired outcome for temporary frost protection.

Foundation Monitoring

Little data is available on the use of on-site organics to provide temporary frost protection for a construction project; therefore, two prepared foundation pads were instrumented with thermistor strings and monitored for temperatures over the winter, in addition to monitoring air temperatures.

Woody plants, including small trees up to 0.3 m in diameter, were chipped/shredded during the 2007 construction season. Selected pads were covered with roughly 1 m of this material which was then covered with plastic sheeting to reduce the potential for natural convection. Thermal simulations were conducted to assist the contractor in determining the thickness of recycled on-site organics necessary for temporary frost protection.

Temperatures were monitored throughout the 2007/2008 winter. The temperatures plotted in Figure 3 show that the chips were effective at preventing building pads from freezing. Figure 3 also suggests some possible heat generation due to organic decomposition.

References

American Society of Civil Engineers (ASCE). 2001. *Design and Construction of Frost-Protected Shallow Foundations.* ASCE 32-01.

Pleistocene Sand-Wedge, Composite-Wedge, and Complex-Wedge Growth in Flanders, Belgium

G. Ghysels
Department of Geography, Ghent University, Krijgslaan 281-S8, Ghent, Belgium
I. Heyse
Department of Geography, Ghent University, Krijgslaan 281-S8, Ghent, Belgium
J.-P. Buylaert
Nordic Laboratory for Luminescence Dating, Department of Earth Sciences, University of Aarhus, Risø National Laboratory, DK-4000, Roskilde, Denmark
A.S. Murray
Nordic Laboratory for Luminescence Dating, Department of Earth Sciences, University of Aarhus, Risø National Laboratory, DK-4000, Roskilde, Denmark
D. Vandenberghe
Department of Geology and Soil Science, Ghent University, Krijgslaan 281-S8, Ghent, Belgium
F. De Corte
Laboratory of Analytical Chemistry, Institute for Nuclear Sciences, Ghent University, B-9000 Ghent, Belgium
P. Van den haute
Department of Geology and Soil Science, Ghent University, Krijgslaan 281-S8, Ghent, Belgium

Introduction

Reconstruction of former periglacial environments in Europe heavily relies on the identification of relicts and pseudomorphs of thermal-contraction-cracking wedges in soils (Vandenberghe & Pissart 1993). During the past seven years, a large number of these wedge-shaped sedimentary structures have been identified in lowland Belgium (Ghysels & Heyse 2006, Ghysels 2008). Wedge forming processes have been carefully reconstructed, providing new information on Pleistocene palaeoenvironmental and palaeoclimatic conditions of the Flemish sandy lowlands. Investigation methods included field observations, sedimentological analysis, and optically stimulated luminescence (OSL) dating.

Results

A key observation includes the identification of composite-wedge pseudomorphs, relict sand wedges, and complex wedges. Their appearance was variable. Some structures showed a typical wedge shape (Fig. 1), while others appeared as irregular features with branching sand veins and bundles (Figs. 1, 2). The majority of the wedges comprised a laminated infill, although some showed a massive infill. Besides mature wedge forms, elementary sand-filled veins and groups of sand-filled veins similar to Murton's (1996) sand veins in Canadian sand sheets were also identified. The veins and wedges penetrated Weichselian aeolian and fluvio-aeolian sand sheets (Fig. 3), but sometimes extended into underlying Tertiary sands and clays (Figs. 2, 3).

All these structures suggest thermal-contraction-cracking of frozen soils in a former cold periglacial environment. Their windblown infill points to sand transport on a sparsely vegetated ground surface with a limited snow cover during wedge growth (Murton et al. 2000).

Discussion

The results point to a greater complexity of wedge-forming processes and palaeoenvironments compared to those of previous studies. The latter stressed the dominance of ice-wedge pseudomorphs (e.g., De Moor et al. 1978, Heyse 1983, 2000, Vandenberghe & Pissart 1993, Huijzer & Vandenberghe 1998). Therefore, former reconstructions may have been biased towards conditions suitable for ice-wedge growth. Sparse vegetation and snow covers during wedge growth may also have favored efficient cooling

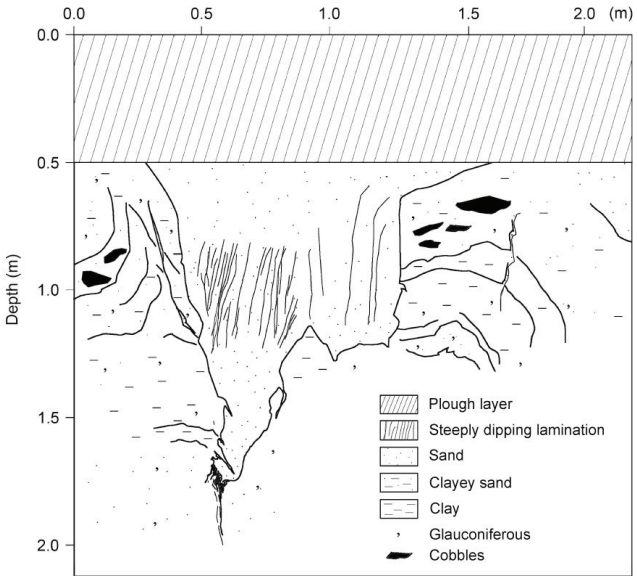

Figure 1. Vertical cross-section of a composite-wedge pseudomorph in Belgium (Ghysels & Heyse 2006). Note the upturned host sediments and the vertical laminated infill, pointing to the progressive infilling of thermal contraction cracks with sand, sand-ice, and ice. Downturned host strata and steeply-dipping tongues of host sediment likely formed as ice melted (Murton & French 1993).

Figure 2. Vertical cross-section of a complex wedge comprising a relict sand wedge (AAL4) which dissects an older composite-wedge pseudomorph (AAL3), Low-Belgium. Numbers refer to the OSL ages (Buylaert et al., accepted).

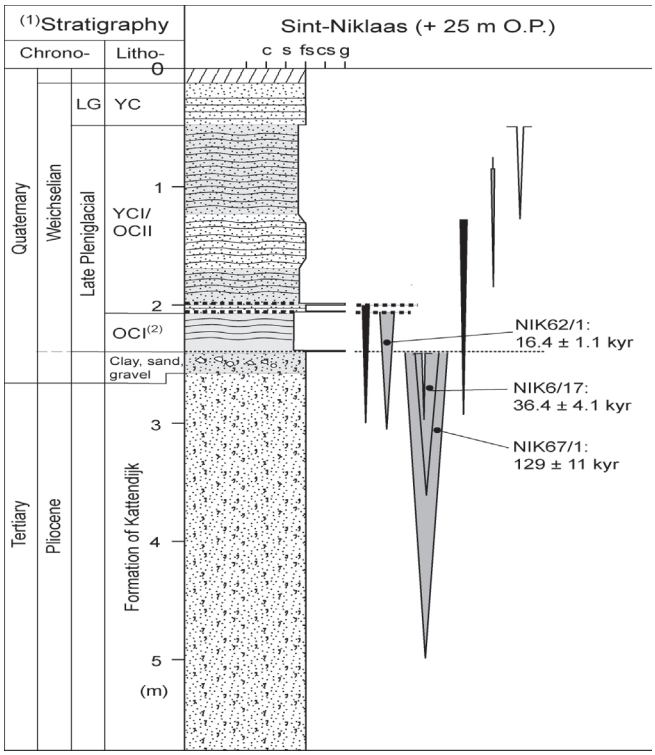

Figure 3. Schematic cross-section of Quaternary deposits showing different wedge levels. Grey wedges indicate wedges with a composite infilling. OSL dates are also indicated (in kyr: kiloyear).

and contraction of the frozen soil due to the lack of an insulating boundary layer (Murton & Kolstrup 2003). As a consequence, it cannot be excluded that wedges grew at higher mean annual air temperatures (MAAT ≤ -3°C) than previously suggested (e.g., MAAT ≤ -6°C in Huijzer & Vandenberghe 1998).

Finally, OSL dating of the aeolian wedge fillings provides direct age estimates for these cold-climate soil processes. The majority of the results points to extensive thermal contraction cracking during Marine Isotope Stage (MIS) 2 (Late Pleni-Weichselian–Lateglacial), peaking around 15,000 and 20,000 years ago (Fig. 2). A few data even suggest the possibility of earlier phases of wedge growth (during MIS 3 or Middle Pleni-Weichselian and MIS 6 or Saalian) (Fig. 3).

References

Buylaert, J.-P., Ghysels, G., Murray, A.S., Vandenberghe, D., De Corte, F., Heyse, I. & Van den haute, P. Accepted. Optical dating of relict sand wedges and composite-wedge pseudomorphs in Flanders (Belgium). *Boreas*.

De Moor, G., Heyse, I. & De Grootte, V. 1978. An outcrop of Eemian and Weichselian deposits at Beernem (N.W. Belgium). *Bulletin de la Société belge de Géologie* 87: 27-36.

Ghysels, G. 2008. *Bijdrage tot de Studie van de Kenmerken, de Genese en de Datering van Periglaciale Polygonale Wigstructuren in België*. Unpublished PhD Thesis, University of Ghent, 266 & 357.

Ghysels, G. & Heyse, I. 2006. Composite-wedge pseudomorphs in Flanders, Belgium. *Permafrost and Periglacial Processes* 17: 145-161, doi:10.1002/ppp.552.

Heyse, I. 1983. Cryoturbation types in eolian Würm Late Glacial sediments in Flanders, Belgium. *Polarforshung* 53: 87-95.

Heyse, I. 2000. Fossil periglacial remnants in the Beernem-Mouton excavation in Flanders (Belgium). *Biuletyn Peryglacjalny* 39: 53-68.

Huijzer, B. & Vandenberghe, J. 1998. Climatic reconstruction of the Weichselian Pleniglacial in northwestern and central Europe. *Journal of Quaternary Science* 13: 391-417.

Murton, J.B. 1996. Morphology and palaeoenvironmental significance of Quaternary sand veins, sand wedges, and composite wedges, Tuktoyaktuk Coastlands, western Arctic Canada. *Journal of Sedimentary Research* 66: 17-25.

Murton, J.B. & French, H.M. 1993. Thaw modification of frost-fissure wedges, Richards Island, Pleistocene Mackenzie Delta, Western Arctic Canada. *Journal of Quaternary Science* 8: 185-196.

Murton, J.B. & Kolstrup, E. 2003. Ice-wedge casts as indicators of palaeotemperatures: precise proxy or wishful thinking? *Progress in Physical Geography* 27: 155-170.

Murton, J.B., Worsley, P. & Gozdzik, J.S. 2000. Sand veins and wedges in cold aeoilan environments. *Quaternary Science Reviews* 19: 899-922.

Vandenberghe, J. & Pissart, A. 1993. Permafrost changes in Europe during the Last Glacial. *Permafrost and Periglacial Processes* 4: 121-135.

Response of Arctic and Subarctic Soils in a Changing Earth (RASCHER) – Project of IPY: Methodology, Activity, Results

Sergey V. Goryachkin
Institute of Geography, Russian Academy of Science, Moscow, Russia
John M. Kimble
Soil Consultant, Addison, NY, USA
Nimazhap B. Badmaev
Institute of General & Experimental Biology, Russian Academy of Science, Siberian Branch, Ulan-Ude, Russia
Marek Drewnik
Jagiellonian University of Krakow, Krakow, Poland
Dmitri G. Fedorov-Davydov
Institute of Physico-Chemical & Biological Problems of Soil Science, Russian Academy of Science, Puschino, Russia
Stanislav A. Iglovski
Institute of Ecological Problems of the North, Russian Academy of Science, Ural Branch, Arkhangelsk, Russia
Elena M. Lapteva
Institute of Biology, Komi Scientific Centre, Russian Academy of Science, Syktyvkar, Russia
Galina M. Mazhitova
Institute of Biology, Komi Scientific Centre, Russian Academy of Science, Syktyvkar, Russia
Nikita S. Mergelov
Institute of Geography, Russian Academy of Science, Moscow, Russia
Vladimir E. Ostroumov
Institute of Physico-Chemical & Biological Problems of Soil Science, Russian Academy of Science, Puschino, Russia
Eva-Maria Pfeiffer
Institute for Soil Science, Hamburg University, Hamburg, Germany

RASCHER (Response of Arctic and Subarctic Soils in a Changing Earth) is the International Polar Year (IPY) project which involves over 20 specialists from different countries. It addresses how climate variability and change can affect the soil systems of the Polar Regions and their sustainability with a changing climate. To provide accurate projections of the impact of climate change requires improved knowledge of its components and their linkages. Soil has both very inert and changeable parameters which are altered differently because of climate change. RASCHER mainly focuses on the study of temporal change of labile soil characteristics (temperature, carbon fluxes and other gas fluxes, microbiota, and microfauna) and of more stable soil characteristics (mineral composition, organic matter content and quality, morphological features, taxonomical status) in different kinds of frontiers (treeline, tundra-bog border, southern border of permafrost, contact zone, and the permafrost table in a profile), which are expected to be changed first due to climate change. The field studies are carried out in the different regions of the Arctic and Subarctic and also in high mountainous landscapes of temperate regions. Their aim is to make a "snapshot" of the current status of soil characteristics in 2007–08. It allows comparison of the inventory data gained in the IPY with results of studies to be carried out at the same locations 30–40 years later, and assessing if any climate-induced change of soil biota will take place. The variability of soil characteristics is taken into account.

The role of thermal factor in composition and functioning of the biotic complex of tundra soils (microbiota, microfauna, and mesofauna) as well as the selective role of negative temperatures on the structure of soil microbiocenoses and the influence of cryogenesis on adaptive functions of soil microorganisms are studied both in the field and in a laboratory, using traditional and new (DNA analysis) methods. For study of the character of polar soil microbocenoses, samples from permafrost-affected soil —Cryozem of the tundra ecosystem of the Lower Kolyma—have been collected and analyzed. The obtained data of the analysis of DNA show that the microbial population of these soils concerns in 14 groups that characterize this soil as the one with high biodiversity comparable with soils of more southern latitudes.

For the inventory study of the soil mesofauna, soil samples in the Vorkuta tundra (northeast of Europe) on soil catena from top to the bottom part of a slope have been collected. Invertebrates have been allocated only from the samples of various layers of the organic horizon. In Barber's traps, there have been caught representatives of five groups (Coleoptera, Hymenoptera, Lepidoptera, Homoptera, Diptera) from a class of insects and species of a class of *Aranei*. Representatives of *Coleoptera* are related to the top and middle part of a slope, while those of *Diptera* are found at the middle and bottom parts of the studied slope. Larvae of *Diptera* have mainly been met in soil samples of the middle part of a slope. In soil microfauna alongside with *Collembola*, there also have been identified ticks: *Gamasidae* and *Oribatei*. The last ones have been found at all sites of the slope mainly in the warmest top

part of soil litters. *Gamasidae* and *Collembola* in the top and middle part of the slope have been met in the whole mass of peaty horizons, while in the wettest bottom part of the slope, they are mostly at the top part of the organic horizons. The general number of *Collembola* in tundra permafrost-affected soils is low. On the average in the top part of the organic horizon, it is nearby 15,300 sp./m^2, and in the bottom part – 1,130 sp./m^2. At the same time the number of *Collembola* depends on the part of the slope. The wettest bottom part of a slope is characterized by a maximum of *Collembola* which are concentrated in the top part of a litter, while the maximum quantity of *Gamasidae* (2,800 sp./m^2) and *Oribatei* (8,400 sp./m^2) is related to the middle part of the slope.

The frontier studies concern the non-stability of the soil thermic regimes, shrinking of isolated patches and the northward retreat of permafrost-affected soils, and the assessments of possible soil change related to vegetation transformation on the base of soil studies (carbon fluxes, humus quality, mineral composition, etc.) in different types of ecotones (forest-tundra, tundra-bog, meadow-tundra).

In the Vorkuta tundra, the constant deepening of the permafrost table was observed. Leveling of the permafrost surface revealed that the ground subsidence due to thaw was 18 cm per 7 years, thus the subsidence rate is 2.5 cm/year. The average increment (396 measurements per year) of the soil layer reached 20 cm, and if adjusted to the subsidence is 38 cm per 7 years. Thus, the average thickness of the permafrost involved annually into soil formation is 5.5 cm.

In the tundra of the Lower Kolyma River, the general tendency for decrease of the permafrost table was also revealed, but the process seems to be more complicated and has more fluctuations. It is the result of the influence of 2 factors: (1) lower permafrost temperature at the Eurasian Northeast, and (2) various processes with negative feedbacks resulting in thaw mitigation.

At the southern part of the Cryolithozone, in Buryatia, in 1907–08 in undisturbed Gelic Chernozems, the permafrost table was identified at a depth of 1.5–1.6 m; in the 1960s, 2.0–2.1 m; at present time, 2.5–2.75 m. In loamy Gelic Luvisols, the permafrost at the beginning of the previous century was found at a depth of 1.2–1.3 m; in 1960–70s, 1.5–1.6 m; at present time, 2.2–2.5 m.

The analysis of archives and personal data revealed a shift of the southern permafrost boundary in the region northward from Arkhangelsk since 1933 to 2000. During 67 years, the southern border of the sporadic permafrost has moved northward 20–30 km.

The monitoring of the "forest-bog" ecotone in the sub-arctic zone of the Arkhangelsk region has been conducted. Besides the well-known phenomenon of northern soils bogging, it revealed the ecotone sustainability based on negative feedbacks.

The study of soil and geomorphic processes has been conducted in formerly permafrost-affected Tatra Mountains, which are the highest part of the Central European Carpathians (2655 m a.s.l.). The Tatra Mountains are not glaciated, and nowadays, the presence of permafrost has not been found. However, these mountains are subjected to intense geomorphic processes (rock falls, rock slides, debris and grain flows, solifluction, gelifluction, and others). The soils studied have been localized in the alpine zone (1800–2200 m a.s.l.), where the most intensive geomorphic processes occur (cryo-nivale zone). The soils studied are shallow and contain a considerable amount of clast. They are subjected to the podzolization process, and they can be characterized by thick humus horizons. Slow geomorphic processes (solifluction, soil creep) modify the upper part of the soil profile, comprised of humus horizons and eluvial horizons. The influence of these processes depends on the participation of the phenomena associated with the freeze-thaw action concerning the ground ice. Along with the increased importance of frost action in the movement of regolith, the degree of soil modification increases. The most profound transformation of the soil cover occurs in the case of gelifluction. Within the forms, which developed as a result of secular processes (protuberances, bench terraces, lobes), the soils are modified, although without leading to essential changes in their properties. The soil affected by gelifluction have the properties and morphology of Fluvisols. Catastrophic processes (rock slides, debris and grain flows) cause strong transformation of soil cover and uniformity of soil mass. Further development of soil depends on the geomorphic position; it is different within erosion zones and different within accumulation zones; so the soils above the upper timberline in the Tatra Mountains are young forms. In relatively stable areas or those subjected to only moderate geomorphic processes, they often display the features of polygenesis associated with changing climatic and geomorphic conditions.

The other part of the frontier studies is the detailed analysis of soil process at the interface of the soil and permafrost tables. It concerns the study of the biochemical and geochemical barrier on this interface and the study of the process of cryogenic lateral transportation at the contact zone of the soil and the permafrost table. This interface is the zone of high concentration of organic matter and other compounds, including pollutants. These detailed physico-chemical studies allow for a determination of the fate of these materials as affected by permafrost thawing due to climate change or anthropogenic impact.

The important feature of the cryogenic structure of the transitional layer is the zone of concentration of labile substances which are situated in the zone of the segregative ice. In depressions of the permafrost surface, there are local zones of accumulation of labile substances—cryogenic geochemical traps. The chemical analysis showed that the general salinity and composition of soluble substances concentrated in these traps differ from the composition of intrasoil ice. The differences observed can be explained by cryogenic transformation of suprapermafrost water and selective penetrability of the cryogenic geochemical barrier.

Local accumulation of labile substances in geochemical permafrost traps is the essential part of geochemical balance. If the soil thawing depth increases, then the elements concentrated in permafrost geochemical traps could escape into the surface-water flow.

Monitoring of the Floodplain Talik Downstream From the Ust'-Srednekan Reservoir

S.A. Guly, V.M. Mikhailov
North-Eastern Research Station of the Melnikov Permafrost Institute, SB RAS, Magadan, Russia

In the continuous permafrost area of northeastern Asia, taliks exist only in river valleys and under large lakes. Many of them develop due to intensive convective heat exchange with rivers and occupy the entire floodplain. A generally accepted indicator of such taliks are phytocenoses of thick mixed woods in which large deciduous trees (*Chosenia arbutofolia* and *Populus Suaveolens*) are often most abundant. These woods stand out sharply against the background of sparse growths of trees (almost exclusively larch) dominating in the lower belt of mountains and over flat interfluves (Fig. 1). Many authors, following Vaskovsky (1958), call them an expressive name—tundra-forest—which accentuates the depression of trees.

The largest floodplain talik begins in the Kolyma River valley between Ust'-Srednekan and Seimchan, and extends downstream for more than 500 km, somewhat lower than Ziryanka (Fig. 2). Its width varies from 2.5–3 to 4–5 km or more. Thus, in this reach of the Kolyma River floodplain, a unique natural complex exists, the main constituents of which are the outstandingly huge block of unfrozen ground and the vast woodland north from the taiga forests.

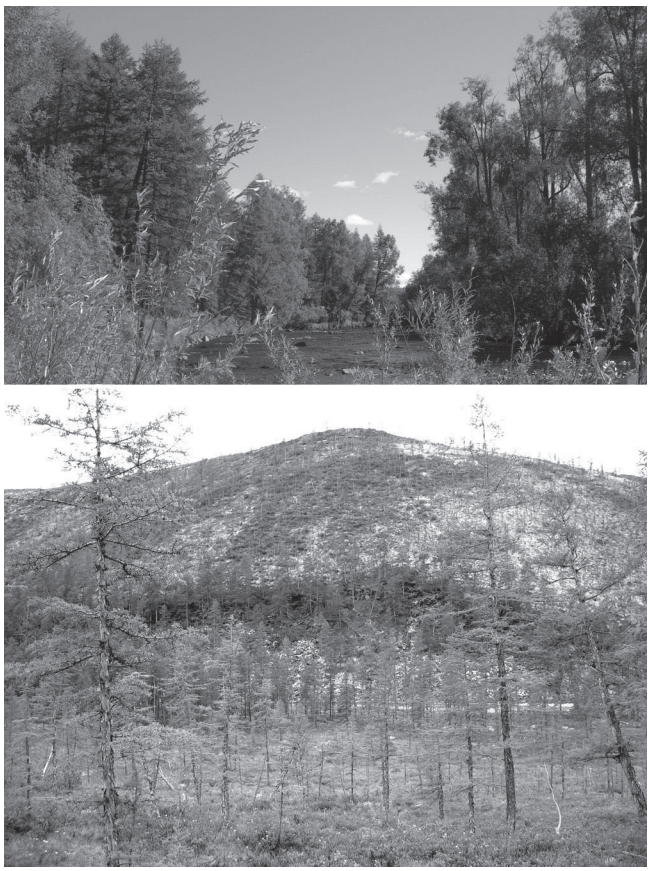

Figure 1. Two typical landscapes of northeastern Asia: mixed forest on a floodplain talik (above) and dominating tundra-forest (below).

In a few years the hydroelectric power station will be put into action 14 km upstream from Ust'-Srednekan. It is common knowledge that reservoir regulations induce significant decreases in temperature and discharge of rivers downstream from dams during summer. Such changes cannot but influence the hydrothermal regimes of contiguous aquifers.

Convective heat exchange is caused by a two-way water exchange (developing due to very high alluvium permeability); in each "elementary" river segment, infiltration of water into ground is accompanied by groundwater recharge. The resulting heat flux into a floodplain talik (q_{conv}) is defined by the formula (Mikhailov 2002):

$$q_{conv} = C(\omega^{-}T - \omega^{+}T_f) ,$$

where C is water volumetric specific heat; ω^{-} is specific (i.e., related to the unit river surface area) rate of water infiltration into alluvium; ω^{+} is the same, only of groundwater recharge into a river; T is water temperature in a river; and T_f is weighted mean groundwater temperature ("weights" are point rates of recharge). Hereafter all dimensions are in SI; specifically, water exchange characteristics ω^{-} and ω^{+} are measured in $m^3/(s\cdot m^2)$. Water surface area may vary greatly over short time periods, so the influence of convective heat exchange on the thermal regime of a talik is better described by the product of q_{conv} by a river width (B).

Characteristics of water exchange do not depend substantially on river discharge, while B is directly related to it. Therefore, both above-mentioned changes will diminish the amount of heat supplied to the Kolyma River floodplain with unpredictable consequences for the talik.

The situation has no precedent because never before was

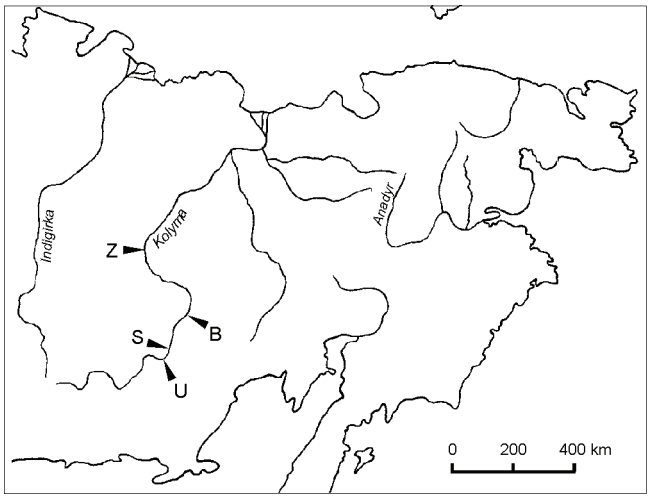

Figure 2. Locations of the gauging stations on the Kolyma River: U – Ust'-Srednecan; S – Seimchan; B – Baligichan; Z – Ziryanka.

a river dam constructed upstream from a floodplain talik; so there is no way to tell how much these changes can influence the natural complex under discussion. Very probably, they will cause reduction of the talik followed by degradation of the woods. To prevent such a trend of developments, it is necessary to perform continuous monitoring of the talik condition downstream from the dam and, in the case of a real threat, to propose efficient ways to reduce the damage to a minimum. Unfortunately, the methods traditionally used in permafrost science are hardly suitable for accomplishing even the first of these aims, because a reasonable degree of accuracy requires numerous measurements that are very labor consuming. Less laborious biological methods are only capable of ascertaining the ecological disturbance when it becomes irreparable.

The most practical approach is based on our recent research of convective heat exchange between rivers and contiguous aquifers by means of estimates of rivers' heat balance (Mikhailov 2002, 2008). Accounting for all commonly considered components, the residual is total heat flux into ground (q_{gr}) of which the conductive constituent is virtually a negligible part (Mikhailov 2002). All other heat fluxes can be calculated accurately enough, thus the same is true for the sought quantity. Long-term estimates of q_{gr} were made for large sections of 6 rivers (Mikhailov 2008). As a result, the general patterns of seasonal variation of this value have been established. One of these sections is located on the Kolyma River between Seimchan and Baligichan (see Fig. 2). It belongs to the upper part of the floodplain talik under discussion, subjected to the strongest influence of the reservoir regulations.

Developing further this approach, the pattern of variations of q_{gr} in this section can be determined as dependent on hydrometeorological conditions during the whole period of observations. Comparison of these data sequences with those obtained after the dam construction will bring to light the influence of reservoir regulations. The results of such analyses will become more and more reliable with time. As a first approximation, a steadfast tendency of decrease of q_{gr} (all other factors being equal) will be indicative of the forthcoming reduction of the talik.

Apparently, the only way to increase heat transfer to the floodplain talik is either by specifying additional flushes from the reservoir or manipulating the parameters of the regular ones (e.g., needed for the shipping). But it is a comprehensive analysis of the dynamics of the river temperature and discharge, together with the q_{gr} values, that can enable a rational choice of optimal periods and minimal durations and volumes of the flushes.

The most essential advantages of the approach discussed are the following:

1. Decrease of q_{gr} precedes any significant changes of both the talik size and—all the more—the conditions of floodplain phytocenoses. It gives time to elaborate and discuss with the authorities proposals for necessary adjustments in the reservoir regulations.

2. Analysis of the fundamentally new information obtained in the course of monitoring will undoubtedly improve our knowledge of regularities of convective heat exchange in river valleys. Besides the basic significance, in the practical aspect it will make the aforesaid proposals more realistic.

3. The most necessary part of data for estimating q_{gr} is standard hydrometeorological information. Additional research will be needed only to improve the accuracy of the results obtained and (probably) to verify the fact of the talik reduction.

It is also important that the Ust'-Srednekan hydroelectric power station will function together with the existing one (Kolymskaya station). Such a complex is far more flexible than a single station and in principle allows for more considerable adjustments. This offers grounds for optimism as regards the acceptability of the would-be proposals for governmental and economic bodies. In that case, we may have a good example of sensible compromise between conflicting interests and demands based on improved knowledge of the functioning of natural complexes.

References

Mikhailov, V.M. 2002. Quantitative methods of indication of floodplain taliks (theoretical premises). Kriosfera Zemli (Cryosphere of Earth) 6: 20-28 (in Russian).

Mikhailov, V.M. 2008. Convective heat exchange between rivers and floodplain taliks. *Proceedings of the Ninth International Conference on Permafrost, Fairbanks, Alaska, June 29–July 3, 2008* (this proceedings).

Vaskovsky, A.P. 1958. New data on the distribution limits of cenoses-forming trees and shrubs in the Far North-East of the USSR. In: Materials on Geology and Minerals in the North-East of the USSR 10: Magadan, 187-204 (in Russian).

Retrogressive Thaw Slump Impacts on Inconnu Spawning Habitat in the Selawik River, Alaska

Raymond Hander
U.S. Fish and Wildlife Service, Fairbanks Fish and Wildlife Field Office, Fairbanks, AK, USA
Kenji Yoshikawa
Institute of Northern Engineering, Water and Environmental Research Center, University of Alaska Fairbanks, USA
Nathan Olson
U.S. Fish and Wildlife Service, Selawik National Wildlife Refuge, Kotzebue, AK, USA

Introduction

One of the most dramatic changes and concerns of climate warming is the increased rate of thawing permafrost and its related environmental shifting, such as changing the hydrological regime of river systems. The Kotzebue Sound area of northwestern Alaska is widely recognized as one of the most ice-rich and thaw-sensitive areas in Alaska (Fig. 1). In particular, glaciated areas are prone to develop retrogressive thaw slumps (RTS) by the thawing of buried glacial ice bodies.

In the spring of 2004, a large RTS occurred in the upper Selawik River drainage above important inconnu *Stenodus leucichthys* spawning habitat within the Selawik National Wildlife Refuge (Refuge) (Fig. 2). This event changed the water from a clear to a glacial-colored river that was noticed by Refuge personnel and persons from Selawik. The Selawik River is habitat for a number of whitefish species, including inconnu that support an important subsistence fishery and occupy an important ecological role in the Kotzebue, Alaska area.

Little is known about the physical spawning habitat requirements for inconnu, especially sensitivity to the accretion of sediments. There is potential that sediment could fill interstitial spaces between the gravel and cobble substrate where fertilized eggs need to settle, overwinter, and mature.

Since 2004, the RTS has continued to erode and influence the river with no apparent end in sight. The RTS is caused by ice-rich permafrost degradation resulting in slope failure (Jorgenson & Osterkamp 2005). Also, increasing thermokarst activity has been identified in a 5,000 km^2 survey area in the adjacent Noatak National Preserve by Bowden et al. (2007).

Preliminary RTS analysis

We attempted to provide an estimate of the volume of sediment/ground ice that has eroded into the Selawik River from the RTS since 2004 using stereophotogrammetric analysis methods of aerial remote sensed imagery (Fig. 3).

This analysis indicated that approximately 25,000,000 to 60,000,000 kg of sediment were released from the RTS in the 2007 melting season. Since 2004, the RTS was discharging 267 g/L of suspended sediments and discharging more than 100 L/sec from thawing permafrost during the melting season. At the inconnu spawning area in August 2007, deposited sediment was observed, and suspended sediments were measured to be at least 375 mg/L.

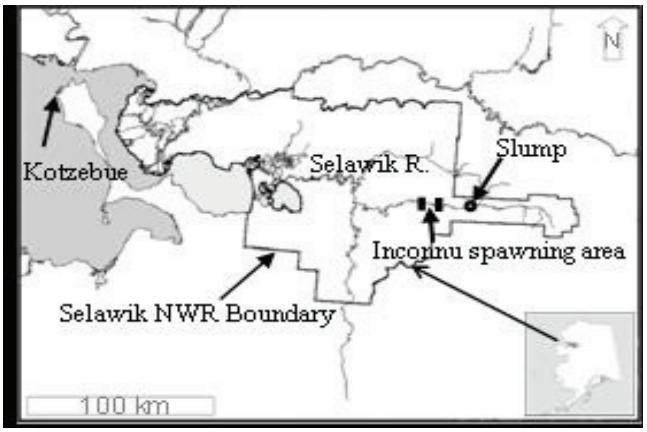

Figure 1. Map of the Selawik River, inconnu spawning area, and the retrogressive thaw slump location.

Figure 2. Selawik River retrogressive thaw slump, 2005. White circle is around a person and provides a slump-size scale.

Inconnu habitat and RTS monitoring and research

Impacts to the Selawik River inconnu population may not be known until the age cohorts from eggs deposited during sediment discharge years reach maturity and return to spawn in about 7 to 12 years (Brown 2000). Work is planned to assess the spawning habitat area for silt accretion on the spawning ground. Also, assessment of inconnu egg distribution relative to stream substrate characteristics will be explored to gain an understanding of specific habitat(s) where eggs reside for overwintering and maturation.

Continued RTS analysis in 2007 will include assessing the

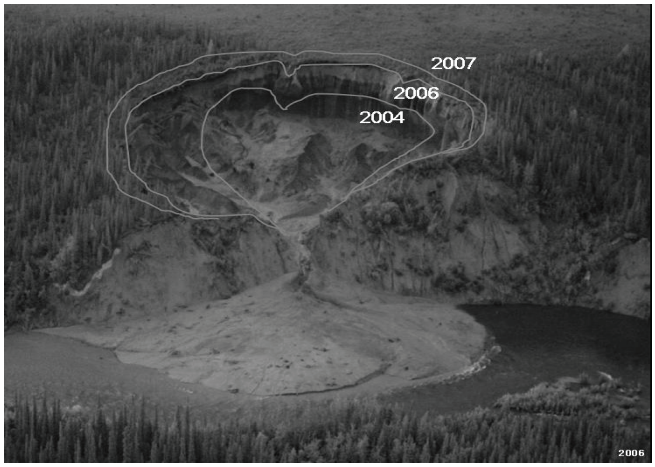

Figure 3. Selawik River retrogressive thaw slump progression from 2004 to 2007.

spatial and temporal distribution of the amount of suspended sediment, profiling river bed geomorphology, assessing spatial distribution of the RTS sediments deposited since 2004, and estimating the total volume of the suspended sediments and discharge volume.

The life expectancy of the RTS is dependent upon its reaching a stable thermal condition induced by the overburden material cover and more stable angles of the RTS walls. Lantuit & Pollard (2005) indicated that it often takes 5 to 10 years for the floor of a slump of dimensions of 100 m and more from the headwall to stabilize.

Acknowledgments

We thank the Selawik National Wildlife Refuge for field support and University of Alaska Fairbanks, Water and Environmental Research Center staff members and students for help with laboratory analyses and field support.

References

Bowden, B., Gooseff, M., Jones, J., Balser, A. & Lawler, J. 2007. *Thermokarst Distribution and Characterization in the National Park Service Arctic Network.* Unpublished progress report.

Brown, R.J. 2000. *Migratory patterns of Yukon River inconnu as determined with otolith microchemistry and radio telemetry*. M.S. Thesis, University of Alaska Fairbanks.

Jorgenson, M.T. & Osterkamp, T.E. 2005. Response of boreal ecosystems to varying modes of permafrost degradation. *Canadian Journal of Forest Research* 35: 2100-2111.

Lantuit, H. & Pollard, W.H. 2005. Temporal stereophotogrammetric analysis of retrogressive thaw slumps on Herschel Island, Yukon Territory. Natural *Hazards and Earth System Sciences* 5: 413-423, European Geosciences Union.

Waters, T.F. 1995. *Sediment in Streams: Sources, Biological Effects, and Control*. Bethesda, Maryland: American Fisheries Society Monograph 7, 251 pp.

Climatic Change and Permafrost Stability in the Eastern Canadian Cordillera

Stuart A. Harris
Faculty Professor, Department of Geography, University of Calgary, Calgary, T2N 1N

Introduction

Permafrost is the result of cold climatic conditions, so the stability of the climate is crucial to permafrost stability. It has been predicted by modeling that Alaska and the Yukon Territory should exhibit the maximum degree of climatic warming in the next century (Anisomov & Poliakov 2003), but Harris (2007) and Sergeev (2007) found that the available climatic data from the most reliable government sources indicated no strong warming trends in large parts of these areas. This paper explores the matter further by extending the study south along the Canadian Cordillera and relating the results to the evidence of associated permafrost stability.

Sources of Data

When commencing the study of permafrost distribution in the Eastern Canadian Cordillera in 1974, weather stations equipped with temperature recorders were used at key sites together with ground temperature cables. Observations are continuing at the key stations (Fig. 1), which provide a record of the mean annual air temperature (MAAT), the seasonal thawing index (STI= the sum of the positive mean daily air temperatures from January 1 to December 31, inclusive) and the seasonal freezing index (SFI= the sum of the negative mean daily air temperatures from July 1 to June 30). The data represent the only available long-term climatic data from high altitudes south of the 60th parallel. The network was expanded north into the Yukon Territory, where the data supplement the data collected by the AES up to 1993 (AES 1993) and the climatic data from the Class 1 weather stations run by the U.S. National Weather Service. These are the best available data sources for northwest North America.

Results

Figure 2 shows the regional pattern of climatic change since 1980, based on the published climatic data (Harris 2007) and the present study. Along the Arctic coast of Alaska, the east slope of the Cordillera and the Mackenzie Valley, and in northern British Columbia, there is evidence for substantial warming. This manifests itself in thawing of permafrost north of the crest of the Brooks Range (Osterkamp & Romanovsky 1999) and east of the crest of MacMillan Pass along the North Canol road (Kershaw 2003). The SFI has been decreasing and the MAAT and STI, increasing since 1980.

The main block of the mountains across central and southern Alaska and the Yukon Territory, as well as south of 52°25′N in the Eastern Cordillera, shows only minor long-term changes in MAAT. The SFI has been decreasing since 1972 in the Watson Lake area, though both the STI and SFI have increased slightly since 1985 at Tuchitua. The permafrost landforms such as palsas and lithalsas show negligible signs of degradation except where beavers have raised the local water level resulting in degradation of the adjacent landform, for example, at Wolf Creek (Lewkowicz 2003) and at Fox Lake, or where human activity has altered the water level (Marsh Lake, north shore, 2007) or through road construction, east of Tagish, Y.T. Where the water level is lowered artificially, the ground temperatures in the landforms cool, and the landforms grow in area (Fig. 3) as at Tuchitua. Kershaw (2003) thought that the west side of the MacMillan Pass was also warming due to slow degradation of two floating palsas, but the ponds in which they are found are becoming shallower and, therefore, warm up more in summer. The peat mounds nearby are not showing increasing ground temperatures, and the nearby large palsa fields on the floodplain of the MacMillan River are not showing evidence of degradation. It is concluded, therefore, that there is a climatic divide along the crest of the mountains separating the Northwest Territories from the Yukon Territory.

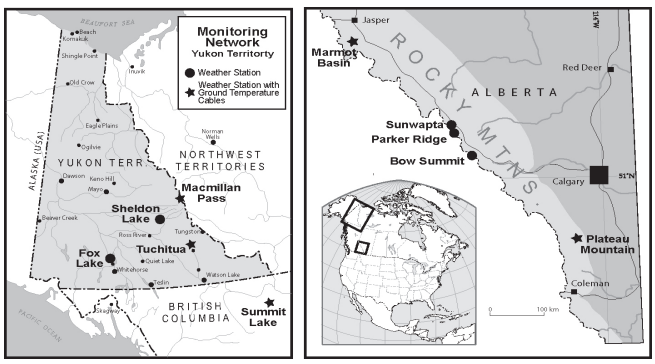

Figure 1. Location of the study sites.

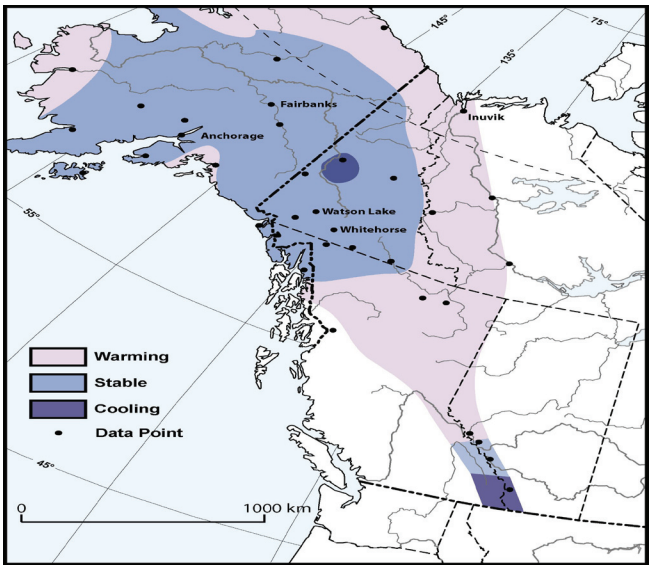

Figure 2. The regional pattern of temperature changes from 1970 to 2006 (partly after Harris 2007).

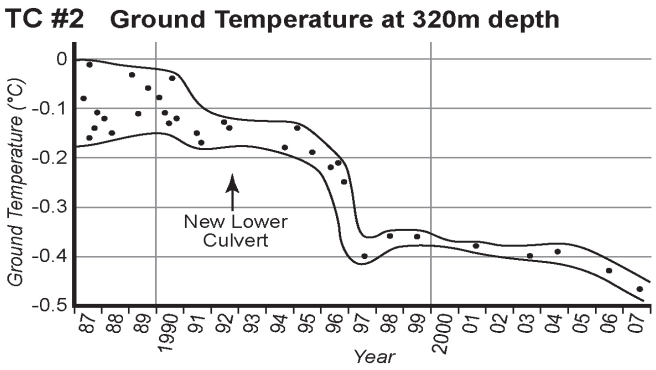

Figure 3. Ground temperature changes at 320 cm depth after the lowering of the adjacent water table, Tuchitua.

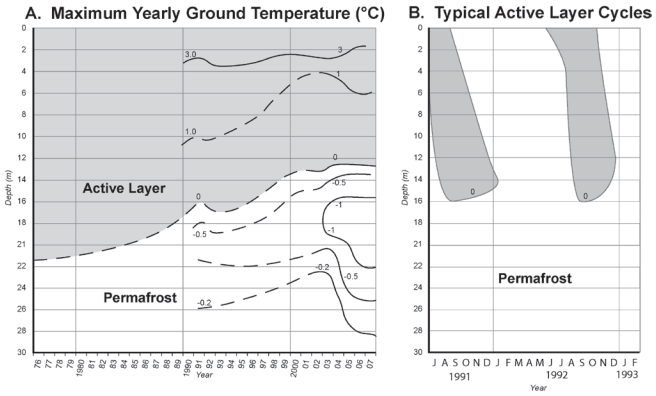

Figure 4. Changes in maximum annual ground temperature a n d active layer, as measured on a yearly basis (A) and on a daily basis (B).

The Summit Lake site showed a spectacular increase of 4.85°C in MAAT between 1982 and 1994 followed by relative stability. The SFI decreased by 40% while the STI increased by 50%. In about 1992, large thaw-flow slides appeared on the hill slopes at 1200 m elevation, and these started to appear up to 1400 m by 2004. The active later thickness increased from 1.5 m in 1982 to >5 m in 2007. The warming decreases southwards to Jasper, where there is only a minor increase in MAAT (0.6°C in 27 years). SFI has decreased considerably as has the mean annual snowfall, but the STI has increased. South to Calgary, the MAAT has remained unchanged with both STI and SFI decreasing (see also Clark et al. 2000).

Plateau Mountain exhibited a decrease in MAAT from 1974 until 1990, but has been fairly stable since then. Both the SFI and STI decreased. The active layer has decreased in thickness, and the upper part of the permafrost has cooled in response to these changes (Fig. 4).

Causes

The first obvious result is that the climatic changes are local rather than global. In the main mass of the mountains of Alaska and Yukon, inversions of air with their associated cloud cover, steam fog in the fall when the air temperature over lakes is lower than the water temperature, and cold air drainage serves to buffer the valleys from climatic changes (Harris 2007). Along the Arctic coast, changes in surface cover from snow to soil and water enhance the effects of any warming.

Almost all stations indicate a decrease in the SFI, this being most marked at Summit Lake. This appears to indicate a weakening of the air pressure north of the 60th parallel, resulting in warmer air and the associated jet stream moving further north as far as Summit Lake from its previous position further south (see also Nkemdirim & Budikova 2001). The cP air mass is thinner and moves further east rather than swinging south along the mountain front

Acknowledgments

Roger J.E. Brown of the Building Research Division, National Research Council of Canada funded the original study. It has also been funded in some years by the Geological Survey of Canada (Alan Heginbottom and Sharon Smith) and NSERC operating Grant A-7483. Parks Canada, Alberta, and BC Parks kindly provided the necessary collecting permits.

References

AES. 1993. CD-Rom of the climatic data collected by the Atmospheric Environment Service at Canadian Weather Stations.

Anisomov, O.A. & Poliakov, V.Yu. 2003. GIS assessment of climatic change impacts in permafrost regions. *ICOP 2003, Permafrost* (1): 9-14.

Clarke, J.S., Yirode, E.K., Burns, N.D. & Astatkie, T., 2000. Regional climate change: trend analysis and precipitation series at selected Canadian sites. *Canadian Journal of Agricultural Economics* 48: 27-38

Harris, S.A. 2007. Reaction of continental mountain climates to the postulated "global warming," evidence from Alaska and the Yukon Territory. *Earth Cryosphere* 11(3): 78-84 (in Russian).

Kershaw, G.P. 2003. Permafrost landform degradation over more than half a century, MacMillan/Caribou Pass region, NWT/Yukon, Canada. *ICOP 2003, Permafrost* (1): 543-548.

Lewkowicz, A.G. 2003. Palsa dynamics in a subarctic mountainous environment, Wolf Creek, Yukon Territory, Canada. *ICOP 2003, Permafrost* (1): 163-168.

Nkemdirim, L.C. & Budikova, D. 2001. Trends in sea level pressure across western Canada. *Journal of Geophysical Research* 106(D11): 11801-11812.

Osterkamp, T.E. & Romanovsky, V.E. 1999. Evidence for warming and thawing of discontinuous permafrost in Alaska. *Permafrost and Periglacial Processes* 10: 17-37.

Idealized Modeling of the Impact of Atmospheric Forcing Variables on Mountain Permafrost Degradation

Christian Hauck
Institute for Meteorology and Climate Research, Karlsruhe Institute of Technology (KIT), Germany
Nadine Salzmann
National Center for Atmospheric Research (NCAR), Boulder, USA

Introduction

The high-mountain Alpine cryosphere is a particularly sensitive system to climate change due to its proximity to melting conditions. In view of probable accelerating rates of ongoing changes concerning atmospheric, surface, and subsurface processes in mountain regions (IPCC 2007), a great need for increased understanding of permafrost degradation processes and corresponding new modeling tools has been identified. Traditional mountain permafrost model approaches focus on spatial distribution models, using physically-based or empirical and statistical approaches to predict the permafrost distribution over larger areas (e.g., Noetzli et al. 2007).

However, to predict possible future changes in the permafrost distribution, the link between small-scale subsurface characteristics, including latent heat processes and predictions from climate models, has to be established. Whereas there is a steadily increasing number of studies using Global and Regional Climate Model (GCM, RCM) simulations to assess permafrost evolution and its impact in arctic regions (e.g., Anisimov & Nelson 1997, Stendel et al. 2007), similar efforts for mountainous terrain have only started very recently (Salzmann et al. 2007a, b). Thereby, regional to local climate scenarios, and especially mountain regions, are among the most ambitious areas for simulating future climate conditions (e.g., Frei et al. 2003). In most GCM/RCM simulations, small-scale processes and influencing variables such as surface characteristics, a realistic snow cover, topography, and lithospheric heterogeneities, as they are typical for mountain regions, cannot be included (Stendel et al. 2007).

Among those influencing variables, the duration of a significant snow cover plays a special role, as it determines the amount of energy exchange between atmosphere and ground and the degree of coupling between both spheres (Hoelzle & Gruber 2008). Climate warming, therefore, can only act upon the permafrost during the snow-free period, which is usually restricted to the summer months in many regions of the European Alps.

On the other hand, the strong decoupling of atmosphere and permafrost during most of the year can be used to simplify the necessary linking procedure between RCM results and subsurface models. The focus of this study is to use idealized modeling of the impact of changes in air temperature and snow cover duration on the subsurface permafrost temperatures. In a next step, permafrost-relevant information (e.g., possible trends concerning air temperature or snow cover duration) from control and scenario time series of RCM simulations can be extracted using the approaches described by Salzmann et al. (2007a).

Atmospheric Forcing Variables

Figure 1 shows a typical example of the influence of net radiation and snow cover on ground temperatures in mountain permafrost regions. The example is taken from the 2900 m high-altitude permafrost station Schilthorn, Swiss Alps, where a more than 100 m thick permafrost layer exists (Hauck 2002, Hilbich et al. 2008). Figure 1a shows the total ground temperature change with time within the uppermost 10 m of a borehole. During the time when a significant snow cover was present (Fig. 1c and vertical black lines), temperatures within the uppermost 10 m of the borehole remained almost constant, as the ground temperature regime was effectively decoupled from atmosphere. After melting of the snow cover in June, temperature variability in the borehole is high, coinciding well with the observed variability of the radiation balance (Fig. 1b). This agreement confirms the dominant role of the radiation balance for ground temperatures in mountain permafrost terrain in the European Alps.

The only exception is seen right after the beginning of snowmelt in May, where small-scale variability of the total ground temperatures is present (Fig. 1a). Scherler et al. (submitted) showed that this feature is most probably due to infiltrating meltwater from the snow cover.

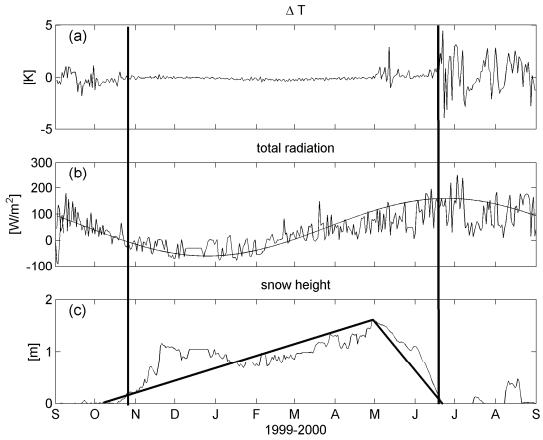

Figure 1. (a) Total temperature difference per day in the uppermost 10 m in the borehole, (b) net radiation at the energy balance station, and (c) snow height at Schilthorn, Swiss Alps.

Approach

For idealized simulations, the annual variability of radiation (or air temperature) can be approximated by a sinusoidal variation, as indicated in Figure 1b. Similarly, the evolution of the snow cover can be approximated by a continuous linear increase in early winter and a sharp linear decrease in early summer (Fig. 1c). For idealized modeling of the impact of atmospheric forcing on the evolution of mountain permafrost, only four atmospheric parameters need to be varied:

1. accumulated summer air temperature (e.g., approximated by the amplitude of the sinusoidal curve);
2. air temperature at the beginning of the permanent snow cover (autumn);
3. time of the buildup of the permanent snow cover; and
4. time of vanishing of the permanent snow cover.

The rationale for this approach can be further illustrated by analyzing multiyear time series of air temperature and snow cover duration (Fig. 2), as well as comparing them to subsurface temperatures. This was done in detail by Hoelzle & Gruber (2008) for two sites in the Swiss Alps (including Schilthorn), indicating that snow cover duration and air temperature are indeed the dominant forcing variables for permafrost temperatures and active layer thickness.

Our approach focuses on determining subsurface temperatures, water, and ice content evolution with a one-dimensional coupled heat and mass transfer model simulating mass and energy balance of the soil-snow-atmosphere system (COUP-model, Jansson & Karlberg 2001). This model has been successfully applied to simulate water and energy at Schilthorn (Scherler et al. submitted). As a first step to using downscaled RCM scenario time series, we use idealized atmospheric forcing time series to analyze the possible impacts of increasing summer air temperatures, for example, or a shift in the snow cover duration on the permafrost temperatures. In a next step, these characteristics will be extracted from simulated RCM scenario time series for longer time scales. For the idealized simulations, combinations of the four atmospheric parameters listed above will be used.

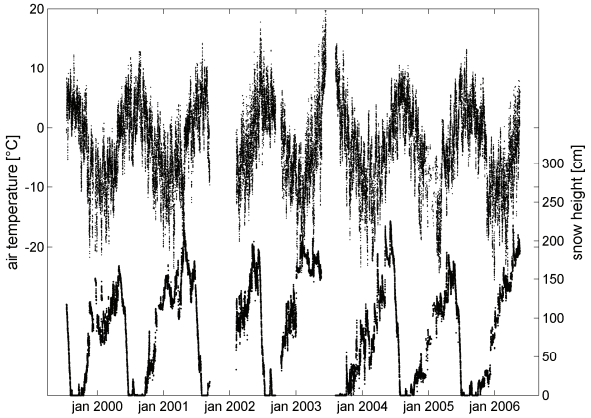

Figure 2. Air temperature and snow height at Schilthorn, Swiss Alps, between autumn 1999 and 2006 (data courtesy of M. Hoelzle and PERMOS).

References

Anisimov, O.A. & Nelson, F.E. 1997. Permafrost zonation and climate change in the Northern Hemisphere: results from transient general circulation models. *Climatic Change* 35: 241-258.

Frei, C. et al. 2003. Daily precipitation statistics in Regional Climate Models: Evalution and intercomparison for the European Alps. *J. Geophys. Res. 108*(D3): ACL 9-1– 9-19.

Hauck, C. 2002. Frozen ground monitoring using DC resistivity tomography. Geophysical Research Letters 29(21): 2016, doi:10.1029/2002GL014995.

Hilbich, C. et al. 2008. Monitoring mountain permafrost evolution using electrical resistivity tomography: A 7-year study of seasonal, annual, and long-term variations at Schilthorn, Swiss Alps, *J. Geophys. Res*. 113: F01S90, doi:10.1029/2007JF000799.

Hoelzle, M. & Gruber, S. 2008. Borehole and ground surface temperatures and their relation to meteorological conditions in the Swiss Alps. *Proceedings of the Ninth International Conference on Permafrost, Fairbanks, Alaska*.

Intergovernmental Panel on Climate Change (IPCC) 2007. *Climate Change 2007: The Physical Science Basis*. Summary for policy makers, 18 pp., http://www.ipcc.ch/.

Jansson, P.-E. & Karlberg, L. 2001. *Coupled Heat and Mass Transfer Model for Soil-Plant-Atmosphere Systems*. Stockholm: Royal Inst. of Technology, Dept. of Civil and Environmental Engineering, 321 pp.

Noetzli, J., Gruber, S., Kohl, T., Salzmann, N. & Haeberli, W. 2007. Three-dimensional distribution and evolution of permafrost temperatures in idealized high-mountain topography, J. Geophys. Res. 112 (F2): F02S13, doi:10.1029/2006JF000545.

Salzmann, N. et al. 2007a. The application of Regional Climate Model output for the simulation of high-mountain permafrost scenarios. *Global and Planetary Change* 56 (1–2): 188-202.

Salzmann, N. et al. 2007b. RCM-based ground-surface temperature scenarios for complex high-mountain topography. *J. Geophys. Res.* 112: F02S12, doi:10.1029/2006JF000527.

Scherler, M. et al. Submitted. Investigation of meltwater infiltration into the active layer of an alpine permafrost site on Schilthorn, Switzerland. *Water Resources Research.*

Stendel, M. et al. 2007. Using dynamical downscaling to close the gap between global change scenarios and local permafrost dynamics. *Global and Planetary Change* 56(1–2): 203-214.

A Method for the Analysis of the Thermal Permafrost Dynamics

M.A. Hidalgo, J.J. Blanco, M. Ramos, D. Tomé
Physics Department, University of Alcala, Spain
G. Vieira
Centre for Geographical Studies, University of Lisbon, Portugal

Introduction

Antarctica is one of the most sensitive areas to climate change in the world. This is close to the upper limit for permafrost viability and, therefore, studying the distribution and the state of the permafrost, we can monitor climate evolution. Livingston Island (62°39′S, 60°21′W – South Shetland archipelago) is located 50 km west of the Antarctic Peninsula. Almost 90% of the island is glacierized, and the rest has a seasonal snow cover, coinciding with the periglacial domain.

Experiment Description

The Incinerador borehole drilled in quartzite bedrock has a depth of 2.4 m with a diameter of 90 mm. There is a logger chain inside the borehole pipe. Since January 2004, the chain is composed of 6 loggers placed at different depths: 5, 15, 40, 90, 150, and 230 cm. The time interval between consecutive measurements is 1 hour and the accuracy of the dataloggers (tiny talk Gemini Co.) is 0.2°C.

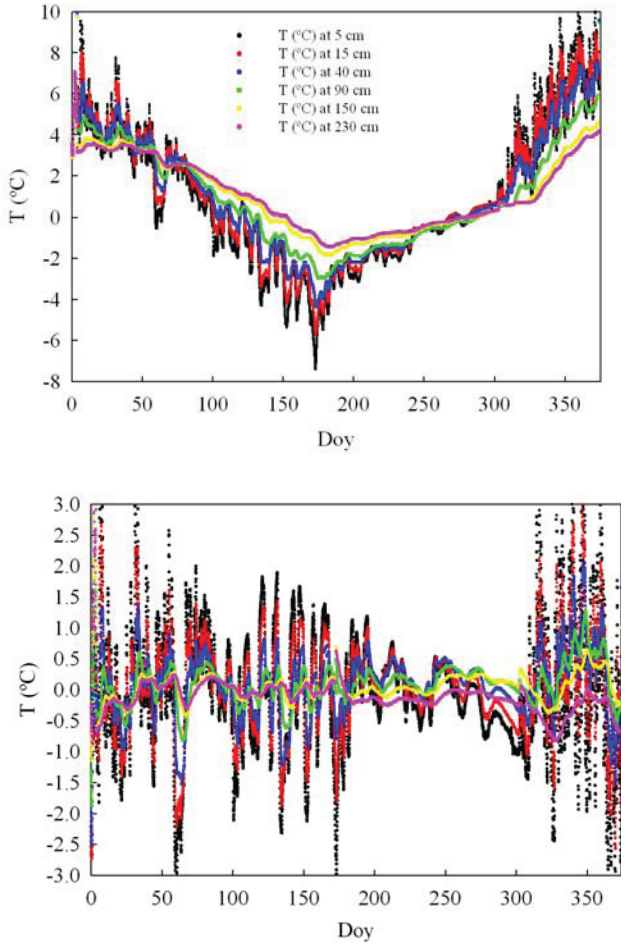

Figure 1. Temperatures recorded during the year 2005 at the different depths (indicated with the legend insert): (1a) the original data, (1b) the data after detrending.

Data Analysis

In Figure 1a, we show the temperatures at the different depths mention above recorded during the year 2005 as a function of the day of year (doy).

Previous to the FFT analysis, a detrending process over the data corresponding to every record was made (Fig. 1b). After that, the FFT power spectrum obtained is shown in Figure 2.

Model Description

The study of the permafrost and thermal regime of the active layer require the knowledge of their thermal diffusivity. This parameter is the key to understanding the thermal response of the soil—in particular, the exponential attenuation of the temperature wave with depth and the lag in phase. (In all the presented study, we assume that there are no thermal sources along all the depths considered).

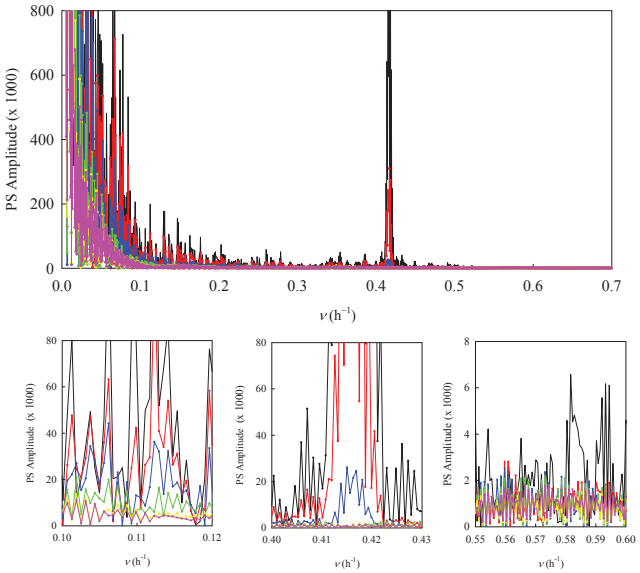

Figure 2. Power spectrum from the FFT analysis made over the detrending data of Figure 1b: (2a) the power spectrums in all the frequency range for the different depths (the colour legends are the same as in Figure 1; (2b)–(2d) details at different frequency ranges.

The temperature regime is determined by the well-known heat conduction equation:

$$\frac{\partial T}{\partial t} = a^2 \frac{\partial^2 T}{\partial z^2} \quad (1)$$

where T is the temperature, t and z the time and depth variables, respectively, and a the thermal diffusivity, given by

$$a = \sqrt{\frac{\kappa}{c\rho}}$$

with κ the thermal heat coefficient, ρ the soil density and c its specific heat. Our starting point is the resolution of equation (1) with the single harmonic boundary condition $T_n(z=d,t)=0$ and $T_n(z=0,t)=T_n^0 \cos(\omega_n t)$. Using the separation variables method, the solution of equation (1) is given by the expression

$$T_n(z,t) = T_n^0 \frac{\sin(\gamma_n(d-z))}{\sin(\gamma_n d)} exp(-i\omega_n t)$$

where

$$\gamma_n = \sqrt{\frac{\omega_n}{2a^2}}(1+i)$$

Developing the solution, we obtain

$$T_n(z,t) = \frac{T_n^0}{\left(\cosh^2\beta_n - \cos^2(\beta_n)\right)} \times \times \left[A_n \cos(\omega_n t) + B_n \sin(\omega_n t)\right] \quad (2)$$

where

$$A_n = \sin(\alpha_n)\sin(\beta_n)\cosh(\alpha_n)\cosh(\beta_n) + + \cos(\alpha_n)\cos(\beta_n)\sin h(\alpha_n)\sinh(\beta_n)$$

and

$$B_n = \sin(\alpha_n)\cos(\beta_n)\cosh(\alpha_n)\sinh(\beta_n) - - \cos(\alpha_n)\sin(\beta_n)\sin h(\alpha_n)\cosh(\beta_n)$$

with

$$\alpha_n = \sqrt{\frac{\omega_n}{2a^2}}(d-z) \text{ and } \beta_n = \sqrt{\frac{\omega_n}{2a^2}}d \quad (3)$$

adding now all the harmonics corresponding to the temperature data recorded at the depth z=0 (and consequence of its Fourier analysis), $T(z=0,t) = \sum_n T_n^0 \cos\omega_n t$, and also considering the boundary condition $T(z=d,t)=0$.

Hence, we can predict and reconstruct the expectable temperature record at any depth, using the linear superposition principle. Simultaneously, this solution allows us to estimate the behaviour of the diffusivity at different depths (see below).

Discussion

Although snow in the surface is thought to be a low-pass filter for the temperature signal (Goodrich, 1982), we find that the dependence of the diffusivity with depth is complex and determinant for interpreting the experimental data. Thus, looking at the results of the FFT power spectrum analysis of the temperature signal at different depths (Fig. 2a–2b), it is clearly seen the strong dependence of the thermal wave with frequency. Figure 2b shows the results for frequencies around $\nu_n \approx 0.11$ Hz , where an almost linear decay of the corresponding amplitude T_n is observed, according with its linear dependence with depth reflected in the term α_n. On the other hand, to explain the tendencies shown for the amplitudes at frequencies $\nu_n \approx 0.41\ h^{-1}$ and $\nu_n \approx 0.55\ h^{-1}$ we necessarily assume an increase of the term β_n with depth, what implies a decrease of the diffusivity with it. This non-uniform diffusivity is a consequence of the variation of some of the magnitudes, and depends on the density, the conductivity, or the specific heat. Because it does not seem to justify a significant variation in either density or specific heat in the depths we are considering, the decrease seems to be related to thermal conductivity. Of course, a good knowledge of behaviour of the diffusivity with depth allows a better forecasting of the thermal evolution of the soil.

Using the presented method to analyse temperatures, data recorded in periods of several years will allow us to make a precise determination of the soil properties under interest, the evolution of the active layer, and their implication on climate. Thus, we will develop a tool implemented with the commercial program IDL with which we will analyse automatically the behaviour of the active layer. Even more, we will extend the presented model, taking into account thermal sources along the depth of interest, which could be very interesting for the study of the evolution of the active layer in soils.

Acknowledgments

This research was founded by the Spanish Ministerio de Educación y Ciencia project, reference code: POL2006-01918/CGL.

References

Blanco, J.J. et al. 2007. Active layer apparent thermal diffusivity and its dependence on atmospheric temperature (Livingston Island, Maritime Antarctic). *U.S. Geological Survey and the National Academies*, USGS OF-2007-1047, Extended Abstract.

Goodrich, L.E. 1982. The influence of the snow cover on the ground thermal regime. *Canadian Geotechnical Journal* 19: 421-432.

Hauck, C. et al. 2007. Geophysical identification of permafrost in Livingston Island, Maritime Antarctica. *Journal of Geophysical Research* (in press).

Ramos, M. & Vieira, G. 2003**.** Active Layer and Permafrost Monitoring in Livingston Island, Antarctica, first results from 2000 and 2001. In: M. Phillips, S.M. Springman, & L.U. Arenson (eds), *Permafrost* 2: 929-933. ICOP 2003. A.B. Balkema. Rotterdam.

Ground Truth Observations of the Interior of a Rock Glacier as Validation for Geophysical Monitoring Datasets

Christin Hilbich
Department of Geography, University of Jena, Germany
Isabelle Roer
Department of Physical Geography, University of Zurich, Switzerland
Christian Hauck
Institute for Meteorology and Climate Research, Karlsruhe Institute of Technology (KIT), Germany

Introduction

Monitoring the permafrost evolution in mountain regions is currently one of the important tasks in cryospheric studies, as little data on past and present changes of the ground thermal regime and its material properties are available. In addition to existing borehole temperature monitoring networks, techniques to determine and monitor the ground ice content have to be developed. A reliable quantification of ground ice is especially important for modeling the thermal evolution of frozen ground and for assessing the hazard potential due to thawing permafrost- induced slope instability.

Near-surface geophysical methods are increasingly applied to detect and monitor ground ice occurrences in permafrost areas. Commonly, characteristic values of electrical resistivity and seismic velocity are used as indicators for the presence of frozen material. However, validation of the interpretation of geophysical parameters can only be obtained through boreholes, limited to vertical temperature profiles. Ground truth of the internal structure and the ice content is usually not available.

During the construction of a ski track in summer 2007 we had the unique opportunity to conduct geophysical measurements (Electrical Resistivity Tomography [ERT] and Refraction Seismic Tomography [RST]) on a partly excavated rock glacier near Zermatt (Valais, Swiss Alps) and to calibrate the data with direct observations. (For further description of the study site, impacts, and investigations, see Maag et al. 2008 and Wild et al. 2008).

Rock Glacier Composition

The general stratigraphy of rock glaciers is described by several authors (e.g., Barsch 1996, Burger et al. 1999) as a sequence of 3 main layers: (1) The uppermost 1–5 m consist of big boulders riding on (2) an ice-rich permafrost layer (with 50–70% ice and ca. 30% finer-grained material (Barsch 1996), which is creeping downslope. (3) The lowermost layer consists of larger rocks, which were deposited at the rock glacier front and subsequently overrun by the other layers. Despite numerous investigations of rock glaciers worldwide, direct observations of the internal structure of rock glaciers are rare. More detailed studies on stratigraphy result from direct observations in boreholes (e.g., Haeberli et al. 1998, Arenson et al. 2002) and indirect geophysical data (e.g., Vonder Mühll 1993, Hauck 2001, Maurer & Hauck 2007).

Observed composition of the Gornergrat rock glacier

Trenches cut during the construction of the ski track (up to 12 m) provided insight into the composition of the blocky active layer, a frozen mix of blocks, fine sediment and ice underneath, followed by a massive ice core. To validate the geophysical data, the respective fractions of rock, ice, water, and air were roughly estimated by visual inspection (Table 1).

Table 1. Estimated fractions (f) of rock, ice, air, and water for different layers observed during the final construction stage.

	f_{rock}	f_{air}	f_{water}	f_{ice}
Active layer (2-3 m)				
Coarse blocks	0.6-0.7	0.3-0.4	0	0
Mix of blocks and fine sediment	0.8	?	?	0
Intermediate layer (3-5 m)				
Blocks with interstitial ice	0.5	0	0	0.5
Lowest observed layer				
Massive ice with few blocks	0.2-0.4	0	0	0.6-0.8

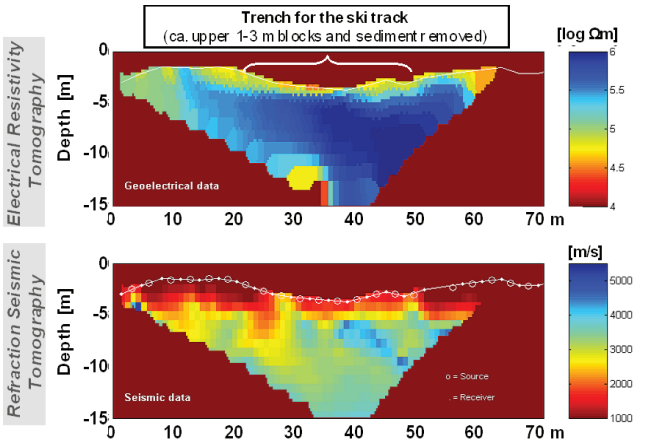

Figure 1. Inversion results for electrical resistivities and *P*-wave velocities obtained at the survey line.

Geophysical Data

In the beginning of the construction of the ski track, while only little material had been removed so far, we conducted ERT and RST measurements on a longitudinal profile (70 m) in the upper part of the rock glacier (Fig. 1).

High resistivity zones coincide with high velocity zones, indicating a high ice content within the rock glacier, especially in the upper (right) part of the profile. The active layer is clearly delineated by smaller resistivities and velocities in the uppermost 2–3 m of the profile. In the central part, the active layer had already been disturbed by the construction work.

Quantification of Material Properties

The Four Phase Model (FPM)

The indirect nature of geophysical soundings requires a relation between the measured variable (electrical resistivity, seismic velocity) and the rock/soil, water, air, and ice contents. The so-called Four Phase Model (FPM) (Hauck et al. 2008) determines volumetric fractions of these four phases from tomographic electrical and seismic datasets. It is based on geophysical mixing rules for electrical resistivity and seismic *P*-wave velocity. Observed resistivity and velocity data are used as input data on a two-dimensional grid (Fig. 1).

Application of this model to the geophysical dataset of the rock glacier allows for an estimation of the total fractions of ice, water, air, and the rock matrix with non-intrusive methods. Direct observations from the trenches cut for the ski track provide a unique opportunity to validate the FPM results and to evaluate the performance of the model.

Modeled composition of the Gornergrat rock glacier

Dominant materials calculated by the FPM are rock and ice with an average ratio of about 50%:40%. The contents of air and water are negligible below the uppermost 3 m, and do not exceed 10% (water) and 40% (air) within the active layer.

A critical parameter is the resistivity of the pore water ρ_W, which has to be prescribed beforehand. This parameter was measured in the field, but yielded 2 different values: 274 Ωm for melted ice (from a previously frozen ice sample), and 69 Ωm for collected meltwater, running out of the rock glacier. The FPM was calculated for both values, resulting in distinct differences for the content of unfrozen water: up to 10% (for 274 Ωm), and less than 5% (for 69 Ωm). Consequences for the other phases are small; only a slight increase in ice content is observed for higher values of ρ_W, but with a slightly lower saturation of the available pore space.

Separated into active layer and the underlying ice core, the respective fractions can be averaged (Table 2).

Discussion

A comparison of modeled and observed (visually estimated) fractions of all four phases in the trenches cut for the ski track yields a very good accordance in terms of geophysical identification of solid (ice, rock), gaseous, and liquid phases. The differentiation between ice and rock is difficult, since seismic velocities of both phases can be very similar. Also, it has to be noted that direct observations/estimations were only made in several outcrops, and showed considerable small-scale heterogeneity of the rock-ice distribution. However, despite the remaining uncertainties of the FPM, the preliminary results seem realistic in terms of identification of the four phases and their relative distribution.

In a further step, relative changes of electrical resistivities and seismic velocities derived from geophysical monitoring data will be used to estimate total seasonal or annual changes in the contents of ice and unfrozen water to quantify permafrost degradation due to climate change.

Table 2: Calculated fractions of rock, air, water, and ice.

	f_{rock}	f_{air}	f_{water}	f_{ice}
Active layer	0.4-0.6	0.3-0.4	0.02-0.08	0-0.4
Ice core	0.4-0.5	0	0-0.03	0.4-0.6

References

Arenson, L., Hoelzle, M. & Springman, S. 2002. Borehole deformation measurements and internal structure of some rock glaciers in Switzerland. *Permafrost and Periglac. Process.* 13(2): 117-135.

Barsch, D. 1996. *Rockglaciers: Indicators for the Present and Former Geoecology in High Mountain Environments*. Berlin, Springer.

Burger, K.C., Degenhardt, J.J. & Giardino, J.R. 1999. Engineering geomorphology of rock glaciers. *Geomorphology* 31(1–4): 93-132.

Haeberli, W., Hoelzle, M., Kääb, A., Keller, F., Vonder Mühll, D. & Wagner, S. 1998. Ten years after drilling through the permafrost of the active rock glacier Murtèl, eastern Swiss Alps: answered questions and new perspectives. *Proceedings of the Seventh International Conference on Permafrost*, *Yellowknife, Canada*.

Hauck, C. 2001. *Geophysical Methods for Detecting Permafrost in high Mountains*. Mitt. der Versuchsanst. für Wasserbau, Hydrol. und Glaziol. der Eidg. Tech. Hochsch. Zurich, Nr. 171: 204 pp.

Hauck, C., Bach, M. & Hilbich, C. 2008. A 4-phase model to quantify subsurface ice and water content in permafrost regions based on geophysical datasets. *Proceedings of the Ninth International Conference on Permafrost, Fairbanks, Alaska, 29 June–3 July 2008.*

Maag, C., Wild, O., King, L., Baum, M., Klein, S. & Hilbich, C. 2008. Permafrost characteristics and climate change consequences at Stockhorn and Gornergrat (Swiss Alps). *Proceedings of the Ninth International Conference on Permafrost, Fairbanks, Alaska, 29 June–3 July 2008.*

Maurer, H. & Hauck, C. 2007. Geophysical imaging of alpine rock glaciers. *Journal of Glaciology* 53(180): 110-120.

Vonder Mühll, D.S. 1993. *Geophysikalische Untersuchungen im Permafrost des Oberengadins*. ETH Zürich, Diss. ETH Nr. 10107: 222.

Wild, O., Roer, I., Gruber, S., May, B. & Wagenbach, D. 2008. Scientific opportunities and environmental impacts related to ski run construction, Zermatt, Swiss Alps. *Proceedings of the Ninth International Conference on Permafrost, Fairbanks, Alaska, 29 June–3 July 2008.*

Internal Structure of Rock Glacier Murtèl Delineated by Electrical Resistivity Tomography and Forward/Inverse Modeling

Christin Hilbich
Department of Geography, University of Jena, Germany

Introduction

Rock glacier Murtèl (Engadine, Swiss Alps) is one of the most intensely investigated rock glaciers worldwide. Borehole temperatures have been recorded since 1987 (Vonder Mühll & Haeberli 1990, Haeberli et al. 1998, Vonder Mühll et al. 1998, Vonder Mühll et al. 2007), providing one of the longest temperature records in Alpine permafrostFrom the broad range of investigations on this rock glacier, it has been learned that:

- The rock glacier Murtèl consists of a considerable amount of massive ice (up to 80–100% in a ca. 25 m thick layer below the active layer) (Vonder Mühll & Haeberli 1990).
- The active layer depths vary only slightly throughout the years (by max. 0.5 m) (Vonder Mühll et al. 2007).
- Rock glacier creeping is generally rather slow with velocities between 5 and 15 cm/a (determined over the period 1987–1996) (Kääb et al. 1998).
- A shear zone exists in 30 m depth, where most of the horizontal movement is concentrated (Arenson et al. 2002).

Apart from the borehole observations, no direct observations of the interior exist at rock glacier Murtèl. However, indirect information could be inferred from geophysical measurements (Vonder Mühll 1993, Hauck & Vonder Mühll 2003, Maurer & Hauck 2007).

In general, rock glacier Murtèl is considered an active rock glacier under stable conditions. The internal structure is assumed to be homogeneous without any distinct degradation phenomena.

Geoelectrical Monitoring

In summer 2005 a longitudinal Electrical Resistivity Tomography (ERT) monitoring profile was installed at rock glacier Murtèl. The horizontal distance of the profile is 235 m (crossing the borehole and the tongue). Results from the ERT monitoring give rise to an interesting inhomogeneity in the central part of the rock glacier.

The general resistivity pattern (Fig. 1) clearly confirms the stratigraphy derived from borehole measurements: the active layer is represented by relatively low resistivities between 15 and 30 kΩm in the upper 3 m. Beneath the active layer there is a sharp increase in resistivities to values between 500 kΩm and 1.9 MΩm, indicating the presence of massive ice. In the central part of the rock glacier, this pattern is interrupted by a vertical anomaly with smaller resistivity values (300–400 kΩm). The monitoring results indicate that this feature is much more pronounced in summer than in winter.

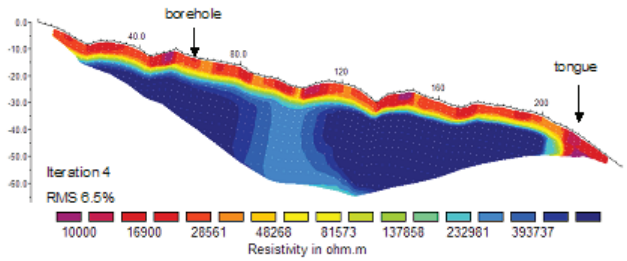

Figure 1. ERT tomogram from rock glacier Murtèl, measured on August 17, 2006.

To assess whether this anomaly is an artefact of the inversion process (cf. Hauck & Vonder Mühll 2003) or produced by a real structural inhomogeneity the resistivity distribution of the rock glacier was analysed by means of synthetic datasets and forward/inverse modeling using the software Res2DMod and Res2DInv (Loke & Barker 1995, Loke 2002). In forward/inverse modeling approaches, apparent resistivities are calculated from a synthetic model of the assumed resistivity distribution. The resulting inversion result can then be compared to the corresponding inversion result of the measured data. If the results are similar in terms of both resistivity distribution and total values, the synthetic model can be evaluated as a realistic model of the subsurface resistivity distribution.

This procedure was performed for a variety of geomorphological situations that may explain the inhomogeneity within rock glacier Murtèl.

Best results were obtained for a simulated crevasse in the massive ice body of the rock glacier, which is, at least partly, filled with unfrozen water. This result is surprising, as the rock glacier does not show indications of disintegration at the surface. An interpretation of this feature in terms of a degradation phenomenon seems likely, but cannot be supported by other data from the rock glacier.

Conclusions

The forward/inverse modeling showed that the resistivity anomaly in the central part of the rock glacier is very likely due to a crevasse-like structure within the ice core. These findings are of interest in the context of the observed speed-up of many rock glaciers in the Alps, which is often associated with disintegration of the surface and the formation of crevasses (Roer et al. 2005, Kääb et al. 2007). Since comparable developments (speed-up, formation of crevasses at the surface) are not known for rock glacier Murtèl so far, further studies are necessary to verify the assumptions resulting from forward/inverse modeling.

References

Arenson, L., Hoelzle, M. & Springman, S. 2002. Borehole deformation measurements and internal structure of some rock glaciers in Switzerland. *Permafrost and Periglacial Processes* 13: 117-135.

Barsch, D. 1996. *Rock Glaciers – Indicators for the Present and Former Geoecology in High Mountain Environments*. Berlin: Springer.

Burger, K.C., Degenhardt, J.J. & Giardino, J.R. 1999. Engineering geomorphology of rock glaciers. *Geomorphology* 31(1–4): 93-132.

Haeberli, W., Hoelzle, M., Kääb, A., Keller, F., Vonder Mühll, D. & Wagner, S. 1998. Ten years after drilling through the permafrost of the active rock glacier Murtèl, eastern Swiss Alps: Answered questions and new perspectives. *Proceedings of the Seventh International Conference on Permafrost, Yellowknife, Canada.*

Hauck, C. & Vonder Mühll, D. 2003. Inversion and interpretation of two-dimensional geoelectrical measurements for detecting permafrost in mountainous regions. *Permafrost and Periglacial Processes* 14: 305–318.

Kääb, A., Gudmundsson, G.H. & Hoelzle, M. 1998. Surface deformation of creeping mountain permafrost. Photogrammetric investigations on rock glacier Murtél, Swiss Alps. *Proceedings of the Seventh International Conference on Permafrost, Yellowknife, Canada:* 531-537.

Kääb, A., Frauenfelder, R. & Roer, I. 2007. On the response of rock glacier creep to surface temperature increase. *Global and Planetary Change 56*(1–2): 172-187.

Loke, M.H. & Barker, R.D. 1995. Least-squares deconvolution of apparent resistivity. *Geophysics* 60: 1682-1690.

Loke, M.H. 2002. *RES2DMOD, Ver. 3.01*: Rapid 2D resistivity forward modelling using the finite-difference and finite-element methods.

Maurer, H. & Hauck, C. 2007. Geophysical imaging of alpine rock glaciers. *Journal of Glaciology* 53(180): 110-120.

Roer, I., Kääb, A. & Dikau, R. 2005. Rock glacier acceleration in the Turtmann valley (Swiss Alps): Probable controls. *Norwegian Journal of Geography* 59: 157-163.

Vonder Mühll & Haeberli 1990

Vonder Mühll, D.S. 1993. Geophysikalische Untersuchungen im Permafrost des Oberengadins. *ETH Zürich, Diss. ETH* 10107: 222.

Vonder Mühll, D., Stucki, T. & Haeberli, W. 1998. Borehole temperatures in alpine permafrost: a ten years series. *Proceedings of the Seventh International Conference on Permafrost, Yellowknife, Canada*.

Vonder Mühll, D., Noetzli, J., Roer, I., Makowski, K. & Delaloye, R. 2007. *Permafrost in Switzerland 2002/2003 and 2003/2004.* Glaciological Report (Permafrost) No. 4/5 of the Cryospheric Commission (CC) of the Swiss Academy of Sciences (SCNAT) and the Department of Geography, University of Zurich: 106.

Permafrost Degradation Beneath a Heat-Producing Coal Waste Rock Pile, Svalbard (78°N)

Jørgen Hollesen
Department of Geography and Geology, University of Copenhagen, Copenhagen, Denmark
UNIS, Longyearbyen, Svalbard
Bo Elberling
Department of Geography and Geology, University of Copenhagen, Copenhagen, Denmark
UNIS, Longyearbyen, Svalbard

Introduction

In Arctic areas, permafrost and low annual air temperatures are considered to keep the chemical activity within sulphide-containing waste rocks low. This has led to a general acceptance that permafrost environments are well suited for storing waste rocks. Although temperatures below 0°C reduce the oxidation rate of sulphide minerals, they do not eliminate oxidation (Elberling 2001). Furthermore, the oxidation of sulphide minerals is strongly exothermic producing 1409 KJ of heat for every mole oxidized. Because the oxidation rate of sulphides increases with temperature (Elberling 2005), the release of heat can result in a positive feedback on the oxidation process, causing subsurface temperatures to become self-increasing (Lefebvre et al. 2001). Depending on the local meteorological conditions, the sulphide content of the waste material and the physical design of the waste rock pile, subsurface temperatures can become so high that weathering processes continue year-round within the waste rock pile (Elberling et al. 2007). This is not only important to the overall amounts pollutants released but also to the stability of the permafrost beneath the pile which could be degraded, causing the foundation of the waste rock pile to destabilise.

The objective of this study is to investigate the thermal regime within a coal waste rock pile on Svalbard and to simulate subsurface temperatures due to current weather conditions, physical properties of the waste rock material, and subsurface heat generation. The simulations will be carried out using the one-dimensional heat and water flow model, CoupModel (Jansson & Karlberg 2001), which will be calibrated and validated based on data from the study area. The validated model will be used to investigate how the permafrost beneath the waste rock pile is influenced by the oxidation processes.

Study Site

In this High Arctic study, an abandoned coal waste rock pile near Longyearbyen, Svalbard (78°20′N, 15°40′E) is investigated. Based on data from 1975–2005, the mean annual air temperature of the area is -5.8 ± 1.3°C and the annual amount of precipitation is 187 ± 44 mm, of which approximately 50% falls as snow. Svalbard is located within the region of continuous permafrost with an active layer thickness of 1.0 to 1.5 m. The construction of the waste rock pile was initiated in 1986 and completed in 1990 with a height of 20 m (roughly 200,000 m^3 of waste rock). It stands out in the landscape with steep sides and is highly exposed to winds.

The waste rock pile has previously been described by Elberling et al. (2007). The waste rock material is very coarse and heterogeneous with only 16% ± 6% being less than 2 mm in diameter and 40% being above 100 mm in diameter. It is dominated by 1–10 mm rocks, but contains rocks more than 0.5 m in diameter. Heat production rates due to pyrite oxidation range from 0.5 to 2.5 μW g^{-1} and a significant exponential increase in heat production has been noted with increasing temperatures (R^2 = 0.98, p = 0.001) which is equal to a Q_{10} of 2.6.

Methods

Based on climatic inputs (air temperature, wind speed, wind direction, relative humidity, radiation, pressure, and snow depth), grain size distribution, porosity and microbial and chemical heat production rates from pyrite oxidation, the CoupModel is used to simulate subsurface temperatures within and below the waste rock pile. The model is calibrated using measurements of subsurface temperatures from 1 October 2004 to 19 August 2005 and validated using measurements from 1 October 2005 to 19 August 2006.

Results

Despite freezing air temperatures 240 days per year subsurface temperatures within the investigated pile were stable around 4.3 ± 0.5°C at 7 m depths throughout the year. Seasonal temperature readings indicate that an outer layer of less than 1 m remained frozen during the six-month winter period. Observations of nearby natural permafrost-affected talus slopes confirm that, without subsurface heat generation, only a thin near-surface layer of less than 2 m thaw every summer (Fig. 1).

The CoupModel setup is successfully calibrated and validated. With r^2 values ranging from 0.99 to 0.64 and p values being <0.001, the linear correlations are highly significant in all depths. The mean temperature differences range from 0.04°C to 1.15°.

Simulations show that the underlying permafrost is strongly influenced by the heat from the waste rock pile. The zone of thaw has changed from 1–2 m in 1986 to 25 m in 2006, and in 2006, temperatures are influenced down to a depth of 50 m (Fig. 1).

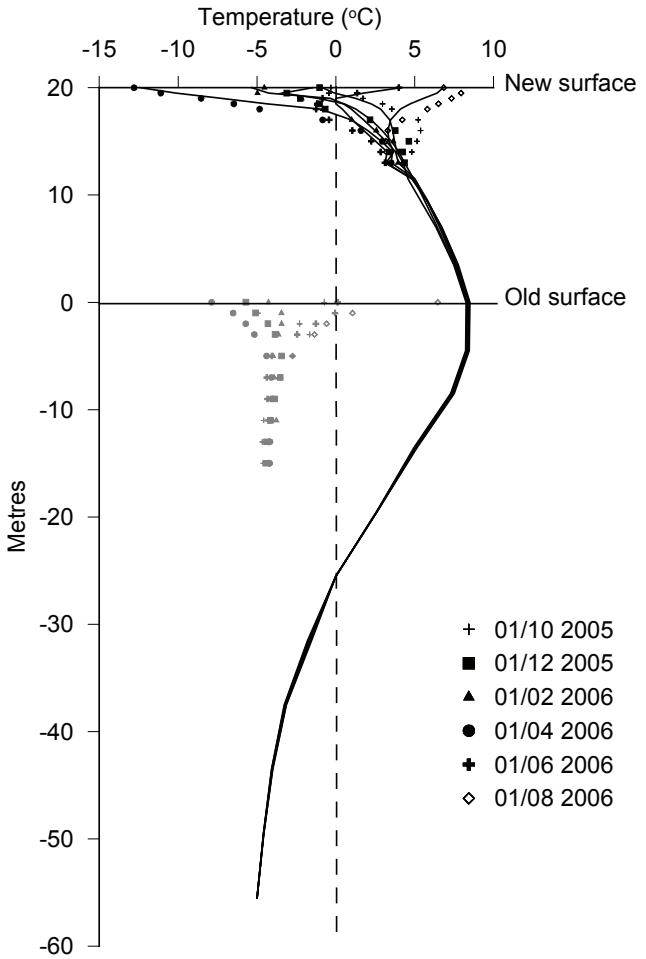

Figure 1. Observed and simulated subsurface temperatures within and beneath the waste rock pile in Bjørndalen (black symbols and lines, respectively). The grey symbols show subsurface temperatures within a nearby talus slope (provided by N. Matsuoka, pers. com., 2008).

Discussion

It is not possible to measure temperatures beneath the waste rock pile; thus the actual thaw depth is unknown.

Observations of the water runoff coming from the pile do show, however, that high concentrations of reduced Fe are coming out at the foot of the pile (Søndergaard et al. 2007). This suggests that water draining from the pile is at least partly infiltrating the newly formed and saturated active layer below the pile.

Many Arctic waste rock piles are located in near-coast regions; thus destabilisation due to permafrost degradation could cause the pollution to spread to the marine environment. There is no evidence that the melting of the permafrost has influenced the stability of the waste rock pile in Bjørndalen. However, as the pile is located on a downward slope the risk still exists, especially if temperatures increase further due to climate change.

References

Elberling, B. 2001. Environmental controls of the seasonal variation in oxygen uptake in sulfidic tailings deposited in a permafrost-affected area. *Water Resources Research* 37: 99-107.

Elberling, B. 2005. Temperature and oxygen control on pyrite oxidation in frozen mine tailings, *Cold Regions Science and Technology* 41(2): 121-133.

Elberling, B., Søndergaard, J., Jensen, L.A., Schmidt, L.B., Hansen, B.U., Asmund, G., Balic-Zunic, T., Hollesen, J., Hansson, S., Jansson, P.E. & Friborg, T. 2007. Arctic vegetation damage by winter-generated coal mining pollution released upon thawing. *Environ. Sci. Technol.* 41(7): 2407-2413.

Jansson, P.E. & Karlberg, L. 2001. Coupled *heat and mass transfer model for soil-plant-atmosphere systems*. Royal Institute of Technology, Dept of Civil and Environmental Engineering, Stockholm, Sweden.

Lefebvre, R., Hockley, D., Smolensky, J. & Gelinas, P. 2001. Multiphase transfer processes in waste rock piles producing acid mine drainage 1: Conceptual model and system characterization, *Journal of Contaminant Hydrology* 52(1–4), 137-164.

Søndergaard, J., Elberling, B., Asmund, G., Gudum, C. & Iversen, K.M. 2007. Temporal trends of dissolved weathering products released from a high Arctic coal mine waste rock pile in Svalbard (78°N). *Applied Geochemistry* 22: 1025-1038.

Patterns in Soil Carbon Distribution in the Usa Basin (Russia): Linking Soil Properties to Environmental Variables in Constrained Gradient Analysis

Gustaf Hugelius, Peter Kuhry
Department of Physical Geography and Quaternary Geology, Stockholm University, Sweden

Introduction

Arctic and subarctic ecosystems harbour large reservoirs of soil organic matter (SOM) and are considered key components in the global carbon (C) cycle (White et al. 2000). To a large degree, this C is found in cryosols and cryic histosols, where subzero temperatures limits decomposition (Davidson & Janssens 2006). We compile and analyse a database describing soil C properties, permafrost conditions, and vegetation in the Usa Basin of Northeastern European Russia. We update previous calculations of landscape soil C storage for the whole Usa Basin and describe general patterns of landscape C allocation with respect to vegetation and permafrost. We analyse a subset of the database in constrained gradient analysis combined with Monte Carlo permutations to determine how an array of environmental variables are linked to site-specific soil quantity and quality.

Study Area

The Usa River Basin straddles the Arctic Circle in Northeastern European Russia, covering some 93,500 km^2. Spruce dominated taiga covers the southern parts of the basin and gradually gives way to open ground in a wide taiga-tundra transition zone. Isolated permafrost first appears in peatlands of this transition zone, but increases as tundra begins to dominate the landscape. The northern lowland parts of the basin are dominated by tundra and peatland with extensive permafrost. Subalpine forests of Larch and Fir grow in the foothills of the Ural Mountains, which denote the eastern border of the basin.

Methods

The analysed database contains soil chemical and physical descriptions from 363 different sites and includes both upland soils and peat. For each site, the soil database lists vegetation cover, soil type (FAO-WRB), depth of soil genetic horizons, top organics, and active layer (if permafrost is present). Carbon storage is calculated to 30 and 100 cm reference depths in mineral soils and to full depth in peatlands. For a subset of the database there is also data on nitrogen (N) content. The C:N ratio of peat decreases as the material is degraded and is considered a useful proxy for quality (Kuhry & Vitt 1996). We also analyse a GIS database of the Usa Basin containing maps of soils (Mazhitova et al. 2003) and permafrost (Oberman & Mazhitova, 2003) as well as 100 m resolution Digital Elevation Model (DEM) and a satellite Land Cover Classification (LCC, 30*30m Landsat TM data, Virtanen et al. 2004). Climate data is interpolated from the 16 km grid of the HIRHAM regional climate model (Christensen & Kuhry 2000).

Analyses

For the purpose of Soil C calculations and upscaling, the Usa Basin is divided into ecoclimatic regions (Fig. 1). The sites in the database are ordered according to region and vegetation. Mean soil C content is then calculated for each vegetation type in the separate regions. We also calculate the proportion of C that is stored in Cryosols. The results are upscaled to full areal coverage using vegetation data from the LCC.

For a subset of lowland sites (n = 68), soil properties are analysed with Redundancy Analysis (RDA). This constrained ordination technique is used to assess the relationships within and between two separate data matrices of response and environmental variables.

For each pedon, a total of nine soil response variables are included: **1–3:** Carbon storage (kgC/m^2) in three depth intervals (0–30 cm, 30–100 cm, and >100 cm); **4–6:** percentage of C that is in top organics, in peat and in permafrost; **7:** Bulk Density (BD, g/cm3); **8–9:** C:N ratio of organic soil horizons and C:N ratio of mineral soil horizons.

The environmental variables permafrost, vegetation, and soil are available from field observations as well as geomatic sources. The Topographic Wetness Index is calculated from a DEM. Climate variables are derived from the HIRHAM model.

We perform RDAs of the response variables, separately using each environmental variable to constrain the ordination (software CANOCO 4.5). The explanatory power of each

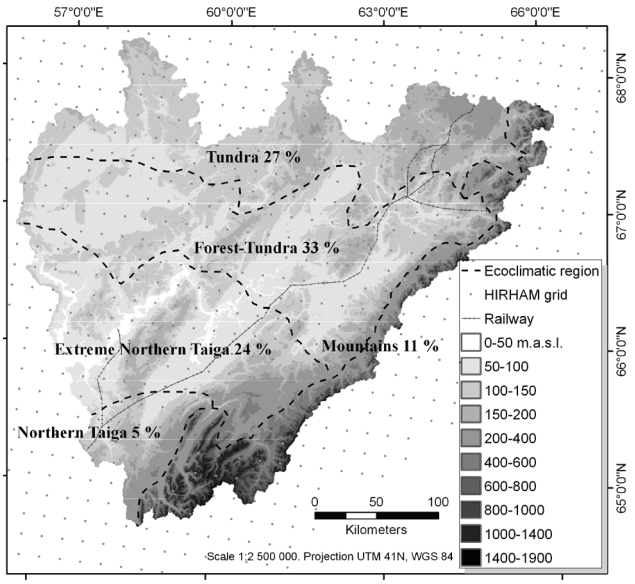

Figure 1. Map showing the coverage of ecoclimatic regions in the Usa Basin with the HIRHAM grid, railway, and topography.

environmental variable is determined through Monte Carlo permutations of the canonical eigenvalues of each RDA (999 permutations).

To further constrain the ordination, the variables that are found to be statistically significant are tested together in a RDA *Monte Carlo forward selection* process (p-value <0.05, Bonferroni correction applied). For this process, the site-corresponding variables from site-specific and geomatic sources were separated and tested in two independent RDAs.

Results

Storage and partitioning

Estimates of soil C storage for 30 cm, 100 cm, and full depth of peatlands in the five ecoclimatic regions are summarised in Table 1. The mean for the entire catchment is 34.8 kgC/m^2 when full depth of peatlands is included. Kuhry et al. (2002) estimated a total storage of 33.0 kgC/m^2 in the Usa Basin for the same depths.

When looking at separate vegetation classes, it is evident that peatlands store a disproportionate portion of soil C. Fen and bog peatlands cover some 30% of the Basin, but hold more than two-thirds of all C. Bogs alone cover less than a fifth, but hold more than half of all C in the Basin.

Carbon storage in permafrost terrain is dominated by bog peatlands. Bogs hold some 90% of permafrost C and >95% of perennially frozen C in the Usa Basin. While there is extensive permafrost underlying northern tundra vegetation, the active layer boundary is generally below the C-rich top organic layer.

Table 1. Area and C storage for regions and whole basin.

Region	Area km^2	30 cm kgC/m^2	100 cm kgC/m^2	Total kgC/m^2
Northern Taiga	4,709	10.4	22.3	31.0
Extreme N. Taiga	22,600	11.2	27.3	38.3
Forest-Tundra	31,245	11.5	27.4	37.3
Tundra	24,720	11.2	27.1	38.1
Mountains	10,210	7.1	12.7	12.8
Whole Basin	93,484	10.8	25.5	34.8

Table 2. Summary of tested environmental variables.

Variable Type	Variable	p-value
Site	Permafrost	*<0.01**
"	Vegetation	*<0.01**
"	Soil	*<0.01**
Climate	Annual mean temperature	0.09
"	July temperature	0.17
"	Summer precipitation	*<0.05*
"	Winter precipitation	*<0.05**
"	Frost index	0.14
Climate / Geomatic	Conrads continentality index	0.48
Geomatic	Permafrost map	*<0.05*
"	Satellite LCC	*<0.01**
"	Soil map	*<0.01**
"	Topographic Wetness Index	0.77

The p-values of variables that were significant when tested separately are in italic. The variables that were further identified in the *forward selection* process are marked with an asterix*.

Constrained gradient analysis

Table 2 summarizes the environmental variables and their significance as explanatory variables. Permafrost, vegetation, and soil are all significant from both site specific and geomatic sources. This indicates that geomatic sources may be used to replace when actual field data is lacking.

Both summer and winter precipitation significantly explains the response variables. While July temperature, mean annual temperature, and the frost index should all affect permafrost occurrence, they are not significant explanatory factors here.

The RDA *forward selection* process further constrains the ordination by removing weak or redundant (collinear) variables. Summer precipitation is highly correlated to winter precipitation and does not contribute to the model. The Permafrost map was partly based on the soil map and satellite LCC, and is also found to be redundant.

Acknowledgments

Much of the material was collected and compiled in the EU 4th Framework TUNDRA project. Further compilation and analyses are funded through the EU 6th Framework CARBO-North project, and a grant of the Swedish Research Council.

References

Christensen, J.H. & Kuhry, P. 2000. High resolution regional climate model validation and permafrost simulation for the East-European Russian Arctic. *J. of Geophys. Res.* 105(D24): 29647-29658.

Davidson, E.A. & Janssens, I.A. 2006. Temperature sensitivity of soil carbon decomposition and feedbacks to climate change. *Nature* 440: 165-173.

Kuhry, P. & Vitt, D.H. 1996. Fossil Carbon/Nitrogen ratios as a measure of peat decomposition. *Ecology* 77(1): 271-275.

Kuhry, P. et al. 2002. Upscaling soil organic carbon estimates for the Usa Basin (Northeast European Russia) using GIS-based landcover and soil classification schemes. *Danish J. of Geog.* 102: 11-25.

Oberman, N.G. & Mazhitova, G.G. 2003. Permafrost mapping of Northeast European Russia based on the period of climatic warming 1970–1995. *Norwegian J. of Geog.* 57(2): 111-120.

Mazhitova, G.G. et al. 2003. Geographic Information System and Soil Carbon Estimates for the Usa River Basin, Komi Republic. *Eurasian Soil Science* 36(2): 123-135.

White, A. et al. 2000. The high-latitude terrestrial carbon sink: A model analysis. *Global Change Biology* 6: 227-245.

Total Storage and Landscape Distribution of Soil Carbon in the Central Canadian Arctic Using Different Upscaling Tools

Gustaf Hugelius, Peter Kuhry
Department of Physical Geography and Quaternary Geology, Stockholm University, Sweden
Charles Tarnocai
Agriculture and Agri-Food Canada, Ottawa, Canada
Tarmo Virtanen
Department of Biological and Environmental Sciences, University of Helsinki, Finland

Introduction

The arctic landscape displays variation on many different spatial scales, and different methods for calculating landscape C pools demand varying approaches to sampling.

In this study we assess the total storage and spatial distribution of soil C in continuous permafrost terrain of Central Canada. The landscape allocation of soil C is assessed using a transect-based soil sampling program carried out in the summer of 2006 at the shore of Lake Tulemalu, northern Kazan Basin (62°55′N, 99°10′W, Fig. 1). We combine and compare three upscaling methods of increasing sophistication: (1) arithmetic mean, (2) transect upscaling, and (3) landscape upscaling. For the latter, we compare land cover and geomorphological landscape elements as spatial proxies for upscaling.

Figure 1. Oblique air photograph facing southwards over the northernmost transect.

Methods

Field sampling and sample analyses

Soils were sampled along three 1 km transects, which were chosen to represent main vegetation types and geomorphology of the landscape. Once the transects were established, however, pedons were collected equidistantly every 100 m without further bias (33 sites). This sampling scheme combined selective representation of what was considered representative with a measure of randomization introduced by small-scale vegetation and micro-topography patterns. Sampling includes upland soils (to 1 m depth) and peat deposits (to mineral contact). At all non-peatland sites, three additional samples of the top organic layer were collected.

Samples from all sites were analyzed in 10 cm depth increments for bulk density and loss on ignition (LOI at 550°C and 950°C) to determine organic content. A subset of samples is tested in an elemental analyzer to accurately determine C and N content. For remaining samples a LOWESS regression model is constructed to translate LOI to C content. The age of basal peat samples from 8 selected sites is determined through radiocarbon dating.

Landscape classification and upscaling

To enable interpretation and landscape upscaling of soil sampling results, we mapped land cover and geomorphology in the larger surrounding area. A land cover classification (LCC) based on Landsat ETM+ imagery was produced and verified using inventoried ground truth points. The classification covers some 400 km^2 around the sampled transects, and the main land cover types are water bodies (35% coverage), fen and bog peatlands (16% and 11%, respectively), dry, moist and wet shrub tundra (6%, 20%, and 8% coverage, respectively), lichen tundra (3.5%) and non-vegetated ground (0.5% coverage). We focus our landscape upscaling on a smaller, 42 km^2, intensive study area, delineated to be representative of the sampled sites. Some 20 km^2 of this is water and will be excluded from the upscaling. A simplified land cover map of this area is shown in Figure 2. A geomorphological map was produced using black and white aerial imagery combined with multispectral satellite scenes. The map identifies features such as recent and relict raised shorelines and separates well-drained upland till soils from local hollows.

In the simplest upscaling method, we calculate an arithmetic mean of soil C storage at all 33 sites. For transect upscaling, the soil sampling results are upscaled according to the proportional distribution of land cover types and landscape elements along the inventoried transects. For the landscape upscaling, we use information from the land cover and geomorphology mapping to calculate total C pool, also assessing land cover and geomorphology proxies separately.

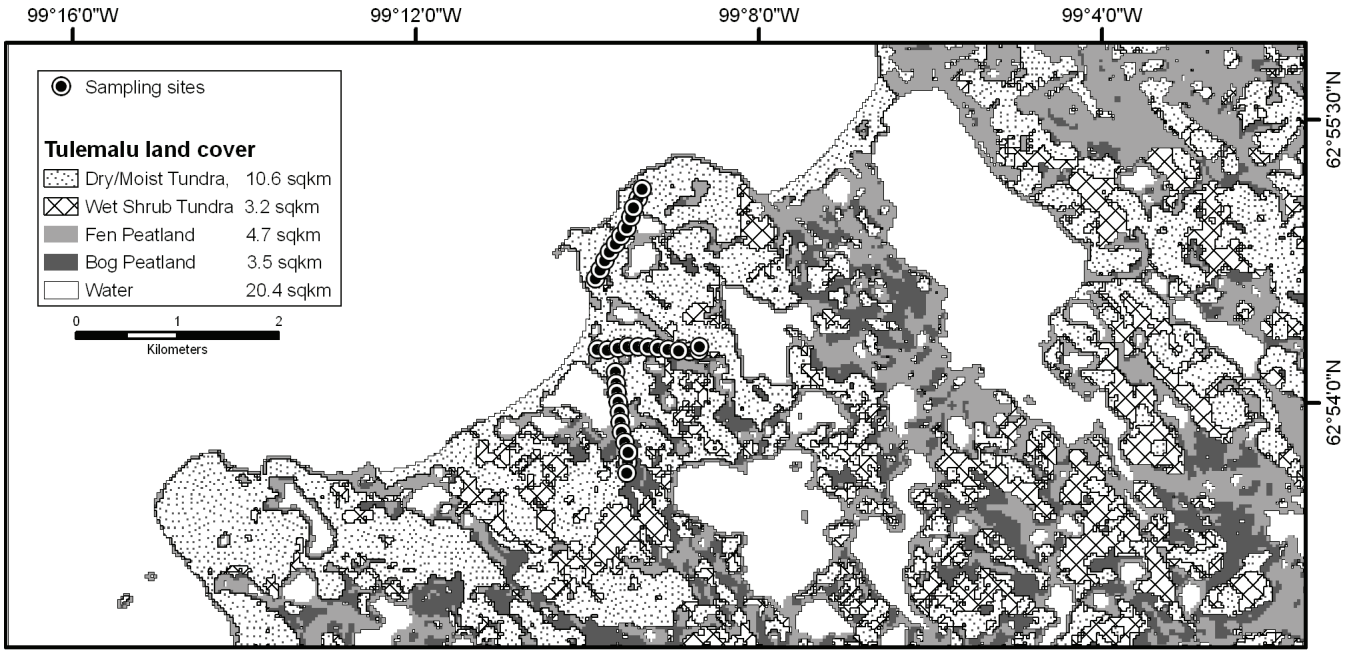

Figure 2. Map of the intensive study area showing land cover and sampling sites. Land cover is simplified with Bare ground, lichen tundra and dry/moist shrub tundra combined into one class.

Table 1. Summary of samples and land cover type coverage

Land cover type	Samples n / %	Organic layer	Transect coverage	Landscape coverage
Dry lichen tundra	3 / 9 %	3 cm	4 %	2 %
Dry shrub tundra	4 / 12 %	5 cm	5 %	9 %
Moist shrub tundra	12 / 35 %	6 cm	34 %	35 %
Wet shrub tundra	4 / 12 %	19 cm	12 %	14 %
Fen peatland	7 / 21 %	32 cm	21 %	21 %
Bog peatland	4 / 12 %	65 cm	21 %	16 %

Results

A summary land cover type representation in samples, transects, and the intensive study area is presented in Table 1. The land cover type Bare ground is only represented at the landscape level (2% of the intensive study area), and is not included. As no lake sediments have been sampled, water is also excluded.

The percentage representation for the three different upscaling techniques is quite similar. Dry lichen and shrub tundra is somewhat over represented in the number of samples collected, while Bog peatlands are under-sampled.

The mean depth of the top organic layers of tundra habitats seem to gradually increase along a moisture gradient. Average peat thickness in raised permafrost bogs is considerably higher than in fen peatlands. Radiocarbon dating shows that bogs are generally older than fens; the oldest basal peat from a bog is 5220 ± 50 C^{14}y BP while the corresponding age for fens is 1405 ± 30 C^{14}y BP.

Preliminary analyses indicate that most of the C is found in fen and bog peatlands. Calculated from arithmetic means, about three-quarters of the C is stored in peat or peaty tundra top organics. The wet shrub tundra stores significantly more C than do moist or dry shrub tundra classes, showing that it is important to make a distinction between shrub tundra classes for the landscape upscaling. Bog peatlands stand out with regard to storage of frozen C.

More than a third of all stored C is perennially frozen beneath the active layer boundary, mainly in histic Cryosols. The soils in the study area are heavily cryoturbated and a tenth of all C is found in cryoturbated soil layers.

An additional objective of this study is to compare average soil carbon storage derived from these intensive landscape analyses with previously published local/regional estimates as well as more general databases such as those provided by The Soil Organic Carbon of Canada Map (Tarnocai & Lacelle 1996).

Acknowledgments

Fieldwork and analyses was supported through a grant of the Swedish Research Council. We wish to thank Ms. Helen Dahlke for her assistance during fieldwork.

References

Tarnocai, C. & Lacelle, B. 1996. *Soil Organic Carbon of Canada Map*. Ottawa, Ontario: Eastern Cereal and Oilseed Research Centre, Agriculture and Agri-Food Canada, Research Branch.

Liquid Water Destabilizes Frozen Debris Slope at the Melting Point: A Case Study of a Rock Glacier in the Swiss Alps

Atsushi Ikeda, Norikazu Matsuoka
Graduate School of Life and Environmental Sciences, University of Tsukuba

Introduction

Positive correlation between temperatures and surface velocities of rock glaciers in various time scales indicates that ground warming accelerates rock glaciers (e.g., Kääb et al. 2007). In particular, rock glaciers lying close to the lower limit of local permafrost occurrence show high surface velocities (>0.2 m a^{-1}) and significant acceleration which appears to follow seasonal to decadal warming trends (Frauenfelder et al. 2003, Roer et al. 2005, Kääb et al. 2007, Delaloye et al. 2008). Such acceleration has been attributed to gradual heat conduction from the ground surface to the creeping layer lying below several meters' depth. In this report, we propose another model of acceleration by water infiltration, based on in situ monitoring of permafrost creep at the melting point (see also Ikeda et al. 2008).

Study Site

The studied rock glacier is the upper lobe of Büz North rock glacier (BNU), located on the northeastern slope of a peak named Piz dal Büz (lat. 46°32′N, long. 9°49′E, 2955 m a.s.l.) in the Upper Engadin, Switzerland (see also Ikeda & Matsuoka 2006 for detailed information). BNU originates from the foot of a talus slope at 2840 m a.s.l. and terminates at 2810 m a.s.l. The horizontal dimension (70 m long and 120 m wide) represents almost the minimum size identified as a rock glacier. The steep frontal slope is 10 m high, sloping at 35°. The upper surface is smooth and the average slope angle is 25°.

A pit and borehole indicated that the major components of BNU are platy shale pebbles and cobbles, the interstices of which are partly filled with sand and silt. Below the frost table, the debris was entirely ice-cemented to the bottom of the hole at 5.4 m depth. The gravimetric ice content of borehole cores (c. 10 cm long) was 50% at 4 m depth and 28% at 5 m depth.

Methods

Inclinometers (BKJ-A-10-D, manufactured by Kyowa Electronic Instruments, Japan) 35 cm long and 2.7 cm in diameter, installed at 4 m and 5 m depths in the borehole on August 9, 2000, measured the deformation of the perennially frozen debris continuously. Each inclinometer sensed inclinations along two directions perpendicular to each other within ±12.2° from the vertical with a resolution of 0.005°. The inclinations were recorded at 3 h or 6 h intervals by a datalogger until August 2, 2007. Ground temperatures (0.1°C resolution) at depths of 0, 0.5, 1, 2, 3, 4, and 5 m were also monitored for the same period.

Downslope inclination at a certain depth was calculated from the sum of the horizontal vectors, which were defined as the tangents of the measured inclinations for the two axes. Strain rates (i.e., vertical velocity gradients) at the two depths were also calculated. Note that inclination for one of the two axes at 5 m depth exceeded the measurement limit on February 3, 2003. From the day to July 2005, the inclination at 5 m depth was estimated from the measured inclination for the other axis using the former linear relationship between the two-axes' inclinations ($r^2 = 0.9995$).

Findings and a Presumed Model

Both inclinometers showed fast continuous deformation (on average, 2.4° a^{-1} and 6.0° a^{-1}) with large seasonal and interannual variations, while the permafrost temperatures remained almost at the melting point (Fig. 1). The movement of the inclinometers coincided with interannual changes in the surface velocities (Ikeda et al. in press). The strain rates at 5 m depth always surpassed those at 4 m depth, both of which had parallel patterns of seasonal variations. The strain rates rapidly increased in the snowmelt periods, indicated by the constant surface temperature at 0°C in early summer. In contrast, the strain rates gradually decreased below a dry snow cover in winter, except for the 2000–01 winter. When the freezing index at the ground surface was small, the decrease in strain rate tended to be small (or even the rate slightly increased in the 2000–01 winter), and the strain rate remained at a large value at the end of the dry snow period (Fig. 2). The highest strain rates at both depths were recorded when the unusually thick snow cover in 2000–01 was melting, whereas the net increases in the strain rates during a snowmelt period were smallest after the extremely snowless 2001–02 winter. In addition, the magnitudes of the acceleration during the snowmelt periods appeared to correlate with the shearing strain (i.e., net deformation) in the preceding dry snow periods.

These phenomena suggest that the frozen debris is permeable to water (mostly from snow melting), although ice-saturated debris is generally regarded as impermeable. The large annual strain rates (>0.1 a^{-1} at 5 m depth) of the coarse debris filled with ice probably result from thrusting up of debris particles over underlying particles within one year. The resulting dilatant deformation probably creates air voids in the frozen debris, a network of which eventually allows water infiltration. The water infiltration accelerates the deformation by reducing effective stress. The refreezing of the pore water, which depends on the cooling intensity in winter, decelerates the deformation. The combination of these processes, possibly affected by different amounts of annually developed air voids and available snowmelt water, controls the temporal variations in the deformation.

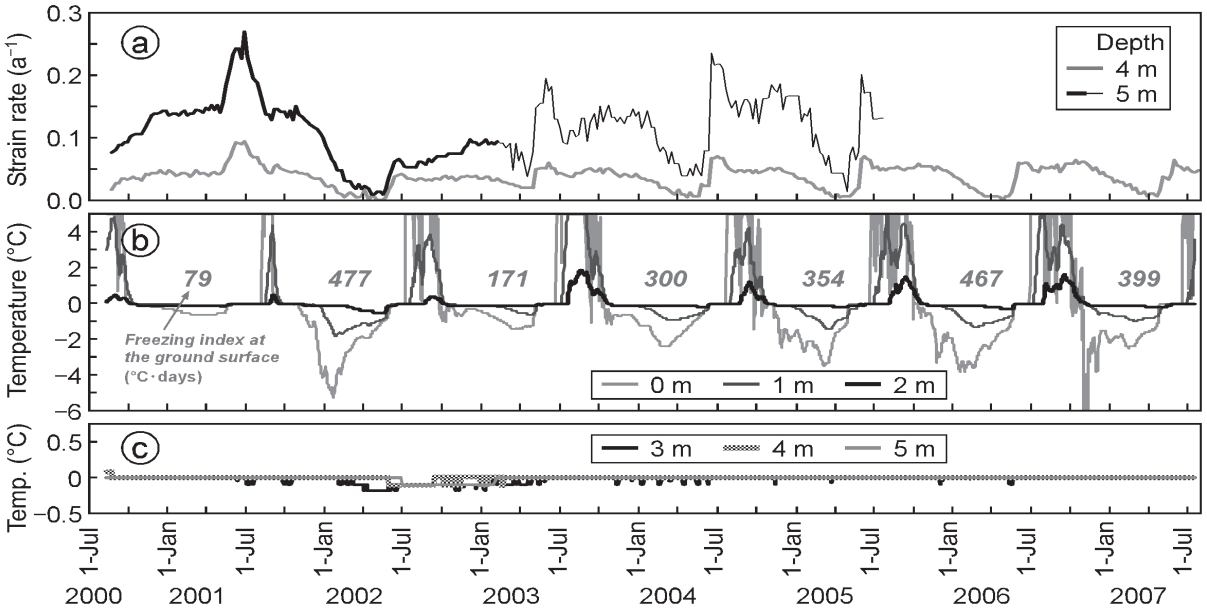

Figure 1. Seven-year records of (a) weekly shearing strain rates, (b) mean daily active-layer temperatures, and (c) permafrost temperatures. The thin line at 5 m depth in (a) is estimated from inclination to one axis after that to the other axis exceeded the measurement limit.

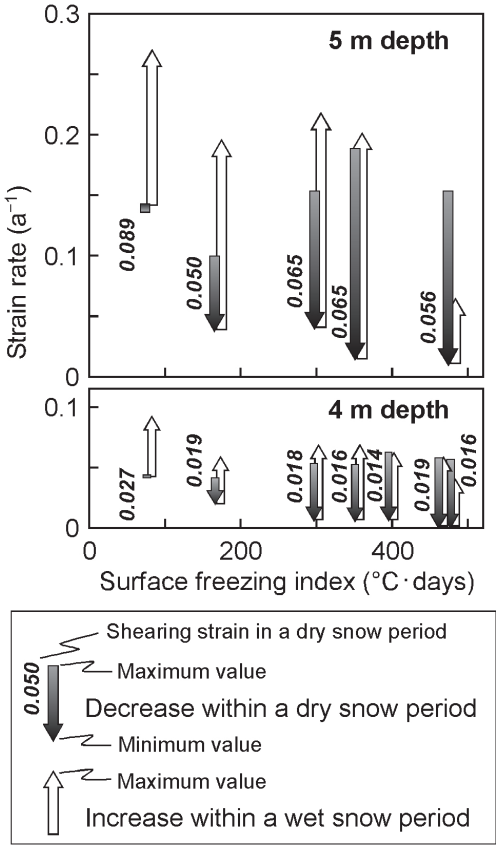

Figure 2. Relationship between surface freezing index and seasonal variations in strain rate. A wet snow period is defined by the constant ground surface temperatures at 0°C in summer and a dry snow period by the preceding subzero temperatures.

References

Delaloye, R., Perruchoud, E., Avian, E., Kaufmann, V., Bodin, X., Hausmann, H., Ikeda, A., Kääb, A., Kellerer-Pirklbauer, A., Krainer, K., Lambiel, C., Mihajlovic, D., Staub, B., Roer, I. & Thibert, E. 2008. Recent interannual variations of rockglacier creep in the European Alps. *Proceedings of the Ninth International Conference on Permafrost, Fairbanks, USA, June 29–July 23, 2008.*

Frauenfelder, R., Haeberli, W. & Hoelzle, M. 2003. Rockglacier occurrence and related terrain parameters in a study area of the Eastern Swiss Alps. *Proceedings of the Eighth International Conference on Permafrost, Zurich, Switzerland, July 21–25, 2003*: 253-258.

Ikeda, A. & Matsuoka, N. 2006. Pebbly versus bouldery rock glaciers: Morphology, structure and processes. *Geomorphology* 73: 279-296.

Ikeda, A., Matsuoka, N. & Kääb, A. 2008. Fast deformation of perennially frozen debris in a warm rock glacier in the Swiss Alps: An effect of liquid water. *Journal of Geophysical Research* 113 (in press).

Kääb, A., Frauenfelder, R. & Roer, I. 2007. On the response of rockglacier creep to surface temperature increase. *Global and Planetary Change* 56: 172-187.

Roer, I., Kääb, A. & Dikau, R. 2005. Rockglacier acceleration in the Turtmann valley (Swiss Alps): Probable controls. *Norsk Geografisk Tidsskrift* 59: 157-163.

TSP NORWAY – Thermal Monitoring of Mountain Permafrost in Northern Norway

Ketil Isaksen
Norwegian Meteorological Institute, Oslo, Norway
Herman Farbrot
Department of Geosciences, University of Oslo, Norway
Bernd Etzelmüller
Department of Geosciences, University of Oslo, Norway
Hanne H. Christiansen
The University Centre in Svalbard, Longyearbyen, Norway
Lars Harald Blikra
International Centre for Geohazards, Oslo, Norway
Kirsti Midttømme
Geological Survey of Norway, Trondheim, Norway
Jan Steinar Rønning
Geological Survey of Norway, Trondheim, Norway

Introduction

Permafrost is widespread in the higher mountains of Norway. Extensive studies in southern Norway show that the lower regional altitudinal limit of mountain permafrost is strongly correlated with the mean annual air temperature (MAAT) and decreases eastward with increasing continentality (e.g., Etzelmüller et al. 2008). However, less information is available on the distribution of permafrost in northern Norway, where most investigations have focused on periglacial geomorphology and, in particular, palsas (Isaksen et al. 2008 and references therein).

In 2002 a permafrost monitoring program was initiated in Troms and Finnmark, which are the two northernmost counties of mainland Norway. A series of miniature temperature dataloggers (MTDs) were installed for monitoring ground surface and air temperatures (Isaksen et al. 2008). A gridded mean annual air temperature map indicates a altitudinal gradient for discontinuous permafrost in northern Norway, decreasing from over 1000 m a.s.l. in coastal sites down to below 400 m a.s.l. in the interior and more continental areas (Etzelmüller et al. 2008).

In March 2007, the Norwegian-founded IPY project "Permafrost Observatory Project: A Contribution to the Thermal State of Permafrost in Norway and Svalbard" (TSP NORWAY) was started. In the following, the project is briefly described, and the first results from borehole thermal profiles are presented.

The TSP Norway Project

The Norwegian-funded IPY project "Permafrost Observatory Project: A Contribution to the Thermal State of Permafrost in Norway and Svalbard" (TSP NORWAY; Christiansen et al. 2007) is a part of the international IPY full project "Permafrost Observatory Project: A Contribution to the Thermal State of Permafrost (TSP)." TSP will obtain a "snapshot" of the permafrost environments as a benchmark against which to assess past and future changes by making standardized temperature measurements in existing and new boreholes throughout the World's permafrost regions. The ultimate payoff is long-term and will serve as validation of current models and understanding of how permafrost conditions are reacting to climate change. Thawing of permafrost in Norway may lead to subsidence of the ground surface, having a substantial impact, for example, on infrastructure and on the stability of mountain slopes.

The main objective of TSP NORWAY is to measure and model the permafrost distribution in northern Norway and Svalbard, including its thermal state, thickness, and influence on periglacial landscape-forming processes.

Establishment of High Altitude Boreholes

Nine 7–31 m deep boreholes were drilled in bedrock in Troms and Finnmark in August and September 2007. In two of the boreholes, a measurement setup with 15–20 thermistors connected to dataloggers and snow depth sensors, with data recording every six hours, was installed. In one of these boreholes (Kistefjellet) the data are transferred by a modem enabling online presentation. The other seven and two existing boreholes were instrumented with MTDs at selected depths. All boreholes were cased. Periodic recalibration of the installed thermistors is possible, and the holes remain accessible for other probes in the future. Furthermore, a series of MTDs were installed for monitoring surface and air temperatures at selected sites.

Results

The first estimate of mean ground temperature (MGT) near the bottom of the boreholes is presented in Table 1. Permafrost is presumably present in one of the boreholes (Guolasjavri 1, Fig. 1). In the remaining boreholes, MGT is near or slightly above 0°C. Snow cover conditions seem to be decisive for the permafrost distribution in the investigated altitude ranges. In addition sediment-covered ground may in some cases experience permafrost conditions due to thermal

Table 1. Key information of the TSP-borehole sites in northern Norway, including the first estimate of mean ground temperature (MGT) near the bottom of the boreholes.

Location	Altitude (m)	Depth (m)	MGT (°C)
Kistefjellet	990	24.8	0.7
Lavkavagge 1	766	14.0	??
Lavkavagge 2	600	30.5	2.0
Lavkavagge 3	492	15.8	??
Guolasjavri 1	786	32.3	-0.1
Guolasjavri 2	814	10.5	<1.4
Guolasjavri 3	780	10.5	0.8
Abojavri 1	761	6.6	??
Abojavri 2	570	30.3	1.1
Iskoras	572	10.7	~0
Trolltinden	848	29.4	0.5

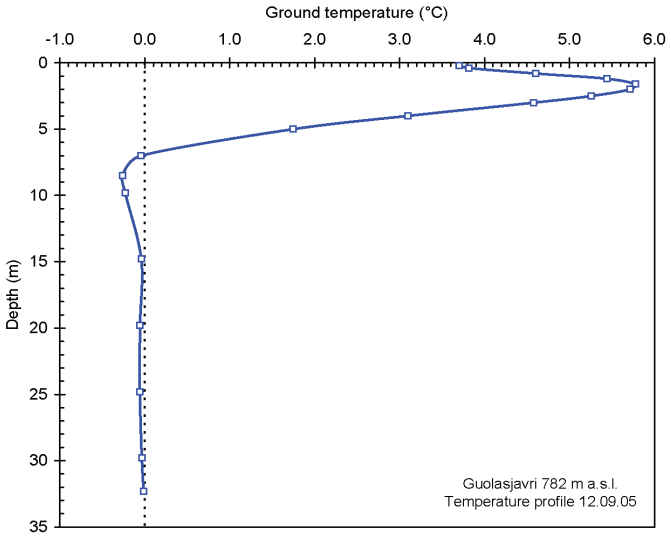

Figure 1. Temperature profile from Guolasjavri 1 borehole, recorded 12.09.2005. Maximum thaw depth is near 7 m.

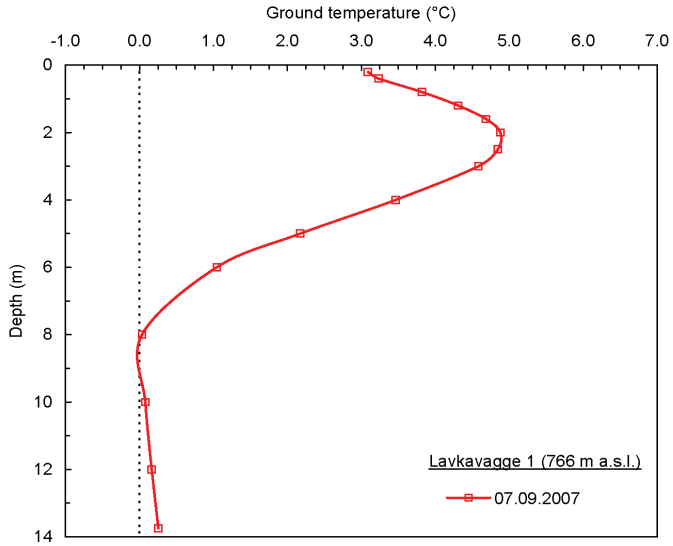

Figure 2. Temperature profile from Lavkavagge 1, recorded 07.09.2007. Seasonal frost reaches a depth of more than 8 m.

offset effects associated with seasonal variation in the heat transfer within the active layer. The seasonal thermal wave may go deep in bedrock, as exemplified by Lavkavagge 1, where seasonal freezing reaches a depth of more than 8 m (Fig. 2).

At Kistefjellet, for example, (Table 1) permafrost is absent. The mean temperature at 24.8 m depth is 0.7°C. The winter snow cover is fairly thick at this site, so permafrost is probably present at nearby wind-swept locations.

Acknowledgements

This study was financed by the Norwegian Research Council IPY program (NFR contract 176033/S30). In addition the study is part of a Norwegian network project, "*Permafrost og ustabile fjellsider,*" established in 2002.

References

Christiansen H. et al. 2007. Permafrost Observatory Project: A contribution to the Thermal State of Permafrost in Norway and Svalbard, TSP NORWAY. *Eos Trans. AGU* 88(52), Fall Meet. Suppl., Abstract C21A-0052.

Etzelmüller, B. et al. 2008. Mapping and modeling the distribution of permafrost in the Nordic countries. *Extended abstracts, Ninth International Conference on Permafrost, Fairbanks, Alaska, 29 June–3 July 2008*.

Isaksen, K., Farbrot, H., Blikra, L.H. & Sollid, J.L. 2008. The distribution of permafrost in Finnmark, northern Norway. *Proceedings of the Ninth International Conference on Permafrost, Fairbanks, Alaska, 29 June–3 July 2008*.

Mapping the Mountain Permafrost in Areas Surrounding Ulaanbaatar City

Ya Jambaljav, A. Dashtseren, D. Battogtokh, D. Dorjgotov
Institute of Geography, Mongolian Academy of Sciences, Ulaanbaatar, Mongolia
Y. Iijima, M. Ishikawa, Y. Zhang, T. Kadota, T. Ohata
Institute of Observational Research for Global Change, JAMSTEC, Yokosuka, Japan

Introduction

According to the geographical location and to the climatic condition of Mongolia, the dominating parameters for permafrost occurrence are incoming shortwave solar radiation (ISWSR) and ground moisture. Using threshold values, we have generated a permafrost distribution map in areas surrounding Ulaanbaatar city.

Study area

There are three observation sites in our study area: (1) Terelj forest site (Terelj FA) is characterized by north-facing forested slope; (2) Terelj grassland site (Terelj GL) is characterized by south-facing sparse grassed gentle slope; and (3) Nalaikh site is characterized by sparsely grassed plate area with smooth hillocks.

Data used

We used the following data: (1) ISWSR at the Nalaikh automatic weather station (Nalaikh AWS), at Terelj GL AWS), and at Terelj FA AWS (Fig. 1). (2) Mean annual ground temperature (MAGT) on the bottom of seasonal freezing and thawing (BSFT) at the above sites and at Sanjai of the Selbe River basin (Table 1). In 5 boreholes, temperatures were measured by CR-10X dataloggers, data marks, and HOBO dataloggers. (3) DEM data from SRTM. (4) Landsat 7ETM image from August 1, 2001, of 131 path and 027 row. We used the temperature data measured by a HOBO datalogger in a borehole located in Sanjai of the Selbe River valley and the temperature data measured by a HOBO datalogger in a borehole located on top of small pingo near Nalaikh AWS.

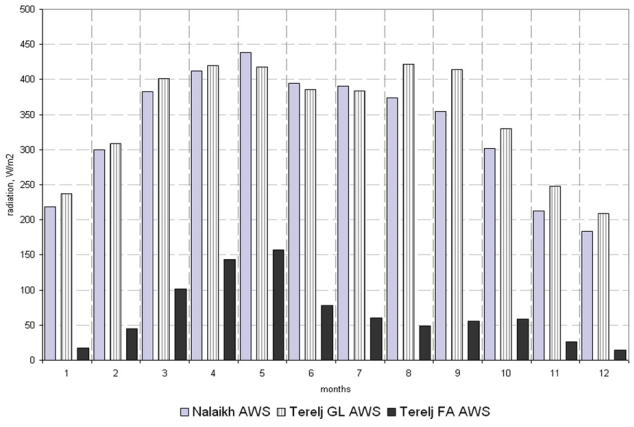

Figure 1. MM of SWSR at Terelj GL AWS, at Terelj FA AWS, and at Nalaikh AWS site.

Table 1. MAGT on BSFT, depth of SFT, and YM of ISWSR.

	Name of sites	MAGT on BSFT, *C	Depth of SFT, m	YM of ISWSR, WM^{-2}
1	Terelj GL	+1.9	4.0	349.3
2	Terelj FA	-1.4	3.5	67.17
3	Nalaikh	-0.14	5.0	330.23
4	Nalaikh pingo	-2.2	1.45	327.67*
5	Sanjai	+1.75	3.2	346.9*

** these data from calculation results*

Table 1 shows the MAGT on BSFT, the depth of seasonal freezing and thawing (SFT), and the yearly mean (YM) of ISWSR

Modeling the Permafrost Occurrence

One of more important criteria of permafrost occurrence or absence is the MAGT at the BSFT. According to Kudryavtsev (1978), the MAGT at the BSFT is the function of multiparameters. Where the MAGT at the BSFT is lower of the zero, permafrost occurs. In contrast, permafrost is absent. *It is the main criterion of our model.* We calculated the monthly mean of ISWSR at selected sites as the following equations (Fu & Rich 2002):

$$R_{income} = \sum R(dir_{\theta,\alpha}) + \sum R(dif_{\theta,\alpha}) \quad (1)$$

where:

$$R(dir_{\theta,\alpha}) = S_{Const} * \tau^{m(\theta)} * SunDur_{\theta,\alpha} * SunGap_{\theta,\alpha} * \cos(AngIn_{\theta,\alpha})$$

$$R(dif_{\theta,\alpha}) = R_{glb} * P_{dif} * Dur * SkyGap_{\theta,\alpha} * Weight_{\theta,\alpha} * \cos(AngIn_{\theta,\alpha})$$

$$m(\theta) = EXP(-0.000118 * Elev - 1.638 * 10^{-9} * Elev^2) / \cos(\theta)$$

$$AngIn_{\theta,\alpha} = \arccos[\cos(\theta) * \cos(G_z) + \sin(\theta) * \sin(G_z) * \cos(\alpha - G_a)]$$

$$R_{glb} = (S_{Const} \sum (\tau^{m(\theta)})) / (1 - P_{dif})$$

where:

S_{Const} – solar constant ($1367 WM^{-2}$)

τ – transmitivity of the atmosphere

θ - solar zenith angle

α - solar azimuth angle

$SunDur_{\theta,\alpha}$ – time durationby sky sector

P_{dif} – the proportion of global normal radiation flux that is diffused

Dur – *the time interval for analysis*

$SkyGap_{\theta,\alpha}$ – *the gap fraction for the sky sector*

Elev – elevation above sea level

G_z, G_s – *surface zenith, azimuth angle*

$Weight_{\theta,\alpha} = (\cos\theta_2 - \cos\theta_1)/Div_{azi}$

θ_1, θ_2 – *the bounding zenith angles of the sky sector*

Div_{azi} – *the number of azimuthal divisions in the sky*

$SunGap_{\theta,\alpha}$ – *gap fraction for the sunmap*

Using equation (1), we calculated the monthly mean of ISWSR at all sites. Figure 2 shows the monthly mean of ISWSR by calculation and by measurement at Terelj GL.

Using the data given in Table 1, we obtained the following regression equation:

$$t_{\xi} = -2.1755 + 0.0116 \; R_{yearly} \quad (2)$$

From regression equation (2) the threshold value below which the permafrost occurs is 187.5WM^{-2}.

Mapping Permafrost Distribution

We generated the map of YM of ISWSR. The YM of ISWSR fluctuates from 50.7WM^{-2} to 409.1WM^{-2}, depending on topography and forests. Mountain permafrost distribution was mapped based on the threshold value of 187.5WM^{-2}.

The permafrost island exists along the small river valleys (valley permafrost) and on the bottom of depression (depression permafrost), where a YM of ISWSR is more than 187.5WM^{-2}. From DEM data, we generated the slope map. From this slope map we have separated the areas with a slope angle between 0–1°. The area with slope angle between 0–1° corresponds to the bottom of depression in Nalaikh. This area of Nalaikh was mapped as a depression permafrost area (relict permafrost). From the slope map we have separated the areas with a slope angle between 0–5°. The areas with 0–5° indicate the small river valleys. In these areas, we have calculated the NDVI and NDWI as follows:

$$NDVI = \frac{NIR - VIS}{NIR + VIS} \quad (3)$$

$$NDWI = \frac{NIR - SWIR}{NIR + SWIR} \quad (4)$$

The areas with high NDVI and NDWI were mapped as wetland areas. NDVI lies between the limits of -0.4667 and +0.7042. A high value of NDVI is between the limits of +0.30 and +0.7042. NDWI lies between the limits of -0.6 and +0.6129. A high value of NDWI is between the limits of 0.0 and +0.6129. The wetland areas overlie the more vegetated areas, and we separated more wetland areas. These areas correspond with the permafrost island areas along the small river valleys.

The study area divides into two areas: permafrost areas and no permafrost areas. The permafrost areas divide into three kinds of permafrost: 1 – mountain permafrost, 2 – depression permafrost (relict permafrost), and 3 – valley permafrost (Fig. 3).

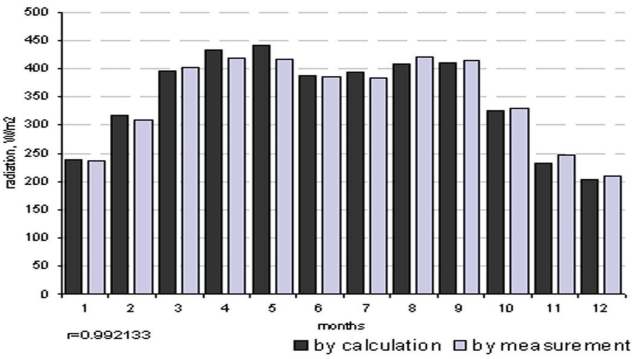

Figure 2. Monthly mean of ISWSR at Terelj GL AWS site.

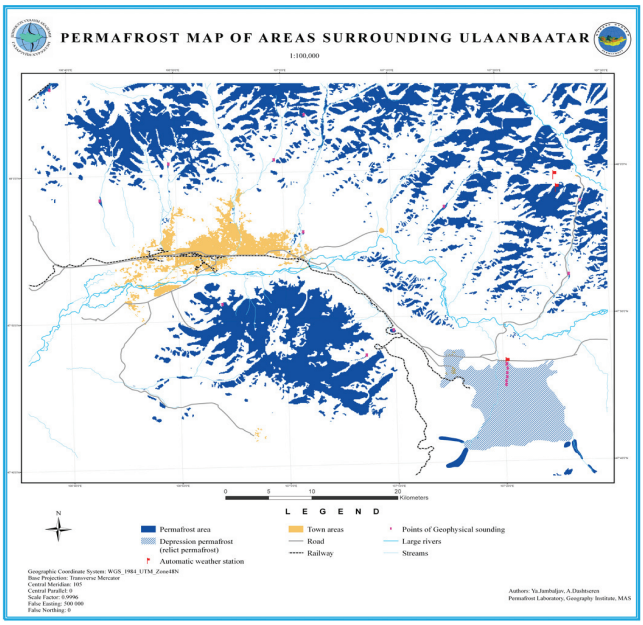

Figure 3. Permafrost map of areas surrounding Ulaanbaatar.

Conclusion

In summer 2007, we carried out the 1D geophysical measurements by instrument AE-72 on 30 more points and excavated 10 pits in our study area for validation of the permafrost distribution. The probability is about 90%.

References

Etzelmuller, B. & Hoelzle, M. 2001. Mapping and Modelling the Occurrence and Distribution of Mountain Permafrost. *Status Report at First European Conference on Permafrost, Roma, Italy, March 2001.*

Fu, P. & Rich, P.M. 1999–2000. The solar analyst 1.0. *User Manual*, Helios Environmental Modeling Institute LLC, USA.

Kudryavtsev, V.A. 1978. *General Geocryology.* Moscow: Moscow University Press, 462 pp.

Historic Change in Permafrost Distribution in Northern British Columbia and Southern Yukon

Megan James
Department of Geography, University of Ottawa, Ottawa, Canada
Antoni G. Lewkowicz
Department of Geography, University of Ottawa, Ottawa, Canada
Sharon L. Smith
Geological Survey of Canada, Natural Resources Canada, Ottawa, Canada
Panya Lipovsky
Yukon Geological Survey, Whitehorse, Canada

Introduction

As a largely climatically-controlled phenomenon, permafrost conditions are impacted by air temperature and precipitation, as well as other local surface and subsurface factors (Smith & Riseborough 1996, 2002). Numerous studies have shown that permafrost should diminish in extent with rising air and ground temperatures (ACIA 2004). However, most of these predictions are based on modeling, and there are very few field-based studies of long-term permafrost change in Canada.

The objective of this study is to directly evaluate the impact of recent climate change on permafrost distribution. We were able to conduct it due to the availability of early baseline permafrost data, which are rare in Canada. In August 2007, we repeated a 1964 permafrost survey undertaken by the late Roger Brown along the Alaska Highway from Whitehorse, YT, to Fort St. John, BC (Brown 1967).

Study Area

It is difficult to demonstrate climate change impacts on permafrost except in very cold permafrost, where temperatures can rise without much thaw, or in areas of very warm and shallow permafrost, where it may thaw completely (Smith et al. 2005). Even warm, shallow permafrost, like that found in the study area, can take several decades to thaw because far more heat is required for phase change than for warming (Smith et al. 2005).

Brown's sites traverse discontinuous permafrost designated as sporadic (underlying 10–50% of the landscape) or isolated patches (underlying 0–10%) (Heginbottom et al. 1995), which can be expected to be the most sensitive to climate change, because a small change in temperature can result in a transition from a cryotic to a thawed state (Kwong & Gan 1994). According to Smith and Riseborough (2002), the southern limit of discontinuous permafrost approximately coincides with a mean annual air temperature (MAAT) of -1ºC. Table 1 shows the MAATs of the principal communities along the study transect east of Whitehorse.

Table 1. MAATs of communities along the study transect.

Community	Latitude	Longitude	Normal MAAT (1971–2000)
Whitehorse, YT	60°42′ N	135°04′ W	-0.7°C
Watson Lake, YT	60°72′ N	128°49′ W	-2.9°C
Fort Nelson, BC	58°50′ N	122°36′ W	-0.7°C
Fort St. John, BC	56°14′ N	120°44′ W	2.0°C

(Environment Canada 2007b)

Methods

Brown described the 60 locations that exhibited permafrost in 1964, as well as some nonpermafrost sites, in such sufficient detail that it was possible to relocate most of them using milepost information, written descriptions, and photographs. This information was retrieved from Brown's 1967 publication, as well as from cartographic and photographic material archived at the National Research Council of Canada. The research was conducted in the month of August so that the depth of the thawed layer would be near its maximum.

Using UTM coordinates for Brown's sites, derived from archived 1965 Alaska Highway maps, we drove along the route until we were within 500 m of the coordinates for a site and continued for 500 m past. We assessed the landscape on either side of the highway until we could confidently match Brown's photographs and descriptions. At some locations we had to examine an area several hundred metres around the UTM coordinates and look for sites most likely to have permafrost (based on vegetation and drainage), which we would investigate. There were several sites that we were unable to relocate due to inadequate descriptions or profound changes in land cover, such as conversion of spruce forest to farm fields. At each relocated site, 2 ground temperature profiles were measured to 1.5 m or until we encountered the frost table. At sites where a frost table was found, 10 ground probings, roughly 1 m apart, were performed to measure active layer thickness.

Further information on ground thermal conditions will be obtained from six climate stations which were set up to measure air temperature, ground temperatures, and snow depths in order to examine the conditions that have allowed permafrost to endure. These data will be downloaded in summer 2008.

Results

The results of this survey demonstrate that significant change has occurred in the last four decades. More than half of the positively located sites which had permafrost in the upper 1.5 m in 1964 along the route as a whole no longer exhibited perennially frozen ground in 2007, and this was true of almost three-quarters of the sites in the route segment to the south of Fort Nelson, BC. In addition, where permafrost was still extant in the upper 1.5 m, active layers on average were deeper than in 1964, even though the survey was undertaken one month earlier in the thaw season.

Climate data show that Brown's survey in 1964 followed roughly 20 years of cooling, especially at Whitehorse (Fig. 1). This cooling continued for another decade, and there was then a rapid rise in temperatures. Changes in active layer thickness and permafrost extent observed during the 2007 revisiting of Brown's sites would have been the result of this 1.5–2.0°C rise in temperature over the past 30 years, as well as any change in precipitation quantities and patterns.

Discussion and Conclusion

Preliminary results suggest that the boundaries of the permafrost zones may have moved substantially northwards since Brown undertook his survey. These results fit with what would be expected given the concurrent air temperature change. However, precipitation is also an important component of climate, and snow depth and duration are significant local factors affecting the ground temperature regime (Smith & Riseborough 1996, 2002). Little is currently known about the snow conditions at the sites, but the climate stations installed in 2007 should reveal relationships between air temperatures, ground temperatures, and snow depths.

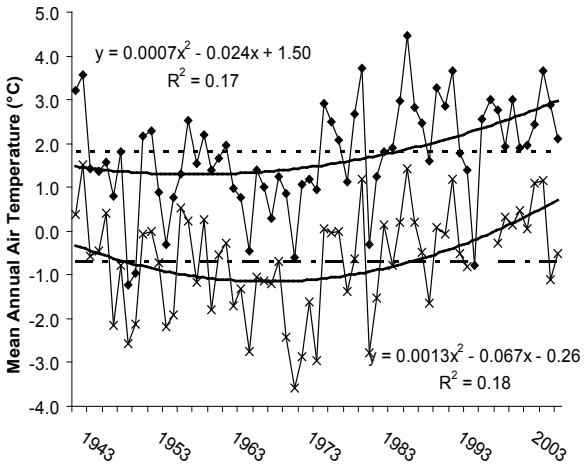

Figure 1. MAATs of Whitehorse, YT (the *x* line) and Fort St. John, BC (the "diamond" line) from 1943–2007 (Environment Canada 2007a). The dashed lines are the long-term MAATs over the time period, and the solid black lines are polynomial lines.

In August 2008, data will be downloaded from the six climate stations and a combination of geophysical techniques and direct drilling will be used to establish current permafrost thicknesses and to install ground temperature cables. This information will be combined with spatial analysis of a highway borehole database on permafrost that is currently being developed at the Yukon Geological Survey.

This study is a step towards filling a research void to provide evidence of loss of permafrost on a multidecadal scale. Careful archiving of information about the research sites should allow repetition of the survey by future generations of permafrost researchers, thus contributing to the legacy of the International Polar Year.

Acknowledgments

Support for this project has been provided by the Federal Government of Canada's International Polar Year Program (Thermal State of Permafrost in Canada), the NSERC Northern Internship Program, the Northern Student Training Program, DIAND, and the Yukon Geological Survey. Catherine Henry provided field assistance.

References

Arctic Climate Impact Assessment (ACIA). 2004. *Impacts of a Warming Climate*. New York: Cambridge University Press, 139 pp.

Brown, R.J.E. 1967. *Permafrost Investigations in British Columbia and Yukon Territory*. Division of Building Research Technical Paper 253. Ottawa: National Research Council of Canada.

Environment Canada. 2007a. *Canadian Climate Data*. http://climate.weatheroffice.ec.gc.ca/climateData/canada_e.html.

Environment Canada. 2007b. *Canadian Climate Normals or Averages 1971–2000*. http://climate.weatheroffice.ec.gc.ca/climate_normals/index_e.html.

Heginbottom, J.R., Dubreuil, M.A. & Harker, P.T. 1995. Canada Permafrost. (1:7,500,000 scale). In: *The National Atlas of Canada*, 5th Edition, sheet MCR 4177. Ottawa: National Resources Canada.

Kwong, Y.T. & Gan, T.Y. 1994. Northward Migration of Permafrost along the Mackenzie Highway and Climatic Warming. *Climatic Change* 26(4): 399-419.

Smith, M.W. & Riseborough, D.W. 1996. Permafrost monitoring and detection of climate change. *Permafrost and Periglacial Processes* 7: 301-309.

Smith, M.W. & Riseborough, D.W. 2002. Climate and the limits of permafrost: A zonal analysis. *Permafrost and Periglacial Processes* 13: 1-15.

Smith, S.L., Burgess, M.M., Riseborough, D. & Nixon, F.M. 2005. Recent trends from Canadian permafrost Thermal Monitoring Network sites. *Permafrost and Periglacial Processes* 16: 19-30.

Improve the Active Layer Temperature Profile Estimation by the Data Assimilation Method

Rui Jin, Xin Li
Cold and Arid Regions Environmental and Engineering Research Institute, Chinese Academy of Sciences

Introduction

The heat and hydrological regimes of the frozen ground, especially its active layer dynamics, have important impacts on the energy and water exchange between the land and atmosphere, runoff, the carbon cycle, and crop growth.

There are two methods widely used in frozen ground research including the physically based model and in situ/ remote sensing observation. However, there are some uncertainties in the model simulation. The observation has instrumental and representative errors as well. The in situ stations are distributed sparsely. Additionally, although remote sensing can provide a regional view, the direct application of remote sensing was to detect the soil surface freeze-thaw status by microwave bands.

Land data assimilation provides a new methodology to merge the observations into the dynamics of the land surface model for improving the estimation of land surface state (Li et al. 2007).

Framework of Active Layer Data Assimilation System

The active layer data assimilation system comprised four components:

1. Model operation: The SHAW (Simultaneous Heat and Water) (Flerchinger & Saxton 1989) model was used to provide the dynamical framework.

2. Observation operator: The microwave radiative transfer model $T_b = e \cdot T_{eff}$ (Liou 1998) was used to convert the predicted model state variable to the simulated brightness temperature.

3. Assimilation strategy: The ensemble kalman filter (Evensen 2003) is a new sequential data assimilation algorithm, which can deal with the nonlinearity and discontinuity of the model.

4. Dataset: It includes atmospheric forcing data, land surface parameters, in situ SMTMS (Soil Moisture and Temperature Measurement System) observation, and SSM/I data.

The assimilation experiments were carried out at AMDO (32.2°N, 91.6°E, 4700 m) station on the Tibet plateau, which is located in the island permafrost region.

Assimilating the 4 cm depth soil temperature observation

The 4 cm depth soil temperature observation was assimilated because it contributed to the microwave emission and was less influenced by the environmental conditions than the soil surface temperature.

The experiment of assimilating hourly 4 cm depth soil temperatures showed the result matched well with the

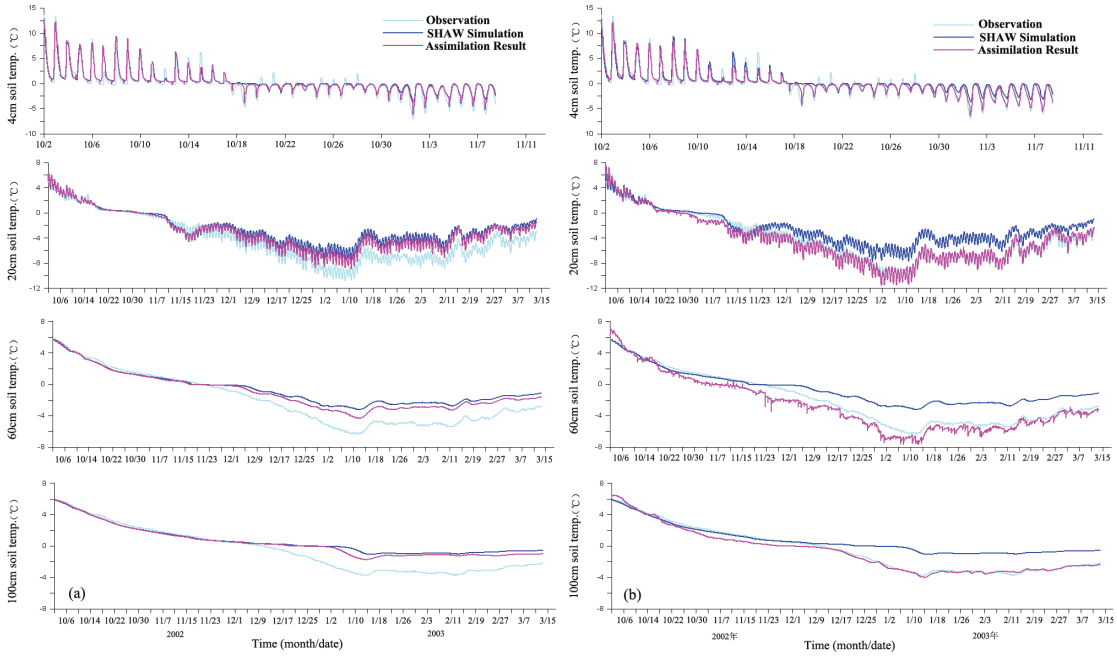

Figure 1. The assimilation result of 4 cm, 20 cm, 60 cm, and 100 cm soil temperature by introducing the 4 cm depth soil temperature observation: (a) the non-diagonal element equals to 0; (b) the non-diagonal element is determined by the model error and the correlation analysis.

Table 1. The soil temperature RMSE (K) of SHAW simulation against the result of assimilating the SSM/I brightness temperature.

Soil Layer (cm) / RMSE (K)	0	4	10	20	40	60	80	100	130	160	200	258
SHAW Simulation	10.09	3.03	2.43	2.07	1.65	1.75	1.67	1.61	1.20	0.81	0.36	0.04
Assimilating SMTMS	8.05	1.61	0.91	0.60	0.99	0.79	0.63	0.38	0.42	0.51	0.31	0.04
Assimilating SSM/I	8.60	1.89	1.23	1.15	1.44	1.06	0.73	0.61	0.62	0.64	0.34	0.04

observations. The RMSE (root mean square error) of the assimilated result of 4 cm soil temperature is 0.16 K, which is significantly less than that (3.03 K) by running the SHAW model alone.

Assimilating the 4 cm depth observation not only improves the state estimation of the corresponding layer, but also can improve the estimation of the whole soil profile state when given reasonable model error covariance matrix (Hoeben & Troch 2000).

Figure 1 showed the assimilation results of the non-diagonal elements equal to zero (Fig. 1a) and equaling the values determined by the correlation analysis (Fig. 1b). For clarity, part of the assimilation result at the 4 cm layer was shown here. The zero non-diagonal elements mean the soil temperature of each layer is independent; only soil temperature at 4 cm can be updated after assimilating the corresponding soil temperature observation. The deep soil temperature can only be influenced slowly by the process of interlayer flow described in the SHAW, so the data assimilation efficiency is very low. The error covariance matrix with non-diagonal elements not equal to zero can play the key role of transferring the updated surface state information to the deep soil quickly, achieving improved estimation of the soil temperature profile. After assimilating the 4 cm depth soil temperature observation, the RMSE of soil temperature decreased 1 K on average, compared to SHAW simulation. The RMSE of assimilation with reasonable covariance decreased about 0.7 K compared to assimilation with covariance as zero.

Assimilating the 19 GHz SSM/I brightness temperature

For the regionally frozen ground research, the available in situ observation is sparse. Remote sensing, especially the passive microwave radiometers, would be a promising observation method because of its frequent revisit cycle and global/regional coverage.

The key to merging the brightness temperature observation into the assimilation system is the microwave radiative transfer model, which can act as the bridge between the model state variables predicted by SHAW and brightness temperature observed by the radiometer. The volume-scattering effect was not considered in the LSP/R model, so the 19 GHz brightness temperatures, having the longest wavelength in the SSM/I frequencies, were chosen as the observations to be assimilated.

After assimilating the SSM/I 19 GHz brightness temperature, the RMSE of soil temperature decreases 0.76 K on average (Table 1). Especially the improvement of 0–100 cm layer soil temperature was obvious, nearly 1–2 K. The improvement by assimilating the brightness temperature is lower than assimilating in situ observation, because the brightness temperature is an indirect observation, and there exist uncertainties in the microwave radiative transfer model.

Conclusion

The one-dimensional assimilation experiments showed that assimilating the in situ observations and the passive microwave brightness temperature can remarkably improve the estimation of a soil temperature profile.

The regional four-dimensional active layer data assimilation system can be developed based on the current one-dimensional system. It will be able to provide soil temperature, water content, ice content, and other datasets with spatiotemporal and physical consistence. The datasets can be used in frozen soil and climate change interaction research, promoting the in-depth and quantitative understanding of frozen soil dynamics.

Acknowledgments

The authors thank the support from the National Natural Science Foundation of China (40701113; 40601065). The data used in the paper are generously provided by the CEOP and NSIDC.

References

Evensen, G. 2003. The ensemble kalman filter: Theoretical formulation and practical implementation. *Ocean Dynamics* 53: 343-367.

Flerchinger, G.N. & Saxton, K.E. 1989. Simultaneous heat and water model of a freezing snow-residue-soil system Ⅰ: Theory and development. *Transactions of the ASAE* 32(2): 565-571.

Hoeben, R. & Troch, P.A. 2000. Assimilation of active microwave observation data for soil moisture profile estimation. *Water Resources Research* 36(10): 2805-2819.

Li, X., Huang, C.L., Che, T., Jin, R., Wang, S.G., Wang, J.M., Gao, F., Zhang, S.W., Qiu, C.J. & Wang, C.H. 2007. Development of a Chinese land data assimilation system: Its progress and prospects. *Progress in Natural Science* 17(8): 881-892.

Liou, Y.A. & England, A.W. 1998. A land surface process/radiobrightness model with coupled heat and moisture transport in soil. *IEEE Transactions on Geoscience and Remote Sensing* 36(1): 273-286.

Long-Term Winter Seismic Vehicle Impacts in Permafrost Terrain

Janet C. Jorgenson
Arctic National Wildlife Refuge, U.S. Fish and Wildlife Service

Seismic exploration was conducted on the coastal plain of the Arctic National Wildlife Refuge, Alaska, during the winters of 1984 and 1985. Approximately 2000 km of seismic line were completed in a 5 x 20 km grid. At least 2000 km of additional trails were created adjacent to the seismic lines by D-7 Caterpillar tractors, pulling ski-mounted trailers between camps. U.S. Fish and Wildlife Service initiated a monitoring program in 1984 to document vegetation and soil disturbance and natural recovery (Felix & Raynolds 1989, Emers & Jorgenson 1997).

Color-infrared aerial photographs were taken of 20% of the trails in 1985 and 1988, and disturbance levels were photo-interpreted at 4914 systematic plots (Raynolds & Felix 1989). A two-stage cluster sample was used to randomly choose 200 of the plots to monitor in the field. Twenty 3-km transects, each consisting of ten 18-m diameter circular plots spaced 300 m apart, were randomly selected. A semi-quantitative system for ranking vehicle disturbance based on vegetation and soil changes was used. Ranks were assigned initially in 1985 by photo-interpretation and subsequently by field evaluations in 1989, 1993, 1998, 2002, and 2005. All plots were visited in 1989. From 1993 to 2005, plots rated as undisturbed in a previous year were assumed to remain undisturbed thereafter and were not revisited.

Disturbance and recovery were summarized by trail type (seismic line or camp-move trail) and vegetation types, which included Wet Sedge Tundra, Moist Sedge-Willow Tundra, Moist Sedge-Dryas Tundra, Moist Sedge-Tussock tundra, Low Shrub Tundra on high-centered polygons, Riparian Shrublands, and Partially Vegetated. The vegetation type Dryas River Terrace was not represented in the 200-plot sample, but data were available from the larger photo-interpreted sample. Ten Dryas River Terrace plots were visited in 2007 to assess recovery.

Snow was usually less than 30 cm deep and did not provide complete protection from vehicle damage. The following summer, most trails had at least some scuffing of vegetation and deeper summer-thawed soil. The greatest damage was destruction of shrubs and sedge tussocks, scraping of ground cover to bare soil, and standing water on trails. Tussock Tundra, Low Shrub Tundra, and Dryas River Terrace were the vegetation types with the highest initial disturbance. About one-half of these plots had medium- and high-level disturbance in 1985. Sedge-Dryas Tundra and Sedge-Willow Tundra were intermediate in disturbance levels, with medium- and high-level disturbance found at about one-third of the plots. Medium- and high-level disturbance was absent in Riparian Shrublands, which collect deep snow, and occurred in <10% of plots in Wet Sedge Tundra. Partially Vegetated areas had no damage.

Recovery was rapid in the first decade as the percentage of disturbed plots decreased from 79% in 1985, to 48% in 1989, and to 11% in 1993. After 1993, the remaining disturbance recovered only slightly. Five percent of plots were still disturbed in 2005. For points that initially had low-level disturbance, recovery was rapid. Twenty-three percent of all points had medium to high levels of disturbance in 1985, and these recovered more slowly.

Figure 1. Repeat photographs of study plot on a trail on Moist Sedge-Dryas Tundra. Parallel ruts and crushed vegetation were evident in 1984, the summer following disturbance (top). An undisturbed reference plot adjacent to this trail had a mean of 37% excess ice content (% volume) near the surface of the permafrost. By 2002, a network of sedge-filled troughs had developed, where melting ice wedges caused ground subsidence (bottom) not seen in the reference plot off the trail.

Vegetation types that tend to have greater amounts of excess ice in the upper permafrost (measured at other plots associated with this study) had the poorest recovery. High disturbance persisted for 23 years only where vehicle traffic had broken the insulating vegetative mat, allowing warming of the soil and permafrost degradation that led to thaw settlement. Changes on these trails included increased moisture, transient increases in nutrient flux, increased cover of a few hydrophytic sedge species, and long-term, large decreases for evergreen shrubs and mosses. In contrast, trails

on the ice-poor gravel substrates of riparian areas (Dryas River Terrace and Riparian Shrublands) did not subside, and vegetation recovered steadily even after severe initial damage.

Tussock Tundra and Sedge-Willow Tundra plots recovered well except for a few that subsided into troughs. Sedge-Dryas Tundra frequently subsided, even when initial disturbance was not high, and over two-thirds of the plots were still disturbed in 2005, with substantial changes in plant community composition (Fig. 1). Low Shrub Tundra and Dryas River Terrace had some low-level disturbance remaining in 2005–2007, mainly patchy subsidence and vehicle ruts that did not subside, with more subtle plant community composition changes.

Figure 2. Repeat photographs of trail on Moist Sedge-Willow Tundra in 1985 (top) and 2007 (bottom). An undisturbed reference plot adjacent to this trail had a mean of 28% excess ice content near the surface of the permafrost. Trail subsidence caused increases in hydrophytic sedges and decreases in all other plants.

Camp-move trails were made by vehicles with higher ground pressure than seismic lines and had more initial damage and slower recovery. By 1989, 32% of seismic trails were still disturbed compared to 64% of camp trails, including 41% at medium- and high-level disturbance. By 2005, all seismic trail plots had recovered to a negligible disturbance level, whereas 10% of the camp trail plots were still disturbed and one-half of those had medium- and high-level disturbance. Overall, 5% of plots were still disturbed in 2005. This translates to 200 km of disturbed trail, out of the original 4000 km of trails.

Previous studies of winter seismic vehicle disturbance in the Arctic predicted only short-term and mostly aesthetic impacts. Long-term monitoring showed that most of the disturbance disappeared gradually, but that impacts to tundra vegetation persisted on a small percentage of the trails up to 23 years after disturbance (Fig. 2).

References

Emers M. & Jorgenson, J.C. 1997. Effects of winter seismic exploration on the vegetation and soil thermal regime of the Arctic National Wildlife Refuge. In: R.M.M. Crawford (ed.), *Disturbance and Recovery in Arctic Lands: an Ecological Perspective.* Dordrecht, the Netherlands: Kluwer Academic Publishers.

Felix, N.A. & Raynolds, M.K. 1989. The effects of winter seismic trails on tundra vegetation in northeastern Alaska, U.S.A. *Arctic and Alpine Res*. 21(2): 188-202.

Raynolds, M.K. & N.A. Felix. 1989. Airphoto analysis of winter seismic disturbance in northeastern Alaska. *Arctic* 42(4): 362-367.

Permafrost Characteristics of Alaska

Torre Jorgenson, Kenji Yoshikawa, Mikhail Kanevskiy, Yuri Shur
University of Alaska Fairbanks, Institute of Northern Engineering, Fairbanks, Alaska, USA
Vladimir Romanovsky, Sergei Marchenko, Guido Grosse
University of Alaska Fairbanks, Geophysical Institute, Fairbanks, Alaska, USA
Jerry Brown
International Permafrost Association, Woods Hole, Massachusetts, USA
Ben Jones
U.S. Geological Survey, Anchorage, Alaska, USA

A new permafrost map of Alaska (see inside of front cover), using a terrain-unit approach for mapping permafrost distribution based on climate and surficial geology, is presented. This map represents the third iteration of a permafrost map for Alaska, following the circum-Arctic permafrost map (Brown et al. 1997), which made minor modifications to the initial map by Ferrians (1965). To map permafrost, we developed a rule-based model that incorporated mean annual air temperatures (MAAT) from the PRISM climate map and the surficial geology map of Karlstrom et al. (1964) modified with some new information on geology. We used terrain-permafrost relationships developed by Kreig and Reger (1982) and our knowledge of permafrost distribution to assign permafrost characteristics to each surficial deposit under varying temperatures.

We coded the map with surficial geology, MAAT, primary soil texture, permafrost extent, ground ice volume, and primary thermokarst landforms. The map focuses on the top 10 m of permafrost, where permafrost can be more readily mapped from surface features, determined by simple field measurements, and where ground ice usually is most abundant. Although we used recent MAAT in our model, we note that permafrost distribution is greatly affected by past climates. We relied on many sources for the effort, but are not able to cite all references in this abstract. The main map shows permafrost thickness values based on Ferrians (1965), Péwé (1975), Osterkamp and Payne (1981), Collett et al. (1989), and others.

The following characteristics are shown on small thematic maps on the inside of back cover:

Ground temperatures (usually measured at depths 20 to 30 m) were obtained from boreholes by V. Romanovsky, G. Clow, K. Yoshikawa, D. Kane, and T. Osterkamp as part of the Thermal State of Permafrost project for the International Polar Year (Brown & Romanovsky 2008). Ground ice volumes were estimated for the upper 5 m of permafrost using terrain relationship from Kreig and Reger (1982) and our field data. Ground ice volume near the surface is higher in colder regions due to active ice wedge formation and ice segregation in fine-grained deposits. Pingo distribution was compiled mostly from the literature and by satellite image interpretation. There are >1500 known pingos in Alaska. In central Alaska and bordering Yukon areas, there are ~760 pingos, mostly open-system. Closed-system pingos predominate in the North Slope, Seward Peninsula, and Noatak regions. The distribution of ice wedges was determined from the literature, from polygonal patterns evident on remote sensing imagery, and from our field experience. Ice wedges actively form in the continuous permafrost zone and are mostly inactive in the discontinuous zone (Péwé 1975). Holocene ice wedges are limited to the top 3 to 5 m of permafrost; large, deep (up to 35 m) syngenetic ice wedges formed during the Late Pleistocene. Thermokarst landforms are abundant in all recent and past permafrost zones (Jorgenson et al. 2008). They are varied, due to differences in temperature, ground ice volume, soil texture, slope, and hydrologic conditions.

The permafrost zones underlie 80% of Alaska, including continuous (29%), discontinuous (35%), sporadic (8%), and isolated (8%) permafrost. Permafrost is absent beneath 15% of the State, with glaciers and ice sheets occupying 4% and large water bodies, 1% of the area.

References

Brown, J.B., Ferrians, O.J., Heginbottom, J.A. & Melnikov, E.S. 1997. *Circum-Arctic Map of Permafrost and Ground-Ice Conditions*. U.S. Geol. Surv. Map CP-45, scale 1:10,000,000.

Brown, J. & Romanovsky, V.E. 2008. Report from the International Permafrost Association: State of permafrost in the first decade of the 21st century. *Permafrost and Periglacial Processes* 19: 255-260.

Collett, T.S., Bird, K.J., Kvenvolden, K.A. & Magoon, L.B. 1989. *Map Showing the Depth to the Base of the Deepest Ice-Bearing Permafrost as Determined from Well Logs, North Slope, Alaska.* U.S. Geol. Surv. Oil Gas Inv. Map OM-222, scale 1: 1,000,000.

Ferrians, O.J. 1965. *Permafrost Map of Alaska*. U.S. Geol. Surv. Misc. Geol. Inv. Map I-445, scale 1: 2,500,000.

Jorgenson, M.T., Shur, Y. & Osterkamp, T.E. 2008. Thermokarst in Alaska. *Proceedings of the Ninth International Conference on Permafrost, Fairbanks, Alaska, June 29–July 3, 2008.*.

Karlstrom, T.N.V. et al. 1964. *Surficial Geology of Alaska.* U.S. Geol. Surv. Misc. Geol. Inv. Map I-357, scale 1:1,584,000.

Kreig, R.A. & Reger, R.D. 1982. *Air-Photo Analysis and Summary of Landform Soil Properties Along the Route of the Trans-Alaska Pipeline System.* Alaska Div. Geol. Geophys. Surv., Geologic Rep. 66, 149 pp.

Osterkamp, T.E. & Payne, M.W. 1981. Estimates of permafrost thickness from well logs in northern Alaska. *Cold Reg. Sci. Tech.* 5: 13-27.

Péwé, T.L. 1975. *Quaternary Geology of Alaska*. U.S. Geol. Surv. Prof. Paper 836, 145 pp.

Comparison of Thermal Regimes in Tundra Virgin and Post-Agricultural Soils of the European Northeast

Dmitry Kaverin
Komi Science Center, Russian Academy of Sciences, Syktyvkar, Russia

Introduction

In tundra, agricultural activity transformed the soils and their properties including temperature conditions. Soil thermal regimes are considered to change into ones having no analogues among virgin soils. We studied thermal properties of tundra post-agricultural and virgin soils. Revealing interannual and seasonal temperature dynamics in these soils is important in view of present climate change.

Regional Background

The research was conducted in upland tundra near the town of Vorkuta (67°30′N; 64°02′E) in the east-European Russian Arctic. The terrain is a rolling plain covered generally with silty loams. The area is attributed to the subzone of southern tundra characterized by the distribution of relatively high shrubs: birch and willow. The area under study belongs to the zone of discontinuous permafrost (Oberman & Mazhitova 2003). Massive islands of permafrost occupy slightly dissected hill slopes and hill summits covered with dwarf-shrub/moss vegetation. Permafrost temperatures vary around -1°C.

Mean annual air temperature (MAAT) is -5.8°C, mean annual thawing degree days (DDT) 1005°C-days, and mean annual precipitation 513 mm.

Objects and Methods

Soil temperature regimes were studied in 2 post-agricultural tundra soils. Two undisturbed soils, one permafrost-affected and another one permafrost-free, served as controls. Grassland soils are located in the landscape position similar to that of the control virgin soils.

Soils under study

(1) Abandoned overgrowing sown grassland, soil Epigleyic Gelisol, grass/dwarf-shrub community, willow covers 7–8% of the site area (2005). Permafrost is at 1.35 m depth.

(2) R2 site of the Circumpolar Active Layer Monitoring network, dwarf-shrub/moss tundra, soil Histi-Turbic Cryosol (Reductaquic), permafrost depth is 100 cm;

(3) Abandoned overgrowing arable land, soil Endogleyi-Stagnic Cambisol, grass-moss community, willow covers only 2% of the site area (2005), no permafrost within 2 m depth.

(4) Shrub-moss tundra, soil Dystri-Stagnic Cambisol, no permafrost within 2 m depth.

Post-agricultural sites were abandoned about 10 years ago, and tall shrubs cover up to 10% of the area. Before abandonment, since 1970s the grasslands were annually harvested with periodic rototilling and fertilizing.

The records were conducted with digital Hobo loggers programmed for 8 measurements daily. Loggers were set at depths of 0, 20, 50, and 80 cm and in the upper layer of permafrost in case of its presence. The study was conducted in the period of 2005–2007.

Results and Discussion

By now, there is not much data about the temperature regime of tundra soils in the European Northeast. Kononenko (1986) studied summer temperatures in virgin and agricultural soils but winter thermal regime was quite poorly characterized. Thermal regimes of the soils were not studied at landscape level.

Continuous soil temperature measurements have been conducted in the area since 1996 by Galina Mazhitova. It was revealed that MAST (mean annual air temperature) in all soils of the area is strongly correlated with snow thickness in winter, with permafrost occurring only in the sites with snow thickness less than 50 cm. A progressive increase in shrub coverage is, therefore, the major MAST-controlling factor. Shrubs effectively intensify snow accumulation, catching the snow redistributed by winds (Mazhitova 2001, 2008).

As in previous years during our study, MAST at depth 0–50 cm was commonly above 0°C in all permafrost-free soils. Negative mean annual temperatures in permafrost-affected soils and positive ones in permafrost-free soils are quite typical for discontinuous permafrost zone (Burn 2004).

Studied permafrost-affected soils (No. 1, 2) are located at the southern windward hill slopes. Shallow snow cover (30–40 cm) and quite thick peat layer (10–20 cm) preserve permafrost within the soil profile. Soils of northern slopes located in the same landscape have no permafrost. Such an inversion is resulted from strong winds blowing in winter.

Until 2006, the site with coldest permafrost-affected soil (No. 2) was characterized with negative MAST down all the profile (Mazhitova 2001, 2008). MAST at a depth of 20 cm was -1.9…0.4°C, 50 cm -0.5…-1.9°C. MAST in the upper permafrost layer was -1.2°C with minimum (-4.4°C) in April.

According to MAST and freezing degree days at depths of 0–50 cm the permafrost-affected soil of the abandoned grassland No. 1 was warmer than the virgin soil No. 2. Thus MAST at a depth of 50 cm was -0.35°C versus -0.5°C in the control soil (2006).

The post-agricultural soil (No. 3) was developed in the former shrubby site similar to that of the soil No. 4. It had lower temperatures in comparison with profile No. 4. Despite the absence of thick shrub vegetation, this grassland soil still had no permafrost and was characterized with positive MASTs at depths of 20 cm and 50 cm (+1 +2°C).

The warmest profile was No. 4. Tall shrub vegetation catching thick snow cover causes relatively higher temperatures in winter. It results in higher MASTs.

In 1996–2005, an increasing trend in MAST was observed in the virgin permafrost-affected soil of R2 CALM site (Mazhitova 2008). It was correlated with an increase in both MAAT and active layer depth during the same period (Mazhitova & Kaverin 2007).

In 2006–2007, negative MAST was changed to positive one in the upper soil layer (0–20 cm). This was quite unusual for permafrost-affected soils, but was correlated with extremely hot summer and mild winter that year. MAAT was -2.8°C in 2006–2007. In the soil of arable land, freezing even did not reach a depth of 50 cm during winter 2006–2007.

Zero curtains which are typical for the research area (Mazhitova 2001) observed both in virgin and post-agricultural soils. Zero curtains could be observed from October till January–February. The longest ones are recorded at a depth of 50 cm and more expressed in the permafrost-affected virgin soil.

Conclusions

Removal of virgin vegetation in permafrost-affected sites does not differentiate thermal properties of soils significantly. Post-agricultural permafrost-affected soils were warmer, but permafrost did not disappear just sinking deeper.

In case of removal, tall-shrub vegetation serving as a heat insulation cover in winter soil thermal regime is getting cooler. And still we do not observe permafrost in the post-agricultural soil of the arable land.

Positive mean annual soil temperatures in the permafrost-affected soil were caused by high air temperatures and considered to be an interannual dynamic.

Acknowledgments

The study was supported by NSF (OPP-9732051 and OPP-0225603) and RASHER project of International Polar Year.

References

Archegova, I., Kotelina, N. & Mazhitova, G. Agricultural Use of Tundra Soils in the Vorkuta Area, Northeast European Russia. In: J. Kimble (ed.), *Cryosols (Permafrost-Affected Soils)*. Berlin-Heidelberg-New York: Springer-Verlag, 673-687.

Burn, C.R. 2004. The Thermal Regime of Cryosols. In: J. Kimble (ed.), *Cryosols (Permafrost-Affected Soils)*. Berlin-Heidelberg-New York: Springer-Verlag, 391-414.

Kononenko, A.V. 1986. *Hydrothermal Regime in Taiga and Tundra Soils in the European North-East*. L: Nauka.

Mazhitova, G.G. 2008. Soil Temperature Regimes in the Discontinuous Permafrost Zone in the East European Russian Arctic. *Eurasian Soil Science* 1: 48-62.

Mazhitova, G.G. & Kaverin, D.A. 2007. Dynamics of seasonal thaw depth and surface subsidence at a Circumpolar Active Layer Monitoring (CALM) site in the European Russia. *Earth Cryosphere* 9(4): 20-30 (in Russian).

Mazhitova, G.G. 2001. Structure-functional organization of soils and soil cover in the European North-East. In: F.R. Zaidelman & I.V. Zaboeva (eds.), *Monitoring of Hydrothermal Regime in Tundra Soils*. S-Petersburg: Nauka, 153-162.

Oberman, N.G. & Mazhitova, G.G. 2003. Permafrost mapping of Northeast European Russia based on period of the climatic warming of 1970–1995. *Norsk Geografisk Tidskrift–Norwegian Journal of Geography* 57(2): 111-120.

Massive Ground Ice in the Norilsk Basin: Evidence of Segregation Origin

O.A. Kazansky
Igarka Geocryological Laboratory, Melnikov Permafrost Institute SB RAS, Igarka, Russia
M.Y. Kushchev
Polar Division, MMC Norilsk Nickel, Norilsk, Russia

The Norilsk Basin is situated in the northwestern part of the Putoran Plateau, between Mt. Lontokoisky Kamen and Mt. Kharaelakh. Surficial deposits which consist of glaciolacustrine clays contain massive beds of ground ice up to 15 m in thickness. As is the case with massive ice bodies elsewhere, the origin of the ice in the Norilsk Basin is controversial. The uncertainty regarding this problem impedes understanding of the spatial distribution patterns of massive ground ice and reduces the accuracy of geocryological predictions.

The results of our research suggest that the ice is of segregation origin. This conclusion is based on the field study of sections, as well as on the experimental and theoretical investigations that have demonstrated the possibility of massive ground ice formation by ice segregation during the development of epigenetic permafrost.

The well-known thermal condition for continued ice lens growth is:

$$q_f = q_w + q_i,$$

where q_f is the heat flow from the base of the growing lens to the permafrost table, q_w is the heat flow to the base of the lens from the underlying ground, and q_i is the heat flow required for removal of latent heat of migratory water.

The physico-mechanical requirement for continued lens growth is that no subhorizontal (normal to the heat flow) low-density zones develop in the frozen fringe where new ice lenses that capture the water flow could initiate.

The hydro-physical condition is that the overburden pressure (σ) must not exceed the maximum crystallization pressure (σ_n). Otherwise, migration of water, through the unfrozen water films, from the unfrozen soil connected with an aquifer will cease.

Physically, the process of continued lens growth can be described as follows. During the period when T_s decreases due to a decrease in the permafrost surface temperature T_o (Fig. 1), the thermodynamic equilibrium in the adsorbed water film between the ice lens and the soil particles is disturbed, and part of the water is changed to the ice phase.

As the unfrozen water film becomes thinner, the crystallization pressure increases, pushing the frozen soil upward (Khaimov-Malkov 1959). At the same time, the chemical potential of the adsorbed water decreases in the soil underlying the ice lens with a definite gradient. In order to balance the chemical potential of the adsorbed water and because of the continuity of the films, water flows from the films of the lower-lying particles to the phase change interface.

When the supply of water is matched by the latent heat removal rate according to the thermal boundary condition, the ice lens will continue to grow. If the heat removal is reduced, the thermodynamic balance will be disturbed due to increased T_s and the ice lens will start to melt, while the water will be forced out to the unfrozen zone. If the heat removal increases and a water deficit develops near the bottom of the lens, the freezing zone will be cooled and new crystallization centres will develop below the lowest lens on which migratory water will subsequently settle, resulting in a new ice lens. In this way, a mineral layer forms between the ice lenses.

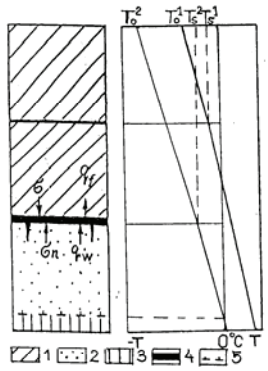

Figure 1. Schematic of the freezing fine-grained soil (Konrad & Morgenstern 1982): 1 – frozen zone; 2 – frozen fringe; 3 – unfrozen soil; 4 – lens of segregated ice; 5 – freezing front.

Any cold wave will be damped at the base of a growing ice lens if it is provided with an adequate supply of water. The wave will not cool the underlying soil until work is done with phase changes. Therefore, in the presence of confined groundwater, continued growth of an ice lens can occur over a long period of time sufficient for the lens to develop into a bed of segregated ice several meters in thickness.

To verify the theoretical concepts considered above, laboratory experiment #15 was conducted in the Igarka permafrost tunnel. Its results corroborate the possibility of continuous growth of a segregated ice lens under the thermal and stress conditions close to those in the field. In the test, a 5.5 cm thick lens was grown in 55 days at a final overburden pressure of 0.25 MPa. Ice lens growth was completely controlled by changing the temperature at the cold side of the sample, simulating the past and present climatic variations. Lowering of the temperature at the base of the ice lens to 0.2°C relative the phase equilibrium temperature corresponding to the applied pressure was allowed. With greater lowering of this temperature, the growing ice lens incorporated soil fragments, resulting in ataxitic (irregular) cryostructure or a

mineral interlayer. Soil and gas inclusions appeared this way in the laboratory-grown ice lenses, which were similar to those observed in natural exposures. The lower the freezing rate is and the larger the soil water pressure is, the better the chance is of continued growth of a segregated ice bed. In the Norilsk Basin, the confined groundwater occurs widely, which easily moves through sandy soils and fissured rocks, providing favourable conditions for the growth of segregated ice.

The transitions between massive ice and ataxitic cryostructure were studied in natural exposures along the Kupets and Norilskaya Rivers, as well as in drill hole cores. In the authors' opinion, such transition between pure ice and ataxitic cryostructure is the only unambiguous evidence so far for the segregated origin of the massive ice beds.

References

Khaimov-Malkov, V.Y. 1959. Thermodynamics of Crystallization Pressure. *Crystal Growth.* Part 2. Moscow: Izd-vo An SSSR, 5-16.

Konrad, J.-M. & Morgenstern, N.R. 1982. Effects of applied pressure on freezing soils. *Can. Geotech. J.* 19(4): 494-495.

Vegetation of Northern West Siberia and its Response to Human-Induced Disturbances

Ludmila Kazantseva
Earth Cryosphere Institute SB RAS, Tyumen, Russia

The significant influence of climate change on ecosystem dynamics was noted long ago (Koloskov 1925, Bocher 1949, Timin et al. 1973, and others) However, long-term ecosystem monitoring in cold regions has been carried out by few researchers (Bliss 1975, Walker 1985, Rannie 1986, Broll et al. 2003). In this connection, the results of long-term ecosystem monitoring at the Nadym site, on which is carried out the conditions of varying climatic and human-induced impact, can be of interest to researchers of arctic and subarctic regions.

The objective of this research is to study vegetation changes under impact of human-induced disturbances. Annual and spatial variability in the structure, species composition, coverage, and frequency of plant species were studied related to changes in seasonal thaw depth and soil temperature.

At the Nadym site located 30 km to the south of the town of Nadym (Moskalenko 2006), detailed descriptions of vegetation on permanent plots are annually carried out, and measurements of seasonal thaw depth and soil temperatures in different landscape conditions are performed.

The zonal vegetation of the Nadym area is birch-larch and birch-pine shrub-moss-lichen light forests. The significant areas are occupied by cloudberry-Labrador tea-peat moss-lichen peatlands and low shrub-sedge-moss bogs. On frost mounds meet cedar Labrador tea-lichen and Labrador tea—peat moss open woodland.

Supervisions were carried out on the 10 x 10 m plots divided grid on meter squares. The plots are situated in natural conditions and in a route of the Nadym-Punga gas pipeline. On each such plot are 100 squares on which the vegetation was described, the soil temperature on a surface and on depth 20 cm was measured, and measurements of seasonal thaw depth were carried out. In a microrelief of plots were described hummocks and space between hummocks and pools; their surfaces were determined with the help of repeated leveling. Microphytocoenoses were registered on dominant species.

The analysis of the received data allowed the compilation of a complete natural and disturbed plots map: spatial structure of microphytocoenoses, microrelief, temperature of soil surface, soil temperature on depth 20 cm, seasonal thaw depth, peat thickness, shrub height.

In Figure 1, two maps of spatial structure show undisturbed and disturbed peat-mineral frost mound results. The microrelief and dominants of microphytocoenoses are shown on these maps.

The vegetation of an undisturbed frost mound is more varied and complicated. There are 3 layers here: (1) shrub layer, height up to 40 cm (*Ledum palustre*); (2) sedge and low

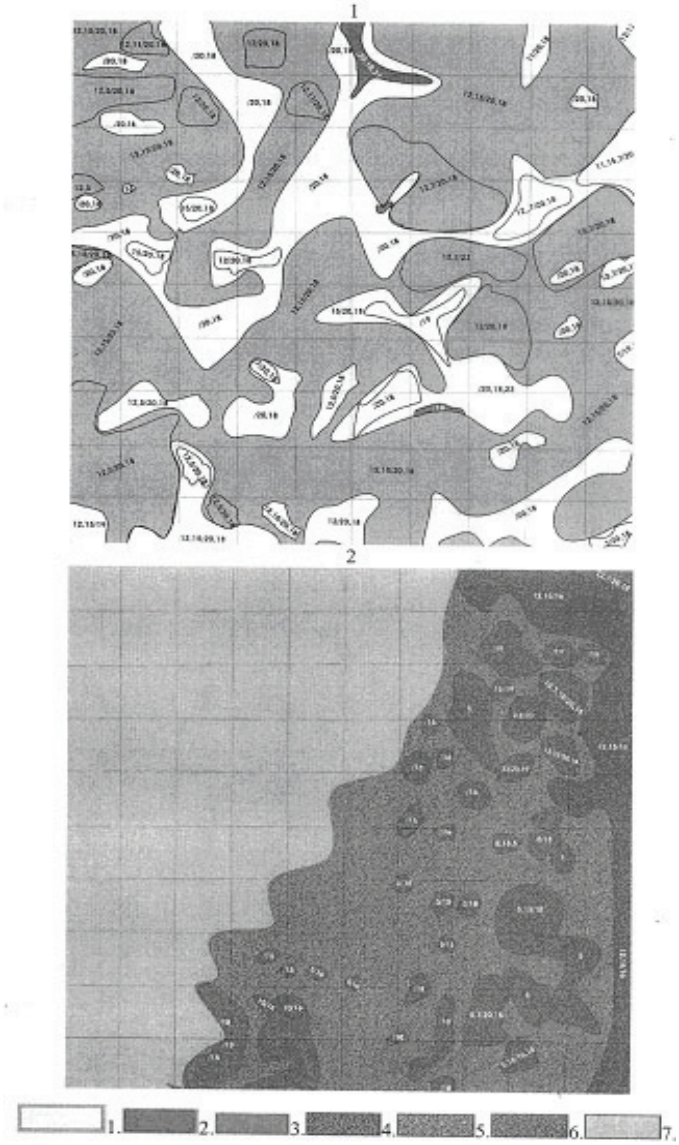

Figure 1. Spatial structure of undisturbed (1) and disturbed (2) frost mound.
Microrelief: 1 – flat surface, 2 – crack, 3 – hummocks, 4 – peaty hummocks, 5 - sandy hummocks, 6 - tussocks, 7 – water
Dominants of microphytocoenoses.
Vascular plants (on the left from line in the index): 4 – Festuca ovina, 5 – Carex globularis, 6 – Juncus filiformis, 7 – Vaccinium vitis-idaea, 8 – Empetrum nigrum, 9 – Dicranum congestum, 10 – Vaccinium uliginosum, 11 – Rubus chamaemorus, 12 – Ledum palustre, 13 – Eriophorum vaginatum, 14 – Andromeda polifolia, 15 – Betula nana, 16 – Pinus sibirica, 17 – Chamaedaphne calyculata.
Mosses and lichen (on the right from line in the index): 18 – Cladina stellaris, 19 – Sphagnum fuscum, 20 – Cetraria islandica, – Cetraria nigricans, 22 – Polytrichum strictum, 23 – Plerozium schreberi.

shrub layer, height up to 10 cm (*Carex globularis, Vaccinium uliginosum)*; and (3) moss and lichen layer (*Cladina stellaris*, *Polytrichum strictum*, *Sphagnum fuscum*).

On a frost mound repeatedly disturbed in 2004 as a result of reconstruction of the gas pipeline, vegetation cover is rare; also it is composed of a small number of species. Vegetation recovery here begins in places where surface peat was kept. More than half of the disturbed plot is flooded with water as a result of infringement of superficial drain by the gas pipeline embankment.

On the natural plot, relative elevations reach 160 cm, and on the disturbed plot, they reach 280 cm due to settlement and flooding of the large part of the plot.

On plot measurements of soil temperature, surface and depth of 20 cm have been carried out. The maps are compiled on the basis of the given temperatures. On the undisturbed frost mound, the maximal temperature of a surface was 14.5°C, on depth 20 cm, -9.7°C; the minimal temperature on a surface was 6.3°C, on the depth 20 cm, -2.7°C. On the disturbed plot, the maximal soil temperature at the depth of 20 cm has increased up to 16°C on peat sites, before covered with lichen, and minimal temperature was 9.5°C. Rise in the soil temperature has made 7°C on the average. Change of temperature influences formation of vegetative cover, the above soil temperature, the more variously specific structure of vegetation on the given site.

Analysis of the given measurements of thaw depth on sites has shown the following: Thaw depth on the undisturbed frost mound was more on the raised sites, occupied with dense Labrador tea; in the space between hummocks occupied with moss-lichen vegetation, thaw depth was less.

The maximal thaw depth was 180 cm; the minimal thaw depth (50 cm) is marked in the frozen crack with lichen cover. According to supervised data, the map of active layer thickness on the undisturbed site is compiled (Fig. 2).

On the disturbed plot, the permafrost table has gone down to a depth of 10 and more meters, according to geophysical works (Ponomareva & Skvortsov 2006).

Measurements of peat thickness have shown that the thickness of peat on a plot changes considerably; it varies in limits from 5 up to 65 cm, depending on the microrelief and vegetation cover. The least thickness of peat is observed on equal sites on which the sedge grows. The greatest thickness of peat is characteristic for peat moss hummocks with cloudberries.

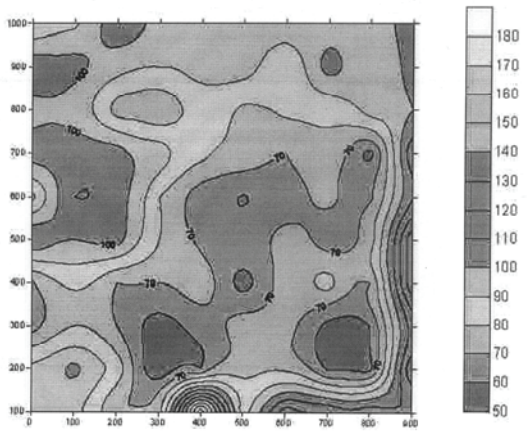

Figure 2. Seasonal thaw depth on undisturbed frost mound (cm).

Human-induced disturbances at construction and operation of the gas pipeline Nadym-Punga in West Siberia rendered significant influence on the vegetation cover and other ecosystem components, which changes are reflected in the complete compiled maps.

These maps can be used for compiling prognostic and ecological maps and also for planning actions related to environment conservation.

Acknowledgments

I thank my colleagues from Earth Cryosphere Institute O.E. Ponomareva, O.L. Opokina, and E.V. Elantsev for help with the fieldwork.

This study was made possible through financial support from the grant of Tyumen governor and the U.S. National Science Foundation (Grants OPP-9732051 and OPP-0225603).

References

Bliss, L.C. 1975. Devon Island, Canada. *Ecolog. Bull*. 20: 17-60.

Bocher, T.W. 1949. Climate, soil and lakes in continental West Greenland in relation to plant life. *Medd. om Gronland*, Bd. 147 (N2,1949): 4.

Broll, G., Tarnocai, C. & Gould, J. 2003. Long-term high Arctic ecosystem monitoring in Quttnir paag National Park, Ellesmere island, Canada. *Proceedings of the Eighth International Conference on Permafrost*, *Zurich, Switzerland, July 21–25 2003*, 1: 85-94.

Koloskov, P.I. 1925. *Climatic Foundations of Agriculture in the Amur Area.* Blagoveshensk: Soviet for Eastern Meteorological Service, 152 pp.

Moskalenko N.G. (ed.) 2006. Anthropogenic changes of ecosystems in West Siberian gas province. *M., RASHN*, 358.

Ponomareva, O.E. & Skvotsov, A.G. 2006. Methods and results of exogenous geological process study in Nadym region of West Siberia. *Proceedings of the International Conference. Tyumen, TGNGU*. 1: 272-274.

Rannie, W.F. 1986. Summer air temperature and number of vascular species in arctic Canada. *Arctic* 39: 133-137.

Timin, M.E., Coller, B.D., Zich, J. & Walker, D.A. 1973. A computer simulation of the arctic tundra ecosystem near Borrow, Alaska. In: *US Tundra Biome Rep*. San Diego State Univ. (73-1): 1-82.

Walker, D.A. 1985. *Vegetation and Environmental Gradients of the Prudhoe Bay Region, Alaska*. Hanover, 239 pp.

Surface Ice and Snow Disappearance in Alpine Cirques and Its Possible Significance for Rock Glacier Formation: Some Observations from Central Austria

Andreas Kellerer-Pirklbauer
Institute of Geography and Regional Science, University of Graz, Austria

Introduction

Active rock glaciers consist of two components: ice (congelation and/or sedimentary ice including "glacier" ice) and lithological material (periglacially and/or glacially-derived rock fragments of different grain size). Considering their long formation period (centuries to millennia) and common climate variability (e.g., temperature, precipitation) in such long time scales, rock glaciers experience strong variations in the rate of nourishment as well as the ratio between ice and debris input to the rock glacier system.

Studies on the climate of rock glaciers reveal that the mean annual air temperature at the rooting zone of active rock glaciers is usually only slightly higher (if at all) than at nearby equilibrium line altitudes (ELA) of normal glaciers and/or the annual precipitation is only slightly lower than at nearby ELA (e.g., Haeberli 1983). This indicates the high sensitivity of rock glacier development to cooler and/or more humid conditions and their close relationship to normal glaciers. However, knowledge regarding incipient formation, entire development period, variations in nourishment rate, and the ratio between ice and rock input seen over a long time span is still far from being complete.

This paper presents data on surface ice and snow disappearance since the Little Ice Age (LIA) at two neighboring cirques in the Central Alps of Austria. Today, one houses a rock glacier and one, a debris-covered glacier remnant. Observations and measurements on thickness variations and thermal conditions of the supraglacial debris cover, on landforms formed from this supraglacial material, and on buried sedimentary ice add to the understanding of rock glacier formation and development.

Study Area and Applied Methods

Kögele Cirque and Hinteres Langtal Cirque

The study area consists of the two neighboring cirques Kögele Cirque (KC) and Hinteres Langtal Cirque (HLC) located in the central part of the Schober Mountains (46°59′N, 12°47′E), Central Alps (Fig. 1). The study area is characterized by crystalline rocks and a continental climate (1500mm at 2000m asl, 0°C mean annual air temperature at 2300 m a.s.l.) causing minor glaciation but a high abundance of rock glaciers. Both cirques are oriented towards the west-northwest, each with comparable high crests and mountain summits (>3000 m a.s.l.) to the south and east (Fig. 1). The HLC is dominated by the Hinteres Langtalkar Rock Glacier (HLRG) which at its front indicates the local lower limit of discontinuous permafrost at 2450 m a.s.l. In contrast, the KC is located some 50 m higher, lacks a rock glacier, but houses a glacier remnant (for details see Kellerer-Pirklbauer & Kaufmann 2007).

Methods

The spatial extent of surface areas covered by glaciers and perennial snow at both cirques was reconstructed for the four stages—c. 1850 (LIA-maximum), 1969, 1997, and 2006—by using morphological evidences (LIA-moraine ridges), air photographs (1969, 1997), and field mapping (Sept. 2006).

Massive sedimentary ice outcrops in the HLC were mapped between summer 2003 and 2007 during fieldwork. In 2006, the thickness of the supraglacial debris mantle in the KC was quantified by digging through and measuring the debris layer to solid ice at 34 sites. These data were used to interpolate the debris cover thickness in the KC, applying the Inverse Distance Weighted interpolator in ArcGIS.

To monitor near-surface temperatures in the supraglacial debris cover, two 3-channel miniature temperature dataloggers (MTLs) (GeoPrecision) were installed in 2006 at 2690 m a.s.l. (KC1) and 2710 m a.s.l. (KC2) in the KC (Fig. 2). Three temperature sensors (PT1000; accuracy +/-0.05°C) were connected to each MTL. The two MTLs operated correctly during the entire period 12.09.2006–25.07.2007, logging values every 0.5 h at depths 0–50 cm (KC1: 0, 10, and 50 cm; KC2: 0, 10, and 20 cm). The lowest sensor at site KC2 was placed at the debris/ice boundary.

Results and Some Related Comments

Surface ice disappearance since 1850

In 1850 A.D., both cirques were covered by glaciers and perennial snow fields covering 0.21 km² of the KC and 0.18 km² of the HLC. In 1969, ice/snow still covered 0.12 km² of the KC and 0.06 km² of the HLC, but by 1997 these values were reduced to 0.06 km² (KC) and 0.01 km² (HLC). In 2006, the extent of surface ice/snow was reduced to a few small patches in the HLC and covered less than 0.01 km² of the KC (Fig. 1).

Supraglacial debris cover and buried sedimentary ice

The supraglacial debris cover in the KC was formed during the last decades by periglacially- and paraglacially-derived sediments from the steadily enlarging supraglacial slopes above the shrinking ice mass. The debris cover is currently relatively thin and increases in thickness down valley, exceeding 70 cm at the lower part of the mapped area (Fig. 2). In contrast to the KC, surface and near-surface (<20 cm), findings of massive ground ice (sedimentary ice judged from the ice appearance) in the HLC are rare and were only noticed at three locations between 2003 and 2007 (Fig. 1). A small lake was observed in the spoon-shaped southern rooting zone of the HLRG in summer 2003 (*2 in Fig. 2), but was absent in the subsequent years. At the upper part of this depression, a narrow massive ice outcrop was seen for the first time in 2006, probably indicating a glacier remnant.

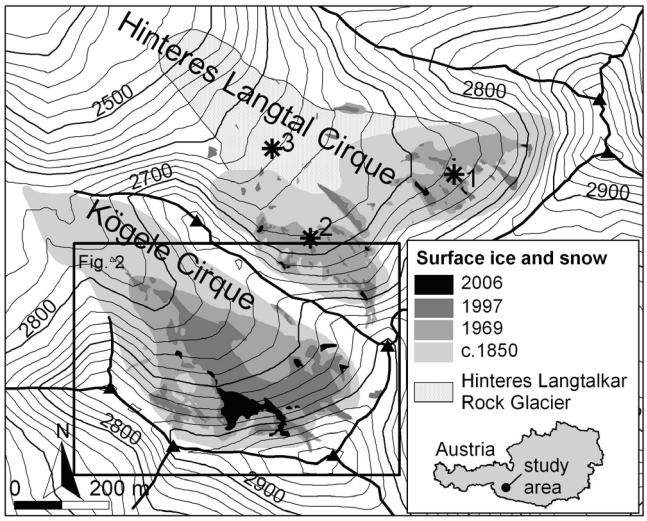

Figure 1. The two cirques Kögele Cirque (KC) and Hinteres Langtal Cirque (HLC) and their extent of surface ice and snow in c. 1850, 1969, 1997, and 2006. The location of the Hinteres Langtalkar Rock Glacier/HLRG (in 2002) is indicated. Findings of sedimentary ice since 2003 in the HLC are asterisked: *1 = in 2006 – below 30 cm of debris; *2 = in 2006 and 2007 – a c. 20 m long and <2 m high massive ice outcrop at the southern rooting zone of HLRG; *3 = in 2007 – below 20–30 cm of debris at the upper edge of a transversal furrow (Viktor Kaufmann, pers. com. 2007).

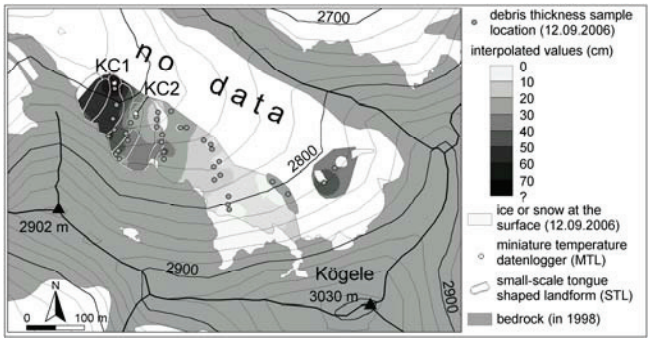

Figure 2. Estimation of the debris cover thickness in the KC, based on 34 sample locations. Locations of the small-scale tongue-shaped landforms (STL) and the two MTLs (KC1 and KC2) are indicated.

Formation of small-scale tongue-shaped landforms

The supraglacial debris cover in the KC does not form a uniform surface. At the southwest margin of the cirque, 9 small-scale tongue-shaped landforms (STL) formed during the last decades are seen on air photographs. Morphometric studies of the STL show heights of the riser of 1–3 m, lengths of 66–125 m, and spatial extents of 859–3276 m². Most of the STL have a down-valley bended appearance in plane view, indicating ongoing movement of the buried glacier remnant. Similar STL features have been observed in the rooting zone of HLRG, hinting a significance of STL for rock glacier nourishment and incipient formation.

Thermal conditions of the supraglacial debris mantle at KC

Data from the MTLs reveal that the mean surface temperature for the period 12.09.2006–25.07.2007 is -1.6°C to -2.4°C at c. 2700 m a.s.l., decreasing with depth (Table 1). The lower temperature at site KC2 seems to be related to longer duration (and thickness?) of winter snow cover. Maximum diurnal temperature fluctuations are >10 K at the surface, 4–5 K at 10 cm depth, 2.2 K at 20 cm depth (at K2 at the ice/debris boundary), and less than 1 K at 50 cm at K1, indicating a substantial damping effect of the debris layer. The lowest sensors at both sites reveal low thawing degree day/TDD values which can be explained by the proximity to the underlying buried ice mass and by a thin active layer at these sheltered locations at such high altitudes.

Table 1. Summarized temperature conditions at different depths at the two sites in the KC for the period 13.09.2006–25.07.2007 (10.5 months) based on MTLs. MPT = mean period temperature in °C; DTF-Max = maximum daily temperature fluctuation during this period in Kelvin; FDD = freezing degree days; TDD = thawing degree days. The snow cover duration was estimated based on low temperature fluctuations (for locations of the MTLs see Fig. 2).

KC1 (snow cover 1.5 months)					KC2 (snow cover 4 months)				
Depth	MPT	DTF-Max	FDD	TDD	Depth	MPT	DTF-Max	FDD	TDD
0	-1.6	11.5	-1010	500	0	-2.4	10.2	-1068	320
10	-1.7	5.3	-924	384	10	-2.8	4.1	-1017	128
50	-2.2	0.8	-742	44	20*	-3.1	2.2	-980	16

*sensor measured at the boundary between debris and glacier ice.

Long-term landscape dynamics: KC versus HLC

The data presented here confirm the fact that, already, slightly different topoclimatic conditions are sufficient to generate over a long time span a rock glacier in one cirque and a normal glacier in the neighbouring cirque. The rate of ice and debris input to the cirque during the past was dominated by the former in the KC, whereas probably by the latter in the HLC. A thin active layer helps to preserve a degrading debris-covered glacier remnant. Subsequent incorporation of such a debris-covered ice mass into a rock glacier body might be regarded as an important nourishment factor; at least this could have been the case at the HLRG.

Acknowledgments

This study was carried out within the framework of the project ALPCHANGE (www.alpchange.at) financed by the Austrian Science Fund (FWF). The air photographs (1969, 1997, and 1998) were kindly provided by Viktor Kaufmann.

References

Haeberli, W. 1983. Permafrost-glacier relationships in the Swiss Alps: Today and in the past. *Proceedings, 4th Intl. Conf. on Permafrost, Fairbanks, AK, July 17–22*: 415-420.

Kellerer-Pirklbauer, A. & Kaufmann, V. 2007. Paraglacial talus instability in recently deglaciated cirques (Schober Group, Austria). *Proceedings, 9th Intl. Symposium High Mountain Remote Sensing Cartography (HMRSC-IX), Graz, Austria, Sept. 14–22, 2006*: 121-130.

Temperatures in Alpine Rock Walls During the Warm Winter 2006–2007 in Austria and Its Significance for Mountain Permafrost: Preliminary Results

Andreas Kellerer-Pirklbauer
Institute of Geography and Regional Science, University of Graz, Austria
Michael Avian
Institute of Remote Sensing and Photogrammetry, Graz University of Technology, Austria
Gerhard Karl Lieb, Matthias Rieckh
Institute of Geography and Regional Science, University of Graz, Austria

Introduction

In a large part of Europe temperatures during autumn and winter 2006–2007 reached a record high. The autumn of 2006 (Sept., Oct., and Nov.) was more than 3°C warmer from the northern side of the Alps to southern Norway if compared to the 1971–2000 average (WMO 2007). The extreme temperature anomaly also affected the high mountains of Austria and caused record temperature values at the Sonnblick Observatory located in the high mountains of central Austria (3106 m a.s.l., 47°03′N, 12°57′E; cf. Fig. 1). At this observatory, the period September 2006 to June 2007 was substantially warmer than the average. Deviations from the mean monthly values of the normal period 1961–1990 are in the range of +2.6°C (Nov. 2006) and +4.9°C (April 2007) with a mean value of +3.2°C for this 10-month period (ZAMG 2007). Comparable extreme atmospheric temperature anomalies are reported to affect near-surface permafrost conditions to depths exceeding 10 m (Isaksen et al. 2007). In particular, monitoring temperature changes in bedrock gives a good indication for the effects of air temperature anomalies on ground thermal conditions (Smith & Riseborough 1996). For this reason, continuous temperature measurements in alpine rock walls for monitoring the effects of climate change on bedrock temperatures (including permafrost) in central and eastern Austria were initiated in summer 2006 within the project ALPCHANGE. Measurements at 9 rock wall sites (RWS) distributed over 5 study areas (SAs) recorded the exceptionally warm 9-month period from 01.10.2006 to 30.06.2007. Preliminary results are presented here.

Study Areas and Instrumentation

Four of the 5 SAs are located in the Hohe Tauern Range, where the highest mountains of Austria reach almost 3800 m a.s.l. At each of the 4 SAs (Dösen Valley, Hintereggen Valley, Hinteres Langtal Cirque, and Pasterze Glacier; Fig. 1, Table 1), 2 RWS with opposed aspects were instrumented with 3 temperature sensors for each rock wall. The fifth SA is located in the eastern part of the Niedere Tauern Range (Hochreichart Cirque), where only one north-facing rock wall at an elevation of 1960 m a.s.l. was instrumented. The 9 RWS are located at elevations between 2220 and 2775 m a.s.l. (3 of them are probably affected by permafrost). All 9 RWS were drilled in different metamorphic bedrock types (Table 1).

To measure bedrock temperatures, 16 mm wide boreholes were drilled at each site 40 cm horizontally into the bedrock by using HILTI drilling equipment connected to an external power set. Due to technical problems, the boreholes at the sites DOV-A, HEV-A, and HEV-B (Table 1) did not reach the intended 40 cm depth. To measure near rock surface temperature, a sensor was installed at 3 cm. The other sensors were installed at depths of 10 and 40 cm (slightly less at the 3 RWS mentioned above) as suggested by Matsuoka (1994). At all RWS, the measurements were recorded every 30 minutes on three-channel miniature temperature dataloggers/MTLs (M-Log6, GeoPrecision). All datasets cover at least the period 01.10.2006 to 30.06.2007. The three sensors are

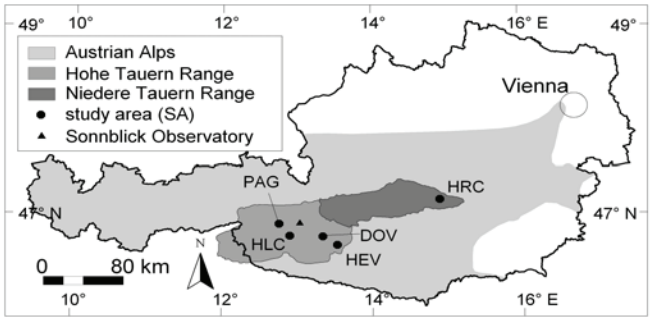

Figure 1. Locations of the 5 study areas in Austria and the Sonnblick Observatory. For abbreviations refer to Table 1.

Table 1. Characteristics of the 9 alpine rock wall sites, where temperature is monitored since summer/early autumn 2006. SA=study area (DOV=Dösen Valley, HEV=Hintereggen Valley, HLC=Hinteres Langtal Cirque, HRC=Hochreichart Cirque, PAG=supraglacial slopes flanking the tongue of Pasterze Glacier); RWS=rock wall site; Bedrock types: GGN=granitic gneiss, AGN=augengneiss, MS=mica schist, GN=Gneiss, CMS=calcareous mica schist; Depths=depths of sensors in borehole.

SA	RWS	Lat.	Long.	Alt. (m asl)	Aspect	Bed-rock.	Depths (cm)
DOV	DOV-A	46°59′N	13°17′E	2630	S	GGN	3,10,32
	DOV-B[1]	46°59′N	13°17′E	2640	N	GGN	3,10,40
HEV	HEV-A	46°55′N	13°23′E	2505	W	AGN	3,10,30
	HEV-B[1]	46°55′N	13°23′E	2530	E	AGN	3,10,30
HLC	HLC-A	46°59′N	12°47′E	2725	SW	MS	3,10,40
	HLC-B[1]	46°59′N	12°47′E	2700	NE	MS	3,10,40
HRC	HRC-A	47°22′N	14°41′E	1960	N	GN	3,10[2],40[2]
PAG	PAG-A	47°05′N	12°44′E	2220	SW	CMS	3,10,40
	PAG-B	47°05′N	12°44′E	2250	NE	CMS	3,10,40

[1] probably with permafrost occurrence (Lieb 1998)
[2] sensor that partly malfunctioned (no data presented in Table 2)

of the PT1000 type with—according to GeoPrecision—an accuracy of +/- 0.05°C, a measurement range between -40 and +100°C and a very high long-term stability (calibration drift <0.01°C/year). Each sensor was connected to the MTL by a teflon cable. After sensors installation, the borehole was refilled with fine quartzite sand and sealed with silica gel to avoid, for example, air circulation in the borehole.

Results and Discussion

Mean temperature values for the 9-month period (MPT), the accumulated freezing degree days (FDD), and the accumulated thawing degree days (TDD) were computed at all 9 RWS for each sensor (Table 2). FDD and TDD equal the number of degree days below and above 0°C, respectively. The results for MPT, FDD, and TDD at the 3 different depths at each RWS are relatively equal, indicating rapid conductive heat transfer in the metamorphic rocks. Maximum value ranges are 0.22°C for MPT (HEV-A), 259 for FDD (DOV-B), and 118 for TDD (HLC-A).

Focusing on the 3 cm values, one might infer that MPT, FDD, and TDD are not correlated with elevation, which can be attributed to differences in the duration of the winter snow cover, aspect, and the small sample size (cf. insert graph in Table 2). The highest location of RWS where positive MPT for the period 01.10.2006 to 30.06.2007 were recorded is located at 2725 m a.s.l., is facing southwest, and was covered by snow for some 3.5 months (HLC-A: 1.55°C). An exceptionally high MPT value of 5.25°C at an elevation of 2220 m a.s.l. with no substantial snow cover was recorded at a southwest-facing RWS (PAG-A). More generally, RWS with absent or short snow cover (1 month or less), located in high as well as lower elevations, reveal positive MPT and relatively low FDD and high TDD values (HEV-A, HEV-B, and PAG-A). In contrary, the lowest MPT (-1.89°C) as well as highest FDD (-679) were recorded at RWS with long snow cover (6 months or more), in north to northeast aspects and in high-elevated permafrost environments (>2640 m a.s.l.). Such conditions have been recorded at HLC-B and DOV-B, where the long-lying snow cover (established around end of November/beginning of December) protected the frozen rock wall from the warm atmospheric conditions during winter and spring.

One might conclude that, based on our data, only rather extreme RWS revealed temperatures during the studied 9-month period 01.10.2006 to 30.06.2007 favorable for permafrost conditions and preservation. Thus, it can be assumed that permafrost regions in central and eastern Austria, with a minor winter and spring snow cover in 2006–2007, experienced very unfavorable conditions. The continuation of our measurements will reveal more details on the significance of this winter over a longer time span.

Table 2. Summarized results of the temperature measurements at all 9 RWS for the period 01.10.2006–30.06.2007: Snow=period with supposed thick snow cover indicated in months; Depth in cm; MPT=mean period temperature in °C; FDD=freezing degree days; TDD=thawing degree days. Insert graph shows relationship between MPT (3 cm) and elevation with respect to snow cover.

DOV-A (Asp. S; Snow 1)			
Depth	MPT	FDD	TDD
3	1.87	-328	839
10	1.93	-312	839
32	1.87	-249	760
DOV-B (Asp. N; Snow 6)			
Depth	MPT	FDD	TDD
3	-1.69	-679	65
10	-1.71	-688	63
40	-1.71	-420	45
HEV-A (Asp. W; Snow 0)			
Depth	MPT	FDD	TDD
3	0.92	-393	646
10	0.91	-384	632
30	0.70	-369	559
HEV-B (Asp. E; Snow 0.5)			
Depth	MPT	FDD	TDD
3	2.11	-249	824
10	2.20	-231	830
30	2.16	-202	791
HLC-A (Asp. SW; Snow 3.5)			
Depth	MPT	FDD	TDD
3	1.55	-302	727
10	1.61	-286	727
40	1.41	-225	609

HLC-B (Asp. NE; Snow 6.5)			
Depth	MPT	FDD	TDD
3	-1.89	-666	149
10	-1.88	-662	148
40	-1.86	-626	118
HRC-A (Asp. N; Snow 0)			
Depth	MPT	FDD	TDD
3	1.99	-303	847
PAG-A (Asp. SW; Snow 0)			
Depth	MPT	FDD	TDD
3	5.25	-101	1535
10	5.42	-81	1560
40	5.10	-37	1429
PAG-B (Asp. NW; Snow 6)			
Depth	MPT	FDD	TDD
3	1.95	-11	544
10	1.77	-28	511
40	1.77	-14	497

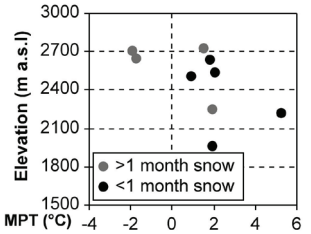

Acknowledgments

This study was carried out within the framework of the project ALPCHANGE (www.alpchange.at) financed by the Austrian Science Fund (FWF).

References

Isaksen, K., Benestad, R.E., Harris, C. & Sollid, J.L. 2007. Recent extreme near-surface permafrost temperatures on Svalbard in relation to future climate scenarios. *Geophysical Research Letters* 34: L17502.

Lieb, G.K. 1998. High-mountain permafrost in the Austrian Alps (Europe). *Proceedings of the Seventh International Permafrost Conference, Yellowknife, Canada, June 23–27, 1998:* 663-668.

Matsuoka, N. 1994. Diurnal freeze-thaw depth in rock walls: field measurements and theoretical considerations. *Earth Surface Processes and Landforms* 19: 423-435.

Smith, M.W. & Riseborough, D.W. 1996. Permafrost monitoring and detection of climate change. *Permafrost and Periglacial Processes* 7: 301-309.

WMO 2007. A warm autumn and winter in Europe. *Newsletter of the World Meteorological Organization* 2007/No. 1: 3.

ZAMG 2007. Present climate data from stations in Austria. http://www.zamg.ac.at (accessed 01.11.2007).

Content and Composition of Organic Matter in Quaternary Deposits on the Laptev Sea Coast

A.L. Kholodov
Geophysical Institute, University of Alaska Fairbanks, USA
Institute of Physical, Chemical, and Biological Problems of Soil Science, RAS, Russia
L. Schirrmeister
Alfred Wegener Institute for Polar and Marine Research, Potsdam, Germany
H. Meyer
Alfred Wegener Institute for Polar and Marine Research, Potsdam, Germany
Ch. Knoblauch
Soil Science Institute of Hamburg University, Germany
K. Fahl
Alfred Wegener Institute for Polar and Marine Research, Bremerhaven, Germany

Introduction

Because of freezing and subsequent preservation of biomass after sedimentation, permafrost areas are considered to be important carbon sinks. Mean TOC contents of frozen Quaternary deposits exposed at the Laptev Sea coast are high and vary between 3.2 to 11.9 wt% (Grigoriev et al. 2004). The organic matter (OM) is preserved in permafrost in the early diagenetic stage of OM maturation. This stage is characterized by a decreasing N content, depletion of products, which have a biological value (carbohydrates, proteins, etc.) and preservation of biopolymers (Bordenave 1993). Deeper thawing caused by climate warming can result in increased decomposition of organic matter and a release of greenhouse gases. This study aims a characterization of the organic matter in different types of Quaternary deposits at the Laptev Sea coast.

The Study Area and Investigated Deposits

Permafrost drilling was carried out on the Bykovsky Peninsula (SW of Lena River Delta) and Cape Svyatoy Nos (NE of Yana River mouth) in 2001 and 2003 (Kholodov et al. 2006). Various types of Quaternary deposits were analyzed from both sampling sites:

1. Middle Pleistocene deposits of the *Kuchchuguy Suite* composed of well-sorted silty loam with numerous thin grass roots. The ice content is in the range from 30 to 50%. The cryostructure is massive. The genesis of these loess-like deposits is still under debate.

2. Late Pleistocene syncryogenic *Ice Complex deposits* of silt or silty loam with sand and peat layers, fragments of twigs and other plant remains, and peat inclusions are characterized by volumetric ice content of up to 80–90% and large wedges (up to 30 m high). The Ice Complex deposits of the Bykovsky Peninsula can be divided into 2 groups: those accumulated due to intensive sedimentation rate and formed under the condition of stable ground surface position. The first group was formed during the MIS-4 and MIS-2 periods. The second group was accumulated during MIS-3 Interstadial. According to previous investigation (Schirrmeister et al. 2002), several periods existed during the MIS-3 time, when rates of sedimentation and freezing decreased and palaeosol horizons were formed over long periods during several thousands of years. The Ice Complex sequences are in places covered by Late Holocene deposits.

3. Late Pleistocene to Holocene *deposits in thermokarst depressions* (alases). The formation of these deposits was a result of thermokarst processes that took place during the Late Pleistocene to Holocene transition period (13–10 kyr BP). This layer can be subdivided into 2 horizons:

a. Taberal deposits, that is, former Ice Complex deposits which were thawed under thermokarst lakes and refrozen after lake drainage. Taberal deposits are silty loams with a volumetric ice content of up to 50%.

b. Lacustrine to boggy (alas) deposits were formed in shallow lakes or in bogs. These deposits are characterized by a high peat and ice (up to 60%) content.

Materials and Methods

The described deposits were cored using a rotary drilling device. The samples were air dried immediately after drilling. Subsequently the material was milled. For determination of TOC and isotopic composition, carbonates were removed from samples by a 1n solution of HCl at 90°C for 3 hours and washed with distilled water.

The following analyses were done:

Water (ice) content and density of soil were determined using a weight method. *Elemental composition* of OM: Total carbon (TC), total organic carbon (TOC), and nitrogen (N) were determined using the VARIO II Element analyzer. *Isotopic composition ($\delta^{13}C$)* was determined with a Finnigan MAT Delta-S mass spectrometer using a FLASH elemental analyzer and a CONFLO III gas mixing system for online determination of the carbon isotopic composition. *Dissolved Organic Carbon (DOC)* was extracted from samples with a $CaCl_2$ solution (4 mM). Subsequently the samples were centrifuged and filtered (0.45 μm) (Zsolnay 2003). *Biomarkers*, to gain better insights into the geochemical composition of the particulate organic carbon n-alkanes (C15 to C37), sterols (sum of 24-Methylcholest-5-en-3ß-ol and

Table 1. Main parameters of organic matter in the investigated deposits.

Type of deposits	n	TC,% *	TOC, % *	TOC/N *	CPI	$\delta^{13}C$, ‰ *;**	DOC (mg gTG) *
Kuchchuguy Suite	14	0.66–1.82 / **1.14**	0.34–1.24 / **0.75**	3.25–9.34/ **6.96**	5–6	-27.28 to -25.70 / **-26.18**	0.13–0.26 / **0.20 (*n*=4)**
Ice Complex	28	0.35–4.53 / **1.91**	0.26–3.89 / **1.48**	1.67–11.38 / **8.75**	–	-27.48 to -23.78 / **-25.34**	0.00–0.95 / **0.36 (*n*=25)**
Taberal deposits	14	0.59–3.28 / **1.64**	0.57–2.65 / **1.08**	0.84–14.63 / **8.44**	4–6	-27.15 to -24.32 / **-25.59**	0.11–0.43./ **0.27 (*n*=9)**
Lacustrine / boggy alas deposits	11	1.01–6.92 / **2.38**	0.93–6.13/ **1.99**	8.20–11.90 / **9.14**	3–5	-26.90 to -23.74 / **-25.33**	0.06–0.61 / **0.27 (*n*=9)**

*Min–max range/average value, ** vs. PDB standard

24-Ethylcholest-5-en-3ß-ol), and fatty acids (carbon length 14 to 30), were analyzed by means of gas chromatography according to Fahl & Stein (1999). The carbon-preference-index (CPI) was calculated after Bray & Evans (1961).

Results and Discussion

The main characteristics of organic matter (TC, TOC, C/N ratio, $\delta^{13}C$, CPI and DOC) in Laptev Sea Quaternary deposits are summarized in Table 1 for the four types of deposits. The mean TC contents are between 1 and 2.5%, most of which (about 60%) is composed of organic carbon. Main differences concerning carbon characteristics between the studied deposit types are lowest TC, TOC, DOC content, C/N ratios and $\delta^{13}C$ values for the Kuchchuguy, whereas Ice Complex, Alas and taberal deposits are similar with regard to their organic composition. The mean $\delta^{13}C$ is about -25.3 to -25.5‰ for these deposits, and very similar ranges let us believe that the ratio between lacustrine/boggy and terrestrial C3 plant remained the same and the degree of reworking is low. The Kuchchuguy deposits, however, are with -26.1‰ slightly lower in $\delta^{13}C$ with similar minimum values, but isotopically lighter (more negative) maximum values. This most likely accounts for the drier conditions and/or higher sedimentation rates during Kuchchuguy deposition, with a lower relative amount of aquatic biomass in the spectrum.

Isotopic composition and C/N ratio indicate a low level of OM decomposition in all investigated deposits. Only buried soils and deposits of the alas complex (both alas and taberal) have C/N values close to the upper (organic) horizons of modern tundra soils. The biomarker data implicate no significant differences between the investigated deposits.

Supply of OM and the grade of its maturity depend on the condition of accumulation. Deposits formed by intensive sedimentation have less OM supply and lowest level of its transformation due to fast burial and subsequent freezing. On the contrary, formed in condition of a stable ground surface, alas deposits and buried soils are characterized by the higher OM supply and level of its maturity.

Conclusion

Frozen Quaternary deposits of the Laptev Sea region are significant reservoirs of low transformed organic matter. The TC content is up to 7 wt%. Most (up to 6 wt%) of this carbon has organic origin and insoluble in water compounds.

Sediments of the highest accumulation rate (Kuchchuguy deposits) have the lowest carbon content and less time to form aquatic organic matter. Decreasing sedimentation rates lead to the accumulation of higher amounts of organic matter from one side and its deeper transformation from another.

Acknowledgments

Current research was supported by RFBR (grant #05-05-64062) and INTAS (YS #04-83-2950).

References

Bordenave, M.L. 1993. *Applied Petroleum Geochemistry*. Enfield, NH: Editions Technip, 524 pp.

Ershov, E.D. 1989. *Geocryology of USSR Eastern Siberia and Far East*. Moscow: Nedra, 515 pp (in Russian).

Fahl, K. & Stein, R. 1999. Biomarkers as organic-carbon-source and environmental indicators in the Late Quaternary Arctic Ocean: problems and perspectives. *Marine Chemistry* 63: 293-309.

Grigoriev, M.N., Rachold, V.R., Hubberten, H.-W. & Schirrmeister, L. 2004. Organic Carbon input to the Arctic Seas through coastal erosion. In: R. Stein & R.W. Macdonald (eds.), *The Organic Carbon Cycle in the Arctic Ocean*. Berlin, Heidelberg, & New York: Springer, 363 pp.

Schirrmeister, L., Siegert, Ch., Kuznetsova, T., Kuzmina S., Andreev, A., Kienast, F., Meyer, H. & Bobrov, A. 2002. Paleoenvironmental and paleoclimatic records from permafrost deposits in the Arctic region of Northern Siberia. *Quaternary International* 89: 97-118.

Zsolnay, A. 2003. Dissolved organic matter: Artefacts, definitions, and functions. *Geoderma* 113: 187-209.

Environmental Controls for the Coastal Processes on Yugorsky Peninsula, Kara Sea, Russia

Artem Khomutov
Earth Cryosphere Institute SB RAS, Tyumen, Russia

Introduction

The study area on Yugorsky Peninsula, coast of the Kara Sea, is noted for active coastal processes (Kizyakov et al. 2006). Dynamics of bluff and thermocirque edges was monitored in 2001–2007, and landscape units were subdivided using satellite image and field data. The paper presents joint analysis of field and remote-sensing data from two key sites: Pervaya Peschanaya and Shpindler. Some aspects of environmental controls for the coastal processes are discussed.

Detailed knowledge of landscape components for remote arctic areas is relatively scarce (Virtanen et al. 2004). Therefore, a combination of remote sensing and field methods was applied to determine response of specific landscape units to coastal processes.

Both key sites were used to work through methods of estimating coastal retreat rate/landscape unit correlation. To understand landscape-coastal process links, a satellite image was classified, and retreat rates at the same plot were measured.

Prior to the field study, main classes were subdivided on a satellite image Landsat 7 ETM+ with 15 m resolution in one panchromatic band. The most suitable combination of multispectral bands was used for accurate identification of classes as specific landscape units subdivided according to the landscape classification of Melnikov (1983). Characteristics of landscape units related to 25 identified classes were based on field studies during the last 3 years (2005–2007). They included descriptions of landforms, vegetation, and active layer depths within each landscape unit. At the coastal bluff and thermocirque edges, retreat was measured in 2001, 2005, 2006, and 2007. Maximum retreat of each of landscape unit was calculated for 2001–2005, 2005–2006, 2006–2007, and for the entire observation period (2001–2007). Then the average annual was calculated by summarizing a maximum retreat for a given landscape during the entire period of measurement divided by 6 years.

Methods

Superposition of the classified satellite image and tacheometric map of the coastal thermocirques at Pervaya Peschanaya and Shpindler key sites shows the following. Landscape resistibility to the coastal processes depends on several environmental factors: slope inclination, moisture/drainage conditions, active layer depth, vegetation complex, and its coverage.

Statistical analysis of the bluff-edge position against landscape units for both key sites provides some indirect retreat rate dependence on environmental controls.

Landscape units subject to coastal processes are subdivided into three groups according to their resistibility to coastal retreat: Irresistible, Medium irresistible, and Resistible. The group of Medium irresistible landscape units is subdivided as a landscape complex, changing its resistibility due to climate change.

Maps for each key site are compiled, showing landscape units, combined into groups marked with different colors depending on their resistibility to coastal processes.

Results and Discussion

Average maximum retreat rates calculated according to the described methodology vary between 1.7– 4.6 m/yr for 6 years. Landscape units are subdivided into 3 groups according to the rate of measured coastal retreat. Irresistible landscapes are those with a maximum annual retreat rate exceeding 7 m/yr. Resistible landscapes are those with a retreat rate less than 3 m/yr. In between are Medium irresistible landscape units. The average maximum retreat rate for a group of Irresistible landscape units is 9.2 m/yr, while the Resistible landscape group shows only 2.4 m/yr average retreat rate. The Medium resistible group is characterized by an average retreat rate of 5.5 m/yr (Table 1).

Landscape components considered as retreat controls are shown in Table 1. They include drainage, slope inclination, surface microrelief, vegetation coverage, and dominating vegetation. Analysis of Table 1 shows that Irresistible landscape units are characterized mainly by slightly poorer drainage conditions compared to Resistible landscapes. As a rule, they are located on steeper slopes, with notable forms of microrelief, such as spot-medallions and hummocks, with rather well-developed vegetation cover and dominating shrubby and mossy complexes. At the same time, landscape units belonging to a Resistant category are generally better drained, level to gently sloping flat surfaces, often bare or poorly vegetated, with graminoid vegetation dominating. Medium irresistible landscape units are characterized by variable landscape features, some of which are closer to the Irresistible type, such as slope inclination and coverage, and some in the middle position between Irresistible and Resistible types.

It should be noted that Medium irresistible are worse drained compared with both extreme types, which means that the combination of even extreme landscape components may cause partial compensation of their effect.

To analyze the role of each retreat rate control, we assigned a numerical score to each of the subdivided environmental factors enumerated in Table 1, based on our experience.

The higher role of the control in retreat rate is presumed, the higher score is assigned. For example, poor drainage (wet surface) is assigned score 3, well drained (dry surface) has score 1. Intermediate drainage is scored as 2.

Table 1. Landscape resistibility to coastal retreat.

Group (average retreat rate, m/yr)	Landscape unit	Average retreat rate, m/yr	Active layer depth range, m	Degree of drainage[1]	Degree of slope inclination[2]	Surface microrelief[3]	Vegetation coverage[4]	Dominating vegetation[5]
Irresistible (9.2)	1	14.6	>1.0	DW	S	H	V	M, Sh, He
	2	8.9	>1.0	D	S	H	BV	Sh, He
	3	8.8	>1.0	D	S	H, SM	V	He, M
	4	8.3	<0.6	DW	G	F	V	M, Se
	5	8.1	0.6–1.0	DW	G	F	V	M, Se
	6	8.0	0.6–1.0	D	L	F	BV	Sh, He
	7	7.6	0.6–1.0	W	G	H, T	V	M, Se
Medium irresistible (5.5)	8	6.6	0.6–1.0	W	G	T	V	Se, M, He
	9	6.3	0.6–1.0	DW	G	F	V	M, Gr
	10	5.95	>1.0	D	S	F	B	
	11	5.9	0.6–1.0	DW	S	H	BV	M
	12	4.95	0.6–1.0	DW	G	F	V	M, Se
	13	4.8	0.6–1.0	D	G	SM	V	M, Sh, Gr
	14	4.1	<0.6	W	L	T	V	M
Resistible (2.4)	15	2.9	>1.0	D	G	H, SM	V	Se, Sh, M
	16	2.7	>1.0	D	L	F	BV	Gr
	17	2.6	>1.0	D	S	F	V	Gr, He
	18	2.4	>1.0	D	L	F	B	
	19	2.3	<0.6	W	L	P	V	Se, M
	20	1.7	>1.0	D	G	F	BV	Gr

[1]D – well drained, DW – poorly drained, W – wet. [2]S – steep, G – gentle, L – level. [3]F – flat, H – hummocky, T – tussocky, SM – with spot-medallions, P – polygonal. [4]B – bare surface, BV – semi-vegetated, V – fully vegetated. [5]Sh – shrubs, He – herbs, Gr – graminoids, M – moss, Se – sedge.

Table 2. Average numerical score analysis of environmental controls.

Groups of landscapes	Environmental controls of maximum retreat rate				
	Dominating vegetation	Vegetation coverage	Degree of slope inclination	Degree of drainage	Surface microrelief
Irresistible	2.4	2.4	2.3	1.7	1.9
Medium irresistible	1.9	2.3	2.1	2.0	1.7
Resistible	1.2	1.8	1.7	1.3	1.5

Scores were summarized and averaged for a group of landscapes as shown in Table 2. Though the table is based on expert judgment, the result expresses an expected pattern: landscape units with a higher retreat rate (Irresistible) according to field measurements show the highest numerical score in all the cases excluding drainage factor, so we consider this approach to give a good qualitative estimate. Analyzing the range of average score for various environmental controls between Irresistible and Resistible landscape groups, we note that the maximum difference (2.4-1.2=1.2, Table 2) belongs to the "dominating vegetation" control, which makes this factor most valuable in determining the degree of resistibility to coastal retreat. Gentle, well-drained slope, though, with moss-shrub vegetation (landscape unit 15) belongs to the category of Resistible landscapes.

Conclusion

Dominating shrubby-mossy vegetation is an indicator of irresistibility of landscapes to maximum coastal retreat, while graminoids indicate the lowest maximum retreat rate. Geomorphological controls are less significant. Most valuable of the geomorphic factors is slope inclination due to gravimetric effect. Microrelief features, such as hummocks and spot-medallions, increase irresistibility of landscape units, especially in combination with steep slopes, because they result from flaws in the active layer.

A combination of environmental controls, even those having a medium numerical score assigned by an expert judgment each, results in a high maximum coastal retreat rate and is a reason for adding this landscape unit in the category of Irresistible.

References

Kizyakov, A.I., Leibman, M.O. & Perednya, D.D. 2006. Destructive relief-forming processes at the coasts of the Arctic plains with tabular ground ice. *Kriosfera Zemli* X(2): 79-89 (in Russian).

Melnikov, E.S. (ed.). 1983. *Landscapes of Cryolithozone of Western-Siberian Gas Province*. Novosibirsk: Nauka Publisher, 166 pp. (in Russian).

Virtanen, T., Mikkola, K. & Nikula, A. 2004. Satellite image based vegetation classification of a large area using limited ground reference data: case study in the Usa Basin, NE European Russia. *Polar Research* 23(1): 51-66.

Carbon Dynamics of the Permafrost Regime, North Slope of Alaska

Yongwon Kim
International Arctic Research Center, University of Alaska Fairbanks, USA
Keiji Kushida
Institute of Low Temperature Science, Hokkaido University, Japan
Masato Shibuya
Graduate School of Agriculture, Hokkaido University, Japan
Hiroshi Enomoto
Department of Civil Engineering, Kitami Institute of Technology, Japan

Introduction

The terrestrial ecosystems, including tundra and boreal forest regions of the Arctic, cover a little less than 18% of Earth's land surface, but they contain more than 40% of all carbon present in the terrestrial biomes (Kasischke 2000), demonstrating about one-third of the carbon sequestered in Pan-Arctic tundra and boreal forests. High-latitude ecosystems are particularly vulnerable to climate change due to the large carbon pools in northern latitude soils. The soil carbon pool estimated for the combined tundra-boreal forest ranges from 21% (Raich & Schlesinger 1992) to 30% (Post et al. 1982) of the global carbon pool.

Recently, Zimov et al. (2006) addressed carbon sequestration from thawing permafrost in the Arctic. The soils of the permafrost region of North America contain 213 Gt of organic carbon—approximately 61% of the carbon in all soils of North America. The soils of the permafrost region of North America are currently a net sink of approximately 11 MtC/yr. The soils of the permafrost region of North America have been slowly accumulating carbon for the last 5–8 thousand years. More recently, increased human activity in the region has resulted in permafrost degradation and at least localized loss of soil carbon.

Considering the wide distribution of permafrost in Alaska's North Slope, the observations of the fluxes of soil CO_2 (e.g., soil respiration) and CH_4, and of the soil carbon/nitrogen contents are extremely significant for a better understanding of soil organic carbon turnover time with the remarkable Arctic climate change (ACIA 2004) on the permafrost regime of Alaska's tundra ecosystem.

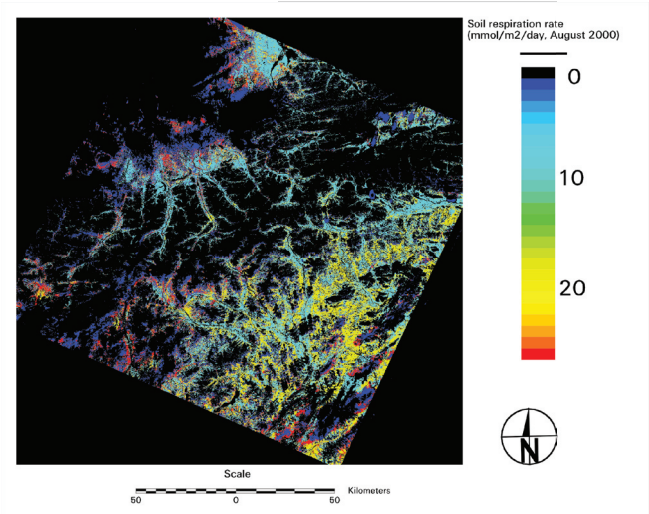

Figure 1. Microbial respiration in subalpine tundra.

Material and Method

Description of study area

The observation sites are shown in Kim & Tanaka (2001), which are coastal tundra (CT) near Deadhorse, upland tundra (UT) north of Toolik Lake station, and subalpine tundra (SaT) north of the Brooks Range along the Trans-Alaska Pipeline during the growing season of 2000/2001. Flux measurements of CO_2 and CH_4 using chambers, soil density, soil water content, and dominant vegetation type and content of soil organic carbon/nitrogen in each site were examined. The chambers used were of two types: one made of transparent material and the other, of nontransparent material. The former is called *light* and the latter is *dark chamber* in this study.

Results and Discussion

Soil respiration and CH_4 flux

Soil respiration consists of heterotrophic (microbial) and root respiration. The average fluxes of CO_2 and CH_4 ranged from -0.058±0.012 (±SE; standard error) in coastal tundra to 0.41±0.08 gCO_2-C/m²/d in upland tundra, and from -1.50±0.33 in subalpine tundra to 1.42±0.23 mg/CH_4-C/m²/d in coastal tundra, respectively. The negative values of CO_2 and CH_4 fluxes indicate photosynthesis and atmospheric CH_4 oxidation. In terms of soil carbon during the growing season, accumulated soil respiration was equivalent to 16±12 and 35±24 gC/m² for light and dark chambers, respectively. It is difficult to estimate seasonal carbon emission for CH_4 flux due to CH_4 oxidation. Gilblin et al. (1991) reported that the soil respiration ranged from 6 to 20 gC/m² in arctic tundra soils during the growing season, and Oechel et al. (1997) measured soil respiration of 4.4 to 44 gC/m² in arctic tussock and wet sedge tundra of Alaska, which is similar to our data during 2000/2001. Figure 1 shows a snapshot of the heterotrophic respiration by soil microbe of soil respiration in alpine tundra using Landsat ETM+ image analysis as well as in situ soil respiration data.

Biomass, soil carbon, and nitrogen

The average content of biomass, carbon and nitrogen,

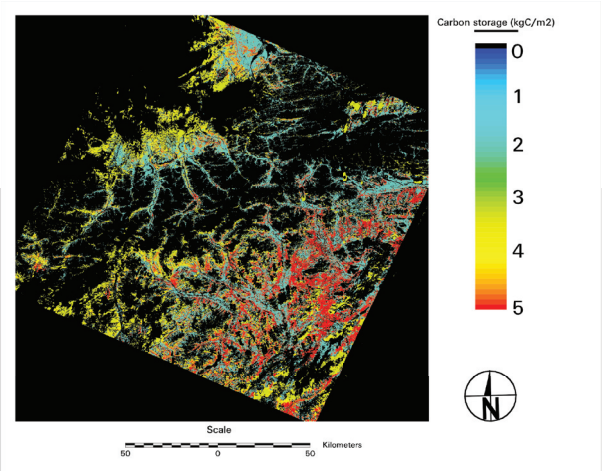

Figure 2. Soil carbon content in subalpine tundra.

and C/N ratio in the upper A0 layer of arctic tundra was 0.13±0.07 kg/m^2, 0.06±0.04 kgC/m^2, 0.001±0.001 kgN/m^2, and 60±18 (n=30), and was 4.31±1.07 kg/m^2, 1.33±1.12 kgC/m^2, 0.053±0.025 kgN/m^2, and 25±3 (*n*=32) in the A0 layer, respectively. The upper A0 layer denotes the layers of shrubs, herbaceous plants, lichen, and moss in surface soils of tundra and boreal forests. Figure 2 shows the soil carbon content in the tundra of Alaska's North Slope during the growing season of 2000/2001.

Turnover time of soil organic carbon

By using soil carbon content and soil respiration from the ground truth data, the turnover time of soil organic carbon on the permafrost regime of Alaska's North Slope varied from 240 years in upland tundra to 570 years in coastal tundra during the growing season of 2000/2001. The coastal tundra is located 32 km south of Deadhorse, which is always saturated by thawed uppermost permafrost water and near-to-peat soil. Thus, it is difficult to decompose the soil organic carbon. Raich & Schlesinger (1992) reported the turnover time was 490 years in the overall tundra of the Arctic. This suggests that the soil organic carbon in tundra is highly vulnerable to intra-tundra regime Arctic warming.

Implication for regional carbon budget

The regional carbon budget in the permafrost regime of Alaska tundra was 0.034±0.025 GtC/season for the light chamber, and 0.074±0.050 GtC/season for the dark chamber during the growing season, respectively, based on 207,000 km^2 of the Alaska tundra area including 73,600 km^2 in subalpine, 62,400 km^2 in the Arctic Foothills, and 71,000 km^2 in the Arctic Coastal Plain. Those are comparable with 0.004 GtC/season in wet sedge and 0.040 GtC/season in the tussock of Alaska's tundra (Oechel et al. 1997).

Acknowledgments

This work was funded by the INIS (IARC-NASDA Information System) and IJIS (IARC-JAXA Information System) projects and in part by the JAMSTEC (Japan Marine Science Technology). We thank Noriyuki Tanaka, Masami Fukuda, Hitoshi Kojima, and Satoshi Tsuda for assisting with the data compilation.

References

ACIA (Arctic Climate Impact Assessment). 2004. *Impacts of a Warming Arctic*. Cambridge: Cambridge University Press, 139 pp.

Gilblin, A.E., Nadelhoffer, K.J. Shaver, G.R. Laundre, J.A. & MaKerrow, A.J. 1991. Biogeochemical diversity along a riverside toposequence in arctic Alaska. *Ecological Monographs* 61: 415-435.

Kasishcke, E.S. 2000. Boreal Ecosystems in the global carbon cycle. In: E.S. Kasishcke & B.J. Stocks (eds.), *Fire, Climate Change, and Carbon Cycling in the Boreal Forest.* New York, NY: Springer, 19-30.

Kim, Y.W. & Tanaka, N. 2001. Temporal and spatial variation of carbon dioxide flux along a latitudinal Alaskan transect. In: T. Nakazawa (ed.), *Proceedings of the 6th International Carbon Dioxide Conference Sendai, Japan:* 465-468.

Oechel, W.C., Vourlitis, G.L. & Hastings, S.J. 1997. Cold season CO_2 emission from arctic soils. *Global Biogeochemical Cycles* 11: 163-172.

Post, W.M., Emanuel, W.R. Zinke, P.J. & Stangenberger, A.G. 1982. Soil carbon pools and world life zone. *Nature* 298: 156-159.

Raich, J.W. & Schlesinger, W.H. 1992. The global carbon dioxide flux in soil respiration and its relationship to vegetation and climate. *Tellus* 44: 81-99.

Zimov, S.A., Schuur, E.A.G. & Chapin, F.S III. 2006. Permafrost and the global carbon budget. *Science* 312: 1612-1613.

Impacts of Climate Warming and Facilities on Rock Temperatures at a Tunnel in High Alpine Continuous Permafrost: Results of Long-Term Monitoring at Kleinmatterhorn, Swiss Alps

Lorenz King
Justus-Liebig-University Giessen, Germany
Clemens Constantin Maag
Justus-Liebig-University Giessen, Germany
Christen Baumann
CEO Zermatt Bergbahnen AG, Switzerland

Introduction

Zermatt is a most popular tourist center in the Swiss Alps, located at approximately 1620 m a.s.l. As the surrounding high mountain ranges often reach above 4000 m a.s.l., the dry and sunny climate generates a high glacier equilibrium line and thus vast unglaciated permafrost areas. Occurrences of sporadic permafrost appear above 2600 m; continuous permafrost exists above 3400 m.

The facilities built on permafrost include hotels, restaurants, mountain huts, railways, funiculars, elevators, or culverts for artificial snow production. In view of climate warming, the subsurface thermal regime requires particular observations, as degradation of permafrost may endanger the proper functioning of these constructions. An appropriate design is crucial and depends on the characteristics of the permafrost occurrences. At present, new constructions and recordings in the continuous permafrost region at Kleinmatterhorn (3820 m) and the previous long-term monitoring at this location enable the study of human influence on this permafrost environment.

Kleinmatterhorn

The mountain peak of Kleinmatterhorn with an altitude of 3883 m a.s.l. is the highest place in the Alps that can conveniently be reached by a cable car and an elevator. The mountain top is located within the continuous permafrost zone. A 176 m long tunnel through the mountain at an altitude of 3820 m and an elevator shaft leading to 3860 m a.s.l. (Fig. 1) present an exceptionally interesting object for permafrost research. Long-term temperature monitoring started in 1998 due to problems caused by refreezing of meltwater in the elevator shaft during a very warm summer. In order to record the bedrock temperatures of the mountain top and the effects of tourist installations, temperature loggers were installed at selected sites of the tunnel.

The permafrost distribution in the Zermatt Valley is quite well known through several studies (cf. references in Philippi et al. 2003). Numerous rock glaciers were the focus of other research projects (Hof et al. 2003, King & Kalisch 1998). Drilling 100 m in depth was carried out on nearby Stockhorn during the EU-project PACE (Harris et al. 2003), indicating a permafrost thickness of 170 m.

At the research site Kleinmatterhorn, air and rock temperatures are monitored at 10 different sites, the

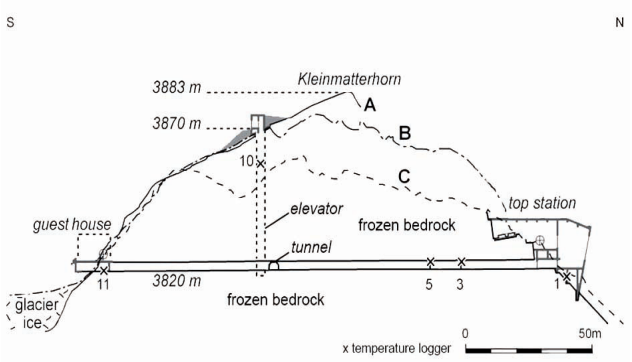

Figure 1. Location of UTL-Loggers (1, 3, 5, 10) at the tunnel system of Kleinmatterhorn mountain peak.

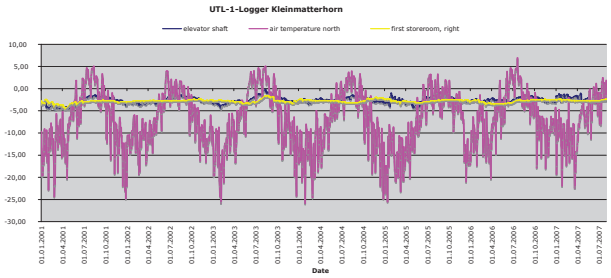

Figure 2. Air, bedrock, and elevator shaft temperatures at Kleinmatterhorn (3820 m) from Jan. 2001 to Aug. 2007.

location of significant loggers are shown in Figure 1. The air temperature (#1) is taken at an undisturbed site near the cable car entrance. Mean annual air temperatures (MAAT) were -8.0°C in 1998 and 1999, attaining -5.7°C in 2006. The mean air temperature in the summer months of July and August 2002 was -0.58°C; it reached +1.98°C in 2003. However, the mean winter temperatures (Dec., Jan., Feb.) also vary considerably with -12.6°C in 2001/02 compared to -15.2°C in 2004/05 and -10.3°C in 2006/07.

Loggers #3 and #5 (located in storerooms that are separated from the passenger tunnel) show small seasonal differences of -2°C and -3°C, with a slightly increasing temperature trend. The elevator shaft temperatures (#10) vary seasonally between -4° and -2°C, however, reaching near zero temperatures in the extremely warm summer of 2003, where also the accumulated positive degree-days are considerably higher than in any other year. Natural ventilation with cold air is a necessary countermeasure to prevent negative effects of heat created by the installations.

Bedrock temperatures around -12°C were reported by Keusen & Haeberli (1983) during the construction phase. The results of the monitoring with 10 loggers since 1998 have proven to be an essential aid for supervising sensitive permafrost areas, thus allowing for preventive measures against the consequences of climate warming and the effects of human activities (heating, inhibited ventilation of cold air etc.) at an early stage.

Actual Construction Activities

One consequence of climate warming in the Alps is that skiing activities tend to concentrate and increase in higher and safer regions. In addition, exceptional attractions help guarantee the success of a tourist resort. The Kleinmatterhorn cable car, constructed from 1976 to 1979, reaches up to 3820 m a.s.l. and arrives at a tunnel cut in the northern wall of the mountain peak. At its southern exit, the ski run starts down to Zermatt.

Currently, three major infrastructure projects are being carried out at the mountain top in order to increase its attractiveness. A new guest house with a larger restaurant will be built at the southern exit of the existing tunnel. The supporting structure will be anchored in the frozen bedrock. From there, two elevators and an ice gallery (cf. Fig. 3) will form a subsurface access to a new "glacier palace" about 15 m below the glacier surface.

The current constructions visualize many engineering and environmental aspects in a sensitive permafrost setting. Future research projects will study the effects on such an intense use of construction and installation for tourism on frozen bedrock and glacier ice, respectively. The mountain guest house accommodating 60 beds will open in late summer of 2008.

At the northern entrance of the tunnel, the construction of a spectacular tower reaching 117 m above the natural mountain top and a viewing platform at an altitude of 4000 m a.s.l. is planned, but has to be approved, consequently providing to the Zermatt resort a sovereign viewpoint.

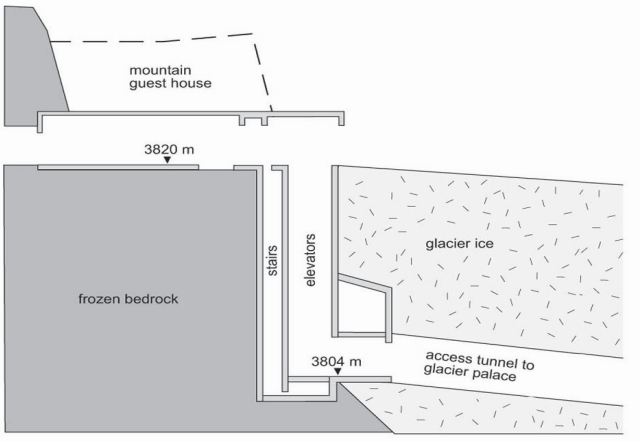

Figure 3. Cross section through guest house, old tunnel (3820 m) and elevator shafts with access to the glacier palace.

Current Research and Future Projects

In February 2008, additional scientific drilling will be carried out in the glacier ice close to the new constructions and at the glacier palace. The mean annual ice temperature will be measured at about 15 m depth. Undisturbed bedrock temperatures near the new construction sites will enable us to establish a good scientific base for new long-term temperature monitoring and 3D modeling of this exceptional mountain peak.

Degradation of permafrost due to both climatic change and an increase in human activity creates a serious challenge for tourist installations, as safety has to be prioritized and ensured in the concerned area. Continuous monitoring will guarantee the required safety.

Acknowledgments

We would like to express our gratitude to Stephan Gruber and Thomas Herz who gave valuable suggestions for fieldwork. The studies were financially supported by the project KI 261/14-1 of the Deutsche Forschungsgemeinschaft.

References

Harris, C., Vonder Mühll, D., Isaksen, K., Haeberli, W., Sollid, J.-L., King, L., Holmlund, P., Dramis, F., Guglielmin, M. & Palacios, D. 2003. Warming permafrost in European mountains. *Global and Planetary Change* 39: 215-225.

Hof, R., King, L. & Gruber, S. 2003. Influence of human activities and climatic change on permafrost at construction sites in Zermatt, Swiss Alps. *Proceeding of the Eighth International Conference on Permafrost, Zurich, Switzerland, July 20–25, 2003*: 65-66.

Keusen, H.R. & Haeberli, W. 1983. Site investigation and foundation design aspects of cable car construction in alpine permafrost at the 'Chli Matterhorn', Wallis, Swiss Alps. *Proceedings of the Fourth International Conference on Permafrost, Fairbanks, Alaska, July 17–22, 1983*: 601-605.

King, L. & Kalisch, A. 1998. Permafrost distribution and implications for construction in the Zermatt area, Swiss Alps. *Proceedings of the Seventh International Conference on Permafrost, Yellowknife, Canada, June 23–27, 1998*: 569-574.

King, L. 1996. Dauerfrostboden im Gebiet Zermatt-Gornergrat-Stockhorn Verbreitung und permafrostbezogene Erschließungsarbeiten. *Zeitschrift für Geomorphologie N.F., Suppl.-Band* 104: 73-93.

Philippi, S., Herz. T. & King, L. 2003. Near-surface ground temperature measurements and permafrost distribution at Gornergrat, Matter valley, Swiss Alps. *Proceedings of the Eighth International Conference on Permafrost, Zürich, Switzerland, July 19–25, 2003*: 129-130.

Differential Estimates of Organic Carbon Pools in Permafrost-Affected Soils of Russia

D.E. Konyushkov, D.I. Rukhovich, N.V. Kalinina, E.A. Dolinina
V.V. Dokuchaev Soil Science Institute, Russian Academy of Agricultural Sciences, Moscow, Russia

At present, a challenge for Russian cryopedologists is to perform differential estimates of organic carbon pools in permafrost-affected soils of Russia on the basis of digitized versions of the 1:2.5 M and 1:1 M scale soil maps. This work is hampered by the absence of adequate databases. For permafrost regions, along with data on the thickness and bulk density of soil horizons and the organic carbon content in them, the databases should include information on the real soil cover complexity, differentiation of thawing depths, the ice content in the soil and the presence of massive ice bodies; the content of gravel and coarser fragments (particularly, for Central and East Siberia); and the depth to the lithic contact. It is important to distinguish between the organic carbon in mineral horizons, the organic carbon in peat layers, and the organic carbon in litter horizons. The organic carbon pool in the transient permafrost layer is a separate problem, as there are little data on the carbon content in it.

Permafrost regions occupy nearly two-thirds of Russia and encompass a wide range of ecosystems with different types of carbon turnover and soil organic carbon (C_{org}) pools: (a) surface accumulation of organic matter in litter, peat, and raw-humus horizons; (b) soil humus accumulation in situ due to the decomposition of root residues; and (c) illuviation of mobile humic substances into humus-illuvial horizons.

The real distribution of C_{org} is a result of various combinations of these processes. A specific feature of permafrost-affected soils is the *cryosequestration of* C_{org} due to (a) cryoturbation and (b) the rise of permafrost table upon the surface accumulation of organic matter, so that the lower part of organic horizons becomes frozen. Another specific feature is the high spatial variability of soil horizons and their intermittent character. In Siberia, these soils are often developed from the residuum of hard bedrock and have high pebble content. The high ice content and the presence of ice wedges are typical of heavy-textured and peat soils. These features should be taken into account in calculations of C_{org} reserves in permafrost regions.

Three major works on carbon reserves in Russian soils are based on different cartographic sources. Orlov et al. (1996) used the *Soil Map of the USSR* (1984, 1:16 M); only major zonal soils were considered. Rozhkov et al. (1996) used a more detailed *Soil Map of Russia and Contiguous Countries* (Gerasimova et al. 1995; 1:4 M); the carbon stored in surface organic horizons and the carbon of soil carbonates were separately calculated. Nilsson et al. (2000) and Stolbovoi (2002) used a generalized version of the *Soil Map of the Russian Federation* (Fridland et al. 1989; 1:2.5 M). The generalized version (1:5 M) contains 168 mapping units and 1300 soil polygons.

In fact, the original map contains 35,000 soil polygons; its legend includes 205 names of individual soils and nearly 100 names of unique soil combinations (soil complexes). The latter are especially typical of the permafrost regions of Russia. The soil cover complexity in the permafrost zone is considerable. Thus, within the permafrost zone of European Russia, 1055 soil polygons encompassing 55 different soils can be found on the 1:2.5 M scale map (Fig. 1). To calculate the reserves of C_{org} on the basis of this map, the attribute database to the digitized version of the map has to be developed.

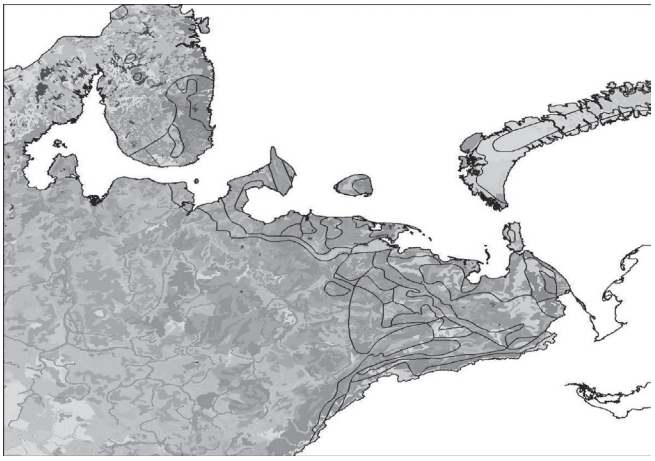

Figure 1. Soil polygons on the 1:2.5 M scale map over the *Circum-Arctic Map of Permafrost and Ground-Ice Conditions* (fragment).

At present, such a database exists for the upper (20 cm thick) soil horizons and, separately, for litters. On this basis, the organic carbon density values used for modeling purposes have been calculated for the European part of Russia (Rukhovich et al. 2007). Figures 2 and 3 illustrate the distribution of C_{org} reserves in the 20 cm thick soil horizons (both mineral and peat soils have been taken into account) and in mineral horizons + litters, respectively. It is seen that the reserves of C_{org} stored in litter horizons play a significant role in the total organic carbon pool within the permafrost zone of European Russia.

However, the database is still incomplete; information on the organic carbon contents and bulk density of the deeper soil horizons is insufficient for final calculations. Information on the content of gravel and coarser fragments is also to be completed for the particular polygons. Finally, in order to calculate C_{org} reserves in the active layer, information on thawing depths is essential.

These problems become more complicated in the case of calculations for the entire permafrost zone of Russia. The database for the map is being developed. The great variability in the soil properties within this vast territory has to be taken into account. A given genetic soil unit may be developed

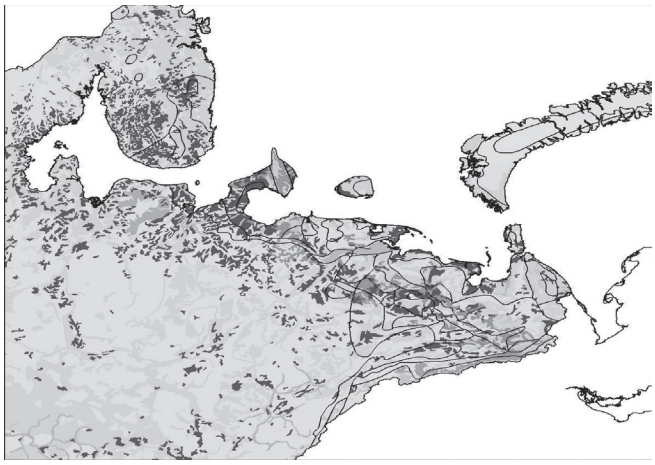

Figure 2. Organic carbon densities in the upper 20 cm thick mineral soil horizons.

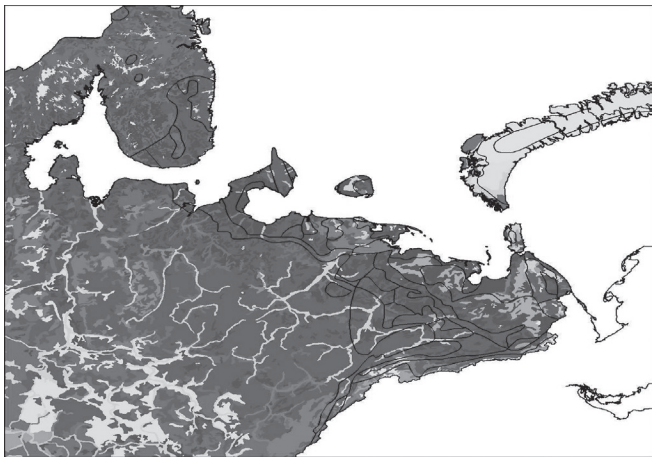

Figure 3. Organic carbon densities in the litters and upper 20 cm thick mineral horizons.

from different parent materials and under somewhat different bioclimatic conditions. As a first approximation, the database is developed for combinations "genetic soil unit + parent material + bioclimatic conditions." In some cases, this information is insufficient. In particular, for mountainous territories and vast plateaus of Siberia, information on the contents of gravel and coarser rock fragments is essential. In calculations of carbon pools for standard depths (50 cm, 1 m), it is also important to take into account the ice content in the soils with a relatively shallow thawing depth and the presence of massive ice bodies and ice wedges in some areas.

Another solid cartographic base for the estimates of organic carbon pools in permafrost-affected soils of Russia is the digitized version of the *State Soil Map* on the 1:1 M scale. This is a much more detailed map. For example, within the European part of the permafrost zone of Russia, 3,427 soil polygons encompassing 155 different soils are shown on this map. In other words, the degree of detail of the 1:1 M soil map is approximately three times higher than that of the 1:2.5 M soil map. It is important that soil polygons distinguished on the 1:1 M soil map display a better correlation with the

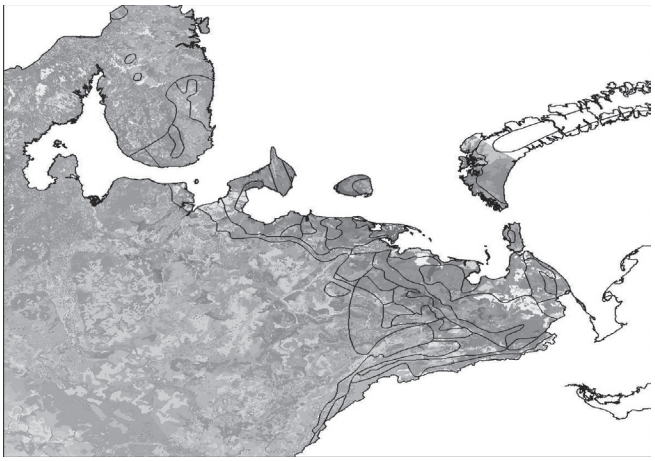

Figure 4. Soil polygons on the 1:1 M map over the *Circum-Arctic Map of Permafrost*.

Circum-Arctic Map of Permafrost, so the use of this map seems to be more promising in the future (Fig. 4).

It is expected that the first results of differential organic carbon estimates for the permafrost zone of Russia on the basis of the digitized version of the 1:2.5 M soil map will be obtained by the end of 2008.

References

Brown, J., Ferrians, O.J. Jr., Heginbottom, J.A. & Melnikov, E.S. 1997. *Circum-Arctic Map of Permafrost and Ground-Ice Conditions.* U.S. Geol. Survey, CP-45. Reston, VA, USA.

Fridland, V.M. (ed.). 1988. *Soil Map of the Russian Soviet Federative Socialistic Republic.* 1:2.5 M scale. Central Administration for Geodesy and Cartography (GUGK), Moscow, Russia, 16 sheets. [In Russian].

Gerasimova, M.I., Gavrilova, I.P., Bogdanova, M.P. et al. 1995. *Soil Map of Newly Independent States.* 1:4 M scale. Central Administration for Geodesy and Cartography (GUGK), Moscow, Russia (in Russian).

Nilsson, S., Shvidenko, A., Stolbovoi, V. et.al. 2000. *Full Carbon Account for Russia.* Interim Report IR-00-021, International Institute for Applied Systems Analysis, Laxenburg, Austria, 180 pp.

Orlov, D.S., Biryukova, O.S. & Sukhanova N.I. 1996. *Organic Matter in Soils of the Russian Federation*. Moscow: Nauka. 256 pp. [in Russian].

Rozhkov, V.A., Wagner, V.B., Kogut, B.M. et al. 1996. *Soil Carbon Estimates and Soil Carbon Map for Russia*. IIASA WP-96-60. Laxenburg, Austria, 44 pp.

Rukhovich, D.I. et al. 2007. Constructing a spatially-resolved database for modelling soil organic carbon stocks of croplands in European Russia. *Regional Environmental Change* 7(2): 51-61.

Stolbovoi, V. 2002. Carbon in Russian soils. *Climatic Change* 55(1-2). The Netherlands: Kluver Academic Publishers, 131-156.

Satellite Observations of Frozen Ground, Snowmelt (1989–2007), and Hydrological Responses at a Discontinuous Permafrost Aquifer (Fort Wainwright, Alaska)

Sarah E. Kopczynski
Cold Regions Research and Engineering Laboratory, Hanover, NH 03755
Joan M. Ramage
Lehigh University, Earth and Environmental Sciences, Bethlehem, PA 18015

Introduction

Snow cover influences permafrost thermal regimes and seasonally frozen ground, and thus impacts groundwater flow, surface runoff, and soil moisture (Ling & Zhang 2003). Within permafrost aquifers, climatic warming will likely increase active layer depth, warm the soil profile, increase soil moisture storage, increase evaporation, cause variable runoff responses, and increase groundwater flux to streamflow (Hinzman & Kane 1992). The aim of this research is to report climate warming impacts at Fort Wainwright and resulting groundwater response over 19 years. Specifically, we investigate timing of spring snowmelt, drawing attention to impacts on permafrost groundwater hydrologic patterns.

Fort Wainwright is located in Interior Alaska east of Fairbanks within the Chena watershed (Fig. 1). Discontinuous permafrost is distributed throughout unconsolidated alluvial sediments and fractured schist bedrock. Groundwater is influenced by the local Chena and regional Tanana Rivers.

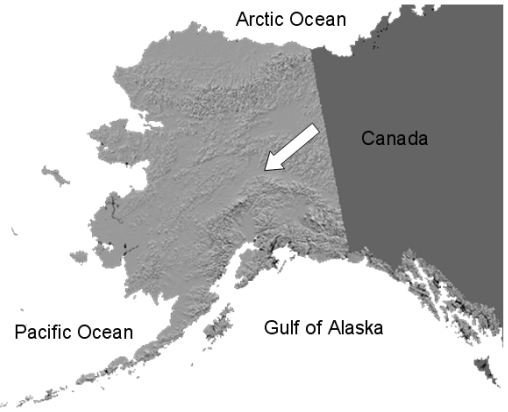

Figure 1. Location of Fort Wainwright, Alaska.

Methodology

Passive microwave remote sensing

This research applies 19 years of multiple daily satellite brightness temperature (Tb) observations of the polar orbiting Special Sensor Microwave Imager (SSM/I) downloaded by online archive. Microwave data measure through darkness, clouds, and precipitation. SSM/I data are used to monitor snowmelt onset and duration (Ramage & Isacks 2002). Snow melts and refreezes when Tb(37V)≥246K and abs(DAV)≥10K. The DAV is the daily amplitude variation of ascending and descending Tb overpasses. Large DAV (>10) indicates melt-refreeze cycles, followed by ripe snow conditions when DAV transitions from abs(DAV)≥10K to abs(DAV)<10.

SSM/I data are used to detect near-surface soil freeze-thaw conditions (Zhang & Armstrong 2001) during 1999. Vertically polarized Tb discriminate frozen from unfrozen ground using a negative spectral gradient (Tb(37V)-Tb(19V))/18<0 together with a cutoff threshold of Tb(37V)<258.2K. Penetration depth is limited to a few centimeters of soil, and observations are only valid when snow cover is absent. Satellite data results are consistent with local thermistor data demarking onset of frozen ground.

Permafrost hydrological responses

Groundwater flow velocities are monitored in situ using high-resolution heat pulse flow sensors throughout the aquifer, which work well in low flow rate higher permeability conditions. Chena and Tanana streamflow are monitored at USGS gauging stations. Soil moisture sensors maintained by UAF provide continuous soil condition records (Hinzman & Lilly 1999).

Results

Between 1989 and 2007, snowmelt onset has occurred 0.86 d/yr earlier (Fig. 2b) with spring snowmelt persisting about 0.7 d/yr longer (Fig. 2c). An example of hydraulic responses to snowmelt (Fig. 3a) in a permafrost-free area and a through-talik in the Fort Wainwright aquifer is shown for 1999–2000. At both sites, rapid snowmelt infiltration causes a soil moisture spike ~8 d before snow is ripe, followed ~10 d later by the local freshet. Soil moisture spikes again during the larger regional freshet. Snowmelt at the permafrost-free site increases flow rates from 2 to 4 ft/d and shifts flow direction 40°. Subpermafrost flow rates respond only to larger basin-wide freshet (1.5 to 4 ft/d), while flow rates at a through-talik respond to both local and regional freshets with peak rates of 1 ft/d and 1.5 ft/d, respectively. Flow directions in the through-talik shift 80° and 100° with each respective freshet. Closed taliks show no statistically significant responses.

Conclusion

This research reports on climate warming impacts at the Fort Wainwright, Alaska, discontinuous permafrost aquifer since 1989. Satellite observations over 19 years show earlier snowmelt (0.86 d/yr) with increasing spring-melt duration (0.7 d/yr). Soil moisture spikes ~8 d before snow is ripe and ~10–20 d before the fluvial freshet. Groundwater velocity increases due to snowmelt infiltration with peak rates of 4 ft/d (permafrost-free site), 4 ft/d (subpermafrost), and ~2 ft/d

in a through-talik. Groundwater velocities in the permafrost aquifer increase during annual active layer freezing when local water levels drop each fall, while there are no comparable responses in permafrost-free areas.

Groundwater velocity measurements are strongly influenced by the timing, magnitude, and duration of snowmelt and ground freezing. These groundwater responses will continue to change as permafrost continues to degrade.

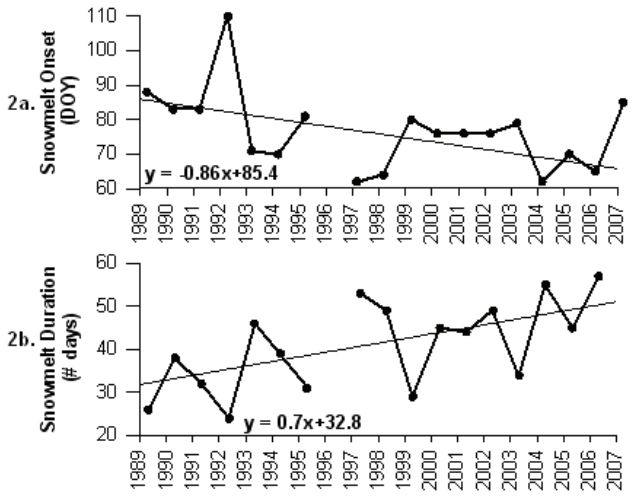

Figure 2. Historical trends in snowmelt onset (a) and duration (b) determined using satellite passive microwave algorithms.

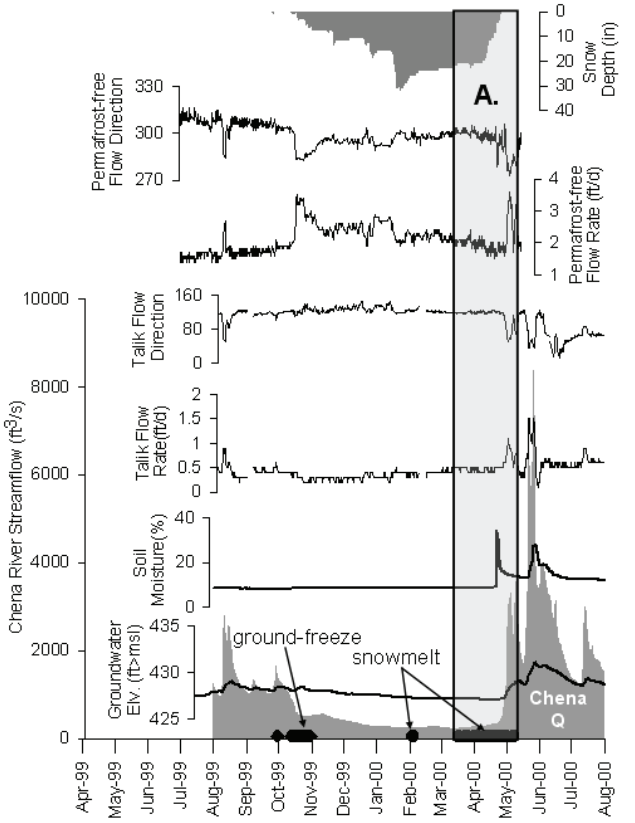

Figure 3. Permafrost-free and through-talik hydrologic responses to ground-freeze and snow melt-refreeze (a) at Fort Wainwright (1999–2000). Snow is ripe after the melt-refreeze interval.

This research establishes long-term baseline observations to underpin investigations of climate warming impacts on permafrost hydrology, and sets the stage for future work to quantitatively model these interactions.

Acknowledgments

This research was funded by NASA Graduate Fellowship NNX06AG08H, U.S. Army Fellowship, NASA Terrestrial Hydrology Grant NNG04GR31G, Lehigh University, U.S. Army Alaska. SSM/I data was provided by the National Snow and Ice Data Center

References

Hinzman, L.D. & Kane, D.L. 1992. Potential response of an arctic watershed during a period of global warming. *Journal of Geoph. Res.–Atmospheres* 97(D3): 2811-2820

Hinzman, L.D. & Lilly, M.R. 1999–2000. Climate data from the Fort Wainwright Hydrology Research. UAF WERC: www.uaf.edu/water/projects/ftww/ftww.html Fairbanks, Alaska. (Ap6009; May99–May00).

Ling, F. & Zhang, T. 2003. Impact of the timing and duration of seasonal snow cover on the active layer and permafrost in the Alaskan Arctic. *Permafrost and Periglacial Processes* 14: 141-150

Ramage, J.M. & Isacks, B.L. 2002. Determination of melt onset and refreeze timing on southeast Alaskan icefields using SSM/I diurnal amplitude variations. *Annals of Glaciology* 34: 391-398.

Zhang, T. & Armstrong, R.L. 2001. Soil freeze/thaw cycles over snow-free land detected by passive microwave remote sensing. *Geoph. Res. Letters* 28(5): 763-766

Low-Frequency Sounding During the Gas Line Engineering Investigations in the Area of the Transition Through Baidaratskaya Bay

A.V. Koshurnikov
MSU-Geophysics, Ltd.
Yu.D. Zykov
The Moscow State University
Yu.V. Kulehsov
Peter Gaz, Ltd.

The main task of this geophysical research was the lateral exploration of frozen and thawed soils in the pipe-laying zone. In that regard, special attention was given to intrasoil ice, thawed soils, and cryopeg detection. Vertical electric explorations were used in the chosen gas pipeline. Vertical electric sounding by a direct current (VES) (Fig. 1), frequency electromagnetic sounding (FS) (Fig. 2), and time domain sounding (TEM) (Fig. 3) were carried out.

To perform the FS, a recently-made hardware system, namely HF-EM, was used. The system includes the generation of square signals with a combination of a discreet set of frequencies from 4 up to 512 kHz. The measuring device and the multiloop frame antenna work simultaneously with the generator. While sounding with VES, a bilateral three-electrode system was used.

Figure.1. VES. Ural, 2006.

Figure 2. FS. Jamal, 2007.

The maximum open pit was 100 m, while the FS sounding distance between the generator and measuring device was 40 m. It takes about 1 minute to measure the signature with the help of FS sounding. Each of these signatures, as *E*

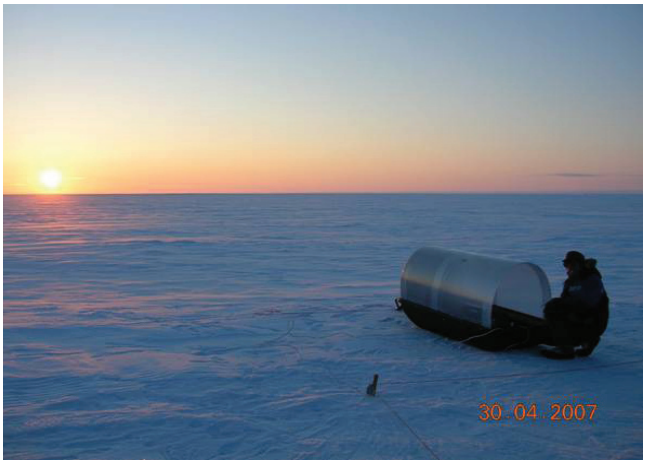

Figure 3. TEM. Jamal, 2007.

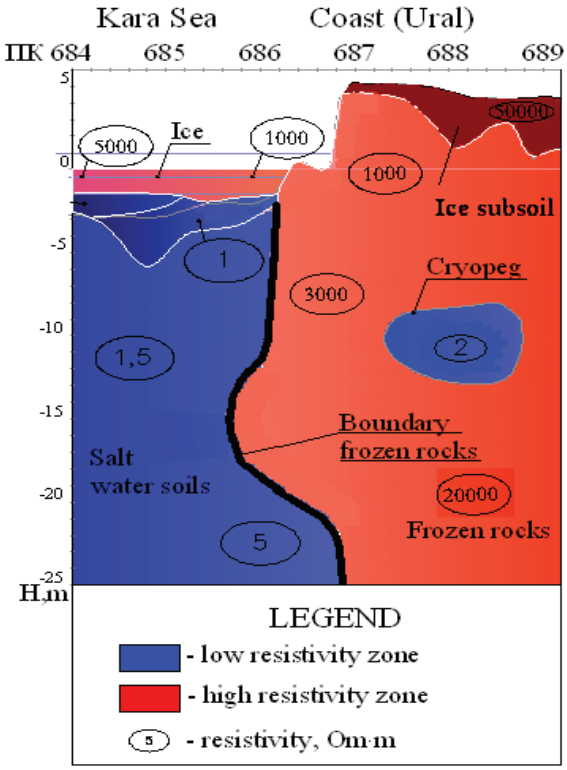

Figure 4. Geoelectric cross section (Ural).

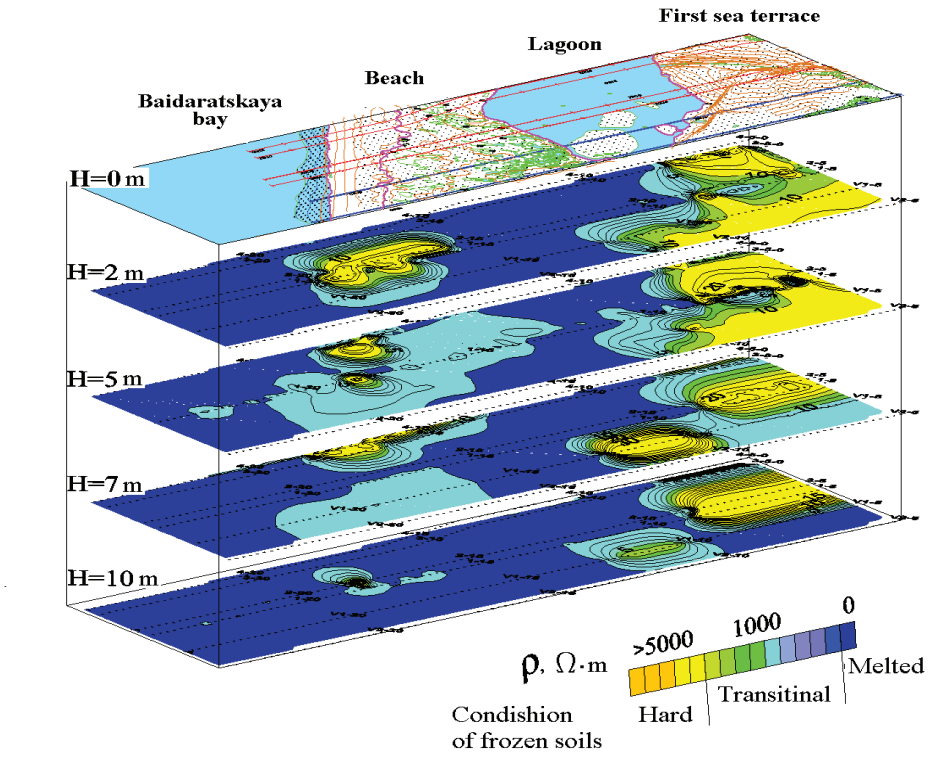

Figure 5. Model of frozen soils condition (Yamal).

against ω, or ρ_ω against ω, can be displayed at the receiver tool screen. For an interpretive translation of the FS data, the EM – 1D programme carrying out 1D inverting ρ_k against ω into simulated resistivity (developed by P. Pushkaryov) was used. The TEM sounding the combine device with square loops sized 20 x 20 (a generator antenna) and 10 x 10 (a receiving antenna) was applied. As a result, it was possible to explore the cut in details to the bottom of 30 m and to solve set tasks.

According to VES data about lithology structure, the maintenance of ice, temperature, and salinity have been obtained (Fig. 4).

According to FS data about position, frozen soil under a beach, a lagoon, and the first sea terrace have been obtained (Fig. 5).

According to TEM, data about deeper borders of thawed and frozen rocks have been obtained (Fig. 4).

The main features of the described methods are as follows:

VES – ability to split the upper part of the cut upon its resistance. But some difficulties are caused due to the presence of a high-resistivity screen (icy subsoil).

FS – ability to map conducting zones (cryopegs); demonstrates the high production, but it is insensitive to the high meanings of resistance.

TEM – ability of depth research.

References

Zykov, Ju.–M. 2007. *Geophysical Methods of Permafrost Studies*. Moscow: Publishing house of the Moscow State University, 272 pp. (in Russian).

Zykov, Ju.D., Buldovich, S., Koshurnikov, A.V. et al. 2007. Opportunity of electromagnetic sounding at geocryology mapping. In: Materials of the international conference "*Cryogenic Resources of Polar Regions" II, Salekhard, 2007*: 149 pp.

Thixotropic Wedges or Frost Cracks: A Review from the Pannonian Basin (Hungary, Europe)

János Kovács
Department of Geology, University of Pécs, Pécs, Hungary
Szabolcs Ákos Fábián
Department of Physical Geography, University of Pécs, Pécs, Hungary
Gábor Varga
Department of Physical Geography, University of Pécs, Pécs, Hungary
István Péter Kovács
Doctoral School of Earth Sciences, University of Pécs, Pécs, Hungary
György Varga
Doctoral School of Earth Sciences, University of Pécs, Pécs, Hungary

Introduction

There is a general consensus about the study and interpretation of soft-sediment deformation structures being helpful in paleoenvironmental reconstructions. During the glacial periods of the Pleistocene, Hungary was subject to a cryogenic environment that produced various relict periglacial features (Dylik 1963, Pécsi 1964, Tarnocai & Schweitzer 1998, Fábián et al. 2000, Kovács et al. 2007). The reason for the cold climate during these glacial periods is Hungary's unique geomorphological setting in the Pannonian Basin. The Carpathians, which surround this large basin, create an almost closed climatic situation, producing climatic conditions not found elsewhere in Europe. In effect, Dylik seems to imply that the climate in Hungary during the glacial periods of the Pleistocene was somewhat similar to the recent climate of the dry tundra regions of North Siberia. According to Maarleveld (1976) and Van Vliet-Lanoë et al. (2004), however, the Pannonian Basin was mostly devoid of continuous permafrost during the Quaternary.

General Setting

In the Pannonian Basin (Fig. 1), the continental crust is thinner and the stress field more complex, owing to a lateral shift to the east of the basin, which is squeezed between the rigid northeast European basement and the Alpine orogene, with transpressional and transtensional phases alternating from the upper Cenozoic to today (Csontos et al. 2002). The present-day seismicity is higher than in northwest Europe, but is still of low magnitude.

As a result of the cold climatic conditions (mentioned above) in the Pleistocene epoch, various types of periglacial features developed and are found in well-preserved relict forms in various deposits. Dylik (1963) summarizes the relict periglacial features of Hungary and discusses their original development, while Pécsi (1964) provides detailed descriptions, including diagrams and photographs, of these features with the locations in which they occur. In the last decade, researchers investigated these cryogenic features for their implication for past climate (Tarnocai & Schweitzer 1998, Fábián et al. 2000, Kovács et al. 2007) and for their distinction between tectonic and periglacial deformation (Van Vliet-Lanoë et al. 2004, Horváth et al. 2005, Magyari et al. 2005).

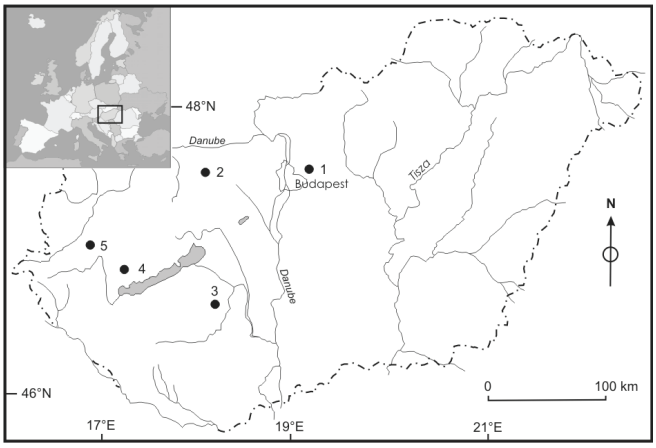

Figure 1. Location of the study sites in Hungary.

Methods

Our interpretation of the periglacial deformations investigated is based on (a) detailed field observations and (b) a synthesis of published data. Polygenetic forms were analysed using criteria defined for the periglacial and seismogenic structures. Sections were cleaned and described using sedimentological and pedological criteria, with respect to the topographical location and available moisture. Samples for grain size analyses and OSL dating were collected from individual fill units, and additional samples were collected for moisture content and background radiation measurement. The samples were dated at the Geological Institute of Hungary.

Results

Thixotropic wedges

Thixotropic wedges, developed in fine sandy-to-pebbly deposits, are formed within the sediment but relatively close to the surface (Montenat et al. 2007). The wedges may be

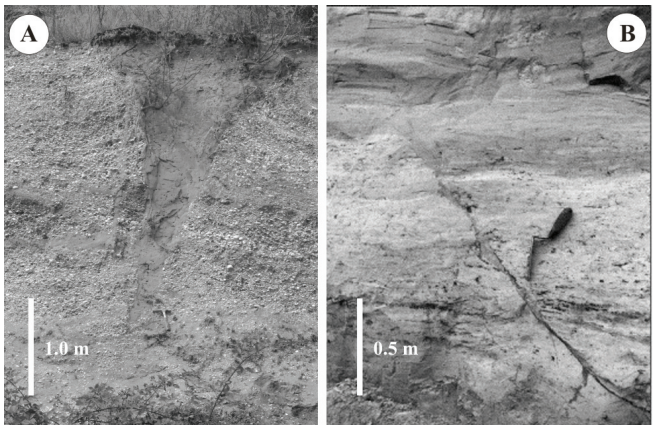

Figure 2. (A) periglacial frost wedge (sand wedge); (B) nonperiglacial synsedimentary transtensive fault (thixotropic wedge).

very narrow and are recurrent (dm to several dm depth); the wedge pattern may be vertically arranged (Montenat et al. 2007). Tension faults (Fig. 2B) are often mistaken for frost (cryodesiccation) fissures, evidence of former ice veins, or even ice-wedge casts, but occur rarely in polygonal networks and extend deeper in depth (Van Vliet-Lanoë et al. 2004). These forms are much narrower than those developed by periglacial thermokarst. Their orientation is parallel or conjugate with tectonic direction (Van Vliet-Lanoë et al. 2004).

Frost wedges

The sand wedges found in the Quaternary sediments have a polygonal system; consequently they are considered sand-wedge polygons. The wedges have an average vertical dimension of 1.5–2.0 m, but some are as much as 3 m (Fig. 2A). The wedge width was measured at right angle of the axial plane of the wedge. Additionally these wedges are 25–30 cm and 50–60 cm or slightly more in width. The sand-filled wedge structures have simple V-shapes with rectilinear or slightly curved sides (convex outward) and pointed toes. The fill of the wedges is subvertically laminated, the sand itself is fine- to medium-grained (1–3 φ) and moderately well sorted. Some wedges near or at the top contain pebbles. The host strata adjacent to a sand wedge is upturned. In plan view, it forms a polygonal network with cracks spaced 2–5 m apart. The cracks are irregular and several meters long.

Conclusions

Several hypotheses for the formation and infill of the wedges were evaluated using detailed physical, stratigraphic, and sedimentological information. The most likely explanation for most of the features is that they are relict cryogenic structures formed by thermal-contraction cracking in permafrost, and filled with wind-blown sediments. The wedges are believed to have formed in the tundra environment that existed in the Pannonian Basin during the coldest parts of the Würm glaciation. Our observations of relict sand wedges support previous inferences for the occurrence of continuous permafrost (which were based on the occurrence of ice-wedge casts and cryoturbations) in Hungary during the Pleistocene. Based on previously reported periglacial features, the local glacial history and OSL dates, these features suggest that the Pannonian Basin was underlain by permafrost during the Late Pleniglacial (22,000–18,000 years ago). We accept that some of the wedge-shaped sedimentary structures may be causally related to paleoearthquakes, but the obvious complexity of the phenomenon requires caution.

Acknowledgments

The authors are grateful to C. Tarnocai and F. Schweitzer for field assistance and useful communications, and to E. Thamó-Bozsó for supervising the OSL measurements.

References

Csontos, L., Benkovics, L., Bergerat, F., Mansy, J.L. & Wórum, G. 2002. Tertiary deformation history from seismic section study and fault analysis in a former European Tethyan margin (the Mecsek-Villány area SW Hungary). *Tectonophysics* 357: 81-102.

Dylik, J. 1963. Magyarország periglaciális problémái. *Földrajzi Értesítő* 12: 453-464.

Fábián, S.Á., Kovács, J. & Varga, G. 2000. Újabb szempontok hazánk periglaciális klímájához. *Földrajzi Értesítő* 49: 189-204.

Horváth, Z., Michéli, E., Mindszenty, A. & Berényi-Üveges, J. 2005. Soft-sediment deformation structures in Late Miocene–Pleistocene sediments on the pediment of the Mátra Hills (Visonta, Atkár, Verseg): Cryoturbation, load structures or seismites? *Tectonophysics* 410: 81-95.

Kovács, J., Fábián, S.Á., Schweitzer, F. & Varga, G. 2007. A relict sand-wedge polygon site in north-central Hungary. *Permafrost and Periglacial Processes* 18: 379-384.

Maarleveld, G. 1976. Periglacial phenomena and the mean annual temperature during the Last Glacial time in the Netherlands. *Biuletyn Peryglacjalny* 26: 57-78.

Magyari, Á., Musitz, B., Csontos, L. & Van Vliet-Lanoë, B. 2005. Quaternary neotectonics of the Somogy Hills, Hungary (part I): Evidence from field observations. *Tectonophysics* 410: 43-62.

Montenat, C., Barrier, P., Ott d′Estevou, P. & Hibsch, C. 2007. Seismites: An attempt at critical analysis and classification. *Sedimentary Geology* 196: 5-30.

Pécsi, M. 1964. Chronological problem of the patterned soils of Hungary. *Biuletyn Peryglacjalny* 14: 279-293.

Tarnocai, C. & Schweitzer, F. 1998. Cryogenic features in Canada and Hungary and their significance for past climate. *Geografia Fisica e Dinamica Quaternaria* 21: 84-92.

Van Vliet-Lanoë, B., Magyari, A. & Meilliez, F. 2004. Distinguishing between tectonic and periglacial deformations of quaternary continental deposits in Europe. *Global and Planetary Change* 43: 103-127.

Potential Inclusion of Vegetation Indices in Mountain Permafrost Modeling

Marian Kremer, Antoni G. Lewkowicz, Michael Sawada, Philip P. Bonnaventure
Department of Geography, University of Ottawa, Ottawa, Canada
Mark Ednie
Geological Survey of Canada, Ottawa, Canada

Introduction

A widely-used method to model the distribution of mountain permafrost employs basal temperature of snow (BTS) measurements as an indicator of the probability of permafrost presence. Multiple regression is used to develop a spatial field of BTS values, and these values are used to predict the distribution of permafrost either through the BTS "rules-of-thumb" or through ground-truthing relationships (e.g., Lewkowicz & Ednie 2004). The best independent variables for modeling BTS values are generally elevation and potential incoming solar radiation (PISR) (e.g., Gruber & Hoelzle 2001, Lewkowicz & Ednie 2004, Ødegård et al. 1999). Multiple regression of BTS against these variables generally results in r^2 values of 0.3–0.4, indicating that there are other important factors affecting BTS values and hence permafrost (Gruber & Hoelzle 2001, Lewkowicz & Ednie 2004), one of which is vegetation.

Vegetation affects the surface offset (Smith & Riseborough 2002) by influencing turbulent energy fluxes, by shading the ground surface in summer and by altering snow distribution in winter, especially in mountain catchments where significant redistribution of snow may occur (e.g., Pomeroy et al. 2006). A small number of attempts have been made to include vegetation in permafrost spatial models using vegetation indices and land cover classifications created from remotely sensed satellite images. However, there is no generally accepted method to represent vegetation for this purpose.

Despite its known theoretical significance, vegetation has proven to be of little importance in the few European mountain permafrost studies that have included it. For example, the Normalized Difference Vegetation Index (NDVI) which was used by Ødegård et al. (1999) in southern Norway did not substantially improve statistical explanation because it was highly correlated with elevation, one of the other independent variables. In Switzerland, Gruber and Hoelzle (2001) used the Soil Adjusted Vegetation Index (SAVI) to correct for the high reflectance of soil in the imagery, but obtained similar results. Without it the r^2 value was 0.386, and with SAVI the r^2 increased by only 0.012 (Gruber & Hoelzle 2001).

Attempts to incorporate vegetation into permafrost modeling using land cover classifications have been more successful. In the Yukon-Tanana Uplands of Alaska, Landsat Thematic Mapper (TM) imagery was used to generate land cover classifications that included types of canopy cover (closed or open) and types of vegetation (coniferous forest, deciduous forest, mixed forest, shrub) (Morrissey & Strong 1986). Using logistic discriminant functions with this classification and data from the thermal band of Landsat TM imagery, which provides similar information to PISR, three classes of permafrost distribution (frozen, discontinuously frozen, and unfrozen) were predicted with reasonable success. In the Mayo region, Yukon, Leverington, and Duguay (1996) also developed a vegetation classification from Landsat TM imagery and used it to test models for predicting active layer depths and the presence or absence of permafrost. The land cover classification was found to be one of the most useful factors for predicting the presence of permafrost. Etzelmüller et al. (2006) combined both land cover classification and NDVI in their multicriteria analysis of mountain permafrost distribution in Mongolia. They found that NDVI was useful only after an initial land cover division into forested and nonforested areas.

Objectives

The goal of this project is to examine which, if any, of the ways discussed above to incorporate vegetation may be suitable for permafrost modeling in the mountains of northwest Canada. Despite their lack of effectiveness in Europe, it is possible that vegetation indices may yet prove useful, given differing patterns of permafrost distribution in relation to vegetation zones. Alternatively, land cover classification or a hybrid approach may be the most effective. By testing models at sites in several climatological zones, we hope to determine if there is a single method that is effective or if adjustments to the methodology must be made to take local vegetation-climate relations into account.

Study Areas

The eight field areas that are being examined for this study represent all the major climatological regions of the southern Yukon and include Wolf Creek near Whitehorse, Johnson's Crossing, Sa Dena Hes mine north of Watson Lake, Faro, Keno, the Top-of-the-World Highway near Dawson, the Ruby Range, and Haines Summit in extreme NW British Columbia. These sites span almost 5° of latitude (59°36′ to 64°05′N), and all fall into zones of discontinuous permafrost (Heginbottom et al. 1995). Elevations in the areas generally vary from about 700 m to 2000 m a.s.l., with the Dawson area extending down to about 320 m. Permafrost is present at higher elevations in all of the areas as well as below tree line in most of them as a result of cold air drainage and hydrological variability.

Results

A preliminary investigation of the relationships between vegetation and the presence or absence of permafrost was undertaken using a dataset collected since 2002 of vegetation descriptions and late-summer probing or temperature profiles in pits at more than 500 mountain sites. Observations were grouped into three vegetation classes that exist in the study areas: northern boreal forest, a shrub tundra zone of willow and birch above treeline, and alpine tundra or bare areas (combined) at the highest elevations.

The percentage of pits exhibiting permafrost for each vegetation type in each study area (organized by increasing precipitation) is shown in Figure 1. The results suggest that precipitation totals may have an impact at the regional scale, but this apparent trend must be interpreted cautiously, as the precipitation values come from low-elevation climatological stations located up to 80 km from the study areas. Organizing the results by latitude (not shown) did not reveal any obvious trends: three sites at virtually the same latitude (Wolf Creek, Johnson's Crossing and Sa Dena Hes) exhibit significant variation in the percentage of permafrost.

Given the link between elevation and vegetation, it is not surprising that the percentage of permafrost is generally higher for alpine tundra sites than for the other two classes. Reasons for the two exceptions (Faro for shrubs and Johnson's Crossing for forest) require further investigation and more field sampling.

The impact of vegetation in affecting the surface offset and, hence, permafrost is best illustrated by the three study areas where shrub sites have the smallest percentage of permafrost (lower than forested sites). This may indicate the importance of trapping snow blown from the tundra above (e.g., Pomeroy et al. 2006) within the shrub zone and the snow's influence on reducing ground heat loss in winter.

These field observations show that vegetation type is highly correlated with elevation, but this brief analysis indicates that it may still affect mountain permafrost distribution independently. It also suggests that these impacts may be site-specific, possibly linked to regional climate. Further investigations of these relationships are planned in order to meet the objectives described above.

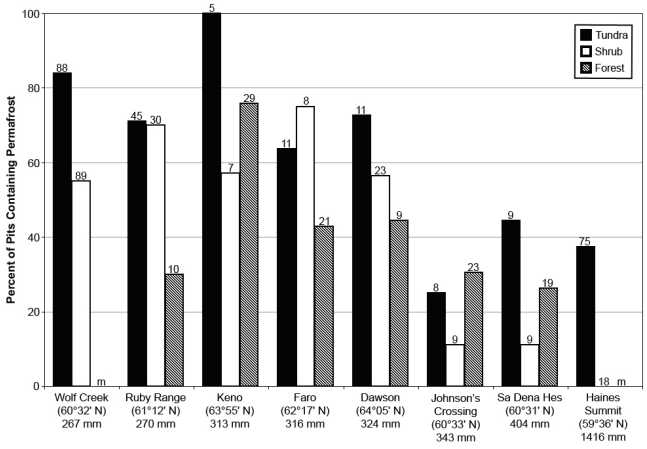

Figure 1. Percent of ground truthing pits that contained permafrost for each vegetation type in each study area. Numbers above the bars indicate the number of pits examined (groups with <5 sites shown as m). Sites organized according to precipitation normals (1971–2000) from the closest climatological station (data source, Environment Canada 2008).

Acknowledgments

Financial support was provided by the Canadian Foundation for Climate and Atmospheric Sciences, NSERC, Geological Survey of Canada, Yukon Geological Survey and the University of Ottawa. Field assistance was provided by Emily Schultz, Dan Odell, and Reid Van Brabant.

References

Environment Canada. 2008. http://www.climate.weatheroffice.ec.gc.ca (accessed February 9, 2008).

Etzelmüller, B., Heggem, E.S.F., Sharkhuu, N., Frauenfelder, R., Kääb, A. & Goulden, C. 2006. Mountain permafrost distribution modeling using a mutli-criteria approach in the Hövsgöl area, northern Mongolia. *Permafrost and Periglacial Processes* 17: 91-104.

Gruber, S. & Hoelzle, M. 2001. Statistical modelling of mountain permafrost distribution: Local calibration and incorporation of remotely sensed data. *Permafrost and Periglacial Processes* 12: 69-77.

Heginbottom, J.A., Dubreuil, M.A. & Harker, P.T. 1995. Canada Permafrost. 1:7,500,000 scale. In: *The National Atlas of Canada*, 5th ed., sheet MCR 4177. Ottawa: National Resources Canada.

Leverington, D.W. & Duguay, C.R. 1996. Evaluation of three supervised classifiers in mapping "depth to late-summer frozen ground", central Yukon Territory. *Canadian Journal of Remote Sensing* 22: 163-174.

Lewkowicz, A. & Ednie, M. 2004. Probability mapping of mountain permfrost using the BTS method, Wolf Creek, Yukon Territory, Canada. *Permafrost and Periglacial Processes* 15: 67-80.

Morrissey, L.A., Strong, L.L. & Card, D.H. 1986. Mapping permafrost in the boreal forest with thematic mapper satellite data. *Photogrammetric Engineering and Remote Sensing* 52: 1513-1520.

Ødegård, R.S., Isaksen, K., Mastervik, M., Billdal, L., Engler, M. & Sollid, J.L. 1999. Comparison of BTS and Landsat TM data from Jotunheimen, southern Norway. *Norsk Geografisk Tidsskrift* 53: 226-233.

Pomeroy, J.W., Bewley, D.S., Essery, R.L.H., Hedstrom, N.R., Link, T., Granger, R.J., Sicart, J.E., Ellis, C.R. & Janowicz, J.R. 2006. Shrub tundra snowmelt. *Hydrological Processes* 20: 923-941.

Smith, M.W. & Riseborough, D.W. 2002. Climate and the limits of permafrost: A zonal analysis. *Permafrost and Periglacial Processes* 13: 1-15.

Thermal Conditions in Martian Permafrost: Past and Present

Mikhail A. Kreslavsky
University of California – Santa Cruz

Present Conditions

Global cryosphere

The temperature of the Martian surface has been monitored by several orbital thermal infrared sensors. These measurements, accompanied by careful and cautious modeling, give rather accurate knowledge of the thermal regime of the uppermost meters of the surface in the present epoch.

The year-average surface temperature on Mars is well below 0°C everywhere on the planet, meaning a thick global cryosphere. The day-average temperature also never exceeds the ice melting point, meaning the absence of the active layer of Martian permafrost in the present epoch.

Observations with orbital gamma-ray and neutron sensors sensitive to the presence of hydrogen in the uppermost meter of the surface have indicated that high latitudes (above ~ 60° in both hemispheres) contain much hydrogen, which obviously means the presence of water ice. This ice is abundant, and its amount in the soil noticeably exceeds 50% by volume. At mid and low latitudes, ice in the upper meter is less abundant or absent. The hydrogen content in equatorial regions is spatially variable and in some regions exceeds 10 wt% water-equivalent by weight. Deeper in the ground, ice may be present virtually everywhere.

Calculations of the ground ice stability against diffusion of water vapor to the atmosphere (e.g., Mellon & Jakosky 1995, Schorghofer & Aharonson 2005) show that the ground ice is stable at high latitudes and unstable at low latitudes; in addition to latitude, surface albedo and thermal properties influence stability.

Patterned ground

High-resolution images reveal a great variety of polygonal patterns (e.g., Mangold et al. 2004), totally covering more than one-quarter of the planet (predominantly at high latitudes). The extent of massive polygonal pattern occurrence somewhat exceeds the limits of the observed high hydrogen content. Polygonal patterns are often forming hierarchical systems of different scales (Fig. 1). These patterns were probably initiated by thermal cracking of ice-rich permafrost. On Earth, thermal cracking of permafrost usually leads to formation of ice-wedge polygons due to seasonal thaw of the active layer. On Mars, seasonal thaw does not occur, and the cracks evolve into sand-wedge polygons and/or sublimation polygons, features, observed in extremely cold and dry terrestrial environments (Marchant et al. 2002).

Thermal cracking of ice-rich frozen soils occurs due to an anomalously high bulk thermal expansion coefficient of the ice-soil mixtures. However, the thermal expansion coefficient decreases with the temperature decrease. Very high seasonal temperature amplitude at high latitudes on Mars favors thermal cracking, while generally low temperatures are not favorable.

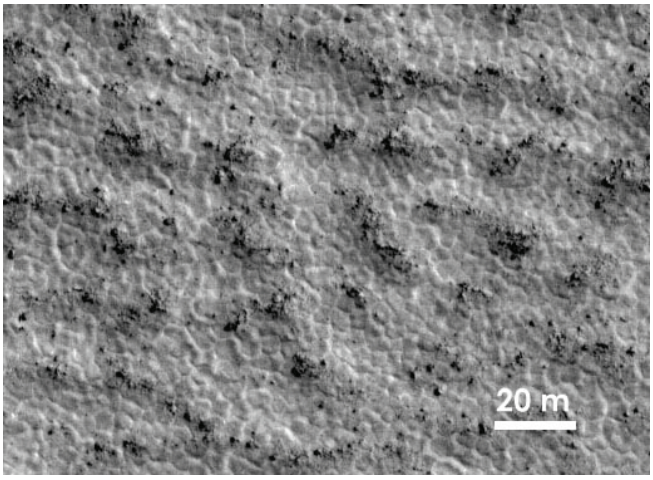

Figure 1. Two scales of polygonal pattern on Mars. HiRISE image PSP_001404_2490, 69°N, 106°W.

The absence of polygons in the *low-latitude* hydrogen-rich regions has been interpreted as evidence for the absence of water ice in the soil (the hydrogen being bound in hydrated minerals). However, in these regions, the seasonal temperature amplitudes are modest (typically, 20–30 K; <50 K in any place) and temperatures (~210 K year average) are very low. The hydrogen-rich regions coincide with the regions of low-thermal-inertia dust cover. This ice-free cover would further reduce the seasonal temperature amplitude at the hypothetical ice table. Formation of the thermal contraction cracks is not probable under such conditions, and their absence cannot be considered as an argument against subsurface ice.

The polygonal patterns at *high latitudes* show remarkable uniformity over large areas, as well as significant regional variability partly correlated with latitude (e.g., Kostama et al. 2006, Levy et al. 2008). The polygon-covered surface at high latitude is almost devoid of small (tens of meters) impact craters, which indicates geologically recent deposition of meters-thick icy material ("mantle") and/or thorough reworking of the surface by cryoturbaton. Thus, patterned ground bears a record of processes related to recent climate change on Mars.

Recent Past

Kostama et al. (2006) found that the crater retention age for tens-of-meters-scale craters in the high northern latitudes is on the order of 100 ka, and is highly variable regionally and latitudinally. Recent measurements of the present-day cratering rate on Mars (Malin et al. 2006, Kreslavsky 2007) make that estimate more certain. Thus the polygonal pattern

records the most recent climate variations and can be used to constrain timing of other recent geological events (e.g., the most recent gully activity).

Stresses causing thermal cracking are proportional to the seasonal amplitude of the surface temperature. At high latitudes on Mars the winter temperature is buffered by condensation of the atmospheric carbon dioxide at ~140 K. Thus, the amplitude of seasonal surface temperature variations is solely defined by the year-maximum day-average temperature. On Mars, weak atmosphere is mostly thermally decoupled from the surface, and the surface temperature is controlled mostly by direct insolation, other contributions being minor. The year-maximum day-average temperature is an increasing function of the year-maximum day-average insolation. Since the winter temperature is the same, the year-average surface temperature is also an increasing function of the year-maximum day-average temperature, and hence, of the insolation. Thus, the year-maximum day-average insolation is a good proxy of the climate signal with regard to cryoturbation and formation of the polygonal patterns.

The insolation regime is controlled by evolution of spin and orbit parameters of Mars. For the recent epoch, these parameters were accurately calculated by Laskar et al. 2004. Figure 2 presents evolution of the year-maximum day-average insolation at high latitudes (70°) in both hemispheres

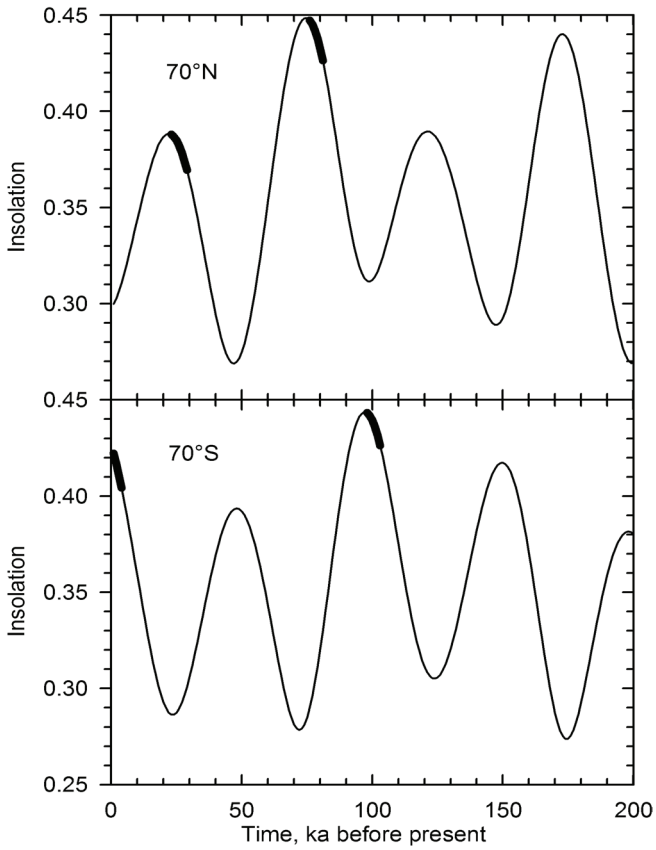

Figure 2. Evolution of the year-maximum day-average insolation (in parts of the martian solar constant) over the last 200 ka for horizontal surfaces at 70° latitude in the Northern (top) and Southern (bottom) Hemispheres. Bold segments show probable most recent periods of intensive polygon formation

over the last 200 ka. Formation of new cracks is expected to be on increasing insolation branches close to the insolation maxima, as marked on the plots (Fig. 2).

In the Southern Hemisphere, the polygon formation can be active at the present time. Older crack systems can have been formed 100 ka ago. If even older polygonal cracks are observed in the southern high latitudes, they may date back to 400 ka ago (not shown in Fig. 2). In the Northern Hemisphere, the most recent insolation peak occurred 20 ka ago, but it was lower than the present-day insolation at the south. The more probable period of activity is 75 ka ago, and it is most close to the age estimates by Kostama et al. 2006. An earlier high insolation peak occurred 275 ka ago.

Applying these results to the geologic studies, we need to keep in mind that the other factors, such as surface albedo (which can change due to painting of the surface with thin layers of fine dust) and thickness of dry layer above the ground ice (which depends on atmospheric water vapor content) can strongly influence the formation of polygonal patterns.

References

Kostama, V.-P., Kreslavsky, M.A. & Head, J.W. 2006. Recent high-latitude icy mantle in the northern plains of Mars: Characteristics and ages of emplacement. *Geophys. Res. Lett.* 33: L11201.

Kreslavsky, M.A. 2007. *Statistical Characterization of Spatial Distribution of Impact Craters: Implications to Present-Day Cratering Rate on Mars*. 7th Conf. on Mars, LPI Contribution No. 1353: 3325.

Laskar, J. et al. 2004. Long term evolution and chaotic diffusion of the insolation quantities of Mars. *Icarus* 170: 343-364.

Levy, J.S., Head, J.W. & Marchant, D.R. 2008. Mars thermal contraction crack polygon classification and distribution: Morphological characterization at HiRISE resolution. *Lunar Planetary Sci. XXXIX*: #1171.

Malin, M.C. et al. 2006. Present-day impact cratering rate and contemporary gully activity on Mars. *Science* 314: 1573-1577.

Mangold, N. et al. 2004. Spatial relationships between patterned ground and ground ice detected by the Neutron Spectrometer on Mars. *J. Geophys. Res.* 109: E08001.

Marchant, D.R. et al. 2002. Formation of patterned-ground and sublimation till over Miocene glacier ice in Beacon Valley, Antarctica. *Geol. Soc. Am. Bull.* 114(6): 718-730.

Mellon, M.T. & Jakosky, B.M. 1995. The distribution and behavior of Martian ground ice during past and present epochs. *J. Geophys. Res.* 100: 11781-11799.

Schorghofer, N. & Aharonson, O. 2005. Stability and exchange of subsurface ice on Mars. *J. Geophys. Res.* 110: E05003.

Collapse of the Bérard Rock Glacier (Southern French Alps)

Jean-Michel Krysiecki
Institute of Alpine Geography, University of Grenoble, France
Xavier Bodin
University Paris-Diderot (Paris 7), Institute of Alpine Geography, University of Grenoble, France
Philippe Schoeneich
Institute of Alpine Geography, University of Grenoble, France

Introduction

In the Mediterranean French Alps, the summer 2006 has been marked by the sudden collapse of the Bérard rock glacier (Parpaillon Range, Alpes de Haute Provence, France), a very rare event and exceptional by the amount of disturbed material estimated to be about 2 millions m^3 (Fig.1).

Located near the southern limits of the European Alpine permafrost, the Bérard rock glacier case is perhaps representative of the potential consequences of mountain permafrost degradation under present global warming, and raises questions about the evolution of ice-debris mixtures on steep slopes; for example, rock glacier under permafrost conditions. An atmospheric warming of 0.5 to 1°C between 1900 and 2000 is indeed currently observed in the Alps (Casty et al. 2005). In the same way, recent observations on thermal evolution of the ground in high mountains (Harris et al. 2003), as well as the occurrence of new and unexpected phenomena, for example, acceleration of rock glacier flow (Ikeda & Matsuoka 2002, Roer et al. 2005, Delaloye et al. 2006, Kääb et al. 2006, Delaloye et al. 2008) or rock glacier collapse (Evin et al. 2007), seem to indicate that mountain permafrost could respond much faster to global warming than expected, and that areas at its lower limits could experience a morphogenetic crisis.

Crucial questions in terms of natural hazards and associated dangers are being raised (Harris et al. 2000): the speed-up of creeping landforms (Kääb et al. 2006), the destabilisation of the frontal part of rock glaciers (Arenson 2002), and an increase of the rockfall activity (Haeberli et al. 1997, Noetzli et al. 2003) and of the frequency of debris flow have already been observed in mountain permafrost areas.

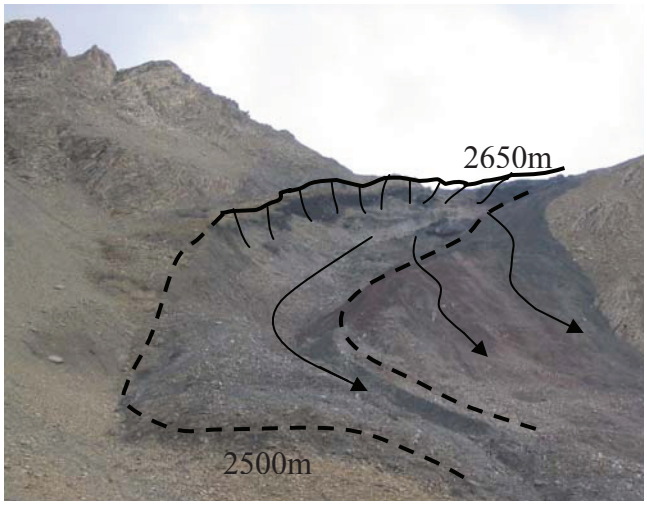

Figure 1. An upward-looking view of the collapsed Bérard rock glacier (July 2007).

In this context, the main objective of our study is to understand the mechanisms that triggered the Bérard rock glacier collapse, which could subsequently gain new insights into the destabilisation of ice-rich deposits on mountain catchments.

The Bérard Rock Glacier Situation

The Bérard rock glacier is located in the Parpaillon Range, one of the southernmost ranges of the European Alps, including the summits of Grand Bérard (3046 m) and La Chalanche (2984 m). Topoclimatic and geomorphological conditions are favorable to permafrost occurrence in this valley.

Methods

Within a larger research project intending to study the consequences of permafrost degradation in the French Alps, a complete monitoring of the site has hence been set up. This includes:

- the geodetic survey (Differential and Permanent GPS) of marked blocks during the summer, in order to quantify the velocity and the characteristics of the movement;
- the use of radar interferometry to reconstruct the history of the event during the previous years and to map the main destabilised areas;
- the interpretation of electrical resistivity and refraction seismic tomographies to assess the physical properties of the internal structure of the rock glacier;
- the analysis of the ice to determine its origin and its main physical properties;
- the survey of the climatic parameters (air temperature, solar radiation, wind speed and direction, snow height) with an automatic weather station; and
- the survey of the thermal state of the ground (with miniature temperature dataloggers) to allow the monitoring of pertinent indicators; for example, mean annual ground surface temperature (MAGST) or mean annual active layer temperature.

First Results

Among the above-mentioned methods, geomorphological study, DGPS results, and ice analyses have given first results.

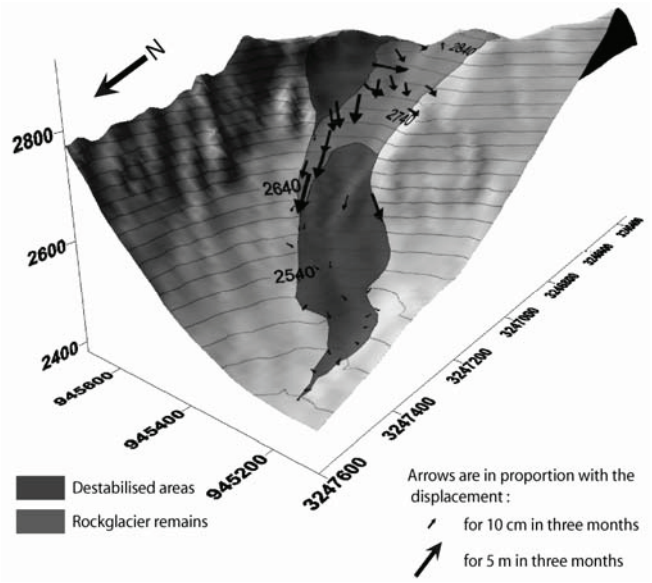

Figure 2. 3-D displacement of marked blocks on the Bérard rock glacier between June and September 2007.

The geomorphological study of the site has already revealed that the breaking of the rock glacier is probably partly related to an underlying rockslide in the schist series, which may have been activated by storms during summer 2006.

First results are DGPS measurements of more than 40 marked blocks on the Bérard rock glacier and the slided mass, in June and September 2007. The 3-D vectors map shows that the slided mass has not experienced important movements during the three surveyed months. *Z* values suggest a general settling (about 5–15 cm), certainly due to the ice melt in debris. Remains of the rock glacier, especially near the collapse area, are affected by large movements (more than 5 m in three months) and the destabilisation is effective as far as the saddle point (displacements are around 1 m in three months). Permanent GPS, located above the scar on a flat area, indicates a mean displacement of 6.4 $mm.day^{-1}$ in the north direction, corresponding to an annual displacement of more than 2 m, which fits with the surrounding DGPS measurements.

Stratigraphic observations on near-surface ice outcrops reveal that Bérard rock glacier has been affected by periglacial and glacial mechanisms. Preliminary analyses of ice structure have revealed the sample to be similar to glacier ice (Vallon, pers. com.). Little Ice Age period is suspected in this mechanism change, but other analyses have to confirm that.

Our study, thanks to the various monitoring devices, has already clarified the respective roles of the meteorological conditions, the recent climatic warming, and the geological settings in the collapse of the Bérard rock glacier. Most of the results are coming during the summer 2008 and will bring new precision on the Bérard rock glacier event.

References

Arenson, L.U. 2002. *Unstable Alpine permafrost: A potential important natural hazard – Variations of geotechnical behaviour with time and temperature.* PhD Thesis, ETH Zurich.

Casty, C. et al. 2005. Temperature and precipitation variability in the European Alps since 1500. *International Journal of Climatology* 25: 1855-1880.

Delaloye, R. et al. 2006. ERS InSAR for detecting slope movement in a periglacial mountain environment (western Valais Alps, Switzerland). *Ninth International Symposium on High Mountain Remote Sensing Cartography* (HMRSC-IX), Graz, Austria.

Delaloye, R. et al. 2008. Recent interannual variations of rock glacier creep in the European Alps. *Proceedings of the Ninth International Conference on Permafrost, Fairbanks, Alaska, 29 June–3 July 2008*.

Evin, M. et al. 2007. Rupture et glissement en masse d'un glacier rocheux dans le vallon du Bérard (Massif du Parpaillon, Alpes du Sud, France) au cours de l'été 2006, Grenoble, *SHF - Section Glaciologie/ Nivologie*.

Gruber, S. et al. 2004. Interpretation of geothermal profiles perturbed by topography: the Alpine permafrost boreholes at Stockhorn Plateau, Switzerland. *Permafrost and Periglacial Processes* 15(4).

Haeberli, W. et al. 1997. Slope stability problems related to glacier shrinkage and permafrost degradation in the Alps. *Eclogae Geol. Helv*. 90: 407-414.

Ikeda, A. & Matsuoka, N. 2002. Degradation of talus-derived rock glacier in the Upper Engadin, Swiss Alps. *Permafrost and Periglacial Processes* 13: 145-161.

Kääb A. et al. 2006. On the response of rockglacier creep to surface temperature increase. *Global and Planetary Change* 56(1–2): 172-187, doi:10.1016/j.gloplacha.2006.07.005.

Noetzli, J. et al. 2003. Mountain permafrost and recent Alpine rock-fall events: A GIS-based approach to determine critical factors. *Proceedings of the Eighth International Conference on Permafrost, Zürich. Swets & Zeitlinger, Lisse.*

Roer, I. et al. 2005. Rockglacier "speed-up" throughout European Alps: A climatic signal? *Second European Conference on Permafrost*, Potsdam, Alfred-Wegener-Stiftung.

Studies of the Freezing Soil Process at the Railway Contact System Supports to Provide Safe Transportation and Operation of Facilities

S.A. Kudryavtsev, D.G.Tsvigunov
Far Eastern State Transport University (FESTU), Khabarovsk, Russia

Introduction

Maintenance and efficient operation of railway power engineering facilities in regions with seasonal freezing and permafrost soils are faced with serious difficulties connected with the bulging of contact system supports. Seasonal soil freezing is one of the major factors taken into consideration for contact system support foundations.

The problem of frost heaving is characterized not only by the number of repaired contact system supports, but also by safe transportation, too. On sections of the Far Eastern railway, which pass through a permafrost area, a large number of contact system supports has to be restored annually. To develop a reliable and stable foundation structure, an exact estimation of thermophysical and stress-deformed conditions of heave-probable soils both at freezing and thawing is required.

Studies of freezing, frost heaving, and thawing of soils and their effect on contact system supports are complicated processes and require further development. Their complexity is first of all explained by a great number of interactive factors, changing in time and space. Studying these processes in natural conditions requires observations for a long period of time, because the data of short-term observations may be accidental.

Thermometric Observations

To check correctness of foundation designs used and search for new decisions in the field of construction, calculations, the utilization of structures, as well as establishing the character of their interaction must be considered. With seasonal freezing soils, monthly thermometric observations have been organized on the Khabarovsk Section of the Far Eastern Railway (8540 km.).

They are:

1. Thermal regime of the soil at the contact system support.
2. Geodesic control of the contact system support position.

To watch the thermal regime, a temperature monitoring system, Thermoscan, had been used. It is designed to do work for measuring temperature in continuous and single regimes.

The Thermoscan set includes a measuring block with a controller, a measuring bus duct with temperature "sensors," a pocket PC, a storage battery, and Thermoscan software.

Numerical Modeling of the Freezing Process

Measurements of the thermo-moisture regime were made with the help of numerical modeling. By analyzing

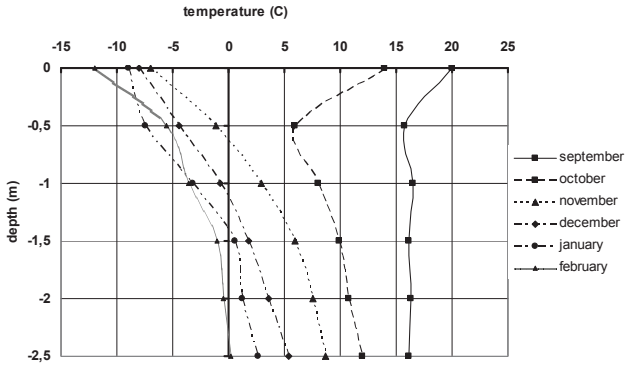

Figure 1. Thermometric observation data.

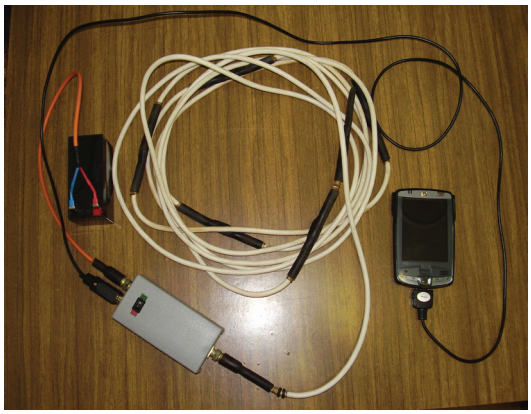

Figure 2. The Thermoscan temperature monitoring system.

the existent models of freezing and thawing of soils, a mathematical model of numerical modeling of freezing, frost heaving, and thawing in an annual cycle has been developed by the method of finite elements in the space set, being a component of the programmed complex "FEM-models."

This complicated geotechnical task is done in two stages: The first stage solves the thermo technical task of defining temperature and moisture fields for each period of time. The second stage solves the task of defining stress-deformed conditions of fundamental soils in the process of freezing and thawing.

We have simulated the process of freezing and heaving of the railway trial sector. Monthly calculations were made for yearly changes of the monthly average temperature in the region. The maximum depth of soil freezing in the contact system support, without principally the thermal insulation layer, was 2.0 m in March.

Deformation of the principal area of the railway bed caused by frost penetration is equal to 6 cm, and horizontal deformation of the contact system support, about 3.5 cm. Use of expanded polystyrene thermal insulation materials lowers the freezing front (zero isotherm) to 1.4 m under the

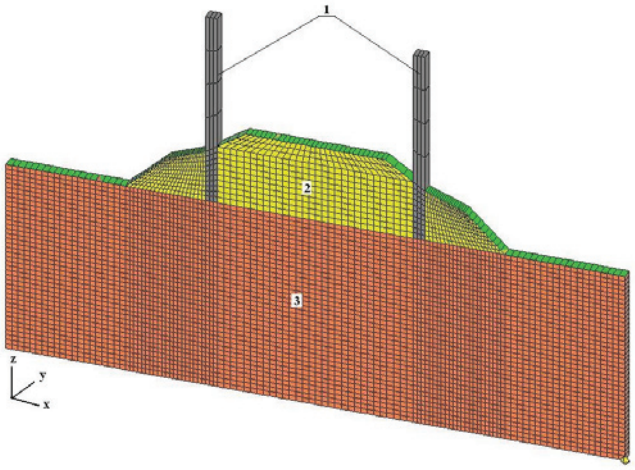

Figure 3. Calculations simulation scheme. 1 – contact system support; 2 – dusty loan embankment; 3 – basement.

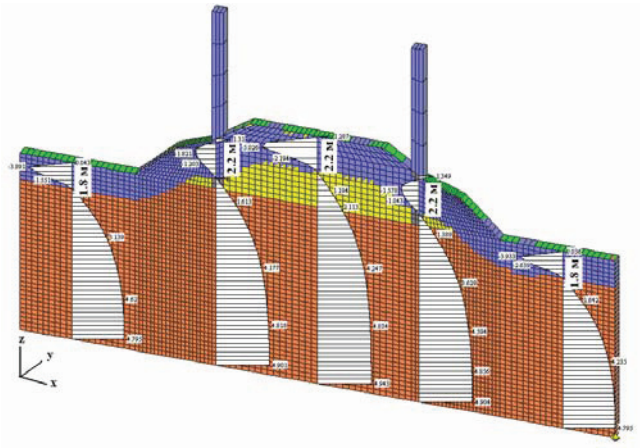

Figure 4. Temperature epures of the embankment body and basement.

center line of the track, and, accordingly, with deformation decrease down to 1.5 cm, frost heaving forces become lower. In the embankment slope, frost heaving forces have a serious effect on the stability of the contact system support, exerting normal and horizontal action, as the zero isotherm catches the foundations. This causes horizontal deformation of the supports, worsening their operational qualities.

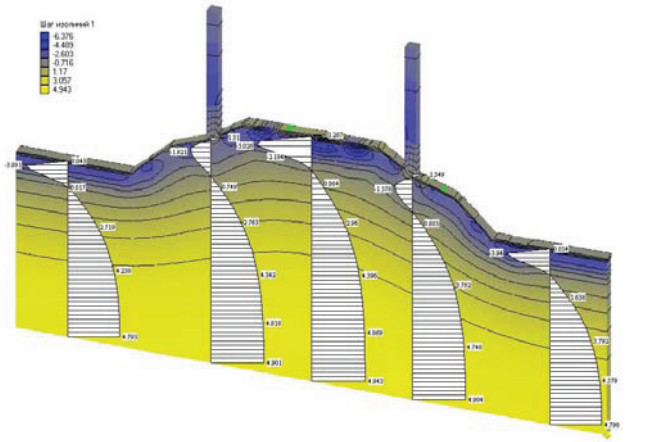

Figure 5. Temperature isolines and epures of the embankment body and basement.

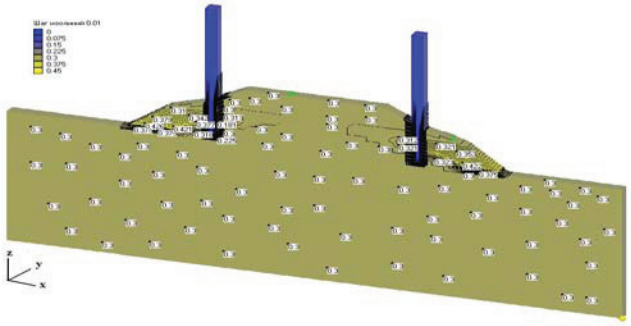

Figure 6. Isolines of moisture distribution in the body of embankment and basement in winter.

References

Kudryavtsev, S.A., Ulitsky, V.M., Paramonov, V.N., Shashkin, K.G. & Lisyuk, M.B. 2003. Contemporary geotechnologies providing safe operation of railway embankments in permafrost conditions. *Proceedings of the Eighth International Conference on Permafrost. Extended Abstracts, Reporting Current Research and New Informational Zurich, Switzerland, 20–25 July 2003:* 167-168.

Temporal Variability in Plant Cover and Carbon Balance of Permafrost-Affected Tundra Ecosystems

Peter Kuhry
Department of Physical Geography and Quaternary Geology, Stockholm University, Sweden

Introduction

The extant tundra in Northeast European Russia is characterized by high spatial variability. Previous studies highlight the fine mosaic of microsites with different vegetation, soil, permafrost, carbon storage, and methane emission characteristics (e.g., Kuhry et al. 2002, Heikkinen et al. 2004). This investigation points in addition to high temporal landscape dynamics in relation to recent climate and/or permafrost changes, which represents a further challenge for the past reconstruction and future prediction of the tundra carbon balance.

Methods

The temporal ecosystem dynamics in a tundra site at Lek-Vorkuta (Northeast European Russia) is traced using high resolution (1–2 cm depth intervals), absolute dating, geochemical, and plant macrofossil analyses of a 22 cm thick top organic sequence in permafrost-affected peaty soil. The LVPS3 profile was excavated from a small hummock in wet tundra (67°40′N, 63°35′E). The upper permafrost table at the time of collection (August 3, 1999) was located at 25 cm. This implies that the entire top organic horizon is located within the active layer. Although the profile at the site showed considerable deformation of the original layers, no evidence was found for complete stratigraphic inversions (Fig 1).

The LVPS3 sequence was dated through a combination of ^{210}Pb dating of the upper 16 cm and ^{14}C AMS wiggle-matching of the lower 7 cm of the top organic deposit. The geochemical analyses of the sequence included bulk density, loss-on ignition (550°C) and carbon/nitrogen ratio measurements. Figure 2 presents the gross stratigraphy of the profile and the samples (intervals and materials) utilized for the different types of analyses performed.

Figure 1. Collection site and material of the LVPS3 profile.

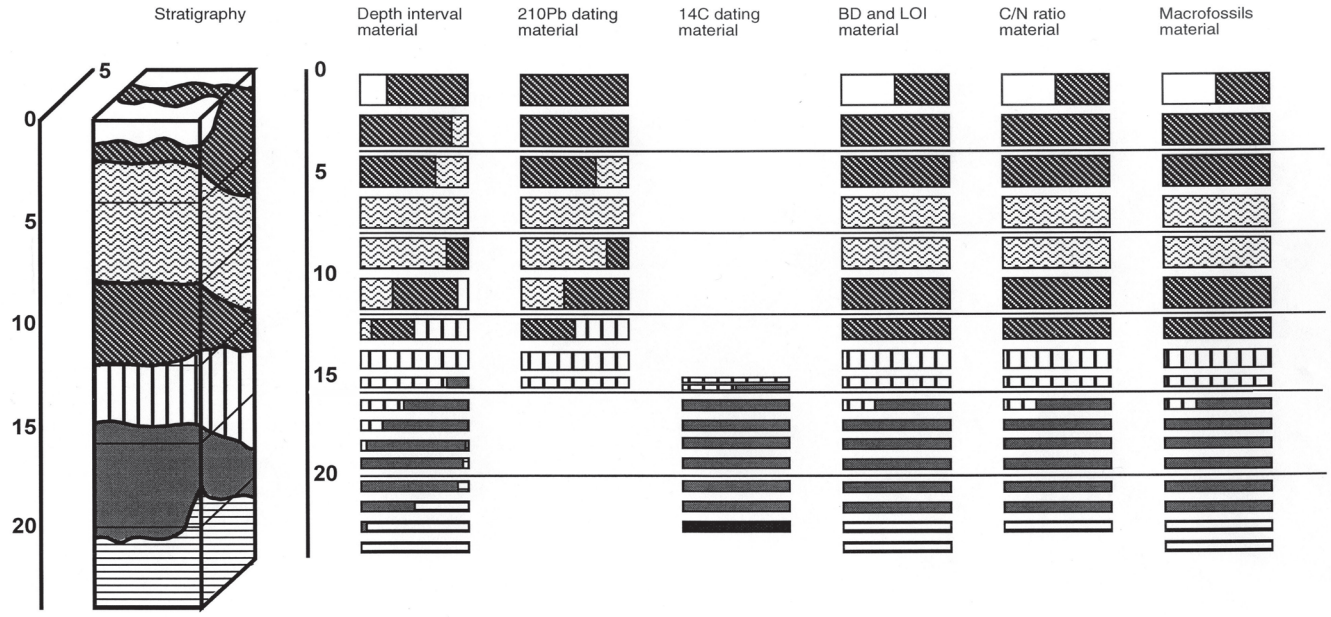

Figure 2. LVPS3 gross stratigraphy and samples analyzed for different analytical procedures. Stratigraphy from base to top: horizontal dash (mineral subsoil); uniform grey (organic soil); vertical dash (monocot peat); diagonal dash, two layers (*Polytrichum/Dicranum* peat); horizontal wave (*Sphagnum* peat); white (present lichen cover).

Results

The most plausible age-depth model suggests that the deposit represents ca. 650 calendar years with a rapidly declining net carbon accumulation rate due to cumulative decay of the organic matter with age. There has been a (near) complete turnover of organic material deposited prior to this time, leaving no evidence of the older history at the site.

Chronological control becomes increasingly more accurate towards the present, allowing a more detailed reconstruction of the timing and duration of successive vegetation phases.

Macrobotanical remains reveal significant changes in surface conditions at the site over time. The first recorded phase, characterized as dwarf-birch tundra, lasted until ca. 1860 AD. At this time the site paludified, resulting in the formation of an *Eriophorum*-dominated wetland. After about 40 years, drier surface conditions developed starting with *Sphagnum fuscum* and culminating in a *Polytrichum/ Dicranum* phase. Wetter conditions reappeared in the 1930s as indicated by *Sphagnum* Sect. Cuspidata. In recent decades the surface became drier again with a *Sphagnum fuscum* phase, followed by the present *Polytrichum/Dicranum*/ lichen phase.

An assessment will be made whether these recent changes in surface conditions can be linked to monitored long-term climate variability in the region. Alternatively, the observed temporal dynamics can be associated with permafrost aggradation following the development of a thick organic layer in the dwarf-birch phase and subsequent differential frost heave/ground subsidence at and in the immediate vicinity of the investigated site.

The final objective is to assess net carbon storage and methane emission characteristics throughout the recent history of the site with the aim to reconstruct the variable net radiative climate forcing originating from this type of dynamical tundra ecosystems.

Acknowledgments

The collection of the material was funded through the EU 4th Framework Environment and Climate Programme (TUNDRA project) and the EU INTAS Programme (PERUSA project). Current analyses of the material are supported by a grant from the Swedish Research Council.

References

Heikkinen, J.E.P., Virtanen, T., Huttunen, J.T., Elsakov, V. & Martikainen, P.J. 2004. Carbon balance of East European tundra. *Global Biogeochemical Cycles* 18, doi:10.1029/2003GB002054.

Kuhry, P., Mazhitova, G., Forest, P.A., Deneva, S., Virtanen, T. & Kultti, S. 2002. Upscaling soil carbon estimates for the Usa Basin (Northeast European Russia) using GIS-based landcover and soil classification schemes. *Danish Journal of Geography* 102: 11-25.

Temperatures of Upper Permafrost in Northern West Siberia

Anna N. Kurchatova, Alexander V. Boytsov
Tymen State Oil and Gas University, Russia
Alexei B. Osokin, Gregory K. Smolov
Gas Company "Nadymgasprom," Russia

Introduction

A monitoring net of permafrost observatories was established in 2004 by the Subarctic Centre (Tyumen State Oil and Gas University) and "Nadymgasprom" Company in Northern West Siberia. The southern part of the submeridian transect is located in continental territory between Nadym and Pur Rivers (Medvezhye and Yubileinoe gas fields); the northern end is situated on Yamal Peninsula (Kharasavay and Bovanenkovo gas-condensate fields). The observational sites are located on the main geomorphological levels of the territory and are presented by different landscapes. Boreholes (from 1 to 3 at observatory, up to 30 m depth) are equipped by automatic systems for temperature measurements made by "GEOTECHCENTRE," Russia. Measurements are taken every 6 hours at the 15s levels. At Bovanenkovo gas-condensate field (Yamal), a soil-climate station (by Campbell Scientific Ltd.) was established in 2006 for registration of standard meteorological parameters and the temperature-moisture regime of the active layer. On the territory of Yubileynoe gas field, 4 CALM sites were created for long-term dynamics of the active layer. The first results of these measurements are presented in this report.

Permafrost Temperatures

Analyses of meteorological data in West Siberia show a general increase in mean annual air temperature for about 30 years mainly due to decreasing of the temperature sum of the winter period. The first publications about the tendency of permafrost warming within the layer of the annual amplitudes appeared in the early 1990s. Long-term research at the geocryological stations in West Siberia (Marre-Sale – Pavlov 1994, and Nadym – Pavlov & Moskalenko 2002) shows the warming tendency of the frozen ground temperature during the last decades. For the last years, relative stability of the annual air temperature is accompanied by an increase in the positive temperature sum that can lead to melting of the ice-bearing permafrost table. And as a result, activity of cryogenic processes or local degradation of frozen ground from the top down at the drained sites in the southern cryolithozone can occur.

Observatories located at weakly drained watersheds of high geomorphological levels composed of mineral soils are the most representative for understanding permafrost's reaction to climate change. Zonal landscapes along the submeridian transect are changed from northern forest to tundra. Local factors can play a main role in the ground temperature regime: In depressions, a formation of snow cover occurs mainly due to the strong wind influence; the high ice content and moss cover provide thermal stability for the frozen peatlands in summer.

The temperature ground regime of the boreholes shows relative stability in different zonal landscapes (Fig. 1A). In the southern cryolithozone, taliks with deep permafrost table are widespread even within watersheds. The first results show that the depth of zero annual amplitude at these sites is about 15 m despite water-saturated sands in the upper part of the soil section. On Yamal Peninsula at the sites composed by clayish sediments, the annual thermal turnover reaches ≈10 m depth, explained by low temperature of freezing and low thermal conductivity of saline marine sediments and widespread cryopegs there. However, at the sandy denuded areas at the high marine terraces, the depth of zero annual amplitude can reach 20 m.

The mosaic landscape structure of forest-tundra has resulted in the high dynamics of the thermal ground state (Fig. 1B, C, D). Sparse growth of larches with dense shrubs is a clear indicator of taliks because of higher snow accumulation (1 m depth and more, I-1; 0.3–0.4 m at the peat bogs, I-2). The zero-temperature regime of the high river terraces has been kept by the warm input of melting snow water and the first liquid precipitation down into the dry frozen sands up to 3–5 m depth despite deep freezing during winter (I-3).

Disturbances of the soil surface (fires and construction) are a more common cause of ground temperature change, and especially of an increase in active layer depth. The substantial increase in the mean annual soil temperature at the base of the active layer within polygonal peatland was caused by a fire and destruction of the moss-lichen cover after the anomalous high air temperature in July 2007 (Fig. 1B, I-2). However, the disappearance of insulating moss cover can also result in fast freezing of the active layer in the beginning of winter, and then to the substantial decrease in soil temperature. We observed the formation of a new frost-cracking system at the other site after a similar fire in 2005.

Acknowledgments

Funding for the research was provided by the INTAS Infrastructure Action (Ref. Nr. 04-87-689) and Tyumen regional grants. We are grateful to the leaders of "Nadymgasprom" Company for the support of drilling and fieldwork, and to Drs. V. Romanovsky and N. Shiklomanov for equipment and assistance in the creation of CALM sites.

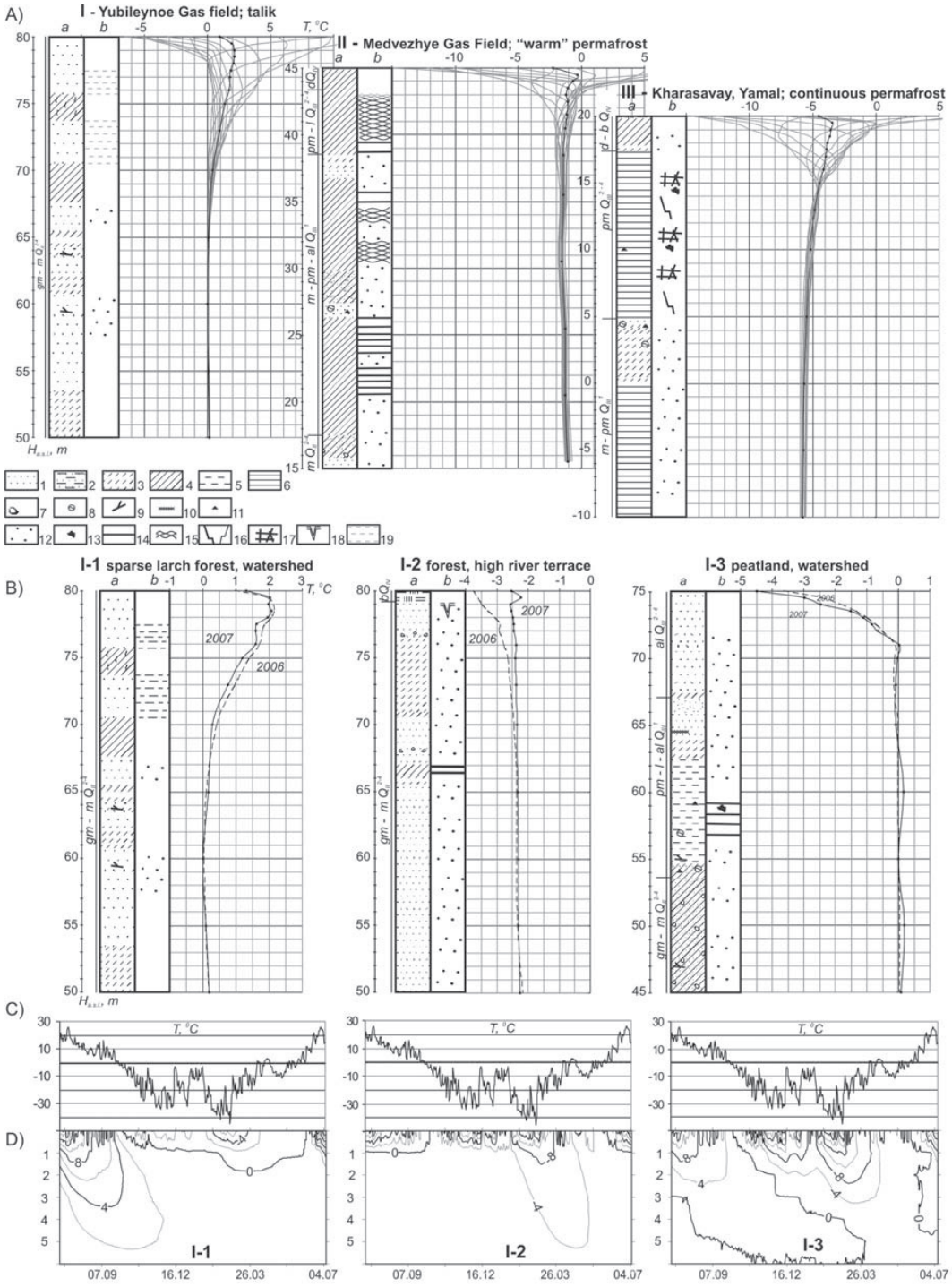

Figure 1. A: Mean annual (black line) and month (gray line) ground temperatures in Northern West Siberia; B: Changes in the mean annual ground temperatures at observatory I (Yubileynoe gas field) in 2006–2007; C: Mean daily air temperature at Novy Urengoy for 07.2006–07.2007; D: Active layer dynamics at observatory I in the different landscapes.
Lithology: 1-sand; 2-silty sand; 3-sandy-loam; 4-loam; 5-silt; 6-clay; 7-pebbles; 8-clayish fragments; 9-wooden remnants; 10-allochtonous peat; 11-carbonized organic debris. Cryostructure: 12-massive; 13-ice agglomerate; 14-layered; 15-reticulate; 16-vertical veins; 17-reticulate-blocky; 18-ice wedge; 19-water saturated soils.

References

Pavlov, A.V. 1994. Current changes of climate and permafrost in the Arctic and Sub-Arctic of Russia. *Permafrost and Periglacial Processes* 5: 101-110.

Pavlov, A.V. & Moskalenko, N.G. 2002. The thermal regime of soils in the north of Western Siberia. *Permafrost and Periglacial Processes* 13: 43-51.

Two-Dimensional Geoelectrical Monitoring in an Alpine Frozen Moraine

Christophe Lambiel
Institute of Geography, University of Lausanne, Switzerland
Ludovic Baron
Institute of Geophysics, University of Lausanne, Switzerland

Introduction

As defined by Haeberli (1979), push moraines are frozen sediments deformed by a glacier advance. In the Alps, push moraines are typically encountered in the margin of small glaciers, at altitudes comprised between 2500 and 3000 m a.s.l., in the belt of discontinuous permafrost (see e.g., Reynard et al. 2003, Delaloye 2004). In order to better know the internal structure and the ice content and repartition of this type of landform, a monitoring of the resistivity variation has been initiated on the Col des Gentianes push moraine (Swiss Alps).

Site Description and Methods

The Col des Gentianes moraine is located at 2900 m a.s.l., on the orographic left side of the Tortin glacier (Fig. 1). A cable car station for ski activity was built on the northern part of the moraine at the end of the 1970s. In October 2006, the road located between the building and the glacier was excavated for ski-run landscaping purposes. Massive ice layers were encountered at depths of 50 cm to 2 m. Congelation and sedimentary ice were present. Ground temperatures have been recorded in a 20 m deep borehole since November 2002 (Lambiel 2006). They attest the presence of permafrost conditions in the moraine, with temperatures of -0.5°C to -1°C between 5 and 20 m depth (Fig. 2).

Two-dimensional (2-D) resistivity imaging is an efficient tool to characterize permafrost extension in recently deglaciated glacier forefields (e.g., Marescot et al. 2003, Kneisel 2004). To provide information on both lateral and vertical variations of the resistivity and to monitor the temporal evolution of the resistivities in the Col des Gentianes moraine, a permanent 2-D electrical profile was installed on the upslope part of the road (Fig. 1). Two acquisitions were carried out on 13 August and on 23 October 2007 with the Wenner-Schlumberger configuration. Data were inversed with the software RES2DINV.

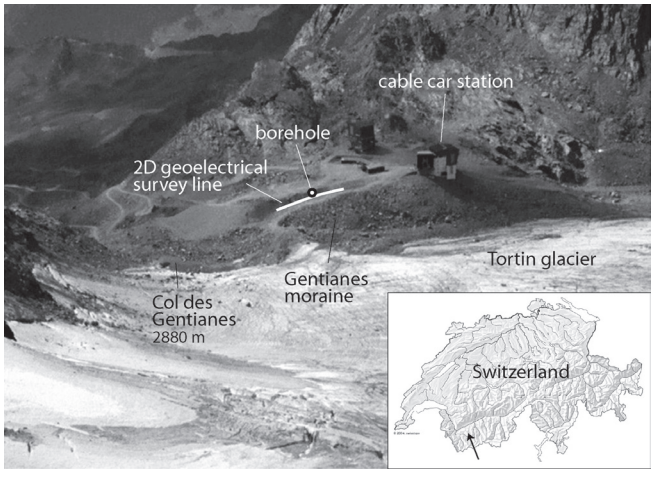

Figure 1. View of the Gentianes moraine with location of the borehole and of the 2-D geoelectrical survey line.

Results and Discussion

The first acquisition (13 Aug. 2007) reveals resistivities overall higher than 5 kΩm, with a clear increase towards the south (Fig. 3). Two lenses of higher resistivities (max. 150 kΩm) are clearly visible near the middle and in the south side of the profile. They probably correspond to massive ice lenses, like those which were observed in the excavation in October 2006. In the centre, resistivities are relatively low (<6 kΩm) below 10 m depth. However, the borehole, which is located near the center of the survey line, indicates negative temperatures throughout the first 20 m of the moraine. Thus, we can conclude that the frozen material is very little resistant in places. Such low resistivities may be explained by an increase of the specific surface. This implies that the deep layers would contain a high proportion of fine-grained sediments.

The second acquisition (23 Oct. 2007) shows a strong increase of the resistivities in the upper layers. The two resistant lenses are still visible, but the resistivities have been multiplied by 2 for the south lens and by 5 for the central one. In the northern half of the profile, at about 6 to 10 m depth, we can observe, on the contrary, a slight decrease of the resistivities.

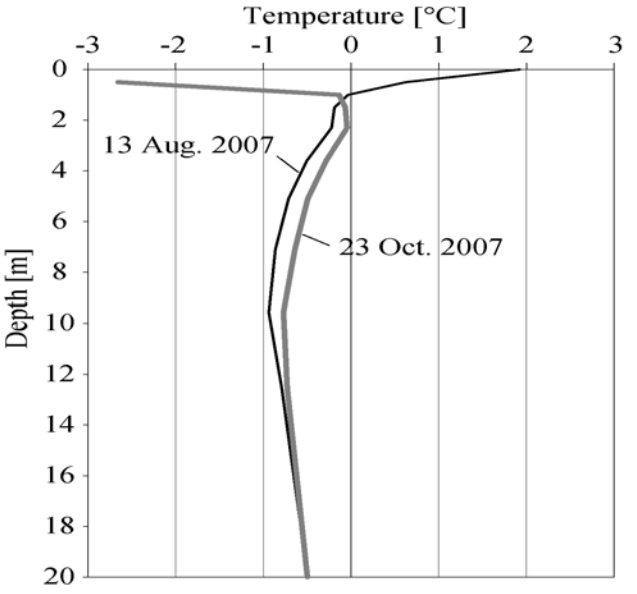

Figure 2. Thermal profiles of the moraine at the time of the two geoelectrical acquisitions.

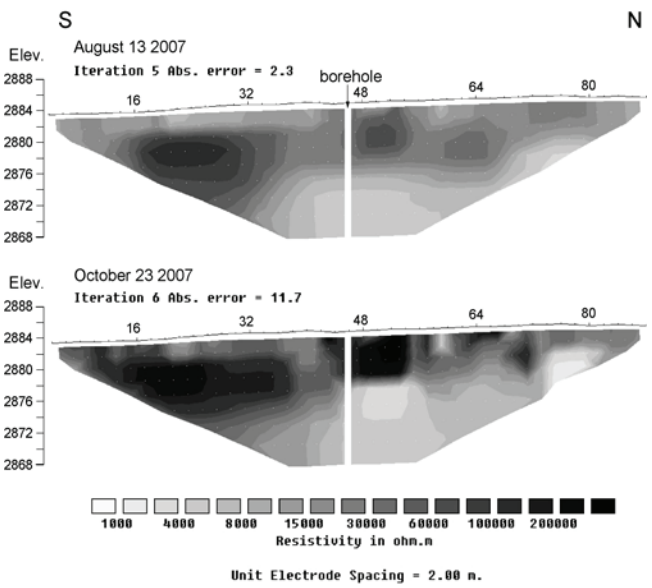

Figure 3. Two-dimensional resistivity profiles on 13 August and 23 October 2007 on the Col des Gentianes moraine.

Borehole data indicate warmer temperatures between 1 and 13 m depth in October than in August (Fig. 2). At the same time, we observe a strong increase in resistivities between the 2 acquisitions up to 6–10 m deep. Now, below 0°C, many studies reported that decreasing temperatures provoke increasing resistivities (e.g., Hauck 2001). Thus, the change in resistivities that we observe cannot be explained by a change in ground temperatures.

A hypothesis which could explain these different resistivities is the existence of 2 completely different climatic conditions during the 2 weeks preceding the 2 acquisitions. In August, the weather was very rainy, whereas October was dry and very cold at the acquisition time. As a consequence, the active layer was probably saturated with unfrozen water in August, whereas it was dry and frozen in October (Fig. 2). This led to higher resistivities at the subsurface. The strong increase in resistivities below the active layer is more difficult to understand, but we can assess that the difference in resistivity contact due to difference in surface humidity played an important role in the inversion process at greater depth.

According to the 2-D resistivity imaging, the ground stratigraphy is very heterogeneous. This is not surprising, insofar as a push moraine is often a complex landform incorporating, for instance, frozen sediments and sedimentary ice from the glacier. The presence of unfrozen lenses cannot then be excluded. Thus, it is possible that water could penetrate the deep layers during the rainy episode of August, which could have provoked lower resistivities.

Finally, the slight resistivity decrease at 6–10 m deep in the center of the profile may be explained by slight warming of the ground between the two acquisitions (Fig. 2).

Conclusion

The measurements show that the internal structure of the moraine is very heterogeneous. Massive ice lenses are probably present above 10 m depth. This assumption is supported by the observation of different ice types (sedimentary, congelation) in an excavation. An unexpected and strong increase in resistivities occurred in relatively deep layers between August and October. Totally different climatic conditions before the acquisitions and the influence of the first layer on the inversion process are probably the only way to explain such differences. However, further acquisitions and modeling of the first layer influence are necessary to validate this hypothesis.

References

Delaloye, R. 2004. *Contribution à l'étude du pergélisol de montagne en zone marginale*. Thèse. Fac. Sciences, Univ. Fribourg, Geofocus 10: 240 pp.

Haeberli, W. 1979. Holocene push-moraines in alpine permafrost. *Geografiska Annaler* 61A(1–2): 43-48.

Hauck, C. 2001. Geophysical methods for detecting permafrost in high mountains. *Mitteilungen der VAW, ETH Zürich,* 171.

Kneisel, C. 2004. New insights into mountain permafrost occurrence and characteristics in glacier forefields at high altitude through the application of 2-D resistivity imaging. *Permafrost and Periglacial Processes* 15: 221-227.

Lambiel, C. 2006. *Le pergélisol dans les terrains sédimentaires à forte déclivité: distribution, régime thermique et instabilités*. Thèse, Université de Lausanne, Institut de Géographie, coll. "Travaux et Recherches," n° 33: 260 pp.

Marescot, L., Loke, M.H., Chapellier, D., Delaloye, R., Lambiel, C. & Reynard, E. 2003. Assessing reliability of 2D resistivity imaging in mountain permafrost studies using the depth of investigation index method. *Near Surface Geophysics* 1: 57-67.

Reynard, E., Lambiel, C., Delaloye, R., Devaud, G., Baron, L., Chapellier, D., Marescot, L. & Monnet, R. 2003. Glacier/permafrost relationships in forefields of small glaciers (Swiss Alps). *Proceedings of the Eighth International Conference on Permafrost, Zürich, Switzerland, July 21–25, 2003*: 947-952.

Impacts of Small-Scale Surface Variations on the Energy Balance of Polygonal Tundra on Samoylov Island, Lena River Delta, Siberia

M. Langer
Alfred Wegener Institute for Polar and Marine Research, Potsdam, Germany
J. Boike
Alfred Wegener Institute for Polar and Marine Research, Potsdam, Germany
K. Piel
Alfred Wegener Institute for Polar and Marine Research, Potsdam, Germany
G. Stoof
Alfred Wegener Institute for Polar and Marine Research, Potsdam, Germany

Introduction

To quantify the magnitude of energy balance variations of a typical polygonal tundra system, two typical polygons at different succession stages were chosen for study. At each polygon site, surface characteristics were analyzed under the aspect of energy exchange processes. The focus rests upon the energy transfer processes due to the emission and absorption of radiation. The study is complemented through the analysis of soil heat fluxes and the corresponding thermal ground characteristics, such as soil heat capacity and conductivity.

Site Description

The investigated polygons have the following characteristics: The center of the first polygon consists of water-supersaturated peat. The groundwater level is at or just above the soil surface. The first polygon rim is elevated 10 cm above the water table. The uppermost soil layers consist of peat with high air content. The soil surface is covered by different moss types associated with dry conditions.

The polygonal crack is 10 cm wide and extends down to the ice wedge. The crack is filled with a combination of water and organic material of hydrophilic mosses.

The second polygonal rim consists of an elevated region and a lower transition zone towards the second polygon center. The soil in this elevated region still holds a considerable air fraction, but has an increased mineral fraction compared to the first polygonal rim. The transition zone shows increasing soil moisture toward the second polygon center. The second polygon center consists of water-saturated peat with the water table just underneath the ground surface. The second polygonal center is dominated by different hydrophilic mosses.

Methods

For detecting variations of the radiation balance, the investigated polygons were instrumented with a radiation scanner system bridging a 10 m transect. The scanner is capable of measuring reflected and emitted shortwave and longwave radiation at high spatial and temporal resolutions of 20 cm and 30 min, respectively.

The system consists of a photo pyranometer and an infrared sensor that were fixed on the scanner wagon 70 cm above the ground surface. An air temperature and relative humidity probe, as well as a photosynthetic active radiation sensor, were attached adjacent to the main sensors. Meteorological variables, such as incoming radiation, were measured at a climate tower located 5 m from the scanner system.

Soil heat fluxes were calculated based on temperature and moisture measurements directly beneath the soil surface at eight different locations along the scanner transect. Two-point temperature measurements were used for thermal diffusivity calculations based on a one-dimensional numerical solution of the heat transfer equation. Soil heat capacities were approximated based upon literature values of different soil types and soil moisture measurements.

Results

The scanner system directly provides surface temperatures and reflected solar radiation fluxes. By estimating surface emissivities, the surface temperatures can be transformed into emitted longwave radiation fluxes. The consistency of the data was controlled by comparing the spatial mean of the emitted and reflected radiation to the radiation measurements at the climate tower.

The scanner system was operated during periods of different weather conditions. The surface temperatures always varied significantly along the profile. At periods of high solar angles the surface temperatures of the dry rims are generally increased compared to the wet locations. During these time spans the polygonal rimes are about 5°C warmer than the wet polygonal centers. Less evident is the reverse situation that occurs during low sun positions, when the wet locations are slightly warmer than the dry polygonal rims. Observed temperature differences are about 3°C. The highest spatial temperature differences were observed during periods of clear sky conditions when radiative transfer is at a maximum.

The observed albedo values also display spatial variations corresponding to the different surface structures. The reflectivity at the rims is about 20% and about 15% at the polygonal centers. These observations are verified through spectrometer data. Instrumentation failures such as sensor

orientation may have strong effects on the measurements. These errors are magnified as measurements decrease in value. Therefore, reflectivity data at periods of low sun angles must be considered with caution. The approximated albedo values are based on midday observations, occurring around 12:00 (local time).

Soil heat flux measurements along the transect display marginal differences within the daily average. More significant are the differences in the diurnal heat flux amplitude, which varies about 10–20 W/m² among the particular locations. The polygonal centers and the crack display more pronounced heat flux amplitudes compared to the polygonal rims. This can be explained by differences in thermal diffusivity due to unlike soil moisture conditions. The varying heat capacities and conductivities lead to higher absorption and re-release of energy at the wet locations.

Discussion

The different surface temperatures indicate variations in the partition of the energy balance at the ground surface. This implies different contributions of sensible, latent, or ground heat fluxes. The results display only slight variations in ground heat fluxes among the different surface structures. Moreover, the comparatively small ground heat fluxes are of secondary importance within the complete energy balance. Thus, the energy partition at the ground surface primarily affects sensible and latent heat processes. Most likely at the dry polygon rims, more energy is available for sensible heat processes, while at the wet polygonal centers, the majority of radiation is consumed through the evapotranspiration process.

Non-Summer CO_2 Measurements Indicate Tundra Ecosystem Annual Net Source of Carbon Double Net Summer Sink

Cheryl Laskowski
San Diego State University, San Diego, CA, USA
George Burba
LiCor, Inc., Lincoln, NE, USA
Walter Oechel
San Diego State University, San Diego, CA, USA

Introduction

The Arctic tundra ecosystems are dominated by winter conditions, but data during the non-summer months is often lacking in Arctic annual carbon exchange estimates. The extreme conditions (temperatures regularly below freezing, low light levels, and snow-covered frozen ground) are often less than ideal for biological processes, and it has been largely assumed that little activity occurs under these conditions (McKane et al. 1997). While winter arctic conditions may not be ideal for high levels of photosynthesis and respiration, biological activity still occurs under snow and in subzero temperatures (Romanovsky & Osterkamp 2000, Sturm et al. 2005). Although there is substantial evidence showing the importance of non-summer periods to Arctic carbon metabolism, the difficulty of making ecosystem measurements under Arctic winter conditions means that estimates of carbon flux rates across the tundra are typically made based solely on summer (June–August) carbon flux data (Kwon et al. 2006, Vourlitis & Oechel 1999).

Annual estimates that ignore the non-summer period are likely to be largely in error with respect to the annual carbon balance (Oechel et al. 1997). Given that snowmelt is occurring earlier (Stone et al. 2002) and the growing season has lengthened (Chapman & Walsh 1993, Keyser et al. 2000), the traditional 10- to 12-week field campaign no longer encompasses even the full snow-free period. Prior attempts to predict annual carbon budgets based on winter field measurements have often lacked continuous monitoring throughout the year, relying on a few data points to model seasonal carbon estimates (Zimov et al. 1996, Oechel et al. 1997). Attempts at continuous monitoring (i.e., through the eddy covariance method) have had limited success while highlighting some of the major limitations. The limitations that have posed the greatest hindrance to continuous monitoring in the past are now diminishing, and include instrument icing (minimized by heaters), instrument operating limits (that have been recently modified to operate at very low temperatures), and mismatch between CO_2 flux estimates and ecological/biological theory (for which there is a new correction provided by Burba et al. 2006).

Methods

Direct and continuous measures of mass (water vapor and CO_2), momentum, and energy exchange were measured near the village of Atqasuk, Alaska, located 100 km south of Barrow, Alaska, during 2006. Net ecosystem exchange was measured using the open-path eddy covariance method and included an open-path infrared gas analyzer (IRGA, Li-7500, LiCor, Inc., Nebraska, USA) and ultrasonic anemometer (R3, Gill Instruments, Lymington, England).

Eddy covariance data were calculated in half-hour data series using the EdiRe program (University of Edinburgh, Edinburgh, England), and applying standard corrections for simultaneous latent and sensible heat measurements (Webb et al. 1980) and quality control techniques (AmeriFlux 2006). Data gaps were filled using techniques outlined in Falge et al. (2001) to represent seasonal/annual carbon exchange estimates. In addition, the data are corrected for an apparent-uptake signal due to heating of the air mass in the absorption path of the IRGA. The correction is modified from Burba et al. 2006, to account for non-vertical sensor mounting angle.

Results

Weather conditions during 2006 were typical of historic climate averages for Atqasuk, Alaska, with July as the warmest month of the year and March, the coldest month (air temperatures of 8.2°C and -29.8°C, respectively). Eddy covariance data availability varied greatly, from a low of 14% in February to a high of 80% in June. Average summer (June–August) data recovery was 71%, and data were primarily rejected due to precipitation events. Average non-summer (September–May) data recovery was 36%, and data loss was mainly due to icing events and conditions outside of the instruments' operating specifications.

Summer carbon flux data showed a distinct diurnal pattern characterized by a midday CO_2 drawdown and slight mid-night release, with the pattern being strongly temperature- and light-dependent. Non-summer diurnal patterns were not evident, due to the lack of intense solar radiation during much of the season.

Cumulative carbon exchange during the summer months resulted in a net uptake of 21.5 g C m^{-2}, whereas the cumulative non-summer carbon exchange showed a net loss of 53.5 g C m^{-2}. This resulted in an annual carbon release of 31.8 g C m^{-2} to the atmosphere (Fig. 1).

Discussion

The results show that non-summer season carbon exchange is not only significant, it can be of greater cumulative magnitude than summer carbon exchange—in this case,

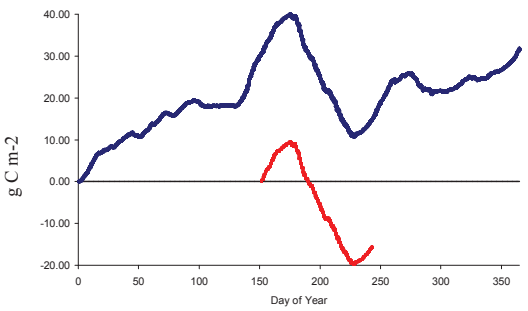

Figure 1. Cumulative carbon exchange for Atqasuk, Alaska, 2006, in g C m^{-2}. Line from day of year 0–365 represents the cumulative annual carbon exchange, while the line from day of year 152–243 (June–August) represents the summer-only cumulatie carbon exchange.

nearly 2.5 times the summer estimate. This also emphasizes the importance of year-round estimates in determining source versus sink activity. Capturing only summer-season carbon exchange would result in a net uptake of carbon rather than a net release. These results indicate that not only is winter carbon emission for tundra ecosystems important in annual carbon estimates, it dominates the annual signal, shifting the net carbon exchange from a sink to a source.

Disproportionately more data were rejected or lost in non-summer months, primarily due to instrument icing. This results in higher uncertainty of non-summer data compared to summer data. Reducing data loss by using heaters or increased site visits may lessen data loss. In addition, the correction factor (Burba et al. 2006) used in this study must be further tested to verify the accuracy of the correction parameters. These features are currently being implemented at this and other sites. However, these data are, to our knowledge, the first near-continuous carbon exchange data for Alaskan Arctic tundra, and provide evidence that not only is the non-summer season important, it may in fact be dominant over summer season net carbon exchange.

Acknowledgments

We would like thank D. Whiteman, R. Bryan, S. Delapena, N. Panzarini, A. Sharma, BASC, VPR, NSB, and NSF's Study of the Northern Alaskan Coastal System's research grant number 046177.

References

Burba, G.G., Anderson, D.J., Xu, L. & McDermitt, D.K. 2006. Additional term in the Webb-Pearman-Leuning correction due to surface heating from an open-path gas analyzer. *Eos Trans. AGU* 87(52), Fall Meet. Suppl., C12A-03.

Chapman, W.L. & Walsh, J.E. 1993. Recent variations of sea ice and air-temperature in high-latitudes. *Bulletin of the American Meteorological Society* 74(1): 33-47.

Falge, E. et al. 2001. Gap filling strategies for long term energy flux data sets. *Agricultural and Forest Meteorology* 107(1): 71-77.

Kappen, L. 1993. Plant activity under snow and ice, with particular reference to lichens. *Arctic* 46(4): 297-302.

Kwon, H.J. et al. 2006. Effects of climate variability on carbon sequestration among adjacent wet sedge tundra and moist tussock tundra ecosystems. *Journal of Geophysical Research-Biogeosciences* 111(G3).

McKane, R.B. et al. 1997. Climatic effects on tundra carbon storage inferred from experimental data and a model. *Ecology* 78(4): 1170-1187.

Oechel, W.C. et al. 1997. Cold season CO_2 emission from arctic soils. *Global Biogeochemical Cycles* 11(2): 163-172.

Romanovsky, V.E. & Osterkamp, T.E. 2000. Effects of unfrozen water on heat and mass transport processes in the active layer and permafrost. *Permafrost and Periglacial Processes* 11(3): 219-239.

Stone, R.S. et al. 2002. Earlier spring snowmelt in northern Alaska as an indicator of climate change. *Journal of Geophysical Research-Atmospheres* 107(D10).

Sturm, M. et al. 2005. Winter biological processes could help convert arctic tundra to shrubland. *Bioscience* 55(1): 17-26.

Vourlitis, G.L. & Oechel, W.C. 1999. Eddy covariance measurements of CO_2 and energy fluxes of an Alaskan tussock tundra ecosystem. *Ecology* 80(2): 686-701.

Webb, E.K. et al. 1980. Correction of flux measurements for density effects due to heat and water-vapor transfer. *Quarterly Journal of the Royal Meteorological Society* 106(447): 85-100.

Zimov, S.A. et al. 1996. Siberian CO_2 efflux in winter as a CO_2 source and cause of seasonality in atmospheric CO_2. *Climatic Change* 33(1): 111-120.

Accelerated Arctic Land Warming and Permafrost Degradation During Rapid Sea Ice Loss

David M. Lawrence
National Center for Atmospheric Research, Boulder, CO, USA
Andrew G. Slater
Cooperative Institute for Research in the Environmental Sciences, Boulder, CO, USA
Robert A. Tomas, Marika M. Holland, Clara Deser
National Center for Atmospheric Research, Boulder, CO, USA

Introduction

In September 2007, the annual minimum sea ice extent shattered the previous observational-record low. CRUTEM3 data indicate that 2007 August to October western Arctic land temperatures were the warmest of the last 30 years (+2.3°C warmer than the 1978 to 2006 average). The striking sea ice decline in 2007 raises the specter that a period of abrupt sea ice loss, such as those simulated in Community Climate System Model (CCSM3) 21st century A1B simulations (Holland et al. 2006), is a distinct possibility. Rapid sea ice loss events (RILEs) in CCSM3 typically last between 5 and 10 years and exhibit negative sea ice extent trends that are roughly 4 times larger than average simulated (or recently observed) trends.

Whether or not the 2007 sea ice record minimum is a precursor of a sustained period of rapid loss remains to be seen, but it provides motivation to assess the potential consequence for adjacent land climate. Here, we evaluate Arctic land temperature response to RILEs in CCSM3. We find that the secular 21st century land-warming trend is augmented by a factor of 3.5 during RILEs, which is likely to have adverse impacts on permafrost. Through idealized experiments with the Community Land Model (CLM), we assess the impact of a RILE and its timing on permafrost. The results presented here are excerpted from Lawrence et al. (2008).

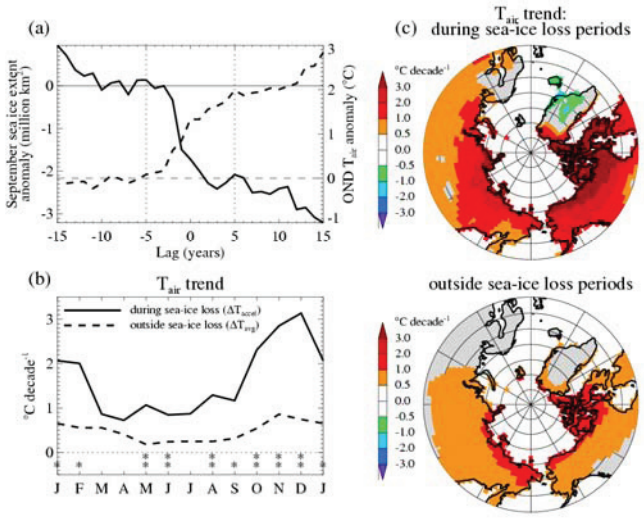

Figure 1. (a) Composite lagged time series of September sea ice extent (solid line) and OND T_{air} (dashed line) over Arctic land area (65°–80°N, 60°–300°E). Composites are centered around the mid-points of the nine rapid sea ice loss events seen in the CCSM3 A1B simulations. Results shown as anomalies from the average of years -10 to -5. (b) Average monthly Arctic land air temperature trends during rapid sea ice loss periods and outside sea ice loss periods. Trend is statistically significant at the 90% (*) and 95% (**) levels. (c) Maps of air temperature trends for OND during and outside abrupt sea ice loss periods.

Arctic Land Temperature Trends During Rapid Sea Ice Loss

Nine RILEs are identified across the eight-member CCSM3 A1B 21st century ensemble (Holland et al. 2006b). By computing a lagged composite of sea ice extent anomalies across the nine events, we form a picture of the typical sea ice extent trajectory during abrupt loss periods (Fig. 1a). A corresponding composite for western Arctic October to December (OND) land T_{air} shows an increase in warming during RILEs (Fig. 1a). Figure 1b shows the western Arctic linear T_{air} trend during and outside RILEs. Warming is accelerated during RILEs throughout most of the year with statistically significant increases in warming rates apparent in the summer and early autumn, likely due to increased open water area, as well as in late autumn and winter, when the thinner ice pack less efficiently insulates the atmosphere from the comparatively warm ocean water below. Accelerated warming spans most of the terrestrial western Arctic juxtaposed to the area of sea ice contraction in CCSM3. It is strongest along the Arctic coast where it is as high as 5°C decade^{-1} in the autumn, but a signal of enhanced warming can extend 1500 km inland (Fig. 1c). Annually averaged, the warming trend during RILEs is 3.5 times greater than outside these periods (1.60°C decade^{-1} versus 0.46°C decade^{-1}).

Impact of Accelerated Warming on Permafrost

To evaluate the impact of abrupt warming and its timing on permafrost, we construct four synthetic trend scenarios based on the results shown in Figure 1. We then use these scenarios to force a version of CLM (Oleson et al. 2004) that includes some improvements in permafrost dynamics, namely explicit representation of the thermal and hydrologic properties of organic soil (Lawrence & Slater 2007) and a 50 m soil column that represents thermal inertia provided by deep ground (Lawrence et al. 2008).

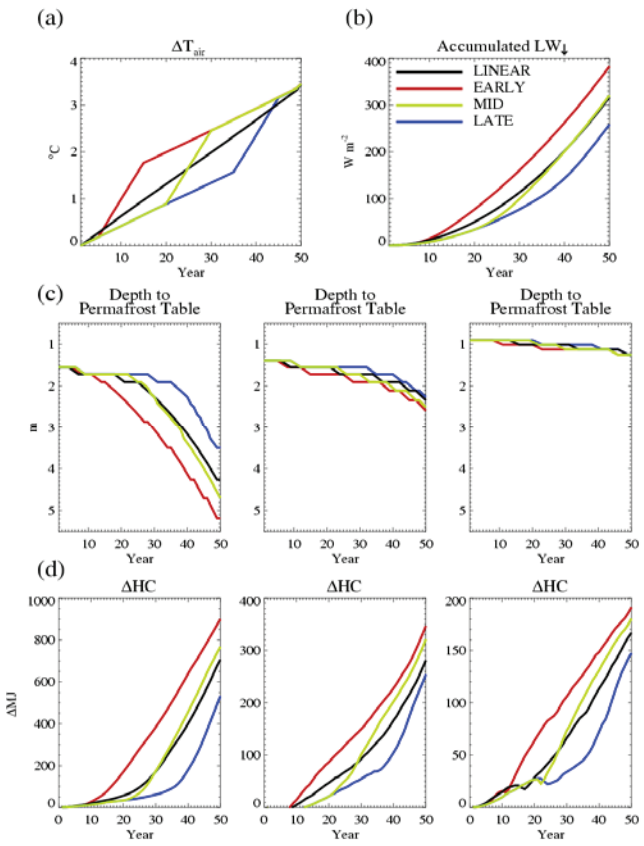

Figure 2. (a) Annual mean T_{air} anomaly time series for the four experiments. Note that monthly air temperature anomalies used in the forced experiments contain the annual cycle structure shown in Fig. 1c. (b) Accumulated LW↓ anomaly time series. (c) Depth to permafrost table (DPT). (d) Change in soil heat content (ΔSHC) for three different initial permafrost states; $\overline{T_{soil}(PT, y=1)}$ = -0.3°C, -1.5°C, and -5.8°C from left to right.

The impact of accelerated warming is shown for three illustrative ground conditions representing differing initial permafrost states (warm to cold) (Figs. 2c and 3d). These cases all exhibit minimal snow depth change (< 10%) over the 50-yr simulation. For initially cold permafrost, the timing of accelerated warming has little influence on the rate of active layer deepening. All four scenarios simulate an ~0.35m deepening of the active layer (Table 1). However, the soil heat content (SHC) gained in EARLY (191 MJ m^{-2}) is 30% larger than in LATE (147 MJ m^{-2}). The additional heat gained in EARLY corresponds to +0.41°C more warming over the 50 m column. The increase in heat accumulation preconditions permafrost for earlier and/or more rapid degradation under continued warming.

For warm permafrost, the timing of accelerated warming has a more dramatic influence. In all four scenarios, DPT increases slowly at first, but accelerates rapidly once a layer of perpetually unfrozen ground forms above the permafrost table (talik) at ~2 m depth. This occurs much sooner in EARLY with accelerated warming instigating talik formation by year 12. By year 50, the warm permafrost soil column in EARLY has absorbed 900 MJ m^{-2}, 68% more than LATE,

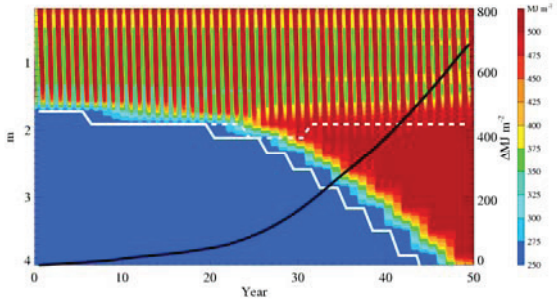

Figure 3. Time series of depth of warming (white solid line) and cooling (white dashed line) fronts from LINEAR experiment for warm permafrost case. Contours indicate SHC. Change in SHC is shown as black line.

and the DPT is 3.6 m deeper compared to only 1.9 m deeper in LATE. Why does talik formation coincide with a strong increase in SHC accumulation rates? Taliks form when the downwelling summer heating wave extends deeper than the corresponding winter cooling wave, thereby preventing the talik from refreezing in winter. Near isothermal soil layers at 0°C beneath the talik also limit cooling from below. At this point, with continued warming, heat accumulates at the maximum depth of the heating wave and permafrost degrades rapidly (Fig. 3).

References

Holland, M.M., Bitz, C.M. & Tremblay, B. 2006. Future abrupt reductions in the summer Arctic sea ice, *Geophys. Res. Lett*. 33: L23503, doi:10.1029/2006GL028024.

Lawrence, D.M., & Slater, A.G. 2007. Incorporating organic soil into a global climate model. *Clim. Dyn.*: doi:10.1007/s00382-007-0278-1.

Lawrence, D.M., Slater, A.G., Romanovsky, V.E. & Nicolsky, D.J. 2008. The sensitivity of a model projection of near-surface permafrost degradation to soil column depth and representation of soil organic matter. *JGR-Earth Surface* (in press).

Lawrence, D.M., Slater, A.G., Tomas, R.A., Holland, M.M. & Deser, C. 2008. Accelerated Arctic land warming and permafrost degradation during rapid sea ice loss. *Geophys. Res. Lett*. (submitted).

Oleson, K.W. et al. 2004. *Technical description of the Community Land Model (CLM)*. NCAR Tech. Note TN-461+STR, 174 pp.

The Sensitivity of a Model Projection of Near-Surface Permafrost Degradation to Soil Column Depth and Representation of Soil Organic Matter

David M. Lawrence
National Center for Atmospheric Research, Boulder, CO, USA
Andrew G. Slater
Cooperative Institute for Research in the Environmental Sciences, Boulder, CO, USA
Vladimir Romanovsky
University of Alaska Fairbanks, AK, USA
Dmitry Nicolsky
University of Alaska Fairbanks, AK, USA

Introduction

Coupled global climate models (GCMs) are advancing to the point that many of the biogeophysical, biogeochemical, and hydrological interactions and feedbacks that are directly or indirectly related to permafrost degradation are or will soon be captured. Here, we describe and analyze improvements in the depiction of permafrost in the Community Land Model (CLM), CLM is the global land-surface scheme that is included in the Community Climate System Model (CCSM). These improvements to CLM represent another step towards a more complete depiction of the integrated Arctic processes in a global modeling system.

In Lawrence and Slater (2005), we presented data from CCSM3 simulations indicating that the extent of near-surface permafrost may contract substantially during the 21st century as arctic temperatures soar. Here, we examine the sensitivity of these near-surface permafrost degradation projections to the incorporation of a deeper soil column and the explicit treatment of the thermal and hydrologic properties of soil organic matter. The results presented here are excerpted from our recently published study (Lawrence et al. 2008).

Model

CLM (for a detailed technical description see Oleson et al. 2004) can be run in both offline mode or as a component of CCSM. The land surface is represented by fractional coverage of lakes, wetland, bare soil, glacier, and up to four plant functional types (PFT) for each grid box. Processes simulated by CLM include heat transfer in soil and snow, hydrology of canopy, soil, and snow, and stomatal physiology and photosynthesis. Fluxes of energy and moisture are modeled independently for each surface type and aggregated before being passed to the atmosphere model. CLM3 includes a five-layer snow model which simulates processes such as accumulation, melt, compaction, snow aging, and water transfer across layers. Simulations with the standard version of CLM are referred to as CONTROL.

Organic soil

Nicolsky et al. (2007) show that accounting for the physical properties of soil organic matter significantly improves soil temperature simulations. In Lawrence and Slater (2007), we describe how organic soil and its impact on soil thermal and hydraulic properties can be implemented into CLM. Briefly, a geographically distributed and profiled soil carbon density dataset for CLM is derived by taking the gridded Global Soil Data Task soil carbon content dataset and distributing the carbon content for each grid box vertically through the CLM This dataset is then used to calculate the organic soil or mixed organic and mineral soil thermal and hydrologic properties for each soil layer. Simulations using this organic matter dataset along with the revised parameterizations are referred to as SOILCARB.

Deep soil

Alexeev et al. (2007) demonstrate that the depth of the bottom boundary condition strongly influences seasonal and longer time-scale soil temperature dynamics. Soil depths of greater than 30 m are preferred to reasonably simulate the annual cycle and decadal trends of subsurface temperatures. We test CLM with soil depths ranging from 25 m to 125 m by adding from 4 to 7 exponentially thicker layers to the original 10 level soil model. Experiments with a deep soil configuration (and organic matter) are referred to as SOILCARB_DS50 and SOILCARB_DS125.

Results

Figure 1 shows annual cycle-depth temperature plots for CONTROL, SOILCARB, and SOILCARB_DS50 compared to observed annual cycle-depth temperatures. The broad qualitative improvements in the simulation are immediately apparent. The active layer thickness (ALT), defined as the depth to which the soil thaws each summer, is much shallower in SOILCARB and SOILCARB_DS50, and its level is in much closer agreement with observations. Soil temperatures below the active layer are also improved, especially in SOILCARB_DS50, where the removal of the zero flux boundary at 3.5 m results in smaller and more realistic seasonal temperature variations at depths below 2 m.

We then force the improved CLM with 6-hourly data from a fully coupled CCSM3 20th and 21st century simulation. The resulting time series of near-surface permafrost extent are shown in Figure 2 for the CONTROL, SOILCARB, SOILCARB_DS50, and SOILCARB_DS125 experiments.

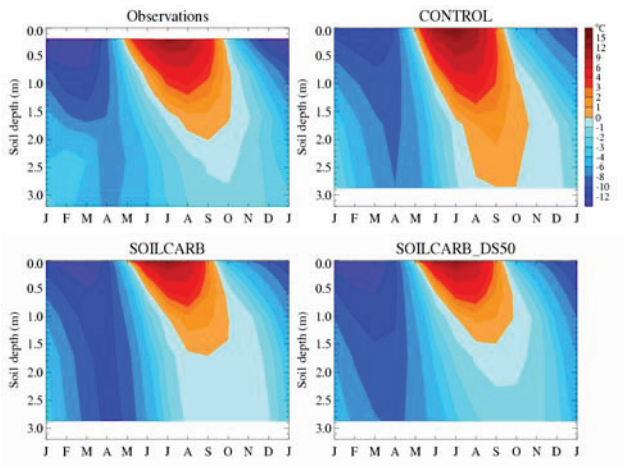

Figure 1. Annual cycle-depth plots of soil temperature averaged for selected stations in Russian soil temperature dataset (Zhang et al. 2001). Stations include those that exhibit perpetually frozen soil in top 3 m. Equivalent locations extracted and averaged over the same time period from offline CLM simulations forced with observed data.

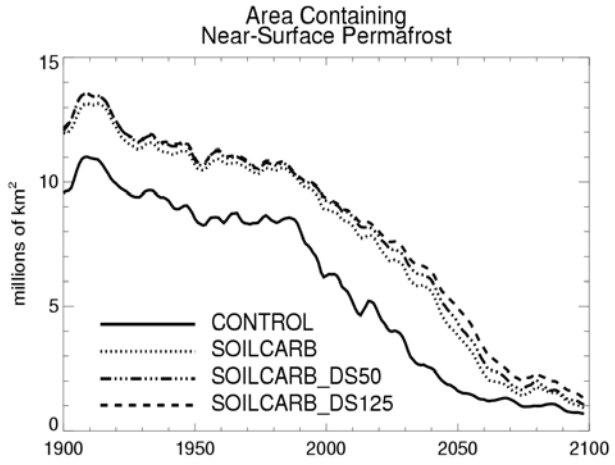

Figure 2. Time series of total area containing near-surface permafrost (north of 45°N and excluding ground underneath glaciers) for selected experiments.

$CONTROL_{CCSM3}$ and $CONTROL_{CLM3}$ are not shown for the sake of clarity, but lie roughly in between the curves for CONTROL and SOILCARB. As noted above, experiments that include soil organic matter are substantially cooler, and near-surface permafrost extent is correspondingly broader. The observed estimates for the area of continuous permafrost (90–100% coverage) and discontinuous permafrost (50–90% coverage) combined are 11.2–13.5 million km^2 (for the region poleward of 45°N (Zhang et al. 2000). The total area simulated in CONTROL is clearly biased low at 8.5 million km^2. In the organic soil and deeper soil column experiments, the area with near-surface permafrost increases to 10.5 and 10.7 million km^2, respectively, which compares reasonably with the observed permafrost extent although still biased a little low.

The rate of near-surface permafrost extent contraction is slower between 1990 and 2040 in SOILCARB (87,000 km^2 yr^{-1} versus 111,000 km^2 yr^{-1} in SOILCARB and CONTROL, respectively). In simulations with a deeper soil column, the average rate of loss decreases further to 81,000 km^2 yr^{-1} and 76,000 km^2 yr^{-1} (1990–2040) in SOILCARB_DS50 and SOILCARB_DS125. However, even though near-surface permafrost degrades at a slower rate in the latter three experiments, the total degradation by 2100 is almost as extensive as that seen in CONTROL.

Although much of the simulated near-surface permafrost degrades in all experiments, it should be stressed that this does not mean that all permafrost disappears. As noted above, each grid box is represented by a single soil column which means that sporadic and isolated permafrost cannot be explicitly detected in the model. For regions where the maximum soil temperature rises above 0°C, but only marginally, it can be assumed that sporadic or isolated patches of permafrost would still be present in the warmer climate. Additionally, for the deep soil experiments, we find that most of the deep permafrost remains at the end of the 21st century.

References

Alexeev, V.A., Nicolsky, D.J., Romanovsky, V.E. & Lawrence, D.M. 2007. An evaluation of deep soil configurations in the CLM3 for improved representation of permafrost. *Geophys. Res. Lett.* 34: L09502, doi:10.1029/2007GL029536.

Lawrence, D.M. & Slater, A.G. 2005. A projection of severe near-surface permafrost degradation during the 21st century. *Geophys. Res. Lett.* 24: L24401, doi:10.1029/2005GL025080.

Lawrence, D.M. & Slater A.G. 2007. Incorporating organic soil into a global climate model, *Clim. Dyn.* doi:10.1007/s00382-007-0278-1.

Lawrence, D.M., Slater, A.G., Romanovsky, V.E. & Nicolsky, D.J. 2008. The sensitivity of a model projection of near-surface permafrost degradation to soil column depth and representation of soil organic matter. *JGR-Earth Surface* (in press).

Nicolsky, D.J., Romanovsky, V.E., Alexeev, V.A. & Lawrence, D.M. 2007. Improved modeling of permafrost dynamics in a GCM land-surface scheme, *Geophys. Res. Lett*. 34: L08501, doi:10.1029/2007GL029525.

Oleson, K.W. et al. 2004. *Technical description of the Community Land Model (CLM)*. NCAR Tech. Note TN-461+STR, 174 pp.

The Influence of Snowdrift on the Geothermal Field of Permafrost: Results from Three-Dimensional Numerical Simulations at a Local Scale

Anne-Marie LeBlanc
Centre d'études nordiques, Université Laval, Québec (QC), Canada
Richard Fortier
Centre d'études nordiques, Université Laval, Québec (QC), Canada
Michel Allard
Centre d'études nordiques, Université Laval, Québec (QC), Canada
René Therrien
Département de géologie et de génie géologique, Université Laval, Québec (QC), Canada

Introduction

Three-dimensional (3-D) numerical simulations of the thermal regime of permafrost were carried out to study the effect of thermal insulation of snow and the impacts of climate warming on the permafrost evolution. The thermal regime of permafrost is closely related to not only the climate variability but also the surface conditions controlling the heat exchange between the ground and the air. Among the parameters affecting the surface conditions, the snow cover is probably the most important because it is recognized as a good thermal insulator preventing the ground cooling in winter (Goodrich 1982). The spatial distribution of snow at a local scale depends on the snow falls, prevailing winds, vegetation, changes in topography, obstacles, and snow removal. While open areas prone to strong winds are characterized by thin snow cover, snowdrifts form in the areas protected from the wind transport and erosion such as depressions, thick embankments, and tall infrastructures. Since the spatial distribution of snowdrifts is highly variable at a local scale, the influence of snowdrifts on the geothermal field of permafrost only can be modeled using 3-D numerical simulation.

Study Site

The Inuit community of Salluit (62°12′N, 75°40′W) is located in the continuous permafrost zone along the southern shore of Hudson Strait, in Nunavik, Canada. The village lies in a valley, and most infrastructures are built on ice-rich marine sediments.

3-D Numerical Simulation

A 3-D finite-element heat conduction model taking into account the phase change was developed to predict the geothermal field of permafrost in the valley of Salluit. The Quaternary deposits and permafrost conditions in the valley were mapped at a scale of 1:2000. These deposits were then divided into 52 vertical layers, with layer thickness increasing from 0.2 m near the surface up to 5 m at a depth of 100 m. The element side varied from 2 to 50 m according to the dimensions of the surface conditions to be simulated. Thermal properties were then given at each voxel of the 3-D model according to the previous mapping. The lower boundary condition at a depth of 100 m corresponded to the geothermal heat flux of 0.03 W/m^2 measured in a deep borehole in the Katinniq plateau, 150 km southeast of Salluit. The complex heat transfer function between the air and the ground was simulated using simultaneous recordings of air and ground surface temperatures at various locations in the valley during two consecutive years. Mean monthly air temperatures from the Canadian Regional Climate Model (Music & Caya 2007) were used to drive the simulations from 1961 to 2100 according to the SRES A2 scenario (IPCC 2000).

Results

Figure 1 shows the predicted mean monthly ground surface temperatures (MMGST) beneath a snowdrift from October 2002 to September 2003 in close match with the observed MMGST at the same location over the same period. The predicted MMGST at this location for the year 2099–2100 is also given in Figure 1. According to SRES A2 scenario, the increase in air temperature of 6ºC over one century, from 2002–2003 to 2099–2100, will shorten the winter period of at least two months. The ground surface will be still snow free in October 2099, and the snowmelt will take place in May 2100; one month earlier than in 2003. The method for predicting the MMGST was based on the assumption that there is no interannual variability in snow thickness and spatial distribution of snow. In the case of a windy environment such as Salluit, this assumption is valid. Even if the variation in snow height was not simulated, the long-term modification in MMGST is similar to the results of the SNOWPACK model presented in Luetschg et al. (2003).

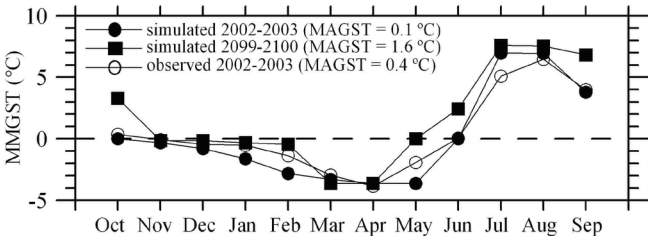

Figure 1. Observed and simulated mean monthly ground surface temperatures (MMGST) beneath a snowdrift.

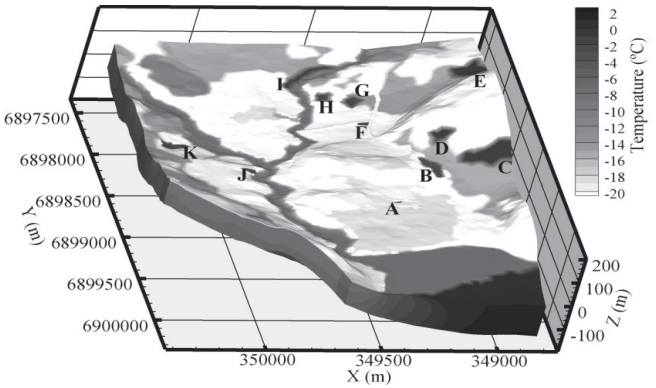

Figure 2. 3-D geothermal model. Snowdrifts *A* to *K*.

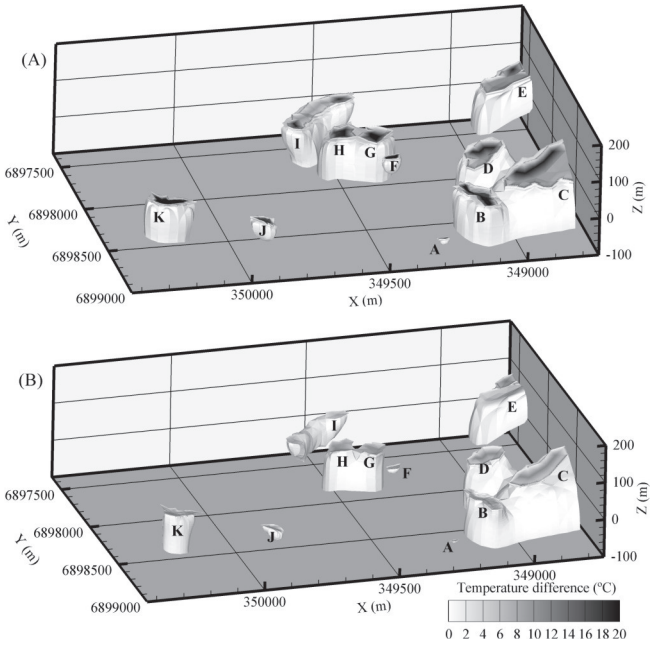

Figure 3. Ground temperature difference between the simulations with snowdrift surface conditions and the bare surface: (A) In January 2005; (B) In January 2100.

The 3-D geothermal model for the month of January 2005 in the valley of Salluit is shown in Figure 2. Among the snowdrifts mapped in the valley, 11 were integrated in the model. They are identified with letters from A to K in Figure 2.

Several numerical simulations were performed for assessing the thermal effect of snowdrifts. The ground temperature difference between the simulations integrating the snowdrift surface conditions and without integrating these conditions is shown in Figures 3a and 3b in January 2005 and 2100, respectively. Ground temperature differences below the cutoff value of 0.5 C are not shown. In 2005, the thermal effect of snow insulation on ground temperatures can reach depths as high as 100 m except for the snowdrifts *A* (16 m), *F* (42 m) and *J* (56 m). The surface area of snowdrift *A* is small, restricting the depth of snow influence on ground temperatures. For similar snowdrift surface area, till and sand transmit the heat more efficiently than clay due to their higher thermal conductivity and their lower water content. The thermal effect of snow on ground temperatures

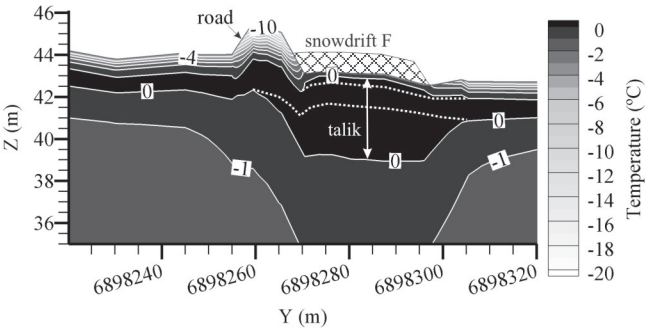

Figure 4. 2-D section of predicted ground temperatures underneath a road embankment and a thick snowdrift in January 2100. The dotted lines are the ground temperatures for a thin snow cover.

is limited, therefore, under the snowdrifts *F* and *J* compared to snowdrift *H* (Fig. 3a) due to the difference in soil types. In 2100, the climate warming will lead to a reduction in temperature difference at the surface: 10°C (Fig. 3b) instead of 20°C (Fig. 3a). The ground volume affected by the snowdrifts will also decrease. In a context of climate warming, the ground temperatures affected by a thin snow cover or under bare surface conditions will increase faster than the ground temperatures beneath snowdrifts.

A 2-D section of predicted ground temperatures underneath a road embankment and a thick snowdrift lying on the right embankment shoulder is shown in Figure 4 to illustrate the major thermal effect of snowdrift. A 4 m thick talik is present beneath the snowdrift, while the talik is only 1 m when considering a thin snow cover (dotted lines). The thermal effect of the snowdrift propagates also underneath the road embankment, inducing a ground warming. However, no attempt was made to take into account the water migration at shallow depths and to accommodate thaw settlement. These two factors can influence the geothermal field of permafrost.

References

Goodrich, L.E. 1982. The influence of snow cover on the ground thermal regime. *Canadian Geotechnical Journal* 19: 421-432.

IPCC 2000. *Special Report on Emission Scenarios*. N. Nakicenovic & R. Swart (eds.). UK: Cambridge University Press, 570 pp.

Luetschg, M., Bartelt, P., Lehning, M. & Toeckli, V. 2003. Numerical simulation of the interaction processes between snow cover and alpine permafrost. *Proceedings of the Eighth International Conference on Permafrost*, *Zurich, Switzerland*: 697-702.

Music, B. & Caya, D. 2007. Evaluation of the hydrological cycle over the Mississippi river basin as simulated by the Canadian Regional Climate Model. *Journal of Hydrometeorology* 8(5): 969-988.

Spatial Variation in CO_2 Release from Arctic Tundra as a Result of Permafrost Thawing and Thermokarst Development

Hanna Lee
Department of Botany, University of Florida, Gainesville, FL 32601-8526, USA
Edward A.G. Schuur
Department of Botany, University of Florida, Gainesville, FL 32601-8526, USA
Jason G. Vogel
Department of Botany, University of Florida, Gainesville, FL 32601-8526, USA

Introduction

One of the biggest potential feedbacks to global climate change from high latitude ecosystems may come from thawing of permafrost, which stores 30% of the total global terrestrial soil organic carbon (SOC) (Gorham 1991). Permafrost thawing may accelerate decomposition of soil organic matter (SOM) and increase carbon dioxide (CO_2) emissions, which could lead to further climatic warming (Oechel et al. 2000). In particular, thermokarst formation in response to permafrost thawing could change C cycling in high latitude ecosystems beyond simple increases in temperature because it has unique effects on soil conditions.

When permafrost thaws and drains in ice-rich areas, it creates localized surface subsidence called thermokarst (Jorgenson et al. 2001). The changes in the ground surface topography can induce variations in soil properties such as soil temperature, moisture content, and nutrient availability (Chapin et al. 2000). Our objective was to determine how permafrost thawing and thermokarst development affect SOM decomposition and ecosystem C exchange. We hypothesized that there will be a positive relationship between the degree of ground subsidence and CO_2 emissions from SOM.

Materials and Methods

Field site

This study was established at the Eight Mile Lake (EML) tundra site located 5 miles outside of Denali National Park. Previous work by Osterkamp and Romanovsky (1999) monitored deep soil temperatures at this site to 27 m belowground for the previous two decades and observed increased permafrost temperatures and thermokarst development (Osterkamp 2007).

Three sites were established at EML as an observational natural gradient study based on the degree of thermokarst development. The observed gradient was divided into three categories: Minimal Thaw, where typical tussock tundra appears least disturbed; Moderate Thaw, where thermokarst development started about 20 years ago; and Severe Thaw, where there were significant surface depressions. Based on 1951 aerial photographs, thermokarst development at Severe Thaw was estimated to be present for at least 50 years (Schuur et al. 2007).

Defining microtopography

We defined the degrees and patterns of depression created by thermokarst using a topographic survey. Twelve transects were established within a 50 m × 50 m plot at each of the three sites, and 600 (±50) points were surveyed. The major independent variable was elevation representing variation in microtopography created by thermokarst; lower surfaces represent subsidence by thermokarst development.

Establishing the plots

A 50 × 25 m subplot was established within the surveyed area at each site. In each plot, 50 equally spaced points were selected and surveyed again with a fine-scale GPS (Trimble 5700) unit within the plot to relate microtopography to soil temperature, moisture, active layer thickness, ecosystem respiration, and photosynthesis.

Soil properties

Soil temperature, volumetric water content (VWC), and active layer thickness were measured across the sites. A handheld soil temperature probe was used to measure soil temperature at 10, 20, and 30 cm during the growing season. VWC was measured at 10 and 20 cm belowground using a soil moisture reflectometer (Campbell Scientific CS616), and a 1/8 inch rod was used as a depth probe to measure active layer thickness.

Carbon emissions

CO_2 flux was quantified 4 times during the summer of 2006 and 2007 at the peak of the growing season to measure net ecosystem exchange of carbon using an IRGA (infrared gas analyzer, LiCOR820) attached to a 40 × 40 × 40 cm plastic chamber. Both dark CO_2 chamber measurement and light measurement were taken covered with a reflecting cloth, completely intercepting light and uncovering the chamber. Dark measurements estimate the rate of carbon emissions from ecosystem respiration, whereas light measurements estimate carbon emissions from ecosystem respiration as well as carbon uptake by photosynthesis. Differences between light and dark measurement served as an estimate of photosynthesis.

Analyses

To compare the effects of microtopography among sites, the plot level elevations were normalized to relative values within each site and semivariograms and correlograms were calculated to mathematically define the surface structure. A multiple regression with stepwise selection was used to obtain the best relationship between microtopography and measured soil and ecosystem properties.

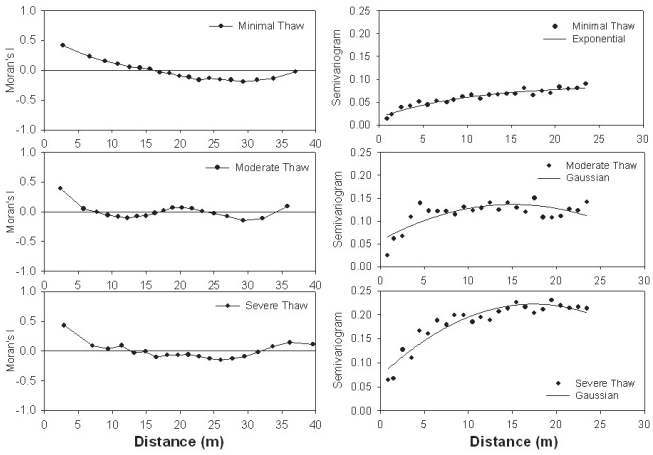

Figure 1. Semivariogram and correlogram of microtopography of the three sites in EML. Semivariograms show autocorrelation of microtopography as a function of distance. Minimal Thaw site has homogeneous surface; Moderate Thaw site has patchy depression within the thermokarst; and Severe Thaw site has large scale depression and is heterogeneous.

Results

Microtopographic patterns

Our semivariogram and correlogram results show that Minimal Thaw site has the most uniform surface pattern of all 3 sites. There are patchy depressions within Moderate Thaw site, while Severe Thaw site shows large-scale heterogeneous depressions that are not autocorrelated over 15 m (Fig. 1).

Soil properties

All of the measured soil properties were significantly correlated to topographic patterns, except for soil temperature due to a measurement error. Among the soil property measurements, VWC showed the strongest relationship with topographic patterns ($p < 0.008$) for all three sites, implying that soil moisture conditions changed the most due to thermokarst development (Table 1).

Carbon emissions

Multiple regression analyses (Fig. 2) showed a negative correlation between ecosystem respiration and micro-topography at Severe and Minimal Thaw sites. Among the environmental variables, the best predictor variable for ecosystem C exchange was VWC from changes in soil properties.

Conclusions

Changes in microtopography created by thermokarst development alter soil properties, especially soil moisture content by redistributing water when the ground surface subsides. Subsided areas showed higher CO_2 emissions; therefore, we suggest thermokarst development may stimulate CO_2 emissions in high latitude ecosystems.

Table 1. Probability of each significant variable in a stepwise regression at each site.

Site	Variables	Step	Sig. Prob.
Minimal Thaw	VWC20cm	1	0.0000
	VWC10cm	2	0.0683
Moderate Thaw	Active Layer	1	0.0000
	VWC20cm	2	0.0000
Severe Thaw	Active Layer	1	0.0000
	VWC10cm	2	0.0008

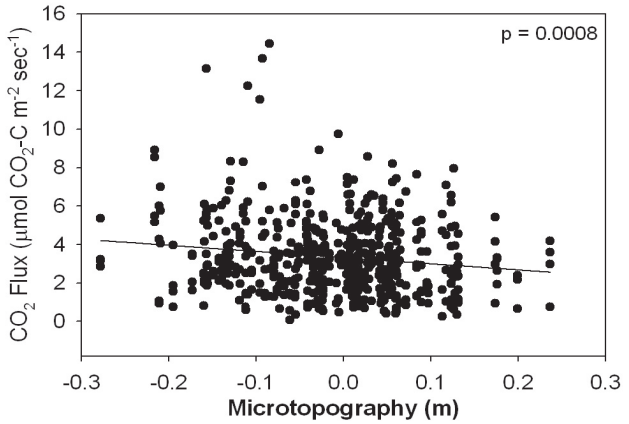

Figure 2. Relationship between microtopography and ecosystem respiration measured using dark CO_2 chamber.

Acknowledgments

We thank C. Staudhammer and M. Lavoie for advice on spatial analysis; UNAVCO for Trimble rental and training. This research was funded by NSF grant DEB-0516326 awarded to EAGS.

References

Chapin III, F.S. et al. 2000. Arctic and boreal ecosystems of western North America as components of the climate system. *Global Change Biology* 6: 211-223.

Gorham, E. 1991. Northern peatlands: Role in the carbon cycle and probable responses to climatic warming. *Ecological Applications* 1: 182-195.

Jorgenson, M.T., Racine, C.H., Walters, J.C. & Osterkamp, T.E. 2001. Permafrost degradation and ecological changes associated with a warming climate in central Alaska. *Climate Change* 48: 551-579.

Oechel, W.C. et al. 2000. Acclimation of ecosystem CO_2 exchange in the Alaskan Arctic in response to decadal climate warming. *Nature* 406: 978-981.

Osterkamp, T.E. & Romanovsky, V.E. 1999. Evidence for warming and thawing of discontinuous permafrost in Alaska. *Permafrost and Periglac. Process* 10: 17-37.

Osterkamp, T.E. 2007. Characteristics of the recent warming of permafrost in Alaska. *Journal of Geophysical Research* 112: F02S02, DOI: 10.1029.

Schuur, E.A.G., Crummer, K.G., Vogel, J.G. & Mack, M.C. 2007. Plant species composition and productivity following permafrost thaw and thermokarst in Alaskan tundra. *Ecosystems* 10: 280-292.

Soil Structural Change Effects on Greenhouse Gas Production and Carbon Loss in Thawing Soils

G.A. Lehrsch
USDA-ARS Northwest Irrigation & Soils Research Laboratory, Kimberly, ID, USA
R.S. Dungan
USDA-ARS Northwest Irrigation & Soils Research Laboratory, Kimberly, ID, USA

Introduction

Freezing alters soil structure, affects microbial populations and activities, increases the emission of greenhouse gases (GHG) such as CO_2 and N_2O, and redistributes the soil solution and its constituents within soil profiles. None of these processes are well characterized, being affected in various ways by the interacting effects of numerous factors, including initial soil water content, freezing rate, and number of freeze-thaw cycles (FTC) experienced (Lehrsch 1998, Lehrsch et al. 1991). As a soil freezes, its soil water is redistributed, at times and in places strengthening aggregates and elsewhere fracturing them. Increases in aggregate stability are thought to be due to clay accumulation or to the precipitation, at particle contact points within aggregates, of soil solution constituents, such as Ca^{2+} or soluble silica (Lehrsch et al. 1991). Experimental evidence for such processes, however, is lacking. Moreover, aggregate breakdown could release soluble organic C (SOC). Increased SOC concentrations in the soil solution, upon thawing, may spur localized microbial activity, increasing GHG emissions. The extent and speed with which soil water is redistributed determines whether these processes will occur and, if so, their extent and significance. The exposing of new fracture surfaces from broken aggregates may increase N_2O flux, since there may then be more nitrogen in the soil solution and more substrate available to support microbial denitrification (Sehy et al. 2004). Since wintertime losses of N_2O from agricultural soils can be 2 to 4 times as great as summertime losses, the study of physicochemical and microbial processes affecting wintertime N_2O flux are critically needed to assess global N_2O budgets (van Bochove et al. 2000). As active layer or seasonally frozen soils thaw, greenhouse gases are emitted but little is known about the effects of freezing-induced soil structural changes upon in situ microbial production of CO_2 and N_2O. Thus, in the laboratory, we characterized the effects of organic carbon, soil water content, and FTC on aggregate stability and the emissions of CO_2 and N_2O from thawing soils.

Methods and Materials

We studied three lots of Portneuf silt loam (Durinodic Xeric Haplocalcid) collected from the 0 to 0.15 m depth of a field site (42°31′N, 114°22′W) located about 2.1 km southwest of Kimberly, Idaho, USA, on 3 October 2007. One lot (hereafter referred to as soil with aged manure) had received about 35 Mg ha^{-1} (dry weight) of dairy manure each spring for 2 y prior to sampling, one lot 35 Mg ha^{-1} of fresh manure at study initiation, and one lot no manure. The Portneuf's Ap horizon contained about 560 g silt kg^{-1}, 220 g clay kg^{-1}, and where no manure had been added, about 9.3 g kg^{-1} of organic carbon (C). When collected, the Portneuf's aggregate stability was about 88%. Field-moist soil (water content of 0.07 kg kg^{-1}) passing an 8 mm sieve was packed to a dry bulk density of 1.15 Mg m^{-3} into 97 mm diameter, 0.13 m long plastic cylinders then, at a temperature of +2° C, slowly wetted to saturation and thereafter drained by tension to a matric potential of -5 or -10 kPa (approximate water contents of 0.48 and 0.37 m^3 m^{-3}, respectively). The packed cylinders, insulated using extruded foam to ensure freezing downward from the surface, in an environmental chamber were then subjected to 0, 1, 2, or 4 FTC, each of which consisted of slow freezing at -7°C for 72 h, then thawing at +2°C for 72 h. The 0, 1, 2, and 4 FTC were chosen for study because (1) the greatest microbial effects occur with the first few cycles, and (2) important structural changes occur with the first few cycles (Lehrsch 1998). The unfrozen controls (0 FTC) were held at +2° C for the entire period of all FTC. A calibrated, infrared photoacoustic detector (Field Gas-Monitor Model 1412, Innova™ AirTech Instruments, Ballerup, Denmark) was used to simultaneously measure CO_2 and N_2O concentrations, after correction for water vapor, in gas samples collected every 8 to 12 h from the 560 ml headspace of intact but thawing cores in sealed containers held at 2, 10, 20, or 30°C for 72 h in an environmental chamber. After each sample had been frozen for the last time but not yet thawed, it was removed from the cylinder and sectioned into 20 to 25 mm thick layers. After each layer was split longitudinally, water content and aggregate stability were measured on one half, and CO_2 and N_2O emitted from the other half using the photoacoustic detector as the soil thawed in a sealed container at 2, 10, 20, or 30°C for 72 h. Before measuring aggregate stability, the frozen soil was thawed at +2°C for 72 h. Thereafter, aggregate stability was measured by wet sieving 1 to 4 mm aggregates in deionized water for 180 s.

Results and Discussion

Soil water and soil structure

Preliminary data revealed that relatively slow freezing at -7°C redistributed the water in the relatively wet soil core (Fig. 1A). Due primarily to thermal potential gradients, water flowed from the 33 mm depth to the 10 mm depth. Compared to the water content at 33 mm, the water content at 10 mm increased about 19%, to a water content of about 0.44 m^3 m^{-3}

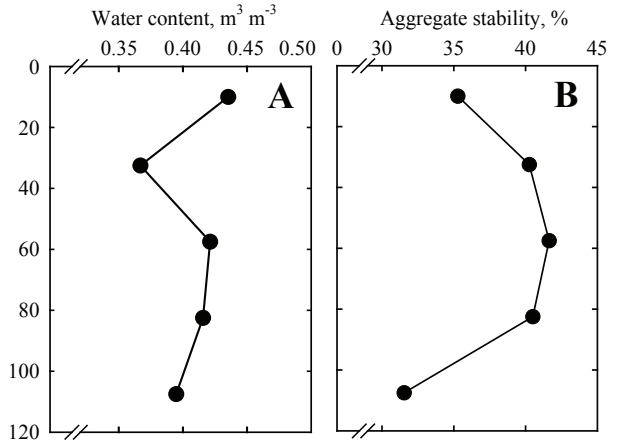

Figure 1. Soil water contents and aggregate stability in a relatively wet core of Portneuf silt loam after freezing at -7°C.

(Fig. 1A). There was little change in water content below 58 mm. Lehrsch et al. (1991) found that water content of 0.34 m^3 m^{-3} in Portneuf silt loam was sufficient to decrease its aggregate stability when it was frozen, then thawed. In this study, at water content nearly one-third greater, structural changes will occur.

Indeed, soil structure near the surface reflected the oft-observed inverse relationship between water content and aggregate stability after freezing (Fig. 1B) (Lehrsch et al. 1991). As water content decreased with depth, aggregate stability increased from 35% at the 10 mm depth to 40% at the 33 mm depth, a 1.14-fold increase. In the middle of the core, however, aggregate stability changed little. The relatively low aggregate stability near the bottom of the core may have been a consequence of difficulty experienced when dissecting the core prior to analysis.

CO_2 and N_2O emissions

Preliminary data revealed that both CO_2 and N_2O concentrations measured in the headspace above intact soil cores increased with time as once-frozen soil containing aged manure thawed at +2°C (Fig. 2). CO_2 concentrations increased by about 200 ppmv (37% greater than ambient) in the first 30 h after air temperatures in the environmental chamber were increased from -7 to +2°C. For subsequent FTC and thawing temperatures of +2°C, CO_2 emissions from intact cores may not be as great. The C pool that provides the substrate for microbial production of CO_2 as repeatedly frozen soils thaw is apparently limited in size, since Herrmann and Witter (2002) found that most CO_2 was produced in the first 4 FTC. Data in Figure 2 also reveal that N_2O concentrations after one incidence of freezing increased by about 5.7 ppmv (more than eight times greater than ambient) in the first 30 h after thawing began. The concentration of CO_2 peaked about 24 h, and N_2O peaked about 26 h after the temperature was increased (Fig. 2). Lysed microbial cells may have provided substrate for microbial denitrification (Sehy et al. 2004).

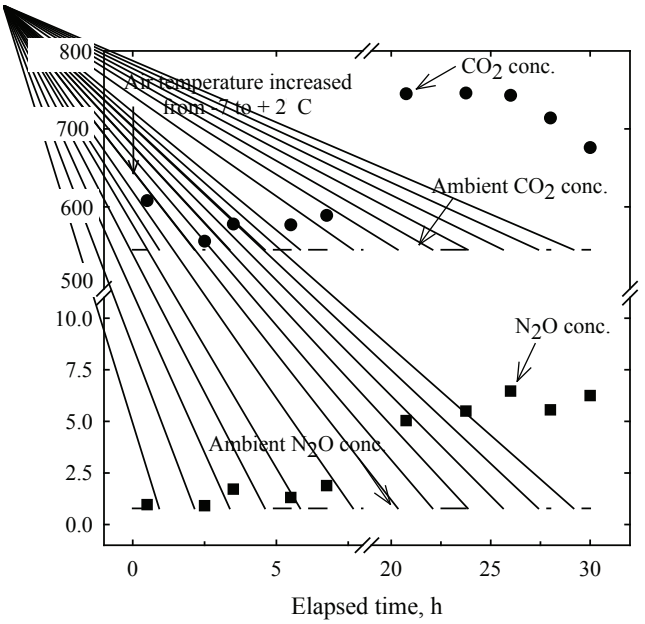

Figure 2. CO_2 and N_2O emissions as a function of thawing time from intact cores frozen once.

Summary

Available data indicate that FTC (1) caused soil water to redistribute and (2) interacted with water content to alter the near-surface aggregate stability of wet soil. Moreover, compared to ambient conditions, emissions of CO_2 increased by a third, and N_2O increased by a factor of eight, each peaking 24 to 26 h after thawing began, from intact cores of soil frozen only once and thawed at only +2°C.

References

Herrmann, A. & Witter, E. 2002. Sources of C and N contributing to the flush in mineralization upon freeze-thaw cycles in soils. *Soil Biology & Biochemistry* 34: 1495-1505.

Lehrsch, G.A. 1998. Freeze-thaw cycles increase near-surface aggregate stability. *Soil Science* 163: 63-70.

Lehrsch, G.A., Sojka, R.E., Carter, D.L. & Jolley, P.M. 1991. Freezing effects on aggregate stability affected by texture, mineralogy, and organic matter. *Soil Science Society of America Journal* 55: 1401-1406.

Sehy, U., Dyckmans, J., Ruser, R. & Munch, J.C. 2004. Adding dissolved organic carbon to simulate freeze-thaw related N_2O emissions from soil. *Journal of Plant Nutrition and Soil Science* 167: 471-478.

van Bochove, E., Jones, H.G., Bertrand, N. & Prevost, D. 2000. Winter fluxes of greenhouse gases from snow-covered agricultural soil: Intra-annual and inter-annual variations. *Global Biogeochemical Cycles* 14: 113-125.

Relation of Active Layer Depth to Vegetation on the Central Yamal Peninsula, Russia

M.O. Leibman
Earth Cryosphere Institute SB RAS, Tyumen, Russia
H.E. Epstein
Department of Environmental Science, University of Virginia, USA
A.V. Khomutov
Earth Cryosphere Institute SB RAS, Tyumen, Russia
N.G. Moskalenko
Earth Cryosphere Institute SB RAS, Tyumen, Russia
D.A. Walker
Institute of Arctic Biology, University of Alaska Fairbanks, USA

Introduction

The purpose of this study was to obtain ground observations in support of remote sensing data. The normalized difference vegetation index (NDVI) and leaf area index (LAI) were measured within a Circumarctic Active Layer Monitoring (CALM) program grid and compared to active layer depth (ALD) measurements. Additional data on active layer properties (soil texture and moisture content), surface features (spot-medallions, hummocks, polygonal pattern and windblown hollows), vegetation complexes, organic mat thickness, and shrub height were analyzed.

The study area is located on the central Yamal Peninsula in the watershed of the Se-Yakha and Mordy-Ykha Rivers. A CALM grid was placed on the top and slope of a highly dissected alluvial-lacustrine-marine plain, affected by landslides with sandy to clayey soils.

Active surface aeolian and landslide processes common in the study area produce vast areas of bare ground. The rate of revegetation and plant succession at such sites related to climate fluctuations was examined through repeated descriptions of vegetation coverage and species in 1993 and 2007.

Previous studies have shown that the main controls of the active layer dynamics are the types of surficial deposits, moisture content in the fall, thickness of organic cover, and air temperature in summer. In general, maximum ALD (1–1.2 m) is found in sands on bare surfaces or with sparse vegetation and low moisture content (up to 20%). Minimum ALD (50–60 cm) is found in peat or clay deposits covered by thick moss and with moisture contents more than 40%.

Methods

The active layer was monitored using a metal probe according to the procedure accepted by the CALM program (Brown et al. 2001) within a grid 100 x 100 m in 10 m increments. Ground and vegetation characteristics were recorded at each grid node. NDVI was measured using a portable ASD PSII spectroradiometer, and LAI was estimated using a LICOR-2000 plant canopy analyzer. NDVI is essentially an index of green, photosynthesizing vegetation, as it strongly depends on the absorption of red light. LAI (as estimated by the LICOR-2000) is the total area of aboveground plant tissue divided by the ground area that is covered by the extent of the plant canopy. Both NDVI and LAI are highly, positively correlated with the mass of aboveground vegetation, and this is true for Low Arctic tundra vegetation (Riedel et al. 2005).

A database was compiled that included ALD, NDVI, LAI, organic mat thickness, shrub height, dominant plant species, and cover of each plant community. The spatial distribution of various parameters was analyzed on a map compiled by interpolation of numerical data between grid-nodes using Surfer software, and field mapping of descriptive data (map not shown).

Active layer measurements in 2007 were accompanied by vegetation descriptions and measurements at each grid-node (121 points and their vicinities were characterized in the database). The data were sorted into three categories of ALD, the averages of all the parameters were calculated, and relations between these averages were analyzed within each category.

Results and Discussion

In general, for the entire CALM grid, the higher the vegetation indices and parameters the lower the ALD (Fig. 1). This result is within the generally accepted effect of vegetation insulation on ground temperatures and ALD (Melnikov et al. 2004).

Analysis of dominant plant species supports the idea that vegetation acts as an insulating mat. Of all the plant groups, moss showed the highest negative correlation with ALD, while lichens and shrubs were more favorable for thawing (or deep thaw was favorable for lichen and shrub growth) (Fig. 2).

Eight vegetation units (Table 1) were recognized within the grid. "Moist grass-sedge-dwarf shrub lichen-moss and green moss hummocky tundra" (#5, Table 1) is most widespread. Partly bare surfaces (#1, 2, 3, and 8, Table 1) are also common, though no bare nodes occurred on the windblown sands, due to recent vegetation recovery.

When the CALM grid was established in 1993, five bare surface grid-nodes occurred in windblown hollows (Leibman 1998). Revegetation of windblown sands started after

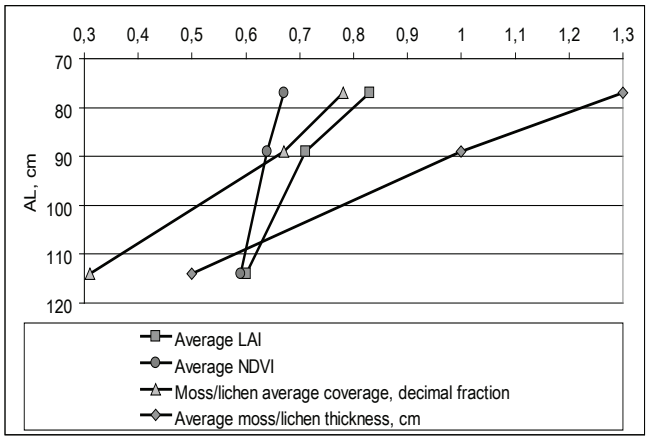

Figure 1. Relation between the active layer depth and average vegetation indices at a CALM grid, research polygon Vaskiny Dachi.

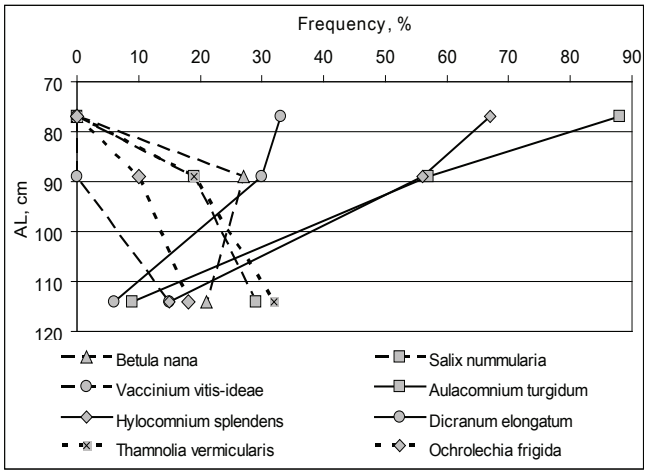

Figure 2. Relation between the active layer depth and frequency of dominant plant species at a CALM grid, research polygon Vaskiny Dachi.

Table 1. Legend for vegetation map of the CALM grid Vaskiny Dachi.

##	Vegetation complex (% bare surface)	Number of grid-nodes
1	Dry blowout sands	0
2	Dry grass-prostrate dwarf shrub-green moss-lichen tundra with spot-medallions (40–60%)	24
3	Dry grass-prostrate dwarf shrub-green moss and green moss-lichen tundra with spot-medallions (10–30%)	12
4	Moist grass-dwarf shrub lichen-moss and green moss tundra	4
5	Moist grass-sedge-dwarf shrub lichen-moss and green moss hummocky tundra	61
6	Moist grass-sedge-low shrub moss tundra	6
7	Wet willow-cotton grass cover	9
8	Moist willow-sedge-grass cover (30–50%)	5

considerable warming in 2000, so the observed revegetation resulted from eight years of change. Shear surfaces of two landslides within the CALM grid were exposed during the landslide event in 1989. Twelve grid nodes became bare surfaces following these events. A survey in 2007 showed that seven grid nodes were entirely revegetated (100% coverage by willow-cotton grass complex, #7, Table 1), and five grid-nodes were partly revegetated (up to 50% coverage by willow-sedge-grass complex, (#8, Table 1) in 18 years.

Conclusion

The active layer depth is negatively related to both LAI and NDVI. This is potentially helpful for mapping active layer depths, using remotely sensed vegetation indices and products. Organic matter coverage and thickness are also negatively related to active layer depth; this is especially true for moss cover. Contrary to the moss species, there is an ordinal relation between ALD and lichen/shrub species.

Temporal patterns of vegetation dynamics on bare surfaces after 10–18 years of revegetation result in the formation of dwarf shrub-lichen cover on dry sandy tops and gentle slopes, willow-cotton grass cover on wet landslide shear surface sites, and willow-sedge-grass cover on moist sites.

Acknowledgments

This research is part of the CALM project funded by the U.S. National Science Foundation (Grant No. OPP-9732051), and the Yamal Land Cover Land Use Change project of the International Polar Year (IPY) funded by NASA Grant No. NNG6GE00A.

References

Brown, J., Hinkel, K.M. & Nelson, F.E. 2001. The Circumpolar Active Layer Monitoring (CALM) program: Research designs and initial results. *Polar Geography* 24: 165-258.

Melnikov, E.S., Leibman, M.O., Moskalenko, N.G. & Vasiliev, A.A. 2004. Active layer monitoring in West Siberia. *Polar Geography* 28(4): 267-285.

Leibman, M.O. 1998. Active layer depth measurements in marine saline clayey deposits of Yamal Peninsula, Russia: procedure and interpretation of results. *Proceedings of the 7th Intl. Conference on Permafrost, Yellowknife, Canada, June 23–27, 1998*: 635-639.

Riedel, S.M., Epstein, H.E & Walker, D.A. 2005. Biotic controls over spectral indices of arctic tundra vegetation. *Intl. Journal of Remote Sensing* 26: 2391-2405.

Rock Glacier Response to Post-Little Ice Age Warming: Spruce Creek Rock Glacier, Ten Mile Range, Colorado, USA

Eric M. Leonard
Department of Geology, Colorado College, Colorado Springs, CO, USA
Stephen G. Weaver
Department of Geology, Colorado College, Colorado Springs, CO, USA
James A. Bradbury
Department of Geosciences, University of Massachusetts, Amherst, MA, USA
Erica E. Langbecker
Department of Geology, Colorado College, Colorado Springs, USA
Jeffrey A. Wollenberg
Department of Geology, Colorado College, Colorado Springs, USA

Introduction

In this study, we use multiple methods to document changes in flow velocity, internal deformation, and surface geometry of the Spruce Creek rock glacier in the Ten Mile Range of central Colorado. Our methods include lichenometry, photogrammetry, and detailed ground surveying. The data provide evidence of strong rock glacier response to both Little Ice Age cooling and post-Little Ice Age warming. Response to warming over the last century appears to have occurred with little lag time.

Methods

Long-term flow variations are evaluated through measurement of lichens (*Rhizocarpon s.l.*) on the rock glacier surface, which provide a record of surface ages, and thus flow rates, spanning the last 2500–3000 years. Lichen measurements are calibrated using a modified version of Benedict's (1993) *Rhizocarpon* growth curve for the Colorado Front Range. Aerial photographs taken at several intervals since 1938 provide a more detailed record of changing flow rates over the last seven decades. Repeated ground surveys begun in the 1985 provide information on changing velocities, strain rates, and strain patterns, and thinning of the rock glacier over the last two decades.

Results

Lichenometry provides only approximate surface ages and thus only approximate flow rates. During the 2000-year interval before about 1600 A.D., mean centerline flow rate at Spruce Creek was approximately 6 cm/yr. The flow rate increased dramatically after about 1600 A.D. For the following three centuries, until the late 19th century, a time interval corresponding to the global peak of the Little Ice Age, mean flow rates were on the order of 40–55 cm /yr. By the mid 20th century, flow rate had declined again to about half of this peak rate, and from the mid 1980s through 2000 A.D., centerline flow rates had declined further to 5.9–10.2 cm/yr on three surveyed transects. Mean flow rates along the three transects over this interval ranged from 4.5 to 6.7 cm/yr. The relatively fast-moving upper portion of the rock glacier, which formed initially during the Little Ice Age, slowed down by 25% between the late 1980s and the late 1990s, and strain rates measured at 12 strain diamonds distributed across the rock glacier declined by an average of 19% over the same interval. Lowering of the rock glacier surface was general, but spatially highly variable, over the period from 1985 to 2000 A.D. Mean surface lowering exceeded 1 m during this period.

Records from the nearest continuously operating meteorological station, at Climax, Colorado, 8–9 km southwest of the Spruce Creek rock glacier, and the more comprehensive records from Niwot Ridge in the Colorado Front Range about 75 km to the northeast, both indicate strong summer warming after the mid 1970s. The velocity and strain rate decreases and surface lowering measured at the rock glacier since the mid 1980s appear to be a response to that warming.

Ongoing Research

During summer 2008, we will resurvey the rock glacier to examine its response to continued warming. Since 2000, summer (June through August) temperatures at Climax have averaged 0.96°C higher than during the initial 15 years of our survey.

Reference

Benedict, J.B. 1993. A 2000-year lichen-snowkill chronology for the Colorado Front Range, USA. *The Holocene* 3: 27-33.

Mapping the Permafrost in China Using Remotely Sensed Land Surface Temperature Data

Xin Li, Shuguo Wang, Rui Jin, Youhua Ran
Cold and Arid Regions Environmental and Engineering Research Institute, Chinese Academy of Sciences Lanzhou 730000, China
World Data Center for Glaciology and Geocryology in Lanzhou, Lanzhou 730000, China

The permafrost area in China is about 1.72×10^6 km^2. The area of altitudinal/mountain permafrost is approximately 1.36×10^6 km^2 (Li et al. 2008), which ranks first in the world in terms of middle- and high-altitude permafrost area. The permafrost in China is very sensitive to climatic warming. Significant permafrost degradation has occurred and is occurring in most permafrost regions in China, and has resulted in an increase of environment fragility and related hazards (Li et al. 2008, Jin et al. 2000, Jin et al. 2006).

Mapping the permafrost is of critical importance therefore. The existing small-scale permafrost/frozen soil maps in China include the map of snow, ice, and frozen ground in China (1:4,000,000) (Shi et al. 1988), permafrost map of the Qinghai-Tibet Plateau (1:3,000,000) (Li & Cheng 1996), the map of geocryological regionalization and classification in China (1:10,000,000) (Qiu et al. 2000), and the map of glaciers, frozen ground, and deserts in China (1:4,000,000) (Wang et al. 2006). In additional, the circum-Arctic map of permafrost and ground-ice conditions (1:10,000,000) (Brown 1998) can be subset to be used as a regional map.

These maps provide a good summary of geocryological research in China; however, there are two weaknesses of these existing small-scale permafrost maps. The first is that the classification systems of these existing maps are inconsistent. All of the legends are continuity-based, but each map uses a different and incomparable map legend itself. The inconsistence is caused, partially, by the ambiguity of the definition of continuity, which is based on the surrounding region it is lying in and, therefore, is scale-dependent (Nelson & Outcalt 1987). Obviously, a consistent and unified legend system is needed for both altitudinal and latitudinal permafrost mapping in China. The lack of it hinders the monitoring and modeling of permafrost.

Another weakness of traditional permafrost mapping is the data unavailability. Global and regional permafrost mapping usually relies on meteorological data. That most commonly used is air temperature, but it is sparse in many permafrost areas, e.g., the Qinghai-Tibetan Plateau. The scarcity of data is an obstacle of high-resolution permafrost mapping.

To address the first weakness, we propose using a stability-based classification system proposed by Cheng (Cheng 1984) to unify the legends of altitudinal and latitudinal permafrost maps. This classification uses temperature criteria, which is more objective than the continuity criteria. It is also more applicable when using GIS mapping technology, because GIS mapping is usually grid-based, which is easy for presenting the existence of permafrost in a grid cell, but not the percentage of permafrost distribution.

To address the second weakness, we propose to use remote sensing data. As stated above, air temperature isotherm is usually used to delineate permafrost zonation. However, many investigators suggested that the air temperature is not an optimal predictor of permafrost distribution, because the very large effects of snow cover and other variables influencing permafrost occurrence are ignored. Instead, land surface skin temperature (LST) should be used (Nelson & Outcalt 1987, Cheng, pers. com.). The LST, though a more ideal criterion, is traditionally more unavailable than air temperature and its heterogeneity is very strong so that extracting LST to data-void regions is more difficult. The remote sensing era has changed this situation. Thermal infrared remote sensing is providing direct observations of LST in high spatial and temporal resolutions, being capable of bridging the gap between permafrost mapping and data unavailability.

The paper aims to develop a new, general, and high-resolution permafrost map of China by applying the thermal stability-based classification system (Cheng 1984) and using remotely sensed LST and snow depth data.

References

Cheng, G.-D. 1984. Problems of zonation of high-altitude permafrost. *ACTA Geographica Sinica* 39(2): 185-193.

Jin, H.J., Li, S.X., Cheng, G.D., Wang, S.L. & Li, X. 2000. Permafrost and climatic change in China. *Global and Planetary Change* 26(4): 387-404.

Jin, H.J., Zhao, L., Wang, S.L. & Jin, R. 2006. Thermal regimes and degradation modes of permafrost along the Qinghai-Tibet Highway. *Science in China D: Earth Sciences* 49(11): 1170-1183.

Li, S.D. & Cheng, G.D. 1996. *Permafrost Distribution Map on the Qinghai-Tibet Plateau*. Lanzhou: Gansu Culture Press.

Li, X., Cheng, G.D., Jin, H.J., Kang, E.S., Che, T., Jin, R., Wu, L.Z., Nan, Z.T., Wang, J. & Shen, Y.P. 2008. Cryospheric change in China. *Global and Planetary Change,* doi:10.1016/j.gloplacha.2008.02.001.

Nelson, F.E. & Outcalt, S.I. 1987. A computational method for prediction and regionalization of permafrost. *Arctic and Alpine Research* 19(3): 279-288.

Qiu, G.-Q., Zhou, Y.-W., Guo, D.-X. & Wang, Y.-X. 2000. *The Map of Geocryological Regionalization and Classification in China*. Beijing: Science Press.

Shi, Y.F. & Mi, D.S. 1988. *Map of Snow, Ice, and Frozen Ground in China, 1:4,000,000*. Beijing: SinoMaps Press.

Wang, T., Wang, N.L. & Li, S.X. 2006. *Map of the Glaciers, Frozen Ground and Desert in China.* 1:4,000,000. Beijing: Chinese Map Press.

The Effect of Spatially Distributed Snow Cover on Soil Temperatures: A Field and Modeling Study

Anna Liljedahl
University of Alaska Fairbanks, USA
Larry Hinzman
University of Alaska Fairbanks, USA
Sergei Marchenko
University of Alaska Fairbanks, USA
Svetlana Berezovskaya
University of Alaska Fairbanks, USA

Introduction

Due to its insulative properties, snow cover has been shown to play a significant role in the 20th century warming of permafrost (Osterkamp 2007, Stieglitz et al. 2003) and thermokarst formation (Osterkamp 2007). Although the effects of snow cover characteristics on soil temperatures have been studied by others (Ling & Zhang 2003, Osterkamp 2007, Overduin et al. 2007, Stieglitz et al. 2003), small-scale geographical variations have been given limited attention. The combination of snow redistribution, hydraulic gradients induced by polygonal features, nutrient limited vegetation, soil mineralization, and respiration impaired by the cold soils calls for a fine-scale analysis to understand the interactions among the Arctic systems and how they would respond to any changes in air temperature and precipitation.

We examine the effects of snow depth and soil thermal properties on micro-scale (>0.6 m horizontal, >0.01 m vertical) soil temperature distribution through field measurements and computer modeling across a single polygon.

Study site

The study site is located inside the boundaries of the Barrow Environmental Observatory (BEO) close to Barrow on the North Slope of Alaska (Fig. 1). The BEO hosts an intensively monitored area called the Biocomplexity site (71°16′47″N, 156°36′2″W), which is a 1 km^2 watershed containing a drained lake basin and low- and high-centered polygons. Sedges and sphagnum moss represent the major vegetation at the Biocomplexity site.

The mean annual air temperature in Barrow during the years 1973–2006 was -12°C with 32% of mean daily air temperatures colder than -20°C. The latter ranged from -45°C to 16°C yr 1973–2006. Adjusted precipitation (Yang et al. 1998) averaged 168 mm/yr with 72 mm falling June–August (1973–2006). Summer 2007 was a warm summer (5.4°C compared to 3.3°C yr 1973–2007) with a low amount of precipitation (24 mm), resulting in unusually dry soils prior to freezing. The Circumpolar Active Layer Monitoring site (Brown et al. 2000), located at the northern end of the BEO, experienced a mean active layer depth of 35 cm yr 1995–2007. The area of focus for this study is a low-centered polygon represented by relatively high (0.5 m) and wide (5 m) rims.

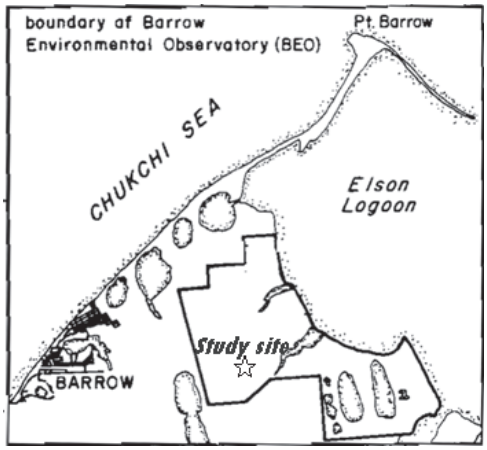

Figure 1. The location of the Biocomplexity site inside the boundaries of the Barrow Environmental Observatory. Original image courtesy of K.M. Hinkel.

Methods

We combined distributed modeling and field observations of snow depth and soil temperatures, focusing on the active layer thermal regime. Output from a snow distribution model was used as input to a soil thermal regime model in both daily and hourly time steps. SnowTran-3D (Liston et al. 2007) provided wind-driven snow depth evolution over topographically variable terrain. Required model inputs include topography, vegetation, and weather data (precipitation, air temperature, humidity, wind speed and direction). In order to simulate the spatially distributed temperatures of permafrost and active layer thickness for the investigated area, both equilibrium and transient models have been applied. The equilibrium model is a spatially distributed permafrost model based on an approximate analytical solution of soil freezing and thawing, which includes an estimation of thermal offset due to the difference of frozen and thawed soil thermal properties (Romanovsky & Osterkamp 1995). The numerical (transient) model simulates soil temperature dynamics and depth of seasonal freezing and thawing by solving nonlinear heat equation with a phase change. In this model, the process of soil freezing/thawing occurs in accordance with the unfrozen water content curve and soil thermal properties, which are specific for each soil layer (Marchenko et al. 2008). The model requires input of

upper (air temperature, snow, and vegetation) and lower (geothermal heat flux) boundary conditions, initial conditions (temperature distribution with depth), soil water content, and soil thermal properties. Topography was resolved in 1 m and 0.04 m horizontal and vertical scale, respectively, with finer pixels available in the near future. Vegetation was mapped into 2.8 m horizontal resolution.

The simulations were validated with field measurements of soil temperature and snow depth. An installation of 116 thermistors (YSI model 44033 and Hobo U23-004) and 29 water content reflectometers (CS616, Campbell Scientific) was made in late September 2007 across the polygon. The thermistors were placed 0.6–20 m apart at three depths per site (1) at the interface of living and dead organic, (2) 7–10 cm below the interface, and (3) at the bottom of the active layer. One soil moisture sensor was placed in the organic layer 7–10 cm below the living and dead organic interface. Thermal conductivity, volumetric specific heat, diffusivity, and temperature were measured with a Kd2Pro sensor (Decagon) throughout the different soil layers in fall 2007.

Results and Discussion

Active layer depths ranged from 18 (troughs) to 46 cm (rims) in 2007 with a mean of 31 cm across the studied polygon. In the thawed polygon soil profile a 2–10 cm thick live moss layer (mean 4 cm) overlaid a 5–25 cm organic layer (mean 10 cm). The thicker moss layers were found in troughs, while the thickest thawed organic layers were found at the inner edge of the rim. Organic layer thermal conductivity in fall 2007 varied between 0.16–0.60 W m^{-1} K^{-1} (n = 68) with moss thermal conductivity from 0.11 to 0.91 W m^{-1} K^{-1} (n = 6). Measurements of moss thermal conductivity could only be obtained at a limited number of sites where ice formation had not occurred. However, five of the six measurements were obtained at the same day, where four sites showed higher thermal conductivities in the moss layer than in the organic layer below (ratio 2.3 to 5.6).

Field measurements showed large variation in near-surface soil thermal properties on short horizontal and vertical scales. Despite relatively small differences in vegetation and topography, a heterogeneous snow accumulation is to be expected due to redistribution by wind. The distribution of winter soil temperatures across the polygon are likely to vary significantly due to the combined effects of snow depth and soil thermal characteristics.

Acknowledgments

The authors are grateful to Matthew Sturm, Robert Busey, Steve Hastings, and B.A.S.C. for field assistance. Financial support was provided by Gålö Foundation, Center for Global Change and Arctic System Research, and the National Science Foundation through the International Arctic Research Center (Grant number 0327664).

References

Brown, J., Hinkel, K.M. & Nelson, F.E. 2000. The circumpolar active layer monitoring (CALM) program: Research designs and initial results. *Polar Geogr.* 24(3): 165-258.

Ling, F. & Zhang, T. 2003. Impact of the timing and duration of seasonal snow cover on the active layer and permafrost in the Alaskan arctic. *Permafrost and Periglac. Process.* 14: 141-150.

Liston, G.E., Haehnel, R.B., Sturm, M., Hiemstra, C.A., Berezovskaya, S. & Tabler, R.D. 2007. Simulating complex snow distribution in windy environments using SnowTran-3D. *J. of Glaciol.* 53(181): 241-256.

Marchenko, S.S., Romanovsky, V.E. & Tipenko, G.S. 2008. Numerical modeling of spatial permafrost dynamics in Alaska. *Proceedings of the Ninth International Conference on Permafrost*, *Fairbanks, Alaska, June 29–July 3, 2008.*

Osterkamp, T.E. 2007. Causes of warming and thawing permafrost in Alaska. *Eos Trans.* 88(48): 522-523.

Overduin, P.P., Boike, J., Kane, D.L. & Westermann, S. 2007. Soil temperatures under a rage of organic and snow covers. *Eos Trans.* 88(52), Fall Meet. Suppl., Abstract C12A-0061, 31:737-747.

Romanovsky, V.E. & Osterkamp, T.E. 1995. Interannual variations of the thermal regime of the active layer and near surface permafrost in Northern Alaska. *Permafrost and Periglac. Process*. 6(3): 313-335.

Stieglitz, M., Déry, S.J., Romanovsky, V.E. & Osterkamp, T.E. 2003. The role of snow cover in the warming of arctic permafrost. *Geophys. Res. Lett.,* 30(13): 1721, doi:10.1029/2003GL017337.

Yang, D., Goodison, B.E. & Ishida, S. 1998. Adjustment of daily precipitation data at 10 climate stations in Alaska: Application of WMO intercomparison results. *Water Resours. Res.* 34(2): 241-256.

The Omnsbreen Glacier: Possible Aggrading Permafrost, Southern Central Norway

Karianne Staalesen Lilleøren
Department of Geosciences, University of Oslo, Norway
Ole Humlum
Department of Geosciences, University of Oslo, Norway

Introduction

The Omnsbreen Glacier is a small (< 0.5 km^2) mountain glacier situated in southern central Norway about 1500 m a.s.l. Presently, the glacier exists approximately 100 m below the regional equilibrium line altitude (ELA), due to local accumulation of wind-redistributed snow.

During the "Little Ice Age" (LIA), the glacier was of a considerable size and extent (approximately 6 km^2) and occupied the whole valley, where today it occupies only parts of the western slope. The maximum size was reached around 1750, as for most of the glaciers in southern Norway (Andreassen et al. 2005). At that time, the effect of snow accumulating by wind on the glacier was significantly reduced because of the glacier's different geometry, filling up the valley.

From the LIA maximum and until around 1930, the glacier remained relatively stable in shape and size. Between 1930 and 1985, however, the bulk of the glacier disappeared. Since then, the glacier has lost mass at a much lower rate compared to the years before, until recent years when the glacier apparently has stagnated with a fairly constant size.

An ongoing study aims at explaining the rapid disappearance of Omnsbreen since 1930 by using local and regional climate data (temperature, precipitation, and wind) and also tries to explain the apparent recent stagnation of the glacier. Couplings between the glacier, the climate, and mountain permafrost is investigated (Lilleøren 2007).

Climatology and Area Description

Location

The Omnsbreen Glacier is located close to Finse (1220 m a.s.l.) at the northwestern margin of the flat Hardangervidda area (Fig. 1). Finse is situated in a transition zone between the marine western coast and the more continental eastern parts of Norway, and has a high mountain climate. The mean annual air temperature (MAAT) was -2.1°C (1970–2000), and the mean annual precipitation in the same period was 1030 mm, according to measurements by the Norwegian Institute of Meteorology at Finse (DNMI 2007).

Temperature

In the before-mentioned ongoing study of the Omnsbreen area, Tinytag-Loggers measuring air temperature, bottom temperature of winter snow cover (BTS), and ground temperature were placed in the area close to the glacier, and the mean difference in air temperature measured between Finse and Omnsbreen was found to be 2.1°C, with the lowest

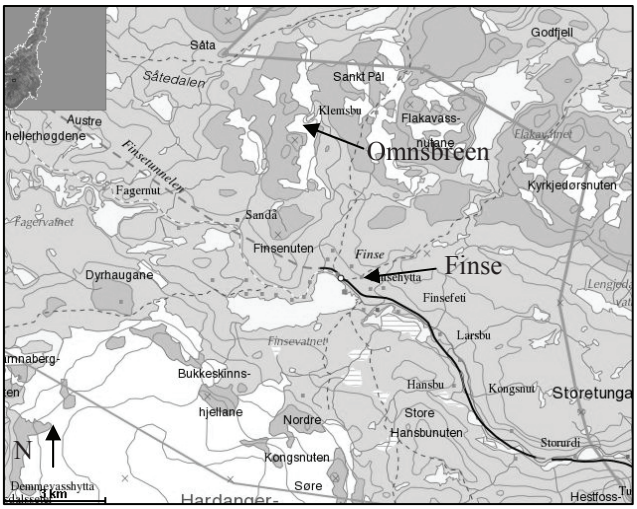

Figure 1. Location of Finse and Omnsbreen, southern central Norway.

temperatures at Omnsbreen for the period 06/08/22 through 07/08/19. The picture is complicated by large temperature inversions in the area, especially during the winter. Finse is situated in a valley bottom that efficiently traps heavy cold air cooled in higher elevations.

Wind

Mapping of snow cover surface forms demonstrated that the mean winter wind direction is from the west or slightly southwest. Omnsbreen's valley has a north–south extension, and snow transported by westerly winds can efficiently accumulate in the valley's east-facing slopes. When studying the wind directions measured by the meteorological station at Finse, it seems like there has been a shift in the wind directions since the 1970s, from a wide directional spread during the winter to a more consistent wind direction from west in the 1980s. This shift also coincides with the reduction in the mass loss from the Omnsbreen glacier.

Permafrost?

Of the loggers measuring the BTS today (four places) in the area earlier covered by ice, one had a stable temperature close to -4°C, which can be interpreted as an indication of permafrost in the area (Fig. 2). The MAAT in the area presumably is too high to allow widespread permafrost, but some sporadic permafrost may exist at this altitude at wind-exposed sites. Situated in a transition area between maritime and continental climate types, the area experiences large differences in snow cover from one year to the next,

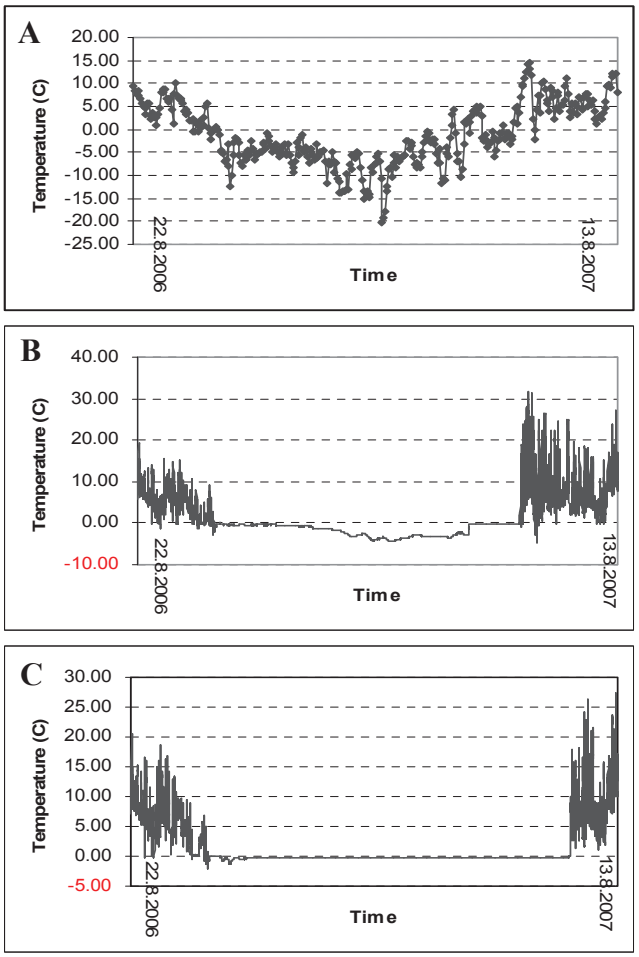

Figure 2. A: Air temperature at Omnsbreen for the period 06/08/22–07/08/13. B: Ground surface temperature (GST) in the Omnsbreen area (1559 m a.s.l.). Snow from mid-October, temperature at ca. -4°C from mid-February to May. C: GST in the Omnsbreen area (1431 m a.s.l.).

including wind-redistributed snow. This situation also changes the permafrost conditions from year to year. In this area, differences in snow cover might be more important for the permafrost distribution than temperature changes, compared to areas further northeast where permafrost is known to exist (Etzelmüller et al. 2003).

The zone covered by ice during the LIA is today characterized by landforms created beneath a warm-based glacier such as flutings, eskers, striae, and crag-and-tails, which indicates non-permafrost conditions at that time. Based on the findings of sporadic permafrost in this area today, the paraglacial zone might be subject to aggrading permafrost (Etzelmüller & Hagen 2005).

Discussion

During the LIA, the Omnsbreen Glacier filled the whole valley. The geometry of the glacier itself probably made accumulation of wind-redistributed snow hard at that time, and it is more likely that the summit areas of the glacier were object to erosion by the wind. As the glacier became smaller, it also became possible for wind-redistributed snow to accumulate in the western parts of the valley. Today's glacier is probably depending on this amount of wind transported snow to exist.

One cannot ignore the possibility that similar wind and topography-induced changes between two stable situations have occurred several times in the history of the Omnsbreen Glacier.

Permafrost

In the following years, time series will be established on BTS, air temperature, and snow cover distribution, considering especially the conditions for permafrost to exist.

References

Andreassen, L.M., Elvehøy, H., Kjøllmoen B., Engeset, R. V. & Haakensen, N. 2005. Glacier mass-balance and length variations in Norway. *Annals of Glaciology* 42: 317-325.

DNMI. 2007. *eKlima*. Oslo: The Norwegian Meteorological Institute.

Etzelmüller, B., Berthling, I. & Sollid, J.L. 2003. Aspects and concepts on the geomorphological significance of Holocene permafrost in southern Norway. *Geomorphology* 52: 87-104.

Etzelmüller, B. & Hagen, J.-O. 2005. Glacier-permafrost interaction in Arctic and alpine mountain environments with examples from southern Norway and Svalbard. In: C. Harris & J.B. Murton (eds.), *Cryospheric Systems: Glaciers and Permafrost.* London: Geological Society, London, Special Publications, 242: 11-27.

Lilleøren, K.S. 2007. *Omnsbreen. Utbredelse og dynamikk under "Den lille istid" og gjennom det 20. århundre.* (English: *The Omnsbreen glacier. Extent and dynamics during the "Little Ice Age" and the 20th century.)*. M.Sc. Thesis. Oslo: Department of Geosciences, University of Oslo.

A Permafrost and Building Foundation Monitoring System to Help Design Adaptable Foundation Structures in a Changing Climate

Michael R. Lilly
GW Scientific, Fairbanks, Alaska, USA
Ron F. Paetzold
GW Scientific, College Station, Texas, USA
Daniel Reichardt
GW Scientific, Anchorage, Alaska, USA

Introduction

Designing foundations for homes and buildings in northern regions will face many challenges in future years as climate changes impact permafrost regions. Permafrost stability may be adversely affected by climate change, and new buildings need to be designed to withstand or adapt for such changing conditions. Past approaches have focused on stabilizing permafrost, making the assumption that the building structure was the primary source for any change in permafrost. As climate changes increase, the potential for associated impacts to foundation systems within the design lifespan of the building will become more common, and the expense and difficulty associated with stabilizing warming permafrost will likely become greater.

The Cold Climate Housing Research Center (CCHRC) was created to promote, develop, and test cold climate building technology. The Center's Research and Testing Facility (RTF) is a 15,000 square foot building designed as a multipurpose structure containing office space, research laboratories, meeting rooms, and a library. The building is located in a setting having shallow permafrost conditions. Additional information about the Center and the RTF may be found on their website: http://www.cchrc.org/.

The RTF was built to adjust to degrading permafrost by having an adjustable foundation system. This is different than past methods, which focus on maintaining frozen conditions. With warming climatic conditions, this places a foundation-stabilization system at odds with the natural state of the environment. The building's foundation is designed with piers that are equipped with 50-ton jacks to keep the building level by compensating for any differential settlement resulting from permafrost degradation.

To help evaluate, respond, and demonstrate this type of foundation system for buildings, a permafrost and active layer monitoring system was installed to help provide data for the life of facility operations. The RTF and the areas beneath and around the building have been thoroughly instrumented to monitor conditions, especially those related to temperature and moisture.

The temperature monitoring network was established to help look at background permafrost conditions, as well as conditions under the building and at various sections of the building foundations that may be impacted by seasonal freezing. The site has a supra-permafrost, unconfined, aquifer in unconsolidated silts. The groundwater flow impacts heat transfer between the building and underlying permafrost. The water-table elevation varies seasonally with snowmelt recharge in the spring. The general groundwater gradient is from west to east.

Additional monitoring includes unfrozen soil-moisture sensors. While the building limits future vertical drainage into the subsurface, annual rising and falling groundwater tables can contribute to the unsaturated moisture levels under the building. Changing permafrost conditions may increase or decrease groundwater fluxes and vertical changes under the building.

A better understanding of the subsurface environment and changing permafrost conditions will be important for future evaluations of the adjustable foundations systems and the transferability to developing cold regions.

Materials and Methods

The depth to permafrost at the building site varies from 3.7 m (12 feet) at the southwest corner to more than 8.5 m (28 feet) on the northeast corner.

Construction began on the RTF in the middle of July 2005. The building was completely enclosed in January 2006 and was completed in September of 2006. Sensors were installed during building construction. Layout of the facility is shown in Figure 1.

Several monitoring wells were drilled into permafrost and allowed to freeze back. The wells can be used for two purposes: measurements of the top of the water-table aquifer and the top of permafrost. A background site was installed away from the facility (weather station site), on the up-gradient side of the building in shallow permafrost, and on the downstream side of the facility, where the maximum impact should come from thermal heat loss from the building. A

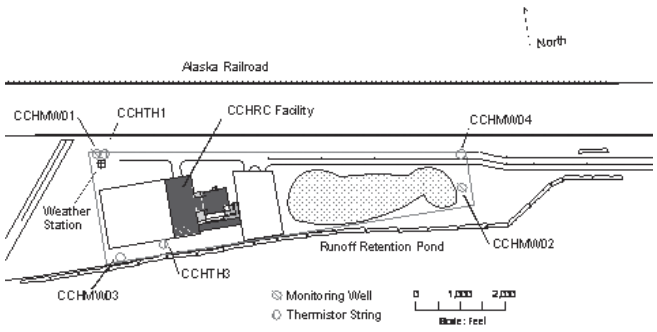

Figure 1. Site location map for CCHRC facility, showing location of observation wells and thermistor borings.

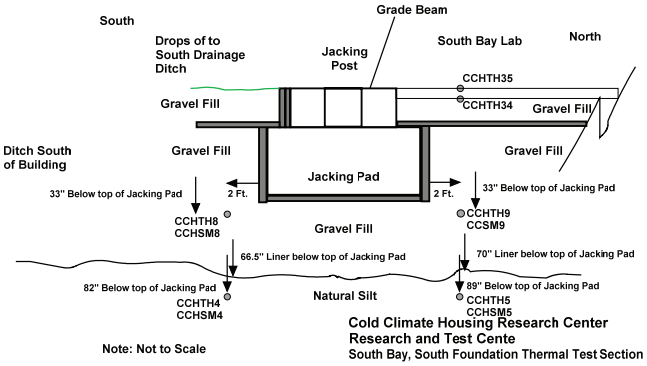

Figure 2. South Bay south foundation thermal test section sensor locations.

number of sensors were also installed under all the building foundation systems to help characterize the heat loss from the building.

Soil temperature is monitored at various points using sensors fabricated with triplicate YSI thermistors or strings of 12 YSI thermistors at a predetermined spacing. The calibration for each sensor was verified. Figure 1 shows the location of two of the thermistor strings: CCHTH1 and CCHTH3.

Soil-water content was monitored with Campbell Scientific, Inc. CS616 TDR-type sensors. These sensors indicate the volumetric amount of unfrozen water content, based on changes in soil bulk dielectric properties.

Water levels in observation wells are manually recorded at selected observation intervals. The groundwater wells are located near the four property corners, as shown on the map in Figure 1.

Sensor readings at each station were controlled and recorded with a Campbell Scientific, Inc. CR1000 datalogger. Data are transmitted hourly to a central processing server though an Internet connection.

Figure 2 shows sensor locations near one of the foundation jacking pad test sections. CCHTH## sensors are temperature sensors consisting of triplicate thermistors. CCHSM## sensors are soil-moisture sensors.

Results and Discussion

The south foundation thermal test section is taken as representative. Figure 3 shows soil temperatures since September 1, 2006, for the sensors in the gravel fill and natural silt to 2.26 m below the top of the jacking pad. The soil temperature did not fall below freezing here.

Figure 4 shows soil-water content since September 1, 2006, for the sensors in the gravel fill and natural silt to 2.26 m below the top of the jacking pad. The sensors in the natural silt, below the gravel fill, show the soil to be very moist, near saturation. The gravel fill is very dry, between about 5 to 7 percent by volume. The graph shows seasonal variability in soil-water content in the silt. The driest time is in the spring. Fall 2007 shows higher soil-water content than the same period in 2006. The monitoring needs to continue in order to ascertain if this is simply seasonal variability, if the soil

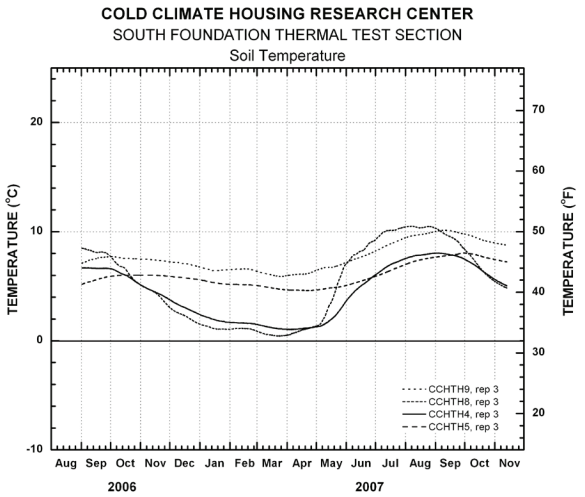

Figure 3. South foundation thermal test section: soil temperature in the gravel fill and in the natural silt.

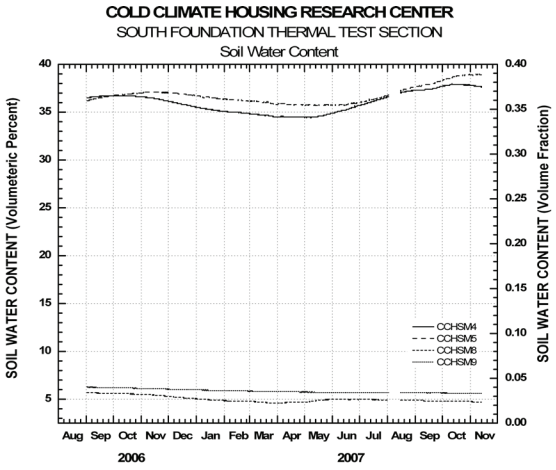

Figure 4. South foundation thermal test section: soil-water content in the gravel fill and in the natural silt.

is getting wetter, or if the soil was dried during construction and is returning to a stable state.

Summary

The CCHRC RTF is a state-of-the-art facility located on shallow permafrost. The building foundation is designed to allow compensation for any differential settlement resulting from permafrost degradation. The building and surrounding area is heavily instrumented to allow soil-temperature and soil-moisture monitoring. The monitoring system is designed for long-term use. Preliminary results are given, but it is too soon to tell if the ground beneath the building has reached equilibrium after the disturbance resulting from the construction.

References

Murton, J.B. & French, H.M. 1994. Cryostructures in permafrost, Tuktoyaktuk coastlands, western Arctic Canada. *Canadian Journal of Earth Sciences* 31: 737-747.

The Role of Permafrost in the 2002 Ten Mile Creek Debris Torrent, Yukon, Canada

Panya Lipovsky
Yukon Geological Survey, Whitehorse, Canada
Crystal Huscroft
Thompson Rivers University, Kamloops, Canada
Antoni Lewkowicz
University of Ottawa, Ottawa, Canada
Bernd Etzelmüller
University of Oslo, Oslo, Norway

Introduction

In June 2002, a catastrophic debris torrent initiated from a moderate north-facing slope in the headwaters of Ten Mile Creek, in central Yukon, Canada. Field evidence indicates that permafrost was a major contributing factor that caused an initial landslide which then triggered the debris torrent. The mechanism of failure in the initial landslide appears to be unique in comparison to other permafrost-related landslides (i.e., retrogressive thaw failures and active layer detachments) documented in the region (Lipovsky et al. 2006, Lipovsky & Huscroft 2007, Lyle 2006).

Setting

The landslide source zone is located at 1084 m elevation, 15 km southeast of the town of Carmacks in central Yukon, Canada (61°58′45.4″N, 136°08′20.7″W). Based on field observations and aerial photograph analysis of the terrain immediately surrounding the source zone, the pre-failure slope is estimated to have been moderately steep (up to 27°) with a typical boreal forest cover consisting of low shrubs, mosses and mature spruce trees.

The landslide left a bowl-shaped scar up to 160 m wide and 100 m long with a steep headwall 12–31 m high (Fig. 1). Springs flow from the base of a secondary slump scar in the floor of this bowl. Following the initial failure, an ensuing debris torrent descended 500 m in elevation and traveled 4.7 km down the narrow *v*-shaped valley of Ten Mile Creek. The main debris lobe came to rest after crossing the South Klondike Highway, clogging its culvert and filling the adjacent ditch with debris. Superelevation measurements taken on a channel bend in the runout zone indicate that the torrent traveled at a maximum velocity of 11 m/s (40 km/hr) with a peak discharge of 1300 m^3/s.

Along much of the debris torrent path, a swath of trees averaging 35 m wide was cleared through mature forest adjacent to the former stream channel. Silty loam diamicton (containing 35–43% coarse fragments) was deposited up to 1.3 m thick along most of the debris torrent path, except within a 600 m long canyon segment confined by steep rock walls. Ongoing remobilization of these deposits by subsequent stream flow has caused sedimentation of local salmon habitat at the mouth of the creek where it flows into Nordenskiold River.

Surficial geological materials exposed in the landslide headwall consist of a stony till blanket up to 12.5 m thick overlying at least 22 m of glaciofluvial sand and gravel exhibiting prominent bedding structures. At numerous locations up to 3.7 km downstream from the source zone, discrete blocks of sandy material deposited by the debris torrent and originating from this lower glaciofluvial unit show intact primary bedding structures. In order to preserve these features over such a long transport distance, the sediment must have been frozen both before and during transport. This implies that in the landslide source zone permafrost must have extended into the glaciofluvial unit found at least 12.5 m below the ground surface.

Local Permafrost Conditions

Ten Mile Creek is located within Yukon's extensive discontinuous permafrost zone. Permafrost is commonly found on north-facing slopes in this region, particularly

Figure 1. Aerial view of landslide source zone showing debris torrent channel exiting at lower left corner. Maximum height of the headwall is 31 m and the bowl is approximately 160 m wide.

beneath thick organic mats associated with boreal forest cover.

Surface probing behind the landslide headwall in late summer 2004 indicated an active layer thickness of 42–86 cm where the organic mat was at least 40 cm thick. Where the organic mat was thinner, the permafrost table was not encountered within 1.05 m of the ground surface, however it was assumed to be present at greater depth. Thermistor measurements and lateral probing into the lower headwall did not detect permafrost in the glaciofluvial unit at this time (ground temperatures 1 m into the face were ~1°C).

DC resistivity surveys conducted in 2006 suggest that permafrost is up to 5 m thick on the gentle north-facing slope behind the landslide headwall, and up to 15 m thick on the steeper north-facing slope adjacent to the landslide source zone (Fig. 1). The resistivity surveys also confirmed the absence of permafrost in the landslide headwall, implying that rapid lateral thaw has occurred since the failure occurred in 2002.

Landslide Failure Mechanism

Unfrozen glaciofluvial sand and gravel exposed in the lower unit of the landslide headwall are highly permeable and porous, with a capacity to store and transmit a large amount of groundwater. This is confirmed by the presence of springs flowing from the floor of the landslide source zone scar. Based on aerial photograph interpretation, these sediments are part of a larger geological unit consisting of bedded glaciofluvial deltaic materials that extend laterally further upslope and capture groundwater from the upper drainage basin. As a result of this geomorphic configuration, the site of the landslide source area represents the location of greatest groundwater convergence within that basin. We hypothesize, therefore, that the base of the impermeable permafrost layer within these sediments confined groundwater flow and allowed high pore pressures to accumulate below the permafrost during the spring snowmelt period in June 2002. During the same time period, no abnormal precipitation was recorded and no earthquakes occurred in the vicinity. We suggest that pore pressures increased until a threshold was reached that allowed rupture or "blow-off" (Cavers 2003) of the unfrozen materials and detachment of the entire permafrost layer above.

We infer that subsequent rapid drainage of stored groundwater supplied a large volume of water which facilitated the catastrophic debris torrent. Similar failure mechanisms are common in non-permafrost areas throughout western Canada where groundwater pressures are instead confined by surficial material stratigraphy rather than by frozen ground (Cavers 2003). Alternatively, the initial movement could have partially blocked a small stream channel to the northeast allowing water to accumulate in a pond. However, we were unable to locate any evidence of such ponding in the field.

Local and regional climatic data show that at least four decades of climate warming have occurred in central Yukon since 1930. Any corresponding permafrost warming and/or thinning may have weakened the permafrost layer and lowered the pore pressure threshold required to initiate a failure and cause detachment. Dataloggers were installed in 2005 to monitor the long-term air and ground surface temperatures above the landslide source zone.

Implications

The results of this study have important implications for future development and land use planning in the area, as the geomorphic setting of the landslide source zone is widespread throughout much of central Yukon. This case study illustrates that significant hazards are associated with this type of landslide. It also highlights the need to perform detailed evaluations of basin characteristics, permafrost conditions, and surficial material stratigraphy several kilometers upslope of any area targeted for human land use. In particular, stream crossing designs and development on fans in permafrost regions should carefully consider the risk of debris torrents triggered by groundwater blow-off failures beneath frozen ground.

Acknowledgments

Funding was provided by NSERC and the University of Ottawa to A. Lewkowicz; by the University of Oslo to B. Etzelmüller; and by the Yukon Geological Survey to P. Lipovsky and C. Huscroft.

References

Cavers, D.S. 2003. Groundwater blow-off and piping debris flow failures. *Proceedings, 3rd Canadian Conference on Geotechnique and Natural Hazards, Edmonton, Alberta, June 9–10, 2003*: 151-158.

Lipovsky, P. & Huscroft, C. 2007. A reconnaissance inventory of permafrost-related landslides in the Pelly River watershed, central Yukon. In: D.S. Emond, L.L. Lewis & L.H. Weston (eds.), *Yukon Exploration and Geology 2006*. Yukon Geological Survey, 181-195.

Lipovsky, P.S., Coates, J., Lewkowicz, A.G. & Trochim, E. 2006. Active-layer detachments following the summer 2004 forest fires near Dawson City, Yukon. In: D.S. Emond, G.D. Bradshaw, L.L. Lewis & L.H. Weston (eds.), *Yukon Exploration and Geology 2005*. Yukon Geological Survey, 175-194.

Lyle, R.R. 2006. *Landslide susceptibility mapping in discontinuous permafrost, Little Salmon Lake, Central Yukon*. M.Sc.E. Thesis. Queen's University, 351 pp.

Carbon Gas Fluxes from Contrasting Boreal Lakes During Intensive Rain Events

Jessica López Bellido
University of Helsinki, Department of Ecological and Environmental Science, Niemenkatu 73, FIN-15140 Lahti, Finland
Anne Ojala
University of Helsinki, Department of Ecological and Environmental Science, Niemenkatu 73, FIN-15140 Lahti, Finland

Introduction

The variability in climate and weather are typical characteristics in the Northern Hemisphere, which by itself already has a strong impact in the hydrology and ecology of freshwater ecosystems. Change in climate variables, such as temperature and precipitation, will definitely impact aquatic species at various trophic levels and alter the physical and chemical processes that act on and within the lake ecosystem. Nevertheless, not only will the extreme seasonality affect the aquatic ecosystems, but also their surrounding areas. For instance, the Nordic region has a vast variety of terrains which contain a significant number and diversity of lakes. This linked pathway makes the lakes vulnerable to changes due to the direct impact from the adjacent terrestrial ecosystem, leading to the reduction or abundance of organic matter which, in turn, significantly impacts aquatic production, that is, agriculture, forestry, and urbanization. Under this process of human disturbance, the flux of gases between land, water, and atmosphere has been radically altered; thus, the increase of greenhouses gases to the atmosphere, mainly of carbon dioxide and methane.

At high latitudes, wetlands (i.e., lakes, ponds, and peatlands) are the key feature of the landscape. Among wetlands, lakes are the most important areas where radical changes in water management or climate can significantly affect the quality of human life. On the other hand, lakes themselves can affect the climate system. Globally, lakes are supersaturated with CO_2 and CH_4 (Cole & Caraco 1998). Lakes in Finland have also been shown to be supersaturated with these greenhouse gases (Kortelainen 2000). They play an important role, therefore, in the exchange of CO_2 and CH_4 at the regional and global scale due to the amount of carbon stored in these ecosystems. This is actually a concern due to the projections in global climate change in Nordic areas, where today's sinks can be turned into sources of carbon dioxide and methane.

In this study, we explored CO_2 and CH_4 fluxes from two lakes with contrasting limnological characteristics in southern Finland: Lake Ormajärvi, a clear-water lake, and Lake Pääjärvi, a humic brown–water system. The main hypothesis was that the two lakes differ in their carbon gas fluxes, where the humic lake, which processes more organic carbon of terrestrial origin, shows larger CO_2 fluxes, whereas CH_4 fluxes were higher from the more eutrophic clear-water lake. Due to the limnological distinctions supposedly resulting in differences in timing and intensity of mixing periods, differences in seasonal flux patterns were examined as well as their relation to biological carbon uptake and carbon mineralization in the epilimnion of the pelagic zone. For instance, it was also hypothesized that fluxes from the clear water Lake Ormajärvi are more closely connected to autochthonous carbon uptake, whereas in the brown-water Lake Pääjärvi, the system is fueled more by allochthonous carbon; thus fluxes and mineralization processes are tied together. Finally, since during the study year 2004 the summertime precipitation in the area doubled from the ordinary 200–220 mm to 413 mm and the extra rain poured down in four events June–July, the opportunity allowed the study of lake response to an extreme weather event.

Methods

Measurements of CO_2 and CH_4 fluxes were based on surface water concentrations as well as gas accumulation in floating closed chambers.

Primary production was measured by the radiocarbon technique, using light/dark bottle incubations (Schindler et al. 1972). Plankton community respiration, that is, biological mineralization of organic carbon, was estimated from the consumption of dissolved oxygen. For final results, the rates of oxygen consumption were converted to rates of CO_2 release using a value of one for the respiratory quotient (RQ) (Wetzel & Likens 2000). To facilitate the comparison between the two different lakes, the data from respiration measurements as well as primary production were areally integrated. Pelagic CO_2 net production due to biological processes was then calculated by subtracting the primary production from the pelagic mineralization.

Results and Discussion

Both lakes presented seasonalities in fluxes, so the gases accumulated under ice and in the hypolimnion were ventilated out in spring and autumn. The annual CO_2 fluxes from Lake Ormajärvi and Lake Pääjärvi were 3.6 mol m^{-2} y^{-1} and 6.1 mol m^{-2} y^{-1}, respectively, and both lakes acted as a source of CO_2. The corresponding values for CH_4 were 24.5 mmol m^{-2} y^{-1} and 18.5 mmol m^{-2} y^{-1}. In terms of global warming potential on annual basis, CH_4 had contributed 7.4% and 19.0% in Lake Pääjärvi and in Lake Ormajärvi, respectively.

The most distinctive results of this study were the overwhelming importance of rain events to gas fluxes. In Lake Pääjärvi, the high precipitation resulted in a large peak in CO_2 and CH_4 fluxes which lasted for a couple of weeks and contributed to 46% in CO_2 and 48% in CH_4 annual fluxes. In Lake Ormajärvi, the contribution of the rainy period to carbon gas fluxes was 39% and 37% for CH_4 and CO_2, respectively. The response of Lake Ormajärvi fluxes to high

precipitation was not as sudden and immediate as in Lake Pääjärvi, but the outcome was more radical, since before the rainy period the lake was autotrophic; that is, photosynthesis exceeded respiration. When the rains started, however, the lake turned to heterotrophy with respiration exceeding photosynthesis. Opposite to Lake Ormajärvi, Lake Pääjärvi appeared net heterotrophic throughout the study period. By thoroughly analyzing the results on biological processes within the lakes, the "extra" CO_2 and CH_4 did not originate from mineralization processes within the lakes, but the gases were flushed into the lakes from the surrounding terrestrial soil and were of allochthonous origin.

Conclusion

This study demonstrated that the link between the catchment and the lake is more immediate than anticipated and is strongly controlled by hydrology. Also, the role of input of CO_2 and CH_4 can be significant even in summertime, when there is an extreme rainfall event. In northern Europe, these kinds of high extremes of precipitation are very likely to increase in magnitude and frequency due to climate change. Thus, for correct estimates of carbon exchange of terrestrial ecosystems, the role of lakes as efflux sites of carbon gases of terrestrial origin should be taken into account.

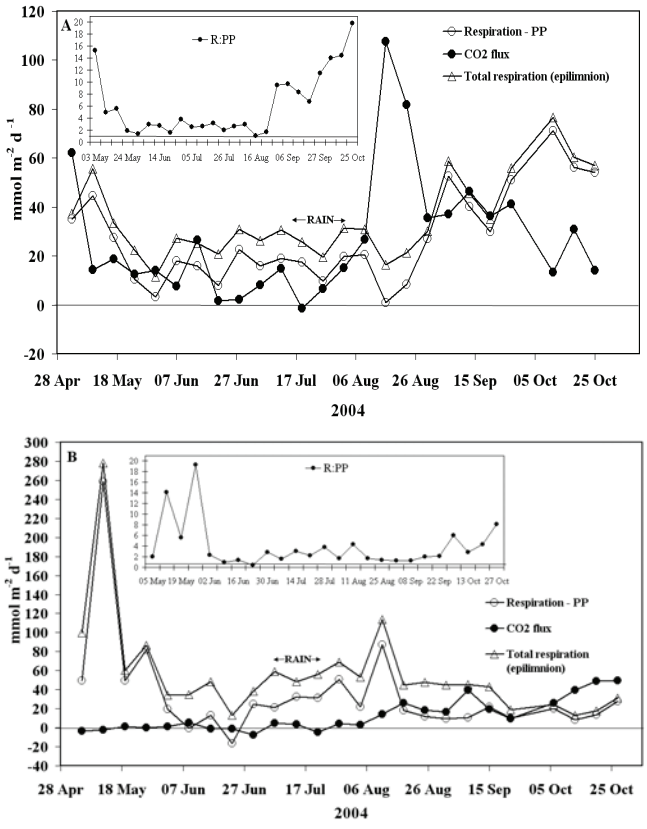

Figure 1. CO_2 net production and community respiration in relation to ΔCO_2 flux in (A) Lake Pääjärvi and (B) Lake Ormajärvi. The period of heaviest rains is shown with arrows. The inserts display R:PP ratios in both lakes.

Acknowledgments

Financial support was provided by NECC (Nordic Center of Excellence for Studies of Ecosystem Carbon Exchange and its Interactions with Climate Ecosystem). Thanks are also to Lammi Biological Station of the University of Helsinki.

References

Cole, J.J. & Caraco, N.F. 1998. Atmospheric exchange of carbon dioxide in low-wind oligotrophic lake measured by the addition of SF_6. *Limnol. Oceanogr*. 43: 647-656.

Kortelainen, P., Huttunen, J., Väisänen, T., Mattsson, T., Karjalainen, P. & Martikainen, P. 2000. CH_4, CO_2 and N_2O supersaturation in 12 Finnish lakes before and after ice melt. *Verh. Int. Ver. Limnol*. 27(3): 1410-1414

Schindler, D.W., Schmidt, R.V. & Reid, R. 1972. Acidification and bubbling as an alternative to filtration in determining phytoplankton production by the ^{14}C method. *J. Fish. Res. Board Can*. 29: 1627-1631.

Wetzel, R.G. & Likens, G. 2000. *Limnological Analyses*, 2nd ed. New York, NY: Springer Verlag.

The Sensitivity of SiBCASA-Simulated Carbon Fluxes and Biomass to North American Interannual Climate Variations

Lixin Lu
Department of Atmospheric Science, Colorado State University, Fort Collins; and CIRES and ATOC, University of Colorado, Boulder, Colorado
Kevin Schaefer, Tingjun Zhang
CIRES and NSIDC, University of Colorado, Boulder, Colorado
Ian Baker
Department of Atmospheric Science, Colorado State University, Fort Collins

Introduction

Simple Biosphere model (SiB2.5) (Sellers et al. 1996a,b) is coupled with Carnegie-Ames-Stanford Approach model (CASA) (Potter et al. 1993, Randerson et al. 1996) to form a new model, SiBCASA, which is capable of simulating diurnal to interannual variations of terrestrial carbon fluxes and biomass at plot to global scales (Shaefer et al. 2008a). While prescribing leaf biomass derived from remotely sensed Normalized Difference Vegetation Index (NDVI), SiBCASA can dynamically allocate carbon to leaf, root, and wood pools, and explicitly calculate autotrophic respiration.

To improve winter-process simulations, Schaefer et al (2008b) improved the snow and soil freeze- and thaw-related algorithms in SiBCASA. These modifications include, incorporating Sturm et al. (1995) snow classification system, adopting the Lawrence and Slater (2005) organic soil model, and extending the soil column depth to 15 m with an increased number of soil layers. These changes greatly improved the SiBCASA-simulated snow density, snow depth, as well as soil temperature, to more realistic ranges with observations.

Study Sites and Experiment Design

Nine eddy covariance flux tower sites (include Barrow, Bondville, Boreas old black spruce, Harvard Forest, Howland Forest, Lethbridge, Niwot Ridge, Park Falls, and Winder River) across a range of the climate-ecosystem zones are selected for initial evaluations of SiBCASA-simulated biophysical and biogeochemical processes (shown in Fig. 1). The meteorological forcings are derived from 32-km grid-spacing North American Regional Reanalysis product spanning 1979 through 2003 at 3-hourly time-step. Modeled carbon fluxes and biomass at these sites are evaluated against tower-observed values. In particular, the parameterizations describing cold-land processes were developed and implemented to better represent the interactions between snow cover, soil thermodynamics, and soil freeze-thaw processes, as well as their influences on carbon cycle over permafrost regions.

A suite of sensitivity experiment is performed by perturbing the atmospheric forcing variables one at a time. Maximum and minimum temperatures are increased and decreased 2°C, while precipitations are increased and decreased 25% of their original values. SiBCASA-simulated carbon fluxes and biomass are also sensitive to the initial conditions

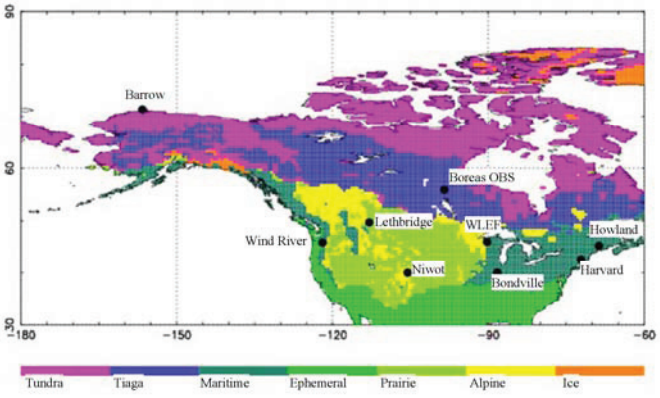

Figure 1. The distribution of nine study sites over the North America domain. These sites are coincident with Ameriflux eddy covariance flux tower sites.

of soil moisture and temperature, snow depth, and initial woody pool size. Statistical analyses are being carried out to understand how these climate perturbations and changes in initial conditions influence the predictions of carbon fluxes and biomass. These experiments, by artificially manipulating the input data to imitate possible future scenarios, will enable us to assess and quantify the sensitivity of North American carbon cycle to large-scale climate change.

Preliminary Results

Heat fluxes

The upper two panels in Figure 2 show SiBCASA-simulated latent and sensible heat fluxes from 1982 through 2004 at the Barrow site. Monthly mean values are plotted to highlight the interannual variations. From year to year, both sensible and latent heat fluxes show changes up to 30% and 40% of their averaged values, respectively. A mid-year latent-heat-flux depression persists throughout the simulation time period, indicating that soil might be drying out due to surface evapotranspiration and soil hydrology before it is replenished by summer rainfalls. The latent heat fluxes share the same sign of temperature changes, up to 30% of their original values when temperature increases or decreases by 2°C. The sensible heat fluxes only vary up to 10% of their original values with the same magnitude of temperature changes as in the latent heat flux experiment, and most importantly, they are in opposite sign of temperature changes. Both heat fluxes respond to precipitation perturbations in much

smaller magnitude and a more non-linear fashion. Most of the time, increased precipitations result in increased latent heat fluxes and reduced sensible heat fluxes, and vice versa. These results imply that the heat fluxes at the Barrow site are more controlled by temperatures than precipitations; it is an energy-limited moist site.

Carbon fluxes and pools

Figure 3 shows clear seasonal cycles and large interannual variability of Net Ecosystem Exchange (NEE) and wood pool modeled by SiBCASA. During summer months, when temperatures increase, the photosynthesis uptake exceeds the respiratory carbon release, resulting in increased net CO_2 uptake. This might be a result of very long daylight hours in Arctic summer. The model shows minimal sensitivity of NEE in winter months, largely because the negligible *R* during very cold winter and the complete shutdown of photosynthetic uptake. In general, increase temperatures and precipitations lead to increased wood pools, and vice versa.

Presently, more detailed statistical analyses are being performed to the results from the SiBCASA sensitivity experiments.

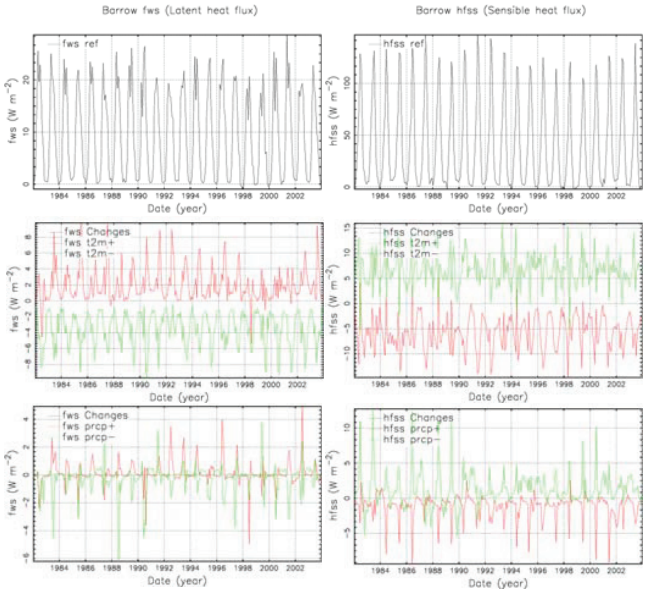

Figure 2. SiBCASA-simulated latent and sensible heat fluxes from 1982 through 2004 at the Barrow site. Also shown are changes in heat fluxes to perturbations of temperatures and precipitations. In these plots, monthly mean values are aggregated from 15-minute time-step model outputs.

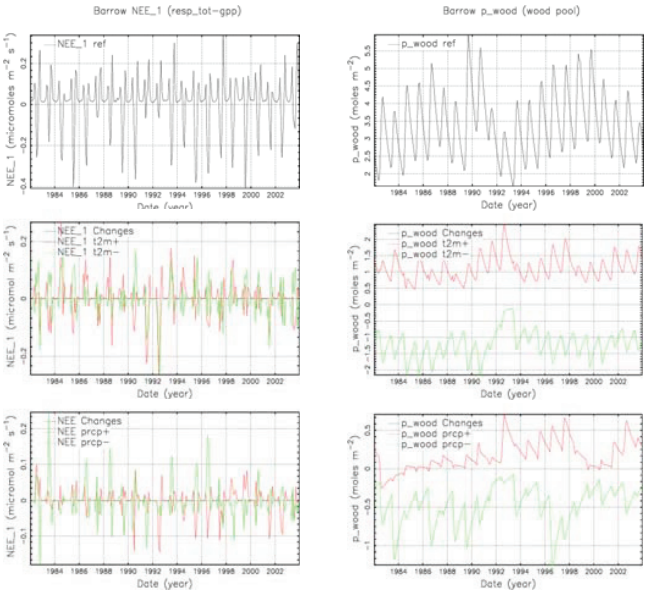

Figure 3. SiBCASA-simulated net ecosystem exchange and wood pools from 1982 through 2004 at Barrow site. Also shown are changes in NEE and wood pool to perturbations of temperatures and precipitations. In these plots, monthly mean values are aggregated from 15-minute time-step model outputs.

Acknowledgments

This study is supported by the U.S. National Aeronautics and Space Administration (NASA) grant NNX06AE65G to the University of Colorado at Boulder.

References

Lawrence, D.M. & Slater, A.G. 2005. A projection of severe near-surface permafrost degradation during the 21st century. *Geophys. Res. Lett*. 32(24): doi:10.1029/2005GL025080.

Potter, C.S., Randerson, J.T., Field, C.B., Matson, P.A., Vitousek, P.M., Mooney, H.A., & Klooster, S.A. 1993. Terrestrial ecosystem production: A process-oriented model based on global satellite and surface data. *Global Biogeochem. Cycles* 7: 811-842.

Randerson, J.T., Thompson, M.V., Conway, T.J., Field, C.B. & Fung, I.Y. 1996. Substrate limitations for heterotrophs: Implications for models that estimate the seasonal cycle of atmospheric CO_2. *Global Biogeochem. Cycles* 10(4): 585-602.

Schaefer, K, Collatz, G.J., Tans, P, Denning, A.S., Baker, I., Berry, J., Prihodko, L., Suits, N. & Philpott, A. 2008a. The combined Simple Biosphere/Carnegie-Ames-Stanford Approach (SiBCASA) terrestrial carbon cycle model. *J. Geophys. Res*. (in press).

Schaefer, K., Zhang, T.J., Lu, L. & Baker, I. 2008b. Applying snow classification system and organic soil properties to the SiBCASA model. *JGR-Atmosphere* (to be submitted).

Seller, P.J., Randall, D.A., Collatz, G.J., Berry, J.A., Field, C.B., Dazlich, D.A., Zhang, C., Collelo, G.D. & Bounoua, L. 1996a. A revised land surface parameterization of GCMs, Part I: Model Formulation. *J. Clim*. 9(4): 676-705.

Sellers, P.J., Los, S.O., Tucker, C.J., Justice, C.O., Dazlich, D.A., Collatz, G.J. & Randall, D.A. 1996b: A revised land surface parameterization of GCMs, Part II: The generation of global fields of terrestrial biosphysical parameters from satellite data. *J. Clim.* 9(4): 706-737.

Sturm, M., Holgren, J. & Liston, G.E. 1995. A seasonal snow cover classification system for local to global applications, *J. Clim*. 8(5): 1261-1283.

Permafrost Characteristics and Climate Change Consequences at Stockhorn and Gornergrat (Swiss Alps)

Clemens Constantin Maag, Oliver Wild, Lorenz King
Justus-Liebig-University Giessen, Germany
Martin Baum, Sebastian Klein, Christin Hilbich
Friedrich-Schiller-University Jena, Germany

Introduction

The Stockhorn-Gornergrat tourist area is of high interest for the study of mountain permafrost and aspects of climate change. Within the EU-project PACE, a 100 m deep drilling located at 3405 m a.s.l. points to a permafrost thickness of about 170 m at the Stockhorn Plateau. Since then, long-term monitoring of the bedrock and permafrost conditions started. A reorganization of the ski region due to changed tourist expectations led to both new ski slopes and cable car connections. The necessary construction work provides the opportunity for new findings of the existing permafrost conditions. Stockhorn qualifies as a salient research area, as it is only marginally affected by the tourist industry yet is within the well-examined Zermatt research area, and only 10 km by airline from Kleinmatterhorn (3883 m a.s.l.) (King et al. 2008). These conditions allow observation of climatic developments due to climate change and construction measures.

Alpine Natural Hazards at Gornergrat

Climate change and accompanying effects like rising temperatures have created new alpine phenomena and dangers. Avalanches, rockfalls and water inclusions may appear more often due to the steady warming of the atmosphere. In 2003, the rise of temperatures resulted in permafrost thaw and exceptional rockfalls (Gruber et al 2004b). As further research projects showed, characteristics of rock walls and their temperature depend not only on the quality of solar radiation and air temperature, but also on their topographic distribution (Gruber et al. 2004).

As the Stockhorn and Gornergrat are highly frequented by large numbers of tourists and skiers, the characteristics of this area must be constantly monitored.

Ground Ice at Kelle

The area Kelle at the northern slopes of the east–west running Gornergrat crest (3135 m) and Hohtälli (3286 m a.s.l.) is well known for its permafrost occurrences. Visible indicators are rock glaciers and perennial snow patches. Scientific studies consisted of measurements of ground temperatures and BTS values (Philippi 2003) and the development of permafrost models (Gruber 2000). In summer 2007, excavation work for a new ski run and a culvert system for artificial snow was carried out, and ground ice was exposed at various sites. The new ski run has a length of 2.5 km and 300 m altitudinal difference, and crosses rock glaciers and rock glacier-like features. Near-surface top layers were removed down to a depth of 8 to 10 m at some places. This offered the rare opportunity to have a look inside these features. The excavation was accompanied throughout 2007 by researchers of different universities. Geophysical measurements were carried out (Hilbich et al. 2007), ice samples taken, and the course of the ski track surveyed (Giessen, Zurich). Melting of the ground ice was already observed during the construction period.

Figure 1. Ground ice of the rock glacier with water conduit for artificial snow production (lower right).

Geophysical Analyses

In order to observe climate-related permafrost degradation, a fix ERT monitoring system was installed at the Stockhorn plateau in summer 2005 (Hilbich et al. 2008) in close co-operation with the PERMOS network (Permafrost Monitoring Switzerland). It enables regular (preferably seasonal) semi-automatic measurements of the apparent electrical resistivity of the ground. The ERT section consists of 55 electrodes with a spacing of 2 m, resulting in a length of 108 m in total. The vertical penetration depth is about 20 m.

Figure 2 shows the computed results of an ERT measurement made in September 2007. The position of the PACE boreholes are marked; however they may have a lateral offset of about 10 m to the ERT line.

In addition, the electrode array was complemented by a coinciding fix transect for refraction seismic monitoring in summer 2007. For the refraction seismic monitoring, one short (2 m spacing) and one long (4 m spacing) section with 24 geophones each were installed to account for both high spatial resolution (at a length of 46 m) and extension across the whole ERT line (96 m).

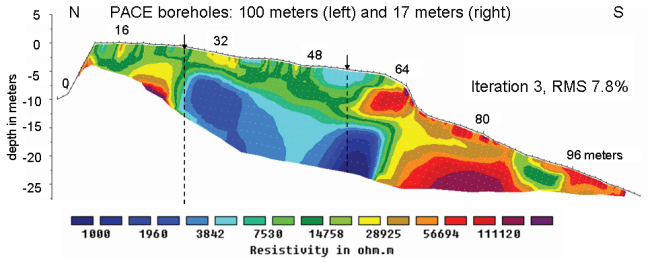

Figure 2. ERT results at Stockhorn Plateau and positions of the PACE boreholes 60/00 (left) and 61/00 (right).

In order to analyze the computed results of the seismic and geo-electric measurements, 4 temperature loggers were installed at a depth of 30 cm, with a lateral offset of about 5 m all along the section.

First results of the geophysical monitoring reveal a pronounced seasonal active layer dynamic up to a depth of about 3 to 5 m. Variations are due to the distinctive topography of the plateau with steeply inclined northern and southern slopes. This characteristic topography also influences the 3D subsurface temperature field, which has to be considered at the interpretation of borehole temperatures.

The combination of both geo-electric and seismic analysis allows the determination of the total content and temporal change of frozen and unfrozen water and air-filled pore space in the subsurface of this plateau (Hauck et al. 2008).

The PACE Monitoring Site Stockhorn

The studies at Stockhorn and Gornergrat directly relate to actual and current aspects of permafrost research under tourist aspects. The various continuous approaches allow a full understanding of the described factors in the high mountain area. Future research will aim at the investigation of the collected PACE data and the embedding into the general research in Valais. The data of both boreholes (100 m and 17 m) will be compared at a depth of 10 m in order to classify the results. Therefore one aspect is to develop a concept for the interpretation of the ongoing measurements under consideration of the natural disturbances and the modeling of corresponding temperature histories. To what extent the overall influence of climate change on both rock and air temperature is intensified by building measures in the alpine regions is of great interest for the tourism industry. A newly structured implementation of this area into the tourist concept generates unique scientific research possibilities due to the rather peripheral location within the Zermatt alpine region.

Acknowledgments

The authors are especially thankful for the support provided by the Zermatt Bergbahnen AG, which made the scientific research possible. Stephan Gruber (Zurich) and Thomas Herz (Giessen) were a crucial help in the data analyses.

References

Gruber, S. 2000. *Slope Instability and Permafrost, a Spatial Analysis in the Matter Valley, Switzerland*. Unpublished master thesis, Germany: Institute of Geography, Justus Liebig University Giessen.

Gruber, S., King, L., Kohl, T., Herz, T., Haeberli, W. & Hoelzle, M. 2004. Interpretation of geothermal profiles perturbed by topography: The alpine permafrost boreholes at Stockhorn Plateau, Switzerland. *Permafrost and Periglacial Processes* 15: 349-357.

Gruber, S., Hoelzle, M. & Haeberli, W. 2004a. Rock-wall temperatures in the Alps: Modelling their topographic distribution and regional differences. *Permafrost and Periglacial Processes* 15: 299-307.

Gruber, S., Hoelzle, M. & Haeberli, W. 2004b. Permafrost thaw and destabilization of alpine rock walls in the hot summer of 2003. *Geophysical Research Letters* 31: doi:10.1029/2004GL020051.

Hauck, C., Bach, M. & Hilbich, C. 2008. A 4-phase model to quantify subsurface ice and water content in permafrost regions based on geophysical datasets. *Proceedings of the Ninth International Conference on Permafrost, Fairbanks, Alaska, June 23–July 3, 2008.*

Hilbich, C. Roer, I & Hauck, C. 2007. Ground truth observations of the interior of a rockglacier as validation for geophysical monitoring data sets. *Eos Trans. AGU* 88(52), Fall Meet. Suppl., Abstracts C21a-0056.

Hilbich, C. et al. 2008. A geo-electric monitoring network and resistivity-temperature relationships of different mountain permafrost sites in the Swiss Alps. *Proceedings of the Ninth International Conference on Permafrost, Fairbanks, Alaska, June 23–July 3, 2008.*

King, L., Hof, R., Herz, T & Gruber, S. 2003. Long-term monitoring of borehole temperatures and permafrost-related data for climate change research and natural hazard management: Examples from the Mattertal, Swiss Alps. *Proceedings of the Eighth International Conference on Permafrost, Zurich, Switzerland, July 20-25, 2003*: 77-78.

King, L. Maag, C.C. & Baumann, C. 2008. Impacts of Climate Warming and Facilities on Rock Temperatures at a Tunnel in High Alpine Continuous Permafrost: Results of Long-Term Monitoring at Kleinmatterhorn, Swiss Alps. *Proceedings of the Ninth International Conference on Permafrost, Fairbanks, Alaska, June 23–July 3, 2008.*

Philippi, S., Herz, T. & King, L. 2003. Near-surface ground temperatures and permafrost distribution at Gornergrat, Matter valley, Swiss Alps. *Proceedings of the Eighth International Conference on Permafrost, Zurich, Switzerland, July 20-25, 2003*: 129-130.

The Microtopography of Periglacial Landforms on Mars

Nicolas Mangold
Laboratoire IDES, CNRS and Université Paris Sud, 91405 Orsay, France

Introduction

The planet Mars is covered by many landforms involving water ice, either at surface or at depth. These landforms are important in studying the geographic distribution of water ice, its temporal variation, and the possibility of freeze-thaw cycles in past epochs. Geologically recent Martian hillside gullies, discovered in Mars Orbiter Camera (MOC) Narrow Angle (NA) images (Malin & Edgett 2000), exhibit characteristic morphologies similar to terrestrial debris flows in mountain or arctic regions, formed by flowing water or water-rich slurries, leading Malin and Edgett (2000) to suggest that they, too, were formed by the action of water. Processes other than water erosion have been proposed to explain the formation of gullies, including the action of CO2-based debris flows (e.g., Musselwhite et al. 2001) and granular avalanches or mass wasting of CO2 frost (e.g., Ishii & Sasaki 2004). The role of liquid water is still debated, especially given the subfreezing mean temperature (-60°C) that might only reach submelting temperatures during high obliquity periods of the past (Costard et al. 2002). The origin of the fluid is also questioned. Various mechanisms for the formation of gullies by water have been proposed, although fundamentally they can be divided into either atmospheric or groundwater processes depending on the source of the water.

Until recently the only available images with sufficient resolution to detect gullies have been MOC NA data, and most previous studies have used this dataset. However, the HiRISE camera of the Mars Reconnaissance Orbiter provides high resolution (<30 cm/pixel) images that allow us a detailed observation of these landforms (Fig. 1). The microtopography can be measured thanks to methods of photoclinometry that use photometric properties of the surface (sun angle, spacecraft position, material property). This enables us to extract topographic profiles at the scale of the image sampling, thus a few tens of centimeters. We apply this method to the recent gullies, and especially to their transverse profile to examine their depth and their levee size. Indeed, the presence of levees and the end of the channel on slopes steeper than 5° are major arguments favoring a plastic or viscous behavior. These parameters help us to estimate the properties of the flowing material (Mangold et al. 2003), such as flow rate and viscosity, showing that a Bingham law might best explain the presence of levees and channels on slopes higher than 10°.

Methods

Photoclinometry can be used to extract topographic data from an image. Photoclinometry is difficult to use in terrains of various albedo like many regions of Mars, but gullies regions are often of regular albedo due to a thin dust mantle which is favorable to this method. Photoclinometric models are developed using the method described by Davis and Soderblom (1984). Models were calibrated using MOLA (Mars Observer Laser Altimeter) profiles as an envelope for the topography, but at the scale of gullies, MOLA data cannot be used directly because MOLA shot data are 300 m spaced. Cross sections for photoclinometry were chosen orthogonal to the flow, enabling us to assume a horizontal profile between both sides of the channel. Indeed, assuming that the flow is in the direction of the main slope, orthogonal profiles should have the same elevation on both sides of the gullies. Sinuous gullies are frequent on this image. Several studies have noted that debris flow levees are commonly higher on outsides of bends than on insides. This characteristic allows us the determination of the velocities of debris flows (Johnson & Rodine 1984). Indeed, the surface of the flow tilts toward the center of curvature of the bend as a result of the radial acceleration of the debris. The consequence of this tilt after the flow is the presence of larger and broader deposits on the outsides of channel bends. The levees are much narrower on the insides of channels bends. According to Johnson and Rodine (1984), the mean angular velocity of the flow inside the bends can be deduced from the radial acceleration a:

$$a = \frac{V^2}{R} \tag{1}$$

with V the velocity, R the radius of curvature. This radial acceleration is also equal to:

$$a = g \cos\alpha \tan\beta \tag{2}$$

with β the tilt estimated from the difference of elevation of levees (g is gravity and α is the slope).

$$V = \sqrt{gR \cos\alpha \tan\beta} \tag{3}$$

This method gives good measurements of velocities on Earth (Johnson & Rodine 1984).

Results

We have measured levees thickness, width, and channel size for different gullies of the selected image (Fig. 1). The method of levees dissymmetry in bends gives us estimates for the flow velocity. The example of Figure 2 shows typical levees size of 1.7 m on one side and 1 m on the other side, implying a tilt of 2.5° of the flow in this bend. The channel thickness is estimated from the average of the levees at 1.2 m. We find flow rates from 1.1 to 2.9 m/s. These values are small especially because of the small radii of curvature of most gullies of only 20 to 40 m. These flow rates also enable us to estimate the viscosity of the flow by using the measured depth, giving values from 200 to 1500 Pa.s. These viscosities

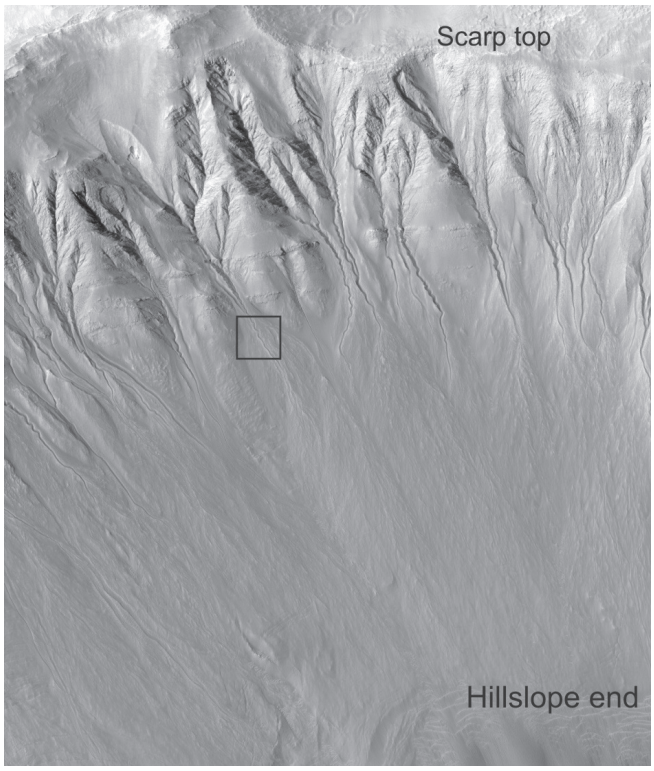

Figure 1. General view of HiRISE image 3464–1380 in Newton Basin. The scarp is about 1 km high. Many gullies are visible showing alcoves in the upward section, channels which typically are found on 10–20° slopes, and large aprons on the downward part. The image is about 2 km large.

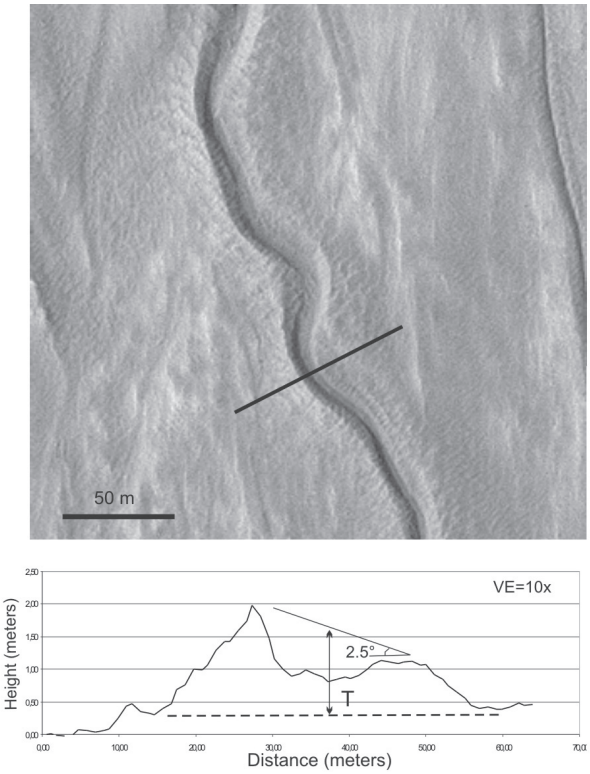

Figure 2. Close-up of Figure 1 on a sinuous channel. The profile shows the topography extracted from photoclinometry. Elevations are exaggerated about 10 times.

and flow rates are typical of viscous debris flows formed by 20 to 40% of liquid water mixed with rocks. This does not exclude other types of material to explain these properties, but excludes granular flows and pure liquid water as a good explanation for the channels observed. More data will be processed as soon as more images become available.

Our study is only preliminary among the large amount of data that are acquired throughout years. We show that the method used is powerful in extraction of material properties from remote sensing data. These results confirm material properties estimates of previous works using MOC images. Given the cold temperatures of Mars, liquid water might form especially from melting of an active layer in summer. Debris flows activity would occur only on the steepest slopes (>20°).

References

Costard, F., Forget, F., Mangold, N. & Peulvast, J.-P. 2002. Formation of recent Martian debris flows by melting of near-surface ground ice at high obliquity. *Science* 295: 110-113.

Davis, P.A. & Soderblom, L.A. 1984. Modeling crater topography and albedo from monoscopic orbiter images 1. Methodology. *J. Geophys. Res.* 89 (B11): 9449-9457.

Ishii, T. & Sasaki, S. 2004. Formation of recent Martian gullies by avalanches of CO_2 frost. *35th Lunar and Planetary Science Conference, 2004,* Abstract 1556.

Johnson, A.M. & Rodine, J.R. 1984. Debris flow. In: D. Brundsen & D.B. Prior (eds.), *Slope Instability*. Wiley and Sons, 257-361.

Malin, M.C. & Edgett, K.S. 2000. Evidence for recent groundwater seepage and surface runoff on Mars, *Science* 288: 2330-2335.

Mangold, N., Costard, F. & Forget, F. 2003. Debris flows over sand dunes on Mars: Evidence for liquid water. *J. Geophys. Res*. 108(E4): 5027.

Musselwhite, D.S., Swindle, T.D. & Lunine, J.I. 2001. Liquid CO2 breakout and the formation of recent small gullies on Mars. *Geophys. Res. Let.* 28(7): 1283-1285.

Coastal Erosion Since 1950 Along the Southeast Chukchi Sea, Alaska, Based on Both GIS and Field Measurements

William F. Manley
INSTAAR, Univ. of Colorado, Boulder, CO 80309-0450
James W. Jordan
Antioch University New England, Dept. of Environmental Studies, Keene, NH 03431
Leanne R. Lestak
INSTAAR, Univ. of Colorado, Boulder, CO 80309-0450
Owen K. Mason
Geoarch Alaska, P.O. Box 91554, Anchorage, AK 99509
Eric G. Parrish
INSTAAR, Univ. of Colorado, Boulder, CO 80309-0450
Diane M. Sanzone
BP Exploration (Alaska) Inc., Anchorage, AK 99519

Coastal environments at high latitudes are experiencing rapid change (e.g., Solomon 2005, Jorgenson & Brown 2005, Mars & Houseknecht 2007). Coastal erosion threatens a variety of nearshore marine, terrestrial, and freshwater habitats, and may be accelerating with Arctic warming. To better understand impacts for national parks in northwestern Alaska, a collaborative study has begun to document coastal change in the southeast Chukchi Sea.

A field-based component includes repeat photography, mapping and description of sediments and landforms, and periodic ground-truth measurements of shoreline change since 1987 at 27 coastal monitoring sites. A geospatial component began with creation of digital orthoimagery over a large area (>6000 km^2) at high resolution (1.0 m or better)

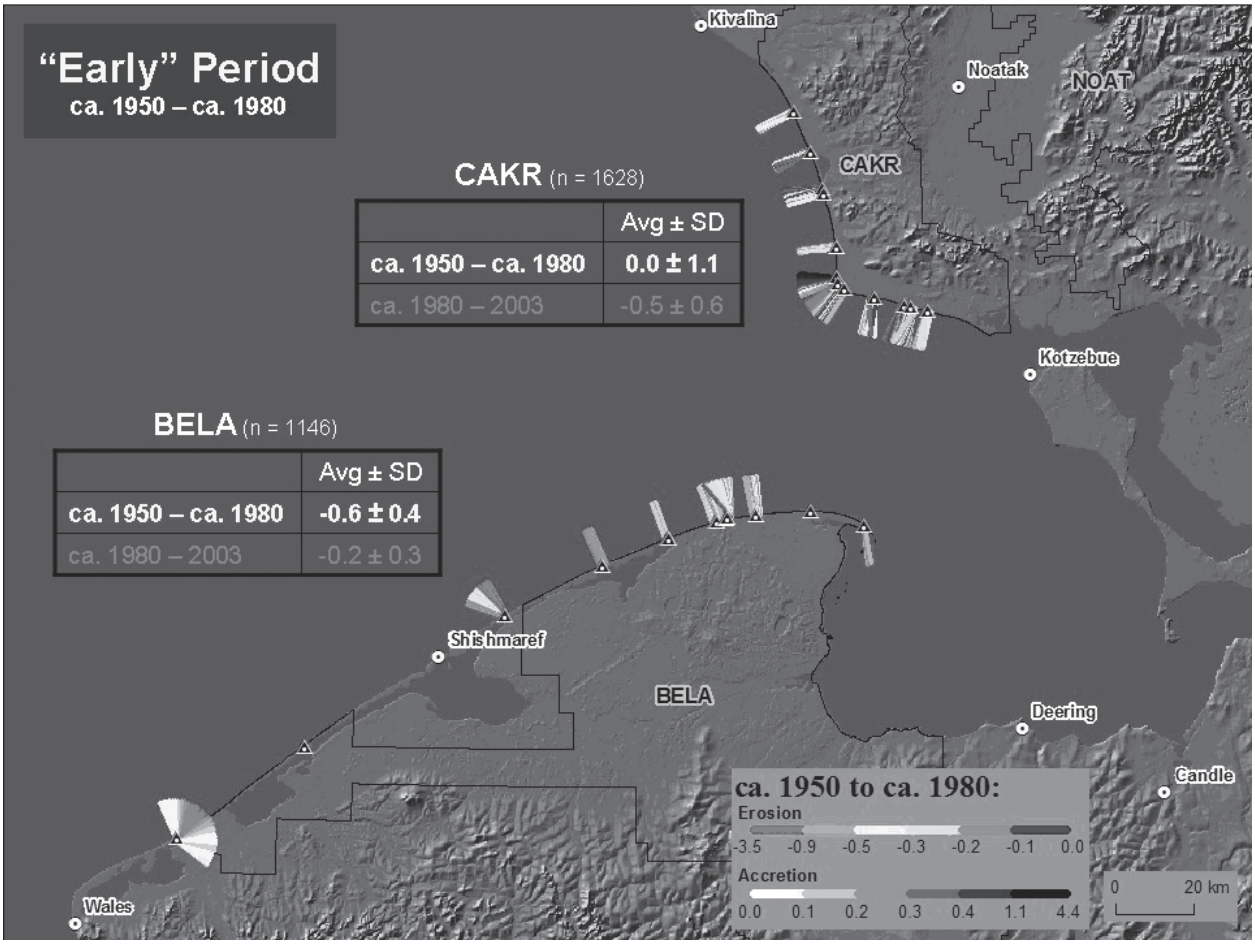

Figure 1. Bluff accretion and erosion near coastal monitoring stations during the "Early" period, from approx. 1950 to approx. 1980 (depending on air photo acquisition dates), in m/yr.

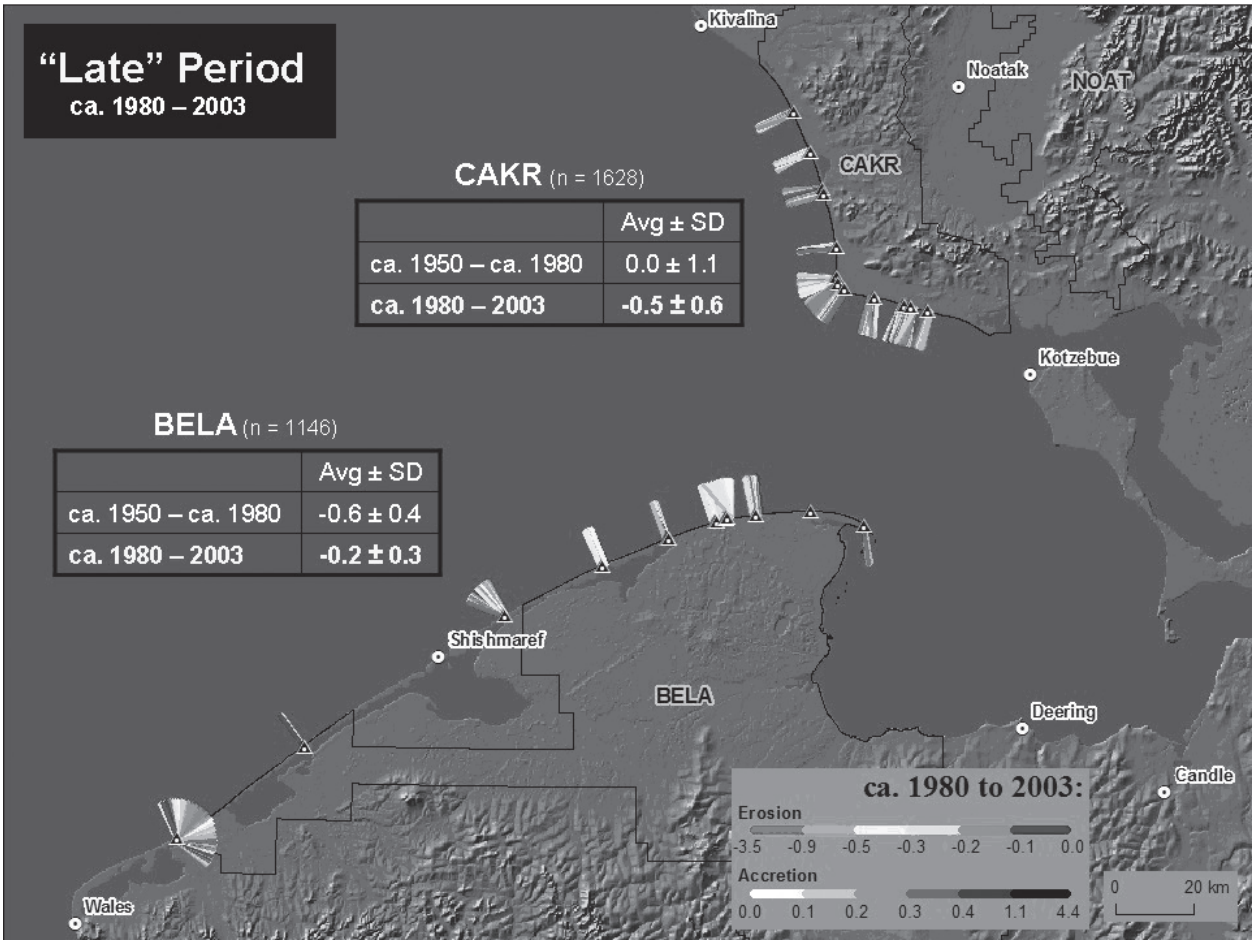

Figure 2. Bluff accretion and erosion during the "Late" period from approx. 1980 to 2003, in m/yr.

for three "timeslices": approx. 1950, approx. 1980, and 2003 (Manley et al. 2007). Spatial analysis of bluff retreat was conducted for selected areas near the monitoring sites using the USGS DSAS extension to ArcGIS (Thieler et al. 2005). Results indicate that the GIS-based measurements have acceptably low errors (+/- 0.1 m/yr or better).

Transects with 20 m spacing reveal high spatial variability related to coastal morphologies and processes (Figs. 1, 2). A comparison of the two time intervals suggests temporal variability also. For example, bluff erosion rates appear to have decreased after 1980 for the north-facing coast of Bering Land Bridge National Park (BELA), while increasing after 1980 for the west-facing coast of Cape Krusenstern National Monument (CAKR). In general, most of the >600 km-long coast from Wales to Kivalina has experienced erosion in the past five decades, with long-term average rates of 0 to -3 m/yr. Direct impacts include beach and bluff retreat, overwash deposition, migration or closure of inlets and lagoons, capture of thaw-lake basins, and release of sediment and organic carbon to nearshore waters. Higher temporal resolution is needed, but the coastal ecosystems in the region appear to be sensitive to the frequency and intensity of storm events, increasing temperatures, permafrost melting, sea-level rise, and the increasing length of the summer ice-free season.

References

Jorgenson, M.T. & Brown, J. 2005. Classification of the Alaskan Beaufort Sea Coast and estimation of carbon and sediment inputs from coastal erosion. *Geomarine Letters* 25: 69-80.

Manley, W.F., Parrish, E.G., Sanzone, D.M. & Lestak, L.R. 2007. *High-Resolution Orthorectified Imagery for the Coastal Areas of Bering Land Bridge NP (BELA) and Cape Krusenstern NM (CAKR)*. Northwest Alaska, Fairbanks, AK: National Park Service, Arctic Network I & M Program. Digital Media.

Mars, J.C. & Houseknecht, D.W. 2007. Quantitative remote sensing study indicates doubling of coastal erosion in past 50 yr along a segment of the Arctic coast of Alaska. *Geology* 35: 583-586.

Solomon, S.M. 2005. Spatial and temporal variability of shoreline change in the Beaufort-Mackenzie region, northwest territories, Canada. *Geomarine Letters* 25: 127-137.

Thieler, E.R., Himmelstoss, E.A., Zichichi, J.L. & Miller, T.L. 2005. Digital Shoreline Analysis System (DSAS) version 3.0: An ArcGIS extension for calculating shoreline change. *U.S. Geological Survey Open-file Report* 2005-1304.

Importance of Changes in Moisture for Geomorphic Responses to Rapid Climatic Warming in the Western Brooks Range and the Arctic Foothills, Northern Alaska: Lessons from the Past

Daniel Mann
Institute of Arctic Biology, University of Alaska, Fairbanks, AK 99775, USA
Pamela Groves
Institute of Arctic Biology, University of Alaska, Fairbanks, AK 99775, USA
Michael Kunz
Arctic Field Office, Bureau of Land Management, Fairbanks, AK 99709, USA

Climate changes between 12,500 and 8,000 ^{14}C yr BP triggered sweeping changes in vegetation cover, slope stability, and floodplain dynamics in the Brooks Range and Arctic Foothills of northern Alaska. Some of these climate changes involved rapid warming, so they provide analogs to the warming predicted for the coming century. Using palynology and radiocarbon-dated basal peats, Mann et al. (2002a) inferred that peat deposition (paludification) began, and shrub vegetation became widespread, ca. 12,500 ^{14}C yr BP, probably in response to a warmer and wetter climate. Stream-bank stratigraphy reveals that increased slope erosion caused rapid alluviation in valleys at the same time that *Populus* trees spread northward along braided floodplains before ca. 11,000 ^{14}C yr BP (Bockheim et al. 2003). During the Younger Dryas (YD) Chronozone (11,000–10,000 ^{14}C yr BP), lake levels fell and streams incised, probably in response to a drier, cooler climate that caused active layers to thin and the erosion of slopes to slow. A hiatus in records of *Populus* suggest that its geographic range contracted during the YD, and pollen records of other species suggest a cooler and drier climate during this interval. Basal peats dating to the YD are rare, suggesting that paludification slowed. Starting ca. 10,000 ^{14}C yr BP, lake levels rose, streams aggraded rapidly again, intense solifluction seems to have occurred, and *Populus* re-invaded the region (Mann et al. 2002a).

Paleoindian people occupied the Arctic Foothills briefly at the close of the YD, though there is increasingly good evidence that they were also present several centuries before the YD began ca. 11,000 ^{14}C yr BP (Kunz & Reanier 1994, Rasic 2000, Kunz, unpubl. data). We speculate that the spread of moist acidic tundra between 10,000 and 8,500 ^{14}C yr BP, along with the wet, organic-rich soils characteristic of the present landscape, caused the Paleoindians and their prey species to disappear from the region.

Floodplain dynamics are of particular interest for understanding the responses of arctic landscapes to climate changes, because they are centers of primary productivity and biodiversity (Walker et al. 2001). Floodplains aggraded at rates of meters/century just prior to 11,000 ^{14}C yr BP and immediately after 10,000 ^{14}C yr BP. Aggradation at such rapid rates must have been accompanied by widespread slope erosion, which suggests intense and widespread thermokarst formations.

Dating of relict alluvial fans in the western Brooks Range suggests several periods of increased deposition from headwater streams over the course of the Holocene. This work is in progress, but currently we have evidence for fan building ca. 4,000 ^{14}C yr BP and ca. 2,000 ^{14}C yr BP. Systematic observations begun in 2005 of floodplains in the western Brooks Range reveal that rapid aggradation is now underway in the headwater reaches of some stream systems. This aggradation is associated with mass movements of several different kinds occurring on hill slopes and in stream channels. Our observations suggest that we are at the cusp of another major ecosystem transition in the Brooks Range.

Most of the landscape-scale changes in the Arctic Foothills during the Pleistocene-Holocene transition involved changes in moisture balance, many imply changes in active-layer thickness, and some occurred very rapidly. The vulnerability of ecosystems in northern Alaska to changes in moisture balance is still evident today in the sensitive threshold existing between sand dunes and the vegetation surrounding them (Galloway & Carter 1993, Mann et al. 2002c). During the Late Pleistocene and early Holocene, the encroachment of marine water caused by rising global sea level was probably a major driver of increasing effective moisture on Alaska's North Slope (Mann et al. 2002b). Today, the moisture balance, which is still poorly constrained by predictive climate models, may be changing under the influences of increased winter snowfalls that accompany warmer winter temperatures, by northward shifts in the summer position of the Polar Front over the western Brooks Range and by net thawing of ice-rich permafrost as the result of warming in both summer and winter. Just as it was during the early Holocene, we suspect that moisture balance will be the key, proximal driver of ecosystem change in northern Alaska and in other arctic regions during the coming century.

References

Bockheim, J.G., O'Brien, J.D., Munroe, J.S. & Hinkel, K.M. 2003. Factors affecting the distribution of *Populus balsamifera* on the North Slope of Alaska, U.S.A. *Arctic, Antarctic, and Alpine Research* 35: 331-340.

Galloway, J.P. & Carter, L. D. 1993. Late holocene longitudinal and parabolic dunes in northern Alaska: Preliminary interpretations of age and paleoclimatic significance. *U.S. Geological Survey Bulletin* 2068: 3-11.

Kunz, M.L. & Reanier, R.E. 1994. Paleoindians in Beringia: evidence from arctic Alaska. *Science* 263: 660-662.

Mann, D.H., Peteet, D.M., Reanier, R.E. & Kunz, M.L. 2002a. Responses of an arctic landscape to late glacial and early Holocene climatic changes: the importance of moisture. *Quaternary Science Reviews* 21: 997-1021.

Mann, D.H., Reanier, R.E., Peteet, D.M. & Kunz, M.L. 2002b. Environmental change and arctic paleoindians. *Arctic Anthropology* 38: 119-138.

Mann, D.H., Heiser, P.A. & Finney, B.P. 2002c. Holocene history of the Great Kobuk Sand Dunes, Northwestern Alaska. *Quaternary Science Reviews* 21: 709-731.

Rasic, J.T. 2000. *Prehistoric lithic technology at the Tuluuk Hill Site, Northwest Alaska*. Master thesis, Department of Anthropology, Washington State University, Pullman, Washington.

Walker, D.A., Bockheim, J.G., Chapin, F.S., Eugster, W., Nelson, F.E. & Ping, C.L. 2001. Calcium-rich tundra, wildlife, and the Mammoth Steppe. *Quaternary Science Reviews* 20: 149-163.

Toward a Permafrost Map of Central Asia

Sergei Marchenko
Geophysical Institute, University of Alaska Fairbanks, USA
N. Sharkhuu
Institute of Geoecology, Mongolian Academy of Sciences, Ulaanbaatar, Mongolia
Xin Li
Cold and Arid Regions Environmental and Engineering Research Institute, Chinese Academy of Sciences, Lanzhou, China
Mamoru Ishikawa
Faculty of Environmental Earth Science, Hokkaido University, Sapporo 060-0810, Japan
Jerry Brown
International Permafrost Association, Woods Hole, MA, USA
Vladimir Romanovsky
Geophysical Institute, University of Alaska Fairbanks, USA
Dmitri Drodzov
Institute of the Earth Cryosphere, Moscow, Russia

Introduction

Although national permafrost maps exist for China, Kazakhstan, Mongolia, and Russia, there is no consistent cartographic or temperature criteria on which to base a unified permafrost map for the more topographically complex regions that prevail in Central Asia. The International Permafrost Association's (IPA) "Circum-Arctic Map of Permafrost and Ground-Ice Conditions" (1:10,000,000) employed an international legend developed primarily for continental (lowland) permafrost regions (Brown et al. 1997). That classification was applied to mountainous and high altitude regions with considerable uncertainties.

The retreat of glaciers and permafrost degradation in Central Asia in recent years is unprecedented as a consequence of warming. Accelerated warming of permafrost in mountainous, highland, and plateau regions of Asia could result in the disequilibria of the water cycle, increased mass wasting processes, and related sediment transport and slope hazards. Without a unified and verified regional permafrost map, these processes cannot be assessed adequately. Mapping, modeling, and monitoring strategies in mountain regions are under development to test and to verify climate-change scenarios and models.

In response to the difficulties involved in classifying and mapping of the region's permafrost, recommendations were approved at the IPA-sponsored International Symposium on Mountain and Arid Land Permafrost, Ulaanbaatar, Mongolia, September 2001 (Brown 2001). These included a request that an international team of experts prepare a unified permafrost map of Central Asia.

The workshop on the distribution and mapping of the permafrost distribution of Central and Eastern Asia was held prior to the Asian Conference on Permafrost, in Lanzhou, China, August 5–6, 2006, and was hosted by the Cold and Arid Regions Environmental and Engineering Research Institute (CAREERI). The workshop participants agreed that conventional mapping and modeling approaches of permafrost in this region recognize both latitudinal and altitudinal permafrost zonation, furthermore, and that the category of mountain permafrost be recognized as a subset of altitudinal zonation or, if appropriate, remain as a separate class. The proposed map should delineate each of these permafrost zones and contain actual and calculated ground temperatures and active layer thickness as point observations. Where available, estimates of ground ice would be included. However, for this next-generation map, classes of ground ice and spatial continuity (percentages) will not be part of the classification.

Mapping of Permafrost in Central Asia

Permafrost classifications

A major difficulty is in reconciling the usage of "continuous permafrost zonation," as it is commonly applied to continental permafrost (greater than 90% of the land surface; see Heginbottom 2002 for a comparison of classification schemes). A comparison of the spatial classifications in use in the four countries is presented in Table 1.

Modeling approach

An alternative approach of altitudinal permafrost mapping is modeling the ground temperature and permafrost distribution using the process-based models. Such an approach allows for spatial and temporal extrapolation of permafrost thermal state and distribution and also is well suited for studies with respect to permafrost response to climate change. But the process-based model requires an extensive set of input data such as meteorological data, surface characteristics (vegetation, snow cover), ground thermal properties, and topography. For the modeling of altitudinal permafrost within the rugged topography of the Altai Mountains, the basic dataset at 100 m resolution for the digital elevation model (DEM) was generated. The spatial permafrost model with a grid box size of 5 km uses gridded fields of monthly air temperature (topographically adjusted

Table 1. Classifications of permafrost continuity for China, Kazakhstan, Mongolia, and Russia.

Country (authors), landform, and region	Principle of permafrost zonation	Terminology for permafrost distribution	Permafrost extent
China			
1.1 Middle height mountain regions in Northeast China (Xu & Guo 1982)	Latitudinal zones	Islands	<30%
		Predominantly continuous	30 – 75%
1.2. Quinghai-Xizang High Plateau (Cheng 1983)	Index or degree of permafrost thermal stability	Lower belt	0°C – -0.5°C
		Middle belt	-0.5°C – -3°C
		Upper belt	< -3°C
1.3. Alpine mountains in West and East China (Zhang et al. 1985)	Altitudinal belts	Islands	
		Predominantly continuous	
Kazakhstan			
High Alpine Tien Shan and Pamirs Mountains (Gorbunov et al. 1996)	Altitudinal subbelts	Sporadic	<30%
		Discontinuous	30 – 90%
		Continuous	> 90%
Mongolia			
Middle height (Altai, Hovsgol, Khangai, & Khentei) mountain and adjacent arid land regions (Gravis et al. 1990, Sharkhuu 2006)	Latitudinal zones	Sporadic	< 1%
		Scattered islands	1 – 5%
		Islands	5 – 40%
		Discontinuous	40 – 80%
		Continuous	> 80%
Southern Russia			
Mountainous regions with depressions and separate plateaus and plains (Ershov 1991)	Latitudinal zones	Southern discontinuous	> -0.5. °C – -2°C
		Northern discontinuous	< -0.5°C – -2°C

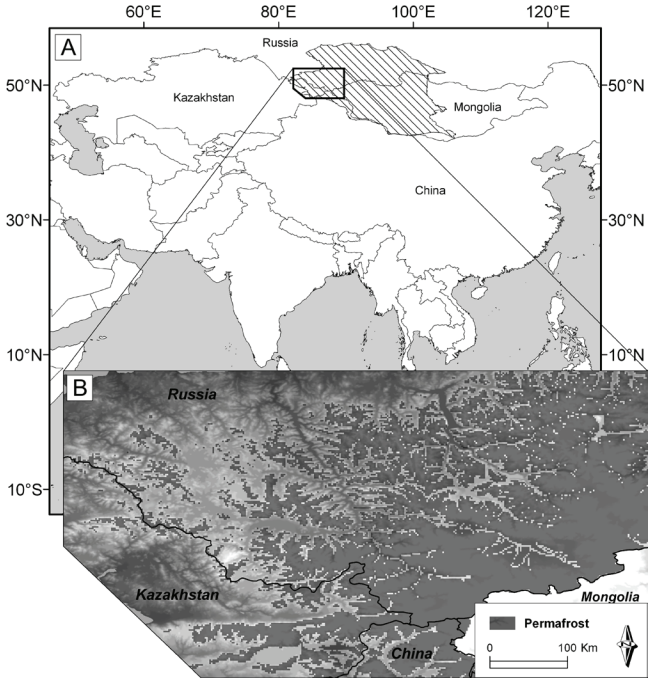

Figure 1. (A) The entire Altai-Sayan region (shaded area) and (B) modeled permafrost distribution within the northwest part of the region.

using the altitudinal air temperature gradients for the various parts of the Altai), incoming amount of solar radiation, vegetation, snow, and soil thermal properties. Figure 1 illustrates the results of the spatially-distributed permafrost model within the northwest part of the Altai Mountains.

Acknowledgments

We thank Alan Heginbottom, Emeritus, Geological Survey of Canada, who provided advice and information on existing classification schemes. We thank all the participants of the two workshops for their interest, discussions, and cooperation.

References

Brown, J. 2001. International Symposium on Mountain and Arid Land Permafrost and Field Excursion in Mongolia. *Frozen Ground News Bulletin* 25: 7-11.

Brown, J., Ferrians, O.J. Jr., Heginbottom, J.A. & Melnikov, E.S. 1997. *Circum-Arctic Map of Permafrost and Ground-Ice Conditions.* U.S. Geological Survey Circum-Pacific Map CP-45, 1:10,000,000, Reston, Virginia.

Cheng, G. 1983. Vertical and horizontal zonation of high-altitude permafrost. *Proceedings of the Fourth International Conference on Permafrost, Fairbanks, Alaska, 1983*: 136-131.

Gravis, G.F., Sharkhuu, N. & Zabolotnik, S.I. 1990. Geocryology and geocryological zonation. *National Atlas of Mongolia. GUGK of Mongolian Republic and* USSR. Ulaanbaatar: Moscow Plates, 40-41, (scale 1:4,500,000).

Heginbottom, J.A. 2002. Permafrost mapping: A review. *Progress Physical Geography* 26: 623-642.

Yershov, E.D. 1991. *Geocryological Map of Russia and Neighbouring Republics.* 16 sheets, 1:2,500,000. Moscow: Moscow State University.

Methane Ebullition During Field-Simulated Lake Expansion and Permafrost Degradation

Olivier Mazéas
University of California, Berkeley, Dept. of Geography 507 McCone Hall #4740, Berkeley, CA 94720-4740, USA
Joseph von Fischer
Colorado State University, Dept. of Biology, Fort Collins, CO 80523, USA
Robert Rhew
University of California, Berkeley, Dept. of Geography 507 McCone Hall #4740, Berkeley, CA 94720-4740, USA

Introduction

The Arctic accounts for 30% of the global emissions of methane (CH_4), a potent greenhouse gas, to the atmosphere (Christensen 1993). Within the Arctic, tundra and lakes are major sources, although they exhibit exceptionally high spatial variability. In arctic lakes, CH_4 ebullition is the major transport mechanism from the sediments to the atmosphere (95%). Ebullition rates are the greatest near the edges of the lakes, where active erosion occurs (Walter et al. 2006). In regions of continuous permafrost, arctic lakes have been expanding in recent decades, owing to permafrost melting and development of thermokarst (Smith et al. 2005). Lake expansion occurs when margins erode into water, supplying large amounts of organic rich material to the sediment-water interface. This allows carbon that was previously stored in the soil (permafrost and active layer) to become bioavailable and subject to decomposition. An increase in arctic CH_4 emissions as a result of permafrost thawing and lake expansion would constitute a positive feedback to arctic warming.

In order to better understand processes associated with lake CH_4 emissions, we conducted an experiment in a thaw lake on the Arctic Coastal Plain during the summer and fall of 2007. Different layers of tundra soil were incubated in chambers at the bottom of the lake, and methane ebullition was monitored.

Material and Methods

Eleven incubations were initiated in mid-July 2007 at a depth of 1 m in Cake Eater Lake, on the Barrow Environmental Observatory (BEO), Alaska. Each experimental chamber consisted of a bucket (yielding an exposed surface area of 0.07 m^2) fixed beneath an inverted funnel equipped with a sampling port to capture and collect the emitted gases.

The nearby tundra soil was vertically stratified in 3 distinct layers, which we extracted separately. First, the unfrozen (upper) section of soil, hereafter called the active layer, was sampled down to the depth of frozen soil, and included live plants and decaying peat material (3 adjacent points, ~20 cm deep and 13 kg each, $n = 3$). Next, the seasonally frozen layer soil (~12 cm thick) was sampled with a mechanical auger, homogenized, and divided into separate buckets (about 8 kg each, $n = 3$). Finally, a layer of permafrost was sampled (~12 cm deep), homogenized, and placed into buckets (about 8 kg each, $n = 3$). Although these soils were initially frozen, the samples thawed before the initiation of the experiment.

In addition to these 9 incubations, 2 others were added for comparative purposes: a control incubation using an empty bucket and another one containing sawdust mixed in with thawed permafrost. This sawdust provided cellulose, which is a major component of plant tissue, and its fermentation was expected to yield substrates for methanogenesis.

Ebullition gas volume determination and sampling were performed at variable time points along an 11-week period, ending on the days of initial lake freeze-up at the beginning of October.

From each gas sample, a 0.5 ml subsample was analyzed using a laser-based analyzer (Los Gatos Research) for methane and carbon dioxide determination. Nitrogen (N_2) was used as the carrier gas, and a calibration curve was run for each sequence (Matheson Tri-Gas grade CH_4).

The initial carbon content was determined using a Carbon-Nitrogen analyzer (NC2100, Carlo Erba). Water and sediment temperatures were recorded using in situ dataloggers, and wind speed and atmospheric pressure were also monitored throughout the experiment.

Results and Discussion

Only the active layer consistently emitted gases via ebullition throughout the experiment, with an average rate of 15 ml day^{-1}. The seasonally frozen and permafrost layers sporadically emitted small volumes of gas (typically 0 to 1 ml per day), with cumulative volumes ~20 times smaller than the active layer. The ebullition frequency was highly variable, and significant ebullition events could not be correlated with any of the environmental parameters monitored.

Daily ebullition events were consistently observed from the active layer incubations from the first day of the experiment, with large ebullition rates (> mean) occurring within 7–15 days and some of the highest rates starting within 3–4 weeks. The replicates show a similar overall trend; however, one replicate could not be monitored after the fifth week of incubation due to technical problems. Ebullition significantly decreased or ceased during the last 7 to 10 days prior to lake freeze-up, a period when the water temperature dropped to between 1 and 0°C. In contrast, no temporal pattern of ebullition rates was observed for the frozen soil layers.

The gas composition of the collected bubbles also differed

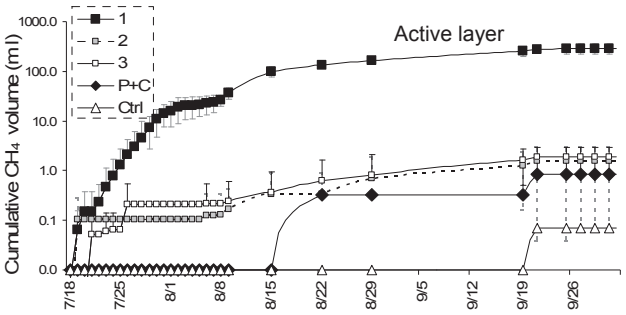

Figure 1. Cumulative CH_4 volume emitted from the beginning of the experiment to the lake freeze-up (logarithmic *Y* axis). Means and error bars are indicated for the replicate incubations. 1: Active layer; 2: Seasonally frozen layer; 3: Permafrost, P+C: Cellulose-enriched permafrost; Ctrl: Control.

between the active layer and frozen layers below. Gas samples from the active layer had CH_4 concentrations that increased gradually during the first two weeks, reaching concentrations in the same range as the ones measured during the following higher gas emission period (~30%). However, when ebullition decreased at the end of the season, slightly higher concentrations (~50% CH_4) were observed. Meanwhile, CO_2 concentrations remained below the detection limit (<0.5%).

The seasonally frozen and permafrost replicates, as well as the cellulose-enriched incubation, were associated with much smaller CH_4 concentrations than the active layer, even when relatively large volumes of gas were emitted. A few samples exhibited high CH_4 concentrations, but were always associated with small ebullition volumes.

Cumulative CH_4 release from the active layer was approximately 160 times higher in the active layer than in the 2 frozen layers (Fig. 1). Meanwhile, cumulative ebullition volumes from the frozen layers were not significantly different from each other. The large variability associated with the seasonally frozen layer was because one of the replicates showed very low emissions, comparable to the control experiment.

Emission rates normalized to carbon content in soil samples were ~50 times higher for the active layer than for the permafrost or the frozen active layer, further demonstrating the unexpected low emissions from the frozen layers (Fig. 2).

Even though there was less carbon in the frozen soil incubations, the particularly low emission from the cellulose-enriched incubation suggests the pattern is not due to carbon limitation, but rather that there are insignificant methanogen or syntrophic organism populations in the formerly frozen soils, even after 11 weeks in the lake, where existing microbes could have colonized the incubated substrates.

We calculated a mean emission rate of 39 mg CH_4 m^{-2} day^{-1} for simulated thermokarst erosion of the active layer. Such a rate is in the range of background ebullition reported by Walter et al. (2006). This corresponds to 0.2 mg CH_4 day^{-1} per kg of active layer.

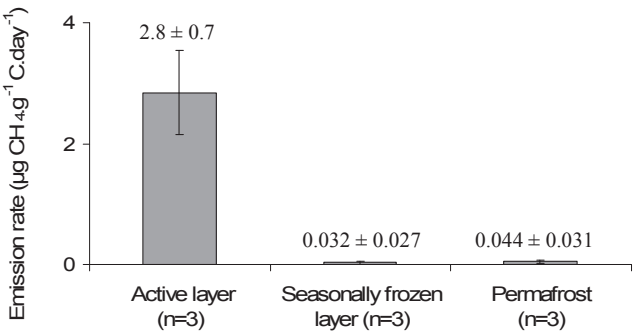

Figure 2. Overall methane ebullition rates in µg CH_4 per day per grams of initial tundra carbon (± standard deviation).

Conclusions

During the first 11 weeks of immersion, the thawed active layer emitted significant amounts of CH_4 while frozen soils only sporadically produced gas bubbles, with CH_4 volumes about 160 times smaller. These low rates could be due to the lack of indigenous methanogen populations in the frozen soils and slow subsequent colonization during the incubation period. The active layer incubations exhibited an average of 39 mg CH_4 m^{-2} day^{-1} during the experiment. This rate is in the range as background ebullition observed by Walter et al. (2006) in Siberian lakes, which is believed to represent 25% of total lake ebullition.

We hope to continue monitoring these incubations over several years and add additional treatments (autoclaved active layer, combined layers, low and high center polygonal tundra) to better define the timing, amplitude, and chemical signatures of methane ebullition as well as its primary physical, chemical, and biological controls. Moreover, we hope to perform additional analyses, such as carbon isotopic determination of CH_4, microbial community characterization, and dissolved oxygen measurements. Similar incubations should also be initiated in larger thermokarst lakes in order to compare ebullition under different chemical and physical parameters.

Acknowledgments

We thank Jerry Brown, the Barrow Arctic Science Consortium, and the Ukpeagvik Iñupiat Corporation for facilitating work at the BEO; A. Kear for gas analyses; and M. Whelan, M. Nguyen, and A. Atwood for field assistance.

References

Christensen, T.R. 1993. Methane emission from Arctic tundra. *Biogeochemistry* 21: 117-139.

Smith, L.C., Sheng, Y., MacDonald, G.M. & Hinzman, L.D. 2005. Disappearing Arctic lakes. *Science* 308: 1429.

Walter, K.M., Zimov, S.A., Chanton, J.P., Verbyla, D. & Chapin III, F.S. 2006. Methane bubbling from Siberian thaw lakes as a positive feedback to climate warming. *Nature* 443: 71–75.

A Provisional 1:50,000 Scale Soil Map of Wright Valley, Antarctica

M. McLeod
Landcare Research, Private Bag 3127, Hamilton, New Zealand
J.G. Bockheim
Department of Soil Science, University of Wisconsin, 1525 Observatory Drive, Madison, WI 53706-1299, USA
M.R. Balks
Department of Earth and Ocean Sciences, University of Waikato, Private Bag 3105, Hamilton, New Zealand

Introduction

During the austral summers of 2005–2007, we mapped soils and permafrost form within Wright Valley, Antarctica, for use at a scale of 1:50,000. Wright Valley, within the McMurdo Dry Valley region of Northern Victoria Land, extends 53 km from the Wright Lower Glacier, a lobe of the Wilson Piedmont Glacier, to the Wright Upper Glacier, an outlet glacier from the East Antarctic ice sheet. The Onyx River flows seasonally from Wright Lower Glacier inland 30 km to Lake Vanda, which is 90 m a.s.l. The study area also includes the Dais, Labyrinth and the North and South Forks. Although many soils have been described in central Wright Valley, they have primarily been used to aid and interpret surficial geologic deposits and assign ages/names to develop a glacial chronology. Renewed interest in environmental classification in a spatial framework (Waterhouse 2001) has led to the demand for soil and permafrost maps of Antarctica. This paper presents preliminary results from those investigations.

Methods

Stereo-pair aerial photographs of Wright Valley were examined with preliminary soil boundaries plotted onto a GIS-based geo-referenced satellite image (http://usarc.usgs.gov/ant-ogc-viewer/declasdownload.htm) and a hill shade image built from a 2 m post-processed resolution LIDAR file (http://usarc.usgs.gov/ant-ogc-viewer/lidardownload.htm) at 1:50,000 scale.

Fieldwork was undertaken to validate the preliminary boundaries and determine the nature of surface geology, soils, and permafrost. About 300 small test pits were excavated, described, and classified following Soil Taxonomy (Soil Survey Staff 2003) and located by GPS. The soil pits were then backfilled. Weathering stage follows Campbell and Claridge (1975), while salt stage follows Bockheim (1990). Soil boundaries were upgraded daily in the field using the GPS and soil pit information. At 118 locations larger pits were dug to at least 70 cm (unless ice-cemented permafrost or boulders were encountered), with the soil being sampled by horizon. Both <2 and >2 mm fractions were weighed, with the <2 mm fraction being retained for analysis.

Analysis for pH, EC, water soluble cations (Ca, Mg, K, Na) anions (Cl, nitrate-N, SO_4) followed methods at http://www.landcareresearch.co.nz/services/laboratories/eclab/eclabtest_list.asp#water. Total soluble salts to 70 cm (TSS_{70}) were calculated following Bockheim (1979).

Results

Broadly, eight groups of soil parent materials have been identified. They are:

- Peleus till, a silty olive-coloured till with few stones and the oldest drift recognized in the valley, was deposited before 3.9 Ma, by a wet-based glacier draining the East Antarctic Ice Sheet.
- Drift from up to 8 westward glacial advances from grounded ice within Ross Sea Embayment.
- Drift from 4 advances (Alpine I–IV) of alpine glaciers along the south valley wall. These drifts are out of phase with the westward flowing glaciers as a result of the snow-gun effect (Prentice 1991), resulting in a complex cross-cutting pattern of surficial geology and in some cases, soil classification.
- Drift from 3 eastward advances of Upper Wright Glacier (which has acted as an alpine glacier) tentatively correlated with Alpine I, IIa and III advances within the lower Wright Valley.
- Rock glaciers in the North and South Forks tentatively correlated with the Alpine IIb advance (Bockheim & McLeod submitted) and two rock glaciers flowing from the south wall of the main valley, immediately to the east of the Dais.
- Alluvium deposited by the Onyx River.
- Colluvium on valley walls and footslopes. Generally, on the north wall, ice-cemented permafrost is not encountered at a soil depth of less than 70 cm (in mid-summer), whereas on the south wall and especially in western reaches, ice-cemented permafrost is commonly encountered at a soil depth of less than 70 cm.
- Bare rock associated with valley walls and valley floor dyke systems. Bedrock consists predominantly of Precambrian to Paleozoic metasediments, granite-gneisses, and lamprophyre and rhyolite porphyry dikes, Devonian-to-Jurassic Beacon Supergroup sandstones intruded by the Jurassic Ferrar Dolerite (McKelvey & Webb 1962).

Soils were classified into the Gelisol order to the family level (Soil Survey Staff 2003); mineral soils with one or more horizons that are cryoturbated are classified as Turbels. Soils without cryoturbation are Orthels. Both suborders are divided into Great Groups on the basis of soil climate and other soil properties. Within Wright Valley soils are both hydrous and anhydrous conditions, as it is soil moisture conditions that are classified rather than atmospheric conditions. Therefore, the soils are classified as Haplorthel/Haploturbels, where ice-cemented permafrost first occurs within 70 cm of the soil

surface or as Anhyorthel/Anhyturbels, where ice-cemented permafrost first occurs below 70 cm. Gelisols were further subdivided into subgroups on the basis of presence or absence of soluble salts (e.g., salic, gypsic, nitric, petrosalic, and petrogypsic).

Discussion

Although 8 broad groups of parent materials have been identified, the soil pattern is also strongly influenced by soil climate. At low elevation (<100 m) from the east along the valley floor to the western end of Lake Vanda, the valley lies within coastal Zone 1 (Marchant & Denton 1996), where the climate is relatively mild, with precipitation at Vanda station approximately 80 mm y^{-1}. Especially near the coast, the precipitation allows recharge of soil water lost to evaporation. Thus ice-cemented permafrost remains close to the soil surface, and soil development is hindered (Bockheim 1979). Similarly, where soil water is recharged from the Onyx River or on foot slopes below a meltwater source, ice-cemented permafrost remains close to the soil surface (McLeod et al. 2008). Generally, in these locations a Typic Haplorthel/Haploturbel association is mapped in recognition of the cryoturbated zones, creating patterned ground around flat-centred polygons.

With increasing age of drift material, and away from the influence of soil moisture recharge, aerosol salts accumulate in the soil, developing firstly increased total salts within the soil until a salic horizon (Soil Survey Staff 2003) develops. When the salic horizon is ultimately cemented, "Petro" subgroups are classified. It follows, therefore, that the combination of a Salic Subgroup under a Haplorthel Great Group is unlikely to occur.

Salt accumulation in the soil profile is relatively low at the coastal eastern end of the valley and highest in the central valley, where we recorded an indurated salic horizon with TSS_{70} of approximately 10 500 mg cm^{-2}. Towards the western end of the valley and in the North and South Forks, salt accumulation does not appear to be so great, possibly because of the low precipitation and the consequent low aerosol deposition of salts.

Soils with a water table were described from two different zones. In the hyporheic zone of the Onyx River, predominantly Typic Haplorthels were mapped, whereas in a bouldery hyporheic zone near the terminus of the Onyx River, a Typic Aquorthel was identified that contained low chroma mottles. In contrast, adjacent to Don Juan Pond in the South Fork, groundwater is sufficiently salty to prevent freezing, and Salic Aquorthels with TSS_{70} of approximately 4000 mg cm^{-2} were described.

Acknowledgments

This work was partially funded by the New Zealand Foundation for Research, Science, and Technology under contract C09X0307. Antarctica New Zealand provided logistical support.

References

Bockheim, J.G. 1979. Ice core and ice cement effects on soil development, eastern Wright Valley, Antarctica. *New Zealand Journal of Geology and Geophysics* 22(4): 487-493.

Bockheim, J.G. 1990. Soil development rates in the Transantarctic Mountains. *Geoderma* 47: 59-77.

Campbell, I.B. & Claridge, G.G.C. 1975. Morphology and age relationships of Antarctic soils. Quaternary Studies. *Royal Society of New Zealand Bulletin* 13: 83-88.

Marchant, D.R. & Denton, G.H. 1996. Miocene and Pliocene Paleoclimate of the Dry Valley region, Southern Victoria Land: A geomorphological approach. *Marine Micropaleontology* 27(1–4): 253-271.

McKelvey, B.C. & Webb, P.N. 1962. Geological investigations in northern Victoria Land, Antarctica –Geology of Wright Valley. *New Zealand Journal of Geology and Geophysics* 5(1): 143–162.

McLeod, M., Bockheim, J.G. & Balks, M.R. 2008. Glacial geomorphology, soil development and permafrost features in central-upper Wright Valley, Antarctica. *Geoderma*. In press.

Prentice, M.L. & Matthews, R.K. 1991. Tertiary ice sheet dynamics: The snow gun hypothesis. *Journal of Geophysical Research* 96(B4): 6811–6827.

Soil Survey Staff 2003. *Keys to Soil Taxonomy*. U.S. Department of Agriculture, Natural Resources Conservation Service. soils.usda.gov/technical/classification/tax_keys/keysweb.pdf

Waterhouse, E.J. 2001. A state of the environment report for the Ross sea region of Antarctica. *Ross Sea Region 2001*. New Zealand Antarctic Institute, Christchurch .

Improving the Parameterization of Snow Processes to Model the Implications of Shrub-Tundra Expansion on Soil Temperatures

Cecile Menard
Centre for Ecology and Hydrology, Wallingford, UK
Richard Essery
School of GeoSciences, University of Edinburgh, UK
Douglas Clark
Centre for Ecology and Hydrology, Wallingford, UK

Introduction

Field observations, satellite remote sensing, and models suggest that the recent warming of the Arctic has caused an increase in shrub cover (Sturm et al. 2005, Jia et al. 2006, Tape et al. 2006). This change in vegetation structure is expected to significantly affect snow distributions and interactions between the land surface and the atmosphere, with consequences for the hydrology, ecology, carbon, and energy balances of the region. Shrubs capture wind-blown snow, increasing snow depths, and decreasing winter water losses through sublimation. The low thermal conductivity of snow insulates the soil, deepening the active layer and affecting the permafrost regime. Thus, snow/permafrost interactions will be at the core of feedback loops leading to further shrub expansion. For example, warmer winter soil temperatures lead to increased microbial activity and hence to greater nutrient availability, which will further stimulate shrub growth (Chapin et al. 2005, Tape et al. 2006). Carbon cycling will also be affected, although the environmental effects of greater shrub abundance are uncertain. Sturm et al. (2005) suggest that the Arctic may become a carbon sink because of increasing production of above-ground shrub biomass. On the other hand, thawing of permafrost is expected to liberate large amounts of carbon currently sequestered in frozen organic soils (Solomon et al. 2007).

Land surface models (LSMs) are required to calculate energy and water fluxes between the land and the atmosphere in global climate models (GCMs), but the representation of cryospheric processes is generally crude in current LSMs. In this paper, two different snow schemes are tested offline to assess the implications for soil processes of the predicted northward expansion of shrub-tundra.

Methods

Field site

Meteorological measurements and soil temperatures were obtained at two sites in the Wolf Creek Research Basin (60°36′N, 134°57′W), Yukon Territory, Canada (Pomeroy et al. 2004):

1. An alpine tundra site (1615 m a.s.l.), characterized by 0.01–0.3 m tall vegetation (willow, dwarf birch, grass, and lichen) and bare rock, within the widespread discontinuous permafrost zone (Lewkowicz & Ednie 2004). Soil temperatures were measured at 3 cm depth.
2. A shrub tundra site (1250 m a.s.l.), with 0.4–3 m tall vegetation (willow, sparse white spruce, dwarf birch and grass), within a sporadic discontinuous permafrost zone. Soil temperatures were measured at 11 cm depth.

Data for the one-year period starting on 1 August 1998 are used here. Air temperatures at both sites were similar from November to February, but the alpine site was generally 2°C colder than the shrub tundra site for the rest of the year. Because the alpine site is more exposed, the annual average wind speed was greater by 2.3 ms^{-1}. Although the snowfall is almost the same at the two sites, increased wind ablation and reduced trapping by shrubs give lower snow depths at the alpine site. The importance of snow insulation is reflected in differences in soil temperatures; the greatest differences occurred in March, for which average soil temperatures were -9°C at the alpine site but -4°C at the shrub tundra site. Summer differences were smaller, and down to 0.4°C in June and August (7°C at the alpine site and 6.6°C at the shrub tundra site).

Model parameterization

Snow depths and soil temperatures at the two sites have been simulated with the JULES (Joint UK Land Environment Simulator; Blyth et al. 2006) LSM using two different snow schemes. Simulations were first performed with the present version of JULES, which represents snow as a composite with the top soil layer. The insulating properties of snow are incorporated by adjusting the thermal conductivity and thickness of the layer (Cox et al. 1999). The temperature of this top layer is taken to be at the layer midpoint, whether snow is present or not, hence it may reflect the soil or the snow temperature depending on snow depth. A new snow model using a multilayer representation of snow has now been developed for JULES. Simple representations of snow compaction, and retention and refreezing of liquid water, all of which were neglected in the original model, have been included.

Model results

Figures 1 and 2 compare simulated snow depths and soil temperatures with measurements. Simulations with the original snow model underestimate winter soil temperatures, particularly for the alpine site where the measurement depth lies within the model's composite snow-soil layer, but also for the shrub tundra site where the measurements are below this layer. The greater snow insulation simulated by the new model greatly improves the soil temperature simulations,

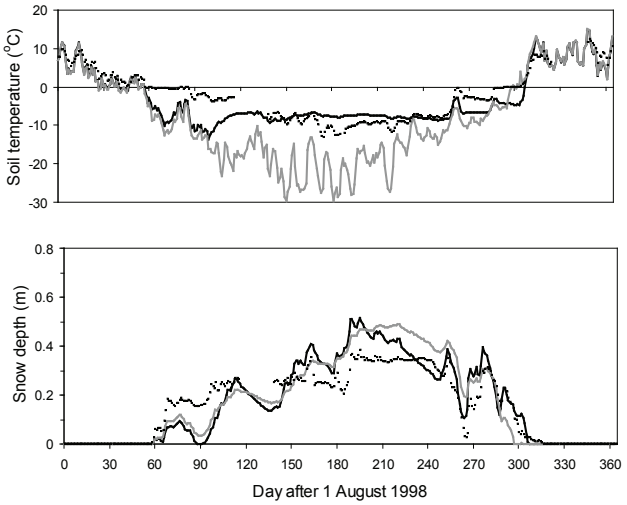

Figure 1. Daily average soil temperatures and snow depths from observations (dotted lines), the composite snow model (grey lines), and the multilayer snow model (black lines) for the alpine site.

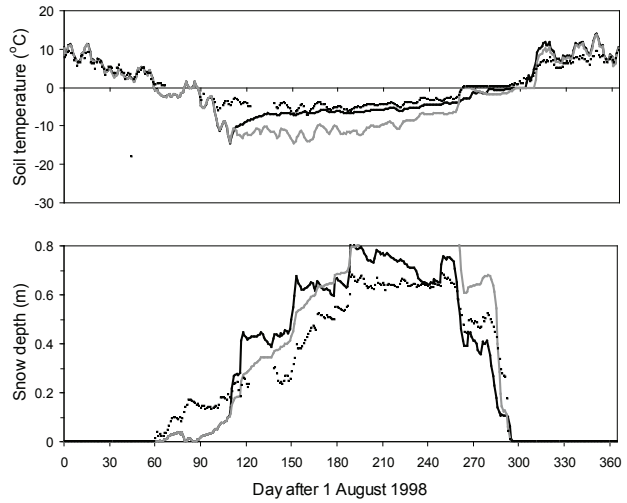

Figure 2. As Figure 1, but for the shrub tundra site.

except for periods such as November when the simulated snow depth is underestimated at both sites.

Additional runs will be made to assess how much of the soil temperature variation between sites can be explained by meteorology and how much by vegetation cover. One way to address this will be to perform simulations with vegetation characteristics at one site used as model input at the other.

Acknowledgments

Field data were supplied by John Pomeroy, University of Saskatchewan. Cecile Menard is supported by a NERC studentship.

References

Blyth, E.M. et al. 2006. JULES: a new community land surface model. *IGBP Newsletter* 66: 9-11.

Cox, P.M. et al. 1999. The impact of new land surface physics on the GCM simulation of climate and climate sensitivity. *Climate Dynamics* 15: 183-203.

Chapin, F.S. et al. 2005. Role of land-surface changes in Arctic summer warming, *Science* 310: 657-660.

Jia, G.J., Epstein, H.E. & Walker, D.A. 2006. Spatial heterogeneity of tundra vegetation response to recent temperature changes. *Global Change Biology* 12: 42-55.

Lewkowicz, A.G. & Ednie, M. 2004. Probability mapping of mountain permafrost using the BTS method, Wolf Creek, Yukon Territory, Canada. *Permafrost and Periglacial Processes* 15: 67-80.

Pomeroy, J., Essery, R. & Toth, B. 2003. Implications of spatial distributions of snow mass and melt rate on snowcover depletion: observations in a sub-arctic mountain catchment. *Annals of Glaciology* 38(1): 195-201.

Solomon, S. et al. (eds.). 2007. *IPCC 2007, Climate Change 2007: The Physical Science Basis. Contribution of Working Group I to the Fourth Assessment Report of the Intergovernmental Panel on Climate Change*. Cambridge: Cambridge University Press.

Sturm, M. et al. 2005. Winter biological processes could help convert arctic tundra to shrubland. *Bioscience* 55: 17-26.

Tape, K., Strum, M. & Racine, C. 2006. The evidence for shrub expansion in Northern Alaska and the Pan-Arctic. *Global Change Biology* 12: 686-702.

Pyrogenic Dynamics of Cryosols and Carbon Pools in Open Forests of Northeast Eurasia

N.S. Mergelov
Institute of Geography RAS, Moscow, Russia

There is no sufficient data on fires and postpyrogenic functioning of ecosystems at the north tree boundary at the Kolyma River Lowland (Russia). Our studies carried out in larch open forests of the northeast part of this region (69°N, 161°E) showed that fires are among the major factors influencing vegetation and soil successions. All loamy cryohydromorphic soils (Turbic, Turbi-Saprihistic, Gleyi-Turbic & Endogleyi-Turbi-Histic Cryosols; Gelic Gleysols) formed at watersheds on loess-icy complex sediments represent various stages of postpyrogenic development.

The most mature ecosystem of the study site is old (quasi-climax) larch open forest (~ 200 years old). Postpyrogenic recovery of vegetation occurs through various nonstable ecosystems: highly productive dense larch forest (30–60 years old), larch open forest (60 years old), treeless areas with grass and low shrubs (15–40 years old), and others (Fig. 1).

The strong fire in combination with absence of seeds for tree reproduction could lead to formation of treeless areas with low shrub-grassy vegetation, stable to larch reproduction during at least 30 years. In later stages, larch appears in such areas forming open woodlands.

The trend of postpyrogenic succession depends primarily on the type (ground or crown fire, ground fires prevail) and intensity of fire. Among others important factors is the availability of the sufficient amount of viable seeds. In the presence of surplus amounts of seed, the plant succession could develop through the stage of highly productive dense larch forest, which subsequently thins out.

The trends in transformation of soil cover generally for initial postpyrogenic stages (increase of the active-layer thickness, increase of soil moisture due to the melting of ice lenses and wedges, intensification of cryoturbations and gleyic processes) differ significantly in the later stages and depend on direction of postpyrogenic plant succession (Fig. 2).

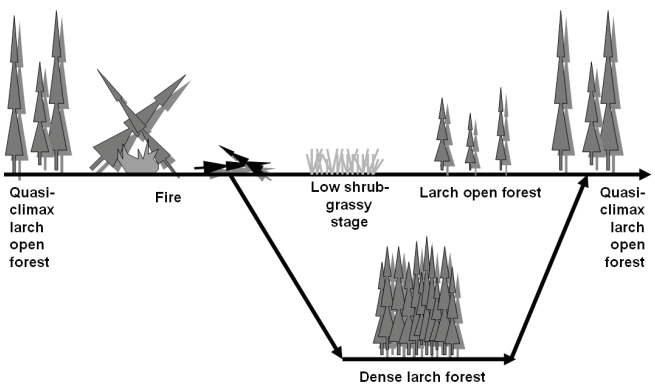

Figure 1. Sequence of postpyrogenic succession change.

Development of dense larch forest with thick lichen-low shrub–moss ground cover leads to a more stable state of the soil cover since thermokarst processes are not so intensive. Active-layer thickness strongly decreases (from 120–140 cm to 30–50 cm). Morphological gleyic and cryoturbation features are not strongly expressed in the soil profile. Due to autoregulation of the ecosystem, dense larch forest thins out. This process is accompanied by raising of diversity of the ground vegetation: the share of mosses decreases while the share of lichens increases. The ground vegetation of mature larch open forest comprises regular low shrub-moss and moss-lichen parcels-polygons. The difference in thermal capacity of mosses and lichens—parcel-forming plants, leads to heterogeneity in thawing depth, which varies also on a regular basis. The average active-layer thickness under low-shrub moss parcel is 25 cm; under moss-lichen parcel is 45 cm.

The treeless areas with low shrub-grassy vegetation even 30–40 years after the fire have high active layer thickness of 90–120 cm, thermokarst processes are still active, and polygonal microtopography is formed. Thermokarst

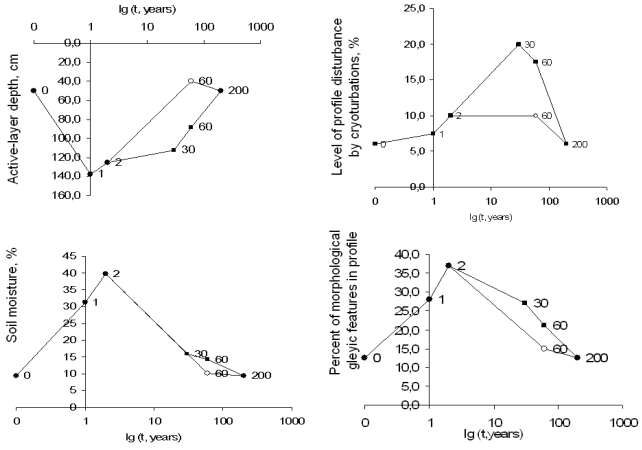

Figure 2. Soil properties alteration in dependence to fire age and/or type of postpyrogenic succession.
● = consecutive postpyrogenic development of larch open forest;
o = development through stage of dense larch forest
Legend:

Time passed after the last fire (years)	Postpyrogenic stages of vegetation recovery
1	Burn without arboreal vegetation
2	Burn without arboreal vegetation
30	Burn without arboreal vegetation (low shrub-grassy stage)
60	Larch open forest
60	Dense larch forest
200	Old (quasi-climax) larch open forest

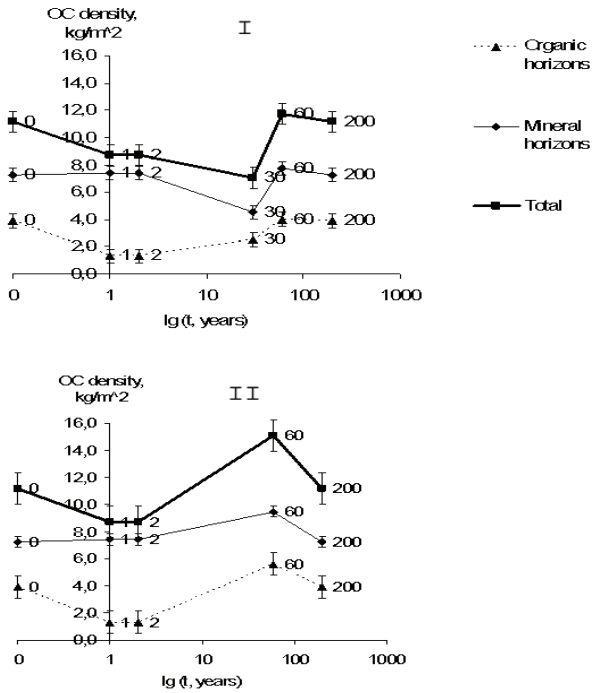

Figure 3. Alteration of OC densities in organic and mineral horizons in dependence to fire age and/or type of postpyrogenic succession (for the legend see Fig. 2).
I – consecutive postpyrogenic development of larch open forest
II – development through stage of dense larch forest

depressions (1–4 m in diameter) indicate an intersection of ice wedges, which partially melt when vegetation is destroyed during the fire. The soil profiles are strongly disturbed by cryoturbations.

Postpyrogenic successions of vegetation and soils are cyclical. This fact provided an opportunity to estimate dynamics of soil features including organic carbon (OC) densities (in similar lithological and geomorphological conditions) (Fig. 3).

OC densities in mineral horizons were calculated for the 50 cm layer. OC storage in organic horizons was estimated for its actual thickness. "Expected" postpyrogenic reduction of OC density is most significant in organic horizons (from 3.9 to 0.5 kg C/m^2). However, 60 years after the fire, OC density reached its initial values in larch open forest and even exceeded initial values in a highly productive ecosystem of dense larch forest (Δ = 1.7 kg C/m^2) with thick moss cover stimulating active peat accumulation. Alteration of OC densities in mineral horizons is less evident. For the larch open forest ecosystem 30 years after the fire, the reduction was fixed (Δ = -1.6 kg C/m^2); however, at the next measuring point (60 years after the fire), an intensive increase has been revealed (Δ = 2.5 kg C/m^2). Such "unobvious" change was primarily induced by two factors: active layer thickness and cryoturbations. According to our data, in a 30- to 60-year period after the fire, active layer thickness decreases, reaching its initial values; at this time cryoturbations reach the highest intensity. Cryoturbations in the presence of two conditions—close permafrost table and already formed thick organic cover—most intensively enrich mineral horizons with organic matter. A similar trend was observed for the succession developing through the stage of dense forest.

Thus, the influence of fires on soil carbon pools has a dual nature: in the first stages, "expected" dramatic reduction of carbon pools in organic horizons and less expressed in mineral horizons; in the later stages, postpyrogenic effect of organic matter accumulation on the mineral surface and OC enrichment of mineral horizons due to intense recovery processes in the ecosystem.

References

Tarabukina, V.G. & Savvinov, D.D. 1990. Influence of fires on cryogenic soils. *Novosibirsk*: 120 pp.

NORPERM: The Norwegian TSP Permafrost Database

Kirsti Midttømme
Geological Survey of Norway, NGU
Geir Strand
Geological Survey of Norway, NGU
Håvard Juliussen
Department of Geology, The University Centre in Svalbard, Norway
Hanne H. Christiansen
Department of Geology, The University Centre in Svalbard, Norway

Introduction

According to the IPY data policy, all data from IPY projects should be stored in international data repositories, ensuring long-term preservation and sustained access. Also, the increasing amount of ground temperature data in Norway and Svalbard collected as part of different projects needs to be managed and stored centrally in a standard format database. The Geological Survey of Norway (NGU) is the managing institution for geological data in Norway, and is thus the obvious institution to host the Norwegian ground temperature database. A Norwegian permafrost database—NORPERM—is thus being developed at NGU as part of the IPY project "Permafrost Observatory Project: A Contribution to the Thermal State of Permafrost in Norway and Svalbard (TSP NORWAY)" (Etzelmüller et al. 2008). This database will include temperature data from about 40 existing boreholes, hundreds of miniloggers measuring shallow ground temperatures, Bottom Temperature of Snow (BTS) campaigns, and from similar research projects such as the CRYOLINK project (Etzelmüller et al. submitted). NORPERM will be the important data legacy from the TSP NORWAY project.

Data Sources – The TSP NORWAY Project

The observatories and data of the TSP NORWAY project are used as templates for NORPERM. There are two main permafrost observatories in TSP NORWAY: Troms in northern Norway and Nordenskiöldland in Svalbard (Fig. 1). Within the observatories, individual measurement sites (boreholes, miniloggers, etc.) are grouped together at specific so-called permafrost locations (e.g., mountains, valleys, etc.). Temperature data to be included in NORPERM are ground temperatures in 10–20 m deep boreholes, shallow ground temperatures using miniloggers, and traditional BTS data. There are 11 TSP boreholes in northern Norway and around 15 in Svalbard. Data from in situ periglacial process monitoring, geodetic surveys and/or remote sensing of landform dynamics, and periglacial landform ages are also collected in the TSP project and may be included in the database.

Extensive datasets on ground temperature exist, mainly from southern Norway, from previous permafrost projects such as the PACE project and the Dovrefjell monitoring programme (Etzelmüller et al. submitted), and from several PhD theses.

NORPERM – Structure and Access

The structure of NORPERM is shown in Figure 2. NORPERM is structured with "permafrost location" at the first level, corresponding to the locations where measurements are clustered. Overview information on climate, large-scale geomorphology, geology, etc., and photos are included at this level. At the next level are boreholes, (with either continuous temperature logging or sporadic manual measurements),

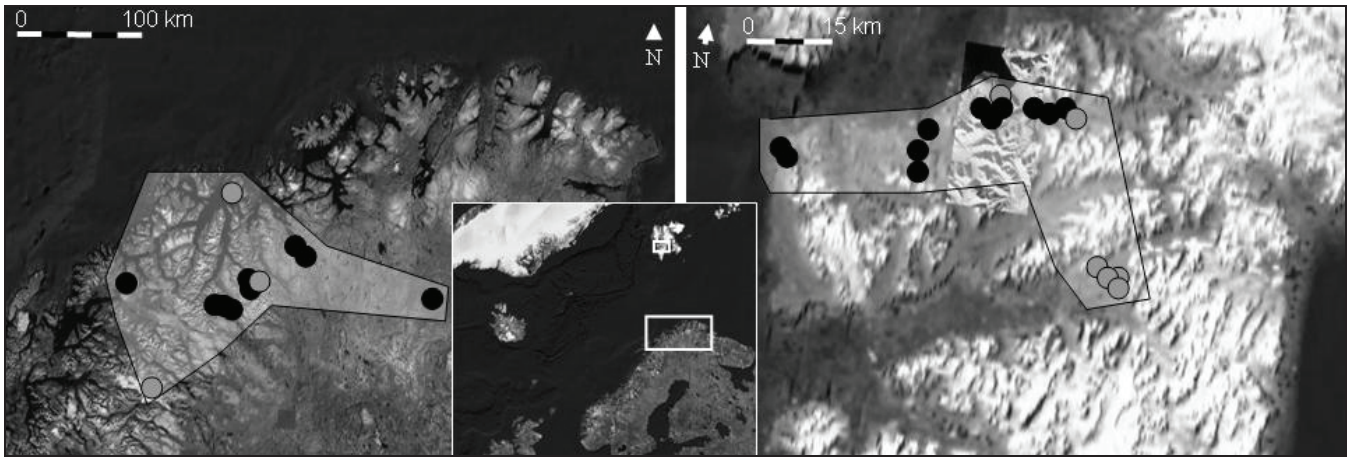

Figure 1. Left: the Norwegian part of the North Scandinavian Permafrost Observatory (69–70°N). Right: the Svalbard Nordenskioldsland Permafrost Observatory (78°N). Locations of TSP (black dots) and existing (grey dots) boreholes are shown. Based on Google Earth.

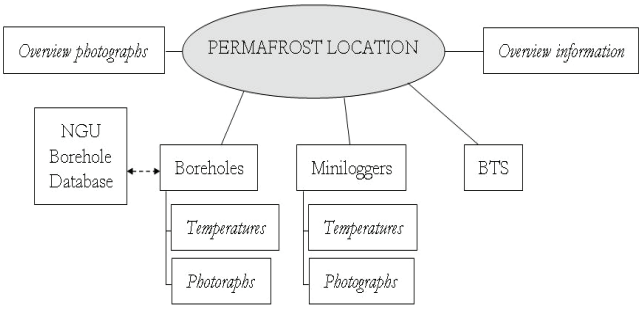

Figure 2. Overview of the structure of the NORPERM database.

shallow ground temperatures recorded with miniloggers, and BTS datasets. Photographs and summary graphics are included for each borehole and minilogger. The boreholes will also be registered in the national borehole database, which is under construction at NGU. Information and core samples from more than 6000 boreholes from mining exploration will be available through this service, and potential boreholes with negative ground temperatures will be included in NORPERM.

Relevant geographic, meteorological, geological, and geophysical data for the permafrost locations, existing at other institutions and available through Norway Digital (a national public cooperation of digital data between Norwegian national institutions), are linked to the NORPERM database. Metadata and data structure for boreholes follow the international standard format, and will be included in the International Global Terrestrial Network of Permafrost (GTN-P), which is the official international database for the international TSP IPY project. Data will be quality checked by TSP project scientists to ensure data quality.

NORPERM will be accessible through the websites of TSP NORWAY (www.tspnorway.com) and NGU (www.ngu.no). The dissemination of information is based on technologies for Internet distribution established through Norway Digital. Web map service (WMS) data will show the permafrost localities on both topographical and geological maps. Downloaded data will be available in standard formats as graphical plots, tables, pictures or "facts sheets."

Future Development

Current map visualization in NORPERM is in 2D. We aim at presenting NORPERM data in 3D in the near future, following guidelines given by a working group on visualization techniques at NGU. We also plan to present our results through Google Earth, as other types of IPY data are.

Three boreholes have been equipped with modem. Thus, real-time borehole temperature data will be available through our webpage (www.tspnorway.com).

References

Etzelmüller, B., Farbrot, H., Humlum, O., Christiansen, H.H., Juliussen, H., Isaksen, K., Schuler T., Ødegård, R. & Ridefelt, H. 2008. Mapping and modeling the distribution of permafrost in the Nordic countries. *Extended Abstracts of the Ninth International Conference on Permafrost, Fairbanks, Alaska, 29 June–3 July 2008*.

Potential Subsidence from Thawing of Near-Surface Ground Ice, Outer Mackenzie Delta Area, Northwest Territories, Canada

P.D. Morse
Department of Geography and Environmental Studies, Carleton University, Ottawa, ON, Canada
C.R. Burn
Department of Geography and Environmental Studies, Carleton University, Ottawa, ON, Canada
S.V. Kokelj
Water Resources Division, Indian and Northern Affairs Canada, Yellowknife, NT, Canada

Introduction

The outer Mackenzie Delta area (OMD), on the southeast coast of the Beaufort Sea, is within the continuous permafrost zone, and typically, permafrost occurs in unconsolidated sediments with greater than 20% visible ice content in the upper 15–20 m of the ground (Heginbottom et al. 1995). Kendall Island Bird Sanctuary (KIBS), OMD, protects 623 km^2 of wetland habitat important to migratory waterfowl and other birds, 60% of which is less than 1.5 m above mean sea level (Mackay 1963). Research on near-surface permafrost (NSP), defined here as the uppermost meter of permafrost, is necessary because of potential climate change impacts on ground conditions, specifically warming of permafrost (Smith et al. 2005) and sea level rise, which is currently 3.5 mm/a at Tuktoyaktuk (80 km east of KIBS) (Manson et al. 2005). Significant natural gas reserves have been identified beneath KIBS, and there are numerous other exploration leases in the region. Development of these resources would require construction of production platforms and distribution pipelines. Permafrost degradation in the OMD may lead to inundation and loss of both wildlife habitat and terrain for infrastructure construction.

The objective of this research is to estimate the potential subsidence from permafrost degradation at KIBS by (1) determining ground ice content of NSP in various surficial units; (2) determining the active layer thickness at each sample location; and (3) calculating the subsidence expected as the active layer thickens.

Surficial Units and Ground Ice

Ground ice contents were assessed in five surficial units within the two physiographic subdivisions at KIBS (Mackay 1963, Rampton 1988): (1) Tununuk Low Hills at the southwest, a rolling upland terrain usually less than 50 m above mean sea level, interspersed with broad, poorly drained depressions, covering approximately 30% of the area; and (2) Big Lake Delta Plain, a flat alluvial wetland, with numerous intersecting channels and lakes that may flood in spring or with storm surges. Tununuk Low Hills is a mosaic of thermokarst lake beds (TK), gravely sandy hills, ridges and terraces (G), ice-thrust hills and ridges (I), and till plains (TP). The physiography is due to Wisconsinan-advance glacial modification of permafrost in Pleistocene marine and fluvial deposits, post-glacial retreat with NSP aggradation, early Holocene thermokarst activity, and subsequent development of aggradational ice (Rampton 1987, 1988, Burn 1997). Big Lake Delta Plain, which consists of fine-grained river deposits (F), was exposed following the Wisconsinan glacial maximum through to the middle Holocene, and subsequently inundated by sea level rise or thermokarst lake development. It was then re-exposed between 0.5–1.5 ka ago due to fluvio-deltaic infilling and possible lake drainage (Rampton 1987, Taylor et al. 1996). Ground ice in F developed under saturated conditions with an aggrading surface from sediments deposited annually by spring flooding (Kokelj & Burn 2005).

Surficial Units and Ground Ice Sampling

The uppermost 1 m of permafrost was sampled at 72 sites in KIBS in 2006 and 2007. Cores were collected with a 5 cm diameter CRREL drill, and were sectioned into 10 cm intervals. Samples were collected along transects previously established within TK, G, I, TP, and F surficial units, and at a few other locations. Active layer thickness at each site was measured by probing the late-summer thaw depth (20–27 August 2007) (Mackay 1977).

Core sections were thawed, re-moulded, and allowed to settle. A saturated sediment layer with supernatant water on top was collected in a beaker, and excess-ice content was estimated with (Kokelj & Burn 2005, Eq. 1):

$$I_C = [(W_V*1.09)/(S_V+(W_V*1.09)]*100, \quad (1)$$

where I_C is the excess-ice content (%), W_V is the supernatant volume, and S_V is the saturated soil volume. The sample was then oven dried at 105°C to determine gravimetric moisture content (G_W).

Relation Between Surficial Units and Ground Ice

All surficial units had high ice content, with higher I_C in the upper 50 cm of permafrost (Table 1). Lowland NSP (F) was of higher ice content, 34%, than the uplands, on average 24%. In the uplands, the highest mean ice content in the uppermost 100 cm of permafrost was in TP, and the lowest was in G, but G also had the biggest range. In places, the ice content in organic-rich deposits at the base of hill slopes exceeded the hilltop ice content by an order of magnitude.

Table 1. Summary statistics for mean I_C (%) of the upper 50 and 100 cm of permafrost in surficial units of the OMD.

Surficial unit	Mean	Median	Min.	Max.	S.D.
F (n = 19)					
Upper 50 cm	36.6	36.8	20.0	53.5	9.7
Upper 100 cm	34.1	32.8	18.6	46.3	7.4
TK (n = 8)					
Upper 50 cm	26.0	23.3	16.6	38.2	8.0
Upper 100 cm	25.7	26.0	13.4	37.9	8.6
G (n = 16)					
Upper 50 cm	24.8	19.5	1.3	60.0	17.8
Upper 100 cm	20.2	19.2	0.8	39.5	12.3
I (n = 9)					
Upper 50 cm	23.2	24.1	7.8	36.3	8.9
Upper 100 cm	22.6	23.8	7.2	37.8	8.5
TP (n = 10)					
Upper 50 cm	32.7	34.1	20.9	47.6	8.4
Upper 100 cm	28.6	28.7	10.5	46.6	11.4

*n = number of cores used. Samples from hill slopes are not included.

Potential Near-Surface Permafrost Subsidence

Subsidence (*S*) due to a thermal disturbance was estimated for each surficial unit using mean upper 50 cm I_C (Table 1), and active layer thickness increases of 30% and 70%, respectively, after Mackay (1970, Fig. 3):

$$S = \{AL_1 /[(100 - I_C)/100]\} * \{I_C /100\}, \quad (2)$$

where AL_1 is the increase in active layer thickness (cm).

Predicted subsidence in the surficial units at KIBS (Table 2) is highest in F, yielding 26 cm of water with a 70% increase in active layer thickness. The greatest amount of subsidence in uplands occurs in TP, while subsidence in the remaining units is nearly uniform.

Subsidence is likely underestimated because I_C does not account for the 10% volume of air bubbles commonly found in larger ground ice bodies. Additional subsidence would likely occur from consolidation of thawed soil. In addition, the release of water would impact terrain stability in unconsolidated sediment, and thermal erosion would likely occur on slopes with modification of drainage patterns (Mackay 1970).

Conclusions

1. High ice content (>20% I_C) occurred in the uppermost 1 m of permafrost in all surficial units in KIBS, and ground ice content was highest in the uppermost 50 cm at the base of the active layer.

2. The highest ground ice content was in F, which accounts for nearly 60% of the habitat at KIBS.

3. An increase of 70% in active layer thickness F, which is typically less than 1.5 m above mean sea level, would decrease the elevation by 26 cm, and increase the chances of inundation during storm events.

Table 2. Thermokarst subsidence estimates based on mean active layer thickness (AL) and mean upper 50 cm I_C for surficial units of the OMD.

Surficial unit	Increase in thickness of active layer (cm)	Total depth of thaw (cm)	Subsidence (cm)
F (n = 19; AL = 64)			
30% increase	19	30	11
70% increase	45	71	26
TK (n = 8; AL = 35)			
30% increase	10	14	4
70% increase	24	33	9
G (n = 16; AL = 49)			
30% increase	15	20	5
70% increase	34	45	11
I (n = 9; AL = 48)			
30% increase	14	18	4
70% increase	34	44	10
TP (n = 10; AL = 47)			
30% increase	14	21	7
70% increase	33	49	16

*n = number of cores used. AL = mean active layer thickness (cm). Samples from hill slopes are not included.

References

Burn, C.R. 1997. Cryostratigraphy, palaeography, and climate change during the early Holocene warm interval, western Arctic coast, Canada. *Canadian Journal of Earth Sciences* 34: 912-925.

Heginbottom, J.A., Dubreuil, M.A. & Harker, P.A. 1995. Permafrost. In: *National Atlas of Canada,* 5th ed.

Kokelj, S.V. & Burn C.R. 2005. Near-surface ground ice in sediments of the Mackenzie Delta, Northwest Territories, Canada. *Permafrost and Periglacial Processes* 16: 291-303.

Mackay, J.R. 1963. *The Mackenzie Delta area, N.W.T., Canada.* Ottawa: Department of Mines and Technical Surveys, Geographical Branch Memoir 8, 202 pp.

Mackay, J.R. 1970. Disturbances to the tundra and forest tundra environment of the western Arctic. *Canadian Geotechnical Journal* 7: 420-432.

Manson, G.K., Solomon, S.M., Forbes, D.L., Atkinson, D.E., & Craymer, M. 2005. Spatial variability of factors influencing coastal change in the Western Canadian Arctic. *Geo-Marine Letters* 25: 138-145.

Rampton, V.N. 1987. Surficial Geology, Mackenzie Delta. Map 22. In: B.R. Pelletier (ed.), *Marine Science Atlas of the Beaufort Sea: Geology and Geophysics*. Ottawa: Geological Survey of Canada Miscellaneous Report 40.

Rampton, V.N. 1988. *Quaternary geology of the Tuktoyaktuk Coastlands, Northwest Territories*. Ottawa: Geological Survey of Canada Memoir 423, 98 pp.

Taylor, A.E., Dallimore, S.R. & Judge, A.S. 1996. Late Quaternary history of the Mackenzie–Beaufort region, Arctic Canada, from modelling of permafrost temperatures. 2. The Mackenzie Delta – Tuktoyaktuk Coastlands. *Canadian Journal of Earth Sciences* 33: 62-71.

Vegetation and Permafrost Long-Term Monitoring in the West Siberia Subarctic

N.G. Moskalenko, O.E. Ponomareva, G.V. Matyshak, P.T. Orehov
Earth Cryosphere Institute, Moscow, Russia
L.A, Kazantseva, E.V. Ustinova
Earth Cryosphere Institute, Tyumen, Russia

Long-term ecosystem monitoring in cold regions was carried out by few researchers (Timin et al. 1973, Bliss 1975, Bocher 1949, Broll et al. 2003, Burgess et al. 1999 and others). In this connection, results of long-term vegetation and permafrost monitoring since 1970 at the Nadym site in the West Siberia North can be of interest for researchers of Arctic and Subarctic regions.

The observation site is located 30 km south of the town of Nadym in the West Siberia northern taiga. This site is found on a flat boggy surface of the fluvial-lacustrine plain (third terrace) with altitude ranging from 25 to 30 m. The plain is composed of sandy deposits interbedded with clays, with an occasional covering of peat. Permafrost underlies the area sporadically. Patches of permafrost are closely associated with peatlands, tundras, mires, and frost mounds.

The annual geobotanical descriptions are carried out on fixed plots and transects in natural and disturbed conditions. Observations over vegetation dynamics were accompanied by soil descriptions, microclimatic observations, microrelief leveling, and measurements of permafrost temperature and seasonal thaw depths.

Flat peatland with a *Rubus chamaemorus-Ledum palustre-Sphagnum fuscum-Cladina stellaris* community is dominant on the fluvial-lacustrine plain (Fig. 1A). For this community, the complex horizontal structure caused by the presence of hummocks, interhummocks, pools, and in this connection, significant spatial variability of seasonal thaw depths (from 0.5 m in inter-hummocks up to 1 m and more in pools) is characteristic.

At the peatland in the first years after vegetation removal, cotton grass-cloudberry groupings formed over only 20% of the surface. Within 15 years on the disturbed peatland, continuous cloudberry-cotton grass-*Polytrichum-Sphagnum* cover had formed. This cover within 30 years, as a result of surface settlement, downturn of permafrost table up to 2–3 m, development of thermokarst, and bogging, was replaced by cotton grass-peat moss cover. The generated fragment of cotton grass-peat moss bog is present 35 years after disturbance (Fig. 1B)

The carried-out definitions of plant biomass have shown that, as compared with boggy communities in tundra communities, the biomass on the disturbed sites increased 2.5 times.

In this tundra, a *Ledum palustre-Betula nana*-lichen-*Polytrichum* plant community developed, replaced within 30 years after disturbance by a *Betula nana-Ledum palustre-Sphagnum*-lichen plant community, which developed here. On disturbed hummocky tundra, downturn of the permafrost table, rise in ground temperature, appearance of surface settlements, and formation in them of pools are observed; during the winter period, snow capacity has increased. It has been accompanied by a sharp increase in vegetation structure of *Betula nana* participation, having an average height of 1 m, and also *Polytrichum* mosses. The participation of these species has led to a substantial increase in plant biomass that was reflected in biodiversity, and abundance and biomass of small mammals in the disturbed tundra.

Evolution of soils on the disturbed flat peatland goes on in bog type, and bog oligotrophic soils are formed here. On the peatland, there are changes of hydrothermal regime and, as a consequence, changes of intensity and orientation of such major soil processes as respiration and transformation of organic material.

Background gas emission from the soil surface was measured. After that active layer left and measurements of gas emission from a permafrost surface directly after its opening and in 24 hours were carried out. On all investigated plots, sharp emission of the investigated gases (CO_2, CH_4), on some orders exceeding background emission, was observed (Table 1).

Measurements of ground temperatures in boreholes on the natural and disturbed peatland have shown (Fig. 1C) that distinctions in temperatures in natural and disturbed conditions have appreciably increased at a depth of 1 m (on 0.5°C). Temperature rise at a depth of 5 m was small, and at a depth of 10 m, it is not traced yet. Also we can see that the depth increase in ground temperature (on 0.8°C) for the period from 1972 to 2007, caused with rise in air temperature, is well defined. According to the Nadym weather station for 1970–2006, the trend in rise of air temperature has reached 0.04°C in a year.

The leveling of a peatland surface was carried out along a fixed transect once a year—at the end of August–the beginning of September—when seasonal thaw depth reaches maximum and surface position reflects the long-term process of frost heave. Marks of a surface were determined concerning a deep reference point.

It is established that the surface of flat peatland tested spasmodic rise in severe winters 1985, 1999, and for 32 years became 67 cm higher than in the beginning of observations. A feature of flat peatland frost heave is the rise of uniformity in the area. After 1999, the surface rise slowed down. The

Table 1. Gas emission (CH_4) from permafrost surface under disturbances (mg/m^2 per hour).

Landscape	Background	In 24 hours
Flat peatland	0.0624807	0.4265244
Palsa peatland	0.0003942	0.1820547

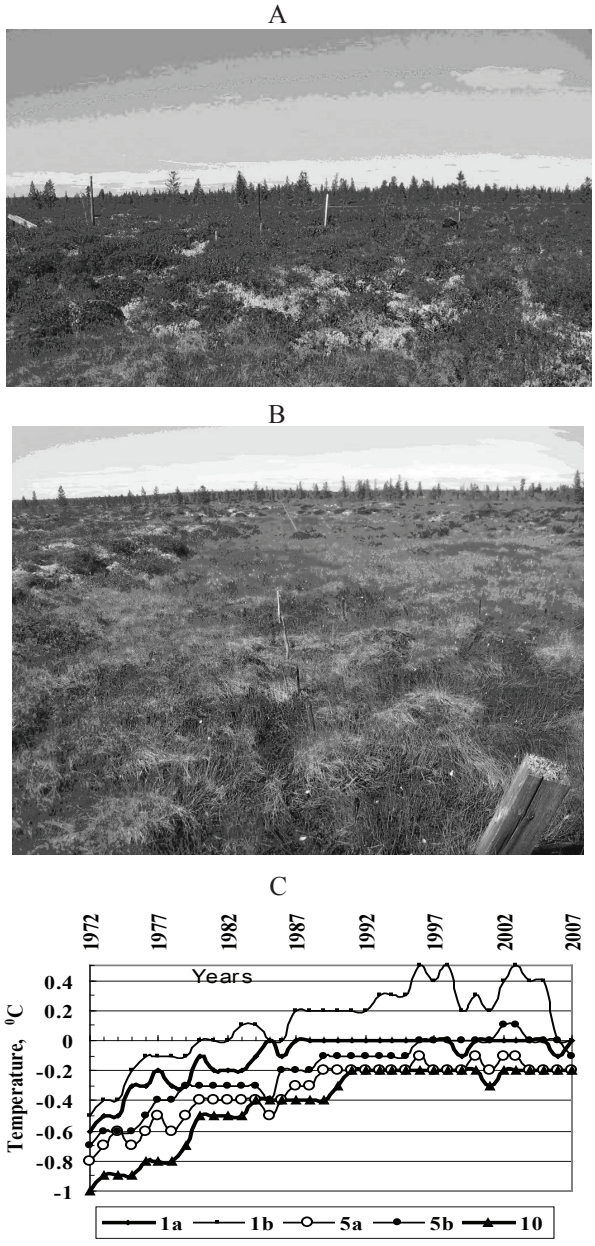

Figure 1. *Rubus chamaemorus-Ledum palustre-Sphagnum fuscum-Cladina stellaris* plant community on undisturbed peatland (A); *Eriophorum russeolum-Sphagnum Lindberg*ii plant community 33 years after removal of vegetation cover (B); and ground temperature (°C) in natural (a) and disturbed (b) conditions at the depths of 1, 5, and 10 m.

surface of flat peatland in recent years has become more stable (Fig. 2). These changes, as a whole, reflect a decrease in intensity of long-term frost heave, owing to climate warming and an increase of natural temperature background at human-induced impact.

Acknowledgments

This research was funded by the Polar Earth Science Program, Office of Polar Programs, National Science Foundation (ARC-0632400, ARC-0520578)

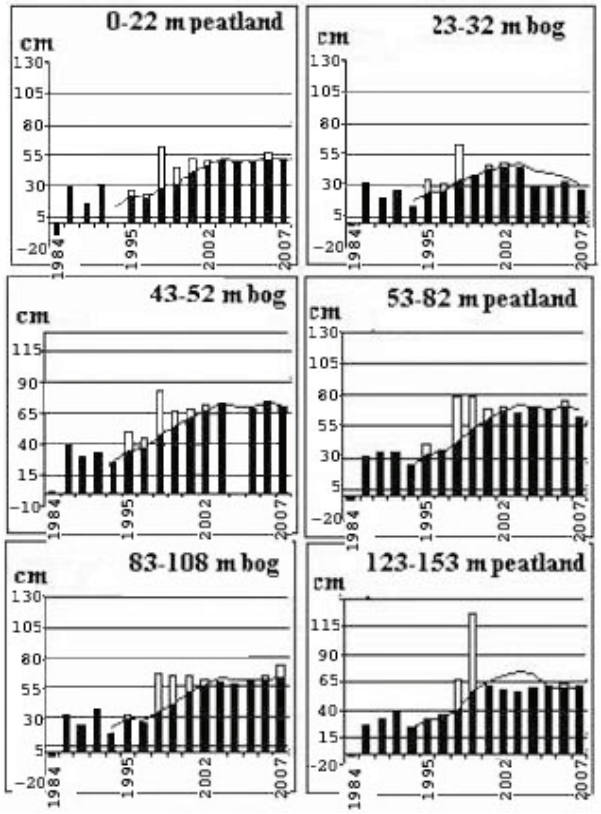

Figure 2. Diagram of changes of surface position along transect from its position in 1984 on data of repeated leveling and trend lines.

References

Bliss, L.C. 1975. Devon Island, Canada. *Ecolog. Bull*. 20: 17-60.

Bocher, T.W. 1949. Climate, soil and lakes in continental West Greenland in relation to plant life. *Medd. om Gronland* 147(2): 4.

Broll, G., Tarnocai, C. & Gould, J. 2003. Long-term high Arctic ecosystem monitoring in Quttnir paag National Park, Ellesmere Island, Canada. *Proceedings of the Eighth International Conference on Permafrost, Vol. 1, Zurich, Switzerland, 21–25 July 2003*: 85-94.

Burgess, M., Tarnocai, C., Nixon, N.M. et al. 1999. Active layer depth, and soil and ground temperature monitoring in permafrost areas of Canada. *Monitoring of Cryoshere.* Pushchino, 92-93.

Timin, M.E., Coller, B.D., Zich, J. & Walker, D.A. 1973. A computer simulation of the arctic tundra ecosystem near Borrow, Alaska. In: *U.S. Tundra Biome Rep. N 73-1*, San Diego State University: 1-82.

The Influence of Shrubs on Soil Temperatures in Alpine Tundra

Isla H. Myers-Smith
University of Alberta, Edmonton, Alberta, Canada
David S. Hik
University of Alberta, Edmonton, Alberta, Canada

Introduction

With a warming climate, northern ecosystems will face significant ecological changes such as permafrost thaw, increased forest fire frequency, and shifting ecosystem boundaries, including the spread of tall shrubs into tundra. In northern mountain ranges such as those in the southwestern Yukon, the shrub line will likely advance up mountain slopes with climate warming. In the last 50 years, rapid shrub expansion has been documented in arctic Alaska (Sturm et al. 2001a, Tape et al. 2006) and the Northern Yukon and NWT (Trevor Lantz, pers. com.) using repeat aerial photography. Paleoecological evidence suggests that tall shrubs last invaded tundra ecosystems in Alaska and northwestern Canada between 7,000 and 12,000 years ago, during the warm post-glacial period (Ritchie 1984). Growing season temperatures are again warming in Alaska and western Canada (Stafford et al. 2000), and concurrent with this trend, satellite imagery shows a greening of the Arctic (Stow et al. 2004). The correlation between warming and greening has been used to link climate change with shrub expansion (Sturm et al. 2001a); however, the exact mechanisms driving shrub increase are probably more complex. A combination of changes in nutrient mineralization, snow depth, microclimate, (Sturm et al. 2001b) disturbance (Trevor Lantz, pers. com.), and species interactions are most likely all contributing factors to shrub expansion patterns on the landscape

Influence of shrubs on soil temperatures

Increased shrubs in arctic and alpine tundra alter the partitioning of solar energy during the growing season, the distribution and physical characteristics of snow in the winter (Liston et al. 2002), and soil thermal dynamics year-round (Sturm et al. 2001b, Sturm et al. 2005a). In the winter, snow trapping by shrubs can insulate soils (by trapping heat) and has been proposed as a positive feedback mechanism promoting the expansion of shrubs in the Arctic (Sturm et al. 2001b, Sturm et al. 2005a). During spring, dark-colored shrubs that extend above the snow alter the albedo and accelerate local snowmelt (Sturm et al. 2005b, Pomeroy et al. 2006). In summer, shading by shrubs decreases soil temperatures under shrub canopies (Pomeroy et al. 2006). Though complex, the interactions between shrubs, snow, and soil warming may act as a positive feedback to shrub expansion (Fig. 4, Chapin et al. 2005). In addition, winter soil warming may enhance nutrient cycling and reduce soil carbon stores (Mack et al. 2004).

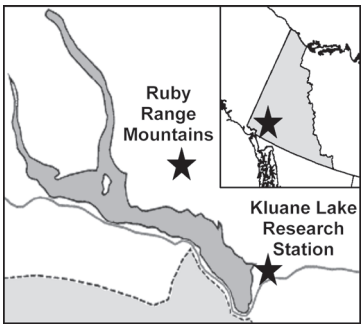

Figure 1. Map of the study region and the Ruby Range Mountain field site.

Study Site

The field site is located in the Ruby Range Mountains (61°20′N, 139°17′W, Fig. 1) adjacent to Kluane Lake. This area of the southwest Yukon is located at the convergence of the coastal and arctic air masses, and as a result, climate change could lead to increased variability in winter temperatures and precipitation. The study area varies in elevation, aspect, and proximity to glaciers, making it an ideal location to test a shrub expansion hypotheses.

Methods

To measure the influence of snow-capture by shrubs on soil warming, we manipulated willow (*Salix* spp.) cover to compare soil temperatures beneath plots with (a) intact shrubs, (b) shrubs removed, (c) artificial vegetation canopies, and (d) adjacent, shrub-free tundra. In September 2007, 6 artificial shrub and tundra plots were constructed by cutting down shrubs and affixing them to stakes in the soil in adjacent shrub-free tundra (Fig. 2).

The 6 manipulation plots and paired control monitoring plots are instrumented with snow stakes with iButton Thermochron temperature loggers (Dallas Semiconductor Corporation, Dallas, Texas, USA) at 2, 5, 25, 50, 100, and 150 cm along their length, and with Hobo micro station 12-bit temperature sensors (HOBO, Onset Computer Corp., Massachusetts, USA), installed at 2 and 5 cm below the soil surface. This experiment will test whether shrubs trap more snow than the adjacent tundra, whether this snow melts out earlier in the spring season, and how much the trapped snow insulates the soil.

Initial Results

Over the growing season of 2007, shrub plots were significantly cooler than tundra plots (for DOY 160 to 244, at 2 cm depth: 1.5°C cooler under shrubs, $F_{1,172} = 33.9$, $p < 0.001$, at 5 cm depth: 1.3°C cooler under shrubs, $F_{1,172} = 25.7$, $p < 0.001$, Fig. 3).

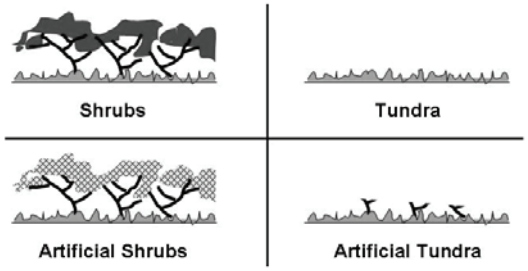

Figure 2. Manipulative experiment.

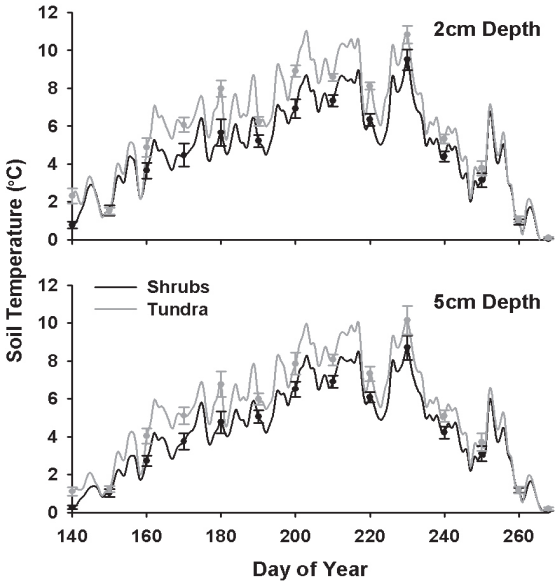

Figure 3. Mean daily soil temperatures (±SE) at 2 cm and 5 cm depth under shrub and tundra plots (n = 12).

Since the manipulation was conducted at the end of the 2007 field season, we were only able to collect one week of experimental data. During the last week of September, both the shrub and artificial shrub plots were cooler than the tundra and artificial tundra plots; however, these comparisons are not statistically significant. Data from the 2007–08 winter season will indicate whether shrub canopies trap more snow and if insulation results in soil warming.

Discussion

Increasing shrubs in arctic and alpine tundra will alter microclimates and soil thermal dynamics (Sturm et al. 2001b). Cooling of summer soil temperatures may reduce decomposition and resulting carbon loss. Warming of winter soils may, however, increase decomposition, accelerate nutrient cycling and promote the further expansion of shrubs (Sturm et al. 2001b, Sturm et al. 2005a). This study attempts to quantify the impact of shrubs on soil thermal dynamics. Shrubs cool soils during the growing season (Pomeroy et al. 2006 this study); however, the contribution of shrubs to winter soil thermal dynamics has been little explored in the literature. By manipulating shrub cover (removing above ground woody biomass and erecting artificial shrubs), the insulation provided by a shrub canopy and trapped snow can be isolated from the influence of understory vegetation and soils. If increasing shrubiness is resulting in warmer winter soils, this may lead to enhanced nutrient cycling and reduced soil carbon stores; however, the 2°C summer cooling may offset a winter warming response. By the summer of 2008, we will have collected data for a full winter season, and will be able to determine snow trapping and soil warming potential of willow shrubs in the alpine tundra of the Kluane Region.

Acknowledgments

We would like to thank Jodie Pongracz, Catherine Henry, Eric Vezeau, and Mark Wong for field assistance. Funding was provided by NSERC, NSTP, C/BAR, Yukon College NRI, the Alberta Ingenuity Fund, and ANIA's Grant-in-Aid Program.

References

Chapin, F.S. III, Sturm, M., Serreze, M.C. et al. 2005. Role of land-surface changes in Arctic summer warming. *Science* 310: 657-660.

Liston, G., McFadden, J.P., Sturm, M. & Pielke, R.A. 2002. Modelled changes in arctic tundra snow, energy and moisture fluxes due to increased shrubs. *Global Change Biology* 8: 17-32.

Mack, M.C., Schuur, E.A.G., Bret-Harte, M.S. et al. 2004. Ecosystem carbon storage in arctic tundra reduced by long-term nutrient fertilization. *Nature* 431: 440.

Pomeroy, J.W., Bewley, D., Essery, R. et al. 2006. Shrub tundra snowmelt. *Hydrological Processes* 20: 923-941.

Ritchie, J.C. 1984. Past and present vegetation of the far Northwest of Canada. University of Toronto Press: Toronto, Canada.

Stafford, J.M., Wendler, G. & Curtis, J. 2000. Temperature and precipitation of Alaska: 50 year trend analysis. *Theoretical and Applied Climatology* 67: 33-44.

Stow, D.A., Hope, A., McGuire, D. et al. 2004 Remote sensing of vegetation and land-cover change in Arctic Tundra Ecosystems. *Remote Sensing of Environment* 89: 281-308.

Sturm, M., Racine, C. & Tape K. 2001a. Increasing shrub abundance in the Arctic. *Nature* 411: 546-547.

Sturm, M., McFadden, J.P., Liston G.E. et al. 2001b. Snow-shrub interactions in Arctic tundra: A hypothesis with climatic implications. *Journal of Climatology* 14: 336-344.

Sturm, M., Schimel, J., Michaelson G. et al. 2005a. Winter biological processes could help convert arctic tundra to shrubland. *BioScience* 55: 17-26.

Sturm, M., Douglas, T. Racine, C. & Liston, G.E. 2005b. Changing snow and shrub conditions affect albedo with global implications. *Journal of Geophysical Research* 110: doi:10.1029/2005JG000013.

Tape, K., Sturm M. & Racine C. 2006. The evidence for shrub expansion in Northern Alaska and the Pan-Arctic. *Global Change Biology* 12: 686-702.

Estimation of the Extent of Near-Surface Permafrost in the Mackenzie Delta, Northwest Territories, Using Remote Sensing

T.-N. Nguyen, C.R. Burn, D.J. King
Department of Geography and Environmental Studies, Carleton University, Ottawa, ON, Canada
S.L. Smith
Geological Survey of Canada, Natural Resources Canada, Ottawa, ON, Canada

Introduction

Based on air temperature, permafrost should be continuous in the Mackenzie Delta (MD), northwest Canada (Henry & Smith 2001). However, the most recent Permafrost map of Canada, using sparse ground temperature data, classifies the MD as having discontinuous permafrost (Heginbottom et al. 1995). There has been little fieldwork investigating permafrost extent within the delta, yet, the determination of near-surface permafrost (NSP) extent, defined in this study as permafrost within 3 m from ground surface, is important for land-use planning, as terrain behaviour varies between frozen and unfrozen ground (Smith et al. 2001).

The objectives of this research were (1) to assess if the spatial distribution of near-shore vegetation associations can be used to predict NSP presence in the MD and, if so, (2) to apply remote sensing techniques to map these vegetation communities and estimate the proportion of ground underlain by NSP.

Vegetation and Permafrost in Mackenzie Delta

The MD stretches 200 km north–south and 60 km east–west (Mackay 1963). It is an alluvial landscape intersected by a network of channels and thousands of lakes, and is subjected to annual flooding. Spatial variation in channel shifting, flooding, and sedimentation is expressed by patterns of vegetation (Gill 1973).

Horsetail (*Equisetum* spp.) communities are the typical emergent plant associations, while Willow-horsetail (*Salix-Equisetum*) communities can be found with increasing distance from stream channels. Alders (*Alnus* spp.) are located at slightly higher elevations than the Willow-horsetail communities, since alder species are less tolerant of sedimentation. Spruce (*Picea glauca*) forests represent the climax community south of tree line. North of tree line, sedges (*Carex* spp.) and horsetails are common adjacent to channels, and Willow-horsetail and *Salix richardsonii* are widespread on more elevated sites (Pearce 1998).

In the MD, the thermal effect of water bodies and the shifting nature of channels affect the age, distribution, temperature, and thickness of permafrost (Smith 1975). On point bars, taliks have been recognized near channels by various authors (Gill 1973, Smith 1975). The presence of a talik, where winter freeze-back does not reach the top of permafrost, is due to the slow establishment of permafrost beneath newly exposed ground, and to deep snowdrifts blown off the channels and trapped in near-shore willow stands (Dyke 2000).

Vegetation and Permafrost Sampling

Field sites were selected so that several representative vegetation classes were present at each site. A line transect methodology was adopted for vegetation sampling and permafrost probing. A total of 52 transects were laid in summer 2006. The majority of transects were between 100 m and 200 m long depending on the width of the vegetation zones found at each site. Transects were established perpendicular to the shoreline and crossing the successional sequence of vegetation (Fig. 1). Vegetation was sampled using point and line-intercept methods and was identified at the genus level for shrubs and trees, and at the functional-type level for herbs. Plant presence and frequency were calculated to provide an indication of how dominant a plant type is in a community. The ground was probed using water-jet drilling to detect NSP in each vegetation association. Since the active layer thickness rarely exceeds 1.5 m in the MD, NSP was considered absent if unfrozen ground was recorded to 3 m depth (Kokelj & Burn 2005).

Relation Between Vegetation and Permafrost

There was a clear association between presence of permafrost in the upper 3 m and different vegetation communities. On point bars and alluvial islands, Horsetail

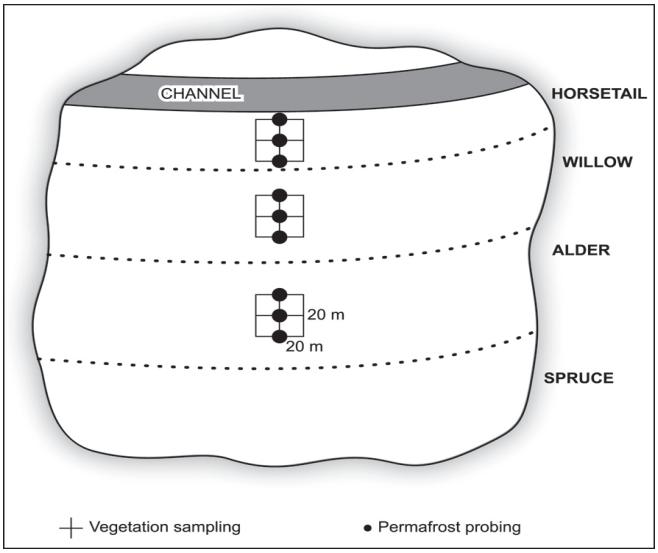

Figure 1. In each 20 m x 20 m plot, the water-jet drilled hole in the centre was complemented with two others. Each plot was assigned a single NSP presence or absence label based on the rule of majority. Spruce forests were not the focus of this research since the presence of permafrost is ubiquitous there with thin active layer thicknesses (Kokelj & Burn 2005).

Table 1. Relation between NSP and vegetation associations.

Vegetation association	Presence of NSP (% of plots)
Southern delta	
Horsetail (n=8)	0
Willow-horsetail (n=19)	0
Alder (n=25)	96
Central delta	
Horsetail (n=11)	9
Willow-horsetail (n=20)	10
Alder (n=26)	100
Northern delta	
Horsetail-sedge (n=18)	100
Willow-horsetail (n=12)	17
Salix richardsonii (n=15)	100

and Willow-horsetail communities were not associated with NSP. NSP was present beneath all other vegetation associations and in other land surface types (Table 1).

Image Data Analysis

Permafrost cannot be directly imaged by airborne or satellite-based sensors, but its presence may be inferred from surface characteristics, especially vegetation. In this study, SPOT-5 images of the MD, captured in July 2006 with a nominal ground pixel size of 10 m x 10 m, were classified for vegetation characteristics associated with NSP. Using relations of these characteristics with field survey data, the proportion of ground underlain by NSP was estimated.

In addition to spectral data produced directly by SPOT-5, data transformations such as vegetation indices, texture analysis and PCA were used to generate additional image information for classification. Training and testing data were chosen randomly among field sampled plots. Maximum Likelihood classifications were used to generate maps of vegetation associations with accuracies above 80%.

Estimation of Near-Surface Permafrost Extent

To estimate the extent of NSP in the MD, the land surface was categorized into three types: (1) Alluvial islands (AI), (2) Point bars (PB), and (3) all other types. PB occupied about 18% of the land surface and the extent of AI in the southern delta was calculated to be about 5%. The extent of NSP in the delta is:

$$\sum_{i=1}^{d}\left(\sum_{j=1}^{L}\left(\sum_{k=1}^{n} V_k * P_k\right)\right) \quad (1)$$

where d are the delta regions, L the land surface types, n the vegetation classes underlain by NSP, V the land fraction occupied by n, and P the land fraction occupied by L.

In the southern delta, 93% of the land surface was found to be underlain by NSP. Zones with presence of NSP represented 95% and 96% of the land surface in the central and northern delta, respectively.

Conclusions

1. On point bars and alluvial islands, Horsetail and Willow-horsetail communities were not associated with NSP. NSP was present beneath all other vegetation associations and in other land surface types.
2. Zones with presence of NSP represent 93%, 95%, and 96% of the land surface in the southern, central, and northern delta, respectively. This indicates that the MD is part of the continuous permafrost zone.
3. The technique developed in this study was useful in the mapping of NSP over large areas in a dynamic environment and could form the basis of a mapping tool that could be used to aid in land-use planning.

References

Dyke, L.D. 2000. Shoreline permafrost along the Mackenzie River. In: L.D. Dyke & G.R. Brooks (ed.), *The Physical Environment of the Mackenzie Valley, Northwest Territories: a Baseline for the Assessment of Environmental Change*. Ottawa: Geological Survey of Canada Bulletin 547: 143-151.

Gill, D. 1973. A spatial correlation between plant distribution and unfrozen ground within a region of discontinuous permafrost. *Proceedings of the Second International Conference on Permafrost, Yakutsk, U.S.S.R., July 13-28, 1973*: 105-113.

Heginbottom, J.A., Dubreuil, M-A. & Harker, P.A. 1995. *Permafrost. National Atlas of Canada,* 5th ed.

Henry, K. & Smith, M.W. 2001. A model-based map of ground temperatures for the permafrost regions of Canada. *Permafrost and Periglacial Processes* 12: 389-398.

Kokelj, S.V. & Burn, C.R. 2005. Near-surface ground ice in sediments of the Mackenzie Delta, Northwest Territories, Canada. *Permafrost and Periglacial Processes* 16: 291-303.

Mackay, J.R. 1963. *The Mackenzie Delta Area, N.W.T., Canada*. Department of Mines and Technical Surveys, Geographical Branch, Memoir 8.

Pearce, C.M. 1998. Vegetation patterns and environmental relationships in an Arctic riparian wetland. In: S.K. Majumdar, E.W. Miller & F.J. Brenner (eds.), *Ecology of Wetlands and Associated Systems*. Pennsylvania Academy of Science, 258-280.

Smith, M.W. 1975. Microclimatic influences on ground temperatures and permafrost distribution, Mackenzie Delta, Northwest Territories. *Canadian Journal of Earth Sciences* 12: 1421-1438.

Smith, S.L., Burgess, M.M. & Heginbottom, J.A. 2001. Permafrost in Canada, a challenge to northern development. In: G.R. Brooks (ed.), *A Synthesis of Geological Hazards in Canada.* Ottawa: Geological Survey of Canada Bulletin 548: 241-264.

Employing a Coupled Permafrost Water Balance Model to Study Possible Changes in Permafrost

D.J. Nicolsky
Geophysical Institute, University of Alaska Fairbanks PO Box 757320, Fairbanks, AK 99775, USA
V.E. Romanovsky
Geophysical Institute, University of Alaska Fairbanks PO Box 757320, Fairbanks, AK 99775, USA
M.A. Rawlins
Jet Propulsion Laboratory, California Institute of Technology, Pasadena, CA 91109, USA

Introduction

Thawing and freezing of arctic soils is affected by many factors, with air temperature, vegetation, snow accumulation, and soil moisture among the most significant. Here we describe the coupling of a Permafrost Model (Sazonova & Romanovsky 2003, Nicolsky et al. 2007) and the pan-Arctic Water Balance Model (PWBM, Rawlins et al. 2003), developed at the University of Alaska Fairbanks and the University of New Hampshire, respectively. Additionally, we present resultant simulated soil temperature and moisture dynamics, depth of seasonal freezing and thawing, river run-off, and water storage across the pan-Arctic. The coupled models simulate the snow/ground temperature with a 5-layer snow and 23-layer soil model. In the soil model, the layers thicken with depth and span a 60 m thick column. The PWBM has two soil storage zones: a root zone that gains water from infiltration and loses water via evapotranspiration and horizontal and vertical drainage, and a deep zone that gains water via root zone vertical drainage and loses water via horizontal drainage. Forcing data (i.e., air temperature, precipitation) are taken from ERA40 datasets and from several of the IPCC 4th Assessment model simulations of future arctic climate. We validate our model simulations by comparing soil moisture and thermal profiles with observational data collected within the pan-Arctic.

Coupling of Two Models

The coupling captures thresholds and non-linear feedback processes induced by changes in hydrology and subsurface temperature dynamics, and hence helps us to study the spatial and temporal variability of permafrost dynamics as well as potential future alterations to permafrost and the terrestrial arctic water cycle. Through explicit coupling of the Permafrost Model with the PWBM, we are able to simulate the temporal and spatial variability in soil water/ice content, active layer thickness, and associated large-scale hydrology that are driven by contemporary and future climate variability and change. Choosing appropriate climate forcings is clearly a significant challenge.

Acknowledgments

This research was funded by ARCSS Program and by the Polar Earth Science Program, Office of Polar Programs, National Science Foundation (OPP-0120736, ARC-0632400, ARC-0520578, ARC-0612533, IARC-NSF CA: Project 3.1 Permafrost Research), by NASA Water and Energy Cycle grant, and by the State of Alaska.

References

Nicolsky, D.J., Romanovsky, V.E., Alexeev, V.A. & Lawrence, D.M. 2007. Improved modeling of permafrost dynamics in a GCM land-surface scheme. *Geophysical Research Letters* 34: L08501.

Rawlins, M.A., Lammers, R.B., Frolking, S., Fekete, B.M. & Vo¨ro¨smarty, C.J. 2003. Simulating pan-Arctic runoff with a macro-scale terrestrial water balance model. *Hydrological Processes* 17: 2521-2539.

Sazonova, T.S. & Romanovsky, V.E. 2003. A Model for Regional-Scale Estimation of Temporal and Spatial Variability of the Active Layer Thickness and Mean Annual Ground Temperatures. *Permafrost and Periglacial Processes* 14(2): 125-139.

Influence of a Hydrothermal Soil Regime on the Radial Increment of Larch and Pine in Central Yakutia

Anatoly N. Nikolaev
Permafrost Institute, SB RAS, Yakutsk, Russia

Introduction

Central Yakutia (eastern Siberia, Russia) has a dominant growth of larches, for it is situated on the area of permafrost distribution. According to sustainable zoning of permafrost soils of Yakutia, the observed area refers to the Central Yakutia taiga-alas provinces of permafrost and pale soils (Elovskaya & Konorovskiy 1978). It has severe, long, and low-snow winters and hot, short, and droughty summers with significant insolation, low annual and winter temperatures, high seasonal and daily amplitudes, and small amount of deposits (Gavrilova 1973). Hydrothermal soil condition is one of the important factors influencing tree species growth. Long-term observation of the thermal soil regime in Central Yakutia has enabled the use of tree-ring chronology not only to reveal the relations between radial increment, atmospheric temperature, and precipitation, but also to analyze the influence of the hydrothermal soil regime on growth and development of larch (Nikolaev & Fyodorov 2004, Fyodorov et al. 2007).

Materials and Methods

Tree-ring chronology was examined at Spasskaya Pad and Tyungyulyu, 25 km northwest and 45 km northeast from Yakutsk accordingly, in Central Yakutia, the scientific stations of Institute of Biological Cryolitozone Problems of the SB RAS.

Due to the fact, that Spasskaya Pad site has areas of larch and pine forests nearby, it was possible to carry out the comparative analysis of the growth of these two species in conditions of permafrost. The forest areas are situated in the Lena and Amga interfluve, which has one of the most droughty climates in Central Yakutia. The width of year rings was measured with the LINTAB-III measuring instrument (Rinn 1996) in the laboratories of cryogenic landscapes of Melnikov Permafrost Institute SB RAS. Dendroclimatology standard research and the analysis technique were applied during dating and construction of tree-ring chronology (Vaganov et al. 1996, Shiyatov et al. 2000, Holmes 1983, 1998, Methods … 1990, Rinn 1996). As a result, we got 2 generalized tree-ring chronologies on the station Spasskaya Pad, one of which is for larch kayander (*Larix cajanderi Mayr.)* (SPPV) and the other for scotch pine *(Pinus sylvestris L.)* (SPP12), which have been constructed. Other tree-ring chronologies on larch have been made up at station Tyungyulyu (TYNG).

The comparative analysis of larch and pine growth depending on external conditions at Spasskaya Pad station was carried out. It is known that these two species are the basic forest-forming ones in Central Yakutia. Growth of trees is influenced not only by climatic factors such as atmospheric temperature and deposits, but also hydrothermal soils conditions. Larch prefers moderately fertile and moderately moistened loamy ground, and grows worse in dry and crude areas. In contrast to larch, pine grows on well aerated dry sandy and sabulous soils.

The soil temperature condition influence on radial trees increment at Spasskaya Pad was analyzed. Here data from Pokrovsk meteorological stations were used. This meteorological station has more homogeneous data in comparison with data of the Yakutsk meteorological station, which has some series disorder as a result of its relocation in 1930, 1952, and 1964 (USSR Climate Directory 1975) and soil condition changes since 1989 caused by an increase in subterranean water.

Results and Discussion

Correlation analysis of larches tree-ring chronology from Spasskaya Pad with soils temperature conditions at various depths shows that considerable correlation occurs during winter period. The higher the soil temperatures, the faster soils warm up, which promotes timely beginning of active tree growth in the vegetation beginning. Summer temperatures do not limit radial trees increment. During this period trees have enough amount of heat for favorable growth.

The similar analysis of pine radial increment has shown, that winter soil temperatures until the end of May have a positive relation to radial tree increments both at active layer table and zero annual amplitudes of active layer at 20 cm and 120 cm depth. A positive influence of temperature occurs in spring months in soil layers at 40–80 cm, which leads to early soil thawing and the beginning of pine growth processes. However, unlike larch, a significant negative influence of summer months' temperature on pine growth occurs at some depths. Probably this is due to a significant deficiency of soil water content in drier soils, where heats causes a drying up effect.

The correlation analysis of larch tree-ring chronology at Tyungyulyu with soil temperature conditions at different depths shows the presence of significant correlation; it is the same for Spasskaya Pad at winter period. It is also revealed, that the soil's summer temperature value has no significant influence on radial tree increments. In some cases, the soil high temperature means its negative relation with larch growth, which features for pine from Spasskaya Pad.

Correlation analysis of tree-ring chronology for larch with soil water content changes was carried out. Results show good correlation occurs during the whole vegetative period. However, it is necessary to note that the most significant ratios fall at the autumn period of the previous season. This

is due to the fact that larch in the beginning of the vegetative period uses the cumulative soil water reserve of the previous year. Thus water content of the soil's upper layers, that is, up to 50 cm, during its seasonal freezing shows significant correlation with the radial larch increment. Also soil water content of September and October at depths of 80–100 show good correlation with the annual increment It is possible to explain this by the fact that the larch root system basically uses water from the soil bottom lifts by the end of the vegetative period, since during summer, soil thawing passes gradually and is accompanied with dehydration of the soils upper horizons.

Conclusions

Thus, it is possible to approve that radial larch increment on permafrost soil is closely related to the active layer soil temperature and water content during the vegetative season. It is also significant that the application of dendroclimatological research technique helped to receive interesting results while studying the reaction of forest-forming species to climatic and soil conditions in the zone of permafrost distribution.

Acknowledgments

The research is executed with support of the grant of the Russian Federal Property Fund 06-05-96117 (r_vostok_a) and the integration project of SB RAS #71.

References

Elovskaya, L.G. & Konorovskiy, A.K. 1978. *Zoning and Melioration of Permafrost Soils in Yakutia.* Novosibirsk: Nauka, 175.

Fyodorov, P.P., Nikolaev, A.N. & Desyatkin, A.R. 2007. Revealing of hydrothermal soil regime influence on Larch radial increment in Central Yakutia. *Proceedings of Conference on New Dendroecological Technique*, *Irkutsk*.

Gavrilova, M.K. 1973. *Climate in Central Yakutia*. Yakutsk: Yakutsk Book Press, 120 pp.

Holmes, R.L. 1983. Computer-assisted quality control in tree-ring dating and measurement. *Tree-ring Bulletin*, 44: 69-75.

Holmes, R.L. 1998. *Dendrochronology Program Library-Users Manual-Laboratory of Tree-Ring Research*. Tucson, Arizona USA: University of Arizona, Updated September 1998 (the electronic version).

Methods of Dendrochronology. 1990. In: E. Cook et al. (eds.), *Application in Environmental Sciences.* Dordrecht: Kluwer Acad. Publ., 394 pp.

Murton, J.B. & French, H.M. 1994. Cryostructures in permafrost, Tuktoyaktuk coastlands, western Arctic Canada. *Canadian Journal of Earth Sciences* 31: 737-747.

Nikolaev, A.N. & Fyodorov, P.P. 2004. Influence of climatic factors and thermal permafrost soils regime of Central Yakutia on Larch and Pine radial increment (by the Example of Spasskaya Pad station). *Dendrology* 6: 1-11.

Rinn, F. 1996. *Referense Manual. Computer Program for Tree Ring Analysis and Presentation*. TSAP version 3.5. Heidelberg, Germany, 264 pp.

Shiyatov, S.G., Vaganov, E.A., Kirdyanov, A.V., Kruglov, V.B., Mazepa, V.S., Naurzbaev, M.M. & Khantemirov, R.M. 2000. *Dendrochronology Technique*. 1: Bases Dendrochronology Basic Foundation. Tee-ring Data Acquisition Tutorial and Methodological Manual. Krasnoyarsk: KrasGU Press, 80 pp.

Vaganov, E.A., Shiyatov, S.G. & Mazepa, V.S. 1996. *Dendroclimatological Research in the Ural-Siberian Subarctic Region*. Novosibirsk: Nauka, 246 pp.

Soil Temperature. 1975. In: USSR Climate Directory, 4th ed., Vol. 8. Yakutsk: Yakutsk Hydrometeorological Service Board Press, 570 pp.

The Effect of Soil Moisture and Ice Content on the Thermal Conductivity of Organic Soil Horizons Underlain By Discontinuous Permafrost

Jonathan A. O'Donnell
Department of Biology and Wildlife, University of Alaska Fairbanks
Vladimir E. Romanovsky
Geophysical Institute, University of Alaska Fairbanks
Jennifer W. Harden
United States Geological Survey, Menlo Park, CA
Kenji Yoshikawa
Water and Environmental Research Center, University of Alaska Fairbanks
A. David McGuire
Institute of Arctic Biology, University of Alaska Fairbanks

Introduction

Permafrost temperatures in Alaska have warmed in recent decades in response to changing climatic conditions at high latitudes (Lachenbruch & Marshall 1986, Osterkamp & Romanovsky 1999). In Interior Alaska, where forests are underlain by discontinuous permafrost, mean annual ground surface temperature (MAGST) often exceeds 0°C, yet permafrost can exist in a stable state (< 0°C) due to thermal offset (the difference between MAGST and mean annual permafrost surface temperature, or MAPST; Burn & Smith 1988). Thermal offset persists because the thermal conductivity of ice is greater than that of water, so soils conduct heat more effectively in winter than in summer.

Soil thermal models typically use a fixed thermal conductivity value for frozen and thawed soils. This bimodal approach, however, may be too simplistic to accurately predict soil temperatures and active layer depth (Overduin et al. 2006). Thermal conductivity of organic soil horizons varies considerably with moisture and ice content and is a critical control on active layer depth (Yoshikawa et al. 2003). Organic horizon type, which varies in bulk density, moisture field capacity, and extent of decomposition, may also influence thermal conductivity values. The primary objective of this study is to evaluate the effects of soil moisture and ice content on the thermal conductivity of three organic horizon types from black spruce forests of Interior Alaska.

Methods

We conducted a laboratory experiment to examine the effects of moisture and ice content on the thermal conductivity of organic soils collected from black spruce forests underlain by permafrost. Soil samples were collected from three moderately drained and three poorly drained black spruce forests in Interior Alaska. Organic soils were divided into three distinct horizons (live/dead moss, fibric, mesic/humic), that differ with respect to bulk density and extent of decomposition. Feather moss (*Hylocomium splendens and Pleurozium schreberi*) was the dominant moss species from the moderately drained stands, whereas *Sphagnum* spp. (most commonly *S. fuscum)* dominated forest floor cover in the poorly drained stands.

In the lab, all samples (n = 5 per site per horizon, total = 90 samples) were saturated and dried at air temperature, during which time we weighed each soil block and measured thermal conductivity using a KD2 Pro Thermal Properties Analyzer (Decagon Devices, Inc., Pullman, WA, USA) to generate a thermal conductivity—moisture content relationship for each sample from each horizon type. Measurements of thermal conductivity as a function of ice content are in progress. In 2005, we measured VWC in the field near Hess Creek, Alaska, using ECH2O probes (Decagon Devices, Inc., Pullman, WA) in replicate plots. Following field measurements, all probes and soil blocks were calibrated (O'Donnell et al. in review).

Results

Volumetric water content (VWC) of feather moss species, such as *Hylocomium splendens*, is generally around 10% (by volume) during summer months (Fig. 1). VWC of *Sphagnum* spp. is generally higher, ranging from 15–40% (by volume; Fig. 1).

We observed strong positive and linear correlations between thermal conductivity and organic VWC across all

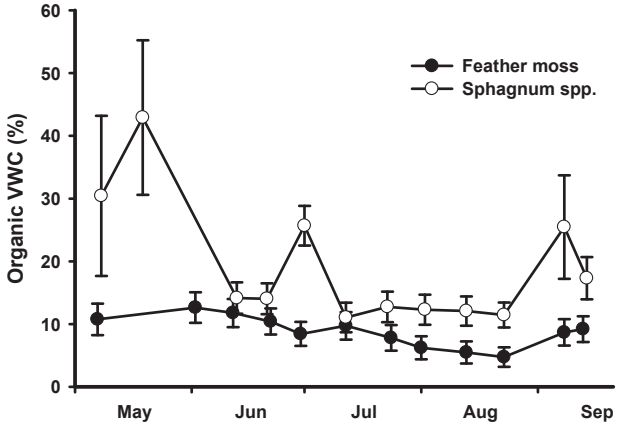

Figure 1. Seasonal variation in volumetric water content (VWC) of fibric organic matter near Hess Creek, Alaska (O'Donnell el al. in review).

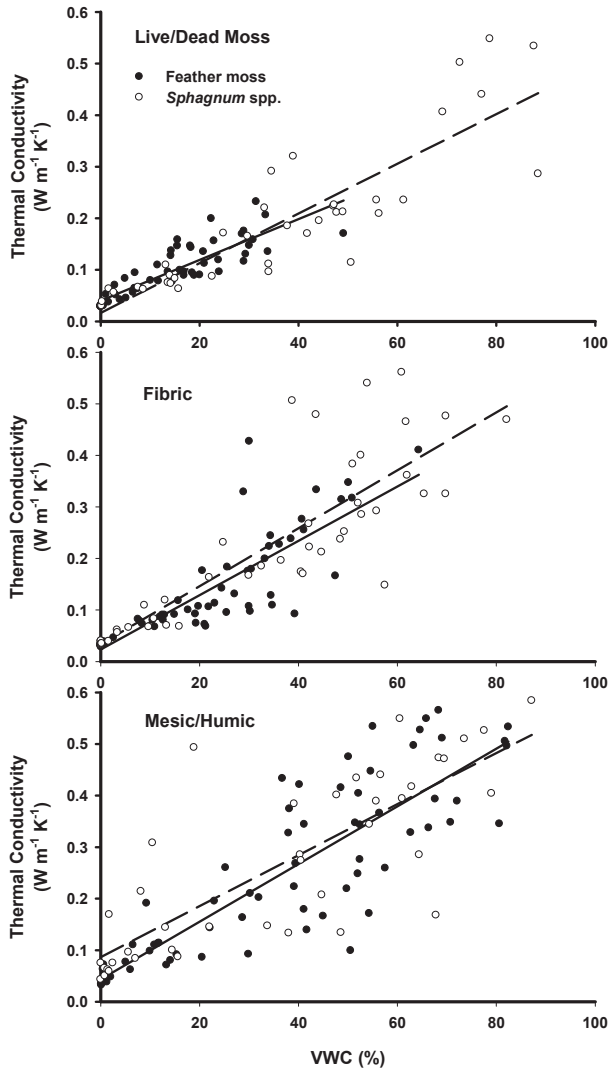

Figure 2. Linear regressions between thermal conductivity and volumetric water content in live/dead moss (top panel), fibric organic matter (middle panel), and mesic/humic organic matter (bottom panel). The regressions were fit separately for feather moss (solid line) and Sphagnum (dashed line).

organic horizons and moss types (range of R^2 values: 0.53–0.76; all P values < 0.0001). Increasing VWC of feather moss from 10 to 40% increased thermal conductivity nearly three-fold, whereas increasing VWC of Sphagnum from 10 to 60% increased thermal conductivity by five-fold (Fig. 2, top panel). We did not observe a very strong difference between feather moss- and *Sphagnum*-derived organic matter (fibric, mesic/humic). On average, increasing VWC of fibric horizons by 50% resulted in a four-fold increase in thermal conductivity (Fig. 2, middle panel). Similarly, increasing VWC of mesic/humic horizons by 70% resulted in a three-fold increase in thermal conductivity values (Fig. 2, bottom panel).

Discussion

Thermal conductivity of organic soil horizons in black spruce forests of Interior Alaska is positively correlated with moisture content. Thus, during the summer, variability in soil moisture content will greatly influence rates of heat transfer from surface to deep soil layers (Yoshikawa et al. 2003). During winter, heat fluxes through the active layer are primarily governed by ice content. However, unfrozen water can persist in deep peat and mineral soils during freeze-up and cooling of the active layer, modifying soil thermal properties and heat transfer (Romanovsky & Osterkamp 2000). Increased unfrozen water content during winter may reduce the thermal offset and increase the potential for permafrost thaw.

To evaluate the stability of permafrost in black spruce stands of Interior Alaska, we have developed a simple model to predict thermal offset (modified from Kudryavtsev 1981). This approach combines field measurements of soil moisture with laboratory measures of thermal conductivity and moisture, reported here. A comparative analysis of the observed thermal offset values with calculated values is currently in progress and will be discussed.

References

Burn, C.R., & Smith, C.A.S. 1988. Observations of the "thermal offset" in near-surface mean annual ground temperatures at several sites near Mayo, Yukon Territory, Canada. *Arctic* 41: 99-104.

Kudryavtsev, V.A. (ed.) 1981. *Permafrost*, short edition. MSU Press (in Russian).

Lachenbruch, A.H., & Marshall B.V. 1986. Changing climate: Geothermal evidence from permafrost in the Alaskan Arctic. *Science* 234: 689-696.

O'Donnell, J.A., Turetsky, M.R., Harden, J.W., Manies, K.L., Pruett, L.E., Shetler, G. & Neff, J.C. In review. Interactive effects of fire, soil climate and moss on CO2 fluxes in black spruce ecosystems of interior Alaska.

Osterkamp, T.E., & Romanovsky V.E. 1999. Evidence for warming and thawing of discontinuous permafrost in Alaska. *Permafrost and Periglacial Processes* 10: 17-37.

Overduin, P.P, Kane, D.L., & van Loon, W.K.P. 2006. Measuring thermal conductivity in freezing and thawing soil using the soil temperature response to heating. *Cold Regions Science and Technology* 45: 8-22.

Romanovsky, V.E. & Osterkamp, T.E. 2000. Effects of unfrozen water on heat and mass transport processes in the active layer and permafrost. *Permafrost and Periglacial Processes* 11: 219-239.

Yoshikawa, K., Bolton, W.R., Romanovsky, V.E., Fukuda, M. & Hinzman, L.D. 2003. Impacts of wildfire on the permafrost in the boreal forests of interior Alaska. *Journal of Geophysical Research* 108: (D1): 8148, doi:10.1029/2001JD000438.

.

Irreversible Damage? Human Activity, Cumulative Impacts, and Recovery Rates of the Antarctic Soil Environment

Tanya A. O'Neill
Department of Earth and Ocean Sciences, University of Waikato, Hamilton, New Zealand
Megan R. Balks
Department of Earth and Ocean Sciences, University of Waikato, Hamilton, New Zealand

Antarctic soils are vulnerable to disturbance because of their physical properties and extremely slow natural recovery rates due to the low temperatures and, in many regions, low levels of precipitation. As most human activities (tourism and national science programs) are concentrated in ice-free regions, the potential for human impacts on the soil landscape is great. Ice-free areas make up less than 0.4% of the total area of the continent, but are home to the majority of the historic huts, research stations, and biologically-rich sites, thereby attracting a short-sharp influx of tourists and science personnel each summer. Consequently, as continent-wide tourist numbers top 30,000 for the 2007/2008 summer season (www.iaato.org), concerns about cumulative effects, and the ability of the most frequented sites to recover after human disturbance, are also increasing.

Current information is insufficient to accurately predict how or to what extent the physical features at particular sites may be affected by repeat visits. This knowledge gap will impede our ability to effectively manage sites of value, and may consequently prove detrimental to the natural assets of the Antarctic ice-free regions.

This poster introduces a doctoral study that seeks to bridge the gap by quantifying the cumulative impacts of human activities on soils in the Ross Sea Region. Specific objectives are to (1) investigate the accuracy of EIAs (Environmental Impact Assessment) at predicting impacts of human activities on the Antarctic soil environment; (2) quantify the relationship between soil vulnerability (based on a soil vulnerability index), cumulative impact, and soil rates of recovery; and (3) elucidate a chronology of visible changes in the site "foot-print" at high human-impacted sites. Through this research we will establish baseline data relating to soil recovery rates in the Antarctic, an area of limited previous study. We will investigate sites where an EIA was conducted (such as the Greenpeace World Park base at Cape Evans, pipelines from McMurdo to Scott Base and beyond, and the proposed wind generation site on Crater Hill), and reassess the impacts on the soil environment following the completion of the activity to test the accuracy of EIA predictions. Such a detailed investigation into the effectiveness of the current EIA scheme with respect to *forecasted impacts* has not been conducted before. For our cumulative impact and recovery rate studies, we have deliberately chosen sites where the nature and timing of the disturbance have been well constrained, so recovery rates can be quantified (such as reassessing the K123 excavation pits and campsites in the Wright Valley, formed over three field seasons; and resurveying the 1992 Scott Base active-layer disturbance site of Campbell and others). In year three of this project, we will apply our Ross Sea Region methodologies to sites in the Antarctic Peninsula, where tourism and human disturbance is of an exponentially higher magnitude. Key heavily visited sites to investigate could include but not be limited to Barrientos Island (Aitcho Islands group), Hannah Point, Livingston Island, and Baily Head, Deception Island. Such comparisons could be used to model the likely impacts of the Ross Sea Region to increased tourist loading and associated pressures.

Our approach will begin to provide the basis for predicting how the Antarctic terrestrial environment will react to future human disturbance and climate change. It will assist environmental managers and Antarctic decision makers by allowing better predictive and managerial capability. There is the potential to document impacts of global warming on the terrestrial environment (soil and permafrost degradation), particularly in the warming Antarctic Peninsula. In the longer term there is the potential to produce a continent-wide map of ice-free regions using soil environment vulnerability classes based on cumulative effects and rates of recovery. This would involve the international coordination of resources to produce a GIS overlay of spatial information ranking soil vulnerability. Improved soil vulnerability data could be used by decision makers to identify or redefine Antarctic Specially Managed Areas (ASMA), Antarctic Specially Protected Areas (ASPA) (assist in developing or refining site specific guidelines), areas that are more resilient, could potentially have preference over others on the tourism itinerary, and identify others to focus future monitoring efforts. This information would be invaluable to the Committee for Environmental Protection (CEP) and aid in their Comprehensive Environmental Evaluation (CEE) assessment.

It is hoped that advancement of knowledge in the field of cumulative impacts will improve the highly criticized area of cumulative impact monitoring within the EIA system of the Madrid Protocol (1991). It is also hoped that this study will contribute to a more comprehensive tourism management system that will better incorporate tourism activities into the current EIA system. which coupled with an internationally standardized and quality EIA prior to an activity commencing, and coordinated environmental monitoring post-event, will ensure all possible environmental protection mechanisms are in place to preserve the integrity of the natural assets of the Antarctic ice-free regions.

The Role of Sea Ice in Coastal and Bottom Dynamics in the Baidaratskaya Bay

S.A. Ogorodov
Lomonosov Moscow State University, Faculty of Geography, Moscow, Russia

Sea ice, as a zonal factor associated with the high-latitude position of arctic seas, plays an important role in the evolution of their coastal zone. The ongoing development of oil and gas fields and the construction of relevant engineering facilities in the coastal and shelf areas (navigation channels, water scoop, terminals, drilling platforms, submarine pipelines) require new information on the effect of sea ice on the dynamics of coasts and sea floor. The effect of sea ice on coastal and bottom dynamics is one of the most important factors that determines the selection of a site for pipelines crossing from an offshore slope to land, method and a value of pipeline deepening. In Russia, special studies of sea ice impacts (first of all, the effect of ice gouging) were carried out in the areas of construction of submarine pipelines: the Baidaratskaya Bay of the Kara Sea (Fig. 1), the Pechora Sea, and the Sakhalin Island shelf.

The so-called "Nothern-Europe Gas Pipeline" must directly connect Russia and Germany through the bottom of the Baltic Sea to 2011. To provide gas for this pipeline, the project "Yamal-Europe" pipeline design, which lines would cross the Baidaratskaya Bay of Kara Sea, was renewed. Since 2005 and in connection with renewing of the project, investigations on coastal zone dynamics and sea ice effects was continued after a 10-year break.

Ice gouging is a destructive mechanical impact of ice onto the underlying surface. This impact onto the shore and bottom of the arctic seas is due to ice dynamics and mobility, hummocking, and formation of grounded hummocks, and it is controlled by hydrometeorological factors and coastal topography. In the Baidaratskaya Bay, the sea ice impact is observed in the coastal zone within the altitudes from first meters above the sea level down to 26 m depths.

Sea coasts are subjected to ice impact during the periods of both ice formation in autumn and fast-ice destruction and seas clearing of ice in spring. The relief of coasts composed of coarse debris material features a wide occurrence of ridges formed under the ice-push effect (Fig. 2). In autumn and in early winter, young sea ice (20–40 cm thick) can be pushed onto land during periods of surge. While moving, this solid ice cover cuts off beach sediments and forms ridges of unsorted material from it.

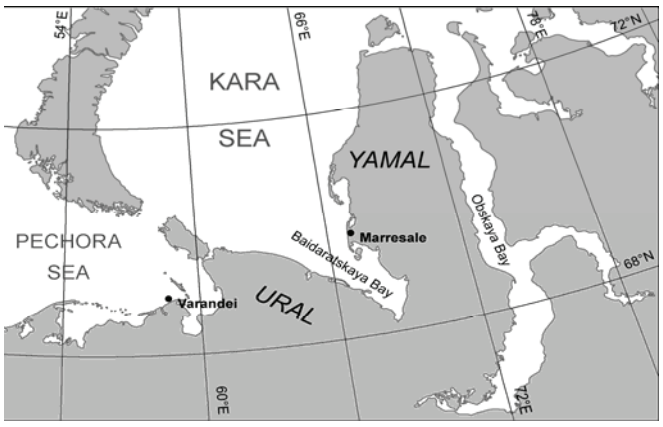

Figure 1. Location of research area

On maritime lowlands that can be flooded during high storm surges, sea ice can be brought inland as far as tens and even hundreds of meters, causing surface and building destruction.

The mechanical action of ice on the sea bottom lasts from the onset of ice formation until the sea is completely free of ice. After young ice freezes to the sea floor in the water edge zone, this new strip of ice serves as a protective buffer. The ridges of hummocks closest to the coast develop above submarine bars. Because of decreased sea depth over these bars, they become the centers of hummocking; hence, the number of hummock ridges commonly corresponds to the number of submarine bars. Due to the onshore pushing impact of sea ice, ice gouges in this zone are mostly oriented normally to the coastline (Fig. 3).

Further in the sea, the pattern of hummock ridges and barriers is irregular and controlled by hydrodynamic factors, particularly by the location of the fast ice edge during periods when storm wind is blowing. Storm winds destroy the fast ice edge and form a new ridge of hummocks or single-grounded hummocks. The ice gouges plowed in this case are either chaotic or parallel to the coastline. This is due to the prevailing along-shore drift of hummock formations. The fast ice edge (within Baidaratskaya Bay, at about 10–15

Figure 2. Ural Coast of Baidaratskaya Bay; ice-pushed ridge.

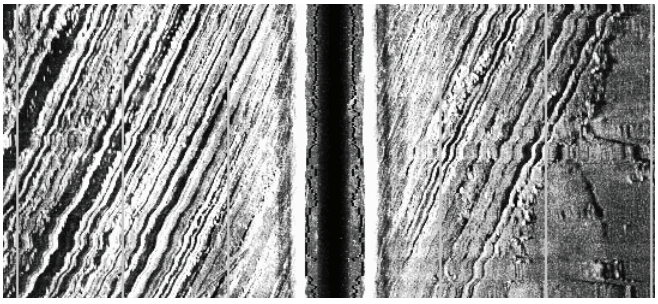

Figure 3. Sonar record at 12 m depth: Parallel and normally oriented to the shore ice gouges formed by multi-keels ice dam.

m depth) is the zone where ice impact on the sea floor is the strongest. Here, hummock ridges and barriers reaching the floor develop during the whole winter.

Within a beyond-fast-ice polynia up to 19–20 m depths sea ice influence on the bottom is also high, since hummocks frozen into the ice fields drift here during the winter as single large bergs which have high kinetic energy due to their mass. As a result, the largest ice gouges can reach 1.8 m deep, 10–40 m wide, and several km long (Fig. 4). They are oriented conformably with the direction of tidal currents—lengthwise the Baidaratskaya Bay.

The main method of indirect estimation of ice gouging intensity is the estimation of density and deepness (Fig. 5) of ice gouges. Meanwhile, the lifetime of such forms essentially can vary according to sea depth, types of sediment, and duration of the dynamically-active period; so the question about sea ice gouging intensity of the coasts and bottom is directly connected with the problem of safety of ice gouging forms.

Investigations on the Baidaratskaya Bay, Kara Sea, show that the frequency of occurrence and the density of ice-gouging forms is the largest at 17–19 m depth; but that does not mean that the intensity of ice gouging is lower in shallow depths with rarer occurrence and smaller depths of ice gouges.

The effect of coastal hummock ridges and barriers on beaches and in shallow areas (down to a depth of 7–10 m) can be traced only immediately after fast ice is destroyed. The life period of ice-gouged forms developed on sand beaches and shallow areas is very short—until the first summer storm. These forms, whose depth is mainly < 0.5 m here, commonly disappear with first strong waves in summer and autumn. Therefore, as a rule, the age of ice gouges in shallow areas does not exceed one year. Due to high hydrodynamic activity here, the gouges quickly smooth over, and the gouge density in shallow areas is lower than in the zone of the fast ice edge.

At depths of 14–16 m, the occurrence and density of gouges turn out to be lower than at higher depths, though ice gouging is the most intense (most of the mobile systems of hummocks and grounded hummocks are formed here). The above situation is due to more active hydrodynamics at smaller depths, where the effect of waves still manifests itself and the velocities of tidal currents are higher. Due to this, the gouges can exist over several years here (as distinct from their short existence in shallow areas), gradually smoothing over and vanishing. The lifetime of ice gouges is substantially determined by proportion between the freezing period and the dynamically-active period, and hence differs in diverse seas. For example, in the Pechora Sea, with a dynamically-active period two times longer in comparison with the Kara Sea, it is quite difficult to find ice gouges at the same depth. Another significant factor for the lifetime of a gouge is wave action. While comparing ice gouges at Baidaratskaya Bay at 12–14 m depth, the fewer number of gouges in the western part as compared with the eastern one is obvious. Indeed, the frequency of strong waves higher than 3 m, which can transfer sediments at stated depths, is a few times higher on the western coast as compared with the eastern one.

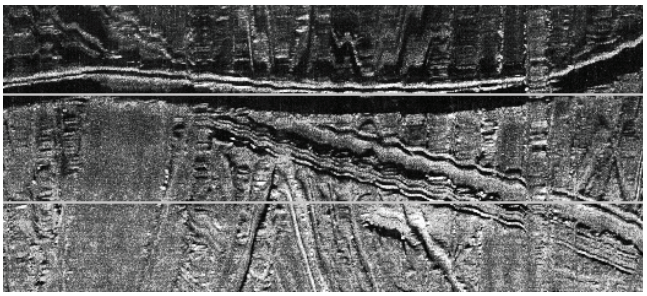

Figure 4. Sonar record, 19 m depth: Largest and deepest ice gouges.

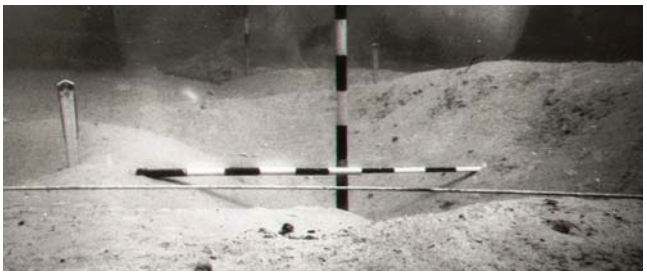

Figure 5. Winter underwater photo at a depth of 7 m: ice gouge deepness measurement. Stamukhi generated holes and gouges will become level by the first strong summer storm.

Deeper than 19 m, the ice gouges occur rather frequently. However, ice formations, particularly grounded hummocks, rarely occur at these depths. This situation is caused by low hydrodynamic activity and low sedimentation rates. Under such conditions, the gouges, especially large ones, can exist on the floor surface over decades. Thus, low intensity of ice gouging is compensated by a long life of gouge forms. This "accumulation" effect gives a wrong idea of high intensity ice gouging here.

The depth of ice-gouging forms depends not only on sea depth, ice thickness, and intensity of sheer stress, but also on composition and the state of bottom deposits. The safety of ice gouging forms probably depends also on plasticity, mobility, and granulometric composition of sediments. Attempts to find regularity between field data about occurrence and density of gouges on the one hand and the type of sediments on the other hand were not successful, except single examples of correspondence. Observations show that ice gouges, especially large ones, have considerable lengths, sometimes up to several kilometers; that is, hummocks can constantly gouge the bottom for a long time due to their large kinetic energy. Therefore hummocks can gouge bottom sections with rather different characteristics of the sediments.

Solifluction Phases During the Late Holocene in Sierra Nevada (Southern Spain)

Marc Oliva
Department for Physical and Regional Geography and Landscape Research Laboratory, University of Barcelona
Lothar Schulte
Department for Physical and Regional Geography and Landscape Research Laboratory, University of Barcelona

Introduction

Sierra Nevada, at latitude 37°N in southern Spain, is the highest massif in the Iberian Peninsula, reaching 3478 m a.s.l. at the Mulhacén peak and concentrates an important number of solifluction features. Dynamic control shows that nowadays most of these solifluction lobes are inactive and a few are weakly active.

The present climate conditions do not trigger intense solifluction processes, although sedimentological profiles of several lobes show enhanced solifluction activity during the last millennia. The alternation of edaphic layers and solifluction deposits implies different environmental conditions and reflects climate variations during the Late Holocene; colder and/or wetter periods promote solifluction, while warm periods induce soil formation.

Headwaters of Rio Seco and San Juan Valleys have a significant number of vegetated solifluction lobes. We have analysed the stratigraphy of many of them, and we provide the first chronology for solifluction activity during the Late Holocene in the southernmost last glaciated massif in Europe (Schulte et al. 2002).

Materials and Methods

Sedimentological and pedological studies according to the FAO system (2006) were carried out on more than 30 lobes placed between 2500–3000 m in these two valleys. A bulk sample of 0.5 kg was taken from each horizon or unit; laboratory analyses were done in the Institute of Geography of the University of Bern (Switzerland) on dry and sieved samples (< 2 mm).

For grain size measurements, organic matter was oxidized with 30% H_2O_2, and micro-aggregates were dispersed with Na_2CO_3. Silt (2–63 μm) and clay (<2 μm) fractions were determined with a Micromeritics SediGraph 5100 system, and sand fractions (63–2000 μm) were quantified by wet sieving. Organic carbon (OC) and the ratio C/N were measured with an Elemental Analyzer. The amorphous and crystalline pedogenic iron (Fe_o and Fe_d) were extracted according to Mehra & Jackson (1960). For AMS dating purposes, pollen grains from organic layers were concentrated and processed in the Angstrom Laboratory of Uppsala (Sweden).

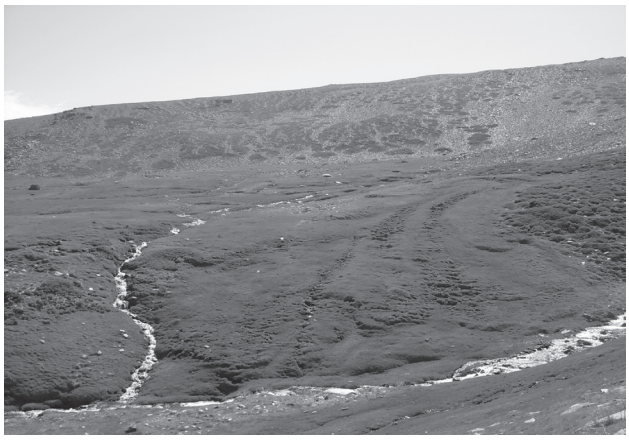

Figure 1. Solifluction lobes in San Juan valley.

Results

Solifluction phases are characterised by high percentage of gravels, a sandy loam fine fraction, and low OC contents (Fig. 2), while edaphic layers have a finer matrix with little amount of gravels, high OC contents (up to 30%) and increasing Fe_d values, depending on soil development intensity and weathering.

We present the lithostratigraphy of a solifluction lobe radiocarbon dated in San Juan Valley (Fig. 3), near late-lying snow patches with abundant supply of water. The bottom of the lobe corresponds to an organic layer that was buried by a solifluction deposit characterised by a high percentage of gravels and low OC contents, perhaps during the Neoglacial period. The warm climate conditions dominant during the Roman Warm Period and the Medieval Warm Period induce edaphic processes and peat formation (OC up to >25%) at this altitude. During the Little Ice Age, solifluction is reactivated with two pulses of significant percentage of gravels and decrease in OC values. In between these slope deposits, there is a thin organic layer, probably developed at the end of the 17th and beginning of the 18th centuries, a relatively

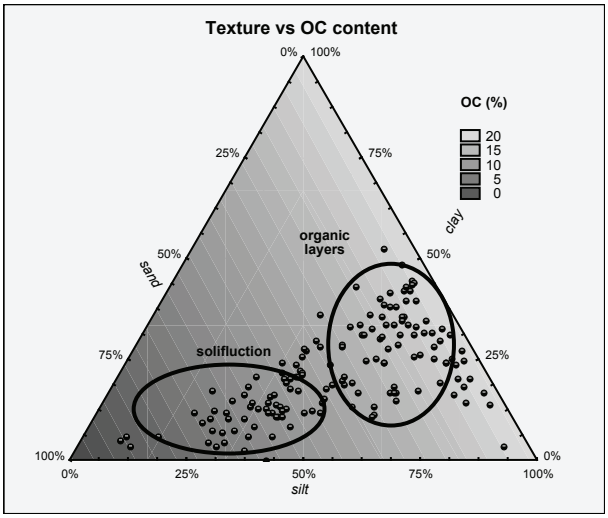

Figure 2. Comparison between texture and OC content in solifluction deposits and edaphic layers.

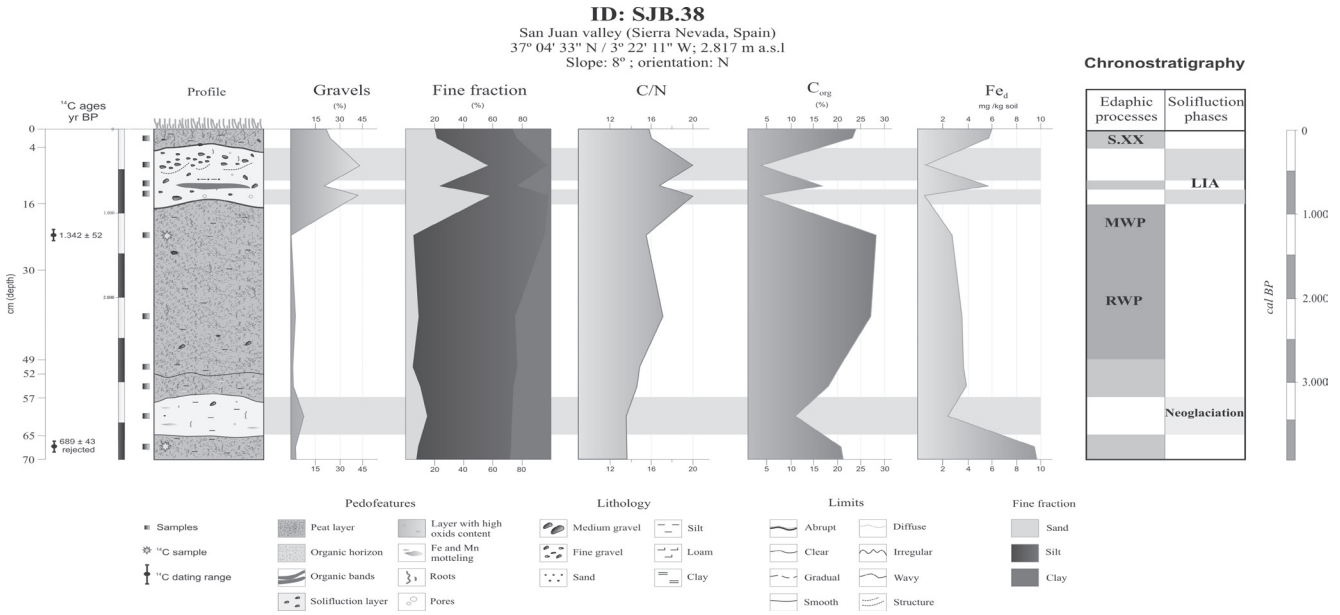

Figure 3. Lithostratigraphy of a solifluction lobe in San Juan Valley.

warm period in Andalusia (Rodrigo et al. 1999). The upper organic horizon of this vegetated lobe is the consequence of the increasing temperature trend of the 20th century.

Conclusions

Considering the chronostratigraphy of several lobes we can deduce different solifluction phases during the Late Holocene in Sierra Nevada: ?–3400, 3000–2700, 1400–1200, 650–300 and 250–100 cal. yr BP. Especially widespread are slope deposits corresponding to the two main pulses of the Little Ice Age (650–300 and 250–100 cal. yr BP) and the Neoglaciation (?–3400 and 3000–2700 cal. yr BP), mostly the two main Holocene solifluction phases in Sierra Nevada. On the other hand, intense soil development and peat formation was dominant during the Roman Warm Period (2700–1400 cal. yr BP) and the Medieval Warm Period (1200–650 cal. yr BP). These Late Holocene solifluction phases match with other mountain environments timing, such as in the Alps (Gamper 1983, Veit 1988), and correlates either with regional (Jalut et al. 2001) and global proxies (Stuiver & Braziunas 1993), suggesting the sensitivity of geomorphic processes in this high semiarid massif to Holocene climate variability.

Acknowledgments

This research was financially supported by the Spanish Ministry of Education, projects AP-2004-4548 and Fluvalps-3000 (CGL2006-01111).

References

FAO. 2006. *Guidelines for Soil Description*. UN, 133 pp.

Gamper, M.V. 1983. Controls and rates of movement of solifluction lobes in the eastern Swiss Alps. *Proceedings of the Fourth International Permafrost Conference. Fairbanks, Alaska, July 18–22, 1983:* 328-333.

Jalut, G., Esteban-Amat, A., Bonnet, L., Gauquelin, T. & Fontugne, M. 2000. Holocene climatic changes in the Western Mediterranean from South-East France to South-East Spain. *Palaeogeogr., Palaeoclimatol., Palaeoecol*. 160: 255-290.

Mehra, O. & Jackson, M. 1960. Iron oxide removal from soils and clays by dithionit-citrate systems buffered with sodium bicarbonate. *Clays and Clay Minerals* 7: 317-327.

Rodrigo, F.S., Esteban-Parra, M.J., Pozo-Vázquez, D. & Castro-Diaz, Y. 1999. A 500-year precipitation record in Southern Spain. *International Journal of. Climatology* 19: 1233-1253.

Schulte, L., Marcos Garcia-Blanco, J.de, Gómez Ortiz, A, Palacios Estrema, D., Tanarro Garcia, M., Fernández Fernández, A. & Ramos Sainz, M. 2002. Evolución Glaciar y periglaciar del Circo del Mulhacén (Sierra Nevada, Península Ibérica). *Publicaciones del Instituto Geológico y Minero de España*. Serie Geología 1: 491-499.

Stuiver, M. & Braziunas, T.F. 1993. Radiocarbon and 14C ages of marine samples to 10,000 B.C. *Radiocarbon* 35: 137-189.

Veit, H. 1988. Fluviale und solifluidale morphodynamik des spät- und postglazials in einem zentralalpinen flusseinzugsgebiet (Südliche Hohe Tauern, Osttirol). *Bayreuther Geowissenschaftliche Arbeiten* 13: 1-167.

Block Fields, Block Slopes, and Rock Glaciers: A Polygenetic Block Accumulation on the Schafstein (Rhoen Mountains, Germany)

Ch. Opp
Philipps-University Marburg, Germany

Introduction

Different forms of block accumulation are widespread in Central European Mid-Mountains. In most of the cases, they are described as block slopes (German: *Blockhalden*) and block fields (German: *Blockmeer*) and other German terms; in rare cases they are described as rock glaciers (Zurawek 2002).

The biggest known extension of block accumulation located in Germany is the basaltic hill of the Schafstein, in the central part of the Rhoen Mountains. This block accumulation was described in the 1960s by Mensching (1960), who called it *Blockmeer*, and in the 1990s by Halfmann (1991), who called it *Blockhalde*.

The first step of this study was to collect information from literature about the features of different forms of block accumulation (cf. Table 1).

Results

With the help of a self-developed mapping method, different features (cf. Table 1) of the Schafstein block accumulation were surveyed, for instance, block forms on the surface, weathering features, etc. The structure and the thickness of the block accumulation were measured with the help of refraction seismic techniques. For measuring air temperature below and between the blocks, dataloggers were used. Rock and soil samples were taken to determine the mineralogical composition with regard to weathering differences and transport mechanisms.

The small-scale survey of the block forms shows that the central part of the Schafstein block accumulation has edged blocks at the upper part and shaped blocks at the bottom of the block accumulation. A special feature at the bottom of the block accumulation is a characteristic wall and depression structure, with more than 30° inclination between the walls (cf. Fig. 1), caused by different tensions of different ice cement-saturated parts of the block accumulation. Refraction seismic measurements have proved that the central part of the block accumulation has a thickness of about 30 and 40 m. During summer time, when air temperature was about 30°C, we measured -1°C air temperature in between the block

Figure 1. Wall and depression structure in the central part of the block accumulation, the fossil rock glacier.

Table 1. Features of different forms of block accumulation (block field, block slope, and rock glacier), compiled after Däuble (2004, changed) from different literature sources.

Feature	Block field	Block slope	Rock glacier
General feature: accumulation of blocks with only a few or no amount of fine particles, with only rare or no vegetation cover			
Size	no details	some 10 m up to some 100 m long, >20 m broad	60...1500 m long, 60...3000 m broad
Thickness	no general details; mostly >1 m	no general details; some meters	10...100 m
Slope inclination	<20°	>20°	seldom more than 10°; border slopes 35°
Relief location	on plateaus and slopes; not necessarily closely connected to the source of blocks	below a bare rock	on slopes
Block size	no general details, different	at least head size, >2 m	mostly 0.6...1 m
Block form	edged or shaped	edged	no details
Block formation	in situ chemical and physical weathering with transport	in situ chemical and physical weathering with transport	physical weathering, primarily by frost
Block transport	solifluction, sliding	falling, sliding	cohesion transport of the ice cement
Surface structure	no details	no details	longitudinal and transverse bulges, depressions
Necessary climate	tropic or periglacial	periglacial, arid, semi-arid	periglacial

Figure 2. Rock glacier features on the bottom of the north and northwest slope of the Schafstein block accumulation.

accumulation (Opp 2005). Nearly all studied features prove that the central part of the Schafstein block accumulation represents a fossil rock glacier (cf. Fig. 2), while the western part represents a block field, and the eastern part is a block slope.

Acknowledgments

The author is especially grateful to Mrs. Däuble (Berlin) and Dr. M. Gude, who were included in the field research.

References

Däuble, F. 2004. Blockmeer–Blockgletscher–Blockhalde? *Ergebnisse neuer Untersuchungen am Schafstein/ Rhön*. Unpubl. FB Geographie, Marburg, 162 pp.

Halfmann, J. 1991. Die Struktur der Vegetation auf periglazialen Basalt-Block-Halden des hessischen Berglandes. *Dissertationes Botanicae* 168: 212 pp.

Mensching, H. 1960. Periglazial-Morphologie und qurtäre Entwicklungsgeschichte der Hohen Rhön und ihres östlichen Vorlandes. *Würzburger Geographische Arbeiten* 7: 39 pp.

Opp, Ch. 2005. Geographische Beiträge zur abiotischen Ausstattung des Biosphärenreservats Rhön. *Beiträge Region und Nachhaltigkeit* 2: 71-83.

Zurawek, R. 2002. Internal structure of a relict rock glacier, Sleza Massif, Southwest Poland. *Permafrost & Periglacial Processes* 13: 29-42.

Occurrence of Permafrost and Ground Frost Phenomena in Mongolia

Ch. Opp
Philipps-University Marburg, Germany

Introduction

Because of the climatic peculiarities and of the extreme continental location, the formation of permafrost and ground frost phenomena in Mongolia are widespread (Opp & Barsch 1993). Most of them belong to different forms of discontinuous and periodic permafrost. Types of ground frost occur in dependence from the zonal climatic, soil, and vegetation conditions. Zones of ground frost are distinguishable by their location above the sea level, by their area, by their spatial share, by their distribution within the zone, and by the thickness of the permafrost (cf. Table 1).

On the basis of observations, measurements, and interpretations during five field trips between 1989 (Barsch et al. 1993) and 1998 (Opp 1998, 2005), selected results are imparted.

Results

Seasonal average periods of freezing of discontinuous permafrost were established between October and May. The corresponding periods of thawing were established from late April until late September (cf. Fig. 1). The processes and periods of freezing and thawing can differ in dependence from the site conditions. Such examples were proved in dependence from the exposition (northern and southern slopes), or in river valleys (cf. Fig. 2) Characteristic differences of temperatures and pH values between the top and the bottom position of thufurs (earth hummocks) were analysed.

The degradation of many thufur fields in Mongolia is caused by climate (warmer winters) and land use changes (higher share of grazing animals) during the last decade.

Thermokarst bank erosion is caused by deep thawing during the summertime and lateral erosion by river water. The erosion rate of bank caving processes is much higher at the natural levee side in southern exposition than at other river bank positions. Within the river valley of the Orkhon River, south of the city of Darkhan, a maximum value of 1.5 m per year of backward erosion of the river bank, caused by permafrost degradation, were measured (Opp 1998, 2006). This "fluvio-cryo-thermo-erosion" of the river banks is a characteristic phenomenon of many rivers in northern Mongolia.

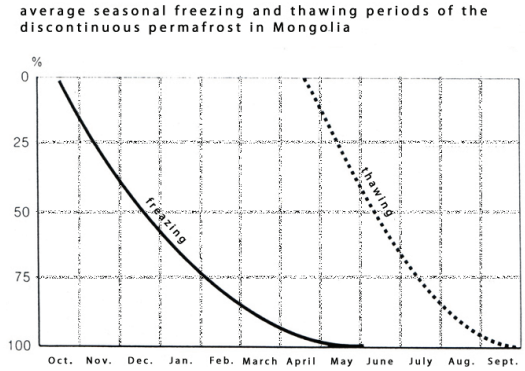

Figure 1. Average seasonal freezing and thawing periods of discontinuous permafrost within the Orchon catchment (northern Mongolia).

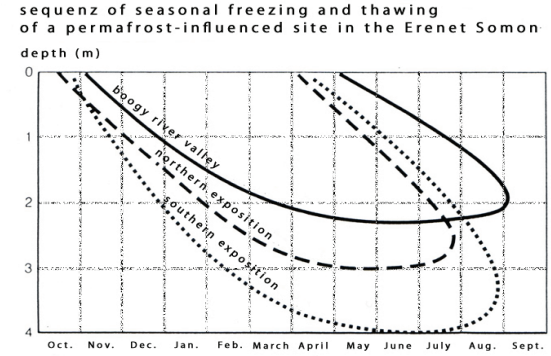

Figure 2. Sequence of seasonal freezing and thawing of a permafrost-influenced site near Erdenet (northern Mongolia).

Table 1. Selected features of the belts of frozen ground in Mongolia (Source: National Atlas of Mongolia, Ulan Bator, 1990).

belts of frozen ground	altitude a.s.l	area		portion within the permafrost area	dominant maximum thickness of permafrost		temperature in 20 m depth
			portion within the country		in valleys	on slopes and on watersheds	
	(m)	(km²)	(%)	(%)	(m)	(m)	(°C)
discontinuous permafrost	1200–2800	175,280	11.2	40–80	20–500 (bis 1000)		-5 bis +1
discontinuous permafrost	700–2600	350,560	22.4	1–40	5–50 (bis 100)	5-20	-5 bis +5
sporadic permafrost	600–1900	460,110	29.4	<1	5–10	-	-5 bis +5
seasonal ground freezing	600–1800	579,050	37	-	-	-	+3 bis +10

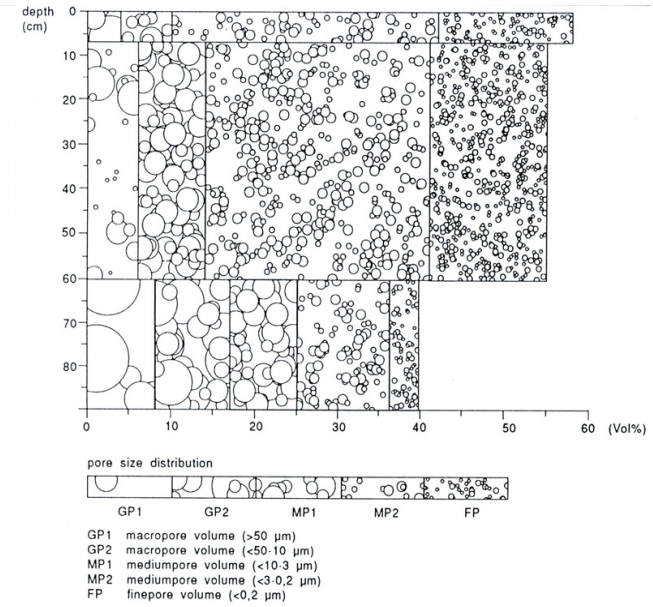

Figure 3. Pore size distribution of a Gelic Fluvisol (Turbel) within the Orkhon floodplain (northern Mongolia).

A warmer climate and an intensive use of pastures of the river valleys are the main reasons for permafrost and ground frost degradation in Mongolia. Effects on soils were proved with the help of cylinders measuring specific soil-physic parameters (pore volume, pore-size distribution, soil density, saturated vertical water conductivity) which, for example, allow statements about natural and man-made soil degradation and ground frost degradation processes. Though the pore volume in the upper soils of these sites is on average bigger than 50%, it is striking that their macro pore volume content is very small. The percentage of quickly-draining coarse pores is zero (cf. Fig. 3).

One reason for this seems to lie in the permafrost of the subsoil. The permafrost table during the summer measurement was at a depth of 90 cm.

Systems of polygonal ice wedges were observed on wet meadows near the river. A different distribution of the soil moisture of the ice wedges—wetter margin of the polygon, drier core of the polygon—was established by the different colouring of the grass. Besides that, ice wedge gaps of a width of 10 up to 40 cm are typical for a soil surface which was deformed by ice push and shrinking. The biggest ice wedge gaps (depth and width) were found in direct proximity of the Orkhon River.

Acknowledgments

The author is especially grateful to Prof. Dr. Barsch (Potsdam), Dr. Böttcher (Magdeburg), Dr. Tulgaa (Ulan Bator) and Mr. Enktuvshin (Ulan Bator), who were included in the field research.

References

Barsch, H., Opp, Ch. & Steinhardt, U. 1993. Geoökologische Probleme in der Waldsteppe der nördlichen Mongolei. *Potsdamer Geographische Forschungen* 3: 1-89.

Opp, Ch. & Barsch, H. 1993. Geomorphological processes in the Mountain Forest Steppe of Northern Mongolia. *Z. Geomorph. N.F., Suppl.-Bd*. 92: 145-157.

Opp, Ch. 1998. Bodenökologische Aspekte dauerfrostbeeinflusster Standorte in der Mongolei. *Mitteilungen Deutsche Bodenkundliche Gesellschaft* 88: 121-124.

Opp, Ch. 2005. Natürliche und nutzungsbedingte Land- und Bodendegradationsprozesse, untersucht am unteren Orchon (Nord-Mongolei). *Erforschung Biologischer Ressourcen der Mongolei* 9: 475-494.

Opp, Ch. 2006. Natural and land use caused land and soil degradation processes, a case study from the lower Orkhon region (northern Mongolia). *Proceedings of the Conference "Soil as a connecting link – function of natural and anthropogenic ecosystems in transition." Irkutsk September 4–7, 2006*: 480.

Reaction of Northern Taiga Ecosystems on Human-Induced Degradation of Permafrost in West Siberia

P.T. Orekhov
Earth Cryosphere Institute, Moscow, Russia, 744001

The development of the oil and gas industry has a considerable effect on permafrost ecosystems. Major and highly dynamic human-induced changes of the Western Siberia ecosystems have been caused due to the establishment and maintenance of the transport infrastructure of the oil and gas industrial system. Even a single facility, such as a main gas pipeline due to its length, is likely to have a drastic effect on ecosystems of different natural environment zones. The study of human impact on permafrost ecosystems appears to be especially urgent, taking into consideration an indirect effect of the disturbed vegetation, soil, and micro-topography on permafrost conditions.

This investigation has been conducted within the area of the Nadymsky Station of the SB RAS (Siberian Branch, Russian Academy of Science) Earth Cryosphere Institute, located in the northern taiga subzone of Western Siberia. The site occupies the area of sporadically distributed permafrost, and it is characterized by varied permafrost conditions. The permafrost patches are found in peat bogs, hilly lands, and frost heave areas. Mean annual temperatures of rocks vary within a range of +1.0 to -2.0°C.

Tundra ecosystems are widespread in peat bogs of the northern taiga. Perennially frozen grounds under the tundra ecosystems are referred to as the continuous permafrost zone. The temperature of perennially frozen ground varies from -0.5 to 1°C. A thickness of a seasonally thawed layer is within the range of 0.8 to 1.2 m in peat and mineral frost heave mounds and 0.5 to 0.7 m in peat mounds.

Associations of tundra plants such as grass, dwarf shrubs, moss, and lichen make up the specific vegetation cover of peat bogs. Dominant plants among those are *Ledum palustre, Vaccinium vitis-idaea, Rubus chamaemorus, Carex globularis, Cladina stellaris, C. rangiferina, Sphagnum fuscum,* and *Polytrichum commune* (Moskalenko 1999). In the almost complete ground cover of the undisturbed tundra ecosystems, lichens appear to be prevailing, that is, *Cladina stellaris and C. Rangiferina.* Apart from those, *Cetraria islandica* is commonly found among the ground cover plants together with *C. cucullata* and peat mosses. Foliage cover of the ground vegetation makes up 70%. The prevalent dwarf shrubs are presented by *Ledum palustre, Betula nana, and Vaccinium vitis-idaea.* Commonly found are *Vaccinium uliginosum*, *Carex globularis*, and *Rubus chamaemorus.* Foliage cover of the grass-and-dwarf shrub layer is 40–45%. The frost peat mounds vegetation cover is comprised of *Polytrichum strictum, Cladonia coccifera,* and *Cladina stellaris; Rubus chamaemorus* is abundant in the grass-and-dwarf shrub layer. In the natural tundra ecosystems, a total abundance of small mammal populations on average makes up 16.9 ± 1.1 species/10 pitfall trapnights. Biomass of small mammals is 259.4 ± 25.6 g/10 pitfall trapnights (Fig. 1).

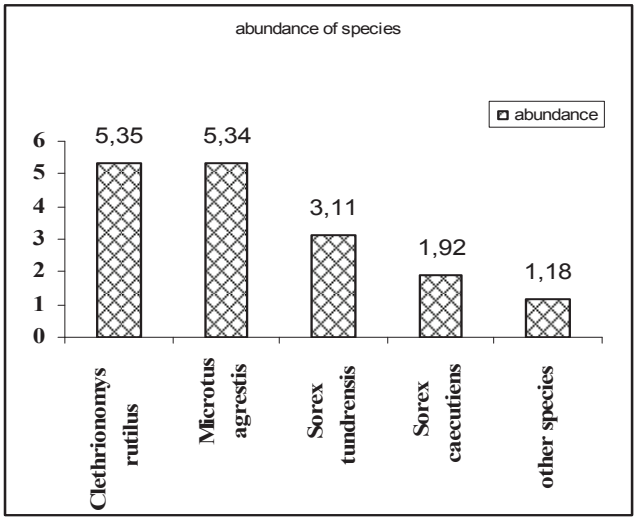

Figure 1. Abundance of small mammal species in the natural tundra ecosystems.

In 1971 in this area, the route was cleaned up to lay the gas pipeline Nadym-Punga. As the route was cleaned up, the vegetation cover was removed, the micro-topography was disturbed, and the upper peaty layer was withdrawn. The pipeline was laid in-ground with the earth fill made later. The pipeline laying lead to disturbance of the tundra ecosystems that resulted in an increase of water due to deteriorated drainage conditions, an increased number and enlarged area of hollows, bog formation, thermokarst activation, and finally, in peat surface subsidence with the top layer of the permafrost ground being dipped down to 6 m and, in areas with a thinner permafrost layer, being completely degraded.

Secondary ecosystems formed by 32 years after the occurrence of the primary disturbance. Ground cover of the secondary ecosystems has mosses prevailing, that is, *Polytrichum commune* and *Cladina stellaris. C. rangiferina* is not commonly found. Foliage cover makes up about 75%. Apart from those, species found in the ground cover are *Cetraria islandica* and *C. cucullata*. Among dwarf shrubs covering 40–45% of the ground surface*, Betula nana, Vaccinium uliginosum*, and *Empetrum nigrum* are growing abundantly. Species commonly found include *Calamagrostis Langsdorfii, Carex canescens, C. Globularis, Eriophorum russeolum, and E. vaginatum*. It should be noted that there are species which started growing abundantly along the pipeline, particularly, *Betula tortuosa* (height 5–7 m), *Salix viminalis* (height 3–5 m), and *Alnus* fruticosa, and these are species not specific for the tundra ecosystems (Sorokina 2003). Temperatures of top soil layers in September go up to 9.1°C.

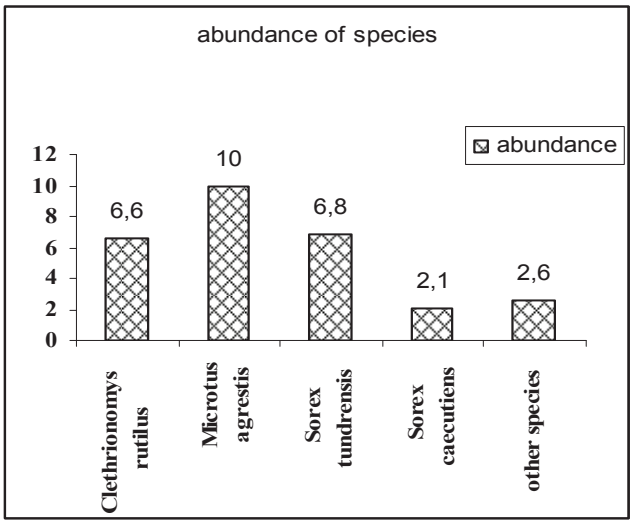

Figure 2. Abundance of small mammal species in the secondary ecosystems.

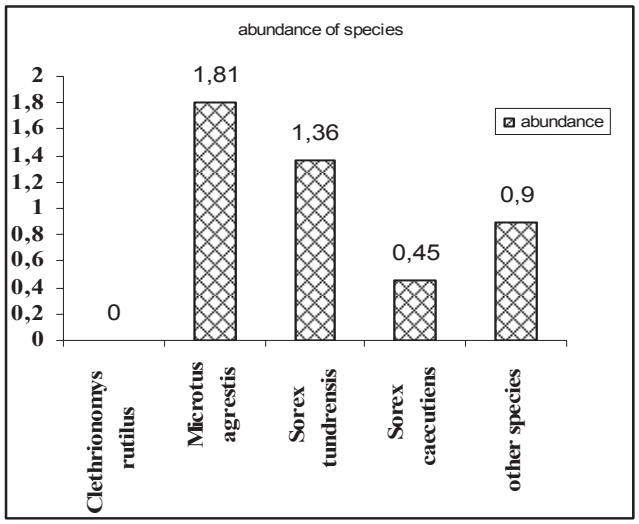

Figure 3. Abundance of small mammal species in the areas disturbed for the second time.

The comparative analysis applied to a community of small mammals has shown that the secondary ecosystems have significant growth of the species richness index that increased by 23.6% and the Shannon's diversity index that increased by 8.5%. A total abundance of small mammal populations on average makes up 28.1 ± 1.3 specisis/10 pitfall trapnights (Fig. 2). Biomass of small mammals is 522.2 ± 62.7 g/10 pitfall trapnights. A change has been observed in the dominance structure of small mammal communities (*Anthropogenic Changes* 2006). These changes in the population of small mammals of the secondary ecosystems compared to the natural ecosystems are associated with a great diversity of habitat conditions formed under the action of human-induced factors, particularly change in the hydrothermic condition of soils and formation of phytocenoses, having a greater variety of species.

In 2004 the gas pipeline was modified with the pipe replaced, which caused once again a disturbance of the secondary ecosystems. In 2005 the areas disturbed for the second time were partly flooded, followed by a formation of small, elongated lakelets up to 1.3 m deep, in which single species of *Utricularia sp.* were found. After the water level subsided as a result of the embankment being washed out in the third year after the secondary disturbance, sparse sedge-and-sphagnum groups were observed to form including single species of *Rubus chamaemorus*. A temperature of the soil top layer varies +4.5°C to +5.6°C. After the secondary disturbance occurred, the total abundance of small mammal species became 4.5 ± 0.9/10 pitfall trapnights. Biomass of small mammals is 60.9 ± 6.3 g/10 pitfall trapnights (Fig. 3).

With construction of pipelines, human-induced transformation of landscapes leads to change in ecosystem components such as vegetation, soil, topography, and rock top layers. This results in a change of snow cover dynamics, hydrological condition, and heat exchange in the bottom atmospheric layer. This in turn leads to impoundment, to change in thickness of seasonally frozen and seasonally thawed layers, to strengthening or weakening of a number of human-induced processes, and to reduced permafrost top layers, and in rare cases, to their degradation. Finally, there will be secondary ecosystems formed that differ considerably from the original ecosystems by multiple parameters.

Acknowledgments

I thank Elena A. Slagoda, Dmitry S. Drozdov, and Nataliya G. Moskalenko from the Earth Cryosphere Institute for logistic support. This research was funded by the grant of the Tyumen governor and the NASA Yamal LCLUC Project.

References

Moskalenko, N.G. (ed.) 2006. *Anthropogenic Changes of Ecosystems in West Siberian Gas Province*. Moscow: Earth Cryosphere Institute, 358 pp.

Moskalenko, N.G. 1999. *Anthropogenic Vegetation Dynamics in the Permafrost Plains of Russia*. Novosibirsk: Nauka, 280 pp.

Sorokina, N.V. 2003. *Anthropogenic Changes of West Siberia Northern Taiga Ecosystems*. Tyumen: Avtoreferat of candidate dissertation, 24 pp.

Geocryology (Permafrost) Course at the University of Alaska Fairbanks

T.E. Osterkamp
Geophysical Institute, University of Alaska Fairbanks

Early years

Professor Ebb Rice developed a course on Arctic Engineering during the 1960s at the University of Alaska Fairbanks. This course was the inspiration for a series of courses in engineering and science dealing with snow, ice, and permafrost. A course on the physics of ice was developed by Professor T.E. Osterkamp in 1970 and taught during the early 1970s. This was followed by a series of separate special topics courses on snow, ice, and permafrost.

These special topics courses evolved into Physics 643 (Physical properties of snow, ice, and permafrost) taught in 1974, Physics 693 (Physical properties of sea ice) taught in 1975, and Physics 693 (Permafrost: Physical properties and processes) taught in 1976.

Eventually, these courses evolved into separate courses on snow and ice (Professor Benson), glaciers (Professor Harrison), sea ice (Professor Osterkamp), and permafrost (Professor Osterkamp). Professor Weeks took over the sea ice course when he came to the university in the mid-1980s. The permafrost course was taught for the second time in 1979 through the Department of Geology and Geophysics, and I taught it every other year since then until 1997, when I retired. Professor Romanovsky has taught the course since then using my course notes as a basis.

Nature of the course

From the beginning, the permafrost course was seen primarily as a materials science course about permafrost, its physical properties, and physical processes occurring within it. It was designed to provide students with the necessary scientific background to understand and study permafrost. Materials science courses bring together a number of disciplines (physics, chemistry, geophysics, geology, engineering) to study a single material. A relatively large amount of background information had to be provided because there was an unusual diversity of student preparation and because the selected topics were often not covered in previous courses.

The course was designed for science and engineering students at the advanced undergraduate and beginning graduate student level and for research personnel with specialties in other areas. Minimum preparation for the course included mathematics at the level of ordinary differential equations and at least senior standing in the sciences or engineering. Topics included soil physics, especially thermodynamics; thermal, electrical, and mechanical properties; and heat and mass flow processes, particularly those related to freezing and thawing. Solved problems and applications from the fields of engineering, mining, geology, environmental physics and geophysics were used to illustrate the course material. The course material was developed primarily from published papers. A fairly comprehensive literature survey was provided as a guide to additional reading.

Problems were developed for the purposes of providing exposure to additional topics, to illustrate certain points, and to allow the students to test their understanding of the material. The table of contents is reproduced below.

PERMAFROST: PROPERTIES AND PROCESSES*

T. E. Osterkamp

Table of Contents

I have most of my lecture notes for the course transcribed and will have a few CDs available for people who are teaching courses on permafrost.

Potential Use of Rock Glaciers as Mountain Permafrost Indicators in Yukon Territory, Canada

Amaris Page
Department of Geography, University of Ottawa, Ottawa, Canada
Antoni Lewkowicz
Department of Geography, University of Ottawa, Ottawa, Canada
Panya Lipovsky
Yukon Geological Survey, Whitehorse, Canada
Jeff Bond
Yukon Geological Survey, Whitehorse, Canada

Introduction

Analysis of the distribution of active rock glaciers is widely accepted as a way to establish the lower boundary of mountain permafrost. Rock glaciers have been used in this capacity for modeling probable permafrost distribution, mainly in Europe (e.g., Imhof 1996, Lambiel & Reynard 2001, Frauenfelder 2005, Etzelmüller et al. 2007, Fukui et al. 2007, and others). All of these models have examined permafrost distribution over relatively small areas.

We are beginning a similar project in Canada's Yukon Territory. A key difference from previous research is the spatial extent over which the study is being conducted. Currently the distribution of rock glaciers and their activity status are being examined in the southern half of the territory, an area of approximately 250,000 km^2.

A second difference between this and the European research is that in North America, rock glacier distribution may represent only the lower limit of *high elevation* permafrost. Permafrost also occurs in lower elevation valley bottoms due to a combination of temperature inversions due to cold air drainage (Lewkowicz & Ednie, 2004), and ecological interactions associated with surface hydrology. This situation does not occur in Europe, where rock glacier distribution can be used to model the full extent of permafrost in mountainous areas.

Our broad goal is to use the distribution of rock glaciers as an independent means of testing mountain permafrost probability models. This abstract focuses on potential sources of information and current knowledge of rock glacier distribution.

Methodology

Rock glacier location data for this research will be derived mainly from the Yukon Geological Survey's surficial geology maps (see Fig. 1 for map coverage). Rock glacier origins and activity status will be determined by examining their morphology on aerial photographs and remotely sensed imagery. Rock glaciers will be classified as active, inactive, or relict. Their distribution will be assessed at various scales and the usefulness of the rock glaciers for determining probable permafrost distribution in southern Yukon will be evaluated. A sub-sample of the rock glacier population will be visited and their origins and activity status verified in the field.

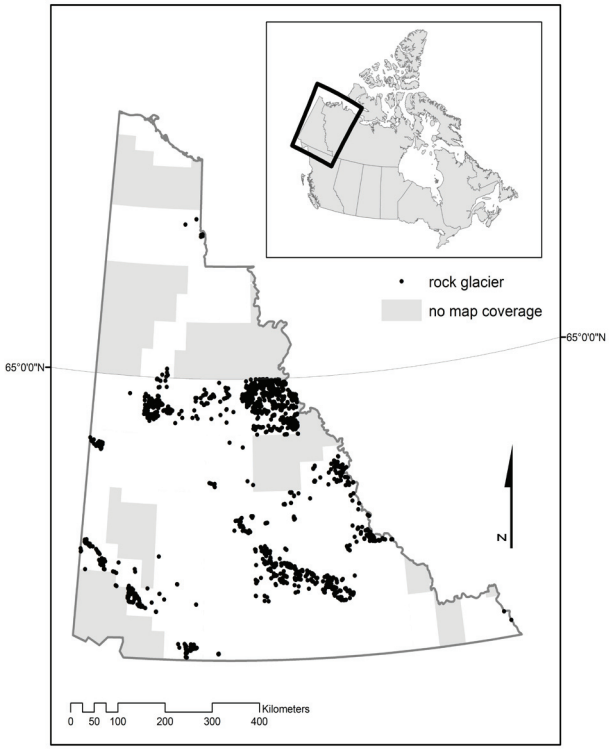

Figure 1. Study area showing surficial geology map coverage (white) and distribution of known rock glaciers (black dots) in the Yukon Territory. According to Heginbottom et al. (1995) discontinuous permafrost becomes continuous at about 64°45′N in this region.

Approximately 1650 individual rock glaciers have been identified to date on maps at scales of 1:25,000 to 1:250,000, which cover roughly 75% of the Territory south of 65°N (the zones of discontinuous permafrost in the Yukon). Verification that the complete population has been mapped will be undertaken for selected areas using aerial photographs. An indication that the maps may not show all the features, possibly because of differences in scale, is that Sloan and Dyke (1998) state that more than 1100 rock glaciers are present in the Selwyn Mountains alone.

Rock glacier density, elevation, and aspect will be compared in different parts of the Territory. Figure 1 shows that there is considerable variation in density with most rock glaciers concentrated in the NW- to SE-trending Selwyn Mountains, Pelly Mountains and Kluane Ranges. Densities in these areas can reach 1 rock glacier per 4 km^2. Extraction of other

parameters, such as orientation, elevation and dimensions, is in progress. Variability in these will be examined, and the possibility of their correlation with climate factors will be studied. From this it is expected that trends in high elevation permafrost distribution will be evident.

Depending on the outcome of the assessment described above, the rock glacier inventory may provide the basis for a permafrost distribution model, or it may be used to verify the results of other models such as those being produced by BTS investigations (Lewkowicz & Ednie 2004, Lewkowicz & Bonnaventure 2008, Bonnaventure & Lewkowicz in review).

Implications

This research is expected to produce the first rock glacier inventory for the southern Yukon, and may additionally be used to create the first permafrost probability map based on geomorphic indicators in the same region. Large-scale permafrost distribution mapping has thus far been carried out using only very general interpolation between existing climate stations with only qualitative consideration of topography (Heginbottom et al. 1995). This project aims to compare methods, improve accuracy, and develop a means of including topographic effects in Canadian permafrost mapping.

Acknowledgments

This research is being funded by the Canadian Foundation for Climate and Atmospheric Sciences.

References

Bonnaventure, P.P. & Lewkowicz, A.G. (in review). Mountain permafrost probability mapping using the BTS method in two climatically dissimilar locations, northwest Canada. *Canadian Journal of Earth Sciences*.

Etzelmüller, B., Farbrot, H., Gudmundsson, Á., Humlum, O., Tveito, O.E. & Björnsson, H. 2007. The regional distribution of mountain permafrost in Iceland. *Permafrost and Periglacial Processes* 18(2): 185-199.

Frauenfelder, R. 2005. *Regional-scale Modeling of the Occurrence and Dynamics of Rockglaciers and the Distribution of Paleopermafrost*. Schriftenreihe Physische Geographie Glaziologie und Geomorphodynamik, 45, Geographisches Institut der Universität Zürich; Zürich.

Fukui, K., Fujii, Y., Mikhailov, N., Ostantin, O. & Iwahana, G. 2007. The lower limit of mountain permafrost in the Russian Altai Mountains. *Permafrost and Periglacial Processes* 18(2): 129-136.

Heginbottom, J.A., Dubreuil, M.A. & Harker, P.T. 1995. Canada – Permafrost. 1:7,500,000 scale map. *National Atlas of Canada* (5th ed.). Natural Resources Canada.

Imhof, M. 1996. Modelling and verification of the permafrost distribution in the Bernese Alps (Western Switzerland). *Permafrost and Periglacial Processes* 7(3): 267-280.

Lambiel, C. & Reynard, E. 2001. Regional modelling of present, past and future potential distribution of discontinuous permafrost based on a rock glacier inventory in the Bagnes-Hérémence area (Western Swiss Alps). *Norsk Geografisk Tidsskrift – Norwegian Journal of Geography*, 55(4): 219-223.

Lewkowicz, A. & Bonnaventure, P.P. 2008. Interchangeability of mountain permafrost probability models. *Permafrost and Periglacial Processes* 19(1): in press.

Lewkowicz, A. & Ednie, M. 2004. Probability mapping of mountain permafrost using the BTS method, Wolf Creek, Yukon Territory, Canada. *Permafrost and Periglacial Processes* 15(1): 67-80.

Sloan, V. & Dyke, L. 1998. Decadal and millennial velocities of rock glaciers, Selwyn Mountains, Canada. *Geografiska Annaler*, 80A(3-4): 237-249.

Soil Carbon Distribution in the Alaska Arctic Coastal Plain

Erik Pullman
University of Alaska Anchorage, Kachemak Bay Campus, 533 East Pioneer Ave., Homer, AK 99603
M. Torre Jorgenson
ABR, Inc. – Environmental Research and Services, P.O. Box 80410, Fairbanks, AK 99708
Yuri Shur
University of Alaska Fairbanks, Civil and Environmental Engineering, P.O. Box 755900, Fairbanks, AK 99775

Introduction

The accumulation of soil carbon in arctic soils represents a globally significant sink of atmospheric carbon that is both formed and maintained by development and accretion of permafrost. Much of this near-surface carbon currently sequestered in permafrost can be incorporated into the active layer through surface disturbance (Pullman et al. 2007) and thermokarst processes related to climate change (Jorgenson et al. 2006). Most recent estimates sample only the active layers or top 100 cm of soil (however, see Bockheim & Hinkel 2007) or are based on samples taken from a limited number of geomorphological terrains.

In this study, we have used a landscape-classification approach to sampling in an area of the North Slope Coastal Plain of Alaska covering 850 km^2 (Fig. 1). The terrain units, surface forms, and vegetation communities of the landscape in this area were classified through aerial photo interpretation and extensive field surveys. Samples for soil carbon were distributed across the major terrain types identified across the study area. Total soil carbon results for each terrain unit were then applied to the terrain map and a total carbon inventory was calculated for the study area.

Methods

Sample collection

Soil cores were collected during the summer in 2001–2003 in the NPR-A area. An intact soil plug was removed down to permafrost. Intact 3-inch (7.5 cm) soil cores in permafrost were collected using a specially-designed soil corer attached to a portable power head. At each location, we attempted to core into the underlying sand sheet and locate sediments with less than 10% visible ice. We postulate that this may represent the syngenetic/epigenetic boundary within the existing permafrost. At each soil pit, soil stratigraphy, texture, and color were described from the intact, frozen soil core. Cryogenic structures were described according to Shur and Jorgenson (1998). Visual ice content was estimated for each stratigraphic section. Soil textures were grouped into lithofacies classes based on similarities on particle size distribution and depositional patterns (Pullman et al. 2007). Frozen soil samples were taken every 10–20 cm (within stratigraphic sections) along the entire length of the core. Sample volumes were measured in the field by taking three measures of core length (at equidistant intervals around the circumference) and three measures of core circumference (at the ends and midpoint of the core length). Unfrozen core material was removed prior to measurement. Mean length and circumference values were used to calculate the cylindrical core volume. Core samples were then placed in labeled ziplock freezer bags for transport. A total of 47 cores and bank exposures were included in this analysis, with total sample depths ranging from 1.8 to 4 m. Most cores extended to 2.7 m.

Field samples were weighed and thawed at room temperature. Excess water was decanted off the sample once all solids had settled to the bottom of the sample bag. Soils were oven-dried to a constant weight at 60°C. A subsample of the homogenized dried soil was submitted for total carbon and nitrogen analysis to the Palmer Soils Laboratory (Palmer, Alaska).

Soil carbon calculations

Soil carbon content was calculated for each stratigraphic section within individual cores, and then summed over 100 cm and 200 cm. Stratigraphic sections that extended through the 100 cm and 200 cm depths were split for the purposes of calculating total carbon for these specific depths. Since we did not sample every stratigraphic section of every core, estimates of the carbon content in unsampled sections were made to obtain total carbon stocks for each core. A stratigraphic method was used to reduce variability that could be introduced by a length-weighted mean method. In this study a total of 612 stratigraphic sections were identified in 46 cores. Of these sections, 476 were sampled for %C content. Measurements on a majority of these sections (400) were made for sample volume, excess ice volume, dry soil density, and water content. Using data from the sampled stratigraphic sections, we were able to calculate mean carbon contents for stratigraphic sections that were missing data for either % carbon, dry density, or both. For stratigraphic sections missing % carbon measures, we used the mean %C of the section's lithofacies class (Table 1). For sections missing dry density measures, sample dry density was calculated using a regression of dry density based on %C of active layer samples multiplied by the % excess ice (from the visual field estimate). For the minority of stratigraphic sections with neither density nor %C measures, we used a value of both %C and dry density, based on calculated means of the appropriate lithofacies class.

Mean carbon stocks for each terrain type were applied to the terrain map of the study area to show the spatial distribution of carbon in the active layer, top 1 m, and top 2 m of soil across the study area to produce a distribution pattern of total

carbon in terrestrial areas of the landscape Terrain types that were not samples include water bodies (lakes, ponds, rivers, and streams) and some of the less-common terrain types.

Results and Discussion

Overall, older surfaces with less-active depositional environments had the largest soil carbon stocks (Fig. 1). Mean accumulation of surface organic material was least in ice-poor thaw basin margins (8.0 cm), eolian inactive sands (11.3 cm), and alluvial-marine deposits (11.1 cm), and greatest in ice-rich thaw basin centers (32.2 cm) and margins (48.8 cm).

Carbon stocks were greatest in alluvial-marine deposits and thaw basin centers, and lowest in eolian inactive sands and basin margins. A general trend of increasing soil organic carbon with decreasing depositional activity was seen across the study area. Soil carbon stocks were lowest in riverine terrain units (active riverbeds, active overbank, and inactive overbank deposits) and highest in thaw basin and and alluvial-marine deposits. In riverine terrains, mean (± s.d.) carbon stocks in the top 1 m of soil ranged from a low of 10.2 ± 7.8 kg C/m² in meander active riverbed deposits to 20.0 ± 2 kg C/m² in delta inactive overbank deposits. In thaw basin terrains, the range was 37.8 ± 3.9 kg C/m² in ice-poor margin deposits to 41.7 ± 13.4 kg C/m² in ice-rich center deposits. Alluvial-marine deposits, which experience minimal deposition or erosional activity, had the highest soil carbon stocks (58.2 ± 16.5 kg C/m²). When calculated in the top 2 m, large increases in carbon stocks were seen in all terrain units (Fig. 1). These data represent conservative estimates of total soil carbon stocks, because additional soil carbon may be present beyond our sampling depths, especially in ice-rich thaw basin centers and alluvial-marine terrains. Our estimates of carbon stocks fall into the range of other recently published accounts (Ping et al. 2002, Bockheim & Hinkel 2007) of carbon stocks in the top 1 m (Ping et al. 2002) and 2 m (Bockheim & Hinkel 2007) of soil on the Arctic Coastal Plain. However, this study includes a wider variety of terrain types and includes carbon-poor soil types that have not been previously sampled.

Soil organic carbon data for sampled terrain units were combined with an existing terrain unit map of a portion of the Western Beaufort Coastal Plain to produce a distribution map of soil organic carbon. As additional terrain unit maps in this area become available, we plan to expand the carbon distribution map and generate a regional soil carbon estimate based on the current dataset. Based on previous soil surveys in the area, this data can be applied to approximately 7000 km² of the Beaufort Coastal Plain. In addition, this data can be combined with thaw settlement estimates across the same area to identify terrain units where sequestered carbon may be incorporated into the active layer under the conditions of a warmer climate or human disturbance.

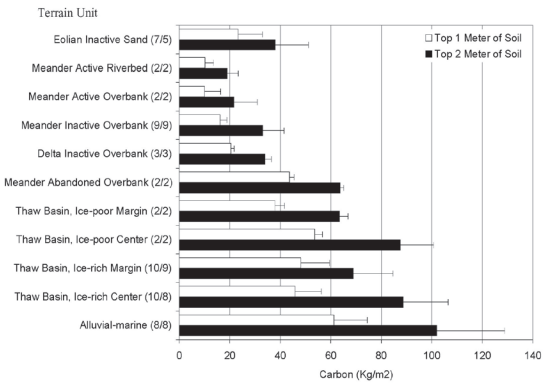

Figure 1. Mean carbon content of soils in common terrain units of the Arctic Coastal Plain, Alaska. Error bars represent standard deviation and numbers in parenthesis show the sample size (number of cores) used to calculate 1 m and 2 m soil organic carbon.

Acknowledgments

This research was funded by ConocoPhillips Alaska, Inc. and managed by Caryn Rae, Senior Biological Consultant. John Shook, Tim Cater, Gerald Frost, Luke Mcdonagh, and Jennifer Mitchell assisted with the fieldwork and soil processing.

References

Bockheim, J.G. & Hinkel, K.M. 2007. The importance of "deep" organic carbon in permafrost-affected soils of Arctic Alaska. *Soil Science Society of America Journal* 71: 1889-1892.

Jorgenson, M.T., Shur, Y. & Pullman, E.R. 2006. Abrupt increase in permafrost degradation in Arctic Alaska. *Geophysical Research Letters* 33: L022503.

Ping, C.L., Michaelson, G.J., Kimble, J.M. & Everett, L. 2002. Chap. 47. Soil organic carbon stores in Alaska. In: R. Lal, J.M. Kimble, & R. Follet (eds.), *Agricultural Practices and Policies of Carbon Sequestration in Soils*. CRC Press LLC, 485-494.

Pullman, E.R., Jorgenson, M.T., and Shur, Y. 2007. Thaw settlement in soils of the Arctic Coastal Plain, Alaska. *Arctic, Antarctic, and Alpine Research*, 39: 468-476.

Shur, Y. & Jorgenson, M.T. 1998. Cryostructure development on the floodplain of the Colville River Delta, Northern Alaska. *Proceedings of the Seventh International Conference on Permafrost, Yellowknife, Canada*: 993-999.

The 2007 "Anaktuvuk River" Tundra Fire on the Arctic Slope of Alaska: A New Phenomenon?

Charles Racine
U.S. Army Cold Regions Research Laboratory (Retired), 219 E. King Street, Edenton, NC 27932, USA
Randi Jandt
Bureau of Land Management, Alaska Fire Service, Fort Wainwright, AK 99703, USA

Introduction

A 1000 km^2 (256,000 acres) tundra fire started by lightning, burned from mid-July to early October 2007, and drew national attention as the largest Alaskan wildfire of the year and the largest North Slope tundra fire in recorded history. It burned from 68.7° to 69.5°N latitude (-150.5° longitude) in the east-central North Slope foothills just south of the Colville River. It doubled the known acres burned north of 68° since records have been kept by Alaska Fire Service (around 1950). As with the melting of Arctic Ocean ice and the expansion of shrubs across the tundra, there has been speculation about whether large fires in arctic tundra are more evidence of climate warming in the north (*Anchorage Daily News*, Sept 28, 2007). The objective of this paper is to place this fire and tundra fires in general in the historical context of wildfire in Alaska.

We used published reports and an online spatial database (afsmaps.blm.gov) of fires between 1956 and 2007 to analyze the extent of tundra fires north and west of tree line. The database shows the latitude-longitude of fire starts, area burned, date of detection, and date when declared out, and displays perimeters of larger fires (>400 ha).

Inferences about the longer term tundra fire regime can be made from pollen and charcoal in lake bottom sediments and suggest that burning increased coincident with the transition from herb tundra to shrub tundra about 13.3 to 14.3 ka BP (Higuera et al. 2008). However, it is noteworthy that fossil charcoal in lake sediments or other paleo-evidence of fire *north* of the Brooks Range is generally lacking for the past 5000 years.

Tundra fire locations

Figure 1 shows all recorded tundra fires (1956–2007) north of 68°N. The AR (Anaktuvuk River) fire is outlined in the right center of the map west of the Alaska Pipeline. Several tundra fires are concentrated along the Noatak River (west side of map) near 68°N, but only 10 recorded fires including the AR fire have been reported north of 69° on the North Slope. Tundra fires occur almost annually north and west of tree line in the Seward Peninsula and the Noatak River Valley, where they are much more common than on the North Slope. Larger tundra fires in these three regions are listed in Table 1.

Of the 10 tundra fires reported north of 69°, four others were >400 ha, occurring in 1993 and 1977 on the western Arctic Slope (Fig. 1, Table 1). Prior to 2007, no large tundra fires had occurred on the east side of the North Slope. One other large tundra fire (Sagavanirktok), in addition to the AR fire, occurred in this area in 2007 (just east of the Alaska Pipeline, Fig. 1).

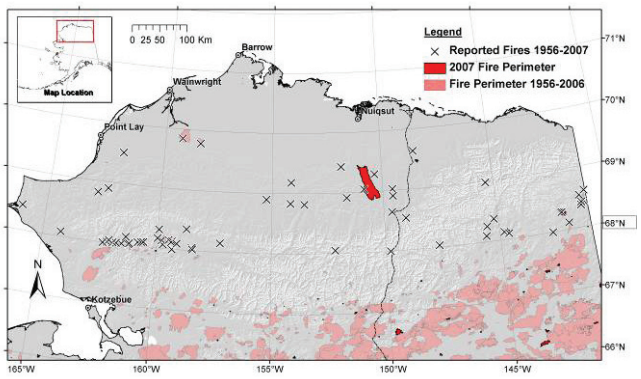

Figure 1. Map of northern Alaska showing locations of all reported fires from 1956–2007 north of 66°N latitude. The *X*s mostly denote smaller tundra fires (<400 ha) north of 68°. The Anaktuvuk River fire is strongly shaded, and the perimeters of large forest fires south of the Brooks Range are lightly shaded.

Tundra fire size

Only one other tundra fire—in 1977 in the central Seward Peninsula—was as large (1,000 km^2) as the AR fire (Table 1). The second largest fire on the North Slope was 330 km^2. Most tundra fires are small (<400 ha), particularly in comparison with boreal forest fires, which can cover 2000 to 6000 km^2 or more (Kasischke et al. 2002). Some of these forest fires are outlined in Figure 1. Racine et al. (1985) analyzed tundra fire size in the Noatak watershed showing that, of 79 fires between 1956 and 1983, almost half were less than 10 ha in size.

As surface or ground fires, tundra fires are easily stopped by rivers and streams and can be more easily extinguished by small rain or fog events or even nightly humidity. Tundra fire flame lengths are typically 2–8 m compared with 15–30 m in black spruce crown fires. Therefore, firebrand production and spotting potential across natural firebreaks are much reduced. The AR fire was confined between the Itkillik and Nanushuk Rivers, but burned a long distance (70 km) from north to south between these two rivers.

Tundra fire timing

The AR fire was started by lightning on July 16, and was declared out on October 6. No other tundra fires are known to have burned this long (almost 3 months) and late into the fall, although the nearby 2007 Sagavanirktok fire, about 90 km northeast of the AR fire, began on September 7, and

burned to October 9 (Table 1). The AR fire initially remained fairly small and was even thought to be "out" in early August, but roared back to life during record warmth and drought in early September and burned to October 5, when the area was blanketed by snow. The other large tundra fire of the same size at Imuruk Lake in the Seward Peninsula (Table 1) burned for over two months from July 9 to September 12. It has been proposed that late-season fires would burn deeper and would be more severe because the active layer deepens, allowing deeper drying of the organic mat.

The AR fire was the largest fire of the 2007 Alaska fire season. The largest fire year on record was 2004 when 6.5 million acres burned statewide, but only a few minor tundra fires were recorded. The year 1977 appears to be the only large Alaska fire year (ranked sixth), when there were both extensive large tundra and boreal forest fires. A total of 2.5 million acres burned with about 0.7 million acres (2800 km^2) resulting from tundra fires in the Seward Peninsula and Noatak River regions (Table 1).

Implications for permafrost

Tundra wildfire results in warmer soil temperatures and initially deeper thaw for several years following fire. Thawing is the result of (1) the removal of all or a portion of the insulating organic soil layer, (2) lowered surface albedo, (3) increased soil moisture, and (4) a longer thaw period as a result of earlier snowmelt and delayed fall freeze-back (Liljedahl et al. 2007).

Table 1. Characteristics of some large tundra fires in three regions of Alaska north and west of tree line.

Fire Name	Year Dates	Fire Size (km^2)	Lat.	Long.
North Slope	1956–2007	2113		
Anaktuvuk	2007 7/16–10/5	1000	69.3	150.5
Sagavanirktok	2007 9/7–10/9	13	69.5	148.3
B678	1993 7/22–8/18	330	69.9	159.1
B480	1993 7/3–8/17	67	69.8	158 2
Kokolik R.	1977 7/26–8/7	46	69.5	161.8
Seward Penin.	1956–2007	5229		
Imuruk Lake	1977 7/9–9/12	1000	65.5	163.0
Niagra Ck.	1997 7/22–9/25	300	65.5	164.5
Coffee Creek	1971 6/29–7/22	210	65.3	164.6
Chicago Ck.	1990 8/8–9/11	220	66.0	162.2
Wagon Wheel	1977 7/9–8/5	180	65.0	162 8
Noatak River	1956–2007	1881		
Mission Lowland	1977 7/15–8/18	458	67.5	162.5
Uvgoon	1999 6/26–8/3	354	67.8	162.7
Noatak Canyon	1977 6/24–7/4	121	68.0	161 7

On flat terrain, thaw depths generally return to pre-fire levels within 10 to 25 years (Racine et al. 2004). However, where slopes are steep, as on river banks and back slopes, tundra fires have been observed to cause subsidence, massive thaw, erosion, and even exposure of ice wedges. Where permafrost is "warm" or discontinuous, as on the Seward Peninsula, the effects of tundra fire on permafrost may be greater (Liljedahl et al. 2007, Racine et al. 1983).

Discussion

By far most wildfire in Alaska occurs in the Interior boreal forests between the Brooks Range and the Alaska Range, where an average of 2869 km^2 burned annually from 1960 to 2000 (Kasischke et al. 2002). Boreal forest fires of 1000 km are not uncommon. Total tundra area burned from 1956 to 2007 is largest for the Seward Peninsula (5229 km^2) (Table 1). The total for the North Slope (2113 km^2) is strongly influenced by the one 1000 km^2 AR fire.

Clearly the factors that determine the frequency and extent of tundra fires are different from those that control boreal forest fire. Lightning frequency, climate, and fuels are different north and west of tree line. Tundra fires are likely more climate-driven than fuel-driven. In the fall of 2007, a large temperature anomaly (10°C warmer than usual) and sunny dry weather along the Arctic Coast possibly associated with an ice-free Arctic Ocean was reported at the December 2007 AGU meeting (arcus.org/press/).

However, the expansion and increase in shrubs predicted and measured in the Alaskan Arctic may also affect the tundra fire regime (Higuera et al. 2008). Separating the effects of climate change and warming from those of fire disturbance and succession remains a major problem, in part because changes in vegetation and disturbance regime are linked.

References

Higuera, P.E. et al. 2008. Frequent fires in ancient shrub tundra: implications of paleorecords for arctic environmental change. *PLoS ONE* 3(3).

Kasischke, E.S., Williams, D. & Barry, D. 2002. Analysis of the patterns of large fires in the boreal forest region of Alaska. *Int. J. of Wildland Fire* 11:131-144.

Liljedahl, A. et al. 2007. Physical short-term changes after a tussock tundra fire, Seward Peninsula, Alaska. *J. Geophys. Res., Earth Surface* 112: doi:10.1029.

Racine, C. et al. 1985. Tundra fire regimes in the Noatak River Watershed, Alaska: 1956–83. *Arctic* 38: 194-200.

Racine, C. et al. 1983. Permafrost thaw associated with tundra fires in NW Alaska. *Proceedings of the 4th Internatl. Conf. on Permafrost. Nat. Academy Press,* 1024-1028.

Racine, C. et al. 2004. Tundra fire and vegetation change along a hillslope on the Seward Peninsula, Alaska, USA. *Arctic, Antarctic and Alpine Res.* 36: 1-10.

Ice Wedge Thermal Regime in Northern Victoria Land, Antarctica

Rossana Raffi
Department of Earth Sciences, "La Sapienza" University, Roma, Italy
Simone Sega
Department of Earth Sciences, "La Sapienza" University, Roma, Italy

Introduction

A study on the ice wedge thermal regime in northern Victoria Land, Antarctica, was conducted by installing dataloggers at three selected sites. Two of the sites are located in the Terra Nova Bay area, near Baker Rocks (74°12′27″S, 164°50′01″E, 11 m a.s.l.) and Boomerang Glacier (74°30′13″S, 163°50′10″E, 874 m a.s.l.). The third site is located near Mount Jackman (72°23′07″S, 163°10′49″E, 1326 m a.s.l.) in the Freyberg Mountains (Fig. 1).

Testo Testor 171-4 dataloggers, equipped with NTC sensors (±0.2 accuracy), were installed in the Terra Nova Bay sites. At the Mount Jackman site PT100 sensors (±0.1 accuracy) mounted on a Campbell CR1000-XT datalogger were used. In each installation, four sensors took hourly temperatures of the air, the ice wedge top and bottom, and the ground surface. The air temperature was measured at a height of 180 cm above the ground at Baker Rocks, 110 cm at Boomerang Glacier, and 155 cm at Mount Jackman. The ground surface temperature was measured at a depth of 2 cm. The ice wedge top and bottom were measured, respectively, at a depth of 50 cm and 133 cm at Baker Rocks, 38 cm and 83 cm at Boomerang Glacier, and 35 cm and 85 cm at Mount Jackman.

Data were collected during the period from 1 February 2004 to 31 December 2006 at Baker Rocks and Boomerang Glacier, and from 1 February 2006 to 31 December 2006 at Mount Jackman (Fig. 2).

The purpose of the study was to provide new data on the ice wedge thermal regime, and to verify if thermal conditions at the sites can trigger ice wedge cracking.

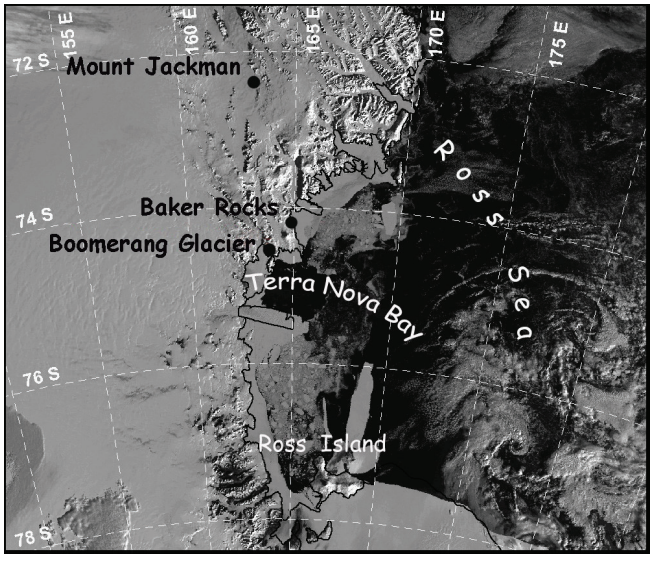

Figure 1. Location of the study sites. Satellite image by Italian Antarctic National Research Program.

Ice Wedge Thermal Regime

Air temperature

The mean annual air temperature (MAAT) during the period from 1 February 2004 to 31 January 2006 was -21.1°C at Baker Rocks and -16.3°C at Boomerang Glacier. The mean air temperature, calculated over 11 months, was -23.3°C at Mount Jackman.

According to Burn (1990), ice wedge cracking is primarily controlled by the winter temperature regime. During the winters of 2004, 2005, and 2006, the mean air temperatures, calculated from April to September, were -25.5°C, -28.4°C, and -28.8°C, respectively, at Baker Rocks, Boomerang Glacier, and Mount Jackman. The lowest monthly mean air temperatures most often occurred in May and July (Fig. 2), with lows below -45°C at Baker Rocks and Boomerang Glacier, and -50°C at Mount Jackman. Moreover, frequent, large temperature fluctuations occurred throughout the winter seasons, with either sharp drops or rapid increases in air temperatures.

In the Arctic, the correlation between sharp air temperature drop, ground cooling rate and ice wedge cracking was fully documented by the field studies of different authors (i.e., Mackay 1993, Allard & Kasper 1998, Fortier & Allard 2005). According to the authors, atmospheric cooling events of major amplitude were taken into account, and their mean values were calculated. Applying this method at the study sites revealed that mean air temperature drops of 18°C, 16.6°C, and 19.3°C, over mean periods of 33.3 hours, 47.7 hours, and 26 hours, at mean air cooling rates of -2.1°C/h, -0.4°C/h and -0.7°C/h, occurred, respectively, at Baker Rocks, Boomerang Glacier, and Mount Jackman. These

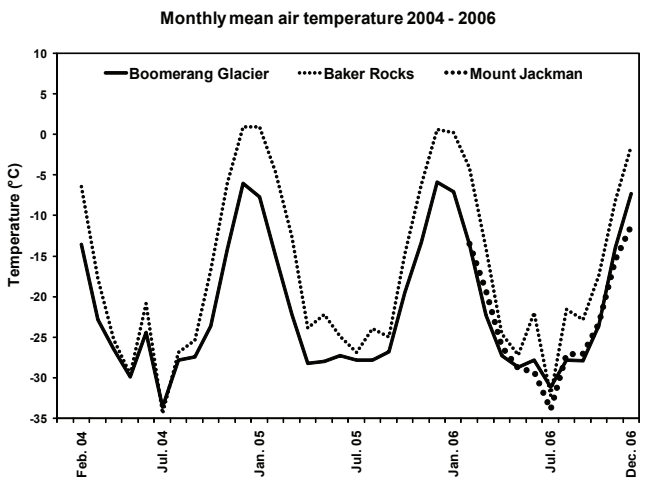

Figure 2. Monthly mean air temperature for 2004–2006 at the ice wedge polygon sites: Baker Rocks (11 m a.s.l.), Boomerng Glacier (874 m a.s.l.), and Mount Jackman (1326 m a.s.l.).

values exceed the 4-day temperature drop rate of 1.8°C/d, reported by Mackay (1993), which favored ice wedge cracking on the western Arctic coast. They also exceed the mean drops of 7.9°C, over mean periods of 18 hours, at a mean air cooling rate of -0.5°C/h measured before cracking events by Fortier and Allard (2005), at Bylot Island in the eastern Canadian Arctic Archipelago.

Ground temperature

The mean annual ground surface temperature (MAGST) was -17.1°C at Baker Rocks and -20.4°C at Boomerang Glacier. The mean ground surface temperature, over an 11-month period, was -22.4°C at Mount Jackman.

During winter seasons the mean ground surface temperature (MGST) was -28.6°C at Baker Rocks, -29.8°C at Boomerang Glacier, and -33.1°C at Mount Jackman. Temperatures with lows below -40°C were recorded at all sites.

The mean annual temperature of the top of the ice wedge was -15.3°C at Baker Rocks, -20.2°C at Boomerang Glacier. A mean value of -21.3°C was recorded at Mount Jackman over an 11-month period. During the winter months, ice wedge top temperatures were consistently below -20°C at Baker Rocks (mean value -21.7°C) and Boomerang Glacier (mean value -26.8°C), and below -25°C at Mount Jackman (mean value -28.4°C).

The ground surface thermal regime closely follows that of the air, with similar large and rapid fluctuations in temperature. Mean ground cooling rates (MGCR) of -28.6°C/d, -4.8°C/d, and -12.4°C/d at the surface, and of -0.4°C/d, -0.5°C/d, and -1.3°C/d at the ice wedge tops were obtained, respectively, at Baker Rocks, Boomerang Glacier, and Mount Jackman. These rates exceed the MGCR before frost-cracking episodes of -0.3°C/d at the surface and -0.2°C/d at the permafrost table, reported by Fortier & Allard (2005).

Discussion

The analysis of the thermal regime at the ice wedge polygon sites revealed that, in winter, the temperatures of the air and on the tops of the ice wedges fell below -30°C and -20°C, respectively. These values exceed the limits at which thermal-contraction cracking is known to occur in the Arctic (Lachenbruch 1966, Allard & Kasper 1998, Fortier & Allard 2005). Comparison of the cooling rates of the air and ground with those measured by Mackay (1993) and Fortier & Allard (2005) at the time of cracking events shows that thermal conditions at the study sites are more severe than those identified in the Arctic areas, and they most likely can trigger ice wedge cracking. This is also supported by the existence of open cracks observed, both in the ice wedges discussed in this article and in many others excavated during summer field surveys in northern Victoria Land (Raffi 2003).

At present, no field data of snow cover are available; however, we can infer that there was no thick snow cover at the three sites because throughout winter seasons, the daily ground surface temperatures were almost always lower than the daily air temperatures. When the opposite occurred, daily ground surface temperatures only remained higher than the air temperature for very brief periods (from a few hours to a few days), and then quickly decreased. The strong katabatic winds, with gusts reaching speeds of more than 200 km/h in winter, prevent snow accumulation and its insulating effect on the ground.

Acknowledgments

This research was carried out within the Italian Antarctic National Research Program. Thanks are due to Dr. R. Bono, CNR-ISSIA of Genova, I, and to Dr. U. Gentili, Climate Project, ENEA, Roma, I, for the field maintenance of the thermometric stations.

References

Allard, M. & Kasper, J.N. 1998. Temperature conditions for ice-wedge cracking: field measurements from Salluit, northern Québec. In: A.G. Lewkowicz & M. Allard (eds.), *Proceedings of the Seventh International Permafrost Conference, Yellowknife, Canada, June 23-27, 1998*. Centre d'études nordiques, Québec: Université Laval, Collection Nordicana 57: 5-12.

Burn, C.R. 1990. Implications for palaeoenvironmental reconstruction of recent ice-wedge development at Mayo, Yukon Territory. *Permafrost and Periglacial Processes* 1(1): 3-14.

Fortier, D. & Allard, M. 2005. Frost-cracking conditions, Bylot Island, Eastern Canadian Arctic Archipelago. *Permafrost and Periglacial Processes* 16(2): 145-161.

Lachenbruch, A.H. 1966. Contraction theory of ice-wedge polygons: a qualitative discussion. *Proceedings of the First International Permafrost Conference, Lafayette, Indiana, November 11-15, 1963*. Washington, DC: National Academy of Sciences-National Research Council, publication no. 1287: 63-71.

Mackay, J.R. 1993. Air temperature, snow cover, creep of frozen ground, and the time of ice-wedge cracking, western Arctic coast. *Canadian Journal of Earth Sciences* 30: 1720-1729.

Raffi, R. 2003. Ice wedges in the Terra Nova Bay region (northern Victoria Land, Antarctica). Distribution and morphological features. *Terra Antartica Reports* 8: 143-148.

Soil Thermal and UV Radiation Monitoring on a Maritime Antarctic Permafrost Area by Means of REMS (Rover Environmental Monitoring Station-Mars Science Laboratory) Sensors

M. Ramos
Department of Physics, University of Alcalá, Spain
J. Gómez, E. Sebastian, J. Martín, C. Armiens
Astrobiological Center (INTA-CSIC), Spain
J.J. Blanco
Department of Physics, University of Alcalá, Spain
M.A. de Pablo
Department of Geology, University of Alcalá, Spain
D. Tomé
Department of Physics, University of Alcalá, Spain

Introduction

The present climatic characteristics of Mars induce the extensive presence of permafrost areas in this lonely planet (Carr 2006). Therefore, environmental parameters that are included in Martian rover missions are the focus for monitoring thermal characteristics and soil surface evolution in order to understand the active layer thickness and the energy balance between the soil and the atmosphere.

On the other hand, the intensity of the incoming UV radiation on the soil level is a key parameter of Mars habitability. Nevertheless, Mars conditions are quite different to those observed on the Earth's surface. On Earth, a deep ozone absorption band centered at 2550Å prevents most of the UV radiation from reaching the surface, whereas on Mars, at least in low latitudes and in summer at high latitudes, the full solar flux at wavelengths greater than 1900Å falls unattenuated onto the surface.

The REMS (Rover Environmental Monitoring Station) is an environmental station designed by the Centro de Astrobiología (Spain) with the collaboration of national and international partners (CRISA/EADS, UPC and FMI), which is part of the payload of the MSL (Mars Science Laboratory) NASA mission to Mars (http://mars.jpl.nasa.gov/msl/overview/).

This mission is expected to be launched in the final months of 2009, and mainly consists of a rover with a complete set of scientific instruments; the rover will carry the biggest, most advanced suite of instruments for scientific studies ever sent to the Martian surface.

Five sensors compose the REMS instrument: ground (GT-REMS) and air temperatures, wind speed and direction, pressure, humidity and ultraviolet radiation (UV-REMS). It also includes all the electronics and software required by sensor read out, signal conditioning and data transmission to the rover. Wind vector, air temperature, and humidity and ground temperature sensors are located in small booms which are attached to the rover mast, while the ultraviolet sensor is on the rover deck and pressure inside the rover body and connected with external ambient by a small opening (see Fig. 1).

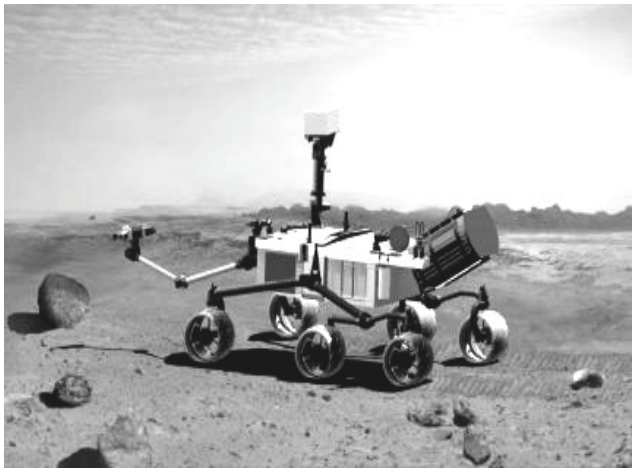

Figure 1. Mars Science Laboratory rover (MSL).

MSL is the third rover generation sent to Mars and is the first time that a rover is equipped with an environmental station to characterize the local micrometeorology and its effect on soil surface, as well the first time that ultraviolet radiation at surface level will be recorded.

Antarctic field test

In the 2007–08 Spanish Antarctic program, our scientific team has included a field test related to the REMS sensor and its behavior on permafrost areas in the surroundings of the Spanish Antarctic Stations (SAS) that are built on Livingston and Deception Islands (Maritime Antarctica).

Livingston and Deception Islands are located in the sub-Antarctic South Shetland Archipelago at (62°39′S; 60°21′W and 62°43′S, 60°57′W). The climate at sea level is cold oceanic, with frequent summer rainfall in low areas and a moderate annual temperature range. The climate reflects the strong influence of the circum-Antarctic low-pressure system (King et al. 2003).

Data from different stations on King George Island (South Shetland Archipelago) show the mean annual air temperature (MAAT) to be approximately -1.6°C near sea level and the annual precipitation to be about 500 mm.

Permafrost in the South Shetland Islands is widespread

above the Holocene raised beaches (ca. 30 m a.s.l.) (Serrano & López-Martinez. 2000). Meteorological and geophysical data indicate, however, that environmental conditions in the islands are marginal for the maintenance of permafrost (Hauck et al. 2007).

Instruments and Methods

A simplified model of the REMS GT and UV sensors are part of the experiment deployed on Antarctica. The model tries to reproduce the conditions measurement of REMS on Mars.

This experiment is composed of some standard meteorological sensors and the photodiodes and thermopiles corresponding to the REMS model (Table 1). All the sensors are mounted on a 1.8 m mast and include a Pt100 air temperature with solar protection shield at the top of the mast and a Kipp and Zonnen CNR1 net radiometer for measuring infrared (CG3) and solar short wave (CM3) radiation at 1.5 m high. REMS GT and UV sensors and its amplification box are at 0.7 m high, and finally two Pt100 sensors are in close contact with the soil surface in the angle of view of the GT-REMS thermopiles.

In the case of the GT-REMS sensor, the model uses the first two bands of REMS thermopiles (8–14 μm and 16–20 μm), and their physical disposition is essentially similar to the flight model. The thermopiles have been previously calibrated using a similar setup to the one described in the REMS calibration plan. Finally, the internal thermopile temperature sensors RTD are also sampled in order to recover the IR energy coming out from the ground surface.

For the UV-REMS sensor the Antarctic experience used only the bands A, B, and C, and contrary to those used in REMS rover (Vazquez et al. 2007). The sensor output signals are sampled by the datalogger model Squirrel 1250 of the company Grant with a general sample period of 5 min, which is the result of averaging samples every minute.

Experiment Objectives

Finally the main objectives of this experience are the following:

1. To compare the soil thermal evolution, measured directly with a good soil thermal contact Pt100 thermoresistences, with the temperature register by means of the GT-REMS thermopiles installed in a mast.

Table 1. Expected signals and system resolution.

Channel	*Range*	*Expected signal*	*Resolution*
UV-A	335-395nm	50μW/cm^2	30nW/cm^2
UV-B	280-325 nm	10μW/cm^2	24nW/cm^2
UV-C	220-275 nm	100nW/cm^2	1,2 nW/cm^2
GT-A	8-14μm	±20ºC	0.012ºC
GT-B	16-20μm	±20ºC	0.061ºC
CG3	5–50 μm	+250 W/m^2	5 W/m^2
CM3	305–2800 nm	1000 W/m^2	5 W/m^2
Pt100		±20ºC	0.015 ºC

2. To analyze the active layer thermal behavior and its effect on the soil surface temperature on a well-known site where we are measuring thermal and mechanical evolution of the active layer by means of CALM (Circumpolar Active Layer Monitoring) protocol (Ramos & Vieira 2003, Ramos et al. 2007).
3. To develop a method that allows us to obtain, with only soil surface and atmosphere temperature data, information about the thermal active layer regime on the surface of Mars.
4. To check the UV-REMS response under Antarctic conditions by registering the UV radiation incoming on soil surface by means of three sensors in the range of A, B, and C spectral bands.

References

Carr, M. 2006. *The Surface of Mars*. Cambridge: Cambridge University Press, 307 pp.

Hauck, C. Vieira, G. Gruber, S. Blanco, J. & Ramos, M. 2007. Geophysical identification of permafrost in Livingston Island, maritime Antarctica. *J. Geophys. Res.* 112: F02S19, doi:10.1029/2006JF000544.

King, J.C. Turner, J. Marchall, G.J., Connolley, W.M. & Lachlan-Cope, T.A. 2003. Antarctic Peninsula variability and its causes as revealed by analysis of instrumental records, in Antarctic Peninsula climate variability. In: E. Domack et al. (eds.), *Antarctic Research Series* AGU 79: 17-30.

Ramos, M. & Vieira, G. 2003. Active layer and permafrost monitoring in Livingston Island, Antarctic. First results from 2000 to 2001. In: M. Phillips, S.M. Springman & L. Arenson (eds.), *Proceedings of the Eighth International Conference on Permafrost, Balkema Publishers, Lisse, Zurich*: 929-933.

Ramos, M., Vieira, G., Gruber, S., Blanco, J.J., Hauck, C., Hidalgo, M.A., Tomé, D., Neves, M. & Trindade, A. 2007. Permafrost and active layer monitoring in the Maritime Antarctic: Preliminary results from CALM sites on Livingston and Deception Islands. *U.S. Geological Survey and The National Academies, USGS OF-2007-1047, Short Research Paper 070*, doi:10.3133/of2007-1047.srp070.

Serrano, E. & López-Martínez, J. 2000. Rock glaciers in the South Shetland Islands, Western Antarctica, *Geomorphology* 35: 145-162.

Vázquez, L. Zorzano, M.P. & Jiménez, S. 2007. Spectral Information Retrieval from Integrated Broadband Photodiode Martian Ultraviolet Measurements, *Optics Letters* 32(17): 2596-2598.

Characterizing Polar Landscapes from Multispectral and Hyperspectral Imagery

Justin L. Rich
State University of New York at Buffalo, Department of Geology, Buffalo, New York, USA
Bea Csatho
State University of New York at Buffalo, Department of Geology, Buffalo, New York, USA
Erzsébet Merényi
Rice University, Department of Electrical and Computer Engineering, Houston, Texas, USA
Brian Bue
Rice University, Department of Electrical and Computer Engineering, Houston, Texas, USA
Chien-Lu Ping
University of Alaska Fairbanks, School of Natural Resources and Agricultural Sciences, Fairbanks, Alaska, USA
Lynn Everett
The Ohio State University, Byrd Polar Research Center, Columbus, Ohio, USA

Introduction

There is a physically based, conceptual understanding of many of the significant interactions that impact permafrost-affected soils. Our observationally based knowledge however, is inadequate in many cases to quantify these interactions or to predict their net impact. To pursue key goals, such as understanding the response of permafrost-affected soil systems to global environmental changes and their role in the carbon balance, and to transform our conceptual understanding of these processes into quantitative knowledge, it is necessary to acquire geographically diverse sets of fundamental observations at high spatial and often temporal resolution. The main goal of the research presented here is to characterize permafrost-affected landscapes by using multispectral and hyperspectral imagery.

Approach

The sheer amount and the heterogeneity of datasets (e.g., LIDAR, stereo imagery, multispectral, hyperspectral, and SAR imagery) make joint interpretation (fusion) a daunting task. Here remote sensing, pattern recognition, and landscape analysis techniques are combined for the delineation of soil landscape units and geomorphic features and for inferring the physical properties and composition of the surface from a fused dataset consisting of an Advanced Land Imager (ALI), Landsat +ETM (ETM) or Landsat TM (TM) scene, and topographic data with its derivative products.

Exploration of the relationship between the mapped surface units and permafrost conditions on the North Slope of Alaska (Fig. 1) has been undertaken. Since the depth of the permafrost manifests in the active layer on a variety of scales, we apply texture-based, object-oriented multiresolution soft classifications. This allowed for integration of multiple data types within the same surface unit through the use of a region-based segmentation algorithm based on data values and shape properties (Darwish et al. 2003). It is recognized that this type of analysis will lend itself to better characterization of complex landscape units and processes than a pixel-based approach and can help to alleviate traditional spatial analysis quandaries, such as the modifiable aerial unit problem (Burnett & Blaschke 2003) or the effects of hard classifications.

Nonstandard advanced Neural Network architectures to attack tasks, such as the determination of the relevant merits of the data components, have also been utilized. Pixel-level fusion, where the measured values from all experiments for a given location (image pixel) are used as one stack-vector serving as the signature of the material at that location, has been applied. Here, one particular challenge is to determine the relative contributions of the data from the various measurements.

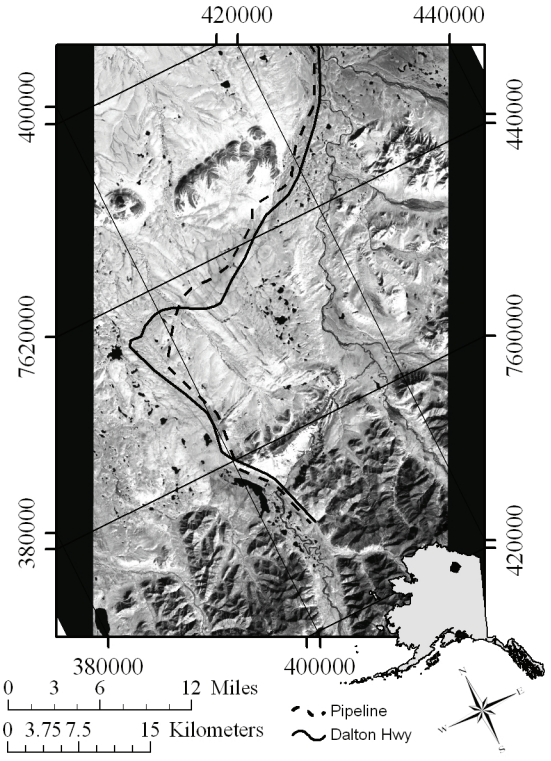

Figure 1. The area of interest in the region of Toolik Lake, Alaska. The location of the Dalton Highway and the Trans Alaska Pipeline are also included for reference.

Results

An example illustrating the concept, from the North Slope of Alaska, using TM, ETM and ALI data, in conjunction with topographic data to develop our object-based model has been undertaken. This analysis was conducted by first processing the data within ENVI (by ITT visual information solutions) to retrieve surface reflectance values and to register the datasets into a common reference system. The results were then imported into Definiens Pro (by Definiens AG) for segmentation and classification based on known surface units such as moist acidic tundra or moist nonacidic tundra (~18 classes total). The results of this segmentation appear to produce objects that correspond well to what has previously been established; however, further work is needed in characterizing class definitions.

By using self-organized manifold learning (SOMs, an unsupervised Artificial Neural Network paradigm), we also clustered a 9-band multispectral image from the ALI instrument. Details of this technique, capabilities, and former analyses are summarized in Merényi et al. (2007) and references therein. We separated 30 different vegetative, soil, and landscape units along the Dalton Highway in the Toolik Lake area. These include various water bodies with different sediment loads, glacial ice, snow, a variety of soils and vegetation. Detailed interpretation is ongoing. This unsupervised segmentation serves to support a detailed supervised classification.

Point-source soils (pedon) data and field spectrometry data have also been acquired at different units to provide ground truth for the satellite image interpretation.

Conclusions and Future Work

Previous studies conducted have utilized datasets that were largely moderate spatial and low spectra resolution. This study is employing datasets that are also moderate spatial resolution, but will be reinforced with high spectral resolution data, resulting in a more accurate assessment of the surface materials and increased confidence in the model. Additionally, by implementing a segmentation of the datasets, it is possible to utilize textual and contextual information that can be lost in pixel-based classifications (Blaschke & Strobl 2001). This type of processing also allows for a more automated processing scheme that can facilitate an efficient temporal study and produce datasets that have undergone the same processing steps with little room for human error. This decreases the amount of time it takes to run an analysis and increases confidence in the model. Preliminary results have shown that image segmentation through a texture-based, object-oriented approach yields landscape unit geometries that appear to correlate well with previously conducted aerial photograph analysis undertaken in the region (Walker 1996).

Field spectral measurements, collected over major land-cover types, indicate that the spectral differences between different landscape units are often minor. Based on high-dimensional intricate signatures, hyperspectral data could provide material discrimination, even in cases of many classes with potentially subtle spectral distinctions. Exploitation of these types of data is a great challenge in itself, both for discovery (unsupervised clustering) and for mapping known species (supervised classification). Fused with other data, this challenge increases. Analysis of hyperspectral imagery resides in our long-term goals, and we hope to report on those at a later date.

Acknowledgments

EM is partially supported by the AISRP (grant NNG05GA94G) of NASA's SMD. BB is supported by NASA GSRP graduate fellowship NNX0AR79H. BC and JR are supported by NASA's ICESat program.

References

Blaschke, T. & Strobl, J. 2001. What's wrong with pixels? Some recent developments interfacing remote sensing and GIS. *GIS Zeitschrift fur Geoinformationssystme* 6(11): 12-17.

Burnett, C. & Blaschke, T. 1994. A multi-scale segmentation/object relationship modeling methodology for landscape analysis. *Ecological Modeling* 31: 737-747.

Darwish, A. et al. 2003. Image Segmentation for the Purpose Of Object-Based Classification. *Geoscience and Remote Sensing Symposium, 2003. IGARSS '03. Proceedings. 2003 IEEE International* 3: 2039-2041.

Merényi, E., Farrand, W.H., Brown, R.H., Villmann, Th. & Fyfe, C. 2007. Information extraction and knowledge discovery from high-dimensional and high-volume complex data sets through precision manifold learning, *Proc. NASA Science Technology Conference (NSTC2007)*, College *Park, Maryland, June 19–21, 2007*: 11pp. ISBN 0-9785223-2-X.

Walker, D.A. 1996. GIS data from the Alaska North Slope. *National Snow and Ice Data Center (Digital Media)*. Accessed 3-15-07.

Contribution of Terrestrial Laser Scanning for Studying the Creep of Mountain Permafrost

François Riff
Geographic Institute of Lausanne University
Christophe Lambiel
Geographic Institute of Lausanne University
Thierry Oppikofer
Institute of Geomatics and Risk Analysis, University of Lausanne

Introduction

Up to now, differential GPS and triangulation using theodolite were the most used terrestrial techniques for measuring the creep of permanently frozen sediment bodies. Recently, the studies of Bauer et al. (2003) and Bodin (2007) demonstrated that terrestrial laser scanning (TLS) offers good opportunities to provide precise measurements on mountain permafrost creep.

This abstract presents positive results of TLS measurements carried out on two permafrost-related creeping landforms located in the Swiss Alps: the tiny Lac des Vaux rock glacier, located in a wider complex slope, and on the Col des Gentianes push moraine (cf. Lambiel 2006). First, the two principal stages of the methodology (data acquisition and treatment) will be presented.

Data Acquisition

TLS is based on the contactless and reflectorless acquisition of a XYZ point cloud of the topography using a time-of-flight principle. The TLS data acquisition stage is relatively quick and easy. However, two recurrent problems were identified using the Optech ILRIS 3D in alpine periglacial landforms:

- The localization of ideal viewpoints is crucial in order to avoid occlusion and too far distances to the object. At a distance shorter than 100 m and with a point cloud resolution better than 5 cm, we were able to identify every object in a unique way. This allows the observation of the movement of the matrix and the bigger blocks. Beyond a distance of about 300 m and a resolution higher than 10 cm, this advantage is lost, but measurement of mass movement is still possible.
- No points can be obtained from snow-covered surfaces, since snow does not reflect the TLS signal.

Data Treatment

The longest stage in the TLS methodology is data treatment with the Polyworks™ software. The raw TLS point clouds need to be cleaned from unwanted objects, unified to a single point cloud and finally georeferenced using GPS points. Sequential TLS point clouds, or TLS time-series, enable the calculation of relative differences, which are related to slope movements (e.g., Oppikofer et al. in review). Positive differences (yellow to red colors in Figs. 1, 2) are related to advances or elevation increases of the creep, while negative differences (blue to pink colors in Figs. 1, 2) are signs of mass loss or depletion.

In addition, the following operations can be carried out:

- Precise volume calculation by creation of parallel cross-sections or use of 3D point clouds.
- Creation of movement vectors by point pair identification. However, using real time kinematics GPS to obtain this kind of information is more practical, faster and more precise than the TLS, but provides only information on selected monitoring points.
- Easy integration of the results in a GIS, since all information is georeferenced.

Results

Lac des Vaux rock glacier

In the upper part of the rock glacier, a distinct blue area (1) indicates a loss of elevation of about 35 cm (Fig. 1). Directly below (2), the light green to yellow colors correspond to positive values, which indicate a general slight increase (5–15 cm) in elevation. Several big blocks even show a positive displacement of about 50 cm. In the lower part (3), the increase in elevation is a bit lower. The GPS data indicates slightly larger displacements.

According to geomorphologic evidence, the successive loss (1) and gain (2-3) in elevation may be the result of

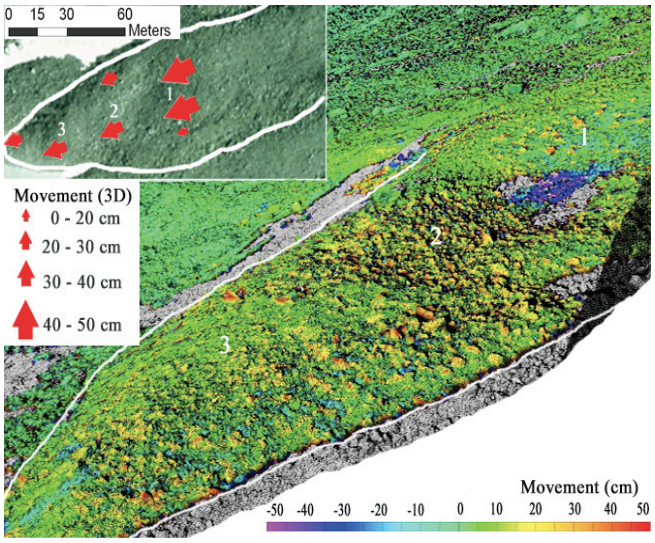

Figure 1. Topographic evolution of the Lac des Vaux rock glacier between 19 July and 16 October 2007, represented with a 50 cm scale. Top left are represented the D-GPS movements extrapolated between the same dates.

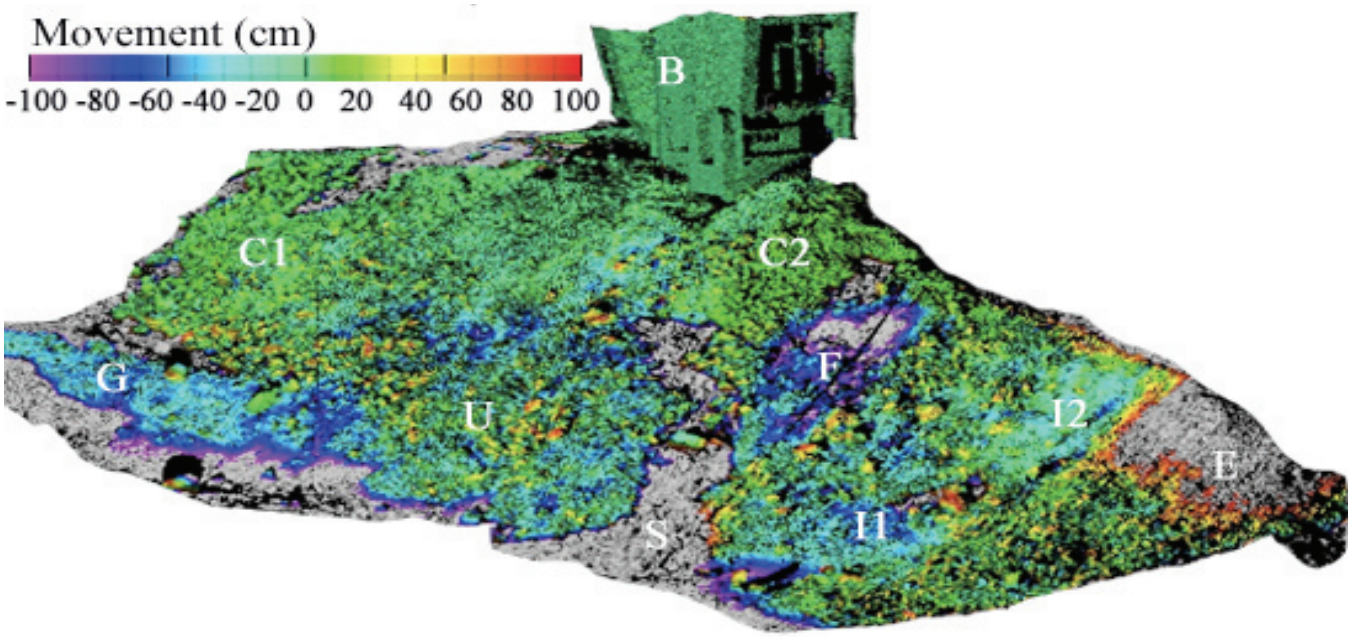

Figure 2. Topographic evolution of the northeast and central parts of the "Col des Gentianes" push moraine between 19 July and 16 October 2007 represented with a 100 cm scale.

a landslide-like development process, as evidenced in destabilized rock glaciers (see Roer et al. 2008). The upper area (1) corresponds to a scar, whereas the lower area (2-3) is the place of a rapid accumulation of materials, with higher destabilization of metric blocks.

Col des Gentianes push moraine

According to geoelectrical measurements and direct observations, the ice content in the moraine is locally important (Lambiel 2006). Generally speaking, all the moraine displays more or less marked movements (Fig. 2). For instance, we can recognize accumulation of materials below a scar (U), a scar of debris flow (F) above an area without any data because of the presence of snow at the time of the first survey (S) and settlement of the moraine due to dead ice melting (I1, I2). C1 and C2 areas are more stable, even if a slight movement (creep) can be observed. The debris-covered glacier at the foot of the moraine is clearly visible (G); (E) is the result of excavation work; and finally, the data confirms the building stability (B).

Discussion and Conclusion

The comparison TLS point clouds evidenced different processes in both investigated landforms, like, for example, permafrost creep, sliding, and settlement due to melting of massive ice. The measurements revealed also that the movement of metric blocks is more important than the displacement of smaller elements, like small rocks and the matrix. Thus, we can conclude that the creeping velocities measured with D-GPS may be slightly overestimated, since, with this technique, large boulders are normally chosen.

Regarding the accuracy of the TLS method, the mean error on sequential TLS point cloud comparisons can be estimated to about 3 cm. This is in the same order of magnitude than with D-GPS. According to the high resolution and precision of the data, the TLS appears to be an efficient technique for studying the creep of mountain permafrost.

References

Bauer, A., Paar, G. & Kaufmann, V. 2003. Terrestrial laser scanning for rock glacier monitoring. *Proceedings of the Eighth International Conference on Permafrost, Zürich, Switzerland, June 2003, 1*: 55-60.

Bodin, X. 2008. Géodynamique du pergélisol de montagne: fonctionnement, distribution et évolution récente. L'exemple du massif du Combeynot (Hautes Alpes*)*. *Thesis. University of Paris-Diderot* (Paris 7), 274 pp.

Lambiel, C. 2006. Le pergélisol dans les terrains sédimentaires à forte déclivité: distribution, régime thermique et instabilités. *Thèse, Université de Lausanne, Institut de Géographie, coll. "Travaux et Recherches"* No. 33: 260 pp.

Oppikofer, T., Jaboyedoff, M. & Keusen, H.-R. In review. Terrestrial laser scanner monitoring of the 2006 Eiger rockslide in the Swiss Alps. *Nature Geosciences*.

Roer, I., Avian, M., Delaloye, R., Lambiel, C., Haeberli, W., Kääb, A. & Kaufmann, V. 2008. Observations and considerations on collapsing active rockglaciers in the Alps. *Proceedings of the Ninth International Conference on Permafrost, Fairbanks, Alaska, 29 June–3 July 2008*.

Extensive Secondary Chaos Formation in Chryse Chaos and Simud Valles, Mars

J. Alexis. P. Rodriguez
Planetary Science Institute, 1700 E. Ft. Lowell Rd., Suite 106, Tucson, Arizona, USA
Ken L. Tanaka
Astrogeology Team, U.S. Geological Survey, Flagstaff, Arizona, USA
Jeffrey S. Kargel
Hydrology & Water Resources, University of Arizona, Tucson, Arizona, USA
David Crown
Planetary Science Institute, 1700 E. Ft. Lowell Rd., Suite 106, Tucson, Arizona, USA
Daniel C. Berman
Planetary Science Institute, 1700 E. Ft. Lowell Rd., Suite 106, Tucson, Arizona, USA

Introduction

The southern circum-Chryse region along the highland-lowland boundary of Mars displays the planet's largest and most complex assemblage of interconnected canyons and channels. The geologic history of this region is key to the understanding of the evolution of crustal volatile release as well as of the nature of the largest condensed surface fluid flows on the planet. Here, large plateau zones have undergone collapse, forming low-lying depressions floored by broken-up and morphologically diverse blocks.

These collapsed terrains, traditionally referred to as chaotic terrains, commonly occur in close spatial association with Martian outflow channels. Martian chaotic terrains and outflow channels have been intensively studied since the 1970s. The consensus is that chaotic terrains represent zones where aquifer destabilization led to ground collapse and to the rapid release of vast amounts of fluids at the surface, which subsequently carved the outflow channels (Sharp 1973). Impact crater densities and geologic relations indicate that both the chaotic terrains and the outflow channels formed during the Late Hesperian Epoch (Scott & Tanaka 1986). An obvious implication of this hypothesis is that the formation of chaotic terrains necessarily pre-dated, but was penecontemporaneous with, the excavation of their associated outflow channels.

Yet, some chaotic terrains formed within the floors of outflow channels, and thus must post-date the excavation of the channel floors they modify. These chaotic terrains, known as secondary chaotic terrains, have been previously described as occurring in the higher outflow channel floors (Rodriguez et al. 2005) . Here, we present a synthesis of the morphologic attributes of a secondary chaotic terrain known as Chryse Chaos that apparently destroyed the southern reaches of the lower outflow channel system of Simud Valles (Fig. 1).

Morphology of Chryse Chaos

Chryse Chaos is located along the lower outflow channel floor of Simud Valles. Its maximum length and width are 700 km and 270 km, respectively, and its surface area is ~0.12 million km^2. Yet, the floor of Chryse Chaos is located a mere ~200 m below adjacent channel floors. Chryse Chaos exhibits a large population of knobs, which are locally closely spaced into clusters (zones outlined by yellow line in Fig. 1b).

The northern margin of Chryse Chaos consists of a prominent break in slope (black, teethed line in Fig. 1b). Our mapping shows that no channels cut down to the chaos floor level and extend north from this break in slope, which forms the downstream margin of the chaotic terrain, suggesting that the formation of Chryse Chaos was not associated with generation of catastrophic floods. In addition, we have not identified any landforms indicative of water ponding such as equipotential terraces (shorelines) along the margins of the

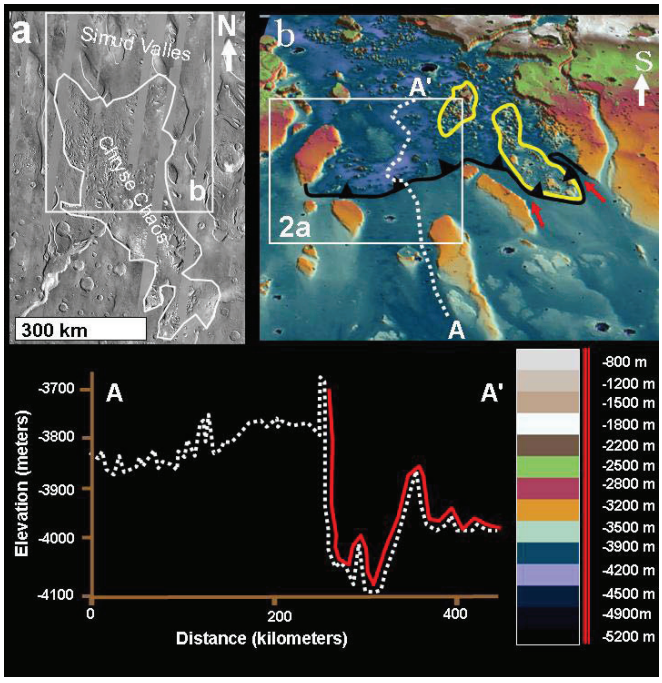

Figure 1. (a) View of Chryse Chaos (part of THEMIS IR mosaic centered at -10.06°N; 322.31°E). (b) View of northern margin of Chryse Chaos. Perspective view of MOLA-based shaded DEM (128 pixels/degree) centered at 13.81°N; 321.15°E and related elevation profile (A-A'). The hachured line shows the location of the break in slope that marks the northern margin of Chryse Chaos. The yellow lines outline collapsed mesas, one of which is flanked by two erosional channels (red arrows). Shown is the location of Fig. 2a.

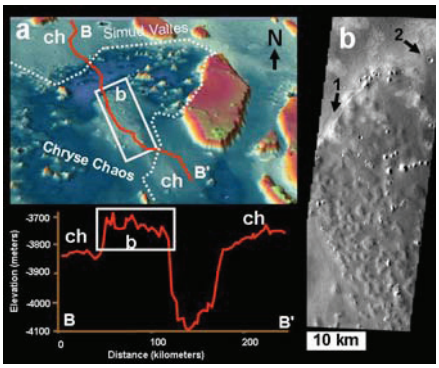

Figure 2. (a) Perspective view of MOLA-based shaded DEM (128 pixels/degree) of the northeastern part of Chryse Chaos (margins marked by white dots) and elevation profile (B-B'). The white box (location of panel b) shows a bulge within the chaos floor, the surface of which is at a higher elevation than proximal channel floors (ch). (b) Close-up of bulge within Chryse Chaos. In the northern margin of the bulge, a graben (arrow 1) transitions into a fractured terrain (arrow 2). (part of THEMIS VIS V19110016 centered at 13.78°N; 322.06°E.

chaotic terrain or of the surrounding high-standing blocks within it, suggesting that bodies of water never ponded within (or, if shorelines formed, they were subsequently destroyed during chaos formation).

A bulge in northeastern Chryse Chaos rises above outflow channel floors both in the regional upslope and downslope directions (see profile in Fig. 2). Nevertheless, its surface does not display surface flow features; instead it has a hilly texture. Its northern margin is marked by a distinct graben and some fracturing (Fig. 2b).

Interpretative Synthesis

To the best of our knowledge, Chryse Chaos is the largest secondary chaotic terrain on Mars and, unlike most chaotic terrains in southern circum-Chryse, its morphology is not diagnostic of flood release and is consistent with a total absence of aqueous fluid emissions.

Location and shape of precursor aquifer

Assuming that (1) the Simud Valles lower outflow channel floor consists of debris flow deposits (Rodriguez et al. 2006) and that (2) Chryse Chaos formed by substrate regional volatile depletion, then an aquifer must have existed within the debris flow deposits and/or within the channel floor materials located at their base. If the maximum dimensions of this aquifer correspond to the extent of Chryse Chaos, then the formational history of this secondary chaotic terrain may be related to:

(a) Deflation of volatile-rich lenses within debris flow deposits: The lower floor of Simud Valles/Chryse Chaos likely consists of sedimentary deposits emplaced by multistage debris flows produced by catastrophic collapse events originating within Ganges, Eos, and Capri Chasmata (Rodriguez et al. 2006). Rodriguez et al. (2006) proposed that instabilities within individual debris flows may have resulted in multiple surges leading to the generation of volatile-depleted and volatile-enriched pulses. Consequently, the lower channel floor within Simud Valles may consist of a mosaic of volatile-poor and volatile-rich geologic materials. Thus, regional volatile deflation of volatile-rich materials may have resulted in, or contributed to, the formation of Chryse Chaos.

(b) Deflation of an aquifer underlying debris flow deposits: Debris flows associated with lower outflow channel activity may have eroded into and then buried an aquifer. Volatile depletion of this putative aquifer could have led to resurfacing of the overlying geologic materials and the generation of Chryse Chaos.

Chaos formation does not appear to have led to the generation of floods, suggesting that its pre-existing aquifer was not under a significant hydraulic head. This can be explained by the fact that the channel floors of Simud Valles form an almost equipotential surface, and as a consequence the aquifer's maximum potentiometric level would correspond to its upper boundary (located at the base of the debris flow deposits).

A case for diapiritic activity

The northern margin of the bulge located in the northeastern part of Chryse Chaos (Fig. 2) displays a graben in close proximity to a cluster of surface fractures, which is indicative of surface extension. Whereas the northern part of the bulge has a smooth texture, its southern part displays extensive surface pitting (Fig. 2b). Moreover, hills appear to be more closely spaced in the southern part of the bulge, where their long axes are aligned parallel to the margin of the bulge (Fig. 2). Assuming that the transition between the smooth hilly zone and the pitted hilly zone is not related to differences in mantle compositional properties, then a difference in the distribution of surface stress could account for this contact. A likely geologic scenario is that the bulge represents the uplifted surface of a large, rising diapir, and that at least some of the hills forming its surface may be the result of undulations along the top of the diapiric plume.

References

Rodriguez, J.A.P. et al. 2005. Outflow channel sources, reactivation, and chaos formation, Xanthe Terra, Mars. *Icarus* 175: 36-57.

Rodriguez, J.A.P. et al. 2006. Headward growth of chasmata by volatile outbursts, collapse, and drainage: Evidence from Ganges chaos, Mars. *Geophys. Res. Lett.* 33: L18203.

Scott, D.H. & Tanaka, K.L. 1986. *Geologic Map of the Western Equatorial Region of Mars*. U.S. Geol. Surv. Misc. Invest. Ser., Map I-1802-A.

Sharp, R.P. 1973. Mars: Troughed Terrain. *J. Geophys. Res.* 78: 4063-83.

Development of Soil Databases on the Territory of Permafrost-Affected Regions in Russia

D.I. Rukhovich, N.I. Belousova, P.V. Koroleva, E.V. Vil'chevskaya, L.G. Kolesnikova
V.V. Dokuchaev Soil Science Institute, Russian Academy of Agricultural Sciences, Moscow, Russia

Soil mapping in Russia has a rich and long history. Since the time of Dokuchaev, a system of soil maps of the country on different scales has been developed. The soil maps in Russia are compiled on very different scales: from the 1:10,000 scale for separate farms to small-scale maps (1:16 M) included in the national atlases.

Soil maps on the scale of 1:1 M and smaller are available for the whole territory of Russia. The 1:1 M state soil map is currently at the stage of its finalization and updating. Both the legends to separate pages of the map and the soil polygons are being updated. Soil maps on the scale of 1:4 M and smaller give the general picture of soil distribution in the country. The number of soil polygons on such maps is relatively small; these maps do not correlate well with the topographic bases and the materials of remote sensing (satellite imagery). The 1:2.5 M map occupies a transitional position in this series of soil maps of Russia. There are 35,000 soil polygons on this map and 305 mapping units in the legend, including 205 soil units and 100 names of different soil combinations (soil complexes).

Traditionally, soil maps for the territory of Russia are published with legends and special explanatory notes. However, these valuable reference materials usually do not contain quantitative information on the soil properties. A thorough study of soil classification systems applied on the maps of different years makes it possible to judge the geographic distribution of soils, but does not allow quantitative calculations and the development of special maps, for example, the maps of soil acidity or the maps of carbon reserves. The absence of quantitative soil characteristics lowers the efficiency of digital versions of soil maps on the territory of Russia. The creation of the geographic information system on Russian soils supplied with necessary attribute databases on the soil properties is one of the challenges for soil geography in Russia.

The soil databases have to include information on the soil profile horizonation and characteristic depths of soil horizons. Thus, podzolic soils are characterized by the following horizonation: O-A2-A2/Bt-Bt-BtC-C. The O horizon O is thin (5–10 cm), slightly decomposed leaf litter; the eluvial horizon A2 is a light-textured horizon with platy structure and very variable (5–50 cm) thickness. The transitional eluvial-illuvial whitish/brown horizon A2/Bt turns into the dark-brown or brown illuvial horizon Bt of 35–55 cm in thickness. The Bt horizon has a heavier texture than the A2 A2/Bt horizons and clear illuviation features in the form of clay coatings. It gradually turns via the BtC horizon into the parent rock C at a depth of 300–350 cm. Quantitative characteristics of the soil properties should be given for every genetic horizon. At present, it is feasible to perform this work on the basis of the "Soil Map of the Russian Federation" on the 1:2.5 M scale (Fridland et. al. 1988, Fig. 1).

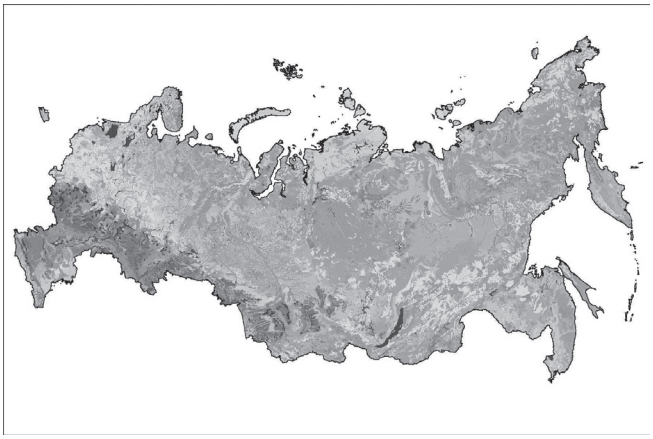

Figure 1. "Soil Map of the Russian Federation," 1:2.5 M scale.

Figure 2. Agroclimatic zoning of Russia.

The unified legend to this map is supplied with information on the horizonation of 205 soil units shown on the map. The legend to the map also contains information on the soil texture and on the character of parent materials. The textural part of the legend consists of 30 units. A given soil unit can be found on parent materials of different geneses and textures. On average, there are three texture classes corresponding to the given soil units. A combination "soil name + texture" gives us about 600 different soils shown on the map. The same genetic unit of soil developed from the parent materials of different textures normally has different quantitative characteristics of its properties, including the thickness of soil horizons, the humus content, base saturation, etc.

Each of the 600 combinations "genetic soil name + soil texture" has its own spatial distribution. Its properties vary in dependence on the particular climatic and geobotanic conditions. The character of climatic conditions can he judged from the special map of climatic zoning of Russia.

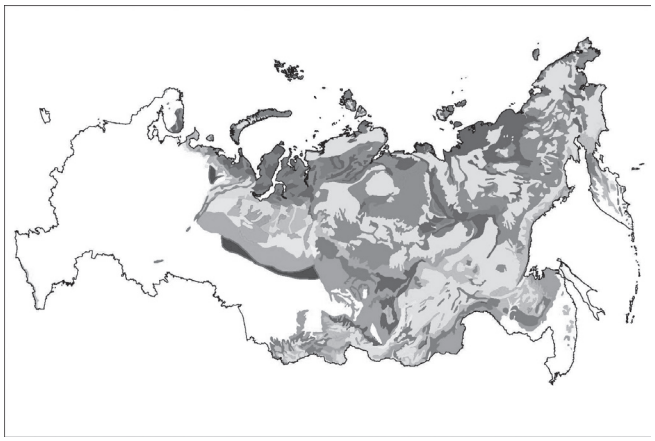

Figure 3. Permafrost distribution in Russia.

Figure 4. Area for which the soil database is being developed.

To reflect the natural variability in soil characteristics, the attribute database to the map should contain information on the range of variation of the particular soil properties. Thus, as a first approximation, the database is developed for 205 soil units in the legend. Then, it has to be refined, and the ranges of variation in the particular soil properties should be reduced with due account for the parent materials and bioclimatic conditions (natural zones). A digitized version of the "Map of the Agroclimatic Zoning of Russia" (Shahshko et. al. 1984) is shown in Figure 2.

One of the factors taken into account in the natural climatic zoning of Russia is the presence of permafrost. The map of permafrost distribution (Brown et al. 1997, Fig. 3) generally corresponds to the natural climatic zoning of Russia, though there are significant differences between the two maps in some regions.

At present, the attribute database to the "Soil Map of the Russian Federation" is being developed in the Dokuchaev Soil Science Institute; particular attention is paid to the territory of Siberia and the Far East of the country (Fig. 4). About 90% of the territory, for which this database is developed, lies within the permafrost zone of Russia.

The database includes information on the soil profiles within the particular combination of major factors: "genetic soil name + soil texture (parent material) + bioclimatic zone." The following information is included in the description of particular soil horizons: thickness, acidity, humus content, exchange capacity, etc. It is important that the soil database (Table 1), corrected for the particular provinces and parent materials from which a given soil is developed (with Podburs [Spodosols] as an example), gives us more adequate information on the values of the particular soil properties.

Table 1.

Natural and agricultural units	Parent rocks	Horizon	Humus content, %
Values from the database for the soil map on the 1:2.5 M scale			
Not differentiated by natural and agricultural zones and parent rocks		O1	21.3–73.0
		Bh	0.2–5.3
		BhC	0.2–2.1
Values from the corrected database			
North Siberia mountain region	acid metamorphic and igneous rocks	O1	60.0
		Bh	2.3
		BhC	1.5
	sandstone	O1	50.0
		Bh	2.0
		BhC	1.5
South Siberian mountain region	acid metamorphic and igneous rocks	O1	50.0
		Bh	3.2
		BhC	2.0

References

Brown, J., Ferrians, O.J., Jr., Heginbottom, J.A. & Melnikov, E.S. 1997. *Circum-Arctic Map of Permafrost and Ground-Ice Conditions*. Reston, VA, USA: U.S. Geological Survey, Circum-Pacific Map Series, CP-45 (ISBN 0-607-88745-1).

Fridland, V.M. (ed.) 1988. *Soil Map of the Russian Soviet Federative Socialistic Republic.* Scale of 1:2.5 M. Moscow, Russia: Central Administration for Geodesy and Cartography (GUGK), 16 sheets (in Russian).

Shashko, D.I., Gaydamaka, E.I., Kashtanov, A.N. et al. (eds.) 1984. *Natural and Agricultural Zoning of Lands of the U.S.S.R.* Map on a Scale of 1:8 M. Moscow, Russia: Central Administration for Geodesy and Cartography (GUGK) (in Russian).

Helical Piles for Power Transmission Lines: Case Study in Northern Manitoba, Canada

Mohammed Sakr
Almita Manufacturing Ltd., Ponoka, Alberta, Canada

Introduction

Helical piles have been used with great success to support power transmission lines. This is mainly due to the fact that helical piles offer significantly higher uplift resistance compared to other deep foundation options combined with their ease in installation in remote areas with relatively small equipment. Moreover helical piles can be loaded immediately after installation. This paper summarizes a case study for helical pile foundations supporting power transmission line located in Northern Manitoba, Canada, in which the site conditions, pile installation, and performance of foundations are described.

Subsurface Statigraphy

Pile load tests were carried out in two different soil conditions including either soft to firm clay or stiff high plastic clay with silt varves that extended along the entire embedded depth of piles. The groundwater level was measured at the existing ground surface. The undrained shear strength parameters obtained from undrained compression (CIUC) triaxial tests are summarized in Table 1. Residual undrained shear strength values were used to estimate the axial capacities of helical piles.

Screw Pile Configuration

Four pile load tests were carried out, including two compression and two uplift load tests. The helical pile configurations used for the pile load test program consisted of two piles with triple helixes spaced at either 2.5D or 3D, where D is the helix diameter, for guy anchors (i.e., to resist uplift loads) and two piles with either triple or four helixes for tower support (i.e., to support compression loads). Helical pile configurations are summarized in Table 2.

Table 1. Soil design parameters.

Soil Type	Undrained Shear Strength, C_u (kPa)	
	Peak	Residual
Soft to firm clay	30	18
Stiff clay	60	30

Pile Installation and Test Setup

The helical piles tested in this study were manufactured and installed by ALMITA Manufacturing Ltd. of Ponoka, Alberta. Helical piles were installed through the use of mechanical torque applied at the pile head. Torque applied at the pile head during pile installation was continuously recorded, and penetration depth was measured. Final measured torque at the end of pile installation and total embedment depths are also summarized in Table 2. The maximum torque measured during installation for triple helix and four helix piles C1 and C2 installed in stiff clay and soft to firm clay were similar. However, the maximum torque for guy anchor, T2, was higher than that of T1 by about 15% due to higher spacing ratio. The embedment depth for triple helix pile was 7.5 m, while the embedment depth for four helix pile was 10.8 m. For guy anchors, the embedment depths were 7.9 m for both piles.

Typical pile load test setup consisted of two reaction piles and a test pile. The reaction piles were positioned at

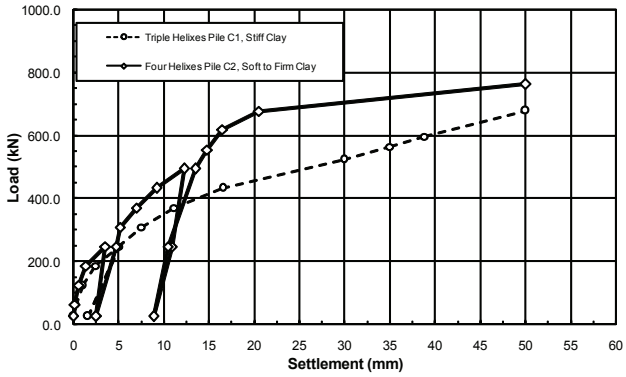

Figure 1. Load vs. settlement curves for axial compression load tests.

Table 2. Summary of pile installation.

Pile No	Pile Configuration		Test Type	Soil Type	Installation Torque kN.m (ft.lbs)	Embedment Depth m
	(Dia. (m) ×Length (m) × No. of helixes × Helix thickness (mm) × Helixes Dia. (m)	Spacing between helixes (m)				
C1	Triple helixes (0.324 × 8.5 × 3× 25.4× 0.813)	2.134	Compression	Stiff clay	94.9 (70,000)	7.5
T1	Triple helixes (0.219 × 8.5 × 3× 19× 0.711)	1.778	Uplift	Stiff clay	52.9 (39,000)	7.9
C2	Four helixes (0.324 × 11.6 × 4× 25.4× 0.864)	2.286	Compression	Soft to firm	94.9 (70,000)	10.8
T2	Triple helixes (0.219 × 8.5 × 3× 19× 0.711)	2.134	Uplift	Soft to firm	61.0 (45,000)	7.9

spacing of 6 m (about 4 helix diameter from the tested pile). Axial pile load tests were conducted according to the ASTM D-1143 Quick Load Test Method for Piles under Static Axial Compressive Load and ASTM D-3689 Quick Load Test Method for Piles under Static Axial Tensile Load. Loads were applied in increments of approximately 10% of the estimated pile capacity in 10-minute time intervals.

Load Test Results

Axial compressive pile capacities

The results of compressive load tests are presented in Figure 1 in the form of load settlement curves. It can be noted from Figure 1 that load settlements were linear at the initial part of the load-settlement curve up to a settlement of about 3 mm and corresponding loads of about 200 kN. At higher settlement levels, piles showed a nonlinear load-settlement followed by plunging failure at settlement of about 50 mm and corresponding loads of 677 kN and 772 kN for piles C1 and C2, respectively. The ultimate compressive load capacities for piles C1 and C2 are presented in Table 3. Cycles were carried out at loads of about 245 kN, and 490 kN indicated that the effect of cyclic loading had a minor effect on the response.

It is noted from Figure 1 that pile C2 with four helixes installed in stiff clay offered higher resistance compared to pile C1 with triple helixes installed in soft to firm clay. This behaviour suggested that the cylindrical shear failure mechanism is mobilized. In cylindrical shear failure mechanism, the load at pile head is resisted by three components including the skin friction along the shaft, the developed cylindrical shear resistance between the helixes, and the surrounding soil and end bearing of the bottom helix (for compression load tests) or the top helix(for uplift load tests). For pile C2 with four helixes, the cylindrical shear resistance component was considerably higher than that of pile C1 with triple helixes due to the larger surface area.

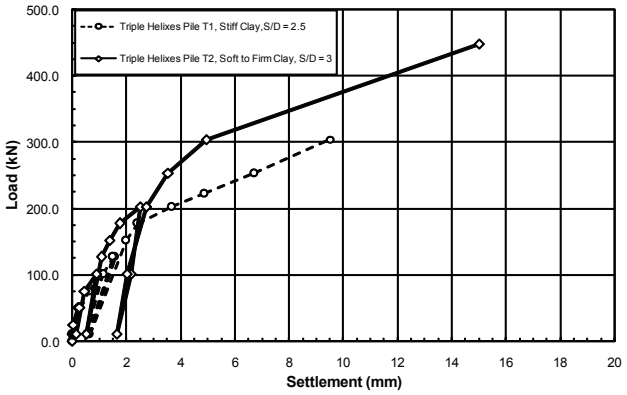

Figure 2. Load vs. displacement curves for axial tension (uplift) load tests.

Table 3. Pile load test results.

Pile No	Soil Conditions	Ultimate Pile Capacity (Q_{ult}) kN	Ultimate Settlement mm
Compression Test Results			
C1	Stiff clay	677	50
C2	Soft to firm	772	50
Tension (Uplift) Test Results			
T1	Stiff clay	370	15
T2	Soft to firm	445	15

Axial tension (uplift) pile capacity

The results of tensile (uplift) load tests are presented in Figure 2 in the form of load displacement curves for piles T1 and T2. Both piles had the same configurations, except pile T1 installed in stiff clay had a triple helixes spaced at 2.5D (1.77 m), where D is the diameter of the helix, while pile T2 installed in soft clay helixes were spaced at 3D (2.134 m). It can be seen from Figure 2 that load displacement curves for both piles were linear at the initial part of the uplift load up to a settlement of about 1 mm and load of about 100 kN. It should be noted that pile T1 installed in stiff clay showed softer response manifested by the larger displacement at the same load level compared to pile T2. However at higher displacement levels, the load-displacement curves were highly nonlinear, and pile T2 reached a plunging failure of about 445 kN at displacement level of about 15 mm (i.e., 2.5% of the helix diameter). The uplift load test for pile T1 was stopped at a load level of about 300 kN, while pile T2 was tested till failure. The ultimate capacity of pile T1 was extrapolated based on the shape of load-displacement curve, and the results are presented in Table 3.

Conclusions

The results of the axial compression and tension load tests performed in soft to firm or stiff clays demonstrated the suitability of helical pile foundations for the power transmission lines in Northern Manitoba. The results of the load testing program confirmed that the helical pile is a viable deep foundation option for construction of power transmission towers in remote areas and demonstrated their advantages.

The results of the full-scale load tests are also used to validate the theoretical model used for helical pile design installed in soft and stiff high plastic clays. The results indicated that the cylindrical shear failure mechanism controls the behavior of helical piles with spacing ratio up to 3 installed in clay materials.

References

ASTM D 1143-81. 1981. Standard Test Method for Piles Under Static Axial Compressive Load (Reapproved 1994). *Annual Book of ASTM Standards* 1997, Vol. 04.08: 95-105.

ASTM D 3689-90. 1990. Standard Test Method for Individual Piles Under Static Axial Tensile Load; (Reapproved 1995). *Annual Book of ASTM Standard,* 1997, Vol. 04.08: 366-375.

Mountain Permafrost Parameters Simulated by Regional Climate Models

Nadine Salzmann
National Center for Atmospheric Research (NCAR/ISSE), Boulder, CO, USA
Christian Hauck
Institute for Meteorology and Climate Research, Karlsruhe Institute of Technology (KIT), Germany
Linda O. Mearns
National Center for Atmospheric Research (NCAR/ISSE), Boulder, CO, USA

Introduction

Permafrost as a thermal phenomenon is strongly affected by the changes in the atmospheric condition (Haeberli & Beniston 1998). However, for a significant time of the year the seasonal snow cover decouples the ground from the atmosphere and thus considerably influences the ground thermal regime (Zhang 2005). As a consequence, permafrost conditions are affected by climatic change twofold: directly by changes in the atmospheric condition, and indirectly by the changes in the duration and dynamics of the seasonal snow cover. The sensitivity of permafrost on these two interacting variables is not clear in detail so far, and neither is how the atmosphere and thus also the seasonal snow cover will change.

Snow accumulation and snowmelt in mountain topography have nonuniform and high spatial variability mainly caused by the local topography, which interacts among others with atmospheric stability, precipitation, moisture distribution, radiation, wind and avalanches. Measuring and modeling of snow parameters in complex mountain topography is thus a challenging task. Among the most promising tools to simulate climate variables in mountain areas are Regional Climate Models (Leung & Qian 2003). Due to their higher spatial resolution compared to GCM, they better resolve the atmospheric dynamics caused by the heterogeneous surfaces such as mountain topographies. The benefits of using RCM simulations for permafrost modeling in complex high mountain topography have been demonstrated by Salzmann et al. 2007a,b. However, the performance of snow representation in RCMs related to permafrost has not been validated in detail so far and most likely differs for different regions and models.

With large projects such as NARCCAP in North America or PRUDENCE and ENSEMBLES in Europe, there is now increasing RCM output available for further use by the impact community. However, the performance of these model outputs must be proven for specific applications because model performance is not simply transferable between variables and regions.

This study aims at investigating the performance of RCMs to simulate seasonal snow cover in mountain environments, with regard on further modeling of subsurface processes.

Study Site and Data

Study site

We focus on a relatively small area (about 500 km2) in the Colorado Rocky Mountains—the Upper Colorado River Basin (UCRB). This basin is surrounded by some of the highest peaks of the Rocky Mountains. Because the streamflow of this area is a major contributor to the Colorado River's annual run off, this area is relatively well equipped with snow measurement stations (see next section).

Data

All RCM simulations used in this study have been performed within the North American Regional Climate Change Program NARCCAP (http://www.narccap.ucar.edu/). Here, we analyze only NCEP-Reanalyses driven runs, since they allow us to compare the RCM output directly with observations. They are all run with a grid spacing of 50 km and cover the UCRB by 10 grid boxes. The following RCM simulations are used here:

- ECPC (Experimental Climate Prediction Center): Scripps Institution of Oceanography, La Jolla, CA, USA.
- MRCC (Modèle Régional Canadien du Climat): Ouranos Consortium, Montreal (Quebec), Canada.
- RegCM3 (REGional Climate Model): UC Santa Cruz, ITCP, USA.

The *observations* we use are point measurement from SNOTEL stations. There are 45 stations located in the UCRB, many of them providing data since 1981.

In addition to the SNOTEL data, we use high-resolution reanalyses (NARR; North American Regional Reanalyses) for comparison purposes. NARR has a grid spacing of 32 km and covers UCRB by 26 grid boxes. NARR data are supposed to be especially valuable for hydrological studies.

First Analysis

We have analyzed the total volume of accumulated precipitation for the individual grid boxes and the average of all grid boxes covering the UCRB. The RCM outputs were compared to SNOTEL and NARR data. The total volume of accumulated precipitation and their temporal distribution showed overall good agreement.

We also compared the 2 m air temperature. The NARCCAP runs simulated generally higher air temperature than NARR, and particularly than SNOTEL.

The results for the annual snow cycles for two time periods are shown in the following Figures. Most obvious are the deviations between NARCCAP (and NARR!) and SNOTEL. Some of these deviations can certainly be explained by grid elevation differences between NARCCAP and SNOTEL, which is also apparent from air temperature, where

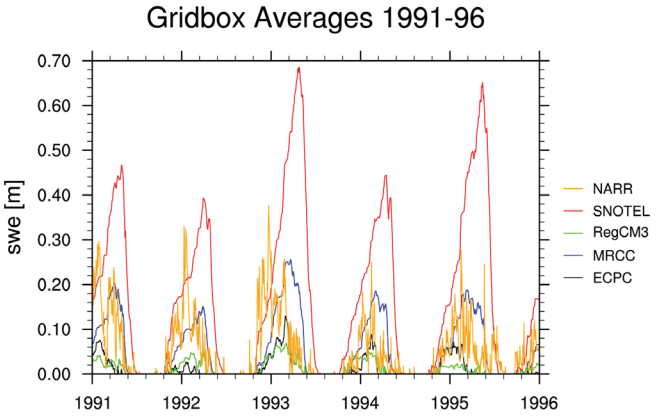

Figure 1.

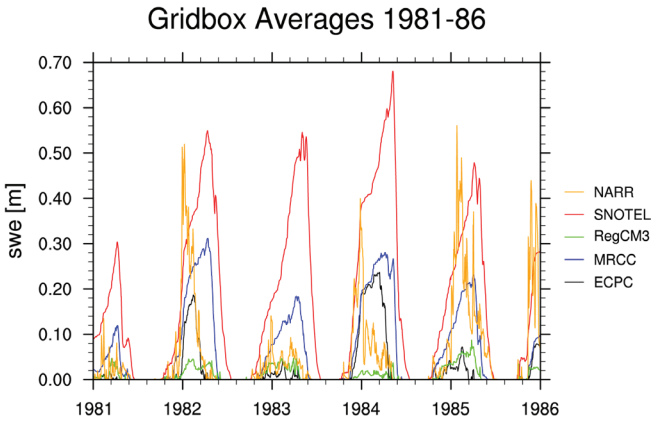

Figure 2.

SNOTEL overall shows lowest temperatures. Furthermore, the SNOTEL sites are generally located where the snow pack lasts long. Therefore, it can be assumed that SNOTEL observations slightly overestimate SWE relatively to the average of SWE over the whole region of the UCRB. Also, RegCM3 produces small SWE values in each year, which partly can be explained by the too-high air temperature that is simulated by RegCM3 (not shown).

Perspectives

For permafrost, among the most significant parameters of the seasonal snow cover are the timing and duration of significant snow depth. Therefore, in a next step, we will compare the duration of the seasonal snow cover and try to associate the deviations to model intern explanations (e.g., air temperature). Furthermore, we will apply the time series of the RCM simulations as input for a water/heat-coupled soil model (COUP; Janson & Karlberg 2004) to simulate ground surface temperatures, which are not provided by the NARCCAP outputs. Similar analyses are planned for the Schilthorn area in the Swiss Alps with RCM simulations from the PRUDENCE and ENSEMBLES projects.

Acknowledgments

This study is financially supported by the Swiss National Science Foundation's program for prospect researcher.

We acknowledge the NARCCAP modeling groups for providing us preliminary simulation results.

NARR data are provided by the NOAA/OAR/ESRL PSD, Boulder, Colorado, USA, http://www.cdc.noaa.gov/

SNOTEL data are provided by Natural Resources Conservation Service, United States Department of Agriculture.

References

Haeberli, W. & Beniston, M. 1998. Climate change and its impact on glaciers and permafrost in the Alps. *Ambio* 27(4): 258-265.

Jansson, P.-E. & Karlberg, L. 2004. *Coupled Heat and Mass Transfer Model for Soil-Plant-Atmosphere Systems*. Stockholm: Royal Institute of Technolgy, Dept. of Civl and Environmental Engineering, 435 pp.

Leung, L.R. & Qian, Y. 2003. The sensitivity of precipitation and snowpack simulations to model resolution via nesting in regions of complex terrain. *J. Hydrometerology* 4: 1025-1043.

Salzmann, N., Frei, C., Vidale, P.L. & Hoelzle, M. 2007a. The application of Regional Climate Model output for the simulation of high-mountain permafrost scenarios. *Global and Planetary Change* 56: 188-202, doi:10.1016/j.gloplacha.2006.07.006.

Salzmann, N., Noetzli, J., Hauck, C., Gruber, S., Hoelzle, M. & Haeberli, W. 2007b. Ground-surface temperature scenarios in complex high-mountain topographies based on Regional Climate Model results. *Journal of Geophysical Research–Earth Surface* 112: F02S12, doi:10.1029/2006JF000527.

Zhang, T. 2005. Influence of the seasonal snow cover on the ground thermal regime: an overview. *Rev. Geophys*. 43: RG4002, doi:10.1029/2004RG000157.

Permafrost Dynamics and Landscape Changes in a Subarctic Peat Plateau, Northern Sweden

A.B.K. Sannel
Department of Physical Geography and Quaternary Geology, Stockholm University, Sweden
P. Kuhry
Department of Physical Geography and Quaternary Geology, Stockholm University, Sweden

Introduction

Perennially frozen peatlands in subarctic regions are sensitive to a warming climate, since permafrost temperatures are close to the 0°C mean annual isotherm. Few monitoring studies have been performed of permafrost dynamics in subarctic peatlands because of their often remote location, the expensive logistics, and the harsh field conditions.

Rapid and extensive permafrost thawing in bogs and mixed mires underlain by permafrost in northern Sweden has been recorded by Christensen et al. (2004). Zuidhoff (2002) conclude that in palsas block erosion, thermokarst and wind erosion are the most important degradational processes involved in the decay. Sollid & Sørbel (1974) found that where frozen palsa plateaus are in direct contact with water, the permafrost core is undermined, causing cracks in the peat. The peat then slips sideways, creating a steep erosion edge. This edge gradually works its way in towards the central part of the palsa.

In a modeling study from Russia, Mazhitova et al. (2004) suggest a 20–30 cm deepening of the active layer in peat plateaus until 2080 as a result of future global warming. It is not only the air temperature that affects the thaw depth; precipitation, snow depth, the ice content in the ground, and other hydrogeological conditions are also important factors for the active layer distribution (Oberman & Mazhitova 2001). Long-term ecosystem monitoring is important for predicting the behaviour of subarctic peatlands under the expected future warmer and wetter climate conditions.

Aim, Methods, and Study Area

The main objective of this project is to study local climate and ground dynamics in a subarctic peat plateau/thermokarst lake complex in order to get a better understanding of how these permafrost peatlands will respond to climate change. Which factors and mechanisms cause the collapse of peat plateaus into thermokarst lakes? Why does the erosion occur only in certain parts of the peat plateau and along certain parts of the thermokarst lake shoreline? How sensitive are these ecosystems to global warming? At the peat plateau/thermokarst lake complex in Tavvavuoma (68°28′N, 20°54′E), northern Sweden, permafrost temperature and landscape dynamics are studied through monitoring of ground temperatures, meteorological data, and snow depth (since 2005), and a time series analysis of aerial photographs and satellite images (from 1963 to 2003). On the peat plateau, snow depth and ground temperatures down to 2 m depth are recorded at 9 different microsites; on the peat plateau, at the eroding edge of the peat plateau, in the thermokarst lake, and in a nearby non-permafrost fen (Fig. 1, 2, 3). A 20 m deep borehole for ground temperature measurements is planned. Air temperature, precipitation, and wind data are recorded on top of the plateau. Snow depth is monitored by using a stationary digital camera that records one image per day.

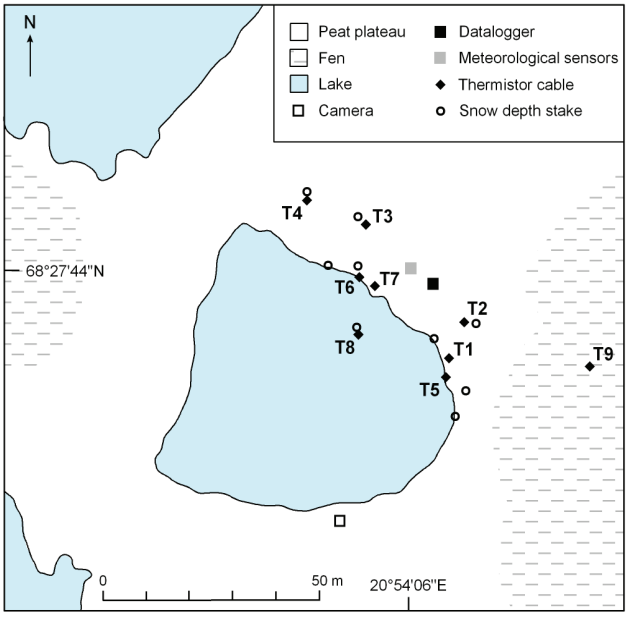

Figure 1. Map showing the location of thermistor cables and snow depth stakes at the monitoring site in Tavvavuoma.

Preliminary Results and Discussion

A comparison of panchromatic aerial photographs with a recent IKONOS image shows that, on a landscape level, major thermokarst drainage has occurred between 1963 and 2003. Along the present thermokarst lake shorelines, field observations show that erosion is active. Ground subsidence of up to 11 cm in 2 years has been observed along the shoreline, whereas the central parts of the monitored peat plateau surface appear to remain stable. The monitoring data are indicating that the permafrost in the peat plateau is thawing out, probably due to recent warming. On the central, dry peat plateau sites, the ground temperatures below 1 m depth are just below 0°C, implying that the peat plateau will be very sensitive to any further increase in temperature. Winter observations indicate very thin snow cover at the top of the peat plateau compared to the edges and in the thermokarst depressions, showing the importance of snow distribution for the permafrost (Fig. 4).

Figure 2. The peat plateau/thermokarst lake complex with monitoring equipment.

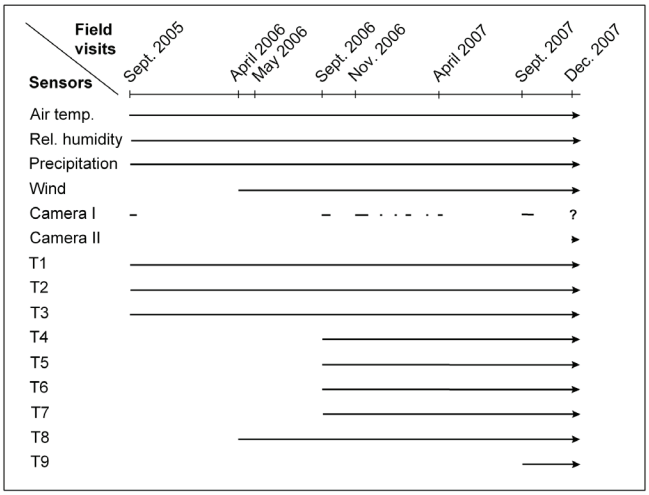

Figure 3. Ongoing monitoring activities at the peat plateau/thermokarst lake complex in Tavvavuoma. Thermistor cables T1 and T5–T7 have thermistors at 2 cm, 10 cm, 25 cm, 50 cm, and 100 cm depth. Thermistor cables T2–T4 and T9 also have thermistors at 150 cm and 200 cm depth. T8 has thermistors located 70 cm, 110 cm, 150 cm, 190 cm, and 230 cm below the lake sediment surface (for location of the thermistor cables, see Fig. 1a).

Warmer temperatures as well as increased precipitation in the winter can cause thawing of the permafrost, resulting in collapse of the peat plateau and increased methane emissions from thermokarst lakes. However, thawing of the permafrost can also result in drainage of thermokarst lakes and renewed peat accumulation.

Acknowledgments

Financial support has been achieved by the Göran Gustafsson Foundation, Foundation Lars Hiertas Minne, Helge Ax:son Johnson Foundation and Swedish Society for Anthropology and Geography. Thanks also to Prof. Peter Jansson at Stockholm University!

Figure 4. Snow distribution at the edge of the thermokarst lake and on top of the peat plateau, December 2007.

References

Christensen, T.R., Johansson, T., Åkerman, H.J., Mastepanov, M., Malmer, N., Friborg, T., Crill, P. & Svensson, B.H. 2004. Thawing sub-arctic permafrost: Effects on vegetation and methane emissions. *Geophysical Research Letters* 31: L04501, doi:10.1029/2003GLO18680.

Mazhitova, G., Karstkarel, N., Oberman, N., Romanovsky, V. & Kuhry, P. 2004. Permafrost and infrastructure in the Usa Basin (northeast European Russia): Possible impacts of global warming. *Ambio* 33(6): 289-294.

Oberman, N.G. & Mazhitova, G.G. 2001. Permafrost dynamics in the north-east of European Russia at the end of the 20th century. *Norsk Geografisk Tidsskrift* 55: 241-244.

Sollid, J.L. & Sørbel, L. 1974. Palsa bogs at Haugtjørnin, Dovrefjell, South Norway. *Norsk Geografisk Tidsskrift* 28: 53-60.

Zuidhoff, F.S. 2002. Recent decay of a single palsa in relation to weather conditions between 1996 and 2000 in Laivadalen, northern Sweden. *Geografiska Annaler* 84A(2): 103-111.

Variable Peat Accumulation Rates in Stable Subarctic Peat Plateaus, West-Central Canada

A.B.K. Sannel
Department of Physical Geography and Quaternary Geology, Stockholm University, Sweden
P. Kuhry
Department of Physical Geography and Quaternary Geology, Stockholm University, Sweden

Introduction

Peatland ecosystems located in the boreal forest and tundra biomes contain a large and significant pool of soil organic carbon. The carbon storage in boreal and subarctic peat deposits is approximately 455 Pg C, representing one-third of the total world pool of soil carbon (Gorham 1991).

As a result of global warming, the highest increases in temperature are predicted to take place at high northern latitudes. For most permafrost regions a reduction in permafrost area and an increase in thaw depth are expected (ACIA 2004, IPCC 2007). Permafrost peatlands are sensitive ecosystems expected to respond rapidly to changes in climate. Since perennially frozen peatlands in the sporadic and discontinuous permafrost zones are already near thawing, they are most sensitive to climate changes (Tarnocai 2006). Climate warming may affect permafrost peatlands in many ways: permafrost degradation, formation of thaw lakes, increased thaw depth, drier peat surfaces, changes in carbon accumulation, methane emissions, plant communities, hydrology, and fire frequency (e.g., Gorham 1991, Zoltai 1995, ACIA 2004).

An increased knowledge of permafrost conditions and carbon accumulation rates in subarctic permafrost peatlands throughout the Holocene is important for understanding how these ecosystems might respond to the predicted future climate changes.

Aim, Study Area, and Methods

The aim of this study is to better understand the long-term carbon dynamics in subarctic peat plateaus in relation to vegetation and permafrost conditions.

Selwyn Lake and Ennadai Lake are located within the low subarctic ecoclimatic region in west-central Canada, where the climate is characterized by very cold winters and short, warm summers (Fig. 1).

The peat profile SL1 (59º53′N, 104º12′W) was collected in the discontinuous permafrost zone from a treed peat plateau bog calving into Selwyn Lake (Fig. 2). The peat profile EL1 (60º50′N, 101º33′W) was collected in the continuous permafrost zone from a polygonal peat plateau on the western shore of a small lake located 1 km west of Ennadai Lake (Fig. 3).

In both peat profiles (SL1 and EL1), vegetation succession and high-resolution peat and carbon accumulation rates have been studied through plant macrofossil analyses and extensive AMS radiocarbon dating. Bulk densities were measured throughout the profiles as well as carbon (C) and nitrogen (N) content.

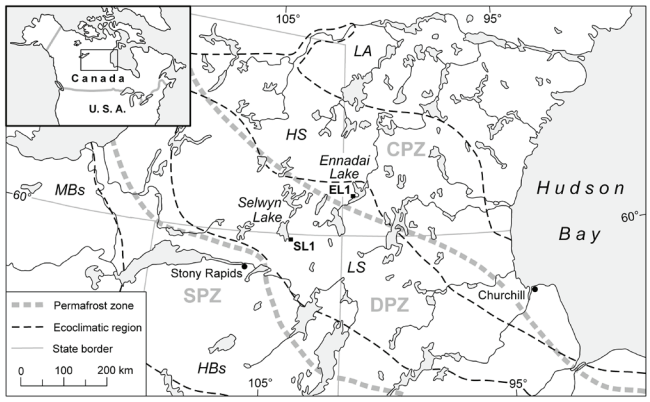

Figure 1. Location of Selwyn Lake and Ennadai Lake, permafrost zonation, and ecoclimatic regions in west-central Canada. CPZ = continuous permafrost zone, DPZ = discontinuous permafrost zone and SPZ = sporadic permafrost zone (after Zoltai 1995). LA = low arctic, HS = high subarctic, LS = low subarctic, HBs = subhumid high boreal and MBs = subhumid mid-boreal ecoclimatic region (after Ecoregions Working Group 1989).

Figure 2. The collection site of peat profile SL1 at a forested peat plateau calving into Selwyn Lake (Photo: © P. Kuhry).

Results and Discussion

Peat formation at the two sites began around 6600–5900 cal yr BP, and permafrost conditions have prevailed in the peat plateaus since permafrost aggradation occurred between 5600–4500 cal yr BP (Sannel & Kuhry in press). An important characteristic of these peat plateaus are the alternating layers of *Sphagnum fuscum* and rootlet peat layers. *Sphagnum* stages represent slightly more moist surface conditions than rootlet stages, which mainly contain roots, *Picea* needles, and leaves from ericaceous shrubs. The long-term peat and carbon accumulation rates for both the studied peat profiles are 0.30–0.31 mm/yr and 12.5–12.7

Figure 3. The collection site of peat profile EL1 at a polygonal peat plateau near Ennadai Lake (Photo: © P. Kuhry).

gC/m^2yr, which is coherent with previously reported data from subarctic Canadian peatlands by Tarnocai (1988) and Gorham (1991).

Extensive radiocarbon dating of the peat profile SL1 shows that accumulation rates are variable over time and that abrupt shifts in accumulation rates occur when the vegetation composition in the peat changes. Vertical peat growth is generally 4–5 times higher in *Sphagnum* peat than in rootlet peat. Also, the net carbon accumulation is 3–4 times higher in *Sphagnum* peat. The lowest accumulation rates are recorded in rootlet layers that have been subjected to fires. *Sphagnum* peat represents 78% of the peat profile height, but only 44% of the time since the peatland was formed (Sannel & Kuhry submitted).

In both EL1 and SL1, C/N ratios in *Sphagnum* peat are relatively high (around 90–140) and remain rather stable throughout most of the profiles, indicating that the organic material that has been incorporated into the permafrost has a low degree of decomposition (Sannel & Kuhry submitted). Persistently dry surfaces as a result of stable permafrost conditions since the peat plateaus developed suggest that these peatlands have been negligible as methane sources throughout their history. Therefore, generally they have represented a negative net radiative climatic forcing over time. However in a future warmer climate, permafrost degradation may cause wetter surface conditions, formation of collapse scars, and thermokarst lakes, and turn these areas into methane sources.

Acknowledgments

Financial support has been given by the K&A Wallenberg Foundation, Ymer-80 Foundation, Royal Swedish Academy of Science, Ahlmann Foundation, Vice-President Central Research Fund, EU GLIMPSE project, and Swedish Research Council.

References

ACIA (Arctic Climate Impact Assessment). 2004. *Impacts of a Warming Arctic*, 1st ed. Cambridge University Press, 139 pp.

Ecoregions Working Group. 1989. *Ecoclimatic regions of Canada, First Approximation*. Ecological Land Classification Series, No. 23. Canada, Ottawa: Sustainable Development Branch, Wildlife Service, Environment, 118 pp.

Gorham, E. 1991. Northern peatlands – role in the carbon-cycle and probable responses to climatic warming. *Ecological Applications* 1(2): 182-195.

IPCC (Intergovernmental Panel on Climate Change). 2007. *Climate Change 2007: The Scientific Basis. Summary for Policymakers*. Geneva: IPCC Secretariat, 21 pp.

Sannel, A.B.K. & Kuhry, P. in press. Long-term stability of permafrost in subarctic peat plateaus, west-central Canada. *The Holocene* 18(4).

Sannel, A.B.K. & Kuhry, P. submitted. Peat growth and decay dynamics in subarctic peat plateaus, west-central Canada. *Boreas*.

Tarnocai, C. 1988. Wetlands in Canada: Distribution and characteristics. In: H.I. Schiff & L.A. Barrie (eds.), *Global change, Canadian Wetlands Study, Workshop Report and Research Plan*. York University, New York: Canadian Institute for Research in Atmospheric Chemistry, 21-25.

Tarnocai, C. 2006. The effect of climate change on carbon in Canadian peatlands. *Global and Planetary Change* 53(4): 222-232.

Zoltai, S.C. 1995. Permafrost distribution in peatlands of west-central Canada during the Holocene warm period 6000 years BP. *Geographie Physique et Quaternaire* 49(1): 45-54.

^{14}C Age of Fossil Wood Remains Buried by an Inactive Rock Glacier, Upper Ticino Area (Southern Swiss Alps)

Cristian Scapozza
Institute of Geography, University of Lausanne, Switzerland
Christophe Lambiel
Institute of Geography, University of Lausanne, Switzerland
Emmanuel Reynard
Institute of Geography, University of Lausanne, Switzerland
Marco Antognini
Natural History Museum of the Canton Ticino, Lugano, Switzerland
Philippe Schoeneich
Institute of Alpine Geography, University of Grenoble, France

Introduction

Within the framework of permafrost investigations in the Southern Swiss Alps of the Canton Ticino (see Scapozza & Reynard in press), eight fossil wood stem remains were found at a depth of 1 m below surface at the front of the Piancabella rock glacier (Fig. 1), situated in the Eastern part of the Blenio Valley (Lepontine Alps of the Ticino, Southern Switzerland).

Previously, ^{14}C datings of soils and moss buried by a rock glacier in the European Alps have been discussed, for example, by Mortara et al. (1992), Giraudi & Frezzotti (1997), Calderoni et al. (1998), Haeberli et al. (1999), and Dramis et al. (2003).

Site and Sampling

The Piancabella rock glacier (46°27′N, 9°01′E) has developed within a former east-facing glacial cirque from perennially frozen scree slopes at 2650–2460 m a.s.l. According to geomorphological observations and mapping, frequency-domain electromagnetic lateral mapping and 2D resistivity profiling (Geonics EM-16R and EM-31), direct current (DC) resistivity vertical soundings, thermal prospecting and space-borne radar interferometry analysis, Piancabella rock glacier is currently inactive (Scapozza 2008). The rock glacier surface is completely lacking of vascular plants.

Eight fossil wood stem remains were found beneath 1 m of coarse blocky sediments (Fig. 2). They were covered with sand and silt. The longest wood stem is 36 cm long and 6 cm large.

Radiocarbon Dating

Necessary preparation and pre-treatment of the sample material for radiocarbon dating was carried out by the ^{14}C laboratory of the Department of Geography at the University of Zurich (GIUZ). The dating itself was done by AMS (accelerator mass spectrometry) with the tandem accelerator of the Institute of Particle Physics at the Swiss Federal Institute of Technology Zurich (ETH).

Radiocarbon dating of the sample PIANCA2 gives a mean conventional ^{14}C age of 845 ± 50 y BP (UZ-5545/ETH-34417). Calibration of the radiocarbon dating, performed with the software OxCal 3.10 (Bronk Ramsey 2005) using the radiocarbon calibration curve IntCal04 (Reimer et al. 2004), gave, with statistical probability of 95.4%, an age of 1040–1280 cal AD (790 ± 120 cal BP).

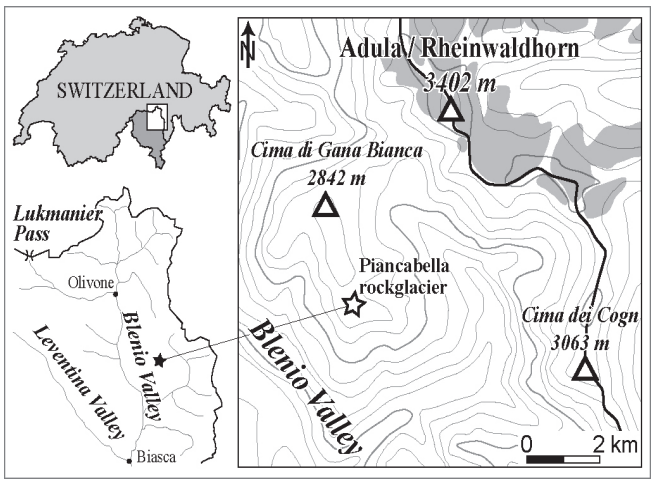

Figure 1. Geographical location of the Piancabella rock glacier.

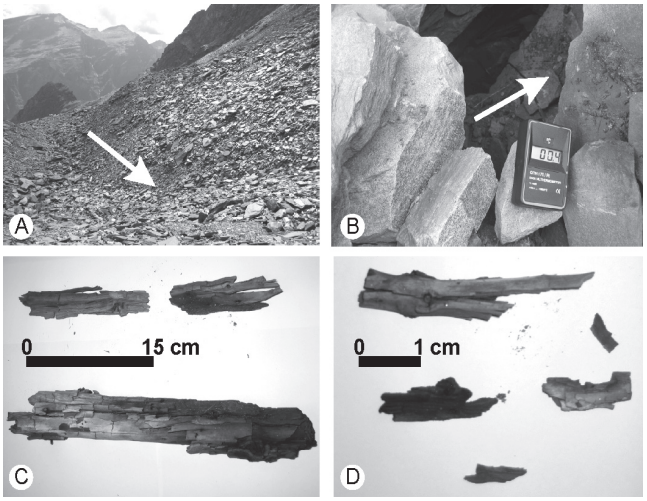

Figure 2. A–B: Sample site. C–D: Wood stem remains.

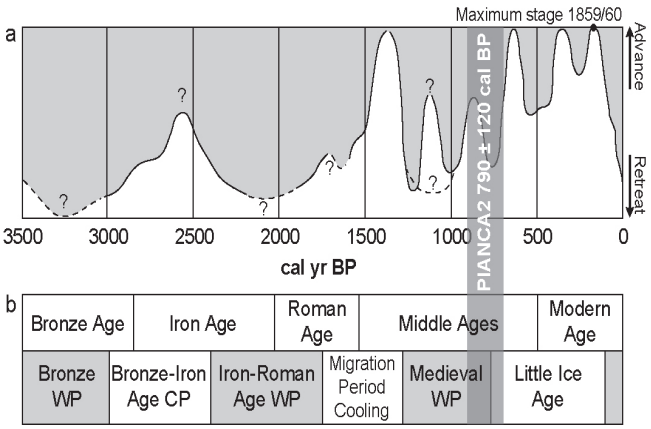

Figure 3. Comparison of the radiocarbon age of the sample PIANCA2 with (a) the Greater Aletsch glacier fluctuations in the last 3500 years, established by Holzhauser et al. (2005), and (b) the chronological and climatic framework of the Swiss Alps since the middle of the Bronze Age (Grosjean et al. 2007). WP: warm/dry; CP: cold/moist.

This age range corresponds to the end of the Medieval Climatic Optimum, a warm and dry period preceding the Little Ice Age cooling period (Grosjean et al. 2007). According to the Greater Aletsch glacier fluctuations established by Holzhauser et al. (2005), the period corresponds to a retreat phase of the alpine glaciers, with a front position similar to today (Fig. 3).

Discussion and Conclusions

Chronologic data suggest that the Piancabella rock glacier probably became inactive during the Medieval Climatic Optimum. The position of the wood remains at the front of the rock glacier confirms that it did not advance anymore after the Medieval Climatic Optimum. If we consider that climatic inactivation stops aggradation of ice in rock glacier permafrost, it confirms that ice within rock glaciers is probably several centuries old and by far predates recent climatic events such as the Little Ice Age, as it was pointed out by Haeberli et al. (1999).

Another hypothesis is possible. During the Medieval Climatic Optimum, the rock glacier front would have been several tens of meters higher in the slope. In this case, wood burial can be interpreted as the result of an advance or a reactivation of the Piancabella rock glacier during the Little Ice Age. Following these hypotheses, wood stems would have been exposed at the soil's surface for several decades before being buried.

The Piancabella rock glacier is currently situated close to the present regional lower limit of discontinuous permafrost (Scapozza 2008). It is, therefore, very difficult to determine which of the two hypotheses is likely realistic. Following the first hypothesis, ^{14}C dating of wood remains found at the front of the Piancabella inactive rock glacier could constitute the first absolute age determination of an alpine rock glacier inactivation.

References

Bronk Ramsey, C. 2005. *OxCal Program, v. 3.10*. Radiocarbon Accelerator Unit, University of Oxford.

Calderoni, G., Guglielmin, M. & Tellini, C. 1998. Radiocarbon dating and postglacial evolution, Upper Valtellina and Livignese Area (Sondrio, Central Italian Alps). *Permafrost and Periglacial Processes* 9: 275-284.

Dramis, F., Giraudi, C. & Guglielmin, M. 2003. Rock glacier distribution and paleoclimate in Italy. *Proceedings of the 8th International Conference on Permafrost, Zurich, Switzerland, July 21–25, 2003*: 199-204.

Giraudi, C. & Frezzotti, M. 1997. Late Pleistocene glacial events in the Central Apennine, Italy. *Quaternary Research* 483: 280-290.

Grosjean, M., Suter, P.J., Trachsel, M. & Wanner H. 2007. Ice-borne prehistoric finds in the Swiss Alps reflect Holocene glacier fluctuations. *Journal of Quaternary Science* 22: 203-207.

Haeberli, W., Kääb, A., Wagner, S., Vonder Mühll, D., Geissler, P., Haas, J.N., Glatzel-Mattheier, H. & Wagenbach, D. 1999. Pollen analysis and ^{14}C age of moss remains in a permafrost core recovered from the active rock glacier Murtèl-Corvatsch, Swiss Alps: geomorphological and glaciological implications. *Journal of Glaciology* 43: 1-8.

Holzhauser, H., Magny, M. & Zumbühl, H.J. 2005. Glacier and lake-level variations in west-central Europe over the last 3500 years. *The Holocene* 15: 789-801.

Mortara, G., Orombelli, G., Pelfini, M. & Tellini, C. 1992. Suoli e suoli sepolti olocenici per la datazione di eventi geomorfologici in ambiente alpino: alcuni esempi tratti da indagini preliminari in Val d'Aosta. *Il Quaternario* 52: 135-146.

Reimer, P.J., Baillie, M.G., Bard, E. & others, 2004. IntCal04 Terrestrial Radiocarbon Age Calibration, 0-26 cal kyr BP. *Radiocarbon* 46: 1029-1058.

Scapozza, C. 2008. *Contribution à l'étude géomorphologique et géophysique des environnements périglaciaires des Alpes Tessinoises orientales*. MSc Thesis, Inst. of Geography, Univ. of Lausanne. Published February 28, 2008, on http:/doc.rero.ch/

Scapozza, C. & Reynard, E. (in press). Rock glaciers e limite inferiore del permafrost discontinuo tra la Cima di Gana Bianca e la Cima di Piancabella (Val Blenio, TI). *Geologia Insubrica*.

Interactions Between Permafrost and the Carbon Cycle

Kevin Schaefer
National Snow and Ice Data Center, University of Colorado
Tingjun Zhang
National Snow and Ice Data Center, University of Colorado
Lixin Lu
Cooperative Institute for Research in Environmental Sciences, University of Colorado
Ian Baker
Department of Atmospheric Science, Colorado State University

Introduction

The net terrestrial carbon flux or Net Ecosystem Exchange (NEE) is the small difference between two large gross fluxes: R – GPP, where *R* is ecosystem respiration and *GPP* is Gross Primary Productivity or photosynthesis. GPP for plant growth removes CO_2 from the atmosphere; R, due to microbial decay of dead plant material, returns CO_2 to the atmosphere. A positive NEE indicates a net flux into the atmosphere, and a negative NEE indicates a net biological uptake of CO_2. Microbial decay is slow in permafrost regions due to low temperatures, resulting in a large buildup of organic material both in the active layer and the underlying permafrost. About 950 Gt of carbon (equivalent to current atmospheric CO_2) was frozen into permafrost during the last ice age, protected from decay and effectively removed from the active carbon cycle (Zimov et al. 2006).

Climate warming across the high northern latitudes has resulted in widespread permafrost degradation (Zhang et al. 2005). Future projections indicate a loss of ~90% of near surface permafrost by 2100 (Lawrence & Slater 2005). As the permafrost thaws, the frozen organic matter will decay, rapidly increasing atmospheric CO_2 in addition to anthropogenic emissions. To predict the fate of this frozen carbon, we must understand how snow cover, soil thermal regime, and soil freeze-thaw processes influence the carbon cycle in regions of permafrost.

To assess these interactions, we simulated permafrost and carbon cycle dynamics across the Northern Hemisphere using the Simple Biosphere Carnegie-Ames-Stanford Approach (SiBCASA) driven by the NCEP reanalysis at 2x2 degrees. Correlations between output model variables identified key relationships between simulated soil temperatures, active layers, photosynthetic uptake, respiration fluxes, and biomass.

SiBCASA computes surface energy and carbon fluxes at 15-minute time steps using the Community Land Model snow and soil models and the CASA biogeochemical model (Schaefer et al. 2008). To improve soil thermodynamics, we (1) added the Sturm et al. (1995) snow classifications to account for depth hoar effects on snow thermal properties; (2) added the effects of organic matter to soil properties to account for the insolating effect of peat; and (3) extended the soil model depth from 3.4 m to 15 m. To reach steady state, we ran three simulations from 1982 to 2007 (75 years total) using the final soil temperatures and soil moistures from one simulation as initial values to the next. We algebraically calculated steady state carbon pool sizes using time average decay rate constants.

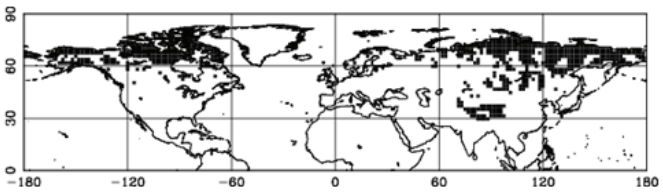

Figure 1. Simulated permafrost in Northern Hemisphere (black).

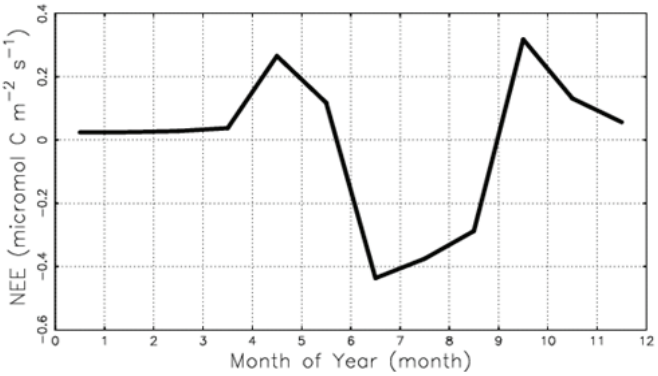

Figure 2. Seasonal cycle in simulated NEE at 70N and 120E.

Results

SiBCASA produced a fairly realistic permafrost distribution for the Northern Hemisphere (Fig. 1). The wave-like pattern in Siberia results from a similar pattern in NCEP precipitation, which is an artifact of the spectral representation of wind fields (Schaefer et al. 2004). Bands of heavy precipitation strongly insulate the soil in winter, resulting in warmer soil temperatures and preventing permafrost formation.

Figure 2 shows a typical seasonal cycle in NEE for a representative point in Siberia (70N, 120E). The NEE shown in Figure 2 is typical in both magnitude and seasonal variation for permafrost regions across both North America and Eurasia. Most permafrost areas are near steady state and the carbon fluxes balanced, meaning that NEE ~ 0 when averaged over several years. All GPP and nearly all R occur in the short arctic summer, peaking at about 6 μmol C m^{-2} s^{-1} in July. GPP is stronger than R in summer due to nearly

continuous daylight, resulting in net CO_2 uptake (negative NEE). In spring and fall, cooler temperatures and shorter days limit GPP, but not R, resulting in a net CO_2 release into the atmosphere (positive NEE). GPP shuts down in winter, but R can continue even in partially frozen soils; so we see positive, but weak NEE in winter.

Winter snow depths modulate the annual NEE cycle by influencing soil temperature and active layer depth. Deeper snows in winter insulate the soil, resulting in warmer soils in spring, which in turn results in deeper active layers the following summer. The timing of snowfall in fall is as important as snow depth: early snows in fall also result in warmer soils in winter and spring and a deeper active layer the following summer.

Winter snow depths affect GPP and R at different times of the year, producing a lopsided, time-delayed effect on the NEE seasonal cycle. Warmer soils and deeper active layers due to deeper winter snow increases R all year, but increase GPP only in late summer, when the active layer is deepest. Increased R due to warmer soil temperatures lead to increased NEE in spring and fall. In summer, increases in GPP overpower increases in R, resulting in increased CO_2 uptake (decrease in NEE).

Our results indicate a strong, time lagged response by the biosphere to changes in winter snow depth. Variations in snow depth in fall and early winter are effectively saved as variations in soil temperature, which in turn influences active layer depth the following summer. Through this memory of the soil temperature and active layer depth, winter snow depths effectively modulate biological fluxes throughout the following summer and fall.

Acknowledgments

This study was supported by the U.S. National Aeronautics and Space Administration (NASA) grant NNX06AE65G to the University of Colorado at Boulder.

References

Lawrence, D.M. & Slater, A.G. 2005. A projection of severe near-surface permafrost degradation during the 21st century, *Geophys. Res. Lett*. 32(24): doi:10.1029/2005GL025080.

Schaefer, K., Denning, A.S. & Leonard, O. 2004. The winter Arctic Oscillation and the timing of snowmelt in Europe. *Geophys. Res. Lett*. 31(22): Art. No. L22205.

Schaefer, K., Collatz, G.J., Tans, P., Denning, A.S., Baker, I., Berry, J., Prihodko, L., Suits, N. & Philpott, A 2008. The combined Simple Biosphere/Carnegie-Ames-Stanford Approach (SiBCASA) terrestrial carbon cycle model, *J. Geophys. Res*. (in press).

Sturm, M., Holgrem, J. & Liston, G.E. 1995. A seasonal snow cover classification system for local to global applications. *J. Clim*. 8(5): 1261-1283.

Zhang, T.J., Frauenfeld, O.W., Serreze, M.C., Etringer, A., Oelke, C., McCreight, J, Barry, R.G., Gilichinsky, D., Yang, D.Q., Ye, H.C., Ling, F. & Chudinova, S. 2005. Spatial and temporal variability in active layer thickness over the Russian Arctic drainage basin. *J. Geophys. Res.: Atmos.* 110(D16): Art. No. D16101.

Zimov, S.A., Schuur, E.A.G. & Chapin, F.S. 2006. Permafrost and the global carbon budget. *Science* 312(5780): 1612-1613.

Surface Offsets and *N*-Factors Across Altitudinal Tree Line, Wolf Creek Area, Yukon Territory, Canada

Emily A. Schultz
Department of Geography, University of Ottawa, Ottawa, Canada
Antoni G. Lewkowicz
Department of Geography, University of Ottawa, Ottawa, Canada

Introduction

Site-specific conditions that control ground heat flow and the surface temperature regime play an important role in determining permafrost occurrence in the discontinuous zone (Smith & Riseborough 2002). These include depth of snow, soil properties, and vegetation cover. As it is currently impractical to fully evaluate the effects of these variables on the energy balance in mountain basins, climate-permafrost relations must be simplified. One method that has recently been attempted is the TTOP model (Juliussen & Humlum 2007), which describes the relationship between the mean annual air temperature and the temperature at the top of permafrost in terms of the surface and thermal offsets (Smith & Riseborough 2002). Key components of this model are *n*-factors, which relate air and ground climate by establishing the ratio between air and surface freezing (winter) and thawing (summer) degree-days, thus summarizing the surface energy balance on a seasonal basis. Here we examine surface offsets and freezing and thawing *n*-factor variability at a number of sites through altitudinal tree line in the southern Yukon.

Study Area and Methods

Air and ground surface temperatures were measured hourly at 10 sites at elevations ranging from 1011–1640 m a.s.l. in and around the Wolf Creek research basin (60°32′N 135°13′W) near Whitehorse. This area is located within the sporadic discontinuous permafrost zone (Heginbottom et al. 1995), but permafrost is predicted to be extensive above 1400 m and continuous on mountain summits (Lewkowicz & Ednie 2004). The basin spans 3 major ecological zones that are mainly related to elevation: boreal forest at elevations below 1100 m, sub-alpine taiga/shrub tundra between 1100 m and 1500 m and alpine tundra above 1500 m (Francis et al. 1997). The measurement sites covered all 3 zones.

Instrumentation at each site consisted of an Onset Hobo Pro 8 datalogger equipped with an internal and external thermistor (accuracy of ±0.2°C). The body of each logger, containing an internal thermistor, was installed just below the ground surface while the external sensor was mounted within a solar radiation shield to measure air temperature at a height of 1.6 m.

Data presented here were collected from October 2003 to August 2006, comprising 3 freezing seasons and 2 thawing seasons. Data, collected at site on a palsa in the middle of the basin since April 2001, provide 2 additional freezing and 2 thawing seasons for analysis.

Snowpack development over the winter was tracked in 2005–06 using iButton miniature loggers, installed on stakes at 10–20 cm intervals (10, 20, 30, 40, 60 and 80 cm) at most of the logger sites. Temperatures were recorded by the iButtons sensors at 4-hour intervals. Differences in the temperature readings of iButtons above and below the snow were used to determine snow depths.

Results

Surface offsets

Surface offsets varied from 0.4° to 3.6°C (Table 1). Offsets for the forested and alpine tundra sites fall within the high and low parts of this range, respectively, while those measured at the sub-alpine taiga/shrub tundra sites cover almost the entire range. The smallest range in values was recorded at the forested sites (1.5°C), slightly smaller than at the alpine tundra sites (1.7°C), where snow accumulation is typically lowest.

Table 1. Surface offsets and *n*-factors at the study sites.

Site / Elevation (m)	Veg. Zone	Max. Snow Depth (2005–06)	Surface Offset (°C)	*nf*	*nt*
T2	boreal forest		2.9	0.29	
1011		70±9 cm	2.1	0.49	0.92
T3			3.6	0.12	
1145		70±9 cm	3.6	0.36	0.92
T4	sub-alpine taiga/shrub tundra		3.1	0.23	
1290		>80 cm	3.0	0.35	0.83
P9			3.8	0.39	-
			2.3	0.57	1.05
			3.0	0.45	1.08
1254			3.3	0.26	0.99
		50±9 cm	3.4	-	-
CR1			2.4	0.49	-
			2.7	0.36	0.91
1260		70±9 cm	2.4	0.56	0.92
CR2			2.8	0.40	-
			3.2	0.31	0.80
1271		50±9 cm	3.6	0.41	1.01
CR3			1.2	0.73	-
			1.0	-	0.95
1363		50±9 cm	2.2	0.55	-
CR4	alpine tundra		0.9	0.70	-
			1.4	0.52	0.86
1457		45±14 cm	2.1	0.51	0.87
CR5					
1495		-	0.4	-	-
Bowl					
1640		-	2.2	0.60	-

N-factors

Freezing factors (*nf*) over the study period ranged from 0.12 to 0.73 (Table 1). Figure 1 demonstrates that *nf* values exhibit a broad relationship with both elevation and vegetation. Values for the forested sites were all <0.40, ranging from 0.12 to 0.36, while those calculated for the tundra sites were all >0.50. Freezing factors for the sub-alpine taiga/shrub tundra zone point to the role of variable vegetation and snow cover close to and below tree line, with values ranging from 0.23 to 0.73 at these sites. Values of *nf* measured at individual sites exhibited significant interannual variability with increases of more than 0.20 at some sites between 2004–05 and 2005–06. Snow accumulation differences likely account for this pattern. Whitehorse recorded a maximum of 47 cm of snow on the ground in 2004–05, but a maximum of only 22 cm in 2005–06 (Environment Canada 2008).

Thawing factors (*nt*) ranged from 0.80 to 1.08, a much smaller range than for *nf* (Table 1). Values of *nt* calculated for the forested sites over the study period were both 0.92, slightly above those calculated for the tundra site (0.86 and 0.87). Sites where *nt* was greater than 1.0 were all situated above 1200 m, and all are located within the sub-alpine taiga/shrub tundra zone. Along the Mount Sima trail, there is a clear transition in *nt* associated with tree line, with thawing factors at the two forested sites (T2 and T3) nearly 0.10 higher than at the sub-alpine site (T4) in 2005.

Discussion and Conclusions

Our results support the findings of Karunaratne and Burn (2004) and the modeling of Smith and Riseborough (2002) that snow depth is the most important variable influencing *nf*, because the low thermal conductivity of snow restricts heat loss from the ground surface. *Nt* values are higher and vary less. They may relate to land cover as suggested by Klene et al. (2001) who obtained the highest values on bare ground and wet tundra sites. Similarly, Taylor (1995) calculated the highest values of *nt* at open sites and lowest at shaded sites, predominantly those located within the forest.

The relationship between surface offset, *n*-factors, elevation, and vegetation in the study area, therefore, demonstrates that trends previously identified in relation to latitudinal tree line also apply to the altitudinal tree line.

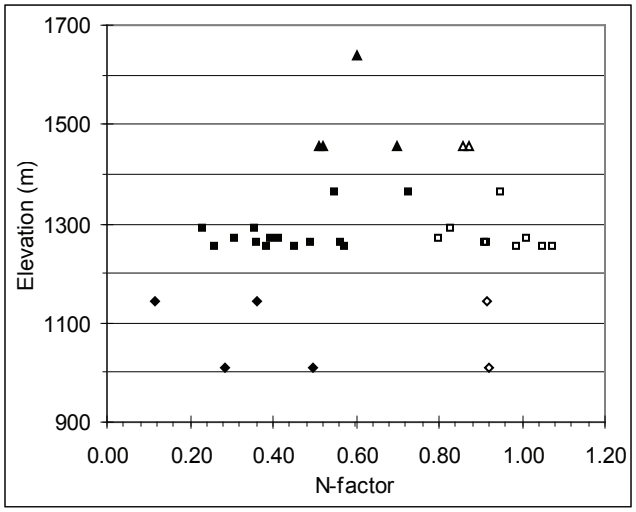

Figure 1. Relationship between elevation, vegetation and seasonal *n*-factors at the study sites (2001–2006). Freezing (filled) and thawing (outlined) factors are shown for the boreal forest (diamond), sub-alpine taiga (square) and alpine tundra (triangle) vegetation zones.

Acknowledgments

This research was supported financially by the Canadian Foundation for Climate and Atmospheric Sciences, NSERC, the Northern Scientific Training Program (INAC), the Geological Survey of Canada, and the Yukon Geological Survey. Logistical support was given by Water Resources Branch, Yukon Government. Field assistance was given by Jim Coates, Phil Bonnaventure, Pauline Favero, and Martina Knopp.

References

Environment Canada. 2008. National Climate Archive [online]. http://www.climate.weatheroffice.ec.gc.ca (Accessed February 9, 2008).

Francis, S., Smith, S. & Janowicz, R. 1997. Intégration des données et la zonation écologique du basin versant du ruisseau Wolf. In: J.W. Pomeroy & R.J. Granger (eds.), *Wolf Creek Research Basin: Hydrology, Ecology, Environment*. Saskatoon: National Water Research Institute, 97-104.

Heginbotton, J.A., Dubreuil, M.A. & Harker, P.T. 1995. Canada-Permafrost. In *National Atlas of Canada,* 5th ed. Ottawa: National Atlas Information Service, Natural Resources Canada. Plate 2.1 MCR 4177, 1:7,500,000.

Juliussen, H. & Humlum, O. 2007. Towards a TTOP Ground Temperature Model for Mountaneous Terrain in Central-Eastern Norway. *Permafrost and Periglacial Processes* 18: 161-184.

Karunaratne, K.C. & Burn, C.R. 2004. Relations between air and surface temperature in discontinuous permafrost terrain near Mayo, Yukon Territory. *Canadian Journal of Earth Sciences* 41: 1437-1451.

Klene, A.E., Nelson, F.E. & Shiklomanov, N.I. 2001. The n-factor in natural landscapes: variability of air and soil-surface temperatures, Kuparuk river basin, Alaska, USA. *Arctic*, *Antarctic and Alpine Research* 33: 140-148.

Lewkowicz, A.G. & Ednie, M. 2004. Probability mapping of mountain permafrost using the BTS method, Wolf Creek, Yukon Territory, Canada. *Permafrost and Periglacial Processes* 15(1): 67-80.

Smith, M.W. & Riseborough, D.W. 2002. Climate and limits of permafrost: A zonal analysis. *Permafrost and Periglacial Processes* 13: 1-15.

Taylor, A.E. 1995. Field measurements of n-factors for natural forest areas, Mackenzie Valley, Northwest Territories. *Current Research 1995-B,* Geological Survey of Canada, 89-98.

The Contribution of Old Carbon to Respiration from Alaskan Tundra Following Permafrost Thaw

Edward A.G. Schuur, Jason G. Vogel, K. Grace Crummer, Hanna Lee, Koushik Dutta
Department of Botany, University of Florida, Gainesville, FL 32601-8526, USA

Introduction

Up to 1670 Pg of soil carbon (C) has accumulated in high latitude ecosystems after the retreat of the last major ice sheets. This soil C has until now been largely protected from decomposition by cold temperature, water-logging, and permafrost. Recent studies suggest that, due to climate warming, these ecosystems may no longer be accumulating C, and in some cases may be losing stored C to the atmosphere. We hypothesize that sustained transfers of C to the atmosphere that could cause a significant positive feedback to climate change will come from old C, which forms the bulk of the soil pool.

Materials and Methods

Field sites

We used radiocarbon ($\Delta^{14}C$) measurements of carbon dioxide to detect the age of C respired from tussock tundra near Denali National Park, Alaska. These measurements were made in the Eight Mile Lake Watershed (63°52′42.1″N, 149°15′12.9″W) on the north slope of the Alaska Range. Ground temperature in a borehole has been monitored for several decades at this site, before and after the permafrost was observed to thaw (Osterkamp & Romanovsky 1999). In this watershed, our study has defined three sites that represent differing amounts of disturbance from permafrost thawing based on observations of the vegetation and the borehole measurements: (1) tussock tundra typical of arctic ecosystems, dominated by the sedge *Eriophorum vaginatum* and *Sphagnum spp* mosses (Minimal thaw); (2) a site near the borehole used for permafrost temperatures, where the vegetation composition has been shifting to include more shrub species, such as *Vaccinium uliginosum* and *Rubus chamaemorus* (Moderate thaw); and (3) a site located where permafrost melted more than several decades ago, now largely dominated by shrub species (Extensive thaw) (Schuur et al. 2007). These three sites are a natural experimental gradient representing the long-term effects of permafrost thawing on C loss. This thawing has occurred without any visible surface disturbance (i.e., fire) and is thought to be an effect of regional climate warming. We made radiocarbon measurements of ecosystem respiration, incubations of soil organic matter, and incubations of aboveground and belowground plant biomass to determine the age and isotopic value of C respired from these sites.

Radiocarbon field measurements

Ecosystem respiration $\Delta^{14}CO_2$ measurements were measured using a modified dynamic flow chamber system analogous to the system used for measuring ecosystem CO_2 fluxes. At monthly intervals during the growing season (May–September), dark, 10 L, plastic chambers were placed over collars in the soil surface. To remove background atmospheric air present when the chamber top is fit to the collar, the air stream is scrubbed with Ascarite. Carbon dioxide was scrubbed from the system at a rate similar to that of soil CO_2 efflux until 2–3 chamber volumes of air had passed through the scrubber, when the CO_2 remaining is almost exclusively soil-respired CO_2. The air stream was then diverted through a molecular sieve to quantitatively trap ~1.0 mg CO_2. In the laboratory, the molecular sieve traps were heated to 625°C to desorb CO_2. Carbon dioxide was then purified and analyzed for $\delta^{13}C$ and $\Delta^{14}C$.

Radiocarbon laboratory measurements

To estimate the contribution of plant respiration, surface litter, and deep, old soil C to surface $\Delta^{14}CO_2$ fluxes, we incubated these materials in the laboratory to determine the isotopic composition of evolved CO_2. We collected 2 replicate soil samples per site down to the mineral soil interface (typically the full August active layer depth) and separated the profiles into 5 depth increments (0–5, 5–15, 15–25, 25–35, 35+ cm). The final depth increment was variable because the total organic layer thickness varied among samples. All samples were split, large roots and stems removed, and the halves kept intact to preserve the soil structure. Soil core splits were incubated in separate glass jars at 3°C and 8°C to determine the temperature sensitivity (expressed as a Q_{10} value) for respiration from these soil. Rates of CO_2 production were then measured daily using an IRGA to monitor the change in CO_2 concentration in the incubation jar headspace over time. Jars were sealed and flushed with moist CO_2-free air when CO_2 concentrations exceed 1%. After 5 days of incubation in the laboratory, the jars were completely scrubbed with CO_2-free air, and respired $^{14}CO_2$ was allowed to accumulate and was then collected for $\Delta^{14}C$ analysis. Similar incubations were made of aboveground and belowground plant parts harvested from 5 x 5cm quadrats during the growing season.

Source partitioning

We estimated the relative contribution of the plant and soil components to the R_{eco} flux using the $\Delta^{14}C$ measurements and a standard statistical modeling approach. The laboratory soil incubations were combined into surface soil (top 2 horizons) and deep soil (lower 3 horizons) components by flux-weighting the soil incubations. To calculate a combined isotope respiration value for the surface and deep soil, the $\Delta^{14}C$ values for the layers that were combined were weighted by (1) the relative CO_2 flux on a per gram dry soil basis, (2)

Table 1. Fluxes and isotopes of carbon dioxide from laboratory incubations of soil organic layers at 15°C.

Site	Soil Layer cm	Carbon Flux μg C gdw^{-1} hr^{-1} (± SE)	Soil Mass $kgdw\ m^{-2}$ (± SE)	Average Summer Temperature ºC	$\Delta^{14}C$ ‰ (± SE)
Minimal	0-5	8.09 (4.21)	3.06 (0.76)	14.0	+101 (7)
	5-15	6.05 (2.14)	5.13 (1.90)	12.2	+96 (13)
	15-25	3.07 (1.64)	8.80 (0.79)	4.7	+53 (6)
	25-35	1.66 (0.23)	14.61 (3.14)	2.0	+48 (1)
	35+	1.26 (0.65)	181.86 (46.21)	0.6	-56 (66)
Moderate	0-5	7.65 (1.31)	3.80 (0.56)	14.0	+94 (11)
	5-15	3.47 (1.73)	5.49 (1.01)	12.2	+78 (23)
	15-25	3.16 (0.71)	10.06 (0.87)	4.7	+35 (10)
	25-35	1.18 (0.28)	17.37 (0.92)	2.0	+25 (4)
	35+	0.38 (0.18)	66.87 (19.27)	0.6	-32 (32)
Extensive	0-5	9.88 (3.38)	3.06 (0.76)	14.0	+101 (7)
	5-15	4.26 (2.00)	5.13 (1.90)	12.2	+96 (13)
	15-25	2.05 (1.01)	8.80 (0.79)	4.7	+53 (6)
	25-35	1.98 (0.58)	14.61 (3.14)	2.0	+48 (1)
	35+	0.46 (0.13)	181.86 (46.21)	0.6	-56 (66)

the relative amount of soil mass in the combined horizons, and (3) by the average field temperature for the horizons (this varied over the season). Plant respiration $\Delta^{14}C$ values measured over the growing season matched the atmospheric values in 2004 (data not shown), and were assumed to follow the atmospheric decline.

Total R_{eco} $\Delta^{14}CO_2$ flux is a combination of surface and deep soil respiration, along with plant respiration. Because there is no single solution that describes the contribution of 3 unknown sources with a single isotope tracer, a standard statistical approach yields a range of possible contributions of the component sources to R_{eco}. Of the sources (plant respiration, surface soil respiration, deep soil respiration), the contribution of the deep soil is the most clearly defined, as demonstrated by the smallest standard deviation and overall range. This is a result of the deep soil having a $\Delta^{14}C$ value furthest away from the $\Delta^{14}C$ value of R_{eco}, thus its contribution to the total is most constrained. While the deep soil C was the only source that could bring the R_{eco} $\Delta^{14}C$ value below that of the current atmosphere,
the $\Delta^{14}C$ values of plant respiration and surface soil respiration were more similar and thus could substitute for one another.

Results and Conclusions

Over the study period, ecosystem respiration radiocarbon values averaged from +35‰ to +95‰ in different months across sites. For soil incubations, surface soil radiocarbon was elevated relative both to ecosystem respiration and the current atmospheric radiocarbon value, demonstrating the significant contribution from C fixed over the past years to several decades (Table 1). The deeper soil, in contrast, had respiration isotope values that averaged below zero, reflecting the significant effect of radioactive decay on the isotope content of deeper soil layers. The plant and soil incubations were combined in a multisource mixing model to determine probable contributions from these different sources to ecosystem respiration. Deep soil respiration generally averaged between 5–15% of total ecosystem respiration, but reached as high as 40% in some months. When aggregated across the growing season, the two sites undergoing more disturbance from permafrost thaw had on average 2–3 times the loss of old, deep C as compared to the least disturbed site. From this isotope partitioning, we determined that the respiration of old C increases following permafrost thaw and contributes towards making these tundra ecosystems net sources of C to the atmosphere.

References

Osterkamp, T.E. & Romanovsky, V.E. 1999. Evidence for warming and thawing of discontinuous permafrost in Alaska. *Permafrost and Periglac. Process* 10: 17-37.

Schuur, E.A.G., Crummer, K.G., Vogel, J.G. & Mack, M.C. 2007. Plant species composition and productivity following permafrost thaw and thermokarst in Alaskan tundra. *Ecosystems* 10: 280-292.

Interactions Between Human Disturbance, Demographics of *Betula Fruticosa* Pall., and Permafrost in the Vitimskoye Upland, East Siberia

I.R. Sekulich
Institute of General and Experimental Biology SB RAS, Ulan-Ude, Russia

The demographic structure of plant coenopopulations is one of the basic estimation criteria of the modern state of species in coenosis, level of vital condition, degrees of their stability, and prospects of development (Harper 1992, Rabotnov 1978, 1985, Uranov 1960, 1975).

Our research was performed on the central part of the Vitimskoye upland, which is located in eastern Siberia (Fig. 1). It is large isolated area which is situated at the southern limit of continuous permafrost. The permafrost is the major ecological factor which determines character and distribution of vegetation here. Communities formed by low birches or birch-shrublands are the most widespread here.

The capacity of permafrost in the research area is from 50–250 m with temperature from 0 to -3°C; depth bedding of permafrost in birch-shrublands in August-September is about 1.0–1.6 m (Vtorushin & Pigareva 1996).

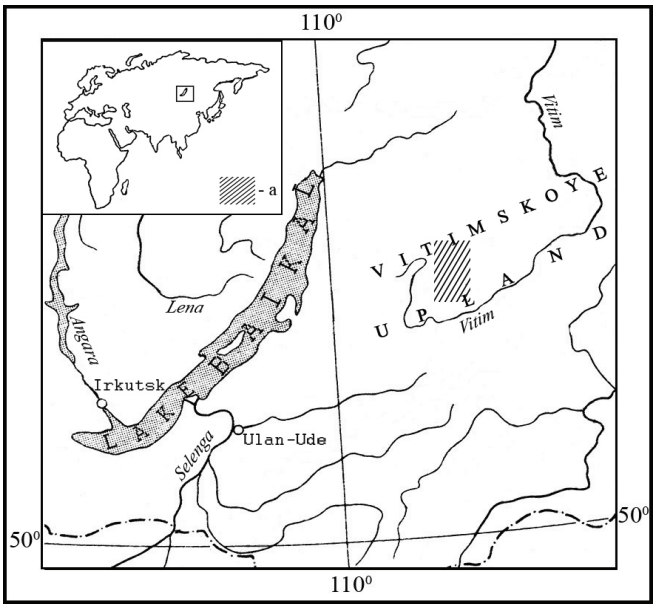

Figure 1. Map of location of researches area: a – research area.

Table 1. Age stages and age groups of the plants.

The age stages	The age groups	The letter code
latent	seed	sm
pre-generative	germ	pl
	juvenile	j
	immature	im
	virginile	v
generative	young generative	g_1
	mature generative	g_2
	old generative	g_3
post-generative	subsenile	ss
	senile	s

The object of our research is *Betula fruticosa* Pall. subsp. *montana* M. Schemberg, the basic dominant of birch-shrublands.

We studied changes of the demographic structure of the coenopopulations of *Betula fruticosa* on sites with partial destruction of vegetative cover as a result of the influence of track transport and pasturing. Research carried out was spent on the model area in 100 square meters on which continuously calculated individuals on age groups.

Rabotnov (1978) had divided the whole life cycle of plants into the following age stages and age groups, which are submitted in Table 1. The letter code of each age group has been offered by Uranov (1960).

The age level of the coenopopulations is estimated by the index of age (Δ) proposed by Uranov (1975) and by the index of effectiveness of the populations (ω) proposed by Zhivotovsky (2001). Values of Δ and ω were calculated by the following formulas:

$$\Delta = \sum n_i m_i \Big/ \sum n_i \quad (1)$$

$$\omega = \sum n_i e_i \Big/ \sum n_i \quad (2)$$

where n_i is the number of individuals of each age group; m_i is the coefficient of the age group, calculated by Uranov (1975); and e_i is the efficiency of plants of each age group, calculated by Zhivotovsky (2001).

Indexes Δ and ω varies from 0 to 1, and the highest value characterized the elder coenopopulation.

In estimating the degree of anthropogenic influence on the demographic spectrum of disturbed coenopopulations, it is necessary to compare them with a base spectrum, which is the modal characteristic of dynamic balance of coenopopulation (Smirnova 1987). The base spectrum coenopopulation *B. fruticosa* on the Vitimskoye upland is full-constituent, has one peak, with absolute maximum on old generative individuals.

It was marked two variants of modification of the demographic structure.

One of them shows an increase in the quantity of pregenerative individuals at the remaining high number of generative individuals. An age spectrum of such coenopopulations has two peaks. As an example, the age spectrum coenopopulation in the community of Multiherboso–Betuletum fruticosae is shown (Fig. 2). The community is situated near to a settlement along a highway and often is exposed to the influence of track-type vehicles.

At the unitary passage of the cross-country vehicle, according to mechanical influence, the integrity of the vegetative cover is broken. As a result of these disturbances,

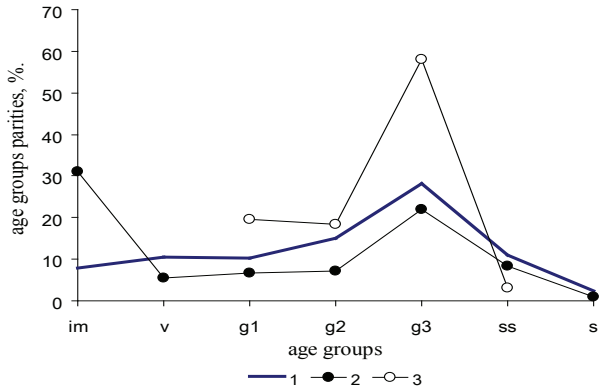

Figure 2. The age spectrums coenopopulations of *Betula fruticosa*. 1 – base spectrum; 2 – community of Multiherboso–Betuletum fruticosae; 3 – community of Kobresio–Betuletum fruticosae. Characteristics of age groups were explained above.

Table 2. The quantity, index of age (Δ) and index of effectiveness (ω) of anthropogenically disturbed coenopopulations of *Betula fruticosa*.

Community	Multiherboso-Betuletum fruticosae	Kobresio-Betuletum fruticosae
The general quantity, pcs./100 m^2	482.3 ± 17.2	23.3 ± 3.2
The quantity of age groups, pcs./100 m^2:		
j	89.4 ± 9.6	-
im	149.4±11.7	-
v	25.9±4.1	-
g_1	32.9±4.3	4.6 ±0.6
g_2	34.1±4.3	4.3 ± 0.5
g_3	105.9±6.4	13.7±2.4
ss	40.0 ±3.9	0.7 ±0.1
S	4.7 ±0.6	-
Δ	0.32	0.65
ω	0.43	0.81

gaps formed, which are the microecotope for renewal *B fruticosa.* There is a rejuvenation of the coenopopulation at the expense of the high number of young individuals (Table 2).

The short-term influence of transport does not effect adult individuals of *B. fruticosa* essentially. At multiple or constant impacts of track-type transports, the adult individuals finally perish, which leads to replacement of birch-shrublands on grassy communities of meadow. This leads to a change of hydrothermal condition of the soil, and the depth of seasonal thawing of permafrost and bogging, thermokarst can develop.

Another variant of anthropogenic changes of the demographic structure occurs with pasturing. As a result of trampling and pasturing, the young individuals of *B. fruticosa* disappear from the structure of the community together with grassy plants. The coenopopulation is presented by old-age plants. The community of Kobresio–Betuletum fruticosae, located on an abrupt slope, can be an example of such kind of coenopopulation. The age spectrum here has one peak, but it is not full-constituent and presented by old individuals (Fig. 2). The number of individuals of *B. fruticosa* in this coenopopulation is low (Table 2).

The low indexes Δ and ω of coenopopulation of *B. fruticosa* occurring in the community of Multiherboso–Betuletum fruticosae shows its invasive character and is considered as young according to "delta-omega" classification (Zhivotovsky 2001). The high indexes Δ and ω in the community of Kobresio–Betuletum fruticosae shows its regressive character and is considered as becoming old.

Thus, human-induced disturbances on the of demographic structure of coenopopulation *B. fruticosa* in birch-shrublands on the Vitimskoye upland promote development of various geocryological processes. When the disturbances of demographic structure are slight, fast restoration of coenopopulation and ecological conditions occurred.

References

Harper, J.L. 1992. *Population of Plants.* Oxford: The Alden Press, 892 pp.

Rabotnov, T.A. 1978. On coenopopulations of plants reproducing by seeds. In: *Structure and Functioning of Plant Populations.* Amsterdam, 1-26.

Rabotnov, T.A. 1985. Dynamics of plant coenotic populations. In: J. White (ed.), *The Population Structure of Vegetation.* Dordrecht, Boston, & Lancaster: Dr. W. Junk Publ., 121-142.

Smirnova, O.V. 1987. *Struktura travjanogo pokrova shirokolistnyh lesov* (*The Grass Layers Structure of Broad-leaved Forests*). Moscow: Nauka, 207 pp. (in Russian).

Uranov, A.A. 1960. Zhyznennoe sostoyanye vyda v rastytel'nom soobshestve (The life state of species in a plant community). *Bulleten' Moskovskogo obshestva ispytatelei pryrody, otdel biologicheskyi* (*Bulletin of Moscow Society of Naturalists, Biological Series*) 67(3): 77-92 (in Russian).

Uranov, A.A. 1975. Vozrastnoi spektr fytocenopopuljacyi kak funkcija vremeny I energetycheskih volnovyh processov (The age spectrum of phytocoenopopulation as a function of time and power wave of processes). *Biologycheskye nauki* (*Biological Sciences*) 2: 7-34 (in Russian).

Vtorushin, V.A. & Pigareva, N.N. 1996. *Kryomorfnye pochvy: perspektivy ich effektivnogo ispol'zovaniya* (*Criomorphic Soils: Prospects of their Effective Utilization*). Ulan-Ude: BSC SB RAS, 295 pp. (in Russian).

Zhivotovsky, L.A. 2001. Ontogeneticheskie sostojanija, effectivnaja plotnost' i klassifikacija populjacyi rastenyi (Ontogenetic states, effective density, and classification of plant populations). *Ecologija* (*Russian Journal of Ecology*) 1: 3-7 (in Russian).

Rock Glacier Distribution in the Absaroka/Beartooth Wilderness, Montana, USA

Zach M. Seligman, Anna E. Klene
Department of Geography, University of Montana, Missoula, 59812, USA

Introduction

Rock glaciers are relatively understudied glacial features found in many alpine environments around the world. Because they are rock-covered and often similar in appearance to talus fields and moraines, their presence and hydrologic significance has gone widely unnoticed (Millar & Westfall 2007). However, they play an important role in alpine environments. Rock glaciers provide a mechanism for transport of headwall debris (Humlum 2000) and, similar to glaciers, can act as a source of year-round water in high alpine catchments where late summer precipitation is minimal (Johnson 2007). Schrott (1996) determined that these features can contribute up to 30% of river discharge during summer months in the Andes.

Additionally, rock glaciers potentially contain significant climatic information within their spatial distribution (Humlum 1998). While a number of studies have focused on these relationships (Kerschner 1978, Brazier et al. 1998, Humlum 1998), a paucity of relevant climate stations often limits such efforts (Brazier et al. 1998). Other research has examined characteristics of rock glacier age (Aoyama 2005), movement (Chueca & Julian 2005), structure (Arenson et al. 2002), and geomorphology (Berthling & Etzelmuller 2007).

In the Absaroka/Beartooth wilderness, rock glaciers number in the hundreds (unpublished data), existing simultaneously with cirque glaciers and permanent snowfields, yet general information about them is sparse, and hydrological research is non-existent. This study will examine the spatial distribution of rock glaciers to understand the relative local importance of topoclimatic and geologic factors. This understanding will allow further investigations into the relationships between rock glacier distribution, ice volume, and downstream ecology. The interplay of these factors has important implications in light of recent and ongoing climatic changes.

Research will be performed in two phases. Phase one includes analysis through GIS and remote imagery, which will explore trends in rock glacier distribution relative to topoclimatic factors. The second phase will be field verification of the digital data, which will subsequently investigate the link between spatial characteristics of rock glaciers and water availability in alpine catchments.

Background

Topoclimatic and geologic controls

Previous research in New Zealand shows that active rock glaciers tend to favor relatively higher elevations and more southerly aspects (Brazier et al. 1998). In the same study, modern distribution of relict rock glaciers favored lower elevations on all aspects. Similarly, Humlum (1998) describes rock glacier presence to be "a complex function of responses to air temperature, insolation, wind, and seasonal precipitation over a considerable period." Just as topoclimatic factors play a major role in ice formation and retention of rock glaciers, lithology has also been shown to be an important component of rock glacier initiation (Johnson et al. 2007). This study will use GIS to compare topoclimatic and geologic controls on rock glacier distribution.

Ice volume and distributional controls

Rock glacier ice volume may also correlate strongly with topographical distribution in the same ways that rock glacier activity is linked to topographical and altitudinal controls (Humlum 1988). As rock glacier activity is dependent on ice volume for its classification, it should follow that ice volume is subject to the same variables that affect rock glacier activity. This study will explore topographical and altitudinal controls on rock glacier ice volume.

Ice volume and vegetation

Investigations of relationships which may exist between rock glacier distribution, ice volume, and downstream ecology can be based upon the relationships currently known to exist between glacial systems and ecological succession in the region. Previous research has looked at vegetative advancement in response to glacial recession in Africa (e.g., Kazuheru 2003). Locally, Hall and Fagre (2003) used models to project vegetation succession patterns of glacial forelands in Glacier National Park, Montana. Perhaps a similar relationship exists for alpine catchments where rock glaciers, instead of ice glaciers, are the dominant glacial feature. This study will estimate rock glacier ice volume in comparison with percentage per area of appropriate vegetation types downhill of the rock glacier terminus.

Implications for climate

Topological and altitudinal distribution of rock glaciers, in itself, has the potential to contain unique climatic information (Humlum 1998). By comparing ages and elevations of active and relict rock glaciers and interpreting changes in equilibrium line altitudes, timing of glaciations and temperature differences have been determined (Millar & Westfall 2007). Regionally, results of vegetative patterns associated with spatial distribution of rock glaciers may also harbor additional climatic information.

Study Area

This study will focus, in the first phase, on the distribution of rock glaciers within Absaroka/Beartooth wilderness area in southwest Montana. Phase two will look at approximately 30 representative rock glaciers within the wilderness area.

Methodology

Rock glaciers were initially identified in the study areas using GoogleEarth software and then were plotted on a printed map. Digital elevation models (10 × 10 m) for each rock glacier of interest will be obtained from the Montana Natural Resource Information System (NRIS). Digital aerial photos will also be obtained from NRIS for the Absaroka/Beartooth Wilderness. Feature Analyst and ArcGIS software will be used with spectral and pattern-recognition techniques to extract rock glaciers from the imagery. Elevation, slope, aspect, vegetation, and insolation estimates will be computed.

Field component

Ground verification will be needed to assess the predictions from the remote imagery. Elevation, slope, and aspect will be recorded in the field. Rock glacier activity, as described by Johnson et al. (2007), will be classified as Class 1 (active), Class 2 (inactive), or Class 3 (relict). Total rock glacier volume and total cirque glacier volume will be estimated by taking GPS coordinates of the perimeters and estimating depth from surrounding topography. Rock glacier mantle volume will be estimated by multiplying the perimeter with the depth of the mantle. Mantle depth will be estimated by making exposures of the ice core and looking for natural ice exposure in the mantle. Total ice volume will be predicted by subtracting the rock glacier mantle volume from the total rock glacier volume.

Vegetation composition will be determined by techniques from Kimball and Weihrauch (2000). Using 100 m^2 plots, percentage per area of several vegetation communities will be determined. Plot information will be gathered below the rock glacier terminus. Elevations of prominent vegetation regimes will be recorded.

Discussion

In phase one, GIS data will be used to analyze trends in rock glacier distribution relative to topographical, altitudinal, and climatic characteristics. Anticipated results of this phase include a tendency toward active rock glacier presence at higher elevations on north-facing slopes. Additionally, estimated rock glacier size, presence of an uphill cirque glacier, and annual insolation will also be examined with relation to altitudinal data, slope, and aspect. It is expected that distribution will represent a complex correlation based on many factors.

Phase two will focus on the field verification of the GIS data and will also look at rock glaciers as elements of water storage in alpine regions. The presence of ice in a rock glacier may act as the only late-summer water available to downslope vegetation. For example, a discrepancy in elevation and percent composition of more xeric species below active rock glaciers might differ relative to relict rock glaciers, which, in effect, do not release late-summer glacial melt.

References

Aoyama, M. 2005. Rock glaciers in the northern Japanese Alps: Palaeoenvironmental implications since the Late Glacial. *J. Quaternary Science* 20(5): 471-484.

Arenson, L., Hoelzle, M. & Springman, S. 2002. Borehole deformation measurements and internal structure of some rock glaciers in Switzerland. *Permafrost and Periglacial Processes* 13: 117-135.

Berthling, I. & Etzelmuller, B. 2007. Holocene rockwall retreat and the estimation of rock glacier age, Prins Karls Forland, Svalbard. *Geografiska Annaler* 89A(1): 83-93.

Brazier, V. et al. 1998. The relationship between climate and rock glacier distribution in the Ben Ohau Range, New Zealand. *Geografiska Annaler* 80A: 3-4.

Chueca, J. & Julian, A. 2005. Movement of Besiberris rock glacier, central Pyrenees, Spain: Data from a 10-year geodetic survey. *Arctic, Antarctic, & Alpine Res.* 37(2): 163-170.

Hall, M. & Fagre, D.B. In press. Where have all the glaciers gone? Modeling climate-induced glacier change in Glacier National Park. *Bioscience*: 1850-2100.

Hughes, P.D., Gibbard, P.L. & Woodward, C. 2003. Relict rock glaciers as indicators of Mediterranean palaeoclimate during the Last Glacial Maximum (Late Wurmian) in northwest Greece. *J. Quaternary Sci.* 18(5): 431-440.

Humlum, O. 1998. The climatic significance of rock glaciers. *Permafrost and Periglacial Processes* 9: 375-395.

Humlum, O. 2000. The geomorphic significance of rock glaciers: Estimates of rock glacier debris volumes and headwall recession rates in west Greenland. *Geomorphology* 35: 41-67.

Johnson, B.G. 2007. The effect of topography, latitude, and lithology on rock glacier distribution in the Lemhi Range, central Idaho, USA. 91: 38-50.

Kazuheru, M. 2003. Vegetation succession in response to glacial recession from 1997–2002 on Mt. Kenya. *J. of Geography* 473(2): 608-619.

Kerschner, H. 1978. Palaeoclimatic inferences from Late Wurm rock glaciers, Eastern Central Alps, Western Tirol, Austria. *Arctic & Alpine Research* 10: 635-644.

Kimball, K.D. & Weihrauch, D.M. 2000. Alpine vegetation communities and the alpine-treeline ecotone boundary in New England as biomonitors of climate change. *USDA Forest Service Proc*. RMRS 15(3).

Krainer, K. & Mostler, W. 2002. Hydrology of active rock glaciers: Examples from the Austrian Alps. *Arctic, Antarctic, & Alpine Res.* 34(2): 142-149.

Millar, C. & Westfall, R.D. Rock glaciers and related periglacial landforms in the Sierra Nevada, CA, USA: Inventory, distribution and climatic relationships. *Quaternary Internatl.*: doi:10.1016/j.quaint.2007.06.004.

Potter, N., Jr. et al. 1998. Galena Creek rock glacier revisited: New observations on an old controversy. *Geografiska Annaler* 80A: 251-265.

Schrott, L. 1996. Some geomorphological-hydrological aspects of rock glaciers in the Andes (San Juan, Argentina). *Z. Geomorph N.F.* 104: 161-173.

Dynamics of the Cryosphere of Northern Tien Shan as a Reaction to Climate Change

Igor V. Severskiy
Kazakh Institute of Geography,
Eduard V. Severskiy
Permafrost Institute of Russian, Academy of Sciences.

On the basis of analysis of long-term observation, data changes of snowiness, glaciation, and thermal regime of seasonally and perennially frozen grounds in the mountains of southeast Kazakhstan (Northern Tien Shan, Dzhunghar Alatau) for last decades are considered.

According to analysis in the testified region, for the last decades the average maximum snow water equivalent (the main component of snow resources) has not changed. Similar results were found for western Tien Shan and Gissar-Alai.

Glacial systems of Central Asia mountains develop in the same direction and have similar rates of modern changes; so for the last decades, the area of glaciers in different regions of Tien Shan, Gissar-Alai, Pamirs and Dzhunghar Alatau has decreased at the average rate 0.8–1.0% per year.

The dimensions and temperatures of the glacier degradation have been determined on the basis of comparison of data of the unified Glacier Inventories, composed by aero-photograph materials and by satellite images for 6 years within the period of 1955 to 1999.

Mean maximum glacial retreat rates at the Northern Tien Shan characteristic of the mid-1970s by the mid-1980s slowed down.

Glacier retreat rate depends to a great extent on its size. A glacier area F = 13–14 km^2 is the threshold. In case of its excess, the self-regulation mechanism of the glacier is so vivid that it neutralizes evidence of all local factors, and its regime is defined by microclimatic conditions of the region.

The regime of each glacier is unique and can differ from not only average data for this type of glacier system, but also from that of a nearby glacier. The differences can be not only significant but also can have a different negative/positive trend. Glacier retreat rate does not depend on its exposition and morphological type. Territorial differences in the retreat rates are defined by the orientation of slopes in reference to the sides of the horizon and the prevailing direction of humid air mass movements, and the location of the region in the mountainous system.

Predominating opinion about the inevitability of glaciers disappearance in Central Asia mountains cannot be accepted as an axiom. Taking into account stability in the rate of precipitation and especially in the rate of snow resources, one can suppose that glaciers in this region will not disappear during this century. Based on our analysis, which takes into account current global warming trends, the glacier area of Balkhash Basin may shrink by about one-third, but will not disappear completely.

Most scientific publications support an opinion that the glacier runoff must increase with glacier retreat due to global warming. Our research shows that the result of modern climate warming is glacier runoff decrease. But despite the reduction of glaciers, annual runoff volumes and the interannual distribution remained unchanged during the last decades. During the same period, norms of atmospheric precipitation and maximum snow water equivalent in the zone of runoff formation remained stable also. All these allow the proposal of the existence of a certain compensation mechanism. Research, based on data analysis of repeated photogrammetric surveys of a group of glaciers and temperature regime of permafrost in Zailiyskiy Alatau, suggests that such mechanism can be an increased (with climate warming) participation of melting waters of ground ice (buried glaciers, rock glaciers, permafrost) in the river runoff.

Taking into consideration, also, the fact that reserves of ground ice in high mountains of Central Asia and Kazakhstan are equivalent to present-day glacier resources and in the Chinese mountains they are two times greater, and also considering that the rates of melting ground ice are much lower than those of the open glaciers, we believe that even if the present-day trends in climate warming are preserved, the above-mentioned compensating mechanism may work during several coming decades as minimum. Hence it can be predicted that the ongoing degradation of glaciers will not cause considerable reduction in the runoff and regional water resources, at least up to the next decades.

Materials from 33 years of geothermal monitoring testify to the ambiguous reaction of perennial and seasonal permafrost to climate changes in the Northern Tien Shan. Regularities of perennially frozen ground distribution and features of spatial changes of depth and character of seasonal freezing of soils in the Northern Tien Shan are reflected in the regional structure of altitudinal geocryological zonality

The total area of perennial permafrost tracts in the subzone with sporadic spreading amounts to not more than 1–2%, it comes up to 30% at insular spreading, it rises up to 70% at intermittent distribution, and at dense one, it is not less than 90% of the total subzone area. There are not any conditions for formation of local masses of permafrost on a southern macro-slope; therefore the subzone of sporadic spreading is absent there. Altitude borders of other subzones are located there on 300–400 m above in comparison with the position on a northern slope.

During the period of 1974–1995, ground temperature in layer of perennial permafrost had increased 0.2–0.5°C, but after that, has been retained at -0.2°C during the last 11 years.

Reaction of strata of seasonal permafrost to climate changes remains ambiguous in different landscape conditions. Seasonal thawing depth increased from 3.2 m in 1974 up to 6.0 in 2001, but then that process stopped. In 2002, the mentioned figure decreased to 4.6 m., and for the last 5 years, it has remained stable, with small interannual oscillations within the limits of 4.6–4.9 m

Since 1975 to 1998, in high mountains (at an altitude of 3000 m), the changing of seasonal freezing depth on slopes on different expositions has not been supervised, but its increase was marked during the last 4 years: by 1.0 m at northern and 0.3 m at southern slopes.

A steady trend of reduction of seasonal freezing depth has been observed in mid-hill terrain up to the top forest border (from 1400–1500 to 2700 m) for the period 1974–1998. Data relating the value of mentioned characteristic on two opposite, but equal by construction, slopes of the central part of the Zailiyskiy Alatau Range at absolute altitude of 2570 m can be viewed here. So during mentioned period, on loamy-detritus soils of the northern slope, the seasonal freezing depth decreased by 25 cm, and on idem ground of the southern one, it reduced by 21 cm.

The tendency in changing of frost penetration depth on northern and southern slopes was not shown for the period since 1975 up to 1998 at absolute height of 3000 m. However, the increasing tendency of seasonal freezing depth on slopes with different expositions has been marked for the last 3 years. That is connected with the reduction of snowiness. Thus, it has increased for 1 m on northern and for 0.3 m on southern slopes.

The revealed tendency of reduction of seasonal frost penetration depth for mid-hill terrains continued till 2002. It has been stable since 2003 to present time, and has been changing just slightly during the years.

Under all other equal conditions, interannual fluctuations of freezing intensity and its depth depend on two factors: distinctions of soils temperatures before frost penetration, and terms ratio between the beginning of ground freezing and snow cover formation.

General glacier recession in the Tien Shan conducts to an output of moraine sediments up to the surface. They are transferring from subglacial status to a subaerial one. This process essentially changes an orientation of cryogenic and post-cryogenic processes on fresh moraines. When small glaciers recede, permafrost moraine layers are released. In subaerial conditions, they are subjected to thawing on 1–2 m depth from the surface during summer seasons; that is, the layer of seasonal thawing appears.

During large glacier receding, long-term frost penetration of the transparent and blind talik systems occurs alongside with the mentioned process. Transformation of the moraines from subglacial to subaerial condition generates a modification of character of relief formation; new processes and effects appear. There is an especially distinguishing thermokarst among them and different modifications.

The thawing of buried ice, accompanied with partial thawing of accommodating permafrost moraines, conducts to subsidence formation, which is filled usually with the water from melted snow. In such a way, thermokarst lakes are forming. Some of the subglacial lakes originate from water-current ponding by the sediments of cryogenic landslips. Thus, fresh moraines are the same kind of arena for intensive formation of lakes of various genesis, sizes, and configurations. There were only 10 lakes, (with the capacity of each one over 10,000 cubic meters) in the middle of 1960 on the northern slope of the Zailiyskiy Alatau. In 1980, that number has increased to 41, and by 1990, to 60. The last 10 years of aero-visual supervision of the glacial belt testify that their quantity significantly increased.

In addition to the lakes, soliflucton processes are developing on fresh moraines, and also active subglacial rock glaciers are forming. Loose, fragmental deposits of fresh moraines increase the supply area of subglacial rock glaciers that had been formed earlier, in that way stimulating the moving of the last ones. Icings are emerged and destroyed; structural grounds are formed; and frost weathering processes are activated on fresh moraines.

Phase Changes of Water as a Basis of the Water and Energy Exchange Function of the Cryosphere

V.V. Shepelev
Melnikov Permafrost Institute, SB RAS, Yakutsk, Russia

Water exists on our planet in all three of its phases within the temperature and pressure ranges found on Earth, resulting in very high activity and extent of phase transitions of water. This involves intensive phase interaction of water, that is, water transfer from the liquid state to the gaseous state and back, from the solid state to the gaseous or liquid state, etc.

Many authors emphasized the importance of the interphase form of water movement. Priklonsky (1958), in his general characterization of groundwater formation, considered such phase changes as evaporation and freezing to be the main types of water movement in the ground. Khodkov & Valukonis (1968), in their discussion of the main types of movement of natural waters, ranked the phase transition of water above other forms of water movement or migration. It is this form of water movement that Vernadsky (1960) had in mind, suggesting the existence of the phase field of the Earth, which encompasses the upper lithosphere and the near-surface atmosphere. The necessity of applying the theoretical knowledge on water physics to investigations of global water cycles was underlined by Sokolov (1966). He noted, in particular, that the role of the cryosphere as a water-exchange system is very high, though remains little studied.

Research on interphase interactions of water is complicated by the fact that all the basic states of water are not phase-homogeneous, but phase-heterogeneous. In other words, the phase mixing effect is inherent in water. In the atmosphere, water is present in liquid, solid, and gaseous states. Similarly, surface ice and ice-rich permafrost contain some amounts of the liquid and gas forms of water. The phase heterogeneity of the basic states of water can be explained by the fact that in nature, there exists no absolutely pure water in either of the states—liquid, solid, or gas. Water in any macroscopic volume is, above all, a dispersion medium in which various microscopic impurities, such as mineral, organic and other solid particles and compounds, are dispersed. The high surface energy of these microscopic particles causes the formation of water microphases on their surface, which intensively exchange water with the surrounding macroscopic medium, determining to a large measure its water- and energy-exchange function.

In the ground, the microscopic phase dispersion of water is boosted, so to say, by the mechanical dispersion of the soil. For example, pellicular water in the zone of aeration is a liquid microphase of water, which actively exchanges water and interacts with the surrounding pore air medium. Similarly, unfrozen interfacial water in ice-rich permafrost can be considered a liquid microphase of water which is in dynamic equilibrium with the pore ice medium. This explains, among other factors, the well-known concept of equilibrium unfrozen water content in frozen ground (Tsytovich 1945, 1959). This concept implies that the unfrozen water content in frozen ground varies with changes in temperature and external pressure of soil or rock. Phase changes of unfrozen water to ice and back occur even under very slight changes in ground temperature or external pressure.

Hence the basic physical states of water reflect only its macroscopic phase homogeneity, characterizing one or another phase of bulk water as a continuum. From the microscopic point of view, the main physical states of water are phase heterogeneous, and this drives the water and energy exchange and other important processes in the Earth's atmosphere, hydrosphere, lithosphere, and, certainly, cryosphere.

Considering the crucial role the phase changes and phase interactions of water play in the cryosphere, and in order to quantify the water and energy exchange function of the cryosphere, it is proposed that the global cycles in climatic circulation of water are distinguished as follows: cryoatmogenic, cryohydrogenic, atmolithogenic, glaciogenic, and cryolithogenic (Table 1).

The *cryoatmogenic cycle* is related to sublimation of water vapour in the atmosphere, that is, the phase changes of water from gas to solid and back, and subsequent falling on the earth surface as large snow and ice formations.

The *cryohydrogenic cycle* is driven by the formation of seasonal river ice, lake ice, icings, and ground ice in the active layer of permafrost and the subsequent melting of these seasonal ice forms, as well as snow cover.

The *atmolithogenic cycle* involves evaporation, condensation and sublimation of water in the zone of aeration, which can be viewed as subsurface atmosphere and where intensive moisture transfer occurs, linking the atmosphere and the lithosphere.

The *glaciogenic and cryolithogenic cycles* are caused by long-term, rather than seasonal, climatic fluctuations. In cold periods, the solid phase of water in glaciers and permafrost increases in volume and mass. Conversely, in warm periods, liquid water resources increase due to melting of glaciers and ground ice. Hence the glaciogenic and cryolithogenic cycles

Table 1. Characteristics of the cryosphere as a water and energy exchange system.

Main water and energy cycles	Mass of water involved in annual water cycle, kg	Energy released (+) or taken up (-), Wt
Cryoatmogenic	$1.0 \cdot 10^{13}$	$\pm 0.9 \cdot 10^{12}$
Cryohydrogenic	$2.6 \cdot 10^{16}$	$\pm 2.75 \cdot 10^{14}$
Atmolithogenic	$0.2 \cdot 10^{11}$	$\pm 0.18 \cdot 10^{10}$
Glaciogenic	$0.25 \cdot 10^{16}$	$- 2.6 \cdot 10^{14}$
Cryolithogenic	$2.5 \cdot 10^{13}$	$- 0.26 \cdot 10^{12}$

have a trend effect on the annual balance of the liquid phase of natural waters, causing a long-term decrease or increase in their volume and sea level.

For quantitative comparison of the cycles identified above, the mass of water involved annually in each water-exchange cycle and the thermal energy released or taken up during the changes in state of water have been estimated based on available information (see Table 1). It should be noted that the water-exchange functions of some of these cycles are as yet little understood and poorly quantified. This is particularly true for the cryoatmogenic and atmolithogenic cycles, thus requiring the establishment of special-purpose research and observation programs to obtain more reliable estimates. As for the rest of the cycles, the quantitative characterization of their water- and energy-exchange function has been based on the analysis of relatively representative data.

The values presented in the table indicate the crucial role of the cryosphere in the global water and energy budget, allowing us to call it a fluctuating cryogenic phase shell of our planet. Further investigations of the water- and energy exchange function of the cryosphere in this perspective will contribute to a better understanding of the role of the cryosphere in total global exchange of energy and matter, and help detect the changes in these processes due to natural factors and human impacts.

Acknowledgments

The author would like to thank Larisa Fedorova and Lilia Prokopieva, Melnikov Permafrost Institute, for assistance in preparation of this manuscript.

References

Khodkov, A.E. & Valukonis, G.Y. 1968. *The Formation and Geological Role of Groundwater.* Leningrad: Izd-vo Leningradskogo Universiteta, 216 pp.

Priklonsky, V.A. 1958. Basic experimental issues in groundwater formation research. In: *Transactions of the Laboratory of Hydrogeological Problems*, Vol. XVI. Moscow: Izd-vo AN SSSR, 86-105.

Sokolov, B.L. 1996. New results of experimental investigation on the lithogenic component of river runoff. *Vodnye Resursy* 23(3): 278-287.

Tsytovich, N.A. 1945. On the theory of equilibrium state of water in frozen ground. *Izvestia AN SSSR, Seria Geograficheskaya* 5–6: 61-67.

Tsytovich, N.A. 1959. Physical processes and phenomena in freezing, frozen and thawing soils. In: *The Principles of Geocryology (Permafrost Studies). Part I. Permafrost Science*. Moscow: Izd-vo AN SSSR, 108-152.

Vernadsky, V.I. 1960. *Selected Papers*. Vol. 4, Book 2. Moscow: Izd-vo AN SSSR, 651 pp.

Near-Surface Stress and Displacement Measurements from Vehicle Passage Over Frozen Ground

S. Shoop
USA-CRREL, Hanover, NH

Introduction

The freezing and thawing process creates extreme strength changes in frost-affected soils. These seasonal changes in strength both benefit and decrement performance of engineered structures and have a particularly severe effect on transportation systems and horizontal construction. We have developed modeling capability for simulating the complicated impact of freeze-thaw layering on transportation systems. These models have been used in several applications: vehicle operations on freezing/thawing ground, seasonal deterioration of unsurfaced roads, freeze-thaw effects on pavement structures, and aircraft operations on frozen ground (Shoop et al. 2006, Haehnel et al. 2005, Parker et al. 2006). An additional challenge occurs in obtaining data for the development and validation of these models. The measurement of stress and strain in soils is problematic even in unfrozen ground, but to use these instruments in frozen ground, they must also be able to sustain the hardships of prolonged cold temperatures on fluid, sensor, and electronic components.

The objective of this project was to build an instrumented test section where we could observe the changes in vehicle-induced stress and displacement at different frost depths. Three test cells, consisting of two feet of sand (SM), silt (ML), and clay (CL) soils were constructed over a well-compacted sand roadbed. The test cells were instrumented for stress or pressure and for displacements, as well as for temperature and moisture profiles. Trafficking of the test sections was done periodically at various frost depths ranging from no frost to over 20 inches of frost.

Instrumentation

Based on a survey of the limited instruments available for stress and strain measurements in soils, few of which had been used within frozen ground, three types of instruments were chosen. For stress measurement, we chose two methods: the National Soil Dynamics Laboratory (NSDL) Soil Stress State Transducer (SST) and a pressure pad by Sensor Products LLC. Soil displacements were measured using extensometers designed by Geokon.

The SSTs are designed by the engineers at NDSL to measure total stress state (Nicols et al. 1987). Three SSTs were obtained on-loan from NSDL. The SST consists of 6 semiconductor pressure sensor transducers installed in a small sphere to measure stress in 3 perpendicular directions and in 3 additional offsets as shown in Figure 1. The sensors are installed with the z direction upward and the x and y directions facing rearward to the left and right side of the approaching vehicle. The six pressure measurements

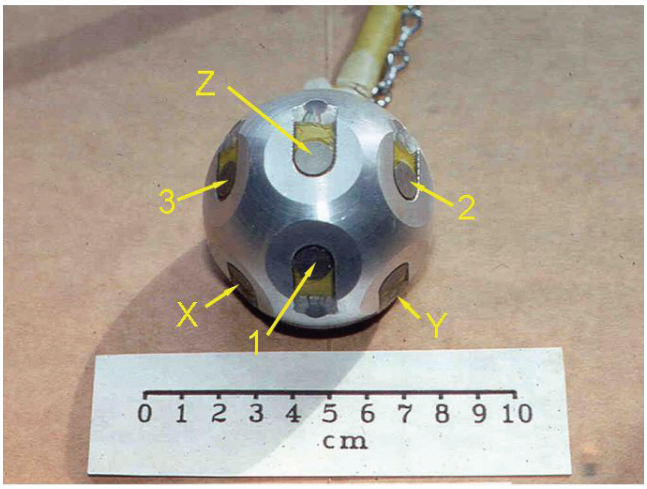

Figure 1. The National Soil Dynamics Laboratory Soil State Transducer (SST) showing the directions of the six pressure sensors.

can be used individually as a measure of pressure in the specific direction, or they can be used in combination and converted to principle stresses with direction cosines or stress invariants. The SST transducers were coated with Teflon to reduce shear on the sensor surface, and the entire sensor was wrapped in plastic and carefully oriented in the soil. The SSTs were installed at five-inch depth within each of the three test soils.

The second stress measurement system was the pressure pads. The pressure pad is a matrix of piezoelectric sensors 19.2 by 19.2 inches with 0.6-inch grid spacing. The sensors are protected with a urethane rubber cover and measure the pressure normal to the pad surface. The pad can capture the tire contact stress distribution as it rolls over the surface, and was specifically designed for use on deformable surfaces, although not to be buried in soil or frozen. Prior to installation in the soil, the pressure pads were tested under vehicle loading while on a hard surface. Two pads were then buried at two inches within the sand and the silt test sections.

The displacement of the soil was measured by installing extensometers modified to measure near-surface displacements. The base of the extensometers was placed below the test soils. Four to six rods of different lengths were fixed to each base, and an anchor plate was attached to the top of each rod as the extensometer was buried. The anchor plates were designed to move with the soil and independent of the other rods in the cluster. Three clusters of extensometers were installed in each test soil: one 6-anchor cluster was placed on the center line of the target wheel path, and two 4-anchor clusters were placed 6 inches to either side of the wheel path center line.

Experiments

The experiments consisted of trafficking vehicles across the test sections during freezing. After several baseline tests were done to make sure all of the instrumentation was working correctly, the ground was allowed to freeze to different depths either naturally or with assistance from freezing panels. At specific frost levels, a vehicle and trailer assembly was driven across the test section and the soil stresses and displacements were measured. Prior to trafficking, the test section was fully characterized by temperature and moisture profiles, density, and various strength measurements.

Results

Even though these instruments had never been used in frozen ground, we were pleased with the performance of all of the instrumentation. The SSTs performed flawlessly during the course of all of the experiments. Although a final reduction of the data into principle stress components has not yet been done, the direction stress data shows the stress from the bow wave in front of each tire, and then the large vertical pressure spike as each tire passes over the sensor. The stress magnitudes clearly diminish as the ground freezes above the sensor and then diminish further as the frost envelopes the entire sensor.

The pressure pads were perhaps the most finicky of the instruments and several of the fine wires within each pad were broken during the course of installation and testing. The configuration of the pads and their calibration were also not entirely suitable for the test conditions so that absolute values of the contact stresses are not reliable. Nonetheless, the trends show the tire contact stresses decreasing and the contact area increasing when the pad is buried, and slight decrease in contact stresses and increases in area as the ground freezes.

As a perfect compliment to the stress measurements, the soil extensometers also show the bow wave prior to each wheel as well as the strong vertical displacement when each wheel passes over the sensor, as shown in Fig. 2. In addition to the displacements measured during trafficking, the extensometers also measure the plastic deformation from the vehicle compacting the soil and the frost heave during freezing.

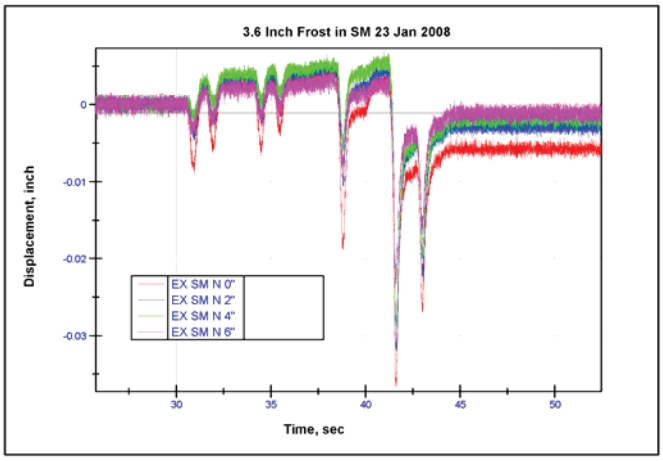

Figure 2. Extensometer data for a four-axle vehicle pulling a multi-axle trailer on sand with 3.6 inch frost (bottom).

Acknowledgments

This project benefited from many engineers and technicians that assisted with design, calibration, and installation of these instruments including Thomas Way and Dexter LaGrand of NSDL, Jason Blume at Sensor Products LLC, Tony Simmonds and Jim McCrae at Geokon, and Glenn Durrell, Chris Williams, Mike Parker, Barry Coutermarsh, Lynette Barna, and Rosa Affleck at CRREL.

References

Haehnel, R., Shoop, S., Affleck, R. & Janoo, V. 2005. Finite element modeling of a thawing pavement structure. *Proceedings, 7th International Conference on the Bearing Capacity of Roads, Railways and Airfields, Trondheim, Norway, 27–29 June.*

Nichols, T.A., Bailey, A.C., Johnson, C.E. & Grisso, R.D. 1987. A stress state transducer for soil. *Transactions of the ASAE* 30(5): 1337-1341.

Parker, M., Barna, L., Shoop, S. & Haehnel, R. 2006. Comparison of Finite Element Model (FEM) data and Single Point Layered Elastic Model (SPLEM) data of a C130 operating on a frozen runway structure. *13th International Cold Regions Conference, Orono, Maine, July*.

Shoop, S., Haehnel, R., Janoo, V., Harjes, D. & Liston, R. 2006. Seasonal deterioration of unsurfaced roads. *ASCE J. of Geotechnical and Environmental Engineering* 132(7): 852-860.

Formation of Frost Boils and Earth Hummocks

Yuri Shur
University of Alaska Fairbanks Department of Civil and Environmental Engineering, Fairbanks, Alaska, USA
Torre Jorgenson
ABR – Environmental Research and Services, Inc., Fairbanks, Alaska, USA
Mikhail Kanevskiy
University of Alaska Fairbanks Institute of Northern Engineering, Fairbanks, Alaska, USA
Chien-Lu Ping
University of Alaska Fairbanks Agriculture and Forestry Experiment Station, Palmer, Alaska, USA

Existing hypotheses of frost boils and earth hummocks formation generally are limited to climatic and active layer processes within a simple two-component system. Based on our field studies and literature review, we have identified two other important factors: vegetation, which affects active layer depth and organic-matter accumulation, and permafrost aggradation, which affects heave and thaw settlement. Accordingly, we have developed a conceptual model of a four-component system involving climate, vegetation, active layer, and permafrost.

A model consists of five stages in the development of frost boils and earth hummocks (Fig. 1). The first three stages describe formation of frost boils, which generally occur in high- to mid-arctic tundra ecosystems. The last two stages depict the evolution of frost boils into earth hummocks, which typically occurs under the slightly warmer climates of the low arctic and taiga regions, or in response to warming climatic conditions.

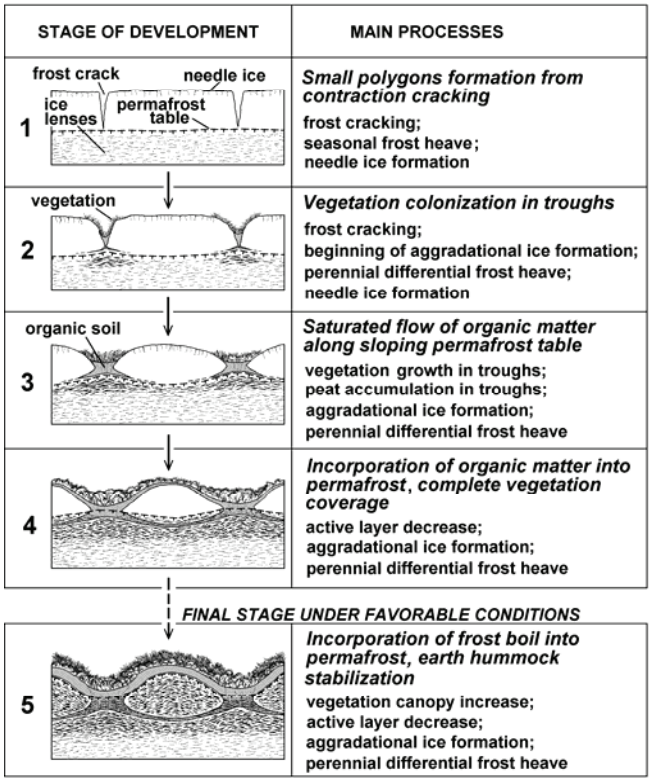

Figure 1. Stages of frost boils and earth hummocks formation. Seasonal segregated ice within the active layer is not shown.

First, small (0.5–3 m) polygons form under a bare soil surface due to frost cracking. This process is typically limited to the high- to mid-arctic, where the low temperatures and thin snow allow sufficient contraction cracking. The contraction cracking generally is limited by the thickness of the active layer because of the small-scale of the features, as opposed to the deeper cracking associated with the larger-scale contraction associated with development of ice-wedge polygons. These small polygonal forms are widespread in the Arctic as noted by ecologists, pedologists and permafrost scientists.

Second, vegetation colonizes the protected microsites of the shallow troughs that develop over the cracks. The surface of frost-boils is usually elevated above the surrounding inter-boil areas, and therefore, is susceptible to wind erosion, especially during winter freeze when the surface becomes elevated by seasonal frost heave. Needle ice prevents vegetation colonization of polygon centers.

Third, further vegetation growth and organic-matter accumulation in troughs change the thermal properties of the soil, causing the depth of the active layer to steadily decrease. In response, segregated ice forms at the top of the aggrading permafrost table, creating an intermediate layer with distinctly different soil and ice morphology (Shur 1988). Gravimetric moisture content in this layer often exceeds 100%. The aggrading ice causes the ground surface to heave. This perennial frost heave differs from seasonal frost heave in the active layer, because it is cumulative and leads to formation of long-term existing features. Features formed by perennial frost heave exist for tens to thousands of years. The differential relief caused by perennial frost heave in frost-boil systems varies from centimeters to decimeters.

At this stage, movement of organic matter from troughs under frost boils becomes important. The permafrost table develops ridges beneath the vegetated areas and concave depressions, or "bowls," beneath the frost boils. Because the permafrost table slopes at the margins of the bowls, organic matter formed in inter-boil areas creeps or flows under saturated conditions into the voids and cracks. There are two possible mechanisms for this gravitational movement of saturated organic matter down to the permafrost table. First, contraction cracks continue to develop, particularly at the interface of the organic matter and the mineral soil. During summer thaw, saturated organic matter, which tends to be moderately or highly decomposed, flows down the cracks.

Second, the thawing of segregated ice, which is formed during fall freeze-back at the top of the permafrost table, leaves voids that are filled with mobile organic matter. Over time, a concave layer of organic matter mixed with mineral soil accumulates at the permafrost table underneath the mineral frost boil. In some boils the organic matter can be discontinuous, but can be traced to its source—the vegetated inter-boil area.

Penetration of organic matter along the bottom of the active layer leads to further decrease in the active layer, aggradation of ice, and incorporation of organic matter in the upper permafrost. This in turn further raises the surface of the frost boil and increases differentiation in seasonal frost heave between boils and inter-boil areas. At this stage, a mature frost boil has developed, and can become the climax stage in the Arctic. While this downward movement of organic matter around frost boils is similar to elements of circulation as described by Mackay's model (1980), there are important differences. In our model, organic moved downward accumulates in the aggrading permafrost. There is no upward movement of solid material, and only dissolved organic can move to the freezing front in winter or desiccated surface in summer.

Fourth, frost boils evolve into earth hummocks when vegetation and organic-rich soil eventually expand to cover the entire surface. This spread may occur over a long time and may be assisted by climate warming. The spread leads to further decreases in depth of the active layer and additional accumulation of aggradational ice above the layer of organic matter, with more accumulation of aggradational ice and more perennial frost heave.

Fifth, sufficient vegetation develops, peat accumulates, and seasonal thaw no longer reaches the base of the former frost boil. Eventually, the thawing front can become limited to the surface peat and no longer penetrates the mineral frost boil. Our previous studies (Shur & Ping 2003, Shur et al. 2005, 2006) explained evolution of the earth hummocks from the frost boils due to growth of vegetation at the surface of frost boil and subsequent accumulation of aggradational ice. Recent observations by Kokelj et al. (2007) support such an explanation.

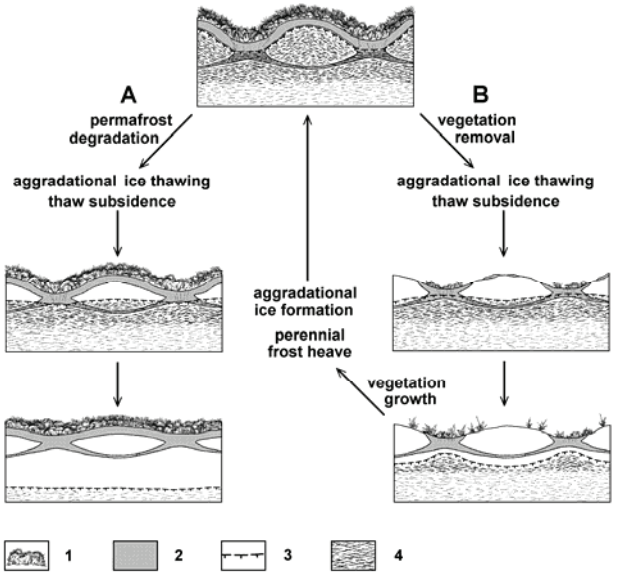

Figure 2. Degradation of earth hummocks due to (A) permafrost degradation and (B) denudation of vegetation, resulting in the regressive frost boils formation. 1 – vegetation; 2 – peat, organic matter; 3 – permafrost table; 4 – ice lenses.

Earth hummocks once fully developed are very sensitive to environmental changes because they evolved in conjunction with ice aggradation below the active layer. Disturbance to the surface, such as by fire, or climate warming can lead to degradation of the extremely ice-rich soil beneath the active layer. In a time scale of hundreds to thousands of years, climate change is the most important process leading to the degradation of the permafrost and earth hummocks (Fig. 2A). In a time scale of years, denudation of vegetation is the leading process in the formation of regressive frost boils. Vegetation recovery, however, can reverse the process and stabilize or restore the earth hummocks (Fig. 2B). Such processes were evident in field observations by Kokelj et al. (2007).

Acknowledgments

Work was supported by NSF grants ARC-0454939 (to YS), ARC-0454985 (to MTJ), EPS-0346770 (to MZK), and OPP-0120736 (to CLP).

References

Kokelj, S.V., Burn, C.R. & Tarnocai, C. 2007. The structure and dynamics of earth hummocks in the subarctic forest near Inuvik, Northwest Territories, Canada. *Arctic, Antarctic and Alpine Research* 39: 99-109.

Mackay, J.R. 1980. The origin of hummocks, western Arctic coast, Canada. *Canadian Journal of Earth Science* 17: 996-1006.

Shur, Y.L. 1988. The upper horizon of permafrost soils. *Proceedings of the Fifth International Conference on Permafrost*, *Trondheim, Norway, August 2–5, 1988*: 867-871.

Shur, Y., Ping, C.L. & Jorgenson, M.T. 2006. Soil formation in frost-boil environment. *Proceedings of 18th World Congress of Soil Science, Philadelphia, Pennsylvania, USA. July 9–15, 2006*. Abstract 106-8.

Shur, Y.L., Ping, C.L. & Walker, D.A. 2005. Comprehensive model of frost boils and earth hummocks formation. *Proceedings of the Second European Conference on Permafrost, Potsdam, Germany, June 12–16, 2005*: 79.

Shur, Y. & Ping, C. 2003. The driving force of frost boils and hummocks formation. *Eos Trans. AGU* 84(46), Fall Meet. Suppl., Abstract C21B-0823.

The Role of Lakes in Carbon Transfers from Permafrost to the Atmosphere: Eight Mile Lake, Alaska

James O. Sickman, Guntram Von Kiparski, William Vicars
Department of Environmental Sciences, University of California, Riverside, Riverside, CA 92521, USA
Edward A.G. Schuur, Jason G. Vogel
Department of Botany, University of Florida, Gainesville, FL 32601-8526, USA

Introduction

In the permafrost-affected watersheds of the arctic and subarctic, dissolved carbon losses can be considerable, accounting for over 37% of net ecosystem production (NEP) in some regions (Judd & Kling 2002). Therefore, dissolved carbon flux may be an important determinant of regional carbon balance in the arctic and subarctic, but more research is needed to understand how these fluxes will respond to warming and whether downstream lacustrine systems can attenuate losses of terrestrial carbon.

The main objectives of our study were to quantify hydrologic losses of carbon along a gradient of permafrost thaw in the Eight Mile Lake watershed and assess the effect of in-lake processes on watershed carbon losses.

Materials and Methods

Field site

The Eight Mile Lake Watershed (EMLW) is located near Healy, Alaska, near Denali National Park. Elevation range in the watershed ranges from 656 to 1057 m, and the drainage area is 1108 hectares. The maximum depth and area of the lake are 3 m and 69 hectares. Within the catchment, plot studies have been initiated across a gradient of permafrost thaw: severely thawed (Old Karst), moderately thawed (New Karst), and not thawed. (Tussock)

Field and laboratory measurements

During 2006, we measured concentrations and estimated fluxes of dissolved organic carbon (DOC) and dissolved inorganic carbon (DIC) at both plot (<5 ha) and watershed (>1000 ha) scales. Stream samples were collected every two-days using ISCO automated samplers during snowmelt (May and June) and manually every week during July through September (surface streams freeze in late September). Soil water was sampled at multiple depths within the tundra active layer using specialized lysimeters called Multisamplers (Martin et al. 2003). Inlet stage was measured in a culvert to a road that bisects the watershed and used to weight lake inlet and outlet chemistry for computation of C fluxes to the lake. Annual runoff was estimated as the difference between watershed precipitation and evaporation.

DOC was measured by high-temperature catalyzed combustion on a Shimadzu TOC 5000. Dissolved CO_2 (the dominant form of DIC in these low pH (<5.6) waters) was determined using headspace equilibration followed by measurement of CO_2 partial-pressure using a LICOR LI820.

Results

Controls on hydrologic carbon fluxes

Soil water DOC concentrations increased significantly along the natural gradient of permafrost thaw in the Eight Mile Lake watershed. (Fig. 1A). In severely thawed soils, concentrations typically ranged from 40 to 60 mg L^{-1}. In moderately thawed soils, DOC concentrations were ca. 30–40 mg L^{-1}, and in unthawed soils, usually 20–25 mg L^{-1}. We observed no strong seasonal trend in soil water DOC. DOC concentrations in the lake inlet responded strongly to hydrology; pulses of DOC were observed during snowmelt runoff (30 mg L^{-1}) and summer rain events. DOC concentrations in the lake outlet were lower and more constant (~10–16 mg L^{-1}) (Fig. 1B).

Dissolved CO_2 in soil water increased with active layer depth with concentrations between 10 to 27 mg C L^{-1} below a depth of 30 cm (Fig. 2C). Dissolved CO_2 concentrations in

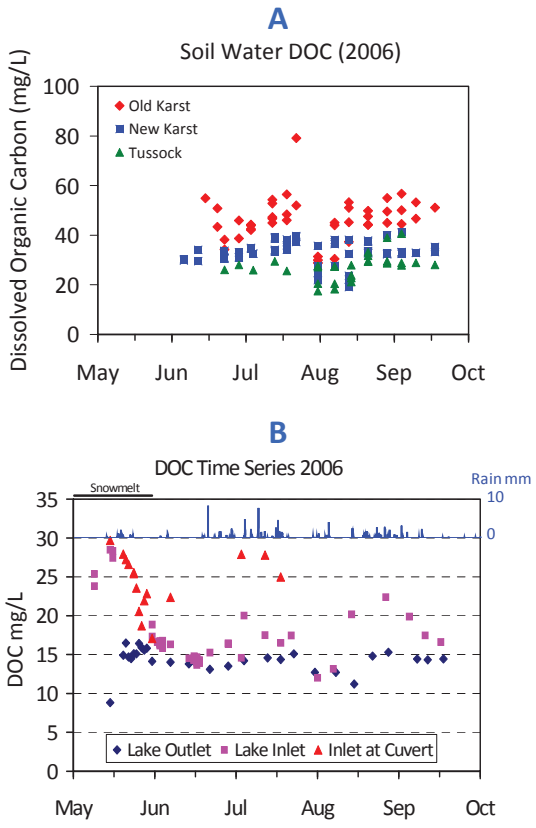

Figure 1. Patterns of DOC concentrations at Eight Mile Lake Watershed during 2006.

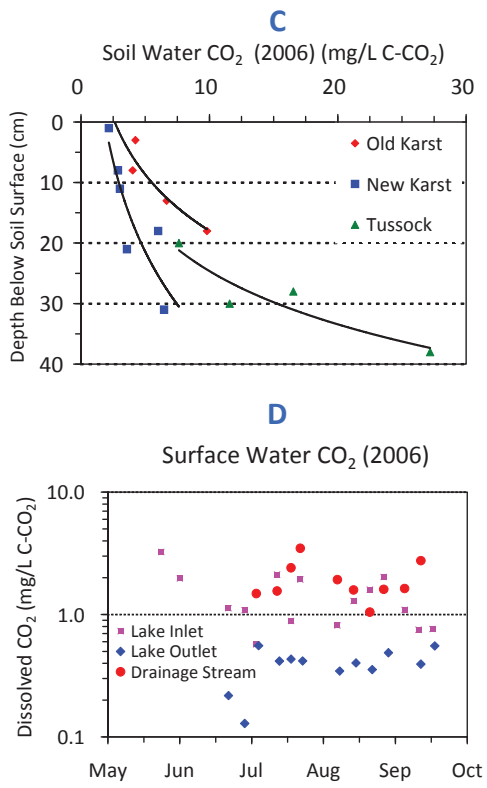

Figure 2. Patterns of DIC concentration at Eight Mile Lake Watershed during 2006.

surface inflows to the lake ranged from ca. 1–4 mg C L^{-1}; at the lake outlet concentrations were <0.5 mg C L^{-1} (Fig. 2D).

Watershed fluxes of water and carbon

During water year 2006, summer rainfall contributed the majority of annual precipitation and runoff (Table 1). Total runoff was estimated to be 19.4 cm. Using lake bathymetry measurements, we computed a lake volume of 1.73 x 10^6 m^3, yielding a mean lake residence time of 0.80 years.

Using stage-weighted inlet and outlet chemistry and estimates of annual runoff, we made a first approximation of the carbon budget for the lake (Table 2). The lake was a strong sink for DOC and CO_2 produced in terrestrial portions of the watershed and was a small net source for POC. Overall, in-lake processing of C accounted for a 50% reduction in watershed yield of C.

Conclusions

At Eight Mile Lake, permafrost thawing, hydrology, and in-lake processes had strong effects on watershed yield of carbon. Concentrations of DOC in soil waters in severely thawed plots were double those in intact tundra. The depth of the seasonal active layer was positively related to dissolved CO_2 concentrations in soil water. Hydrologic flushing (snowmelt and summer rain events) produced spikes in DOC concentration. Waters entering the lake had higher DOC and CO_2 concentrations than waters exiting the lake. Outgassing of CO_2 took place rapidly, while losses of DOC occurred over the course of weeks to months. Preliminary input/output estimates show that the lake consumes about 50% of the carbon entering via runoff.

Table 1. Water balance for the Eight Mile Lake watershed.

Component	Winter/Snowmelt	Summer
Snow/Precipitation Depth (cm)	10.0	22.7
Runoff Coefficient	0.80	0.50
Runoff Depth (cm)	8.0	11.35
Runoff Volume (m^3)	8.86 x 10^5	1.26 x 10^6
Lake Volume/Residence Time	1.73 x 10^6 m^3 / 0.80 years	

Table 2. Dissolved C input/output for Eight Mile Lake. Terrestrial yield is watershed yield at the inlet of the lake. Catchment yield is yield at the outlet of the lake.

Carbon-Flux	Terrestrial Yield (g/m^2)	Watershed Yield (g/m^2)	Net Change Due to In-lake Processes (g/m^2) / % of input
DOC	5.2	2.3	-2.9 / -56%
Dissolved CO_2	0.40	0.07	-0.33 / -83%
POC	0.38	0.59	+0.21 / +55%
DOC + CO_2 + POC	6.0	3.0	-3.0 / -50%

Acknowledgments

We thank Christian Trucco for field assistance. Funding was provided by the National Science Foundation, Division of Environmental Biology.

References

Judd, K.E. & Kling, G.W. 2002. Production and export of dissolved C in arctic tundra mesocosms: The roles of vegetation and water flow. *Biogeochemistry* 60: 213-234.

Martin, J.B., Hartl, K.M., Corbett, D.R., Swarzenski, P.W. & Cable, J.E. 2003. A multi-level pore-water sampler for permeable sediments. *Journal of Sedimentary Research* 73: 128-1325.

Recent Climatic Changes in Yakutia

Yu.B. Skachkov
Melnikov Permafrost Institute, SB RAS, Yakutsk, Russia

Introduction

Yakutia is the largest administrative region of the Russian Federation, occupying an area of 3.1 million square kilometers. Most of the region is underlain by continuous permafrost. Being the product of climate, permafrost is a sensitive indicator of its long-term changes. In view of the predicted permafrost degradation due to global warming and its negative consequences, it is extremely important to gain complete information on recent air temperature variations in the region.

During the past years, several works have been published on the general assessing of climate changes in Siberia and the Far East over different periods of time (Ippolitov et al. 2007, Izrael et al. 2006, Pavlov & Malkova 2005, and others). The present paper continues the previous research made by the author over the period 1966–1995 (Skachkov 2001), and using the new data of the last decade, informs on the current rate of climate warming in Yakutia.

Data and Calculation Technique

To assess trends of the changes of the annual average air temperature (T_{air}) over the period 1966–2005 throughout Yakutia the following actions have been carried out:

1. selection of 29 weather stations with accurate unceasing observation data (Fig. 1).
2. calculation of the linear trend of the air temperature and annual air temperature amplitude and their variance.
3. assessment of the linear trends.

The linear trends significance was estimated with the student criteria by the determination coefficient squared value R^2. The determination coefficient shows the linear trend deposit in the general variation of the analyzed parameter. The parameter variation trend would be considered significant if its confidence level equaled or surpassed 95% ($P \geq 0.95$). With the sample size of 30 years, it conforms to $R^2 \geq 14\%$, and of 40 years, $R^2 \geq 12\%$.

Figure 1. The plan of location of the stations selected for analysis.

The temporal series data of the mean monthly air temperature were used in the analysis. The meteorological observation data were obtained from the climatologic handbook and monthly magazines and also from the USA National Ocean and Atmosphere Agency database (http:www.ncdc.noaa.gov). Trend parameter calculations were performed with Microsoft Excel 97.

Results and Discussion

The mean annual air temperature field analysis shows that T_{air} over the observed area widely varies from -16.7°C (Oymyakon) to -5.6°C (Vitim). High interannual variability of the mean annual air temperature is the peculiarity of extreme continental climate endemic for the major territory of Yakutia. The fluctuations of T_{air} over the observed period in the mean from all stations amount to 4–5°C. The lowest fluctuations of T_{air} (-3.4°C) were noticed in Batamaya, and the highest (-5.6°C), in Tiksi and Chulman.

The global warming started in the end of 1960s over the majority of the Northern Hemisphere including Yakutia. From 1966 to 1989, the warming in this area passed on rather smoothly and had almost zonational increment of the air temperature. The highest increment values (1°C and more) are noticed in central and south Yakutia. Toward the north, there is noticed the decrease of temperature increment. The air temperature trend values of the Laptev Sea shore, island stations and northwest of Yakutia are subzero at this time (Skachkov 2001).

The early 1990s saw spatially variegated temperature increase appear sharply throughout Yakutia. Southward of the latitude 64°N, the air temperature increment amounted to 1.5–2°C and more; northwest and northeast Yakutia was 0.5–1°C. It is significant that the major contribution to the

mean annual air temperature increase pertains to winters that became warmer, especially in central and south Yakutia.

Turning to the data-processing analysis over the period 1966–2005, the trend analysis shows a warming tendency throughout Yakutia, though it is spatially variegated. The trend speed over the area varies from 0.16°C/decade to 0.63°C/decade. The highest trend speed was noticed in central Yakutia, and the lowest, in the regions northward of latitude 64°N. In the arctic regions of Yakutia, the warming is irreducible. The annual air temperature increment appeared mostly due to a rise in the number of warm winters.

The trends comparison for the period 1966–1995 and 1966–2005 shows that the warming rate has decreased and, in some regions, paused during the past decade.

As before (Skachkov 2001), no latitudinal or submeredianal allocation regularity is noticed.

Apart from linear trend parameters assessing the relative contribution of the trend component in the general temperature dispersion, the air temperature increment trends of Yakutia proved to be reliable in 12 points (the annual and winter period values). The reliable trends for the summer period were noticed only in 3 points.

Recently in the scientific literature, there have emerged reports that the current warming in the regions of the Northern Hemisphere is accompanied by a decrease of annual air temperature amplitudes. At the same time, it is noticed that the lowest temperatures grow faster than the highest ones.

Interannual variability is inherent for both mean annual and mean seasonal air temperatures. Therefore the amplitude T_{air}, being one of the most important parameters of the continentality, changes from year to year. The amplitude T_{air} is defined as the difference of the mean warm (T_{sum}) and cold seasons of year (T_{win}). The cold period includes the whole period with subzero temperatures at each station, while the warm period, the period with the above-zero temperatures. At the island Kotelnyi, the most northern station in Yakutia, the warm period lasts only 2 months; at the stations Tiksi, Kjusjur, Jubilejnaja, Cokurdah, and Olenek, the warm period lasts 4 months. At the other stations of the region, summer lasts for 5 months.

The winter air temperature increasing faster then the summer one, the difference (T_{sum} - T_{win}) falls. The most significant and noticeable decrease (to 1.5–2.5°C) descended in central Yakutia.

Conclusion

Significant warming has been noticed in Yakutia during the past decades. The highest air temperature rise in the region occurred in the 1980s. Warming has obviously paused since the mid 1990s in some of the Yakutia regions. There are some points showing a trend of temperature decrease. In general, the 1966–2005 trends notably decrease compared with those of 1966–1995. There has been noticed a fall in continentality over the last decades in central Yakutia.

The insignificant summer period warming almost throughout the republic territory shows minimal cryolitozone reaction to the climate changes that should not cause much alarm. This thesis is also proved with longstanding research (Skachkov et al. 2007).

References

Ippolitov, I.I., Kabanov, M.V. & Loginov, S.V. 2007. Spatial and Temporal Scale of the Observed Warming in Siberia. *DAN* 412 (6): 814-817.

Izrael, Yu.A., Pavlov, A.V., Anokhin, Yu.A., Myach, L.T. & Sherstyukov, B.G. 2006. Estimators of Climate Elements Changes in Permafrost Regions of Russian Federation. *Hydrology and Meteorology* 5: 27-38.

Pavlov, A.V. & Malkova, G.V. 2005. *Recent Climate Changes of the North of Russia: the Album of Small-Scale Maps*. Novosibirsk: Academic Press Geo, 54 pp.

Skachkov, Yu.B. 2001. Present-day variations of air temperature in Yakutia. *Proceedings The Fifth International Study Conference on GEWEX in Asia and GAME, Aichi Trade Center, Nagoya, Japan, October 3-5, 2001*.3: 758-761.

Skachkov, Yu.B., Skryabin, P.N. & Varlamov, S.P. 2007. The Results of 25-years Monitoring Research of Cryolitozone at the Chabyda Station (Central Yakutia). *Proceedings of International Conference Cryogenic Resources of the Polar Regions, Salekhard, June 17-20, 2007*. Puschino, ONTI PNC RAN, 1: 167-170.

Permafrost, Parameters, Climate Change, and Uncertainty

Andrew G. Slater
NSIDC, University of Colorado, Boulder, CO, USA
David M. Lawrence
National Center for Atmospheric Research, Boulder, CO, USA

Introduction

Recently observed changes in the state of permafrost are many and varied. Appearance and disappearance of lakes, degradation of ice wedges, and changes in river channel morphology are several of the processes that have been linked to thawing of permafrost and warming of soil temperatures. Osterkamp (2007) suggests that permafrost at West Dock, Alaska, has warmed about 3.7°C since 1976 and may have warmed greater than 6°C since 1900. While most modeling efforts to assess the effects of future climate change on permafrost and frozen ground indicate that there will be substantial change, the magnitude and extent of the change is still uncertain (e.g., Lawrence & Slater 2005; Zhang et al. 2008). Part of the uncertainty in permafrost simulations can be associated with somewhat external factors such as simulation of snow or specification of soil and vegetation parameters. Here we present a sensitivity study of such inputs and parameters.

Methods

Model

A simple analytic model following the method of Kudryavtsev (Sazonova & Romanovsky 2003) was applied to estimate the current and future state of permafrost. The model produces a steady-state solution under the assumption of constant sinusoidal temperature forcing. The model also accounts for the presence of snow, vegetation, and the organic matter above the mineral soil. The primary inputs to the model are the mean annual air temperature, annual amplitude of air temperature, and the mean snow depth over the winter period. Parameters required by the model include soil texture, so as to compute thermal conductivity and heat capacity as well as estimates of snow thermal conductivity. The model is applied on a 100 x 100 km EASE equal-area grid for the region covered by the pan-arctic drainage basins; this region extends down to 45°N in places.

Data

Temperature data was derived from the ECMWF 40-year reanalysis project. This data has been shown to produce. Average snow depth and density was obtained as the ensemble average from five land surface models (CHASM, CLM, ECMWF, NOAH, and VIC) that had performed 23-year simulations over the region (Slater et al. 2007). The estimates from the models are more consistent with station-based measurements than the available passive microwave satellite data; this is particularly so in the eastern Siberian uplands, where satellite products have known biases. Parameter data for soil texture properties is based on the map of Zobler (1986) and has been used extensively in large-scale modeling experiments. To simplify matters and maintain a conservative estimate of change, soil moisture was prescribed at 99% of saturation.

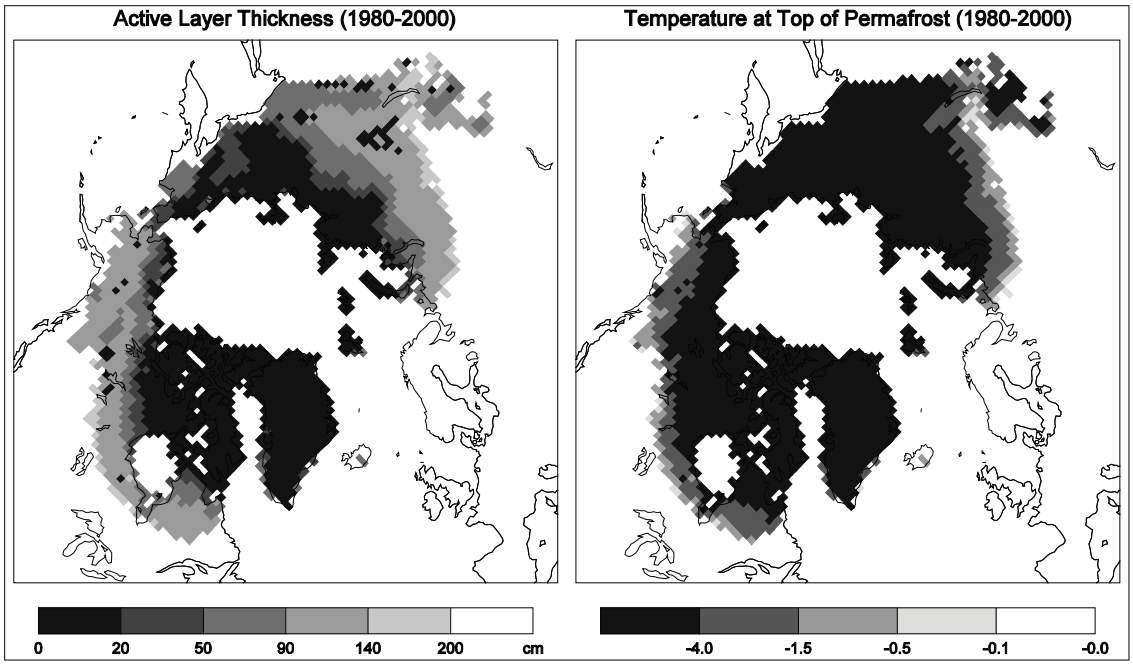

Figure 1. Analytic model simulation of present-day permafrost. Temperature is in degrees Celsius. Disregard results for Greenland.

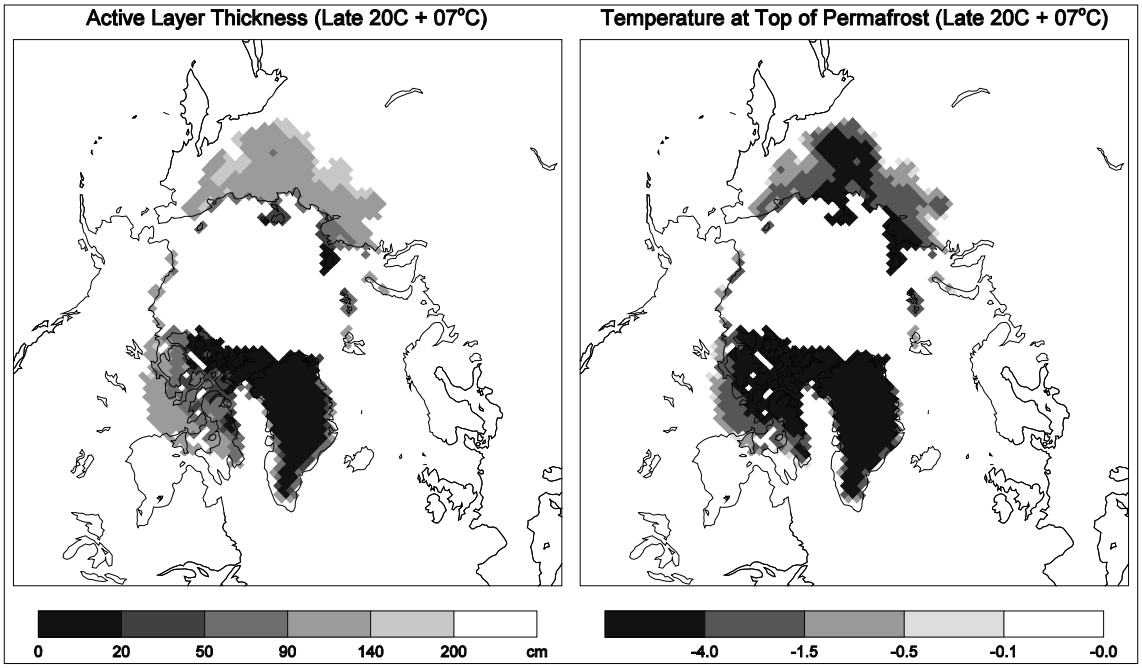

Figure 2. Analytic model simulation of permafrost with a simple climate change scenario of 7°C increase in annual mean temperature.

Results and Summary

Figure 1 shows the results from the analytic model for the late 20th century. Estimates of the active layer depth as well as the mean annual temperature at the top of the permafrost are shown. These results compare favorably to the estimated distribution of permafrost as given by the International Permafrost Association map. Temperature at the top of the permafrost is shown in four ranges that are roughly considered to compare to permafrost zones of continuous, discontinuous, sporadic, and isolated.

Some initial simple experiments were performed in which mean annual temperature was raised by 7°C, which is within the range of changes expected to be seen over the Arctic in the coming century according to IPCC estimates (Fig. 2). Snow depth and cover for these preliminary simulations was kept the same as present day. Estimates of changes in snow depth and cover vary widely, but Räisänen (2008) suggests that there is a likelihood of deeper snow over mid-winter in the high latitudes, as the increased precipitation will still fall in solid phase. This will no doubt have an impact on the future state of permafrost. Further simulations assessing sensitivity to snow and soil will be carried out and presented at the NICOP meeting.

Acknowledgments

This work was partially funded by NSF grants ARC-0229769 and ARC-0531040.

References

Osterkamp, T.E. 2007. Characteristics of the recent warming of permafrost in Alaska, *J. Geophys. Res.* 112: F02S02, doi:10.1029/2006JF000578.

Räisänen, J. 2008. Warmer climate: Less or more snow? *Clim. Dynamics* 30(2–3): 307-319.

Sazonova, T.S. & Romanovsky, V.E. 2003, A model for regional-scale estimation of temporal and spatial variability of active layer thickness and mean annual ground temperatures. *Permafrost Periglac. Process.* 14: 125-139.

Slater, A.G., Bohn, T.J., McCreight, J.L., Serreze, M.C. & Lettenmaier, D.P. 2007. A multimodel simulation of pan-Arctic hydrology, *J. Geophys. Res.* 112: G04S45, doi:10.1029/2006JG000303.

Zhang, Y., Chen, W. & Riseborough, D.W. 2008. Disequilibrium response of permafrost thaw to climate warming in Canada over 1850–2100. *Geophys. Res. Lett.* 35: L02502, doi:10.1029/ 2007GL032117.

Zobler, L. 1986. *A World Soil File for Global Climate Modeling.* NASA Tech. Memo 87802, Natl. Aeronaut. and Space Admin., Goddard Inst. for Space Stud., New York.

Thermal State of Permafrost in Canada: A Contribution to the International Polar Year

Sharon L. Smith
Geological Survey of Canada, Natural Resources Canada, Ottawa, Canada
Antoni G. Lewkowicz
Department of Geography, University of Ottawa, Ottawa, Canada
Christopher R. Burn
Department of Geography and Environmental Studies, Carleton University, Ottawa, Canada

Introduction

Over the past two to three decades, Canadian researchers have established and maintained a permafrost monitoring network consisting of boreholes in which ground temperatures are measured. Data collected from these sites have facilitated documentation of recent trends in permafrost thermal state (e.g., ACIA 2005, Smith et al. 2005, Lemke et al. 2007). The monitoring network is also a key contribution to the Global Terrestrial Network for Permafrost (GTN-P).

The International Polar Year (IPY) provides the opportunity for the Canadian permafrost community and the International Permafrost Association (IPA) to conduct a well-designed global and coordinated multinational programme of permafrost observations in order to explore present conditions and their spatial and temporal variability. It also provides the opportunity to fill gaps identified in the Arctic Climate Impact Assessment (ACIA 2005), such as improved characterization of permafrost-soil-vegetation interactions and the upgrade and maintenance of long-term monitoring networks. Canada is a key contributor to the IPA-led IPY project, the Thermal State of Permafrost (TSP).

In 2007, a collaborative proposal from the Geological Survey of Canada, University of Ottawa, and Carleton University was successful in acquiring funding from the Canadian Government's IPY program for TSP-Canada. This funding along with additional support acquired by the principal investigators and collaborators has facilitated the establishment of new monitoring sites both prior to and during IPY. This paper provides an overview of the TSP-Canada project and summarizes the establishment of new monitoring sites

Objectives of TSP-Canada

Canada's contribution to the Thermal State of Permafrost project will examine the ongoing impacts of climate change on permafrost conditions and meet the following objectives: (1) obtain a set of standardized temperature measurements for all Canadian monitoring sites (snapshot); (2) produce a dataset and map of contemporary permafrost ground temperatures contributing to a global effort; (3) increase the number of monitoring sites prior to and during the IPY; (4) provide data to verify models to improve prediction of future permafrost conditions; (5) examine permafrost-climate linkages and feedbacks to explain observed change and variability in permafrost conditions; and (6) develop outreach products on permafrost change for northerners and present results in scientific papers.

The project builds on an existing network of approximately 100 thermal monitoring sites established over the last two to three decades (see Smith et al. 2003). A key objective of the project is enhancement of the network to fill thematic and regional gaps.

Network Enhancement

New sites

Over the last two to three years, new monitoring sites have been established that contribute to TSP-Canada and GTN-P. Most of these new boreholes are less than 20 m deep, but some extend to depths of 50 m. These new sites consist of cased boreholes in which permanent thermistor cables have been installed.

More than 50 new boreholes have been established in the western Arctic (Fig. 1). The majority of these are located in the Mackenzie Valley and Delta region and were established to provide baseline information essential for design and environmental impact assessment of hydrocarbon development projects. In particular, an important gap north of Norman Wells (north of ~65°N) has been addressed. Sites were also established in collaboration with communities in the NWT and Yukon Territory. Several new boreholes have been established in the central and southern Yukon.

Through collaboration with Parks Canada, seven new boreholes were established in northern Manitoba. These sites are located in Wapusk National Park and York Factory and represent a variety of terrain conditions. They provide better coverage in the area to the west of Hudson Bay.

Dataloggers have been connected to most of the thermistor cables to provide a continuous record of ground temperatures. For sites established prior to summer 2007, preliminary ground temperature data have been collected that provide a baseline against which to measure change. All new sites will be visited in 2008, and this should provide a record of ground temperatures for the first year of IPY.

Plans for additional site establishment

During 2008, further site establishment is planned. Additional sites will be established in the central and southern Yukon. Deep boreholes to depths of 50 to 100 m are proposed with a number of them to be established in collaboration with a mineral exploration company. Efforts

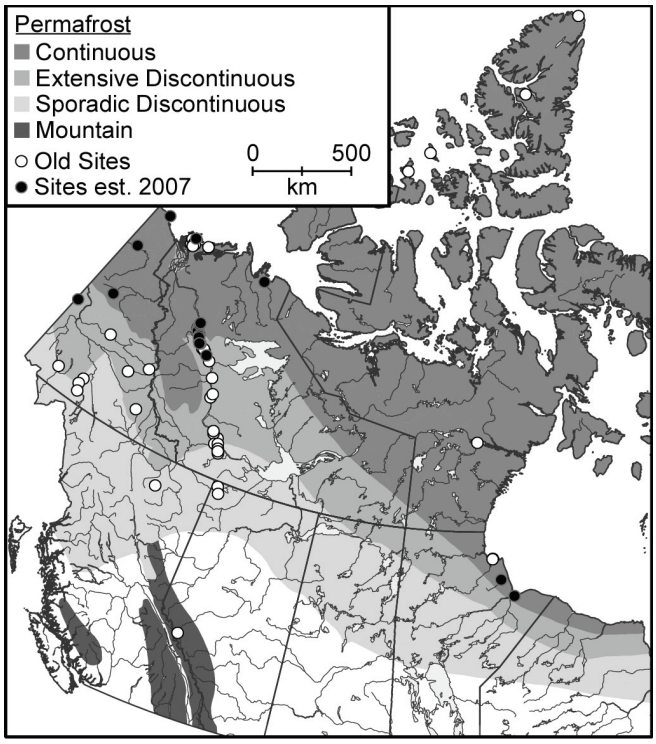

Figure 1. Location of new monitoring sites established in 2007 and older monitoring sites established over the last 30 years in the central and western Arctic. Note: for clarity not all new sites established in the Mackenzie Valley and Delta are shown.

will also be made to locate and re-occupy some boreholes which were drilled in the 1980s by an engineering consulting company and for which historic data are available.

A significant gap still exists in Nunavut. Through collaboration with communities and the territorial government, attempts will be made to establish five to ten monitoring sites to fill gaps in the central and eastern Arctic. Data generated from these sites will also be utilized by the communities for land use planning and development of strategies to adapt to climate change impacts on infrastructure.

Summary

TSP-Canada is the main Canadian contribution to the IPA led IPY project on the thermal state of permafrost. Over the last two to three years, progress has been made towards the objective to establish new monitoring sites in advance of and during IPY. Additional new sites are planned to increase coverage in the central and southern Yukon Territory and the central and eastern Arctic. Preliminary data have been collected from the first IPY year, with further data collection planned between 2008 and 2009. These data provide new baseline information on permafrost thermal state for the Canadian permafrost region and will be utilized to meet the objectives of TSP-Canada.

Acknowledgments

Support for network enhancement has been provided by the Canadian government's IPY program, Natural Resources Canada, Northern Energy Development Memorandum to Cabinet, Canadian Foundation for Climate and Atmospheric Sciences, University of Ottawa, Carleton University, Polar Continental Shelf Project, and NSERC. Sites in the western Arctic were established in collaboration with Indian and Northern Affairs Canada.

References

ACIA 2005. *Arctic Climate Impact Assessment.* Cambridge University Press, 1042 pp.

Lemke, P., Ren, J., Alley, R.B., Allison, I., Carrasco, J., Flato, G., Fujii, Y, Kaser, G., Mote, P., Thomas, R.H. & Zhang, T. 2007. Chapter 4, Observations: changes in snow, ice and frozen ground. In: *Climate Change 2007: The Physical Basis. Contribution of Working Group I to the Fourth Assessment Report of the Intergovernmental Panel on Climate Change,* 337-383.

Smith, S.L., Burgess, M.M., Riseborough, D. & Nixon, F.M. 2005. Recent trends from Canadian permafrost thermal monitoring network sites. *Permafrost and Periglacial Processes* 16: 19-30.

Smith, S.L., Burgess, M.M., Romanovsky, V. & Brown, J. 2003. The Global Terrestrial Network for Permafrost (GTN-P): Status and preliminary results of the thermal monitoring component. Extended Abstracts Reporting Current Research and New Information. In: W. Haeberli & D. Brandova (eds.), *Proceedings of the Eighth International Conference on Permafrost*, *Zurich, Switzerland, July 2003*: 153-154.

Tides as a Possible Reason for Massive Ice Beds Formation

Sergey A. Sokratov, German A. Rzhanitsyn
Faculty of Geography, Moscow State University, GSP–1, Moscow, 119991, Russia

Introduction

The argumentations on the genesis of massive ice beds discovered on wide territories of the Arctic and Subarctic have special meaning for the Russian permafrost scientific community. The critical point of the ongoing discussions turns out to be either marine or glacier origin of the massive ice beds, since this affects in whole the interpretation of the paleo-history of Northern Eurasia (Solomatin 2005). It should be emphasized that the massive ice beds of interest (*plastovye l'dy*) neither are a part of the Russian ground ice classification (Popov et al. 1985) nor a singled-out type of ground ice in the IPA glossary (van Everdingen 2005). From a terminology viewpoint, different genesis of the massive ice beds at different sites is the natural expectation. Recently, these massive ice beds are being classified by expected genetic types (Shpolyanskaya & Streletskaya 2004). However, the disagreement on either buried or in-site origin of seaside massive ice beds, especially, still exists due to uncertainties in explanations of the existence of saline-free massive ice lenses incorporated into salted marine sediments, the isotopic difference between the sea water and the massive ice lenses, and particularly the morphology interpreted as the deformation markings on some of the massive ice beds (Solomatin 2005).

Leaving aside the fundamental question of ice sheet existence over Northern Eurasia, the paleo-climate signal enclosed into the massive ice beds and their bearing strata is the product of the processes responsible for the formation, growth, and melt of an ice body. Since most of the known massive ice beds are found in the former or present coastal zones (Shpolyanskaya & Streletskaya 2004), it is worth considering coastal zones-specific processes as the possible participants in the massive ice beds formation and maintenance. The background of the reported investigation was to test the possibility that periodic natural fluctuations of groundwater level due to upthrust of groundwater runoff by tides play a part in ice lens formation. Such a mechanism, with favorable groundwater freezing climate conditions, allows for formation of saline-free ice lenses from groundwater with close to the atmospheric precipitations isotopic content in the saline marine sediments.

Tides and Groundwater Runoff

The result of field investigations at the White Sea coast (Pon'goma) was the confirmation of the dependence of groundwater level variation on the tidal regime, at least in the case of sandy ground and tides up to 2 m (Fig. 1).

The dependence observed by measurements in dug pits by automatic water level sensors was pronounced up to tens of meters from the shoreline. Figure 1 shows the results of

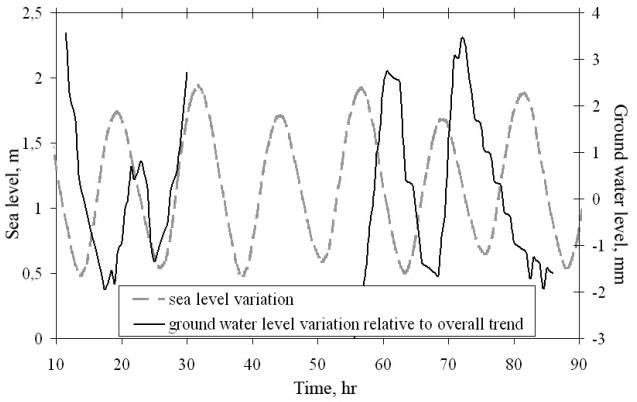

Figure 1. The correlation between sea level variation and groundwater level variation.

the groundwater level measurements in a dug pit 7 m from water's edge at maximal tide, 1 m above the maximal sea level. The variation is extracted from the overall change of groundwater level due to variability in precipitation and snowmelt, and represents about 10% of the overall variability. The delay between the extremums of sea and groundwater level variations is approximately 4 hr. Such dependence was not observed in another area of the coastal zone with clayey and peat grounds, despite high (up to 9 m) tides (Mezenskaya Bay, White Sea).

The field observations also demonstrated strong seasonal variability of the dependence of the groundwater level variability on tides up to disappearance of the propagation of the tides' signal at distance from the shoreline, caused by the amount and unevenness of the groundwater runoff. An important role in the tides' signal propagation was found to belong to the formation of an impermeable seasonally-frozen ground layer near the soil surface. Therefore, it was concluded that the relation between the tides and the groundwater level variation is different for territories with different texture of soil, is determined by the amount of the groundwater runoff and by the activity of tides, and varies considerably in dependence on the soil freezing conditions.

A study of thick deposits of ground ice in exposure at the Ural coast of Baidaratskaya Bay revealed their polygenetic origin. The analysis of the structural characteristics of the ice, however, suggested the possibility of participation of the proposed mechanism in ice lenses formation.

Groundwater Level Variation and Ice Lens Growth

The laboratory studies included modeling of the groundwater level change, periodically introduced upward into two-layer samples with unidirectional frost penetration

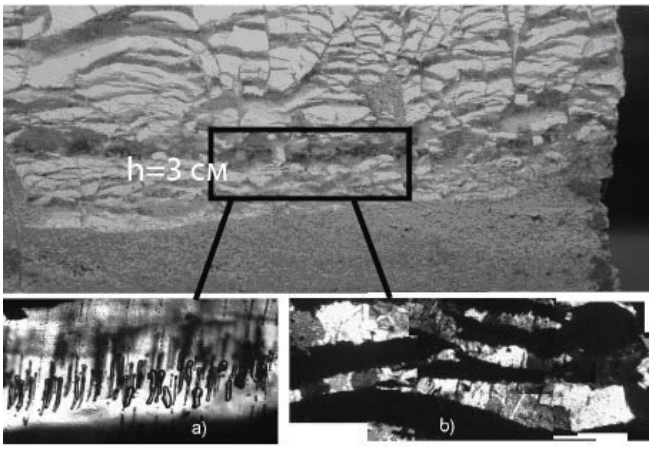

Figure 2. Structure of the ice schlieren near the boundary of the two layers of a sample. The top layer is montmorillonite; the bottom layer is fine sand.

from top downward. The top layers were made from different clay and the bottom layer, from sand (Fig. 2).

The ice-rich horizon and ice lens (up to 1.5 cm thick) were formed near the boundary between the layers during several tens of cycles of the alternating groundwater level variation. The microstructure of the ice filling the fractures in the clay is characterized by subparallel to the schlieren layering related to several stages of ice crystal formation and growth inside the fractures. The ice crystals normally had a columnar structure with the long axes in the heat flux direction regardless of the variation in orientation of the schlieren (Fig. 2a). The gas inclusions in central parts of the schlieren were mainly represented by large elongated allocations, and at the peripheral parts, by chains of small bubbles. Large elongated bubbles were usually oriented subperpendicular to the schlieren's boundaries. Large multilayered schlieren also contained thin chain-like gas inclusions parallel to the schlieren's strike which, together with microcracks, confirm rupturing of already existent ice schlieren and repetitive water freezing inside them (Fig. 2b). The arrangement and form of ice crystals and gas inclusions corresponds to the structural specific of the intrusive ice formed from small amounts of inlet water and is alike to those of the natural massive ice lenses.

Conclusions

The results of the studies verified the possibility of the formation of ice-saturated ground horizons by periodic variation of the groundwater level, with the tides as a possible reason of such periodic variation. A considerable number of conditions required for realization of such a mechanism determines spatial limitations of its manifestation at each time interval. However, long-term variation of sea level against the background of climate change concedes action of the mechanism in past and allows explanation of recent-time distribution of the massive ice deposits over wide territories and at considerable distances from the recent-time Arctic shoreline (Golubev 2007a, 2007b).

Acknowledgments

The project was supported by the Russian Foundation of Basic Research, grant No. 05-05-65115.

References

van Everdingen, R.O. (ed.). 2005. *Multi-Language Glossary of Permafrost and Related Ground-Ice Terms*. International Permafrost Association, 278 pp.

Golubev, V.N. 2007a. Periodicheskie izmeneniya urovnya morya kak faktor formirovaniya plastovykh zalezhei l'da. (Periodic variations of sea level as a factor of the tabular ice formation.) *Kriosfera Zemli* (*Earth Cryosphere*) XI(1): 52-61

Golubev, V.N. 2007b. Rol' morskikh gidrodinamicheskikh protsessov v formirovanii zalezhei plastovykh l'dov na arkticheskom poberezh'e. (The role of sea hydrodynamic processes in formation of the massive ice beds deposits at Arctic shore.) *Materialy Glyatsiologicheskikh Issledovanii* (*Data of Glaciological Studies*) 102: 32-40.

Popov, A.I., Rozenbaum, G.E. & Tumel', N.V. 1985. *Kriolitologiya.* (*Cryolithology*). Moscow: Moscow State University, 239 pp.

Shpolyanskaya, A.N. & Streletskaya, I.D. 2004. Geneticheskie tipy plastovykh l'dov i osobennosti ikh rasprostraneniya v Rossiiskoi Subarktike. (Genetic types of massive ice beds and specific of their distribution in Russian Subarctic.) *Kriosfera Zemli* (*Earth Cryosphere*) VIII(4): 56-71.

Solomatin, V.I. 2005. Gletchernyi led v kriolitozone. (Glacier ice in cryolithozone.) *Kriosfera Zemli* (*Earth Cryosphere*) IX(2): 78-84.

Preservation of the Alaska Highway

Eva Stephani
Department of Geology and Geological Engineering, Université Laval, Québec, Québec, Canada
Daniel Fortier
Institute of Northern Engineering, University of Alaska Fairbanks, Alaska, USA
Yuri Shur
Department of Civil and Environmental Engineering, University of Alaska Fairbanks, Alaska, USA
Guy Doré
Department of Civil Engineering, Université Laval, Québec, Canada
Bill Stanley
Yukon Highway and Public Works, Yukon Government, Whitehorse, Yukon, Canada

Introduction

Road construction in permafrost areas affects the thermal regime of frozen soils via removal of the vegetation, compaction of the soil, road cut, and use of black asphalt pavement, for instance. The thermal degradation of the permafrost causes the ground ice to melt and results in permafrost thaw settlement, as well as subsidence and cracking of pavement. In many northern areas, roads are now showing signs of instability as a result of permafrost degradation, which could be partly due to recent climate warming. According to the IPCC projection of climate warming, this situation will undoubtedly be exacerbated in the future (IPCC 2007).

The Alaska Highway is an essential and widely used communication link between Alaska, Canada, and the southern United States. The highway has a poor driving surface, and some sections of the embankments have experienced substantial settlement. Severe pavement subsidence, longitudinal cracking, and potholes could eventually threaten the structural integrity of the infrastructure. Sections of the Alaska Highway built on ice-rich permafrost might eventually require relocation or replacement with a different design, and sections built on permafrost with a lower volume of ice will require at least rehabilitation. Alternative designs and mitigation measures should be adopted in order to reduce maintenance costs. The Yukon Government has decided to implement a test section at Beaver Creek, Yukon Territory, Canada (62°20′N, 140°50′W). Engineering mitigation measures will be tested to control the degradation of the permafrost. Six techniques will be implemented at the Beaver Creek experimental road site: (1) Air convection embankment (ACE); (2) heat drain; (3) air duct cooling system; (4) thermo-reflective snow shed; (5) grass-covered embankment; and (6) light-colored aggregate bituminous surface treatments (BST).

The Alaska University Transportation Center is responsible for characterizing the stratigraphy at the test site and for determining the geotechnical properties of the permafrost prior to the construction of the road test section. The objectives of this paper are to outline the thaw-susceptible nature of the permafrost at the test site and to illustrate the challenges related to rehabilitation of degraded permafrost under the road embankment.

Methodology

Field methods

Thermal conditions at the Beaver Creek experimental site have been monitored since 1998 by means of thermistor cables. One cable is installed under the center line of the road, one cable is installed in the side slope of the embankment, and one cable is in the natural ground adjacent to the road. Air temperatures also have been monitored.

Drilling and coring operations at the test site were realized during summer 2007 in the natural ground adjacent to the road and in the berms. Permafrost cores from 17 boreholes were collected, sampled, and brought back in a freezer to the University of Alaska Fairbanks for laboratory analyses.

Laboratory methods

The cryostructure and sediment types of soil were identified. Each stratigraphic unit was identified by its pH, electrical conductivity, gravimetric and volumetric ice content, grain-size distribution, and thaw-settlement potential.

Preliminary Results and Discussion

The mean annual air temperature (1971–2000) at Beaver Creek is -5.5°C (Environment Canada 2008). The local extreme maximum was 32.8°C in 1982, while the local extreme minimum was -55°C in 1971 (Environment Canada 2008). The mean annual precipitation is 416.3 mm, of which 123.1 mm water equivalent falls as snow (Environment Canada 2008). Monthly mean air temperatures are 11.9°C, 14°C, and 11.2°C for June, July, and August, respectively. Air temperatures above and below freezing represent an average (1971–2000) of 1532.6 thawing degree-days and 3534.2 freezing degree-days, respectively (Environment Canada 2008).

The coring operations in the natural ground revealed the presence of very ice-rich syngenetic permafrost with buried inactive ice wedges. Three main stratigraphic units were identified: Unit 1 (0–0.5 m) is ice-rich peat. Unit 2 (0.5–6.5 m) is silt, which is ice-rich at the top (>2.0 m), ice-poor below (2.0–3.5 m), and ice-rich in the lower portion (3.5–6.5 m). The top of the ice wedge is located in the ice-poor layer around 2.5 m depth and extends down to at least 6.5 m. Unit 3 (6.5–10 m) is an ice-rich diamicton.

Figure 1. Longitudinal cracking along the shoulder of the Alaska Highway due to degradation of the underlying permafrost. The 1-m shovel (arrow) gives the scale.

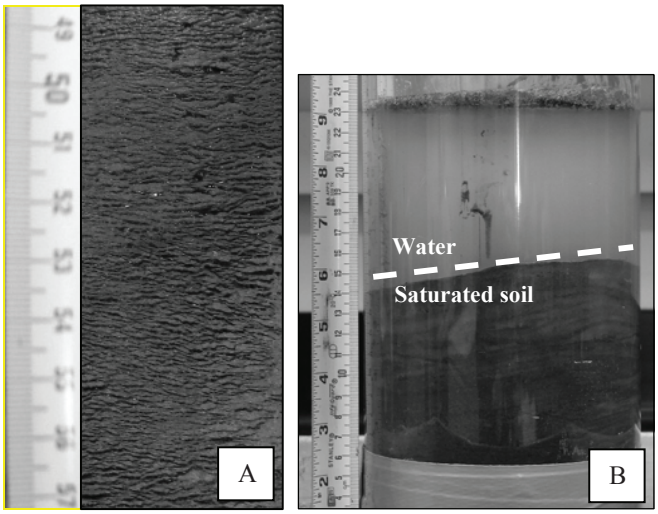

Figure 2. (A) Very ice-rich microlenticular cryostructure typical of syngenetic permafrost. (B) Thaw-settlement-potential test showing excess water upon thawing in the thaw-settlement cell.

In 2004, the maximum thaw depth in the natural ground was 70 cm. The maximum thaw depth under the center line of the road was located in the embankment material. However the mean annual ground temperature just below the embankment was close to the melting point (-0.3°C), and numerous observations (in 2007) of cracks and depressions affecting the central part of the road suggest that the thaw depth now reaches the natural ground where the embankment is thinner. In the side slope of the embankment, the thaw depth was located in the natural ground. Deepening of the active layer in the natural ground under the road creates thaw settlement and subsidence of the embankment (Fig. 1) Drilling realized in 2007 from the berm adjacent to the side slope of the embankment revealed that, locally, the maximum thaw depth can be located as deep as 2.5 m in the natural ground below the base of the embankment. If submitted to warming, these large unfrozen zones will progressively extend towards the center line of the road. The water content measured in the thawed layer under the embankment varied between 221% and 357%. This indicates that these zones are supersaturated due to the melting of ground ice and restricted drainage.

Table 1. Thaw strain values of the stratigraphic units.

Unit	Ice content	Thaw strain
1	Ice-rich	0.35
2 (0.5–2 m)	Ice-rich	0.41–0.61
2 (2–3.5 m)	Ice-poor	0.05
2 (3.5–6.5 m)	Ice-rich	0.43–0.54

The high water content can be explained by the prevalence of permafrost with an extremely ice-rich micro-lenticular cryostructure. This type of cryostructure is typical of syngenetic permafrost and usually has very high settlement potential (Fig. 2). Thaw-settlement tests indicate that the upper part of the permafrost (Units 1 & 2) is highly susceptible to thermal degradation (Table 1). A thaw-settlement test realized on the ice-poor layer of Unit 2 revealed that it is thaw-stable (Table 1). However this layer comprises a widespread network of ice wedges extending in the underlying ice-rich units. Ice wedges are highly thaw-susceptible and their geometric patterns make them prone to thermo-erosion and deep linear subsidence.

Conclusions

Drilling operations revealed the presence of large, unfrozen supersaturated zones under the road embankment. Rehabilitation of thawed permafrost under the road embankment will necessitate refreezing of the sediments. This could be long, due to the large amount of latent heat to extract from the water trapped in these unfrozen zones. Our study indicates that syngenetic ice-rich permafrost is highly susceptible to thermal degradation, especially where ice wedges are present.

Our preliminary results indicate that a detailed spatial geotechnical characterization of the permafrost (e.g., cryostructure, volumetric ice content, grain-size distribution, thaw-settlement potential, thaw-consolidation potential, ground thermal regime) is needed to determine the potential thaw susceptibility of the permafrost to climate warming and to find the proper engineering solutions to control permafrost degradation.

References

IPCC. 2007. *Climate Change 2007: The Physical Science Basis. Contribution of Working Group 1 to the Fourth Assessment Report of the Intergovernmental Panel on Climate Change,* S. Solomon, D. Qin, M. Manning, Z. Chen, M. Marquis, K.B. Averyt, M. Tignor, & H.L. Miller (eds.). Cambridge, UK & New York, USA: Cambridge University Press,

Specific Features of Dynamic Modeling of Processes in the South Siberian Permafrost

V.A. Stetjukha
State University, Chita, Russia

Introduction

The southern Siberian permafrost is unstable because of natural and climatic features of the region. First of all, the condition of soil stability due to external influences results from their high temperature (from -0.1 up to -2°C). Degradation of warm permafrost, even due to small external influences, occurs much more quickly than in other environments. Anthropogenic impacts can easily contribute to this environmental balance.

There are features of soil development due to physical processes in warm permafrost to consider. Traditional models for forecasting the impact on the environment do not give realistic results. They do not adequately model the physical processes in soils, as they do not take into account a number of processes that have an influence on soils. The cumulative impact of these neglected processes is significant. Anthropogenic factors are also not taken into account.

Modeling of Processes

The methods of heat-mass transfer and stress-strain modeling of unstable geocryological systems is presented. The method takes into consideration the adaptation of the model to natural and climatic conditions, and incorporation of technological influences like mining and building. Within a modeling framework, the advanced equations of heat-mass transfer and a technique for their use are developed. The publication is devoted to a process-modeling approach.

The basic process equations are given in an article by Stetjukha (2003a). The model includes the following components: thermo-gradient streams of moisture, the distributed sources and convective streams of thermal energy, a gravitational component for moisture streams, electro-osmotic streams of moisture, and thermal streams caused by electro-osmotic moisture streams. The equations of thermal and water balance on a surface of soil column takes into consideration evaporation, steepness and exposure of slopes, and anthropogenic influences. At the surface boundary, the temperature and moisture balances of a near-surface layer are carried out. The equations are solved in finite difference form.

In conditions of warm permafrost, the total influence of the neglected processes on depth of thawing and freezing that are not taken into account in the majority of traditional models, reaches 75%. Results are confirmed by calculations and comparison with observations.

To determine stresses and strains in soils, the finite element method is again used. In this case, the variable characteristics of loading in time, changeability of soil properties, changing boundary conditions, and temperature deformations are simultaneously taken into consideration.

The proposed technique of forecasting is based on the consideration of several interactions of soil properties and their change with time. This modeling technique differs from others in that it considers mining influences, the cumulative impact of several processes, the application of a system analysis approach, and a new way of considering factors that change with time. The offered model is exposed to continuous change and regulation owing to continuously changing conditions. The mathematical model is exposed to a continuous readjustment in connection with degradation of frozen soils.

The distinctive features of the dynamic model are:

- the coupling of the tasks of heat-mass transfer and geo-mechanics on the basis of developed mathematical models. Thus, researched soils are broken into elements of finite size by grids with common junctions;
- increase in quantity of factors (variables);
- the consideration of complex geometry to capture human-caused changes;
- transformation of impacts in time, caused by the presence of two fronts of freezing, by migration of moisture, by degradation of permafrost;
- ability to adjust, in time, physical-technical parameters of soils: porosity, density, deformation modulus, Poisson's coefficient, an angle of internal friction, coupling forces, tensile and compressive strengths based on change of temperature, humidity and pressure in various points of space. During periods of compression of soils, the thermal capacity, thermal conductivity, coefficient of linear expansion are corrected;
- the consideration of changes in soil properties due to changes in density as a function of their position in the soil profile;
- the consideration of temperature deformations;
- use of the method of combined influences on soil column (Stetjukha 2003b), which provides a determination of extreme values, adverse combinations, and the periods and sequence of loading of separate factors of influences;
- a determination of optimum accommodation of influences in time and space and definition of their optimum quantitative characteristics;
- application of imitating modeling (Stetjukha 2003b) for perfection of preliminary generated mathematical models.

The developed algorithm has the distinctive features shown in Figure 1.

The block model diagram is characterized by an extensive quantity of initial factors. The incorporation of the quantity of the initial data has required statistical processing. Within the framework of the block, the double-step process of correction

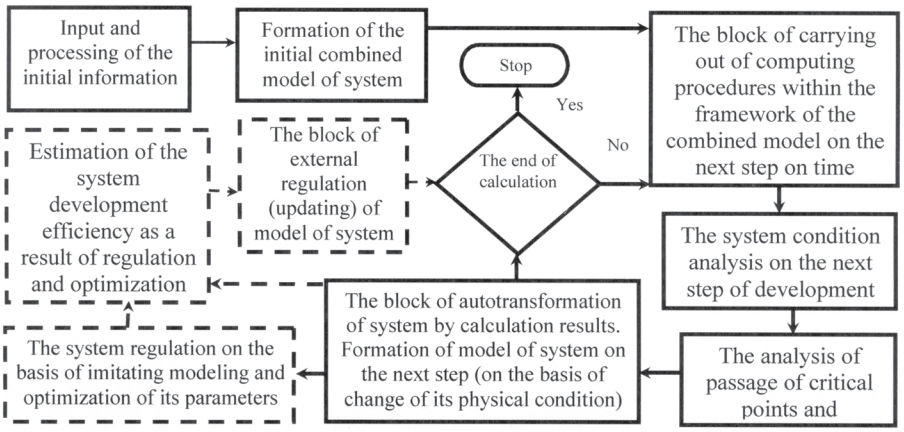

Figure 1. The integrated circuit of calculations with change of model in time.
□ = the common modules of system; ⬚ = the modules used at regulation.

of the complex model is carried out. Preliminary selection of parameters is carried out by generating alternative variants. The correlation analysis of factors provides a procedure of parameter selection on the degree of their importance. From initial analysis results, some parts of the complex model can be removed. Those factors staying are divided into two groups. First, those used in the performance of numerical experiments; second, those used for forming regression equations (Stetjukha 2003b). The second stage of model correction consists in quantitative correction of separate parameters. The algorithm of imitating modeling and optimization of system lays in the basis of this stage.

Computing procedures are carried out under the obvious circuit. It allows tracing the development of processes and inserting corrective changes.

The analysis of the system at each step of calculations takes into account changes of borders between thawed and frozen zones, achievement by soil of a condition of saturation by moisture, etc. The control points are analyzed. Control points are established on restrictions in the use of materials, on design factors, on restrictions of technological process, etc.

The major elements of the model are mechanisms of system adaptation to changed conditions. Thus two stages are allocated. One of them is updating of the model at the next step on the basis of change of a physical condition of system components. New dependences between factors are determined here. The second stage of adaptation of the combined model is its regulation on the basis of results of imitation modeling and optimization. The procedure of imitation modeling and optimization of processes includes performance of numerical experiments on a considered circle of tasks. As a result of regulation, a planned correction of physical-mechanical properties and other parameters of the system on the next step of external forcing are carried out.

Results of Calculation

The described modeling was carried out in an area of construction of a federal motorway, "Amur." Thawing of permafrost imbedded with ice on a slope with an inclination of 34° was predicted. Opening of frozen soils was carried out in the middle of April. The site with an open cut on a slope with the weak soils on 726 km of the motorway was considered. Up to a depth of 1.5 m on a slope, loam is encountered (layer 1); up to a depth of 2.5 m, fine loamy sand (layer 2); up to 4.4 m, loamy sand containing ice (layer 3); up to 5.6 m, fine sand containing ice (a layer 4); up to 6.5 m, loam, including rubble (layer 5); finally, a diorite. The depth and speed of thawing of separate layers during the warm period of the year were determined. Calculations established loss of stability of a slope in the middle of July. The predicted results are confirmed with observation.

The author carried out the forecast of results of impacts on other environments, such as where the soil/vegetation cover has been disturbed, preservation of frozen soils with use of heat insulating materials, shading screens, waterproof screens, and frozen veils (Stetjukha 2003b).

Depth of permafrost thawing under the bottom of the projected channel on a deposit of brown coal on a coal pit was determined. Predicted depth of thaw in 5 years was 5.5 m; in 10 years, 7.8 m. The threat of destruction of the channel is confirmed.

On the basis of the described method, a model of anthropogenic ices mound forecasting (Stetjukha 2003b) is developed.

The offered model of dynamic development of a natural-technological system allows objective estimation of temperature distribution, humidity, pressure, and deformation fields in conditions of changing influences on soil. Forecasting of processes in frozen soil has allowed the development of recommendations on optimum technological circuits of work during various seasons of the year.

References

Stetjukha, V.A. 2003a. Complex analytical modeling of processes in the south Siberian permafrost. *Permafrost*. Zurich, Switzerland: Swets and Zeitlinger Publishers: 1103-1106.

Stetjukha, V.A. 2003b. *Forecasting of a Mining Processes Influence for a Condition of a Permafrost Region Soils*. Chita: Publishing of Chita State University, 192 pp.

Understanding the Filling Process in Ice Wedges Using Crystallography, Isotopes, and Molar Gas Ratios

Mélanie St-Jean
University of Ottawa, Ottawa, Canada
Ian D. Clark
University of Ottawa, Ottawa, Canada
Bernard Lauriol
University of Ottawa, Ottawa, Canada
Paul Middlestead
University of Ottawa, Ottawa, Canada

Introduction

Much still remains unclear about ice wedge formation and filling process. Some researchers have indicated that the primary source of water for ice wedge growth is derived from snow meltwater (Washburn 1980, Lauriol et al. 1995). Other researchers suggest ice wedge growth by hoar-frost accretion in some cases rather than by the traditionally accepted process of water trickling into the wedge during the spring thaw prior to closure of the fissure.

Literature Review and Methodology

In Canada, the discussion concerning the identification of massive ground ice bodies is mostly focused on whether the ice is a remnant of the Laurentide ice sheet, or whether it is derived from segregation/injection processes. The majority of research in this field has been focused on the stratigraphic and petrographic characteristics of massive ground ice. The concentration and molar ratios of CO_2, O_2, N_2, and Ar gases entrapped in the ice, offer an innovative tool that allows differentiation between ground ice of glacial (firnified glacier ice), non-glacial intrasedimental, and surface origin. The principle behind this technique is that molar gas ratios of gases (O_2/Ar and N_2/Ar) entrapped in glacier ice tend to preserve an atmospheric signature modified by firn diffusion and gravitational settling, whereas the molar gas ratios of segregated-intrusive ice are significantly different from those found in the atmosphere and glacier ice due to the different solubilities of the gases in water (Lacelle et al. 2007, Cardyn et al. 2007).

This new extraction technique, modified from Sowers et al. (1997) and Cardyn et al. (2007) could also be useful in better understanding the filling process in ice wedges. The concentrations and molar ratios of atmospheric gases change during dissolution in water. Therefore, ice bubbles will have a gas composition closer to atmospheric air if the filling process involves hoar-frost accretion or snow, while ice bubbles resulting from snow meltwater filling will have a composition closer to gases exsolved from freezing water. An extraction line was built to isolate gases from ice, and a mass spectrometry technique was used to analyze the gas ratios (O_2/Ar and N_2/Ar).

Study Area

Ice samples used in this analysis were collected in northwestern Canada. What distinguishes these sites from others in the Canadian Arctic is that they are located outside and inside the limits of the last Pleistocene Cordilleran glaciation and could represent modern, Holocene, and Pleistocene ice bodies of different origin (see Fig. 1). They are ideal sites to have an extensive range of values of gas ratios. Here we present results that should enable us to distinguish the two different ice wedge-filling processes.

Old Crow, Yukon

A series of ice wedges along the Eagle, Bell, and Porcupine Rivers (Yukon) were sampled on the Holocene terrace to identify their period of growth and source of infiltrating water. Preliminary results from one ice wedge near Old Crow indicate ratios similar to gases dissolved in water, but

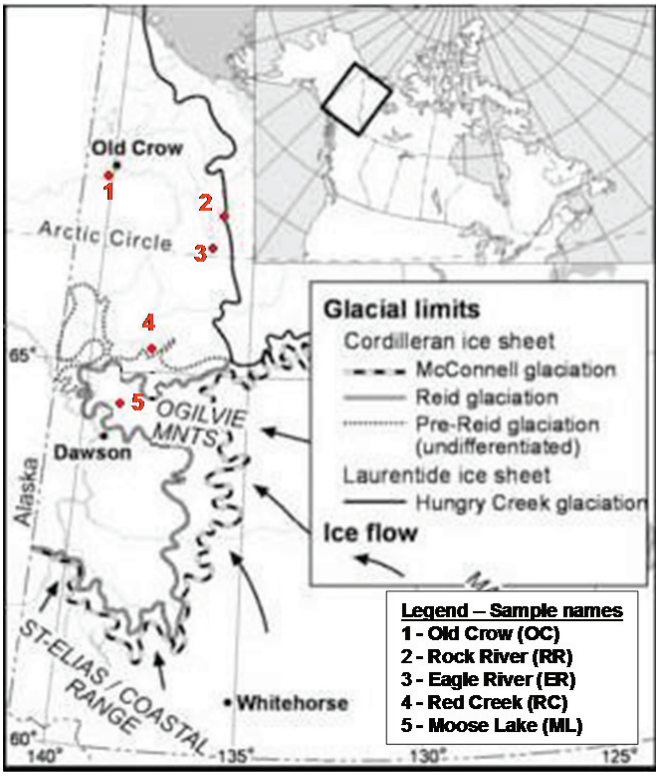

Figure 1. Study area (modified from Lacelle et al. 2007).

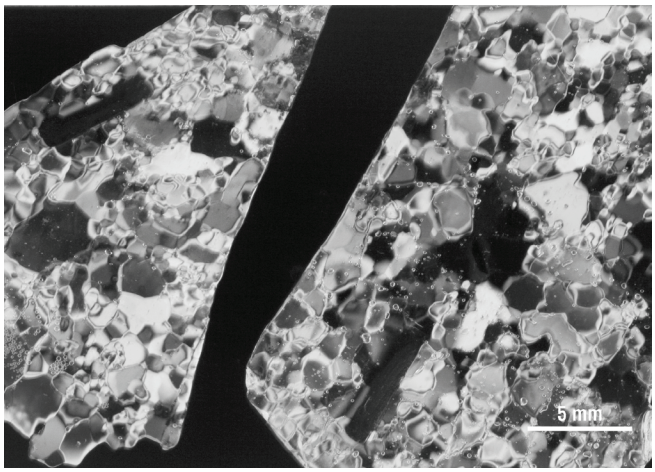

Figure 2. Thin sections from an ice wedge under crossed polaroids.

with significantly less oxygen than usual. Preliminary results of stable isotopes show homogeneity between ice wedge centers and exteriors, indicating climatic stability over this time. The range in $\delta^{18}O$ values of waters (from -24‰ to -26‰) agrees well with the range of modern ice wedges (-27 ‰ to -23 ‰) in the Old Crow area (Lauriol et al. 1995) and in the Richardson Mountains (-29 ‰ to -22 ‰) (Lacelle 2002). The $\delta^{18}O/\delta^{2}H$ signatures are plot below the meteoric waterline, indicating that ice wedges are filled during the later stages of snowmelt.

Ice crystal size (see Fig. 2) ranges from 0.5 to 6 mm in diameter, and the average size is about 2 mm in diameter. *C*-axes show a dispersed pattern. Ice wedge crystal size seems to be constrained by the width of the thermal contraction cracks. Elongated and spherical bubbles follow the foliated structure produced by repeated infilling of vertical thermal contraction cracks. Spherical bubble size ranges from 0.5 to 1 mm in diameter, and elongated bubble size ranges from 0.5 to 5 mm long.

Eagle River, Yukon

Samples of ice and soil were taken on top of the banks of the Eagle River at 372 m. Preliminary results for this site indicate molar gas ratios closer to atmospheric air ratios. The bubbles are bigger than Holocene ice wedge bubbles, and the crystals are similar to those found in glacier ice. Isotopic composition of the water coming from the ice indicates that these ice wedges are possibly older, dating from the Pleistocene ($\delta^{18}O_{water} \approx$ -30‰). A possible explanation for those results could be that the ice found at the Eagle River site is Pleistocene ice wedge ice, filled by snow or hoarfrost accretion. A silty sample between ice wedges is possibly carbonated loess coming from the Mackenzie, because loess coming from Old Crow Flats is not carbonated, and Mackenzie loess is highly carbonated. We can possibly make a connection with big ice wedge remnants of the Arctida loess bridges that can be found in the Laptev Sea (Tomirdiaro 1996). Tomirdiaro describes them as polygonally-veined ice formations developed to incredible size, but in form rather typical ice wedge polygons. These deep cracks were formed by infilling with sublimated and congealed ice, forming ice wedges.

Conclusion

These results should provide a better interpretation of ice wedge formation and filling process, and should be significant to palaeoclimatic interpretation of ground ice in permafrost areas.

Acknowledgments

We wish to thank the G.G Hatch Isotope Laboratory for their support and expertise. Financial support was provided by Natural Science and Engineering Research Council of Canada (NSERC) and by Northern Scientific Training Program (NSTP).

References

Cardyn, R., Clark, I.D., Lacelle, D., Lauriol, B., Zdanowicz, C. & Calmels, F. 2007. Molar gas ratios of air entrapped in ice: A new tool to determine the nature and origin of relict massive ground ice bodies in permafrost. *Quaternary Research* 68(2): 239-248.

Lacelle, D., Lauriol, B., Clark, I.D., Cardyn, R. & Zdanowicz, C. 2007. Middle Pleistocene glacier ice exposed in the headwall of a retrogressive thaw flow near Chapman Lake, central Yukon Territory, Canada, *Quaternary Research* 68(2): 249-260.

Lacelle, D. 2002. *Ground Ice Investigation in the Far Northwest of Canada.* Thesis (M.Sc.). Ottawa: University of Ottawa, 101 pp.

Lauriol, B., Duchesne, C. & Clark, I.D. 1995. Systématique du remplissage en eau des fentes de gel: les résultats d'une étude oxygène-18 et deutérium. *Permafrost and Periglacial Processes* 16: 47-55.

Sowers, T., Brook, E., Etheridge, D., Blunier, T., Fuchs, A., Leuenberger, M., Chappellaz, J., Barnola, J.M., Wahlen, M., Deck, B. & Weyhenmeyer, C. 1997. An interlaboratory comparison of techniques for extracting and analyzing trapped gases in ice cores. *Journal of Geophysical Research* 102: 26527-26538.

Tomirdiaro, S.V. 1996. Palaeogeography of Beringia and Arctida, In: F.W. West (ed.), *American Beginning: the Prehistory and Palaecology of Beringia*. Chicago: University of Chicago Press, 58-69.

Washburn, A.L. 1980. *Geocryology: A Survey of Periglacial Processes and Environments*. New York: Wiley.

Snowmelt in an Arctic Catchment: Application of the Hydrological Model WATFLOOD in a Small Arctic Basin with Different Land Cover Classes

A. Strutzke
Philipps-University Marburg, Germany
Ch. Opp
Philipps-University Marburg, Germany

Introduction

The world's climate change affects arctic areas in many ways. Climate models predict considerable warming for most northern regions, especially the Western Canadian Arctic. As a result, the western Arctic faces a shortened snow-covered season, changes in winter snow cover properties, and changes in timing and volume of snowmelt water runoff. Furthermore, the fragile ecosystem of the Canadian Arctic has to face a huge impact on its vegetation and animal species. Shrubs and trees will expand northwards and to higher elevations, replacing existing plants. Animals dependent on cold temperatures such as polar bears, seals, caribou, and reindeer are forced to move further north.

The objective of this research project is to examine the capability of the Canadian model WATFLOOD to simulate the runoff in Arctic environments. WATFLOOD was developed for and, so far, is mainly used in southern Canadian river systems and large drainage basins. In arctic areas the physical conditions are very different from those in the south: rivers freeze over completely in winter, the soil is permanently frozen (permafrost), and the watersheds in most cases are untouched by human influences. One of the most important aspects of arctic watersheds is that over the long winter, the precipitation falls almost exclusively as snow, which accumulates in the watershed. At the end of winter, snowmelt occurs, and most of the meltwater is released within days out of the basin. The end-of-winter snowmelt creates the highest yearly runoff peak in spring, with little runoff in the short summer that follows.

Modeling small watersheds in the Canadian Arctic is still a young science. The Arctic itself is a data-poor area compared to other well-researched areas in Canada or the world. Applying a hydrological model to arctic areas relies on having measurement stations in the Arctic as well as doing fieldwork to compare the modeled results with the measured data in evaluating the model's ability. The hope with modeling in the Arctic is that scientists will be able to come up with generalized parameter sets that can be used elsewhere in the Arctic where observation stations do not exist.

Results

Considering that WATFLOOD was developed for more temperate regions than the Arctic, the validation runs showed that WATFLOOD was able to simulate runoff in Hans Creek fairly accurately. WATFLOOD produced reasonable meltwater hydrographs in most years by only using WATFLOOD's relatively simple air temperature index algorithm to simulate snowmelt, together with the calibrated soil and channel parameters for Hans Creek. The aspect that WATFLOOD consistently estimates the days of first runoff too early can be explained by two naturally occurring processes that are not specifically addressed in the WATFLOOD model: snow meltwater percolation through the snow cover and snow damming. Both of these processes delay runoff by several days and are not accounted for by the model, leading to the problems in simulating the first day of runoff. Another major problem is the existence of many lakes in the Hans Creek watershed, where the outflow of the basin is located. This plays a huge role in the hydrology of the study basin, slowing runoff considerably. The lake-rich environment might also be an explanation for why WATFLOOD was not able to simulate any runoff from rainstorm events at the end of the summer, even though they were clearly visible in the gauging station.

The water storage in lakes and their particularly complex freezing and melting patterns clearly were a problem for WATFLOOD. One reason for this could be that the land cover class "water," as used for lakes in Hans Creek, was based on snow survey data from the generally very small lakes in the neighboring Trail Valley Creek. Hans Creek, however, holds lakes in a huge variety of sizes, which were all initiated in spring with the same amount of snow water equivalent. This may lead to large modeling errors because of the extensive redistribution of snow during blowing-snow events, which happen especially over lakes. Responsible is a lack of vegetation and the absence of melt/freeze cycles that could stabilize the snow cover. Additionally high wind speed events happen often over the long winter period in this area leading to frequent periods of blowing snow and high sublimation losses.

In a subsequent model series, the model performance was tested using climate data from a long-term observation station in Inuvik, 60 km south of the Hans Creek watershed. While the overall average of total and peak runoff volumes was fairly good, the individual hydrographs for the 15 years used in this series as well as the NSC clearly showed that WATFLOOD could not simulate the runoff accurately for most of the years. Since WATFLOOD was able to predict the runoff of the neighboring watershed Trail Valley Creek (Pohl et al. 2007) using Inuvik climate data, the reason must be sought in the differences between both watersheds. Likely reasons seem to be the bigger size of Hans Creek and

the existence of many lakes and wetland areas in the basin, which considerably slow the runoff because of their storage capacity. The modeling of runoff through lakes and arctic wetland areas could not be processed by WATFLOOD with satisfying accuracy.

Recent Rise of Water Level in Lake Hovsgol in the Permafrost Zone of Northern Mongolia: Trends and Causal Factors

Kazuo Takeda
Obihiro University of Agriculture and Veterinary Medicine, Obihiro, Japan
Hiroji Fushimi
University of Shiga Prefecture, Hikone, Japan
Tatuo Kira
Lake Biwa Environmental Research Institute, Ohtsu, Japan

Introduction

Lake Hovsgol is the largest freshwater lake in Mongolia (Table 1), located on the southern fringe of the east Siberian permafrost zone that supports the so-called "light taiga," or the deciduous conifer forests dominated by larch (*Larix spp.*). Once the larch vegetation is destroyed due to increasing forest fires and the outbreak of pest insects, direct sunshine raises ground surface temperature, resulting in deeper thawing of permafrost in summer.

According to observations at the station of the National Agency for Meteorological (1940–2006) in Hatgal village (on the southernmost shore of Lake Hovsgol) during 67 years, the annual mean temperature has gone up at the rate of 3°C per century with mean annual precipitation of only 200~400 mm/yr. Also noticed is that the water level of the lake has risen by 100 cm during the latest 37 years (Murun Meteorological Station 1970–2006).

As for the cause of such recent rise in water level, it is sometimes suggested that global climate change might be responsible (Kumagai 1998, Kumagai et al. 2006). Namely, the inflow of thawed fossil water from permafrost layers and glaciers brought about by global warming is supposed to be the main source of increasing lake water. This hypothesis, however, lacks concrete evidence because of the absence of continuous reliable records of groundwater supply into the lake.

This paper deals mainly with another causal factor relevant to the lake water level rise, viz. the bottleneck structure at the head of the Egiyn Gol (= river), the sole outlet of the lake. Environmental information related to the water budget of the lake is presented based on field survey around the lake.

Study Methods

Field surveys were conducted at 12 sites (Fig. 1), including 57 observation points during 3 years since 2000. Items observed were depth of active later (at most sites), soil properties such as moisture content, and grain size composition (at some limited number of sites). To find the depth of the active layer, a temperature profile was measured along a vertical hole made by striking an iron rod into the ground. The 0°C isotherm depth was then estimated by extrapolating the profile curve downward. This procedure was done after late August, when the active layer depth approached the seasonal maximum.

About 1.5 km southward from Hatgal at Site L (Fig. 1), the Egiyn River starts draining lake water through a very narrow and shallow bottleneck route, produced by the deposits carried by a tributary river. The structure of riverbeds of the two joining streams, so important for the control of the lake's water budget, was carefully surveyed. Further, as some of groundwater, the flow rate of an inflow stream originating from Har usnii Spring about 700 m from the lake (Site C, Fig. 1) was measured.

Results

On most alluvial beds deposited around the lake, ground surface soil layers generally consisted of silt and clay, fairly rich in mixed round gravel, and relatively dry with a volumetric water content of 10–20%. The estimated maximum depth of the active layer in late summer mainly amounted to 1.5–4.0 m under grasslands (pasture), while it was mainly 1.4–2.0 m under larch forests. The water content of surface soil under larch forests on north-facing slopes was around 22%, whereas it was only 13% on slopes facing the other three directions. However, once such a forest stand had been burned or clear-felled, the depth of active layer increased up to 1.9–5.4 m, owing to increased solar irradiation on the exposed ground.

At Site L, a large tributary river, Ulgen Sair, joins the uppermost stream of Egiyn River (Fig. 2). The stream bed of Ulgen Sair is far larger than the Egiyn stream, about 400 m wide at the confluence, and is entirely filled with fully eroded round gravel. Surface water flow does not exist under normal weather, but in case of concentrated heavy rainfall, vast mounts of debris are carried down by flood water and deposited on and around the confluence with the Egiyn River. For instance, in July 1971, the debris deposits following a heavy rainfall of 71 mm/day (at Hatgal) entirely buried the Egiyn stream, completely cutting off the outflow from the lake (Batsukh et al. 1976). Similar events took place twice in 2003

Table 1. Physical dimensions of Lake Hovsgol (Kurata 1993).

Location	50°27′–51°37′N, 100°51′–101°47′E
Altitude (m)	1,645
Surface area (km^2)	2,770
Maximum depth (m)	267
Mean depth (m)	138
Volume (km^3)*	383
Length of shoreline (km)	414
Drainage basin area (km^2)	4,940
Forest (km^2)**	(2,365)
Pasture (km^2)**	(1,559)
Mountain (km^2)**	(1,016)

* Data (Kumagai 1998); ** Values measured in map.

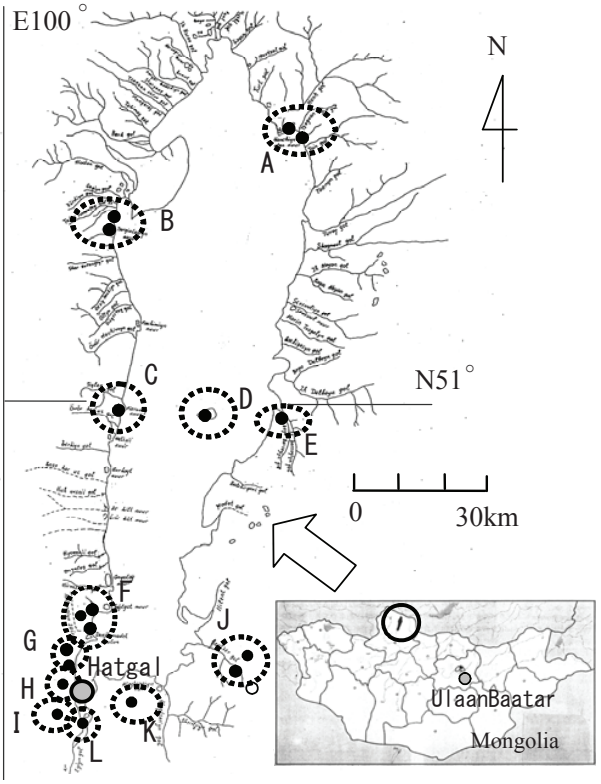

Figure 1. Distribution of the study sites around L. Hovsgol.

and 2006. Owing to such repeated flood disasters, it is difficult for Egiyn River at Site L to maintain a clearly open channel. The outflowing rate at Site L calculated from the current speed measured at stream surface (1.89 m/sec) and the cross-sectional area water channel (26.44 m^2) amounted to 1.58 km^3/yr.

At Site C, the inflowing rate of stream to originate from Har usnii Spring, where the water keeping 4.3~6.2°C flows throughout the year, was measured as 6.05 m^3/s and amounted to 0.19 km^3/yr.

Discussion

Based on the survey results, a depth of active layer was determined, and thereby estimated the increase of water inflow to the lake caused by additional thawing of permafrost due to climate warming. For example, the additional increase of the active layer in the forest area was determined to be 3.5 m, assuming that the forest vanishes and it becomes deeper from 1.9 m to 5.4 m. Using *Vw* 40% as the volumetric water content in permafrost and *Vw* 20% after thawing, the amount of fossilized water to outflow to the lake was estimated to be 1.66 km^3, using the area of forest given in Table 1.

However, such water does not flow out at the same time, but does so gradually for a long time. For example, it is known that the fossilized water keeps flowing out due to thawing of permafrost for several years after a forest fire. If it takes a century for the forest to vanish and the fossilized water flows out by the thawing of permafrost, the outflow of the water is estimated to be only 0.02 km^3/yr. The estimated amount is not even so much in the forest area larger than the pasture or the mountain (Table 1), because of the thin surface soil and abundance of gravel and rocks.

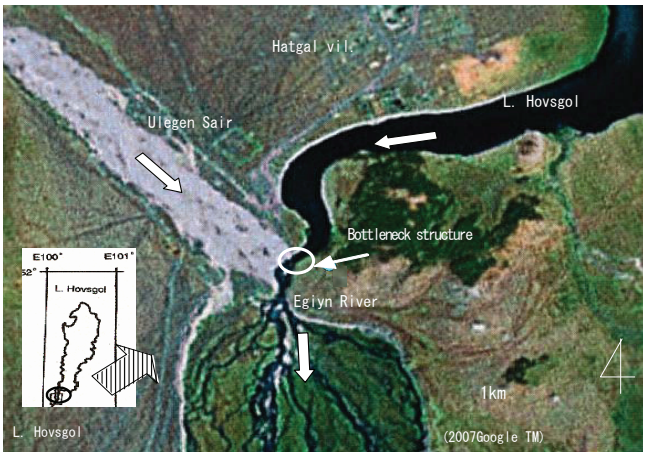

Figure 2. Outflow River, Egiyn River, at the confluence with the tributary river, Ulgen Sair.

The total amount of fossilized water in the drainage basin area is considered to be too small to cause a significant rise in water level, because the amount in the forest area is negligibly small compared with the outflow 1.58 km^3/yr through Egiyn River. Therefore, it is difficult to regard as the main causal factor that the increase of water inflow to the lake caused by additional thawing of permafrost due to climate warming induces the rise in water level.

On the other hand, the draining capacity of the sole outflowing river—Egiyn River—is very unstable, since its uppermost course suffers from vast amounts of sediment carried down by a large tributary stream at times of heavy rainfall, filling the river channel either partly or completely. A close negative correlation was found between the lake's water level and the rate of outflow through this bottleneck in the uppermost part of the Egiyn River.

References

Batsyk, N., Schymeev, V.P. et al. 1976. Surface water and water balance of Lake Khubusgul. In: N. Sodnom & N.E. Losev (eds.), *Natural Conditions and Resources of the Khubusgul Region in the Mongolian Peoples Republic.* Moscow: Nedra, 185-206 (in Russian and Japanese, translated by Dr. Naganawa).

Kumagai, M. 1998. Lake Hovsgol in Mongolia. In: Lake Biwa Research Institute (ed.), *Record of the 16th IBRI Symposium*. Otsu: LBRI, 89-104 (in Japanese).

Kumagai, M., Urabe, J. et al. 2006. Recent rise in water level at Lake Hovsgol in Mongolia. In: C.E. Goulden, T. Sitnikova et al. (eds.), *The Geology, Biodiversity and Ecology of Lake Hovsgol (Mongolia)*. Leiden: Backhuys, 77-91.

Kurata, A. (ed.), 1993. *Data Book of World Lake Environments: Compact-size Ed 1: Asia and Oceania.* Kusatsu: ILEC & UNEP.

Murun Meteorological Station 1970-2006. *Meteorological Data Observed at Lake Hovsgol during 1970–2006.*

National Agency for Meteorology 1940–2006. *Meteorological Data observed at Moron and Hatgal during 1940–2006.*

Effects of Increased Snow Depth on Ecosystem CO_2 Fluxes in Arctic Tundra

Lina Taneva
Environment and Natural Resources Institute, University of Alaska Anchorage
Patrick F. Sullivan
Department of Biology, University of Alaska Anchorage
Bjartmar Sveinbjornsson
Department of Biology, University of Alaska Anchorage
Jeffrey M. Welker
Environment and Natural Resources Institute, University of Alaska Anchorage

Introduction

Shrub expansion into arctic tundra has been documented (Tape et al. 2006) and climate warming and altered precipitation regime have been proposed as possible drivers of plant community composition changes (Sturm et al. 2005). Increases in winter precipitation and deeper snowpack can alter the soil microclimate, leading to warmer soils and deeper active layer, potentially resulting in changes in the carbon, water, and nutrient cycles of arctic ecosystems. Associated changes in plant community composition in tundra ecosystems can further lead to altered ecosystem function. The Arctic represents a large carbon reservoir in the global carbon cycle, and changes in the cycling of carbon in tundra ecosystems with observed changes in biotic and abiotic conditions could have important implications for atmospheric CO_2 accumulation.

The objective of this study was to evaluate the short-term and long-term effects of deeper winter snow depth on ecosystem carbon cycling during the growing season.

Methods

This research was conducted during the 2007 growing season at three moist tussock tundra sites near Toolik Lake, in the northern foothills of the Brooks Range, Alaska, USA. Plant community composition is dominated by the tussock grass *Eriophorum vaginatum,* the shrubs *Betula nana,* and *Salix pulchra*, as well as other short-stature vegetation, mosses and lichens. Snow fences were constructed in 1994 (n = 1) and 2006 (n = 3), in order to increase snow depth in the treatment plots during winter/spring. A naturally occurring shrub patch was used as a reference.

Ecosystem CO_2 flux measurements were taken using a clear plexiglass chamber, connected to a Licor 6200 infrared gas analyzer.

Results

No significant changes in ecosystem C uptake or respiration after one year of snow depth increase were observed, with the ecosystem representing a C source for part of the growing season (Fig. 1). Long-term (13 yr) snow depth increase resulted in greater C uptake rates in treatment plots, whereas no significant changes in ecosystem respiration rates were observed, and both treatment and control plots were a C sink during the growing season (Fig. 1). Ecosystem C fluxes in a nearby naturally occurring shrub patch were lower than those in tussock tundra under ambient or increased winter snow depth, and NEE was near zero (Fig. 1).

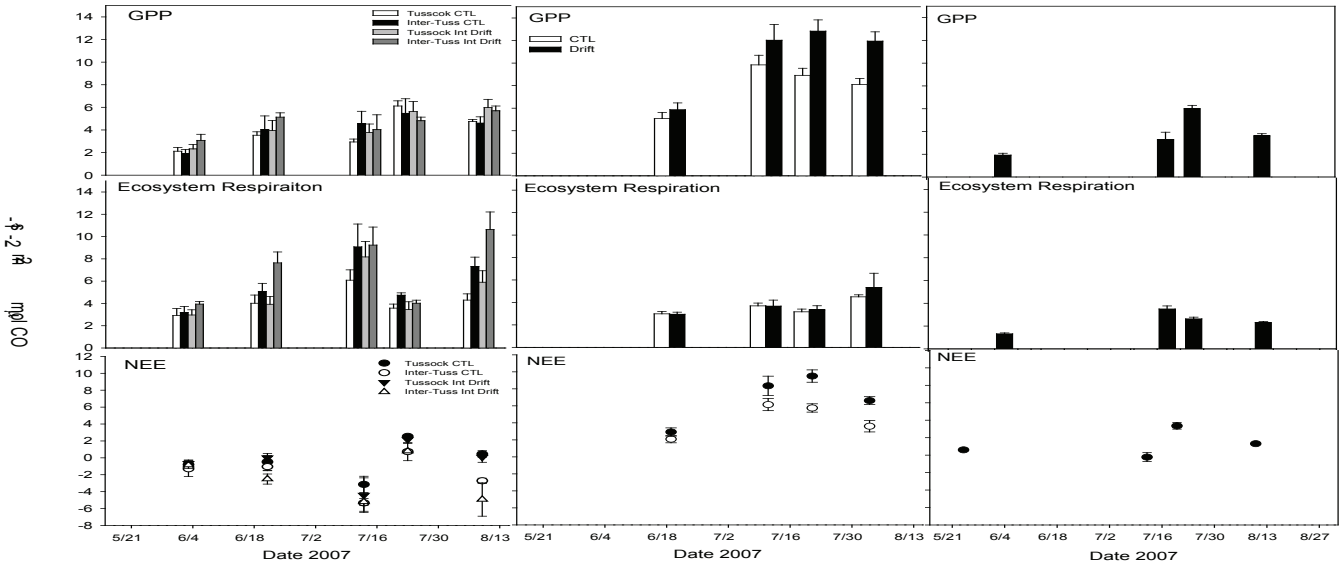

Figure 1. Ecosystem CO_2 fluxes (gross ecosystem productivity [GEP], ecosystem respiration, and net ecosystem CO_2 exchange [NEE]) in tussock tundra after 1 and 13 years of snow accumulation increase, and in a site dominated by shrub (*B. nana*) vegetation without any snow treatments.

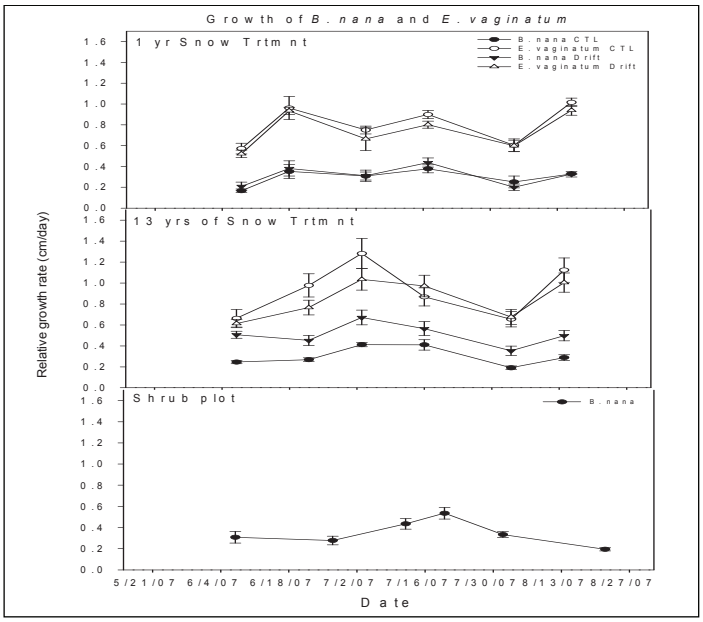

Figure 2. Growing season growth rate of *B. nana* and *E. vaginatum* in a tussock tundra ecosystem after 1 and 13 years of snow accumulation increase, and in a shrub-dominated plot with no snow depth manipulation.

The growth rate of *E. vaginatum* was higher than that of *B. nana*, with no significant changes in growth rates after 1 yr of snow depth increase (Fig. 2). Long-term snow depth manipulation led to a stimulation in *B. nana* growth rate and a trend towards lower *E. vaginatum* growth rates, relative to ambient snow plots (Fig. 2). Rates of *B. nana* growth in the long-term treatment plots were higher than those in the shrub-dominated plot, while growth rates at ambient snow were comparable at tussock tundra and shrub sites (Fig. 2).

Conclusions

Long-term increases (13 yr) in winter snow cover and associated changes in plant community composition (i.e., increases in shrub abundance; Wahren et al. 2005) converted this tundra ecosystem from a source of C to the atmosphere (as reported in Jones et al. 1998 and Oberbauer et al. 2007 after 2, 3, and 4 years of treatment) to a C sink.

Enhanced GEP with deeper snow cannot be explained by increases in shrub abundance alone and suggests altered winter soil processes under deeper snow that may alleviate ecosystem nutrient limitation.

Changes in plant community composition in tundra ecosystems can potentially translate to altered C inputs, storage, and turnover rates in these C-rich and warming-sensitive ecosystems, with subsequent implications for the global C cycle.

Acknowledgments

This research was funded by an International Polar Year grant #0612534 through the Office of Polar Programs at the National Science Foundation. We gratefully acknowledge the staff at Toolik Field Station for camp maintenance and operation. We thank Jeremy Chignell for his help in the field.

References

Jones, M.H., Fahnestock, J.T., Walker, D.A., Walker, M.D. & Welker, J.M. 1998. Carbon dioxide fluxes in moist and dry Arctic tundra during the snow-free season: Responses to increases in summer temperature and winter snow accumulation. *Arctic and Alpine Research* 30(4): 373-380.

Oberbauer, S.F., Tweedie, C.E., Welker, J.M., Fahnestock, J.T., Henry, G.H., Webber, P.J., Hollister, R.D., Walker, M.D., Kuchy, A., Elmore, E. & Starr, G. 2007. Tundra CO_2 fluxes in response to experimental warming across latitudinal and moisture gradients. *Ecological Monographs* 77(2): 221-238.

Sturm, M., Schimel, J., Michaelson, G., Welker, J.M., Oberbauer, S.F., Liston, G.E., Fahnestock, J. & Romanovsky, V.E. 2005. Winter biological processes could help convert Arctic tundra to shrubland. *Bioscience* 55(1): 17-26.

Tape, K., Sturm, M. & Racine, C. 2006. The evidence for shrub expansion in northern Alaska and the Pan-Arctic. *Global Change Biology* 12(4): 686-702.

Wahren, C-H.A., Walker, M.D. & Bret-Harte, M.S. 2005. Vegetation responses in Alaskan arctic tundra after 8 years of a summer warming and winter snow manipulation experiment. *Global Change Biology* 11: 537-552.

Modeling Permafrost Evolution and Impact on Hydrogeology at the Meuse/Haute-Marne Sedimentary Site (Northeast France) During the Last 120,000 Years

Vanessa Teles, Emmanuel Mouche, Christophe Grenier, Damien Regnier
Laboratoire des Sciences du Climat et de l'Environnement, UMR CEA-CNRS-UVSQ, France
Jacques Brulhet, Hakim Benaberrahmane
Andra, Agence nationale pour la gestion des déchets radioactifs, France

Introduction

The Callovo-Oxfordian layer in the eastern part of the Parisian Basin (France) was recognized as a potential nuclear waste repository layer. To evaluate transfers from the host formation to the biosphere, it is important to understand the temporal evolution of the hydraulic boundary conditions of the clayey layer, which means to understand the evolution of the whole hydrogeological system. The Callovo-Oxfordian unit is part of the Parisian Basin consisting of piled up sedimentary units ranging over thousands of meters in depth at maximum and covering the northern half of France. Besides this specific sedimentary geological structure, past permafrost extension differs from Nordic situations, because ice cover remained here very limited in time and depth soon followed by a cold and dry steppic landscape.

A few years ago, Andra (National Agency for Nuclear Waste Management) launched a research program on the geoprospective of the MHM (Meuse/Haute-Marne) site, including the study of the impact of glacial cycles on the underground flow patterns (Andra 2005, Andra 2004, Brulhet 2004).

Recent efforts to study the impact of permafrost on underground flow patterns, modeling of permafrost extension through geological times as well as on going activities, are reported here involving the LSCE (Laboratoire des Sciences du Climat et de l'Environnement) team. This work follows a former phase of pure hydrological modeling of the MHM site.

The studies conducted at LSCE are presented here along 3 major issues: (1) impact of permafrost reconstruction on hydrogeology during the last 120,000 years; (2) 3D thermal modeling of permafrost extensions based on solar radiation evolution (120,000-year period); and (3) coupled thermo-hydrological modeling and role of small-scale surface and subsurface units (valley vs. hill, river, lake, aquifer).

The thermal and hydrodynamic simulations have been performed with the Cast3M code, developed and implemented by the CEA (Atomic Energy Commission), using finite-element or mixed hybrid finite-element formulations.

The extension of the modeled zone is 75 km x 80 km, involving the actual present-time topography and rivers, as well as geological layers (from bottom to surface: Dogger, Callovo-Oxfordien, Oxfordien-Calcaire, Kimmérigien, Cretacé-Barrois) corresponding for the latter to roughly a 500 m depth.

Impact of Permafrost Reconstruction on Hydrogeology During the Last 120,000 Years

The idea behind this first modeling phase (refer to Teles & Mouche 2005) consists in taking reconstructions of permafrost extensions over the last 100,000 years, transfer it into permeability information, and simulate transient flow on the MHM domain with adequate boundary conditions. More precisely, reconstructions from Van Vliet (2004) concerning the MHM region were considered. They involve five development stages with associated time periods: present conditions for 10,000 years BP, installation of a thin permafrost (starting 95 BP), permafrost on hills with free valleys (from 75,000 years BP on), thick continuous permafrost (starting 20,000 years BP), relict permafrost (from 13,000 years BP). Three-dimensional simulations of transient flow were conducted starting from initial conditions close to present state. Freezing causes a stop in the infiltration as permafrost develops, so surface boundary conditions are changed from imposed heads assumed close to the local altitude to no flow conditions. Furthermore, the 3D permeability field is modified to account for the presence of permafrost. Practically speaking, permeability tensors are associated with each mesh element corresponding vertically to harmonic mean between permafrost permeability (arbitrary put at 10^{-13} m/s) and actual geological formation permeability; horizontally, arithmetic mean was considered. Consequently, vertical flow is limited, whereas horizontal flow is directly a function of the vertical fraction of unfrozen formation thickness.

Results show that the flow velocities are reduced as compared with present-state conditions in all geological formations during permafrost phases. This is the result of the stop in the recharge as well as reduction in the permeability. Flow velocity in the aquifers not directly concerned themselves by freezing is roughly reduced by a factor of two.

It should be stressed here, nevertheless, that conditions inferred at the MHM site for the last glacial cycle are very different from conditions reconstructed for more Nordic locations, where the ice thickness was large and lead to a mechanical load onto the geological units. Consequently, increased pressure boosted access of water to deeper zones, though recharge from the surface was actually stopped. The situation at the MHM site is considered best represented as a mere stop in recharge, leading to a pure aquifer drainage situation for deeper units.

3D Thermal Modeling of Permafrost Extensions from Solar Radiation Evolution (Last 120,000 Years)

In a second step (refer to Teles & Mouche 2006), focus was put on the modeling of transient evolution of permafrost extension. Former 3D geometrical features were retained for a thermal modeling approach and identical 100,000-year time period. A purely conductive model was considered with actual geological formation thermal properties, imposed bottom geothermal flux, and transient imposed surface temperature. The latter followed the normalized variation in solar radiation over the time period according to Berger (1978). The modeling of permafrost extension was attempted considering the following refined points: (1) Imposed surface temperature was made dependant from the actual altitude and incident solar radiation (Šafanda 1999). (2) Ground level solar radiation was considered dependant on incident solar radiation, topographic slope and surface orientation (Senkova & Rontu 2003). (3) Imposed surface temperature was affected a positive correction when corresponding to a river mesh to account for heat exchange resulting in the reduction of permafrost development under rivers (the coefficient was chosen constant and its value assessed based on model sensitivity analysis). Simulation results were finally compared to a vertical reconstruction of 0°C isotherm for a deep borehole location. These reference values correspond to a best expert view resulting from in situ analysis, naturalistic considerations, as well as 1D vertical thermal modeling including phase change effects (cf. Courbouleix et al. 1998).

This study remains preliminary in the sense that the 3D model was not further complexified to account for phase-change phenomena and heat advection due to water flow. This is attempted in the third modeling phase. Nevertheless, results show that qualitative evolution of the 0°C isotherm could be well simulated, although quantitative fit requires better constraints on the solar radiation forcing history. This is a critical point, since literature shows that uncertainties in solar radiation histories resulting from existing scenarios remain large, whereas the sensitivity of the thermal model to this input data is very large. For two models considered in the study only differing roughly by a factor of two, permafrost extensions were very different. Consequently, care should be put in the future in increasing the robustness of this forcing term.

Coupled Thermo-Hydrological Modeling of Small-Scale Units

Ongoing efforts consist in (1) developing a coupled TH (Thermo-Hydro) numerical model within our Cast3M code including thermal conduction, convection, and phase change; (2) answering the issue of the level of heat flux actually transmitted to the underground while considering various surface- and subsurface-specific units leading to heat exchange like water bodies (river, lake, aquifer), or including topographic variability (valleys vs. hills); and (3) addressing the issue of spatial and temporal upscaling (e.g., periodic thermal stress, daily, yearly, cycles) to achieve regional modeling for a 120,000-year time period.

These efforts will serve to organize the various mechanisms into a hierarchy, and finally improve the physical and numerical modeling of the impact of glacial cycles on the hydrogeology at the MHM site over geological time scales.

References

Andra. 2005. Dossier 2005. Argile, Référentiel du site de Meuse / Haute-Marne, Tome 3. *Document Andra* n° C.RP.ADS.04.0022.B.

Andra. 2004. *Site Meuse/Haute-Marne, Géothermie*. Inventaire des nouvelles données. *Note Technique Andra* n° C.NT.ASMG.04.0001.

Berger, A. 1978. Long-term variations of daily insolation and Quaternary climatic changes. *Journal of the Atmospheric Sciences* 35(12): 2362-2367.

Brulhet, J. 2004. L'évolution géodynamique (tectonique et climatique) et son impact sur l'hydrogéologie et l'environnement de surface. Site MHM. *Note Technique Andra* n° C.NT.ASMG.03.106.B: 84 pp.

Courbouleix, S., Gros, Y., Clet, M., Coutard, J.P., Lautridou, J.P., Van Vliet-Lanoe, B., Dupas, A. & Cames-Pintaux, A.M. 1998. Simulation de la profondeur du pergélisol au cours du dernier cycle climatique. Utilisation des échantillons du sondage EST106, *Rapport Andra* n° D.RP.0ANT.98.011.

Šafanda, J, 1999. Groundwater surface temperature as a function of slope angle and slope orientation. *Tectonophysics* 306: 367-375.

Senkova, A.V. & Rontu, L. 2003. *A Study of the Radiation Parametrization for Sloping Surfaces*. St. Petersburg: Baltic HIRLAM Worshop, 79-82.

Teles, V. & Mouche, E. 2005. Analyse de sensibilité de la présence d'un pergélisol continu et discontinu sur l'hydrogéologie du secteur, Site MHM. *Rapport Andra* n° C.RP.12CEA.05.001.

Teles, V. & Mouche, E. 2006. Site MHM, Modélisation tridimensionnelle de la distribution du pergélisol au cours d'un cycle climatique. *Rapport Andra* n° C.RP.12CEA.06.001.

Van Vliet-Lanoë, B. 2004. Modèle conceptuel du pergélisol, Site MHM. *Rapport Andra* n° C.RP.0UST.04.002.

Effect of a Snow Fence on the Shallow Ground Thermal Regime, Baker Lake, Nunavut, Canada

Jennifer L. Throop
Department of Geography, University of Ottawa, Ottawa, Canada
Sharon L. Smith
Geological Survey of Canada, Natural Resources Canada, Ottawa, Canada
Antoni G. Lewkowicz
Department of Geography, University of Ottawa, Ottawa, Canada

Introduction

Snow depths on the tundra can be highly variable due to snow redistribution by high winds in relation to topography and vegetation. These differences are an important factor in the spatial variability of the ground thermal regime (Smith & Riseborough 2002). Variations in snow depths substantially affect the heat exchange between the air and ground surface, thereby influencing the surface offset. Changes in amounts of snow cover are expected to accompany a warming climate (ACIA 2005) and may be an important factor in influencing future permafrost conditions.

An instrumented arctic tundra site at Baker Lake, Nunavut, (64°19.6′N, 96°2.5′W) provides the opportunity to investigate the impact of variable snow depths on the shallow ground thermal regime. Baker Lake is in a region of continuous permafrost with thicknesses of up to 200 m (Smith et al. 2005). The site consists of a transect of four shallow boreholes reaching depths of 3 m along a gentle south-facing slope. The installation of a 4 m tall snow fence in 1981 has prevented snow from drifting into the community. This has resulted in a large snowdrift developing downwind of the fence that persists into late July. Our goal is to assess the impact of the snow fence by examining the thermal data collected from two of the boreholes: the site least affected by the snow fence (BH4, representing natural conditions) and the site most affected by the snow fence (BH2, beneath the snowdrift).

Site Description and Methods

The boreholes were drilled in 1997. BH4 is located 400 m upwind of the snow fence, and BH2 is located 45 m downwind, where the large snowdrift forms. These boreholes were instrumented with temperature cables that have thermistors at 50 cm intervals down to 3 m. Manual readings were taken monthly or semi-monthly from 1997 until 2005 and less frequently since 2005. A datalogger was attached at BH4 in 2002 to record temperatures three times daily. A weather station was installed near BH4 in 2002 to obtain air temperature, wind speed, and the natural snow depth for the area. Temperature sensors were installed in 2002 at 2–5 cm depth to provide an indication of the surface temperature.

Surface offsets were calculated for both sites from 2002–2006 by subtracting the mean annual air temperature (MAAT) from the mean annual ground surface temperature (MAGST). The maximum and minimum values at each depth to 3 m were taken from the manual data collected between 1997 and 2005.

Maximum thaw depths were calculated for each year at both boreholes using linear interpolation between sensors located above and below the 0°C isotherm. Thawing and freezing degree-days (TDD and FDD) were calculated using the air temperature data from the weather station at BH4.

Results

The MAAT varied between -8.8 and -12.2°C over the 4 years of continuous records (Table 1). For the same period, the MAGST at BH4 ranged from -5.2 to -8.6°C, giving surface offsets of 2.4 to 4.7°C. At BH2, MAGST was higher, ranging from -0.1 to -2.0°C, producing very large surface offsets of 7.8 to 10.6°C. The difference between the two sites indicates that the ground surface warmed beneath the snowbank by 4-8°C over the 16-year period.

The temperature envelopes (Fig. 1) illustrate that the snowdrift at BH2 has strongly affected minimum ground temperatures down to 3 m. At BH4, these range between -16 and -22°C, whereas at BH2 the range is between -5 and -7°C. There is a difference of approximately 15°C near the surface, and 11°C at 3 m depth. Maximum temperatures on the other hand, are quite similar.

Calculated maximum thaw depths at BH4 averaged 1.84 m for 1997–2005 with a standard deviation of 0.28 m (Fig. 2). The minimum value of 1.25 m occurred in September 1997, and the maximum of 2.17 m in September 2005, giving a range of 0.9 m. Although the results suggest a trend towards increasing thaw depths, the dataset is too short to reach a definitive conclusion. A comparison between thaw depths and the square root of TDD from the nearby Baker

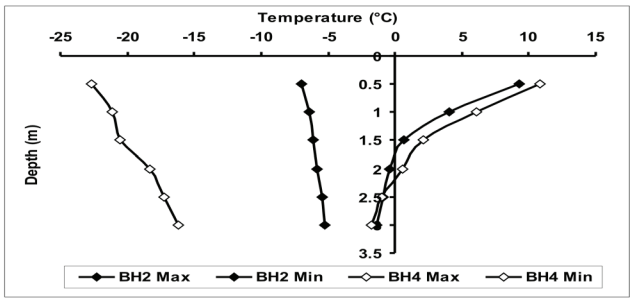

Figure 1. Temperature envelopes (maximum and minimum values) at BH2 and BH4 from the 1997–2005 manual readings.

Table 1. Summary table of data values at BH4 and BH2.

Year (Sept-Aug)	MAAT	Snow Depth Average (cm)	Snow Depth Maximum (cm)	MAGST BH4	MAGST BH2	Surface Offset BH4	Surface Offset BH2
2002–2003	-10.5	18.0	33.2	-8.1	-0.1	2.4	10.4
2003–2004	-12.2	14.6	24.8	-7.6	-2.0	4.7	10.2
2004–2005	-11.5	12.6	36.3	-8.6	-0.9	2.9	10.6
2005–2006	-8.8	28.1	56.1	-5.2	-1.0	3.6	7.8

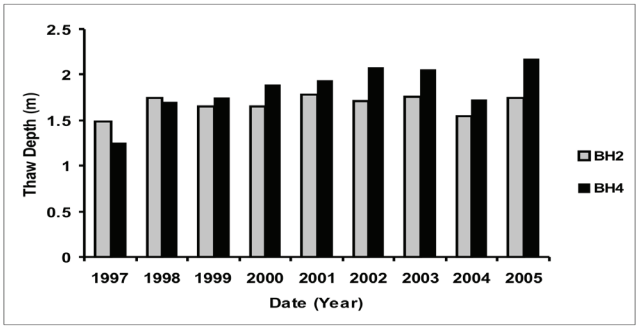

Figure 2. Maximum calculated thaw depths for BH2 and BH4 from 1997 to 2005 using manual data taken approximately three times per month during maximum thaw season.

Lake weather station did not produce a significant linear fit (results not shown).

Calculated maximum thaw depths at BH2 beneath the snowbank averaged 1.67 m with a standard deviation of 0.10 m, and range from a minimum of 1.48 m in September 1997 to a maximum of 1.78 m in September 2001 (Fig. 2). Interannual variability in the thaw depth at this borehole, therefore, was only about 0.3 m, substantially less than at BH4.

The average snow depth at BH4 from 2002–2006 ranged from 13 to 28 cm. The highest value occurred in the winter of 2005–2006, when the maximum depth reached 56 cm at the end of April, at least 20 cm deeper than any of the other three years (Table 1).

The year 2004 had the lowest TDD in the four years of continuous monitoring at the site with a value of 843, whereas 2003, 2005, and 2006 ranged between 947 and 1051.

Discussion

The effect of the snowdrift can be seen clearly in the temperature envelopes in Figure 1. The amplitude of the envelope is much greater at BH4, reaching much lower minimum temperatures showing a more direct link to changes in air temperature. The small amplitude of the envelope and the milder temperatures at BH2 illustrate the muting effect of the snowdrift, dampening the effect of air temperature changes.

The decrease in thaw depth in 2004 reflects the low value of thawing degree-days that year (843) compared to other years. There was not a clear link between interannual differences in snow depths measured at BH4 and surface offsets. The 2005–2006 winter at BH4 had more snow than other years along with the highest MAGST and MAAT. Even though this year had the most snow, the greatest surface offset was in 2003–2004, and that at BH2 was noticeably less than in the other years in 2005–2006.

The result that the deep snowbank produces very large surface offsets and substantially warms the ground surface on an annual basis was also found beneath a snow fence induced snowbank in Barrow, Alaska (Hinkel & Hurd 2006). Similarly, the shallower thaw depths produced by the late-lying snow were observed in Alaska, where in one year their snowbank failed to melt completely.

Conclusion

The long-lasting snow fence induced snowbank at Baker Lake results in the ground surface beneath being warmer than the surrounding area by 4–8°C on an annual basis. However, the snow is so deep that thaw is retarded significantly, and thaw depths average 17 cm less beneath its deepest section than at the control site (BH4). Variability in depths of thaw over 9 years was greater at the control site than beneath the snowbank. There is no evidence from the ground temperature data that warming by the snowbank is causing thermokarst at the site.

Acknowledgments

Support for this project has been provided by Natural Resources Canada, the Canadian Government's Climate Change Action Plan 2000, and International Polar Year Program. Orin Durey, a Baker Lake resident, maintains the site and collects the temperature data.

References

ACIA 2005. *Arctic Climate Impact Assessment*. Cambridge University Press.

Hinkel, K.M. & Hurd, J.K. Jr. 2006. Permafrost destabilization and thermokarst following snow fence installation, Barrow, Alaska, U.S.A. *Arctic, Antarctic and Alpine Research* 38: 530-539.

Smith, M.W. & Riseborough, D.W. 2002. Climate and the limits of permafrost: a zonal analysis. *Permafrost and Periglacial Processes* 13: 1-15.

Smith, S.L., Burgess, M.M., Riseborough, D.W. & Nixon, F.M. 2005. Recent trends from Canadian permafrost thermal monitoring network sites. *Permafrost and Periglacial Processes* 16: 19-30.

Examining the Temporal Variation in Headwater Drainage Networks and Potential for Thermokarst Using Remote Sensing in the Imnavait Basin

Erin D. Trochim
University of Alaska Fairbanks
Douglas L. Kane
University of Alaska Fairbanks
Anupma Prakash
University of Alaska Fairbanks

Introduction

Surficial drainage networks underlain by a confining layer such as permafrost are characterized by significant amounts of overland flow, manifesting features such as water tracks and incised channels as the dominant complex. Variations in routing can occur in the Arctic fresh water hydrological cycle as feedback mechanisms between vegetation and permafrost distribution. Predicting and characterizing potential response is an important component for engineering infrastructure appropriate for the climatic conditions. The Imnavait basin north of the Brooks Range in Alaska is part of a long-term monitoring effort, and provides an opportunity to pair hydrological studies and high-resolution topography models with remotely sensed data, to create a qualitative, spatially distributed perspective.

Water tracks are saturated areas mantled with organic soils which may or may not connect to the channel network (McNamara et al. 1999). Flows are perpendicular to elevation contours, and they often develop a parallel distribution with spacing of approximately tens of meters. The vegetation associated with water tracks is proportional to quantity of water typically present within the channel (Walker et al. 1994). Well-developed water tracks contain the *Eriophorum angustifolium-Salix pulchra* willow community while water tracks of intermittent flow, which are poorly defined, contain shrub facies of the *Sphagno-Eriophoretum vaginati*. subass. *typicum*.

Thawing of ice-rich permafrost or thermokarsting (van Everdingen 1998) in foothills or mountainous areas typically occurs along water tracks; determining the thermal regime of the water tracks will allow the prediction of (if) when a thermokarst may occur. Assessment of whether the water tracks are experiencing shrub expansion, one of the strongest indicators of ecosystem change due to climate change measured to date (Stow et al. 2004), is important for prediction of the future thermal state. Changes in vegetation can result in feedbacks to the thermal state of the associated permafrost, as an increase in density and spatial expansion lower the albedo and allow more energy to be absorbed into the ground (Callaghan et al. 2004). Coupling this effect with potential alterations to landscape as a result of thermokarst activity, including changes in groundwater flow and storage, relief, and discharge patterns and amounts (Grosse et al. 2006), results in the potential to significantly alter the landscape.

Figure 1. Water tracks in the Kuparuk River basin.

The Imnavait basin covers an area of 2.2 km^2. Till from a glacial advance in the middle Pleistocene covers the slopes (Hamilton 1989). Thick permafrost reaching 300 m deep (Osterkamp & Payne 1981), and lack of springs in the basin effectively isolate the basin from deep groundwater sources. Maximum depths of thaw are typically 25 to 50 cm, but can extend to 100 cm with variation in environmental factors including soil type, slope, aspect, and soil moisture (Hinzman et al. 1991).

Aerial photographs from July of 1956, 1978, and 2007 were georeferenced and used to digitize water tracks into three classes to examine the temporal variation in both area and texture over this 61-year period. Water tracks that were least, moderately, and well developed were buffered by 2, 5, and 7.5 m, respectively, to approximate area. Zonal GIS analysis using a 5 m digital elevation model acquired in 2001 was used to examine the variations in slope, aspect, and elevation.

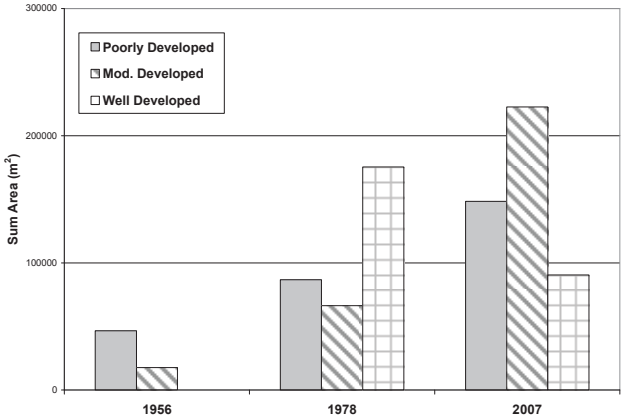

Figure 2. Imnavait Basin water track distribution: 1956, 1978, and 2007.

Table 1. Zonal GIS analysis of water track distribution.

		Elevation (m)			Aspect (°)	Slope (°)
Develop. of WT		*Mean*	*Min*	*Max*	*Mean*	*Mean*
Poorly	*1956*	900.64	874.75	951.13	235.43	4.71
	1978	906.91	878.74	946.2	226.46	4.94
	2007	903.19	873.67	946.72	204.72	4.34
Mod.	*1956*	895.52	873.88	905.44	229.88	3.98
	1978	907.72	897.01	943.24	256.73	5.23
	2007	899.71	871.83	943.55	224.89	4.86
Well	*1956*	0	0	0	0	0
	1978	899.1	872.01	930.11	206.99	4.78
	2007	901.25	874.1	932.03	222.98	5.71

Changes in the distribution of the poorly and moderately developed water tracks both exhibited significant positive linear trends with R^2 values >0.90. The well-developed water tracks show an initial increase from 1956 to 1978 and then a decrease from 1976 to 2007. This may be due to changes in precipitation and soil moisture, which negatively affected species distribution or gradual channel incision which restricted saturated flow to a smaller area.

The mean elevation of water tracks varies with time, climbing initially in 1978 and then decreasing in 2007. This suggests that water tracks initially extend in distribution up the slope, and then expand in density in the lower elevations by 2007. Overall, water tracks in the Imnavait show a southwest (202.5–247.5°) aspect with significant variation only in the moderately developed classes with a shift in 1978 to west (247.5–292.5°). Well-developed water tracks show an increase in mean slope angle with time, supporting the notion that a decrease in overall precipitation or deeper active layer permitting more infiltration would restrict overland flow to the steeper areas.

Analysis of water track distribution and density from 1956 through 2007 showed an increase in both poorly and moderately defined tracks, while the well-developed water tracks decreased in area. This trend corroborates climate warming and may indicate increased amounts of solid precipitation as snow which leave the ground more saturated in the early growing season and, coupled with warming weather, provide ideal conditions for shrub expansion. The effect of the change in climatic conditions and the corresponding shrub expansion in this area on the permafrost will be examined in future work.

Acknowledgments

Many thanks to Matt Sprau for field assistance and Jason Stuckey of the Toolik Field Station GIS program. Funding was provided by a student research grant awarded by the Center for Global Change & Arctic System Research, University of Alaska Fairbanks.

References

Callaghan, T.V., Bjorn, L.O., Chernov, Y., Chapin, T., Christensen, T.R., Huntley, B., Ima, R.A., Johansson, M., Jolly, D., Jonasson, S., Matveyeva, N., Panikov, N., Oechel, W., Shaver, G., Schaphoff, S. & Sitch, S. 2004. Effects of changes in climate on landscape and regional processes, and feedbacks to the climate system. *Ambio* 33(7): 10.

Grosse, G., Schirrmeister, L. & Malthus, T.J. 2006. Application of Landsat-7 satellite data and a DEM for the quantification of thermokarst-affected terrain types in the periglacial Lena-Anabar coastal lowland. *Polar Research* 25(1): 51-67.

Hamilton, T.D. 1989. *Late* Cenezoic glaciation of the Central Brooks Range. In: T.D. Hamilton, K.M. Reed & R.M. Thorson (eds.), *Glaciation in Alaska: The Geologic Record,* Vol. 99. Anchorage, AK: Alaska Geol. Soc., 9-49.

Hinzman, L.D. & Kane, D.L. 1991. Snow hydrology of a headwater arctic basin. 2. Conceptual analysis and computer modeling. *Water Resources Research* 27(6): 1111-1121.

McNamara, J.P., Kane, D.L. & Hinzman, L.D. 1999. An analysis of an arctic channel network using a digital elevation model. *Geomorphology* 29: 339-353.

Osterkamp, T.E. & Payne, M.W. 1981. Estimates of permafrost thickness from well logs in Northern Alaska. *Cold Regions Science and Technology* 5(1): 13-27.

Stow, D.A., Hope, A., McGuire, D., Verbyla, D., Gamon, J., Huemmrich, F., Houston, S., Racine, C., Sturm, M., Tape, K., Hinzman, L., Yoshikawa, K., Tweedie, C., Noyle, B., Silapaswan, C., Douglas, D., Griffith, B., Jia, G., Epstein, H., Walker, D., Daeschner, S., Petersen, A., Zhou, L. & Myneni, R. 2004. Remote sensing of vegetation and land-cover change in Arctic Tundra Ecosystems. *Remote Sensing of Environment* 89: 281-308.

Van Everdingen, R. (ed.) 1998. *Multilanguage Glossary of Permafrost and Related Ground-Ice Terms.* Boulder, CO: National Snow and Ice Data Center for Glaciology.

Walker, M.D., Walker, D.A. & Auerbach, N.A. 1994. Plant communities of a tussock tundra landscape in the Brooks Range Foothills, Alaska. *Journal of Vegetation Science* 5: 843-866.

Detection of Degraded Mountain Permafrost with the Help of GPR Profiling at Mesón San Juan, Mendoza, Argentina

Dario Trombotto Liaudat
Geocryology Ianigla-Cricyt-Conicet, Casilla de Correo 330, 5500 Mendoza, Argentina
Jandyr Menezes Travassos
Observatório Nacional, Rua General José Cristino, 77, 20921-400, Rio de Janeiro, Brazil
Giovanni Chaves Stael
Observatório Nacional, Rua General José Cristino, 77, 20921-400, Rio de Janeiro, Brazil

This work shows the use of ground penetration radar (GPR) for detection of superficial structures of degradation in mountain permafrost imaging in an area of the Central Andes. Andean permafrost can be classified on the basis of topography, hydrology (or estimated ice content), and climate (global warming) (Trombotto 2003). Continuous or quasi continuous Andean permafrost still appears at -2 to -4°C, found on the mountain summits or as "island permafrost" if it appears as an isolated body. Permafrost types could be also subclassified on the basis of more or less than 10% of ground ice content (Brown et al. 1998).

The study area was a permafrost plateau at Mesón San Juan (Fig. 1, 6012 m, 33°30′S and 69°49′W), located on the foot of the glacier and bordering recent moraines at a height of 4400 m a result of the glaciation retreat of the Mesón San Juan summit and the consequent cryoweathering and erosion of the sediments produced by cryogenic phenomena. The Cenozoic volcanic Mesón San Juan with 6012 m are located on the Argentinean-Chilean border, south of Tupungato volcano (6570 m) and Cerro Aconcagua (6962 m), the highest mountain of the Western Hemisphere, in the province Mendoza.

The permafrost plateau at Mesón San Juan is related to the highest parts of the mountain and represents a type of

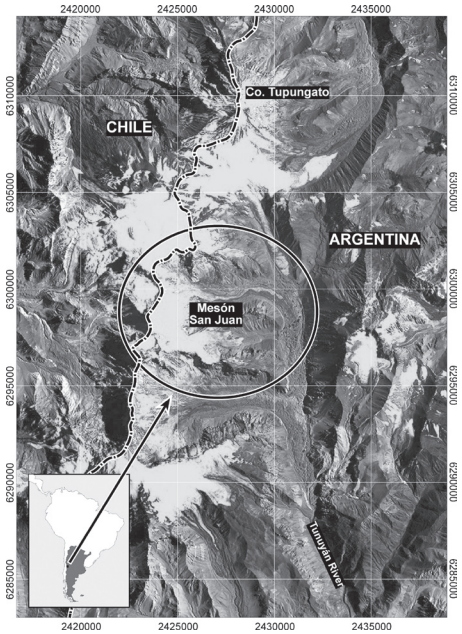

Figure 1. Study area.

cryoplanation surface of polygenetic origin on the foot of the glacier and bordering recent moraines at a height of 4400 m. It falls as glacier-shaped rocky slopes reaching down to 3600 m in the area. The plateau is a result of the glaciation retreat of the Mesón San Juan summit and the consequent cryoweathering and erosion of the sediments produced by cryogenic phenomena.

The GPR data were collected with PULSE EKKO IV equipment with a time window of 2048 ns, a sampling interval of 800 ps, a 1000 V transmitter, and 50 MHz antennae. The antennae were moved along fixed-offset profiles with a constant step size of 0.20 m and kept 2 m apart from each other. We kept the same step size for the central mid-point (CMP) profiles, where each antenna was moved away from another symmetrically in fixed steps of 0.10 m. We concentrate here on two profiles: one fixed-offset that is the result of merging two 51 m long profiles with directions 96º MN and 134º MN, the former along the largest dimension of the plateau; and two CMP profiles. The two mutually perpendicular CMP profiles were deployed crossing at the center point of the first fixed-offset profile. Each CMP profile was 31 m long, one of them having the same direction of the first fixed-offset profile. We also restricted the time-window to 1024 ns, where the signal-to-noise ratio is higher. We adopted a basic processing flux in our data set. After some editing, the time window was chopped off to earlier times, dewowed, low-pass filtered to reduce high-frequency noise, and gained with an automatic gain control.

The periglacial sedimentary cover on the plateau displays an open permeable structure. The thickness of the active layer and the depth to the permafrost table was obtained with 3 superficial holes reaching a depth of 1.20 m. One hole was drilled at the edge of the glaciation in an ice-covered area with transitional sediments from the SE wall of the glacier of the Mesón San Juan, thus correlating with the morainic area. Two holes were drilled further away on cryoplanation surfaces bordering the present glaciation and did not reach a permafrost table, but revealed the presence of a freezing level without any visible ice, which was interpreted as dry permafrost. Temperatures were obtained with Weston thermometers.

The CMP profiles yielded an average velocity of 0.09 m/ns, and a very interesting indication of lower velocity at two-way travel time ≥ 200 ns was discovered. There was a clear transition at 270 ns from a more conductive and inhomogeneous horizon to a less conductive, albeit still

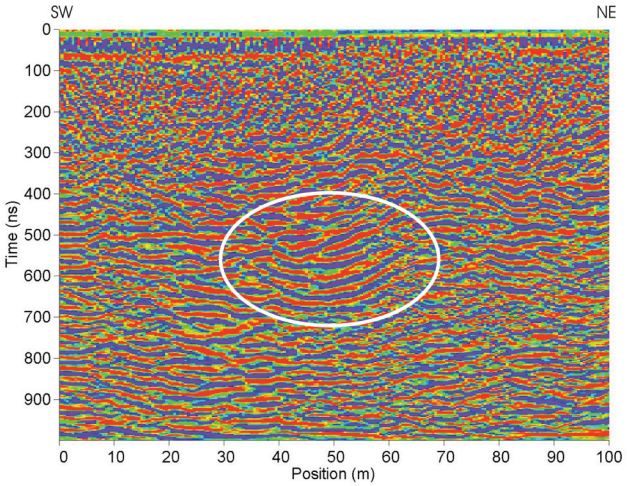

Figure 2. Migrated section with the I-zone.

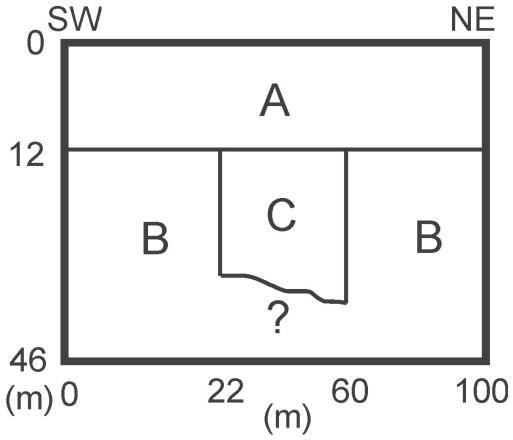

Figure 3. Interpretation of the subsoil at Mesón San Juan.

cluttered, subsurface. Another important characteristic of the section was relatively higher amplitudes seen at later times between 22 and 60 m of reflectors that do not display lateral continuity.

A migrated section, which has conspicuous smiles at later times inside a so-called vertical I-shaped zone located between 22 and 60 m, indicated a significantly smaller phase velocity within it (Fig. 2). The lower velocity I-zone is surrounded laterally by two zones of phase velocity, v = 0.09 m/ns. Moreover the tails of the diffractions in the I-zone indicate that the conductivity is lower compared to the remainder of the section. We found that the I-zone is correctly migrated only with very low velocities like the water velocity, v = 0.03 m/ns for migrating the section. We supposed by weight and low ion contents that it is a region of liquid water probably due to the degradation of permafrost. The I-zone is topped by a cluttered, more conductive horizon, reaching 270 ns or 12 m, that encompasses the active zone formed probably mainly by till and cryogenic sediments.

One explanation for the I-zone is that the segment is a discharge channel linking a suprapermafrost—a laterally discontinuous near-surface system not seen in this work—to a subpermafrost aquifer (Lawson et al. 1996). Most probably the source of that water is the retreating glacier above the plateau that finds its way through the morainic till, which composes the active layer. Figure 3 expresses the interpretation of the frozen and unfrozen subsoil. We expected to find the basement at 45–50 m, but that is beyond the limit of our data.

As already described for other areas (Trombotto et al. 1998), with gradual disappearance of snow patches, the retreat of the Andean glacier fronts generates a considerable input of melting water in the open structure of the Andean cryolithozone, which enhances erosion of suprapermafrost but also allows the water to penetrate through the discontinuities of the frozen soil, thus contributing to the degradation of its internal structure.

Acknowledgments

We would like to thank Dr. Alberto Aristarain (LEGAN) for his financial and logistical support, and José Hernández, José Corvalán, and Rafael Bottero for their technical support. JMT acknowledges a grant from the CNPq.

References

Brown, J., Ferrians Jr., O.J., Heginbottom, J.A. & Melnikov, E.S. 1998. *Cicum-Artic map of permafrost and ground-ice conditions.* U.S. Geological Survey.

Lawson, D.E., Strasser, J.C., Strasser, J.D., Arcone, S.A., Delaney, A.J. & Williams, C. 1996. *Geological and Geophysical Investigations of the Hydrogeology of Fort Wainwright, Alaska, Part I: Canol Road Area*. CRREL Report 96-4, 32.

Trombotto, D. 2003. Mapping of permafrost and the periglacial environment, Cordón del Plata, Argentina. *Proceedings of the Eighth International Conference on Permafrost, Zurich,* Extended Abstracts: Reporting Current Research and New Information, W. Haeberli & D. Brandová (eds.): 161-162.

Trombotto, D., Buk, E., Corvalán, J. & Hernández, J. 1998. Present state of measurements of cryogenic processes in the "Lagunita del Plata," Mendoza, Argentina, Report Nr. II. *Proceedings of the Seventh International Conference on Permafrost, Yellowknife, Canada*. Program, Abstracts, and IPA Reports, Extended Abstracts: 200-201.

Pleistocene and Holocene Periglacial Forms in the Cantabrian Mountains (Northwest Spain)

Dario Trombotto Liaudat
IANIGLA, CONICET, 5500 Mendoza, Argentina
V. Alonso
Departamento de Geología. Universidad de Oviedo. 33005, Oviedo, Spain

Detailed geomorphological mapping of a deglaciated area in the Cantabrian Mountains (CM) has revealed a great variety of periglacial forms that have been ascribed to different cryomeres during and following deglaciation.

The CM, with frequent altitudes around 2000 m, show erosional and depositional glacial features related to the Pleistocene last glacial cycle; distribution of till, erratic blocks and glacially abraded surfaces indicate ice thicknesses up to 400 m in some areas (Alonso & Suárez Rodríguez, 2004), while glacier fronts reached altitudes around 900 m a.s.l. in many of the valleys.

A geomorphological map, at a 1:5000 scale, was made for a sector to the south of the main watershed characterized by a homogeneous bedrock. The map has been analyzed in a regional context.

This zone around El Miro peak, 1985 m, shows a strong asymmetry in processes and forms. Most of them are fossil features. Rock glaciers (Fig. 1), felsenmeer, protalus, boulder lobes, solifluction forms, and talus deposits were developed, from glacially derived material or from cryosediment, on cold slopes.

Warm slopes, slighter or even nonglaciated, developed giant sorted stone stripes (Fig. 2), boulder lobes and stone-banked lobes from cryosediment.

In relation to deglaciation, gravitational slope readjustments took place in cirque zones and mixed landslides partially modified warm slopes; paraglacial alluvial fans were formed in adjacent valleys.

Deglaciation in this zone of the CM was dated to be before 34,000 ± 1400 ^{14}C yr BP in Laguna de Villaseca, at 1305 m a.s.l. (Jalut et al. 2004). But terminal moraine complexes at lower altitudes, formed when glaciers still were 11 km in length in areas with calculated previous ice thicknesses up to 260 m, suggest a long evolution between the beginning of deglaciation and stabilization phases during retreat. Other data worth mentioning (Pallàs et al. 2006) about the close region of the Pyrenees, where an early maximum glacier extent during the last glacial cycle is not excluded, indicate an extensive glaciation at ca. 18–20 ka (MIS 2), coinciding with the global LGM.

Altitude, aspect, preservation degree, and soil development of cryogenic forms around El Miro indicate more than one cryomere, although the lack of datable material has not allowed us to determine a precise time for these cryomeres. A tongue-shaped rock glacier in a cold and low position and giant sorted stripes on warm slopes, both proposed to be coeval with cirque glaciers, suggest continuous mountain permafrost in ice-free areas during deglaciation, when the most important indicators were cryogenic periglacial and not glacigenic. We propose that conditions during deglaciation were probably similar to those of the Pyrenees, where continuous permafrost and important cryogenic landforms with glacier ice at the same time are represented in the *Climex Map of 2002* for the Last Glacial Maximum.

The peak of the periglacial environment in the CM, however, must have occurred after the LGM, with predominantly much drier climatic conditions and benefitting from vaster areas uncovered by ice; discontinuous permafrost, expressed by rock glaciers during the Late Pleistocene or Early Holocene, is likely to have reached 1540 m a.s.l.

Figure 1. Fossil rock glacier.

Figure 2. Giant sorted stone stripes.

At higher altitudes, sparsely vegetated small forms with scarce or no development of soil—lobate rock glaciers, protalus, and boulder lobes—would correspond to more recent times; some of these landforms were probably active during the LIA. The rock glacier fronts end at approximately 1730 m a.s.l.

References

Alonso, V. & Suárez Rodríguez, A. 2004. Evidencias geomorfológicas de la existencia de un pequeño casquete glaciar en la Comarca de Babia Alta (Cordillera Cantábrica). *Revista de la Sociedad Geológica de España* 17: 61-70.

CLIMEX World Maps. 2002. Cartes des Envionnements du Monde pendant les deux derniers extremes climatiques. N. Petit-Maire, Ph. Bouysse (Scientific editors), CCGM, CGMW & ANDRA, France.

Jalut, G., Belet, J.M., García De Celis, A., Redondo Vega, J.M., Bonnet, L., Valero-Garcés, J.M., Moreno, A., Villar Pérez, L., Fontugne, M., Dedoubat, J.J., González-Sampériz, B.L., Santos Hidalgo, L. & Vidal Romaní, J.R. 2004. Reconstrucción paleoambiental de los últimos 35 000 años en el Noroeste de la Península Ibérica: La Laguna de Villaseca (León). *Geo-Temas* 6: 105-108.

Pallàs, R., Rodés, A., Braucher, R., Carcaillet, J., Ortuño, M., Bordonau, J., Bourlès, D., Vilaplana, J.M., Masana, E. & Santanach, P. 2006. Late Pleistocene and Holocene glaciation in the Pyrenees: a critical review and new evidence from ^{10}Be exposure ages, south-central Pyrenees. *Quaternary Science Reviews* 25: 2937-2963.

Permafrost Response to Dynamics of External Heat Exchange: Comparison of Observed and Modeled Data (Nadym-Pur-Taz Region)

Julia Ukhova
Institute of Environmental Geoscience, Russian Academy of Sciences, Moscow, Russia
Alexey Osokin
NadymGazProm, Nadym, Russia
Dmitry Sergeev
Institute of Environmental Geoscience, Russian Academy of Sciences, Moscow, Russia
Julia Stanilovskaya
Institute of Environmental Geoscience, Russian Academy of Sciences, Moscow, Russia

Introduction

The study of thermal state permafrost dynamics in connection with climate conditions has became topical in recent years.

Besides the air temperature, the amount of precipitation and the temperature of permafrost have increased in some areas since the 1960s (Israel et al. 2006, Pavlov et al. 2005). The problem of permafrost state forecast became significant for industrial companies. It requires the organizing of temperature permafrost monitoring. Most measured boreholes are located near industrial and civic constructions that disturb the ground temperature regime dynamics. It is difficult to consider the climatic role in permafrost temperature dynamics by using this data because the influence of construction and business activities is greatly powerful in local aspect. This problem impedes efficient permafrost forecasting because of the difficulty of model accuracy estimation.

Methods

The authors used mathematical modeling for the diagnosis of the man-caused disturbances factor that influences the permafrost temperature regime. We supposed that the codirectionality of modeled and observed temperature trends at low depths proves the weakness of anthropogenic influences in a short time period.

The forecast was done for the Nadym-Pyr-Taz region where climate warming is evident. The air temperatures have been increasing 0.05°C per year in the observed period 1960–1995. We modeled the ground temperature for a one-dimensional system, using the one-layer loamy silt configuration and observed mean monthly values of air temperature and snow cover depth (Fig. 1). We used the meteorological data from the Salekhard met-station, adding constant monthly average corrections in considering microclimatic features of the investigation site. Other climate characteristics were used as long-term average monthly values.

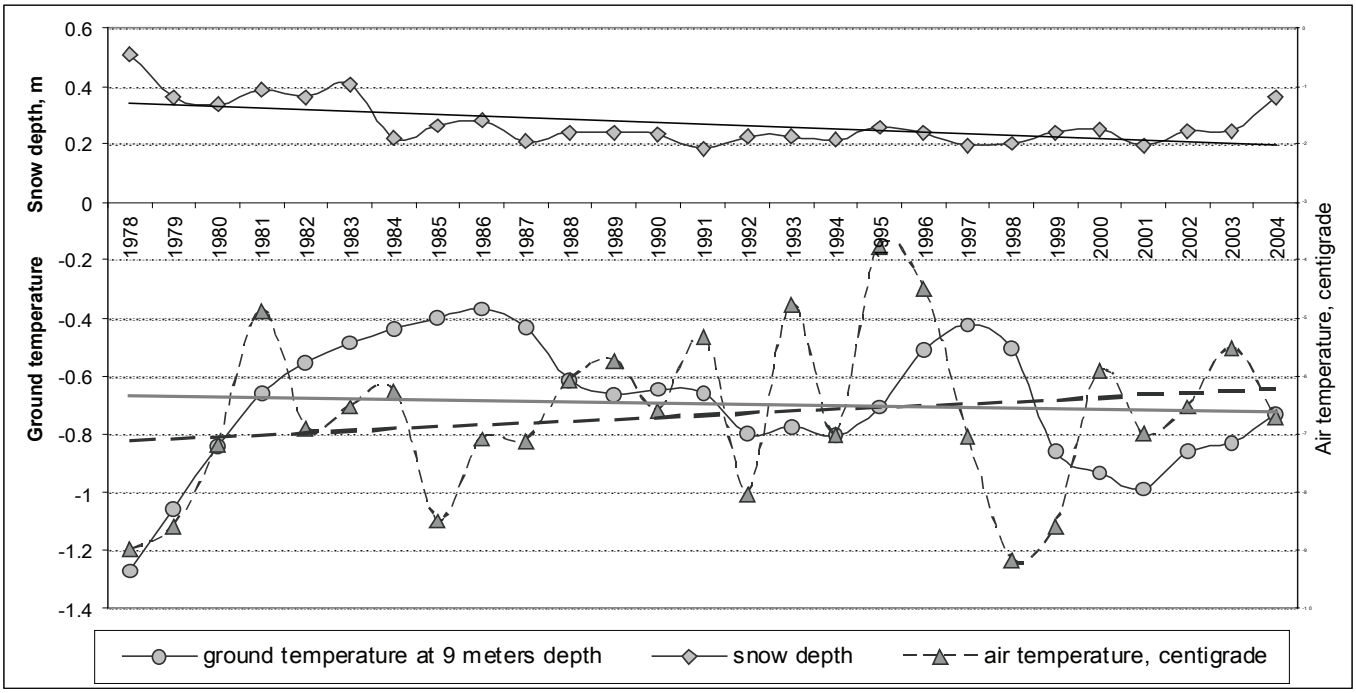

Figure 1. Long-term course of climate characteristics (air temperature and thickness of snow cover) and calculated ground temperature at 9 m depth.

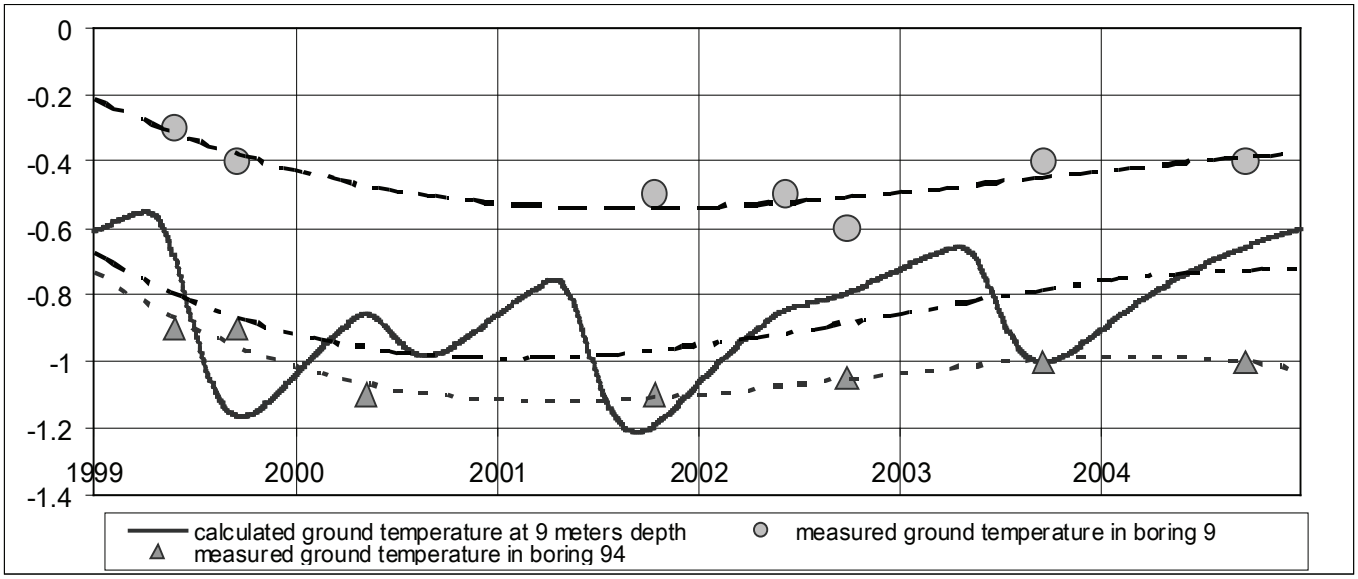

Figure 2. Comparison of measured and modeled ground temperature at 9 m depth.

The mathematical realization of the model was determined by G.S. Tipenko. The calculated values of ground temperature at 9 m depth was obtained and compared with the climate trend.

Results

The course of the modeled ground temperature is conformable to the measured temperature trend in boreholes #9 and #94.

We supposed that boreholes #9 and #94 are located in undisturbed conditions in the industrial area. The disagreement in the absolute value of the ground temperature in these boreholes is determined by the variability of snow cover. The data in detail of snow cover are not available; however, the interannual course of ground temperature at low depths is probably defined by climate dynamics, especially by the snow cover trend.

It is seen that the course of snow cover dynamics in long-range aspect has a stronger influence on ground temperature at low depth when compared with the course of air temperature.

To generalize, the framed and calibrated model of dynamic ground temperature allowed us to forecast the permafrost dynamics, depending not only on air temperature change but also on other factors of surface heat exchange. The model calibration criterion was the agreement fact of the trends rather than the desired accuracy of model parameter. Comparing the model of boreholes in undisturbed and disturbed conditions, the influence of technogenesis cannot be allowed. Thus, the data of climate contribution in the dynamics of permafrost temperature can be obtained. The boreholes that have the different tendency are strongly influenced by building and other man-caused factors.

References

Israel, J.A., Pavlov, A.V., Anokhin, J.A., Myach, L.T. & Chertyukov, B.G. 2006. Statistical estimation of climate components change in permafrost area in Russia. *Meteorology and Hydrology* 5: 27-38 (in Russian).

Pavlov, A.V. 2002. Century anomalies of the air temperature on the Russian North. *Earth Cryosphere* 6(2): 75–81 (in Russian).

Pavlov, A.V. & Malkova, G.V. 2005. *Actual Climate Change on the Russian North: Album of Low-Scale Maps*. Novosibirsk: GEO, 54 (in Russian).

Application of DC Resistivity Tomography in the Alpine Area of the Southern Carpathians (Romania)

Petru Urdea, Florina Ardelean, Alexandru Opaca, Mircea Ardelean, Marcel Török-Oance
West University of Timişoara, Department of Geography, B-dul. V. Parvan, Nr. 4, 300223, Timişoara, Romania

Introduction

During the last decade, the use of geophysical techniques has become increasingly important in geomorphological study and for many geomorphologists, new and exciting tools (Schrott & Sass 2008).

The acquisition of a complex geophysical system, PASI 16GS24, opens new possibilities for performance investigations of some landforms and deposits of the alpine area of the Southern Carpathians—for first time in Romanian geomorphology—and, accordingly, the aim of this paper is to present some results of the application of DC resistivity tomography in alpine area of the Southern Carpathians (Romania). By application of geophysical techniques on different geomorphic deposits, we have the possibility to gain insight into their overall thickness and inner structures, as well as the aspect of the contact surfaces with bedrock (Milmson 1996).

Study area

The Southern Carpathians, or Transylvanian Alps, are the most massive and the highest part of the Romanian Carpathians, having 11 peaks above 2500 m and a maximum elevation of 2544 m in Moldoveanu Peak (Făgăraş Mountains). In the high area of the Southern Carpathians, the geomorphological landscape is dominated by glacial landforms, the detailed characteristics being due to periglacial forms, like rock glaciers, talus cones, and scree slopes, block fields, rock streams, cryoplanation terraces, patterned ground, solifluction forms, etc. (Urdea et al. 2004).

Geophysical investigations were carried out in numerous study areas of the Southern Carpathians in the Făgăraş, Retezat, and Şureanu Mountains (Fig. 1), representative units for the main geomorphological landscapes of Romanian Carpathians. Our investigation focused on rock glaciers, scree slope deposits, late glacial stadial moraines, post-glacial in-filled glacial depressions, solifluction lobes, and fossil patterned grounds (Table 1).

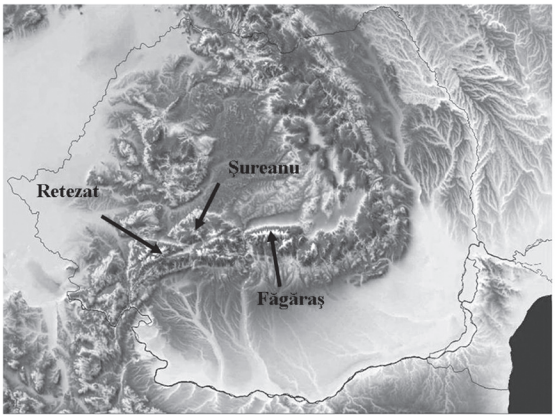

Figure 1. Location of the investigated areas.

Methodology

The PASI system consisted of 32 electrodes with a standard spacing of 5 m. In function of deposits and landforms dipole-dipole, Wenner and Wenner-Schlumberger arrays was used, with a maximum penetration depth of 30 m. The longitudinal profiles were carried, and for rock glaciers were carried also longitudinal and transversal profiles. Due

Table 1. Location of DC resisitivity investigations.

Area & date	Altitude (m)	Latitude Longitude
Scree slopes		
Bâlea Lake (Făgăraş Mts.) 03.07.2007	2088	45°36′06″ N 24°37′10″ E
Văiuga (Făgăraş Mts.) 11.09.2007	2270	45°35′17″ N 24°37′22″ E
Stadial moraines		
Doamnei Valley (Făgăraş Mts.) 04.07.2007	1903	45°36′19″ N 24°35′51″ E
Rock glaciers		
Ana (Retezat Mts.) 22.08.2007	1989	45°21′13″ N 22°52′04″ E
Pietrele (Retezat Mts.) 23.08.2007	2043	45°22′13″ N 22°52′16″ E
Capra (Făgăraş Mts.) 10.09.2007	1928	45°35′20″ N 24°37′19″ E
Postglacial in-filled glacial depression		
Valea Doamnei (Făgăraş Mts.) 04.07.2007	1879 m	45°36′21″ N 24°35′49″ E
Căldarea Berbecilor (Făgăraş Mts. 03.07.2007	1907	45°36′33″ N 24°37′07″ E
Şureanu (Şureanu Mts.) 26.08.2007	1769	45°34′51″ N 23°30′33″ E
Solifluction lobes		
Paltinu (Făgăraş Mts.) 06.07.2007	2372	45°35′52″ N 24°36′25″ E
Patterned grounds (fossil)		
Paltinu – Piscu Negru (Făgăraş Mts.) 06.07.2007	2338	45°35′48″ N 24°36′26″ E

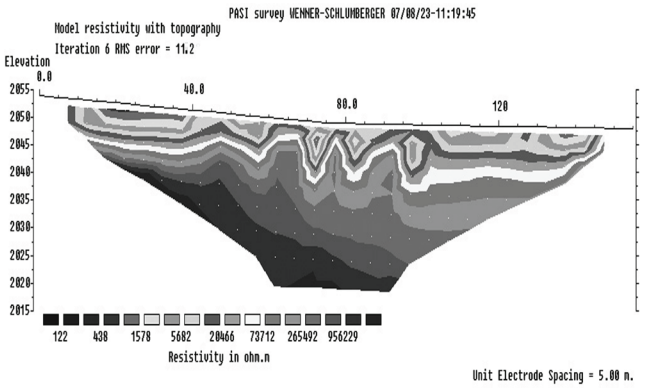

Figure 2. 2-D resistivity longitudinal section at Pietrele rock glaciers.

to the special characteristics, in the case of solifluction lobe and fossil patterned ground, the electrodes were arranged in a different configuration, on equal distance of 1 m, which permits a differentiation of distinct layers of 40–50 cm. Two-dimensional model interpretation was undertaken using the software package RES2DINV (Loke 1999). This software package produces a two-dimensional subsurface model from the apparent resistivity pseudosection.

Results and Interpretation

Application of 2-D electrical resistivity tomography began with measurements in Făgăraş, Retezat, and Şureanu Mountains on different geomorphic landforms, such as rock glaciers, scree slopes, solifluction lobes, fossil patterned ground, and glacial overdeepening depression filled with postglacial sediments. In all cases the results show varying resistivity. Starting with this design, we can know and interpret the structure of different deposits and, importantly, the depth and configuration of the surface contact with bedrock. In the case of scree deposits is the evidence of the presence of quasi-layered structure and some different bodies of rock blocks and/or fines—made by downwash and debris flow processes—with contrasting resistivity (more than 10 kΩ/m and, respectively, less than 2 kΩ/m). For fossil-patterned grounds are revealed undulating layers and elipsoidal bodies of fines, more humid and with low resistivity (500–800 Ω/m). In the case of Ana and Pietrele rock glaciers, electrical tomography reveals typical structures, and, important for permafrost scientists, the presence of ice-rich bodies in the Ana rock glaciers or ice-rich layer on Pietrele rock glaciers, revealed by high resistivities, on the order of more than 900 k Ω/m (Fig. 2).

We must mention that the presence of permafrost in the reported area was indicated by BTS measurements and by the low temperatures (<2°C) of the spring situated on the base of the front of rock glaciers Pietrele (Urdea 1993).

Acknowledgments

The authors are grateful to numerous students from West University of Timişoara for their committed help in carrying and installing the heavy equipment in the field. Financial expenses was supported by National Council for University Research (grant CEEX 738/2006).

References

Farbrot, H., Isaksen, K., Eiken, T., Kääb, A. & Sollid, J. 2005. Composition and internal structures of a rock glacier on the strandflat of western Spitsbergen, Svalbard. *Norwegian Journal of Geography* 59: 139-148.

Loke, M.H. 1999. Electrical imaging suurvey for environ-*mental and engineering studies – a practical guide to 2-D and 3-D surveys*. Copyright by M.H. Loke, Penang, Malaysia.

Milmson, J. 1996. *Field Geophysics*. Chichester: Wiley, 187 pp.

Sass, O. 2006. Determination of the internal structure of alpine talus deposits using different geophysical methods (Lechtaler Alps, Austria). *Geomorphology* 80: 45-58.

Schrott, L., Sass, O. 2007. Application of field geophysics in geomorphology: Advances and limitations exemplified by case studies. *Geomorphology* 93: 55-73.

Urdea, P. 1993. Permafrost and periglacial forms in the Romanian Carpathians. *Proceedings of the Sixth International Conference on Permafrost.* South China University of Technology Press, I: 631-637.

Urdea, P., Vuia, F., Ardelean, M., Voiculescu, M. & Török-Oance, M. 2004. Investigations of some present-day geomorphological processes in the alpine area of the Southern Carpathians (Transylvanian Alps). *Geomorphologia Slovaca* 4(1): 5-11.

Repeated Mapping of the Northern Taiga Ecosystems in West Siberia, Disturbed by Pipeline Construction

E.V. Ustinova
Earth Cryosphere Institute, Tyumen, Russia

Engineering construction in the north of West Siberia leads to disturbances of vegetation cover and changing permafrost conditions. The scale of changes is in direct relation to the degree of human-induced disturbance and landscape properties. Many natural features can be lost under increasing anthropogenic pressure; therefore, solving the problem of rational land usage and wildlife management becomes extremely difficult. The information presented here results from ecosystem monitoring.

Monitoring of disturbed ecosystems has been carried out for 35 years along a gas pipeline located in the subzone of northern taiga at the Nadym field station. Terrain changes are studied every 3–5 years by large-scale repeated mapping of the territory, using contemporary air photos and fieldwork. The last analyses were made in 2006. The greatest environmental disturbances occurred during pipeline construction in 1971–1972 and pipeline replacement in 2004. Smaller changes took place in 1974 in relation to electrical line construction, and in 1983, in adding new fill to the embankment. The service road along the pipeline is reconstructed every year.

Disturbance of natural conditions triggered activation of thermokarst and frost heave. Bog formation in areas ponded by embankments and wind erosion of sand on dry sites also take place. Observations show that in disturbed areas the occurrence of lakes has increased 22%.

The landscape hierarchy was described according to Melnikov (1983) using information on permafrost distribution, topography, and vegetation. A series of digital maps shows natural terrain units (ecosytems) as well as terrain units affected by construction over the time period from 1970 to 2006. These maps are based on air photography of different years and on field surveys. The location of monitoring sites, temperature boreholes, and features related to cryogenic processes are shown as well. The database of boreholes is linked to the maps.

The analysis of the maps compiled for different years revealed changes in the area of human-induced disturbances and trends in ecosystem development under the impact of climatic changes and disturbances (Fig. 1). After construction, the width of the disturbance zone increased differently in the various terrains. The increase in boggy areas due to swamping of the forest ecosystems was determined by comparing the maps of 1970 with those of 1988 (Fig. 1).

During 2004 pipeline reconstruction, pipes were replaced. The histogram (Fig. 2) is based on comparison of the terrain map of 1970, which was prepared prior to construction of a gas pipeline, and the map of 2005. Figure 2 shows that human-induced disturbance has caused an increase of 2.9%

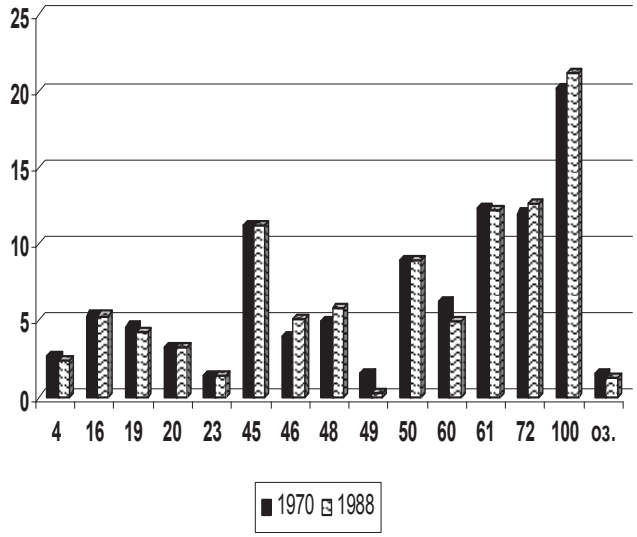

Figure1: Frequency of ecosystems at the Nadym site in 1970 and 1988 years.
4 - dry gentle slopes with birch-pine-cowberry-lichen sparse forests; 16 - flat slightly drained sites with birch-pine-wild rosemary-lichen–moss sparse forests; 19 - flat boggy sites with larch-wild rosemary-moss open forests; 20 - flat boggy sites with hummocky larch-wild rosemary-lichen-moss open forests; 23 - peat-mineral frost mounds with sedge-shrub lichen-moss open larch-pine woodland; 45 - hollows with sedge-moss mires; 46 - hollows and flat sites with tussocky sedge-moss mires; 48 - flat sites with hummocky sedge-peat moss bogs; 49 - flat sites with dwarf shrub-sedge-peat moss bogs; 50 - hollows occupied bogs with dwarf shrub-sedge-peat moss ridges and sedge-moss pools; 60 - flat sites with cloudberry-wild rosemary-moss- peatlands, 61 - flat sites with cloudberry-wild rosemary-moss-lichen peatlands; 72 - palsa peatland with sedge-shrub-moss-lichen cover on palsa and sedge-peat moss on pools between palsa; 100 - flat sites with hummocky tundras with sedge-shrub-moss-lichen cover on hummocks and sedge-peat moss on pools and rare frost boils; 03 - lakes.

in the area of hummocky sites (ecosystem 100), 1.8% in the areas of bogs (ecosystems 45, 46, 48), and 1.5% in the area of palsa peatland (ecosystem 72). Some flat areas (ecosystems 60 and 61) have partly recovered, however, and disturbance decreased by 2.8%.

Most disturbance relates to the removal of vegetation, modification of a microrelief, removal of 10 to 20 cm of peat during clearing of the right-of-way, and partial destruction of vegetation as a result of road transportation. The smaller areas occupy the sites disturbed as a result of caterpillar transport travel, where vegetation, soil cover, and microrelief have been broken only in part. The areas occupied by sites

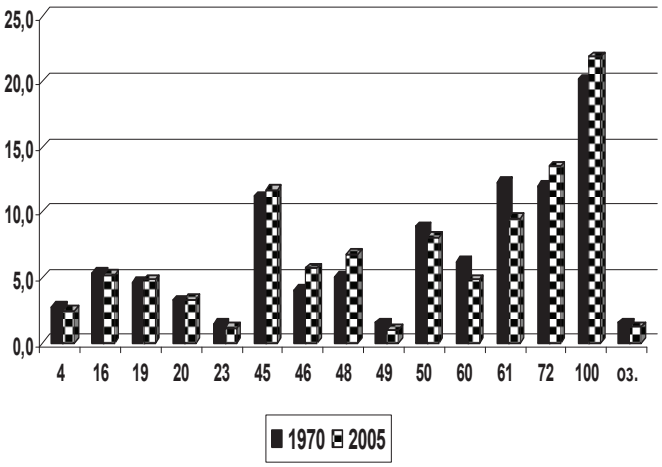

Figure 2. Frequency of ecosystems at the Nadym site in the years 1970–2005.

which have undergone other kinds of disturbance (burial and destruction of vegetative cover as a result of formation leading the removed vegetation), do not exceed 15%.

More often because of various human-induced loadings and various degrees of stability of covers, mosaic groupings are formed, including simultaneously 3–4 types of disturbance. Most all disturbance of all types was in 2004, during reconstruction of a gas pipeline.

Construction of service roads led to sufficient change in the regime of surface water and swamping of the surrounding territory and appearance of new lakes. With time, areas of lakes decrease as a result of swamping. Small frost mounds and palsas up to 1 m in height appeared in the surrounding areas.

Vegetation recovery is on sandy, well-drained sites. Natural recovery on the wet clayey soils is much faster. The highest rate of recovery of the disturbed vegetation takes place on boggy sites, where almost continuous vegetation cover was observed 3–4 years after disturbance. Lack of moisture on well-drained sites is one of the major factors that slow down vegetation recovery.

The degree of ecosystem resistance to recovery can be used for classification and mapping of geoecological hazards. Maps can be used for planning purposes. Maps of ecosystem conditions prepared for different years are a good tool for studying changes in ecosystems; for example, to find the occurrence of new frost mounds on bogs.

Repeated landscape mapping enables us to locate a zone of natural ecosystem disturbance and to trace its changes at the time of observation. Compiled landscape maps can form a basis for geoecological maps and for forecast maps of ecosystems impacted by pipelines and roads construction.

References

Mann, R.E. 1973. *Global Environmental Monitoring System (GEMS). Action Plan for Phase 1.* SCOPE, rep. 3. Toronto, 130 pp.

Melnikov E.S. (ed.) 1983. *Terrain Units of Permafrost Zone of the West Siberian Gas Province*. Novosibirsk: Nauka, 165 pp.

Moskalenko N.G. (ed.) 2006. *Anthropogenic Changes of Ecosystems in West Siberian Gas Province.* M., RASHN, 358 pp.

Forcing Factors of Permafrost Retreat: A Comparison Between LGM and Present-Day Permafrost Extent in Eurasia

Jef Vandenberghe
Institute of Earth Sciences, VU University Amsterdam, The Netherlands
Andrei Velichko
Laboratory of Evolutionary Geography, RAS, Moscow, Russia
Aldar Gorbunov
Permafrost Institute, SD RAS, Almaty, Kazakhstan

In recent years, it has been shown that growth and especially decay of permafrost may have tremendous effects on the environmental conditions of the concerned region. Attributing the cause for changes in permafrost occurrence only to global temperature changes is apparently too simple. There are a number of feedback mechanisms that potentially may induce regional differences in permafrost extension or reduction. In this short note, we expand on the factors that have contributed to the northward displacement of the southern permafrost limit on the Eurasian continent since the last glacial maximum (LGM) and which role potentially may be enhanced in the near future.

For that purpose we have constructed the southernmost extent of the permafrost during the LGM by combining different sources of research, and compared that with the present-day permafrost extent. Mapping the southern limit of permafrost is not as simple as it may look because of several reasons:

- LGM permafrost maps are not always distinctive in describing whether the permafrost is continuous, discontinuous, or sporadic.
- Even when this distinction is made, the definitions of those terms are not always the same in the different papers.
- The age of permafrost indicators of the LGM has often not precisely been defined.
- The altitude plays a decisive role in permafrost distribution, and the distinction between latitudinal and mountainous permafrost may be diffusive (French 1996).
- High altitudes may shift the latitudinal permafrost limit substantially southward.

With these restrictions in mind we (re)constructed for both periods the location of the position of the southern limit of permafrost (including sporadic, island, and discontinuous permafrost) and that of continuous permafrost (Fig. 1).

For the present-day situation, we based us essentially on the Arctic Permafrost Map as compiled by Brown et al. (1998). In the zone of continuous permafrost, regions with mountainous permafrost are included (e.g., in the Ural Mountains and especially in eastern Siberia). The LGM reconstruction is more complicated. For western and central Europe, we used data published by Van Vliet (1996), Renssen & Vandenberghe (2003), Vandenberghe et

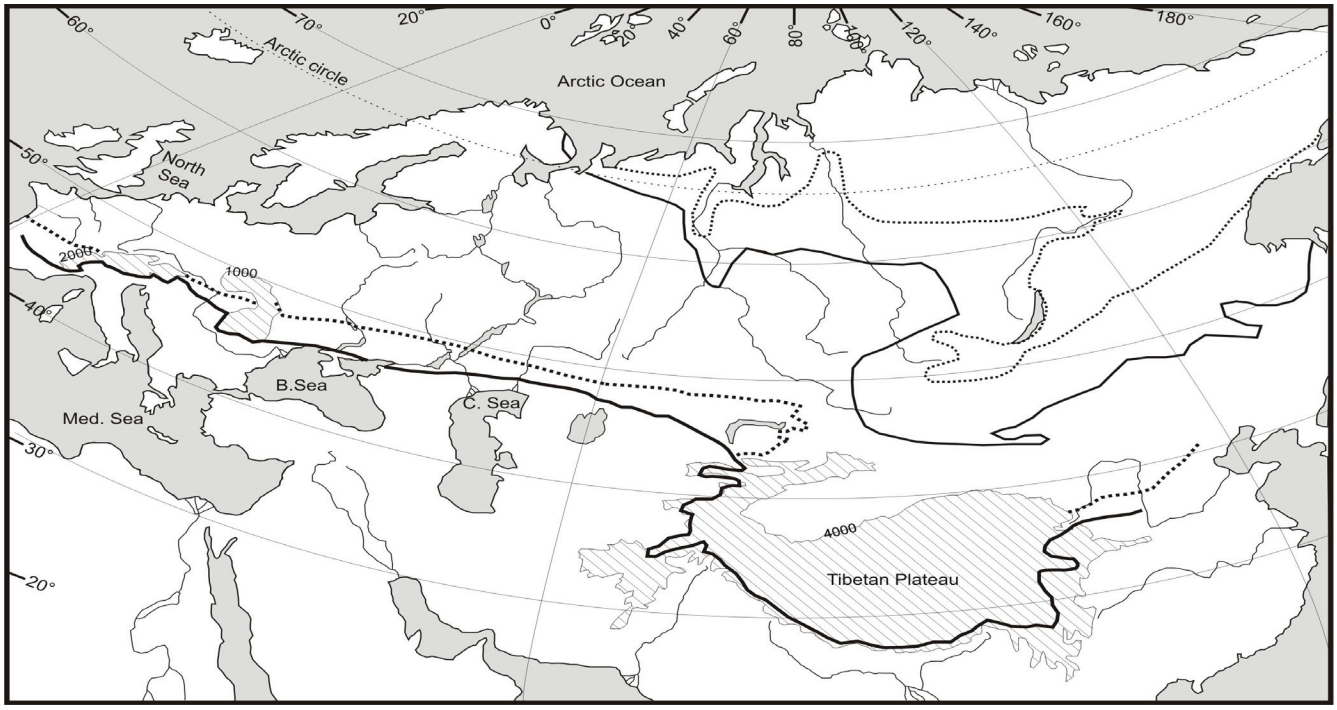

Figure 1. Southern limits of modern permafrost (upper full line) and continuous permafrost (upper stippled line), and LGM permafrost (lower full line) and continuous permafrost (lower stippled line), largely based on Aubekerov & Gorbunov (1999), Vandenberghe et al. (2004a,b) and Velichko (2002).

al. (2004b); for Russia, maps provided by Velichko (2002); for Kazakhstan, a map by Aubekerov & Gorbunov (1999); and for China, data compiled from different sources (e.g., Vandenberghe et al. 2004a). Especially in regions where the boundary between discontinuous and continuous permafrost is crossing mountainous areas, the zone of discontinuous and sporadic permafrost may be very limited in extent and, as such, not exactly defined in the published literature. For the LGM situation, this is the case, for instance, in the southern Central Massif (France), the southern Carpathians, and the southern margin of the Tibetan Plateau.

A few striking results appear from the comparison between LGM and present-day permafrost extension limits. We derive a general, extremely constant west–east orientation of the permafrost boundary during the LGM at around 52°N latitude in lowlands, apart from minor expulsions to the south in upland regions (e.g., Central Massif, Carpathians) and a major southward expulsion due to the mountain permafrost of the Tibetan Plateau. This is in line with the zonal extension of permafrost reported by Huijzer and Vandenberghe (1998) for west and central Europe and by Velichko (1973) for southern Russia. It may be explained by the combined cold sources of sea ice and ice sheets in the North Atlantic Ocean, Arctic Sea, northern Europe, and Siberia. Tracks of westerly winds were shifted towards the south and, in any case, were not able to induce maritime influences on the continent at the latitude of permafrost occurrence (Isarin & Renssen 1999, Renssen & Vandenberghe 2003).

The present-day situation shows a distribution pattern that significantly differs from the LGM pattern. The southern limit of permafrost shows a clear shift to the south from c. 69°N latitude south of Nova Zembla to 66° in west Siberia and 61° in east Siberia (around the Lena River). The latitudinal permafrost occurrence in easternmost Siberia is difficult to determine because of the interference with altitudinal permafrost. This Eurasian permafrost extension is obviously directed by the cold Arctic Sea, while there is no steering at all by North Atlantic sea ice. Maritime influences, through westerlies that transport temperate air from the North Atlantic waters, are diminishing towards the east. On the contrary, warm equatorial waters are entering the North Atlantic Ocean at present by the Gulf Stream.

Thus, both the temperatures over the North Atlantic and the Arctic Sea determine the extent of permafrost over Eurasia. During the LGM the cold (frozen) North Atlantic Ocean and Arctic Sea induced the regular zonal pattern with overall west–east oriented permafrost limit. By now the North Atlantic Ocean change to warmer conditions induced a northward shift of the permafrost limit over Europe, which is gradually disappearing eastward over Siberia.

References

Aubekerov, B. & Gorbunov, A. 1999. Quaternary permafrost and mountain glaciation in Kazakhstan. *Permafrost and Periglacial Processes* 10: 65-80.

Brown, J., Ferrians, O.J., Jr., Heginbottom, J.A. & Melnikov. E.S. 1998. Revised February 2001. *Circum-Arctic Map of Permafrost and Ground-Ice Conditions*. Boulder, CO: National Snow and Ice Data Center/ World Data Center for Glaciology. Digital Media.

French, H.M. 1996. *The Periglacial Environment,* 2nd ed.), Edinburgh Gate: Addison Wesley Longman.

Huijzer, A.S. & Vandenberghe, J. 1998. Climatic reconstruction of the Weichselian Pleniglacial in north-western and central Europe. *Journal of Quaternary Science* 13: 391-417.

Isarin, R.F.B. & Renssen, H. 1999. Reconstructing and modelling Late Weichselian climates: the Younger Dryas in Europe as a case study. *Earth Sci. Rev*. 48: 1-38.

Renssen, H. & Vandenberghe, J. 2003. Investigation of the relationship between permafrost distribution in NW Europe and extensive winter sea-ice cover in the North Atlantic Ocean during the cold phases of the Last Glaciation. *Quaternary Science Reviews* 22: 209-223.

Vandenberghe, J., Cui, Z.J., Zhao, L. & Zhang W. 2004a. Thermal contraction crack networks as evidence for Late-Pleistocene permafrost in Inner Mongolia. *Permafrost and Periglacial Processes* 15: 21-29.

Vandenberghe, J., Lowe, J., Coope, G.R., Litt, T. & Zöller, L. 2004b. Climatic and environmental variability in the Mid-Latitude Europe sector during the last interglacial-glacial cycle. In: R. Battarbee, F. Gasse, & C. Stickley (eds.), *Past Climate Variability through Europe and Africa: PEPIII Conference Proceedings*. Dordrecht: Kluwer, 393-416.

Van Vliet-Lanoë, B. 1996. Relations entre la contraction thermique des sols en Europe du Nord-Ouest et la dynamique de l'ínlandsis Weichsélien. *Comptes Rendus Académie des Sciences de Paris* 322, série IIa: 461-468.

Velichko, A.A. 1973. Paragenesis of a cryogenic (periglacial) zone. *Biuletyn Peryglacjalny* 7: 89-110.

Velichko, A.A. 2002. *Dynamics of terrestrial landscape components and inner marine basins of Northern Eurasia during the last 130,000 years*. A.A. Velichko (ed.-in-chief). Moscow: GEOS Publishing House, 231 pp. (in Russian).

Application of Georadar in the Cryosphere for the Study of Engineering Constructions

Sergey Velikin
Viluy Permafrost Station of the Permafrost Institute, RAS Siberian Branch, Chernishevskii
Rudolf Czhan
Permafrost Institute, RAS Siberian Branch, Yakutsk

The ground-penetrating radar (GPR) method is very useful for the study and monitoring of different engineering constructions foundation beds. The advantages of GPR are mobility, compactness, and possibility of continuous observation. The results of a GPR survey with different day surface preparations—cleaning, surfacing, wettings—are presented. Seasonal peculiarities of the state of ground sections were also taken into consideration for GPR data interpretation. This approach, in some cases, improves the effectiveness of GPR surveys performed in Western Yakutia.

The effectiveness of the GPR method for the study and diagnosis of engineering constructions foundation beds can be improved as a result of special day surface preparation (cleaning**,** surfacing**,** and wetting) before survey. The other factor of GPR data improvement is seasonal observations (Judge at al. 1991). A priori information about lithology of sections, changes of temperature condition in basement soils, and temperatures of the beginning of thawing-freezing gives a key to the effective use of GPR technologies for the study and control of engineering constructions, buildings, and road coverings. Use of georadar sections difference observable in winter and summer time, before and after precipitations, that is, in various temperature-moisture conditions, is very informative (Velikin at al. 2000).

Figure 1 shows the result of a GPR survey along a road with a concrete covering. Measurements were carried out with the same equipment at a present small air-gap (4 cm) between the bottom of the antenna and road (measurements on a support with wheels) and without it (shooting without a support). As shown in Figure 1, in the case of measurements, an antenna radarogramma raised above the road is considerably noisy in comparison with the results of observation without a support that complicates section study.

After clearing road dirt from along the top of Sitikan reservoir dam, GPR data revealed rather detailed elements of the dam structure. Knowledge of the positions of the revealed elements allows supervision of the state of Sitikan dam while conducting building actions (strengthening of a road cloth, cementation of embanked sections weakened during object exploitation). Figure 2 shows the result on GPR data quality of cleaning the Sitikan reservoir ice sheet. After cleaning, the noise level becomes much lower. These data were used for proper determination of the thickness of the underwater part of bank slope anti-seepage filling.

It is important to note that cleaning and smoothing of sounding surfaces sharply improves radarogramm quality due to reduction of the influence of microrelief and a non-uniform covering of study sites with dirt and sleet, which can considerably deform and attenuate signals.

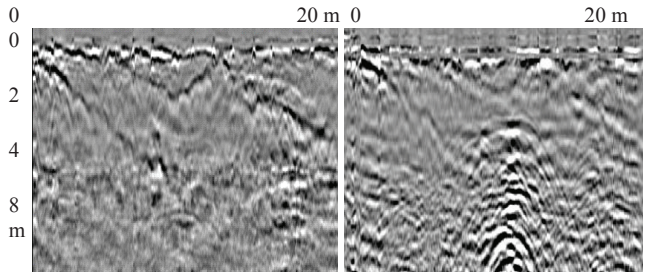

a) b) noise from air electric main

Figure 1. An example of a small air stratum effect (4 cm) between the bottom of antenna (facility SIR2000 antenna FGMOD5106, f = 200 MHz) and probing surface (concrete-surfaced road on frozen foundation): a) georadarogramm with antenna without air-gap (no support); b) georadarogramm with uplifted antenna (4 cm air-gap due to support on wheels).

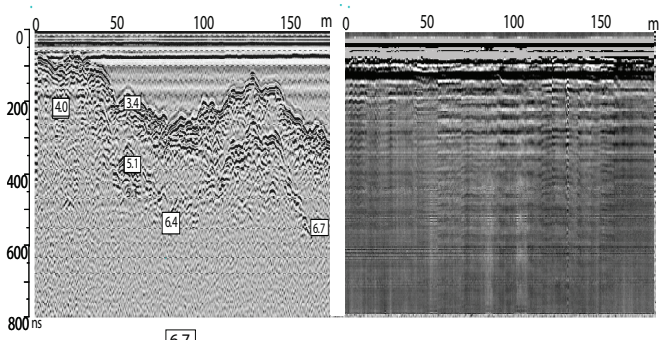

6.7 Depth of reflectors in meters

Figure 2. Georadar observation from the ice sheet of Sitikan reservoir (bottom sediments study). On the left: GPR observation after ice cleaning from sleet mixed with road dust.

Figure 3 presents GPR mapping of the productive horizon basement and reveals details of its structure. This becomes possible only after removal of the soil-vegetative layer, which was a strong screen because of high humidity and presence of a clay sheet.

Among other measures on preparation of probing surfaces, it is necessary to note filling with a fine-grained material and smoothing of a surface of studied structures. In particular at one of the dams in western Yakutia, it revealed with high resolution a weakened zone and a filtration window in the body of the dam (Fig. 4).

During a georadar survey, good effect gives the use of seasonal and weather factors; that is, sounding in freezing and thawing conditions of investigated sections, before and after surface wetting by rainfall.

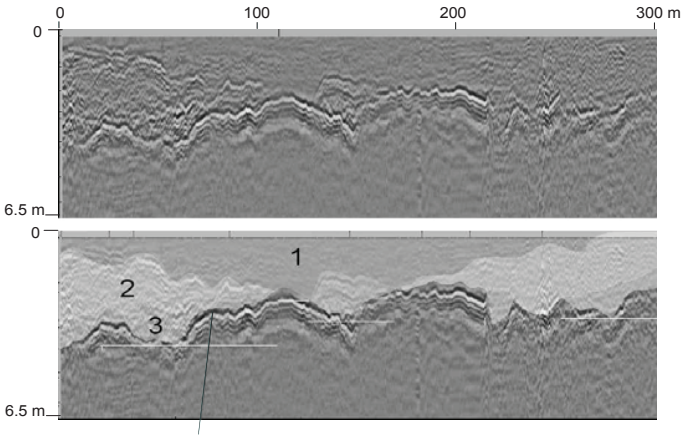

Figure 3. Georadar plot of diamond alluvial deposit from diamond-field in Western Yakutia: a) radarogramm after preliminary processing; b) radarogramm with picked geoelectric horizons corresponding to different soils of terrace sediments.

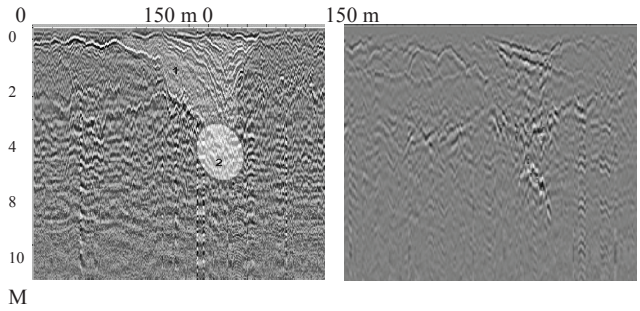

Figure 4. Radarogramm along coping of settling pound. Detecting seepage zone in the body of dam. 1: outline of deconsolidation sink; 2: seepage zone. On the right, road-covered wet mud with broken stone. On the left, road after preparation.

In December 2005 and February 2006, GPR seasonal surveys were performed on a diamond alluvial deposit during winter frost penetration time. It appeared that, in December, the maximum frost penetration and summer maximum thaw depth rather precisely marked out, which has proved to be true by temperature observations. Further in January–February, during further freezing of a section, lithological borders, including the roof and bottom of the productive horizon, distinctly stand out on the radarogramm, which proves to be true by the geological data on cores and description of a prospecting shaft. During processing, the account of a relief of a daytime surface has been carried out, and it has revealed confidently the bottom of the productive horizon, to define its depth and thickness for the moment of the beginning dragging works. Consequently, it was possible to predict the state of soils developed section (time of thawing of productive horizon after filling dragging a foundation trench).

Conclusion

The results presented in our work show that during georadar survey, application of different types of preparation of studied surfaces (cleaning, filling, smoothing, wetting, etc.), as well as using and accounting seasonal- climatic and weather factors, allows productivity increase of GPR survey in many cases.

In spite of that, in a basis of georadar survey is difference of rocks and soils in dielectric permittivity and electro conductivity, the basic character of georadar sections lays, as a rule, reflects mainly lithological boundaries (Finkelshtein et al. 1977, Vladov & Starovoitov 2005). Boundaries associated with the geocryological state frequently have a secondary character and come to light on a radarogramm less precisely. In many cases, basic elements of geocryological structure come to light more brightly during the periods which are not corresponding seasonal geocryological state. In particular, it concerns the boundary of maximal seasonal thawing during intensive freezing.

References

Finkelshtein, M.I., Mendelson, V.L. & Kuteev, V.A. 1977. *Radar-Location of Layered Terrestrial Covers*. Moscow: Soviet Radio, 176 pp. (in Russian).

Judge, A.S., Tucker, C.M., Pilon, J.A. & Moorman, B.J. 1991. Remote Sensing of Permafrost by Ground-Penetrating Radar at Two Airports in Arctic Canada. *Arctic* 44 Supp. 1: 4-48.

Velikin, S.A., Vladov, M.M. & Makcheeva, I.V. 2000. Application georadiolocation method for the study of hydro units in permafrost conditions. In: *Georadar in Russia-2000*. Moscow, MGU: 36-38.

Vladov, M.M. & Starovoitov, A.V. 2005. Introduction to georadiolocation. Moscow: MGU, 165 pp. (in Russian).

A Role of Description of Thaw/Freeze Processes in the Permafrost Zone for Quantifying Fire Weather

Sergey Venevsky
School of Geography, University of Leeds, Leeds, UK
Met Office – Hadley Centre for Climate Prediction and Research, Exeter, UK
Alexey Rubtsov
School of Geography, University of Leeds, Leeds, UK

Introduction

Wild fires happen frequently over northeastern Eurasia. The occurrence of these fires can be monitored from satellite data and shows a large seasonal cycle, together with a strong interannual variation. Several indices are available in the literature and aim at a quantification of fire risk based on various meteorological and soil moisture parameters. In this paper, we evaluate the ability of three such indices at quantifying the occurrence of fires over large areas of Siberia (60°E–140°E, 48°N–72°N). We compare the ability of Reg-FIRM fire weather danger index (Venevsky et.al. 2002) at quantifying the occurrence of fires over large areas of Siberia (60°E–140°E, 48°N–72°N) and estimate a role of thaw-freeze processes for correct description of fires with this index.

Methods

The Reg-FIRM fire danger model was developed by Venevsky et al. (2002) for introducing fire processes in the LPJ and SEVER dynamic global vegetation models (Sitch et al. 2003, Venevsky & Maksyutov 2007). This index is evolved from the Nesterov index, according to Equation (3). The increase in fire risk caused by drier fuel loads is explicitly accounted for in the Reg-FIRM WFDI by an exponentially decreasing function of the soil moisture, *S*. The driving input variables of the Reg-FIRM WFDI are the maximum and minimum daily air temperature ($T_{air}^{\max}$ and $T_{air}^{\min}$ in °C) and the daily soil moisture *S* in the upper soil layer, expressed in relative volumetric units.

We used as input the weather parameters from the ECMWF operational data and the GLC-2000 vegetation classification. We compare these indices to the number of fires detected by the MODIS spaceborne instrument at 8-day time scales over a 4.5-year period.

The Reg-FIRM WFDI would be unrealistic over Siberia, in particular during the spring season, without distinguishing between the liquid and the frozen components of the soil moisture *S*. We replaced *S* in Equation (4) by the liquid fraction of soil moisture S_{liq} , defined by $S_{liq} = (1-\alpha) \times S$, where α is the frozen fraction of soil moisture diagnosed each month from a global run of the HadGEM1 Atmospheric General Circulation Model of the Hadley Center

The frozen fraction of soil moisture, used in the Reg-FIRM WFDI was diagnosed from the output of the HadGEM1 general circulation model (Johns et al. 2006) with a monthly time step. However, the HadGEM1 has a "warm bias" 2°–7°C in the Siberian region so that the predicted thaw is too early by 2–10 days compared to the observed values (Legates & Willmot 1990). This warm bias depends upon latitude, and it is caused by an underestimate of the low cloud fraction, which results in an overestimate of the downward short-wave radiation at the surface. A rough-and-ready correction of the thaw date is given by:

$$d_{mid-month}^{corr} = d_{mid-month}^{old} - (l - 62) \quad (1)$$

where $d_{mid-month}^{old}$ is a mid-month thawing date in a given grid point, $d_{mid-month}^{corr}$ is the mid-month thawing-date day corrected for the warm bias, and *l* is the latitude in degrees. Equation (1) was empirically obtained and accounts for delay in thaw and shift forward of freeze of roughly one day per degree of increasing latitude north of 62°N.

Results

With the frozen water correction, spring fires that are detected by MODIS, are well captured by the Reg-FIRM WFDI. The improvement is quantified by both the averaged correlation coefficients (% of grid cells with positive correlation increased from 55 to 73) and their spatial distributions. This finding confirms the importance of thaw and freeze processes for predicting the occurrence of fires in boreal forests as suggested in previous studies (Venevsky 2006).

References

Johns, T.C., Durman, C.F., Banks, H.T. et al. 2006. The new Hadley Centre climate model HadGEM1: Evaluation of coupled simulations. *Journal of Climate* 19(7): 1327-1353.

Legates, D.S. & Wilmott, C.J. 1990. Mean seasonal and spatial variability in gauge-corrected, global precipitation. *International Journal of Climatology* 10: 111-127.

Sitch, S., Smith, B., Prentice, I.C. et al. 2003. Evaluation of ecosystem dynamics, plant geography and terrestrial carbon cycling in the LPJ dynamic global vegetation model. *Global Change Biology* 9(2): 161–185, doi:10.1046/j.1365-2486.2003.00569.x.

Venevsky, S., Thonicke, K., Sitch, S., et al. 2002. Simulating fire regimes in human dominated ecosystems: Iberian Peninsula case study. *Global change Biology* 8: 984-998.

Venevsky, S. 2006. Estimate of global carbon emissions to the atmosphere from lightning and human induced fires. Integrated Land Ecosystem-Atmosphere Process Study. In: A. Reissell & A. Aarflot (eds.), *Proceedings of the 1st iLEAPS Science Conference, Boulder, Colorado, USA. Report Series in Aerosol Science*. Helsinki, 109-110.

Venevsky, S. & Maksyutov, S. 2007. SEVER: A modification of the LPJ global dynamic vegetation model for daily time step and parallel computation. *Environmental Modelling and Software* 22: 104-109.

Hydrogen and Oxygen Isotope Studies from an Ice Wedge in Svalbard

Helle Vittinghus
Institute of Geography, University of Copenhagen, Denmark and
Department of Geology, The University Centre in Svalbard, UNIS, Norway
Hanne H. Christiansen
Department of Geology, The University Centre in Svalbard, UNIS
Hanno Meyer
The Alfred Wegener Institute, Potsdam, Germany
Bo Elberling
Institute of Geography, University of Copenhagen

Introduction

Svalbard is located in an area of great sensitivity to climate change. Palaeo-climate archives from glaciers have been investigated; however, the longest record analysed dates back 800 years. Ice wedges in Adventdalen are believed to be up to 3500 years old (Jeppesen 2001) and, therefore, possibly contain mid to late Holocene palaeo-environmental information.

Field Site

The Adventdalen Valley is located in central Svalbard. The valley trends east–west and is 3.5 km wide and 27 km long. The permafrost in Adventdalen is continuous, with widespread ice wedges. Polygonal networks are found on the flat terraces along the riverbed and on the gentle valley slopes up to 25° and up to 500 m a.s.l. (Sørbel & Tolgensbakk 2002). They are of variable sizes reaching 10–20 m in diameter. Distinct troughs range from 0.5–5 m across with adjacent ramparts, clearly delimiting the ice wedges below. The oldest age of an ice wedge in Adventdalen is 3685–3640 cal. yr BP (Jeppesen 2001). At the northernmost edge of the terrace at the south side of Adventdalen, thermal erosion of gullies into ice wedges have developed in the river bank cliff. In other places ice wedges are exposed due to river erosion.

Methods

An ice wedge was first exposed in the terrace river cliff in 2003 during stratigraphical studies in outer Adventdalen. This ice wedge was 1.6 m wide, with the top 145 cm exposed. It is a syngenetic ice wedge, reflected by an elevated upper part of the top 10 cm of the ice wedge being only 60 cm wide. Leaves of *Salix* twigs found in the outer part of this ice wedge were ^{14}C AMS dated to 1980–2150 cal. yr BP (Christiansen et al. in prep).

The ice wedge was sampled, cutting horizontally across by chainsaw in winter, to avoid any thawing during cutting and transportation. Ice wedge sampling was designed to capture the isotopic chronology of the vein accumulation and to study vein orientation and/or reactivation event. Since the ice wedge exposure was assumed syngenetic, two sets of samples were taken: one across the widest part of the ice wedge, sampling 107 cm, and one 60 cm above, across the smaller top of the ice wedge, sampling 12 cm.

To capture the horizontal variation in as much detail as possible preferably representing each vein, only a few mm wide samples were necessary. This was achieved by vertical sampling with a microtome from the ice wedge sample blocs in the freezing laboratory at UNIS. Several microtome slices representing 2–3 mm of ice wedge were collected in one sample. The wide ice wedge sample was sampled only in 1–1.5 cm slices, using a standing band saw for ice in the freezing laboratory. This method offered a good opportunity to cut along the vein orientation, since skew cutting was manageable.

The water stable isotopic compositions of $\delta^{18}O$ and δD from the ice wedge samples were determined using a Finnigan MAT Delta-S mass spectrometer by the equilibrium technique at the AWI laboratory. δD and δO^{18} values were calculated by the commercial software ISODAT (version 5.2) and displayed as per mille differences relative to Vienna Standard Mean Ocean Water (V-SMOW) with an internal 1 σ error of better than 0.8‰ and 0.1‰ for δD and δO^{18}, respectively (Meyer et al. 2000).

Results

Results from the ice wedge studies are shown in Figure 1a–d. The grey line in Figure 1b–d represents results from high-resolution sampling from the upper, smaller ice- wedge part. The black line represents the samples from the wider part of the ice wedge. Figure1a shows the general vertical veins, with some veins displaced and some crossings. This shows that, to some extent, a complete horizontal vein pattern could not be assumed to reflect a perfect chronological evolution across the ice wedge, but we believe the overall pattern reflects a symmetrical growth.

Discussion

The horizontal distribution of $\delta^{18}O$ (Fig. 1b) and δD (Fig. 1c) values from the wider part shows, respectively, a peak and a low towards the middle, with descending and ascending values going towards the sides. An overall symmetrical pattern is thus visible, but the values from the smaller part show a more detailed picture, with significantly different values to the samples from the wider part. Thus,

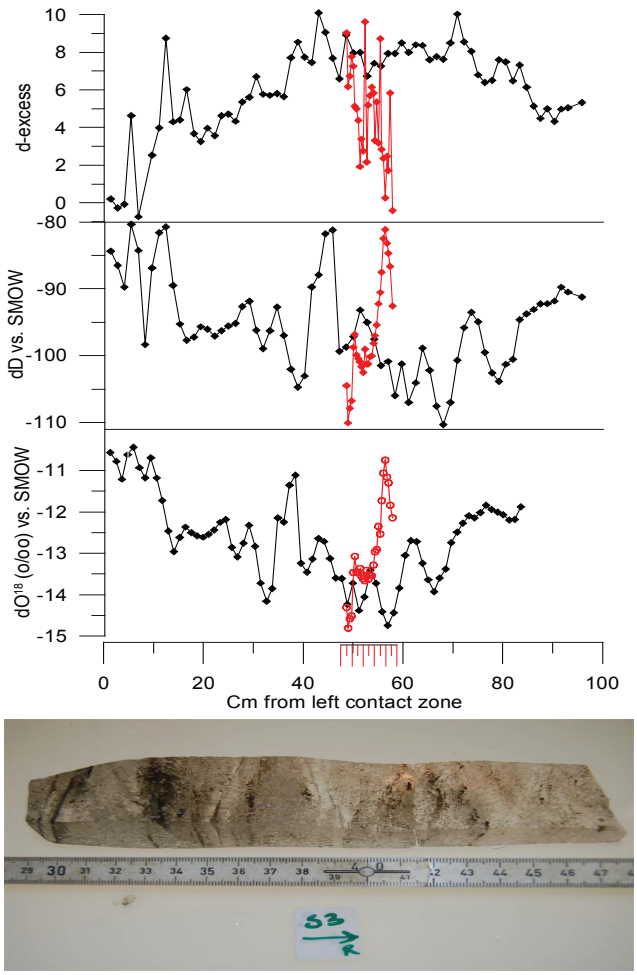

Figure 1. 1a represents the ice wedge part from 28–43 cm from the left contact zone and shows the general vertical vein structure. 1b–d shows the horizontal distribution of $\delta^{18}O$, δD and *d*-excess with the black line representing the wider ice wedge part and the grey line representing the upper, smaller ice wedge part.

the higher resolution samples reveal a more detailed isotopic pattern, and the lower resolution samples from the wider part reflect a mean value of the veins represented in the respective samples. The small vertical distance of 60 cm between the two set of samples is not enough, in this case, to detect a vertical climatic trend, and could account for the similarity (from a climatic point of view) in the isotopic values.

The horizontal *d*-excess signal (Fig. 1d) shows that values from the side sections are too low for a genetic relation with an oceanic moisture source. *D*-excess values in the smaller part range from -0.7‰ to 10‰, with decreasing values towards the sides. The mean value of winter precipitation collected in 2006 in Adventdalen was 7.5‰. Since mean values of winter precipitation should be found in the veins, another moisture source or an altered signal from potential fractionation processes since deposition must be assumed towards the ice wedge sides.

Conclusion

While an overall symmetrical pattern could be interpreted from the horizontal $\delta^{18}O$ and δD variations, a climatic trend during the period of activity was considered detectable. Since a more detailed isotopic pattern was revealed from the higher resolution samples, the lower resolution samples are believed to reflect a mean value of the veins represented in the respective samples. No vertical climatic trend could be seen between the two cores. The veins of the investigated ice wedge are seen to crossing, which most likely complicates palaeo-environmental reconstructions.

References

Christiansen, H.H., Hormes, A. & Snowball, I. (in prep). *High Resolution Late Holocene Loess Record with Syngenetic Ice-Wedges in Adventdalen, Svalbard*.

Jeppesen 2001. *Palæoklimatiske Indicatorer for Central Spitsbergen, Svalbard. Eksemplificeret ved Studier af Iskiler og Deres Værtssedimenter*. M.Sc. Thesis. Svalbard: The University Centre in Svalbard.

Meyer, H., Schönicke, L., Wand, U., Hubberten, H.W. & Frederichsen, H. 2000. Isotopes studies of hydrogen and oxygen in ground ice. Experiences with the equilibration technique. *Isotopes in Environmental and Health Studies* 36: 133-149.

Sørbel, L. & Tolgensbakk, J. 2002. Ice wedge polygons and solifluction in the Adventdalen area, Spitsbergen, Svalbard. *Norsk Geografisk Tidskrift* 56: 62-66.

Vegetation Change and Thermokarst Development: Effects on Ecosystem Carbon Exchange in Upland Tussock Tundra

Jason G. Vogel, Hanna Lee, Christian Trucco, Edward A.G. Schuur
Department of Botany, University of Florida, Gainesville, FL 32601-8526, USA
James Sickman
Department of Environmental Sciences, University of California Riverside, Riverside, CA 92521, USA

Introduction

Thermokarst development generally alters the vegetation composition of an area because of changes in soil temperature and moisture (Camill et al. 2001). In upland tussock tundra, thermokarst depressions are wetter and warmer than undisturbed areas, while areas along the sides of thermokarst are drier due to drainage (Schuur et al. 2007). The changes in soil climate and vegetation composition that occur with thermokarst could affect ecosystem C cycling. Plant growth, or net primary productivity (NPP) and microbial respiration (Rm) of organic matter are both affected by soil climate, and it is the balance between these two processes that determines net ecosystem exchange (NEE). Vegetation composition can directly affect NPP because plant species differ in growth potential, and can indirectly affect Rm because tissue chemistry strongly influences decomposition rates (Chapin & Shaver 1996). Potential C loss from permafrost soils is important to the global C budget because these soils store ~1.6 times more C than is currently in the atmosphere (Schuur et al., in press).

The objective of this study was to examine how vegetation composition and NPP, and thermokarst development may be affecting ecosystem C cycling. In a previous study, we reported that thermokarst depressions in upland tussock tundra apparently caused the loss of tussock-forming species (*Eriophorum vaginatum, Carex bigelowii*) and a gain in deciduous shrubs and mesophilic *Sphagnum* species (Schuur et al. 2007). In this study, we relate these changes in vegetation composition, mortality, and NPP to measurements of seasonal change in ecosystem respiration (Reco), gross primary productivity (GPP), and net ecosystem exchange (NEE).

Materials and Methods

Field site

The study area was in the Eight Mile Lake (EML) watershed in central Alaska. The EML watershed is located 7 miles west of the town of Healy, and is near the north end of Denali National Park and Preserve. Osterkamp and Romanovsky (1999) have monitored permafrost temperatures to 27 m since 1985. Between 1990 and 1998 the permafrost profile warmed by ~0.7–1.2°C, warming that coincided with thermokarst development (Osterkamp 2007). Since 1999, permafrost temperatures have stabilized or slightly decreased (~0.2°C).

A natural gradient study was established within 400 m of the permafrost monitoring borehole. Three sites were located: "Minimal Thaw," where surface topography and tussock tundra vegetation appeared little changed by thermokarst; "Moderate Thaw," where thermokarst development began about 15 years ago; and "Extensive Thaw," where surface depressions are wider and deeper than Moderate Thaw due to a prolonged period (minimum of 50 years) of thermokarst development (Schuur et al. 2007).

Vegetation sampling

Vegetation composition and NPP were sampled in twelve 0.7 x 0.7 m quadrats (chamber base) per site that were distributed in pairs across a 40 m transect The "point frame" method was used to estimate vegetation characteristics, where a thin metal rod is passed vertically through the canopy and the number of interception points with vegetation used to estimate biomass. Site-specific relationships between the number of point intercepts and vegetation biomass were developed in 2004 (Schuur et al. 2007) and applied to surveys in 2004 and 2006. We estimated ground coverage of live and dead mosses and *Eriophorum vaginatum* using the line-intercept method. The five dominant moss groups within the quadrats were identified, including the area coverage of dead *Sphagnum spp*.

Ecosystem carbon exchange

NEE and Reco were estimated with both an automatic and manually operated closed chamber system. The chambers were 0.4 m high and were placed on the same 0.7 x 0.7 areas or chamber bases where NPP and plant species composition were measured. The air inside a chamber was circulated to an infrared gas analyzer (LI-820) and the rate change in CO_2 concentration recorded on either a Campbell CR10x (automatic chamber) or Palm Tungsten C palm pilot (manual chambers). Measurements began in the first few weeks of May and continued until the end of September. Response curves of NEE to light and Reco to temperature were developed and growing season estimates constructed with these response equations. Gross primary productivity was estimated as the difference between growing season NEE and Reco.

Analyses

Multiple regression analysis was used to determine if vegetation characteristics of a chamber base (proportion of dead moss and NPP of functional groups) covaried with chamber level variation in growing season NEE, GPP, and Reco. The best parameters for the regression model were selected based on the maximum coefficient of variation

(adjusted R^2) and Mallow's CP statistics. When a minimum CP statistic and maximum R^2 are selection criteria, the result is the best fit model with the minimum number of parameters.

Results

NPP and ecosystem C exchange

In both 2004 and 2006, NEE, GPP, and Reco measured with the closed chambers were significantly correlated with NPP measured with the point-framing method (Fig. 1a, b, c). These same ecosystem C exchange variables were significantly correlated with active layer thickness, but NPP better described overall variation (not shown). The slope and intercepts of the NPP vs. Reco and GPP relationships were not significantly different between years, but the slope of the NEE lines did differ significantly between years.

Relationship between carbon exchange and specific plant functional groups

We previously reported that across this upland tussock tundra landscape, thermokarst corresponded to a relative decrease in the NPP of graminoids while moss and deciduous shrub NPP increased (Schuur et al. 2007). Here we use multiple regression analysis to examine whether the NPP of individual functional groups corresponded to a change in NEE, Reco or GPP. For NEE, the regression procedure selected a different combination of plant functional types in different years. In 2004, the variance in NEE was best explained with evergreen shrub NPP (+ effect in model) and the coverage of dead moss (- effect in model). In 2006, the variance in NEE was best explained by moss, evergreen shrub, and graminoid NPP. Interestingly, in neither year were deciduous shrubs a component of the NEE model despite the NPP of this functional group generally increasing with active layer thickness (Schuur et al. 2007). Indeed, for GPP deciduous shrubs were also removed from the overall model in both years. This suggests that additional C uptake by deciduous shrubs was effectively replacing the C uptake of the different functional groups that were lost.

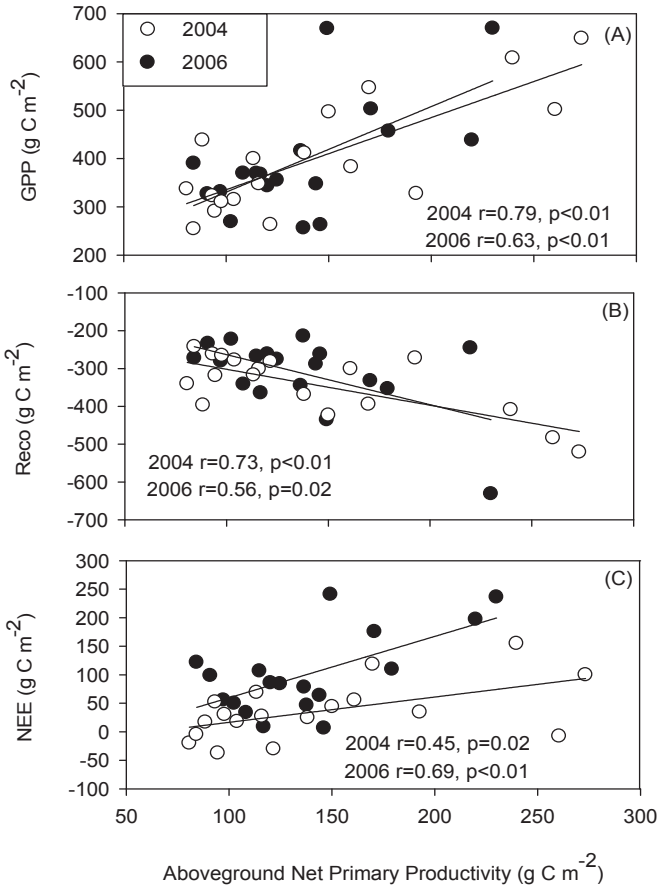

Figure 1. Relationships between growing season aboveground net primary productivity (NPP) and NEE, GPP and Reco across three sites that varied in the degree of permafrost thaw and thermokarst development.

Acknowledgments

We thank Michelle Mack for assistance in processing vegetation samples. Terry Chapin provided laboratory resources. Emily Tissier, Jamie Hollingsworth, and Brian Charlton provided logistical support. Tom Osterkamp undertook the early research that made this project possible, and Guy Adema and Larissa Yocum of Denali National Park and Preserve provided logistical support.

References

Camill, P., Lynch, J.A., Clark, J.S., Adams, J.B. & Jordan B. 2001. Changes in biomass, aboveground net primary production, and peat accumulation following permafrost thaw in the boreal peatlands of Manitoba, Canada. *Ecosystems* 4: 461-478.

Chapin, F.S. & Shaver G.R. 1996. Physiological and growth responses of arctic plants to a field experiment simulating climatic change. *Ecology* 77: 822-840.

Osterkamp, T.E. & Romanovsky, V.E. 1999. Evidence for warming and thawing of discontinuous permafrost in Alaska. *Permafrost and Perigl. Process* 10: 17-37.

Osterkamp, T.E. 2007. Characteristics of the recent warming of permafrost in Alaska. *Journal of Geophysical Research* 112: F02S02, doi:10.1029.

Schuur, E.A.G., Crummer, K.G., Vogel, J.G. & Mack, M.C. 2007. Plant species composition and productivity following permafrost thaw and thermokarst in Alaskan tundra. *Ecosystems* 10: 280-292.

Preliminary Analysis of Anthropogenic Landscape Fragmentation: Tazovsky Peninsula, Russia

Jesse S. Wallace
Department of Geography, University of Montana, Missoula, 59812, USA
Anna E. Klene
Department of Geography, University of Montana, Missoula, 59812, USA

Introduction

As part of the IPA 2007 International Polar Year activities, Moscow State University offered a "Technogenic and Environmental Permafrost Observatories" field course in west Siberia. During this course, students were granted access to three natural gas fields owned by regional subsidiaries of the Russian energy company, Gazprom. The fieldwork addressed the impact of industrial development in permafrost regions, with an emphasis on the evolution of technologies designed to mitigate the problems associated with engineering in arctic environments.

The fragmentation analysis performed as a result of this field course examines these issues by quantifying the degree to which recent industrial development has affected the tundra. Anthropogenic impacts on this region have been discussed at length with regard to ecological consequences (Vilchek & Bykova 1992, Kryuchkov 1993). Ramifications of climate change on both the tundra and an ageing infrastructure have also been examined (Mazhitova et al. 2004). This fragmentation analysis provides additional quantitative information for future environmental assessments of the region.

Study Area

The Tazovsky Peninsula occupies the central north of the Tyumen oblast, surrounded by the Gulf of Ob' as it enters the Kara Sea (Fig. 1). This region lies within the West Siberian Basin, the largest petroleum and natural gas basin in the world (Ulmishek 1998). Underlain by continuous permafrost, the landscape is primarily peat tundra, characterized by mosses, lichens, grasses, and shrub-level bushes (*sphagnum balticum, ledum palustre, carex, betula nana, larix siberica*). Tree growth is restricted to river banks, where increased active layer depths allow more substantial root systems. Average temperatures range from -22°C to -26°C in January, and 4°C to 15°C in July (Russian Climate Server 2007).

History of industrialization

The Yamburg gas-oil condensate field is the largest proven field in the world, accounting for 15% of Russia's total natural gas and condensate reserves (Yamburggazdobycha 2007). Natural gas deposits on the Tazovsky Peninsula were discovered in 1969. In 1982, construction on the settlement of Yamburg began in order to house workers for the developing gas field. Located on the west coast of the peninsula, Yamburg is currently the only urban area in the region. Though there are no permanent residents, the town

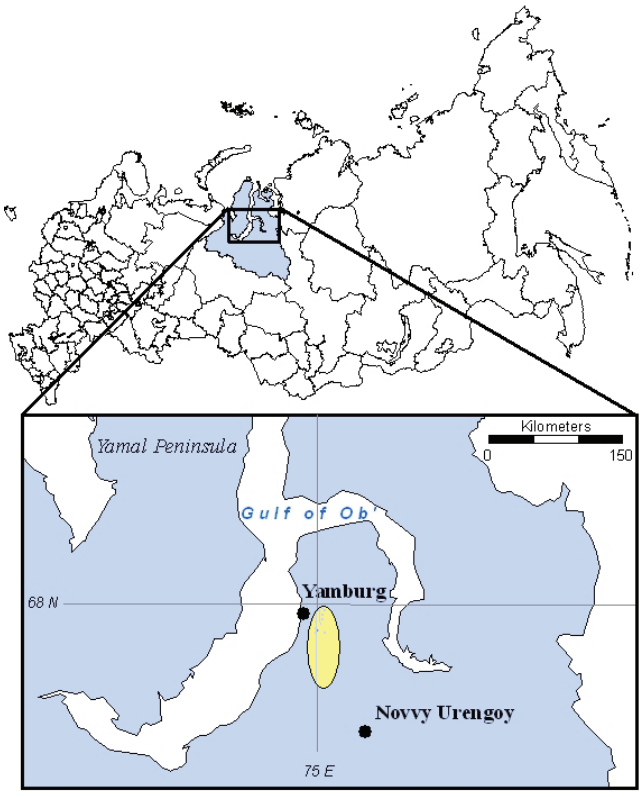

Figure 1. A detail map of the Tazovsky Peninsula shows the towns of Yamburg and Novvy Urengoy. The area to the southeast of Yamburg shows the approximate location of the Yamburg gas-condensate field.

is capable of housing up to 10,000 workers. The natural gas field and related industrial complex spreads to the south and east of the town, covering an approximate area of 8,500 km². In 2007, the estimated annual output of the Yamburg gas field was 10 bln m³, with a maximum capacity of 40 bln m³ (Yamburggazdobycha 2007).

Methodology

Satellite imagery of the study area was collected across a 23-year period corresponding to the inception and growth of the Yamburg natural gas field. Imagery from 1984, 1987, and 1999 were collected by the LANDSAT MSS, TM, and ETM+ sensors respectively. Imagery of 2007 is from the TERRA ASTER sensor.

The imagery was classified according to land-cover, with an emphasis on identifying all areas of anthropogenic impact, including drill pads, processing complexes, roads,

and pipelines. Data collected in the field were used as a validation set for the resulting classification. The areas classified as "industrial" were then used as the basis for the fragmentation analysis.

The FRAGSTATS statistical program has the ability to calculate over 200 fragmentation metrics (McGarrigal & Marks 1995). Each of the classified images of the study region was analyzed within this program to determine quantitative changes as measured by a set of established metrics. Of these, patch count, mean patch size, and edge density are the most efficient in evaluating fragmentation of a region over time (Ritters et al. 1995). While these metrics provide discrete values for each image, it is the change in these values over time that provides the basis for comprehensive fragmentation understanding. In order to put these changes in perspective, the results will be compared to other areas that have undergone similar development. Recent technological advances employed in the construction of the natural gas complex at Zapalyrnoe, to the southeast of the study area, have allowed similar production levels with significantly less infrastructure (Yamburggazdobycha 2007). Correlating fragmentation metrics to production levels at each site provides one avenue of comparative analysis.

Discussion

The ability to trace quantified changes across the study area, from the introduction of industrialization to the present day, offers a unique opportunity to assess the comprehensive impact of anthropogenic development in permafrost regions. Increases in patch count, and decreases in mean patch size, nearest neighbor, and diversity indices at each temporal analysis point provide quantitative evidence of the degree to which the region has been affected. Extension of the analysis potentially allows investigation of a correlation between annual natural gas production at the Yamburg field and key fragmentation metrics. Verification of this correlation offers the possibility of predicting the impacts that future resource development will have on other areas of west Siberia that have yet to be developed. The fragmentation correlation template additionally introduces a vehicle for analyzing the mediating effects of new extraction technologies on regional landscape fragmentation.

Acknowledgments

The field course was made possible through Moscow State University as part of the International University Courses on Permafrost offerings for the International Polar Year. Gazprom and its regional subsidiaries, NadymGasprom and Yamburggazdobycha, granted special access to their fields, and provided generous hospitality throughout the course. The University of Montana provided financial assistance to Dr. Klene through grants and startup funding.

References

Kryuchkov, V. 1993. Anthropogenic loads and the northern ecosystem condition. *Ecological Applications* 3(4): 622-630.

Li, X., Cheng, G. & Xiao, H. 2001. Quantifying landscape structure of the Heihe River basin, northwest China using FRAGSTATS. *Journal of Arid Environments* 48: 521-535.

Mazhitova, G., Karstkarel, N., Oberman, N., Romanovsky, V. & Kuhry, P. 2004. Permafrost and Infrastructure in the Usa Basin: Possible impacts of global warming. *Ambio* 33(6): 289-294.

McGarigal, K. & Marks, B. 1995. *FRAGSTATS: Spatial Pattern Analysis Program for Quantifying Landscape Structure*. Reference manual. Forest Science Department, Oregon State University, Corvallis, Oregon.

North, R. 1972. Soviet northern development: The case of NW Siberia. *Soviet Studies* 24(2): 171-199.

O'Neill, R.V., Krummel, J.R., Gardner, R.H., Sugihara, G., Jackson, B., Deangelis, D.L., Milne, B.T., Turner, M.G., Zygmunt, B., Christensen, S.W., Dale, V.H. & Graham, R.L. 1988. Indices of landscape pattern. *Landscape Ecology* 1: 153-162.

Russian Climate Server. 2007 URL: http://meteo.infospace.ru/climate/html/index.ssi

Ulmishek, G. 2003. *Petroleum Geology and Resources of the West Siberian Basin.* USGS Bulletin 2201-G.

Vilchek, G.E. & Bykova, O. 1992. The origin of regional ecological problems within the northern Tyumen Oblast, Russia. *Arctic and Alpine Research* 24(2): 99-107.

Weller, C., Thomson, J., Morton, P. & Aplet, G. 2002. *Fragmenting Our Lands: The Ecological Footprint from Oil and Gas Development*. Seattle, WA, & Denver, CO: The Wilderness Society.

Yamburggazdobycha, LTD. 2007. Promotional CD-ROM.

Engineering Effect on the Thermal Status of Shallow Ground in Permafrost Regions

Zhi Wen
State Key Laboratory of Frozen Soil Engineering, CAREERI, CAS, Lanzhou Gansu 730000
Yu Sheng
State Key Laboratory of Frozen Soil Engineering, CAREERI, CAS, Lanzhou Gansu 730000
Wei Ma
State Key Laboratory of Frozen Soil Engineering, CAREERI, CAS, Lanzhou Gansu 730000
Qingbai Wu
State Key Laboratory of Frozen Soil Engineering, CAREERI, CAS, Lanzhou Gansu 730000
Bo Huang
Qinghai Provincial Highway Research and Survey Institute, Xining Qinghai 810008, China

Introduction

The construction of an embankment in permafrost regions may induce substantial disturbance on the heat and mass transfer balance between the ground surface and atmosphere, which results in more heat absorption in the embankment. The temperature of the permafrost underneath increases even if permafrost thaws, causing serious problems for embankment due to thaw settlement on the Qinghai-Tibetan Plateau (Wen & Sheng 2003). The thermal status of the embankment affects directly the thermal status of permafrost under the railway embankment, which determines the embankment stability in the permafrost regions, especially ice-rich permafrost regions (Yu & Lai 2002).

Owing to important signification of the thermal regime of the upper soil layer on permafrost stability, many researchers have studied the thermal regime of the natural ground on the Qinghai-Tibetan Plateau (Xu & Ma 1984, Zhang & Zhu 1998). However, there is scarce research on heat balance and annual heat incomes and expenses of railway embankments. To know about the influence of engineering activities on the thermal regime of the natural ground, dynamic monitoring using dataloggers made in Compbell Company for temperature and heat flux in the upper active layer was carried out during August 2002, making it possible to use quantificational method analyses of the influence of engineering activities.

General Situation of the Test Sites

The test site is situated between Kekexili and Fenghuoshan along the Qinghai-Tibetan Railway on the Qinghai-Tibetan Plateau. Dynamic monitor sections of railway embankment and natural ground were set up on August 2002. Each section may measure heat flux and temperature of shallow ground simultaneously. Instruments used in two sections were self-calibrating heat flux sensor, temperature sensor, and datalogger and the readings were taken once half hour. The temperature probe may measure the temperature at the depth of 2.0 cm, 5.0 cm, 10.0 cm, 20.0 cm, and 50.0 cm from ground surface. The depth of heat flux placed was 20.0 cm from ground surface. Taking the difference of heat flux at two sides of the embankment into consideration, there was one self-calibrating heat flux sensor at each side of two sections and the data of heat flux were the even value of two sensors.

Variation Character of Soil Temperature

After railway embankment construction, many conditions were changed compared to natural ground, such as surface conditions (vegetation, albedo, etc.), soil moisture content, and soil component, which affected radiation absorption of surface and its transfer process downwards certainly. As seen in Figure 1, the soil temperature under the embankment surface at a depth of 50.0 cm was 2°C higher than that of the natural ground and had same phase location under similar climatic conditions (embankment testing site was close to natural ground site). Apparently, the phase and variation current of soil temperature was similar between two sites, which was due to some same conditions for two sites, such as climatic conditions, etc., that had nothing to do with engineering activities. However, the soil temperature at the embankment site was 2°C higher than that of the natural ground site if other conditions stayed the same, which was affected by engineering activities distinctly. After engineering construction, vegetation in the natural ground was destroyed, and the soils type, soils component, and its moisture content were changed, which increased the radiation absorption and decreased the evaporation water content. In a word, a high temperature boundary was brought to bear on the surface, which augmented the heat exchange and accelerated the permafrost degradation. Due to engineering activities, thawed core below embankment came into being and thawing settlement began.

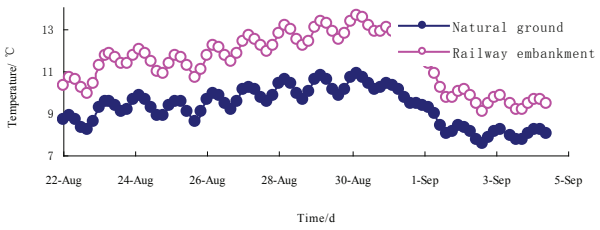

Figure 1. The contrastive temperature curves between the railway foundation and the natural ground at 50 cm depth.

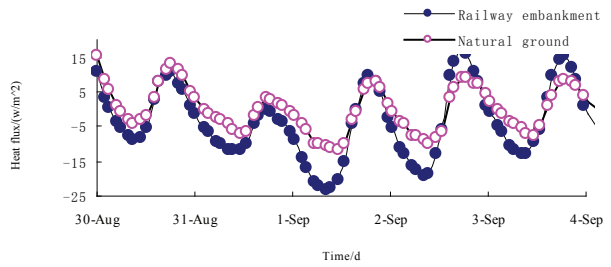

Figure 2. The contrastive heat flux curves between the railway foundation and the natural ground at 50 cm depth in the warm season.

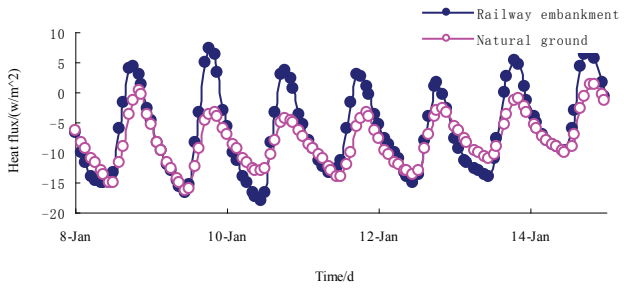

Figure 3. The contrastive heat flux curves between the railway foundation and the natural ground at 50 cm depth in the cold season.

The Variation Character of Soil Heat Flux

Figures 2 and 3 show the soil heat fluxes of two sites at a depth of 20 cm in the warm season and the cold season, respectively. The observed results of soil heat fluxes at two sites showed that there were distinct differences between the embankment site and the natural ground site (Figs. 2 and 3). The soil heat flux at the natural ground site varied mild, while the soil heat flux at the same depth of the embankment site varied great. In addition, the daily amplitude of heat flux at the natural section was smaller than that of the embankment section at the same depth.

It can also be seen from Figures 2 and 3 that there were two processes (heat release state and heat absorption state) for the soil heat flux at a depth of 20 cm in the warm season, whatever under embankment and under natural ground. As for the cold season, the soil heat flux at the natural ground site was in the heat release state invariably. In addition, we also found that the daily variation amplitude of soil heat flux in the cold season was smaller than that in the warm season, and the daily variation amplitude of soil heat flux in the cold season was approximately one-half to two-thirds of that in warm season.

Conclusion

Due to railway construction and instrument fault, long-term observation data were not obtained. Additionally, the moisture content was not monitored. To realize the heat-moisture process of the active layer in permafrost regions, a heat-moisture observation plan will be performed in 2007, when the temperature and the moisture probes will be installed simultaneously. Based on testing results and foregoing analyses, some useful conclusions can be drawn. The soil temperature under the embankment surface at a depth of 50 cm was 2°C higher than that of natural ground, and they had the same phase location under similar climatic conditions, which was affected by engineering activities distinctly. The daily variation amplitude of soil heat flux at the natural ground site was smaller than that of the embankment site, and the variation at the natural ground site was even more. In addition, the soil heat flux at the embankment site was more sensitive to the change of air temperature and tended more to be disturbed by the environment. There were two processes (heat release state and heat absorption state) for soil heat flux at a depth of 20 cm in the warm season, whatever under embankment and under natural ground. The daily variation amplitude of soil heat flux in the cold season was smaller than that in the warm season, and the daily variation amplitude of soil heat flux in the cold season was approximately one-half to two thirds of that in the warm season.

Acknowledgments

The research was supported by a grant of the Western Project Program of the CAS (Grant No. KZCX2-XB2-10), by the Graduate Student Innovation Program of the CAS granted to Dr. Zhi Wen, and by Opening Foundation of State Key Laboratory of Frozen Soil Engineering.

References

Wen, Z., Sheng, Y. & Wu, Q. 2003. Dynamic monitoring of thermal state for shallow ground in Qinghai-Tibetan Railway embankment. *China Journal of Rock Mechanics and Engineering* 22(2): 2664-2668.

Xu, Z. & Ma, Y. 1986. Calculation of soil heat flux on Qinghai-Tibetan plateau and analysis of stability of climate generalization method. Scientific testing paper volume on Qinghai-Tibetan plateau climate. Beijing: Science Press, 35-45.

Yu, W., Lai, Y. & Niu F. 2002. Temperature field features in the laboratory experiment of the ventilated railway embankment in permafrost regions. *Journal of Glaciology and Geocryology* 22(5): 601-607.

Zhang, J., Zhu, B. et. al. 1998. *Process in Climate Science of Qinghai-Tibetan Plateau*. Beijing: Science Press, 78-88.

Long-Term Monitoring of Sensible and Latent Heat Fluxes Using Eddy Covariance at a High Arctic Permafrost Site in Svalbard, Norway

S. Westermann
Alfred-Wegener-Institute for Polar and Marine Research, Potsdam, Germany
J. Boike
Alfred-Wegener-Institute for Polar and Marine Research, Potsdam, Germany
K. Piel
Alfred-Wegener-Institute for Polar and Marine Research, Potsdam, Germany
J. Lüers
Univ. of Bayreuth, Germany, Dept. of Micrometeorology

Introduction

Land-atmosphere interactions are an important element in the energy and water budgets in permafrost regions. The eddy covariance method has proven to be the most reliable way to directly measure sensible and latent heat fluxes (Foken 2006). However, due to the difficult logistics and the extreme environment, very few long-term eddy covariance studies exist in arctic regions (Grachev et al. 2007). Previous measurements on Svalbard, Norway, were limited to the summer season (Lloyd et al. 2001). Here we present long-term eddy covariance measurements of sensible and latent heat fluxes at a High Arctic continuous permafrost site on Svalbard.

Methods

The eddy covariance measurements were performed near Leirhaugen hill, located approximately 2 km southwest of the village of Ny-Ålesund. The site is situated in hilly tundra at the foot of two major glaciers, and is characterized by sparse vegetation alternating with exposed soil and rock fields.

The eddy covariance system consisted of a Campbell CSAT 3D sonic anemometer and a LiCor LI-7500 CO_2 and H_2O gas analyzer, which were sampled at 20 Hz using a CR3000 Campbell Scientific datalogger. The evaluation of the raw data was performed with the software "TK2" (Mauder & Foken 2004) from the University of Bayreuth, Germany. The quality assessment scheme of Foken & Wichura 1996 (see also Foken 2006), which is based on tests for stationarity and integral turbulence characteristics, was used to assess the quality of the flux measurements.

Measurements were collected from April to September 2007, covering a period from late winter until the end of the summer season. To account for the changing height above ground of the flux sensors due to accumulation or melting of snow, the snow depth directly at the EC-site was recorded using a Campbell Scientific SR50 distance sensor. The measured heights above ground ranged from a minimum of 2.0 m to 3.2 m at the end of the snow ablation period. After a complete snow melt, the EC-instruments were lowered to a height of 2.5 m above ground.

The net radiation was recorded at a climate station in the vicinity of the eddy covariance site, so that it is possible to compare the magnitude of the sensible and latent heat fluxes with the radiation balance.

Results

During the entire snow-covered period, either a stable or a neutral near surface atmospheric stratification was recorded, corresponding to z/L (measurement height over Obukhov length) significantly greater than zero or approx. zero, respectively. Hereby, a stable stratification was associated with low horizontal wind speeds of less than 5 m/s, while a neutral stratification was found predominantly for higher wind speeds. Particularly at stable conditions, the use of the eddy covariance method, which depends upon a fully developed turbulence field, is questionable. This was also reflected applying the Foken & Wichura quality assessment: a significant part of the data measured during the snow-covered period was classified as "only for orientation purposes" or "to be discarded" both for the sensible and latent heat flux. The data, which withstood the quality assessment, typically yielded low fluxes of less than 20 W m^{-2}. Hereby, the sensible heat flux was usually negative, corresponding to a sensible flux directed from the atmosphere to the ground (longwave radiation forcing), while the latent heat flux was positive, corresponding to weak but still existing sublimation and/or evaporation processes of snow or melt water.

The appearance of large snow-free patches around June 26 triggered a strong increase of both sensible and latent heat fluxes, with now both fluxes being positive, corresponding to a warming of the tundra surface forced by shortwave radiation. During this period the latent heat flux, with a maximum of 90 W m^{-2}, was more than twice as large as the sensible heat flux, likely due to very wet soil conditions directly after snowmelt. This situation reversed during July, when the tundra increasingly dried up throughout most of the potential fetch area of the eddy covariance site. Around the middle of July, both heat fluxes were approximately equal, the sum of both peaked at values of more than 200 W m^{-2}. Towards the end of July, the sensible heat flux subsequently became dominant over the latent heat flux by approximately a factor of two. The immediate surrounding of the measurement site could then be characterized as moderately damp tundra. From mid of August onwards, both

fluxes decreased steadily. At this time, the latent heat flux with peak values around 50 W m^{-2} was found to dominate once again over the sensible heat flux.

During the polar day season, the sensible and latent heat flux displayed a strong diurnal course with peak fluxes associated with maxima of solar radiation around midday. At the lowest sun angles, around midnight, both fluxes usually decreased to close to zero, but remained positive.

From the completion of snowmelt through the middle of August, the atmospheric stratification (according to the z/L ratio) was found to be either unstable or neutral, resulting in a good data-quality assessment. Towards and after the end (approximately middle of August to September) of the polar day season the general pattern could be characterized as neutral to weak unstable atmospheric stratification during the day and stable atmospheric stratification during the night. The quality assessment still indicated a good data quality during the day, with an increasingly poor data quality during the night.

Discussion

The highest amount of the net radiation was observed around beginning of July to be around 300 W m^{-2}, corresponding with a total of sensible and latent heat fluxes reaching values around 200 W m^{-2}. This clearly shows the importance of the sensible and latent heat fluxes regarding their parts in the whole energy budget of permafrost soils around Ny-Ålesund. Thus, eddy covariance measurements must be regarded as an essential tool in obtaining a complete picture of the energy budget and the allocation of the available energy during the summer period.

At snow-covered times, that is, for approximately two-thirds of a year, the situation is yet more difficult to assess. On the one hand, the quality of a significant portion of the data is questionable according to quality assessment (Foken & Wichura 1996), and only low fluxes were observed. On the other hand, such quality assessment schemes were developed in and for temperate zones, and are therefore not necessarily well suited for conditions found in the Arctic. Furthermore, low but sustained sensible and latent heat fluxes might have to be taken into account in the energy budget of the snow-covered ground. It is of great importance to critically review and possibly modify the evaluation and quality assessment for eddy covariance data for these circumstances.

References

Grachev, A.A., Andreas, E.L., Fairall, C.W., Guest, P.S. & Persson, P.O.G. 2007. SHEBA flux–profile relationships in the stable atmospheric boundary layer. *Boundary Layer Meteorol.* 124: 315-333.

Foken, T. 2006. *Angewandte Meteorologie, Mikrometeorologische Methoden*, (2 and extended edition). Heidelberg: Springer, 326 pp.

Foken, T. & Wichura, B. 1996. Tools for quality assessment of surface-based flux measurements. *Agric Forest Meteorol*. 78: 83-105.

Lloyed, C.R., Harding, R.J., Friborg, T. & Aurela, M. 2001. Surface fluxes of heat and water vapour from sites in the European Arctic. *Theor. Appl. Climatol.* 70: 19-33.

Mauder, M. & Foken T. 2004. Documentation and instruction manual of the eddy covariance software package TK2. *Work Report University of Bayreuth, Dept. of Micrometeorology* Vol. 26, ISSN 1614-8916.

Scientific Opportunities and Environmental Impacts Related to Ski Run Construction, Zermatt, Swiss Alps

Oliver Wild
Department of Geography, University of Giessen, Germany
Isabelle Roer, Stephan Gruber
Department of Physical Geography, University of Zurich, Switzerland
Barbara May, Dietmar Wagenbach
Institute for Environmental Physics, University of Heidelberg, Germany

Background

The building of ski runs and their associated installations are likely to influence the alpine environment and the permafrost present at many of those sites. Therefore, it is important to have a good understanding of the impacts of this construction. As it is impossible to restore the normal environment once the work is finished, the present state should be documented, and information about how the formation of the area and its periglacial landforms took place in the past (e.g., with ice samples) should be gained. During the years after the construction, further research must be conducted to evaluate the degree of change. The research within this article contributes to this knowledge, and preliminary results are presented.

Study Site

During construction for a new ski run at the Gornergrat (Zermatt, Swiss Alps), diverse exposures of ground-ice were created. The site (3135 m a.s.l) is located in the southern Swiss Alps and is part of the Matter Valley. The Zermatt region has a continental climate with 610 mm annual precipitation (MeteoSwiss 30-year average 1961–1990) and strong direct solar radiation.

Located on the northern slopes of the east–west running crest between Gornergrat and Hohtälli (3286 m a.s.l.) is the area called "Kelle" (Fig. 1). Here, the ski run is constructed within the discontinous permafrost zone, which can be expected between 2600 and 3500 m a.s.l., according to King (1996). Regarding permafrost distribution, measurements of the ground surface temperature (GST) and the basal temperature of the snow (BTS), as well as permafrost models have contributed to knowledge about this area (Gruber 2000, Herz 2006).

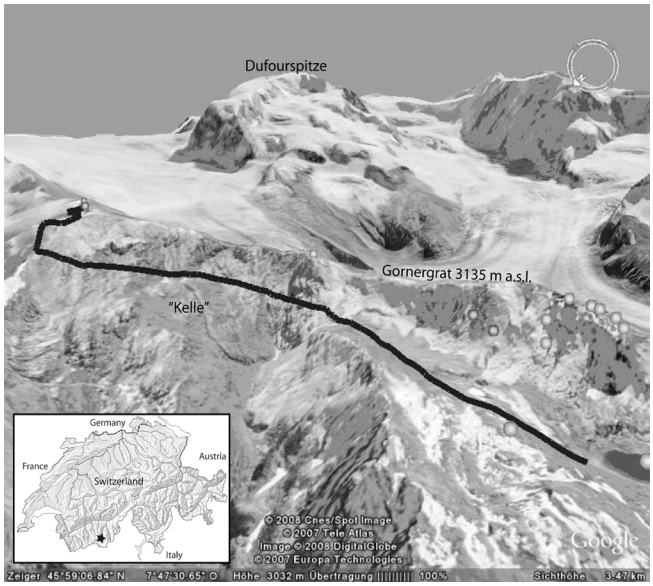

Figure 1. The study site with its new ski run (black line).

Environmental Impacts

During the construction in summer 2007, ground-ice was exposed at various spots in the "Kelle" area. The building of a new ski run with a snowmaking system, commissioned by Zermatt Bergbahnen, was the reason for that. With a length of approximately 2.5 km and an altitudinal difference of 350 m, the track leads through a steep cirque where large masses of rock and sediments had to be moved. Various geomorphological features were affected by these actions. The uppermost part of the track leads through the remaining ice of a small glacier (Fig. 2a), the middle part cuts through a rock glacier (Fig. 2b & 2c), and rock glacier-like features (polygenetic landforms) were influenced in the lowest part (Fig. 2d).

The maximum depth reached is approximately 8 m below the former surface. Due to the removal of the active layer and

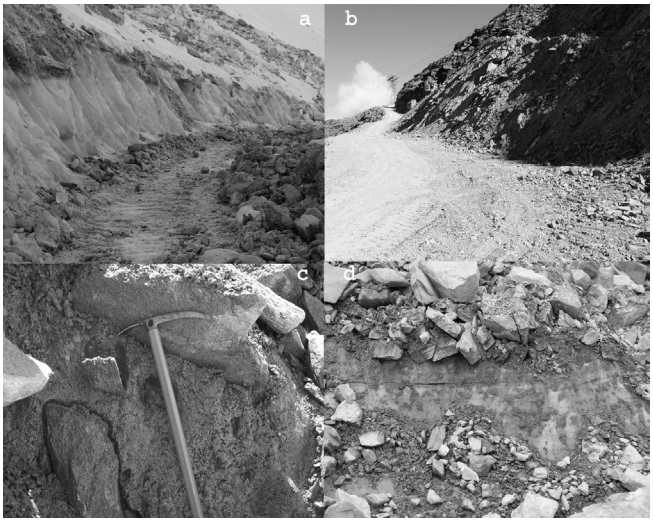

Figure 2. The ice of the remaining glacier (a), the ski track cutting through the rock glacier (b), rocks and ice (c), and an ice core of a polygenetic landform (d).

the exposure of ground-ice, the thermal regime is disturbed. Increased melting during the summer and the formation of a new active layer is expected.

Unique Scientific Opportunities

Even if the interferences with the periglacial system of "Kelle" have negative consequences, it offers great opportunities for permafrost research, which can rarely be found elsewhere. Due to the excavations it was possible to document and map the inside of rock glaciers and other geomorphological features. On the rock glacier, stratigraphy was mapped and compared to geophysical soundings (Hilbich et al. 2008).

Considering the expected effects of a disturbed thermal regime and increased melting, repeated geodetic surveys will be conducted. A geodetic survey of the whole area at the beginning of summer 2008 gives the opportunity to quantify the amount of sediments that has moved in 2007. A second survey in autumn 2008 will show if thaw settlement has occurred. The observed landforms may show different reaction times and degrees of change. It is known that the preparation of ski runs is leading to decreasing temperature in the ground, compared with non-prepared places in the surrounding area (Rixen et al. 2004); however, the removal of a coarse blocky surface layer, which exerts a strong cooling influence, can lead to significant ground warming and permafrost degradation (cf. Herz 2006).

In addition, ice samples were taken at different locations and are currently being investigated (Fig. 3). Three ice samples are inspected for visual features such as air bubbles and grain size prior to first sub-sampling for ice density, total ion content (conductivity), and stable water isotope ($\delta^{18}O$ and δD) measurements. This is expected to lead to information about the dominating processes of ice formation and exchange. Here, tritium analyses are envisaged as well, allowing for estimating any influence of recent water. ^{14}C analysis of organic impurities might help to infer an upper age limit, in case the ice would date back over several centuries.

Preliminary Results

In 2007, this unique opportunity was used to map the permafrost landforms, which is the basis for observation of future changes. Because of the disturbed thermal regime and thawing permafrost, rebuilding of the ski run must be expected for future years.

The pilot analyses of the ice, performed so far, indicate:

- An ice texture broadly similar to non-temperate ice found in Alpine ice caves, as characterized by centimeter-size grains, an ice density close, but still significantly below 0.9 g/cm^3, and few but relatively large bubbles.
- A surprisingly low ion and dissolved impurity content likely due to post depositional snow cover elution and $\delta^{18}O$ values clearly pointing to freeze on of mainly winter precipitation.

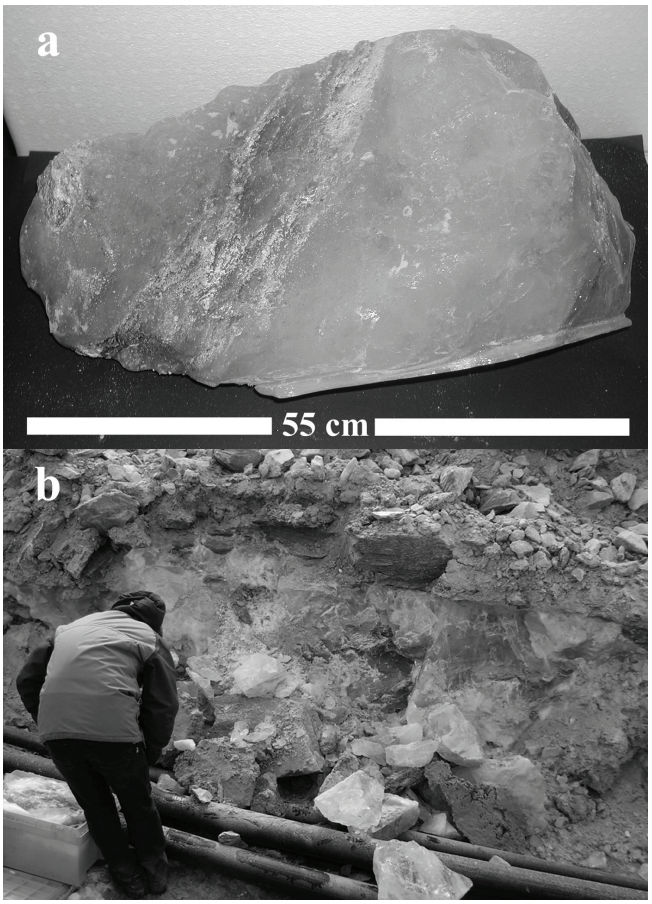

Figure 3. The biggest ice sample (a), which was taken in the ditch for the snowmaking system (b).

References

Gruber, S. 2000. *Slope instability and permafrost: A spatial analysis in the Matter Valley, Switzerland*. Unpublished Master Thesis. Giessen, Germany: Institute of Geography, Justus Liebig University.

Herz, T. 2006. *Das Mikroklima grobblockiger Schutthalden der alpinen Periglazialstufe und seine Auswirkungen auf Energieaustauschprozesse zwischen Atmosphäre und Lithosphäre.* Institute of Geography, Justus Liebig University Giessen, Germany. URL: http://geb.uni-giessen.de/geb/volltexte/2006/3837/

Hilbich, C., Roer, I. & Hauck C. 2008. Ground truth observations of the interior of a rock glacier as validation for geophysical monitoring datasets. *Extended Abstracts, Ninth International Conference on Permafrost, Fairbanks, Alaska, 29 June–3 July 2008.*

King, L. 1996. Dauerfrostboden im Gebiet Zermatt–Gornergrat–Stockhorn: Verbreitung und permafrostbezogene Erschließungsarbeiten. *Z. Geomorph. N.F., Suppl. Bd.* 104: 73-93.

Rixen, C., Haeberli, W. & Stoeckli, V. 2004. Ground temperatures under ski pistes with artificial and natural snow. *Arctic, Antarctic, and Alpine Research* 36(4): 419 – 427.

The Effect of Climate and Permafrost on Tree Line Dynamics in Northwest Russia: A Preliminary Analysis

Martin Wilmking
Saskia Kenter
Jens Ibendorf
University Greifswald, 17487 Greifswald, Germany

Introduction

Tree line dynamics provide important feedback mechanisms to the global climate system by altering albedo and carbon storage at high latitudes. A northward movement of the northern tree line is generally assumed to decrease albedo (Chapin et al. 2005), but increase above-ground carbon storage. However, ecosystem carbon storage might be reduced during tree line advance due to the respiration of (old) soil carbon and thus result in a positive feedback to warming (Wilmking et al. 2006).

Establishment of trees north of tree line requires on the one hand favorable climatic conditions (climate driver) and on the other hand suitable microsite conditions (microsite driver) (Lloyd & Fastie 2002). Suitable microsites are often hampered by the existence of permafrost, and thus ultimately may depend on permafrost degradation. Thus, one main factor controlling carbon storage and tree line advance in many regions is permafrost.

The EU Project "CarboNorth" aims at quantifying the carbon budget in northwest Russia, and as part of this project, the consortium is studying tree line dynamics. This paper reports preliminary results from the dendroecological part of the investigation. Particularly, we were interested in the climate sensitivity of established trees at tree line (climate driver) and in the age structure of seedlings extending beyond tree line from mostly permafrost-free soils to permafrost-influenced soils (microsite driver).

Methods

Field sites were located at northern tree line in northwest Russia at 67.4°N, 62.3°E (R1), 67.2°N, 62.1°E (R2), 67.1°N, 59.5°E (Kho). Each site consisted of a gradient from tree islands on well-drained soil with permafrost pockets, through woodland to treeless tundra underlain by permafrost (conceptional permafrost degradation). Each transect consisted of 3–4 plots (15 x 15 m): (1) forest, (2) dense woodland, (3) open woodland, and (4) tundra. Permafrost depth was measured with a 120 cm long probe (July/August 2007). We collected penetrating tree cores or disks (at root collar level) from every *Picea obovata* tree or seedling within each plot in 7/2007. Samples were prepared according to dendrochronological standards. Age of samples was determined by ring counts and adjusted for sample height. We measured ring-width (LINTAB 5, 1/1000 mm) from all R2 samples including other well-established trees close by and crossdated visually and with COFECHA. We used the program ARSTAN (negative exponential, straight line fits, Huggershoff) to standardize the tree ring series, to remove the biological age trend, and to build site chronologies. We calculated climate-growth relationships of chronologies only, if EPS (expressed population signal) exceeded 0.85. We used mean monthly temperature and precipitation data (1901–2002) from the closest grid point of the gridded CRU-dataset, because the temperature record correlated very well ($r > 0.98$) with the closest station (Khoseda Hard) and records of Pecora ($r > 0.90$) and Nar Jan Mar ($r > 0.87$). Correlation and response functions over time were analyzed with the program DENDROCLIM2002 (Biondi & Waikul 2004); moving window length was 50 years.

Results

Microsite conditions

The active layer depth was generally significantly shallower in the tundra plots compared to woodland and forest plots, which showed similar thaw depths (Fig. 1), often exceeding the depth of the probe. While forest plots were generally well drained, woodland and especially tundra plots were often waterlogged, and trees and seedlings had often established on slightly higher terrain (hummocks).

Age structure

The age structure revealed a striking similarity at all plots at all three study sites, where most individuals had established between 1950 and 1960, and none had after 1982.

Climate-growth relationships at R2

Only one chronology (Forest) exceeded an EPS value of 0.85 during the 20th century and, subsequently, was used for the calculation of climate-growth relationships. The standard chronology showed some significant correlation and responses to temperature, but none was very strong or stable over time. No significant correlation existed with precipitation. The residual chronology showed significant

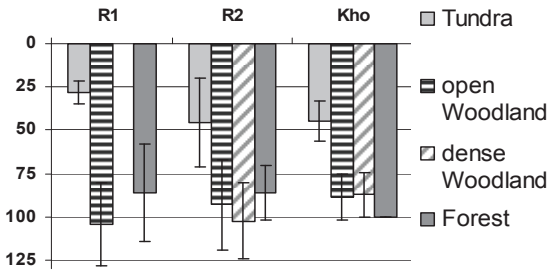

Figure 1. Minimum thaw depth (in cm) across the forest–tundra transect; error bars are standard deviation.

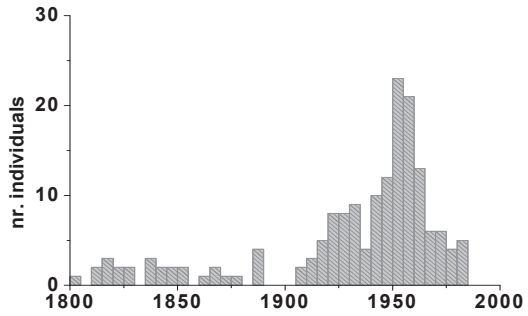

Figure 2. Establishment date of trees and seedlings on all plots since 1800. Note distinct peak between 1950 and 1960.

strong negative correlation and response functions to previous July (mostly consistent over time) and also partly to previous June and August temperatures; and significant strong positive correlation and response functions to current June and July temperatures (inconsistent over time).

All other chronologies did not exceed the 0.85 EPS threshold. Preliminary analyses of individual trees and seedling groups revealed differing growth responses, with increasing influence of precipitation closer to tundra areas.

Discussion and Conclusions

Tree line advance not only depends on favorable climatic conditions, but also on suitable microsites (Lloyd & Fastie 2002). In northwest Russia, where recent warming has not been pronounced and concentrated on spring and summer, no recent establishment in forest or woodland has occurred. In fact, most seedlings established 50–60 years ago in a period of winters warmer than and summers slightly cooler than today. No seedlings have established after 1982, the period of strongest warming in spring and summer. While established trees show positive correlations with warmer summers (growth year), they also show a drought stress-like signal of negative correlations to previous July temperatures, as reported from boreal forest and tree line areas in Alaska (Barber et al. 2000, Wilmking et al. 2004). More analysis is necessary to confirm these results.

The possible influence of precipitation on growth of seedlings in the woodland plots seems to point to the additional influence of microsite conditions on growth. Active layer depth (and thus the distance to the local water table) varies on very small scales, partly following the microtopography, and seedlings often establish on top of hummocks. There, soil temperatures are higher, and no waterlogging occurs. However, the top of hummocks are prone to drying. Preliminary analysis revealed strong, mostly positive correlations of seedling growth with summer precipitation. Higher precipitation might be counteracting drought during the warmest part of the year.

Our preliminary investigation points to a complex interaction between climate (temperature and precipitation) and microsite drivers (active layer depth) for the establishment of trees in the tundra areas of northwest Russia, warranting further investigations. Our plans include the inclusion of two additional sites in the calculation of the climate growth relationships of established trees and seedlings, and a more sophisticated analysis of the actual microsite conditions of each sampled individual.

Acknowledgments

This study was supported by a Sofja Kovalevskaja Award from the Alexander von Humboldt Foundation (M. Wilmking), the German National Scholarship Foundation (S. Kenter), and the EU-Project CARBO-North (6th FP, Contract No. 036993).

References

Barber, V., Juday, G. & Finney, B. 2000. Reduced growth of Alaska white spruce in the 20th century from temperature-induced drought stress. *Nature* 405: 668-72.

Biondi, F. & Waikul, K. 2004. DENDROCLIM2002. A C++ program for statistical calibration of climate signals in tree ring chronologies. *Computers & Geosciences* 30: 303-11.

Chapin, F.S. et al. 2005. Role of land-surface changes in Arctic summer warming. *Science* 310: 657-660.

Lloyd, A.H. & Fastie, C.L. 2002. Spatial and temporal variability in the growth and climate response of treeline trees in Alaska, *Climatic Change* 52: 418-509.

Wilmking, M., Juday, G.P., Barber, V.A. & Zald, H.S.J. 2004. Recent climate warming forces opposite growth responses of white spruce at treeline in Alaska through temperature thresholds. *Global Change Biology* 10: 1724-36.

Wilmking, M., Harden, J. & Tape, K. 2006. Effect of tree line advance on carbon storage in NW Alaska. *JGR* 111: G02023, doi:10.1029/2005JG000074.

Bathymetric Mapping of Lakes in the Western Arctic Coastal Plain, Alaska

Barry Winston
University of Cincinnati, Cincinnati, USA
Kenneth Hinkel
Department of Geography, University of Cincinnati, Cincinnati, USA
Richard Beck
Department of Geography, University of Cincinnati, Cincinnati, USA

Introduction

The Arctic Coastal Plain (ACP) of northern Alaska is characterized by thousands of lakes developed atop continuous permafrost. This region can be subdivided into the Younger Outer Coastal Plain (YOCP), the Outer Coastal Plain (OCP), and the Inner Coastal Plain (ICP) (Hinkel et al. 2005), which are demarcated by ancient shorelines at 23–29 m. a.s.l. and 7 m a.s.l. (Hopkins 1973, Péwé 1975). These subregions can be further differentiated by surficial sediments that reflect the effects of recent geomorphic processes, with fine-grained marine sediments associated with the OCP and YOCP and eolian sand characteristic of the ICP (O'Sullivan 1961, Williams et al. 1978, Williams 1983). Lakes are significantly different among these three subregions with respect to lake surface area, depth, and lake density (Hinkel et al. 2005).

Many lakes on the ACP have depths of less than 2 m (Carson & Hussey 1962). Such lakes are shallow enough that water freezes to the lake bottom during winter and is continuous with the underlying permafrost. However, in the case of deeper lakes, water at depth remains unfrozen. With water temperature above freezing, the underlying permafrost begins to thaw, thereby creating a thaw bulb. The thaw bulb expands and the substrate slowly subsides as it loses volume when pore ice is converted to water. As the lake grows larger and deeper over time, the thaw bulb beneath the lake expands, the underlying permafrost thaws, and the ground subsides further. It is possible for the thaw bulb to reach the maximum depth of permafrost (>300 m) in large, deep lakes, resulting in the formation of an open talik (French 2007).

Several models for lakes on the ACP suggest that these features develop, expand, and drain as part of a cyclical process (Cabot 1947, Carson & Hussey 1962, Everett 1980, Billings & Peterson 1980). However, recent research suggests that lake evolution is more complex and may not be applicable across the entire ACP (Jorgenson & Shur 2007). The goal of this study is to gather basic bathymetric and sedimentological information from these small, deep lakes. They appear to be fundamentally different from the well-studied lakes of the OCP that were used to develop the thaw-lake cyclical model.

Study Area and Methodology

The lakes reported on here are all with 32 km of our base camp at 70°0′N and 153°5′W. They are located within the ICP and are characterized by deep central basins and prominent shelves composed of sand deposits. Bathymetric data were collected along transects from 17 lakes during late summer 2007 to determine general basin depth, slope, and morphological characteristics.

Depth measurements from the lakes were recorded with an Eagle SeaCharter 502c DF iGPS sonar mounted to the stern of the vessel. The sonar was equipped with a 50/200 kHz dual-frequency transducer that was positioned approximately 15 cm below the water surface. The GPS was calibrated to UTM Zone 5 North, NAD-1983 and had a locational accuracy better than 3 m. The data were collected by making a series of transect passes across the lakes, recording both depth and location once every second. The distance between each sample was estimated during post-processing of the GPS locations. The slope was calculated between each pair of samples using the depth measurements.

Results and Conclusions

Out of the 17 lakes sampled, 7 lakes contained deep basins that exceed a depth of 10 m; the maximum recorded depth in one lake was 19 m. These 7 lakes contained shallow shelves that declined into deep basins over short distances. However, the deep basins were not always located in the center of the lake, and several lakes contained multiple basins or exhibited discontinuous basins.

The shelves were very shallow (0.3–3 m), with dunes and ripples apparent in the sandy sediment. The basin floors were relatively flat (1–2°), and the shelf-basin transition area averaged 30°. However, for the 2 transects shown in Figures 1 and 2, a slope of 54° was estimated in Lake A, and a slope of 44° was determined in Lake B.

The sandy lake bottom sediments should have an angle of repose no greater than 35° (Stegner & Wesfreid 1999). However, in the case of the 2 observed lakes, the slope was significantly greater. This suggests that the shelf sediments are bonded by permafrost, since unconsolidated sand cannot maintain the observed slope.

It is not known if the permafrost is syngenetic, and aggraded upward with sediment deposition along the lake margin. The association of the deepest lake basins (~18 m) with oversteepened slopes suggests thaw bulb development and subsidence. However, thaw consolidation is typically not very effective in sandy sediments unless significantly enriched in ice. Jorgenson & Shur (2007) indicate that near-surface sediment cores from this region of the ACP have not evidenced ice oversaturation. Subsequent fieldwork on lakes in the ACP will focus on mapping lake bathymetry,

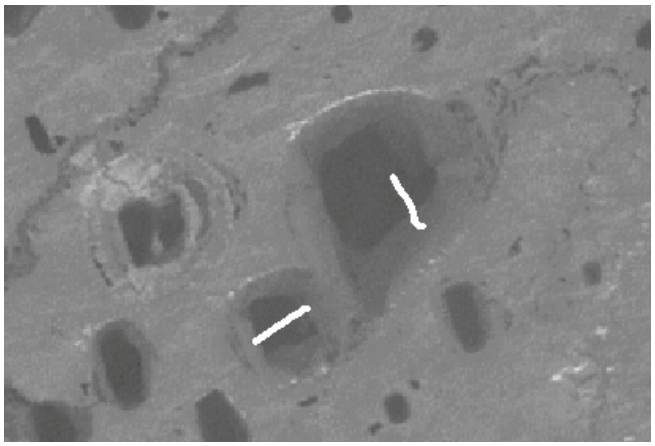

Figure 1. Landsat-7 grayscale image showing two sampled lakes. White lines indicate data acquisition path. For reference, Lake A is on the left; Lake B is on the right.

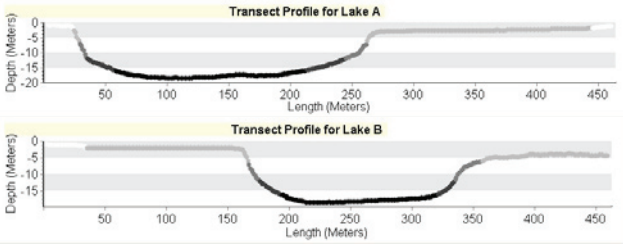

Figure 2. Associated transect profiles. Transect in Lake A is from west to east; transect in Lake B is from south to north.

collecting bottom cores, and conducting ground penetrating radar investigations.

Acknowledgments

This work was supported by the NSF under grants 9732051 & 0094769 to KMH and 0548846 & 0539167 to W. Eisner. Any opinions, findings, or conclusions expressed in this material are those of the authors. We appreciate support from the Barrow Arctic Science Consortium and the Ukpeagvik Inupiat Corporation.

References

Billings, W.D. & Peterson, K.M. 1980. Vegetational change and ice-wedge polygons through the thaw-lake cycle in Arctic Alaska. *Arctic and Alpine Research* 12: 413-432.

Cabot, E.C. 1947. The northern Alaska coastal plain interpreted from aerial photographs. *Geographical Review* 37: 369-648.

Carson, C.E. & Hussey, K.M. 1962. The oriented thaw lakes of northern Alaska. *Journal of Geology* 70: 417-439.

Carter, L.D. 1981. A Pleistocene sand sea on the Alaskan arctic coastal plain. *Science* 211: 381-383.

Everett, K.R. 1980. Landforms. *Geobotanical Atlas of the Prudhoe Bay Region, Alaska.* Hanover, NH: U.S Army Cold Regions Reserve.

French, H.M. 2007. *The Periglacial Environment,* 3rd ed. England: John Wiley and Sons Ltd.

Hinkel, K.M., Frohn, R.C., Nelson, F.E., Eisner, W.R. & Beck, R.A. 2005. Morphometric and spatial analyses of thaw lakes and drained thaw lake basins in the western Arctic coastal plain, Alaska. *Permafrost and Periglacial Processes* 16: 327-341.

Hopkins, D.M. 1973. Sea level history in Beringia during the last 210,000 years. *Quaternary Research* 3: 520-540.

Jorgenson, M.T. & Shur, Y. 2007. Evolution of lakes and basins in northern Alaska and discussion of thaw lake cycle. *Journal of Geophysical Research* (in press).

O'Sullivan, J.B. 1961. *Quaternary geology of the Arctic Coastal Plain, northern Alaska*. Ph.D. Dissertation. Ames: Iowa State University Science and Technology.

Péwé, T.L. 1975. *Quaternary Geology of Alaska*. U.S. Geological Survey Professional Paper 835.

Stegner, A. & Wesfreid, J.E. 1999. Dynamical evolution of sand ripples under water. *Physical Review* 60: 3487-3490.

Williams, J.R. 1983. *Engineering-Geologic Maps of Northern Alaska, Meade River Quadrangle.* U.S. Geological Survey Open File Rep. 83-294.

Williams, J.R., Carter, L.D. & Yeend, W.E. 1978. Coastal Plain Deposits of NPRA, In: K.A. Johnson (ed.), *The U.S. Geological Survey in Alaska: Accomplishments During 1977*. Reston, VA: USGS, Circ. 77-2 B.

Digitizing Regional Permafrost Maps for Central and Eastern Asian Permafrost Mapping

Lizong Wu
Cold and Arid Regions Environmental and Engineering Research Institute, CAS, Lanzhou 730000, China
Xin Li
Cold and Arid Regions Environmental and Engineering Research Institute, CAS, Lanzhou 730000, China
Jerry Brown
International Permafrost Association, P.O. Box 7, Woods Hole, MA 02543, USA

Introduction

Permafrost and seasonally frozen ground regions occupy approximately 24% and 60%, respectively, of the exposed land surface in the Northern Hemisphere. The actual area underlain by permafrost is approximately 12% to 18% of the exposed land area. Accelerated warming of permafrost in mountainous, highland, and plateau regions of Asia will result in disequilibria of the water cycle, increased mass wasting processes, and related sediment transport and slope hazards. Without a unified and verified regional permafrost map, these processes cannot be assessed adequately.

Although national permafrost maps exist for China, Kazakhstan, Mongolia, and Russia, there is no consistent cartographic for mountainous and high altitude regions. The existing classifications based on spatial continuity or percentage distribution and ground ice content have limited application for mountainous or plateau regions. The 2001 International Symposium on Mountain and Arid Land Permafrost held in Mongolia recommends that an international team of experts is required to prepare a uniform map of Central Asia permafrost. A team for central and eastern Asian permafrost mapping was established during the workshop on Permafrost of Central and Eastern Asia held in China (2006). The members agreed to digitize and archive the recent permafrost map, and auxiliary information exists for China, Kazakhstan, Mongolia, and Russia to complete a pilot map with a unified legend. Classification-based temperature and/or thermal stability was recommended to employ in this work (Brown et al. 2006). The WDC for Glaciology and Geocryology at Lanzhou was expected to organize the digitizing of the permafrost maps for the four countries.

Regional Permafrost Maps Resource

China

Permafrost mapping study in China began in the 1960s. After that, regional permafrost distribution maps for Da and Xiao Xing'anling Mountain (1:2,000,000), Tianshan Mountain (10,000,000), and Qilian Mountain (1:10,000,000) were completed in 1980, 1981, and 1983, respectively (Cheng 1999). Permafrost mapping for the plateau regions began in the 1980s; the permafrost map along the Qinghai-Tibetan Highway (1:600,000) was published in 1981, and the permafrost map of the Qinghai-Tibetan Plateau (1:3,000,000) was finished in 1996 (Tong et al. 1983, Li et al. 1996).

Up to now, there are three permafrost maps that exist for all of China's land territory. The first one, entitled "Map of Snow, Ice and Frozen Ground in China" compiled by Yafeng Shi, was published in 1988 (Shi et al. 1988). The "Map of Geocryological Regionalization and Classification in China," at a scale of 1:10,000,000, was published in 2000 (Qiu et al. 2000). The map was digitized by T. Zhang and collected by NSIDC at Boulder. The latest version contained in the "Map of the Glaciers, Frozen Ground and Deserts in China" was published in 2006 at a scale of 1:4,000,000 (Wang et al. 2006). The classification used in these maps is based on spatial continuity or percentage distribution and elevation.

Thermal stability was used to classify permafrost on Tibet by Nan, performed upon the analysis of mean annual ground temperature distribution features from 76 observed data (Nan et al. 2002).

In the last two years, most of these maps have been digitized, and an attempt to merge different sources was carried out at the WDC for Glaciology and Geocryology, Lanzhou to obtain a more detailed permafrost map.

Russian

Beginning in 1995, geocryological maps published in the USSR (former Soviet Union) and Russia were identified and catalogued to form an inventory. This bibliography was compiled in 1998 by Irena Streletskaya and Marina Leibman, Earth Cryosphere Institute Russian Academy of Sciences, Siberian Branch. The detail information can be browsed from the Frozen Ground Data Center of NSIDC (NSIDC).

The "Geocryological Map of Russia and Neighbouring Republics" by Yershov at a scale of 1:2,500,000, with four attached maps at a scale of 1:25,000,000, were published between 1991 and 1996. An English-language description of the map and its compilation procedure are given by Zaitsev et al. (1998).The map divides permafrost zones by both percent of coverage and ground temperatures at the depth of zero amplitude. So the present legends can be used as reference classification in compiling the other permafrost maps.

The map project used is identified only as "conic equidistant projection," and lacks specific information on the projection. After the digitizing of the map, a geometry correction has been conducted.

Kazakhstan

An unpublished map of Kazakhstan was available and presents the distribution of mountain permafrost and legend. Dr. Sergei S. Marchenko from the Geophysical Institute,

University of Alaska Fairbanks, offers the original data of the map. The map divides permafrost zones by both altitudinal belts and ground temperatures (Brown et al. 2006).

A second mapping effort by Marchenko will prepare a modeled map of the four-country Altai Mountain region, showing the computed extent of permafrost and estimated MAGT at 20 m depth.

Mongolia

The "Map of Geocryology and Geocryological Zonation of Mongolia" was derived from the National Atlas of Mongolia and collected by the Frozen Ground Data Center of NSIDC. The Mongolia maps have 14 different terrain classifications determined according to elevation, mean annual air temperature, permafrost thickness and thaw depth, and seasonal frozen ground freeze depth (NSIDC).

Next Step

All of the maps mentioned above have been digitized at the WDC for Glaciology and Geocryology in Lanzhou. The next step is to develop a merged regional permafrost map of central and eastern Asia. A thermal stability-based classification system (Cheng 1984) is proposed to be used.

Acknowledgments

This work is supported by the Ministry of Science and Technology of China project "Data-sharing Network of Earth system" and the NSFC (National Science Foundation of China) project "Environmental and Ecological Science Data Center for West China."

References

Brown J., Marchenko, S., Li, X. et al. 2006. *Report for the Workshop on Classification, Mapping and Monitoring of Permafrost of Central and Eastern Asia*. Lanzhou, China.

Cheng, G.-D. 1984. Problems of zonation of high-altitude permafrost. *ACTA Geographica Sinica* 39(2): 185-193.

Cheng, G. 1999. Glaciology and geocryology of China during the past 40 years: Progress and prospects. *Journal of Glaciology and Geocryology* 21(4): 289-310.

Li, S. & Cheng, G. 1996. *Map of Frozen Ground on Qinghai-Xizang Plateau*. Lanzhou: Gansu Culture Press.

Nan, Z., Li, S. & Liu, Y. 2002. Mean annual ground temperature distribution on the Tibetan Plateau: Permafrost distribution mapping and further application. *Journal of Glaciology and Geocryology.* 24(2): 142-149.

NSIDC. http://nsidc.org/fgdc/

Qiu, G., Zhou Y., Guo, D. et al. 2000. *The Maps of Geocryological Regionalization and Classification in China (1:10,000,000)*. Beijing: Science Press.

Shi, Y. 1988. *Map of Snow, Ice and Frozen Ground in China*. Beijing: China Cartographic Publishing House.

Tong, B., Li, S., Bu, J. et al. 1983. Principle and method of compilation of permafrost map (1:600,000) along Qinghai-Xizang (Tibet) Highway. *Proceedings of the Second International Conference on Permafrost (Selection)*. Lanzhou: Gansu People's Publishing House, 75-80.

Wang T. (ed.) 2006. *Map of the Glaciers, Frozen Ground and Deserts in China (1:4,000,000)*. Beijing: Sino Maps Press.

Challenges of Infrastructure Growth on a University Campus in Discontinuous Permafrost

Frank Wuttig
Shannon & Wilson, Inc.

Introduction

The University of Alaska Fairbanks (UAF) campus is located in a transition zone from the southern edge of a broad upland area down onto lowlands of the Chena and Tanana Rivers (Fig. 1). The campus is underlain by warm discontinuous permafrost.

The main portions of the campus, including Lower Campus and West Ridge, are on a low east–west trending ridge overlooking the lowlands to the south. The distribution and character of the permafrost has affected and continues to affect the development of the campus and surrounding infrastructure.

This abstract describes the geologic and permafrost setting of the campus and surrounding area, and describes some of the effects permafrost has had on design and construction of campus facilities.

The majority of campus development has occurred on the crest or southern slope of the ridge, which is generally free of permafrost and permafrost-related features. Development becomes more challenging in discontinuous permafrost areas north of the ridge crest and on the lowlands south of the ridge. This abstract discusses four campus infrastructure projects impacted by permafrost, as well as challenges and lessons learned from developing the projects.

Geologic and Permafrost Setting

The upland ridge is underlain by loess-covered schist bedrock, and bedrock outcrops are found at the east end of campus. The windblown silt is retransported downslope to the north and south of the ridge crest. The lowlands consist of vegetated floodplains and low benches cut by the Tanana and Chena Rivers. Soils in the lowlands typically consist of interbedded alluvial sands and gravels mantled by silty overbank deposits dissected by filled sloughs and oxbow lakes representing former river channels.

A large, low-angle fan of retransported loess emanating from the nearby Cripple Creek Valley onto the lowland covers the southwest portion of the area. The distal (leading) edge of the silt fan is scalloped where it has been eroded by former channels of the Chena River. Soils along the leading edge of the fan have been mapped as silt-filled meander scars. Terrain units mapped by Pewe (1976) are shown in Figure 1.

The silt fan is generally underlain by continuous permafrost, with a low to moderate ice content, occurring primarily as pore ice with some segregated ice as seams and lenses.

Permafrost on the floodplain is generally discontinuous. Surficial soils on the floodplain have low to moderate ice content. The underlying sands and gravels typically have low moisture contents.

Retransported silt permafrost on the north-facing slopes and in the valley bottoms is typically perennially frozen with moderate to very high ice content in the form of pore ice, segregated ice as seams and lenses, and massive ice associated with ice wedge deposits.

International Arctic Research Center

The International Arctic Research Center (IARC), founded on windblown silt in the West Ridge area of the UAF campus, was originally designed to sit north of Koyukuk Drive in line with the front of the adjacent Elvey building. A portion of the proposed footprint extended into a forested area north of the ridge crest. Exploratory drilling showed the area to be underlain by discontinuous ice-rich silt permafrost. Long-term thaw settlement concerns resulted in a shift of the building footprint to the south into Koyukuk Drive and a reroute of the road south of the structure.

In the first year following construction of the facility, the sidewalk slab in front of the main entry heaved, blocking the front entrance. The slab was constructed on a thin layer of nonfrost-susceptible fill overlying a frost-susceptible silt fill and a silt subgrade. It was postulated that the heaving was likely aggravated by construction water, which was used to compact the silt fill beneath the sidewalk. Heaving has not been a problem in subsequent years.

West Ridge Research Building

The multi-storied West Ridge Research Building (WRRB) is north of the Elvey Building in the West Ridge area of the UAF campus. The structure is north of the east–west trending ridge crest in an area originally developed as a parking area for adjacent buildings. Numerous ground collapses, some more than 7 m deep, have developed along the northern edge of the parking lot, the result of concentrated surface runoff entering thermokarst voids in the subsurface.

Subsurface exploration of the area showed the southern portion of the parking area immediately behind the Elvey Building had suitable conditions for a deep, conventional foundation consisting of thawed and low-moisture-content silt permafrost. The northern portion of the lot was not suitable for construction due to known thermokarst and thaw-unstable silt permafrost. However, the footprint of the structure was extended out into the northern portion of the parking area. During construction, large voids and massive ice representing degrading ice wedges were encountered in the northern portion of the foundation excavation. To reduce the potential for thermokarst collapse beneath the structure

foundation, additional subexcavation to a depth below the anticipated base of thermokarsts and ice wedges was completed and the base of the excavation probed on a tight grid for additional thermokarst voids and ice. The northern foundation wall of the structure was redesigned as a deep grade beam that could span localized settlement in the event undetected thermokarsts were present.

Harper Building

The Harper Building is near the southern edge of the campus along Geist Road. The building is on the floodplain at the leading edge of the silt fan in an area of meander scars. Ice-rich organic silts and inorganic silts were encountered to depths averaging about 3.6 m. Localized peat deposits occurred at the site outside the building footprint. Thaw-unstable sand and silty sands extended to depths averaging 7.3 m; slightly thaw-unstable gravels occurred below this depth. The building is founded on steel pipe adfreeze piles bearing in the underlying gravels. The structure was designed to be elevated to provide a free air space beneath the building and protect the permafrost from thawing.

Since construction, the free air space of the structure was skirted and passively heated, resulting in more than 60 cm of differential settlement beneath the pile and grade-beam-supported floor. Connections to buried utilities, not designed to withstand building settlement, have reportedly failed. Landscaped areas and driveways have experience significant amounts of differential settlement.

Main Entrance Roads

The main entrance to the university at time of the last permafrost conference in Fairbanks in 1983 was along Fairbanks Street off Geist Road. A four-lane overpass was constructed at the railroad tracks along this access. The center span of the three-span bridge is supported on strip footings founded on colluvium and shallow bedrock. The bridge abutments were founded on continuous footings bearing in the embankment fill on either side of the tracks. The north abutment and center piers were founded on thaw-stable soils, whereas the southern approach embankment was constructed on highly thaw-unstable slough deposits at the leading edge of the silt fan. The southern abutment subsequently settled approximately 1 m, rendering the bridge unsafe.

A new access road to the university (Thompson Drive) was constructed across permafrost terrain in 2005 and 2006. The majority of the alignment is located on silt fan deposits, which are perennially frozen and slightly to moderately thaw-unstable. Cleared farm fields were thawed to a depth of 9 m.

Thompson Drive was constructed using experimental passive refrigeration systems in areas underlain by shallow permafrost, including a system of insulation, nonfrost-susceptible fill, and hairpin thermosyphons completely buried in the road bed at the southern end of the project, shoulders ventilated with a layer of coarse rock in the center of the project, and an air convection embankment at the northern end of the project. The bridge over the railroad is founded on permafrost schist bedrock, and alluvial sands and gravels underly the site.

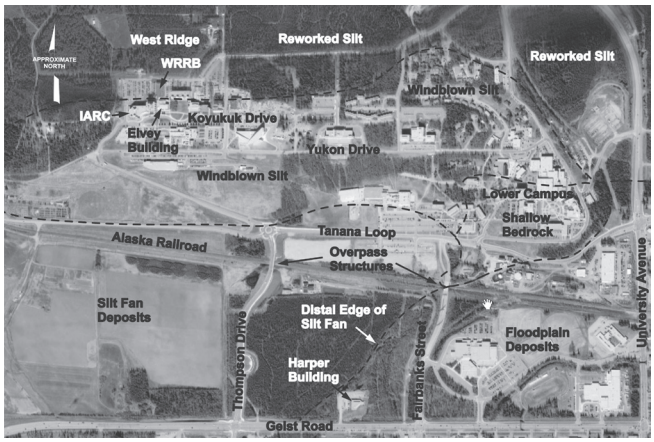

Figure 1. UAF campus and terrain units mapped by Pewe (1976).

References

Pewe, T.L. & Bell, J.W. 1976. Map *Showing Foundation Conditions in the Fairbanks D-2 SW Quadrangle, Alaska*. U.S. Geological Survey Map I-829-E.

Modeling and Monitoring Ecosystem Performance of Boreal Forests in the Yukon River Basin

Bruce K. Wylie
ASRC Research and Technology Solutions, contractor to U.S. Geological Survey (USGS)
Earth Resources Observation and Science (EROS) Center

Li Zhang
SAIC, contractor to USGS EROS

Norman Bliss
ASRC Research and Technology Solutions, contractor to U.S. Geological Survey (USGS)
Earth Resources Observation and Science (EROS) Center

Lei Ji
ASRC Research and Technology Solutions, contractor to U.S. Geological Survey (USGS)
Earth Resources Observation and Science (EROS) Center

Larry Tieszen
U.S. Geological Survey, Earth Resources Observation and Science Center, Sioux Falls, South Dakota

W.M. Jolly
U.S. Department of Agriculture Forest Service, Fire Sciences Laboratory, Missoula, Montana

Introduction

We emphasize the ability to quantify ecosystem processes, not simply changes in land cover, across the entire period of the remote sensing archive (Wylie et al., in press). The method builds upon remotely sensed measurements of vegetation greenness for each growing season. However, a time series of greenness often reflects annual climate variations in temperature and precipitation. Our method seeks to remove the influence of climate so that changes in underlying ecological conditions are identified and quantified. We define an "expected ecosystem performance" to represent the greenness response expected in a particular year given that year's climate. We distinguish "performance anomalies" as cases where the ecosystem response is significantly different from the expected ecosystem performance. Performance anomaly maps and anomaly trends provide valuable information on the ecosystem for land managers and policy makers at 1-km resolution. The results offer a prototype to assess the entire Yukon River Basin, a task slated for completion with our Canadian counterparts for the entire archival period (1984 to current) at 1 km and at 250 m (2000 to current).

Methods

A regression tree model was developed to predict growing season Normalized Difference Vegetation Index (NDVI), or expected ecosystem performance, from nearly 14,000 random pixels, which represents a range of annual climatic conditions and numerous site conditions. We used 1-km Advanced Very High Resolution Radiometer NDVI 7-day composites integrated from April through the first week of October as a proxy for ecosystem performance. Using spatial climatic data and site potential information, annual maps of expected growing season NDVI from 1996 to 2004 were constructed from this model.

Site potential is the historical performance related to elevation, slope, aspect, soils, and other factors. Dry years have lower expected ecosystem performance, and wet years have higher expected ecosystem performance. Areas that do not perform within a normal range determined by the regression tree model's expected error were identified as ecosystem performance anomalies. These anomalies are areas that responded to climatic conditions differently from areas with similar expected ecosystem performance.

The anomalies were validated using Composite Burn Index data from selected fires and Landsat spectral indices across a burned-to-unburned gradient. Linear time series trends in the performance anomaly were mapped based on the significance and sign (positive or negative) of the slope.

Results

Expected ecosystem performance

Regression tree models predicted expected performance from site potential, climate data, and land cover ($R^2 = 0.84$) and showed little bias. Withheld test locations had similar mean standard error of regression values as those of the model development dataset. Regression tree committee models were used, wherein each regression tree model possessed five different regression trees, each trying to improve predictions made by the previous regression tree model. This resulted in over 500 different piecewise multiple regressions being employed.

Ecosystem performance anomaly

Significant ecosystem performance anomalies were determined at 90% confidence intervals of the expected ecosystem performance model. Underperforming anomalies correlated with recent fires. Composite burn index (Epting et al. 2005) from selected fires validated the ecosystem performance results. Landsat spectral indices were also

used to validate performance anomalies across a burned-to-unburned gradient. We investigated trends in post-fire performance anomalies and found that ecosystem performance in burned areas showed varying rates of recovery when compared to climatically-predicted expected ecosystem performance. This indicates that this approach identifies and quantifies post-fire vegetation succession, although ground validation of vegetation and surface cover are needed for further interpretation.

Areas with significant consistent performance anomalies over multiple years are likely boreal forests under environmental stress. Frequency and trend maps of performance anomalies emphasize areas which perhaps experience degrading permafrost, marked by dryness, insect infestations, or disease.

Areas with burn dates prior to the beginning of the study often exhibited positive trends during the study.

Conclusions

Our approach uses climate data to account for interannual variations in ecosystem performance. The ecosystem performance anomalies reflect ecological changes that are caused by factors other than climate or site potential. The underperforming areas documented in this study were strongly associated with burn disturbances. Based on climate, portions of the study reveal that boreal forest performance is declining, and the trend appears more severe with time.

Acknowledgments

The authors would like to thank Barry Baker of the Nature Conservancy for providing domain cluster data (Saxon et al. 2005) used to help map boreal forest site potential. Funding was provided by the USGS Earth Surface Dynamics and Land Remote Sensing programs, with work performed under USGS contract numbers 08HQCN0007 (B.K. Wylie), 03CRCN0001 (L. Zhang), and 08HQCN0007 (N. Bliss and L. Ji).

References

Epting, J., Verbyla, D. & Sorbel, B. 2005. Evaluation of remotely sensed indices for assessing burn severity in interior Alaska using Landsat TM and ETM+. *Remote Sensing of Environment* 96: 328-339.

Saxon, E., Baker, B., Hargrove, W., Hoffman, F. & Zganjar, C. 2005. Mapping environments at risk under different global climate change scenarios. *Ecological Letters* 8: 53-60.

Wylie, B.K., Zhang, L., Bliss, N., Ji, L., Tieszen, L. & Jolly, M. In press. Integrating modeling and remote sensing to identify ecosystem performance anomalies in the boreal forest, Yukon River Basin, Alaska. *Int. J. Digital Earth*.

Impact of Frozen Ground Change on Streamflow Hydrology Over the Lena Watershed in Siberia: A Preliminary Analysis

Daqing Yang, Ipshita Majhi, Doug Kane
Water and Environmental Research Center, University of Alaska Fairbanks
Tingjun Zhang
National Snow and Ice Data Center, University of Colorado

Permafrost limits the amount of subsurface water storage and infiltration that can occur, leading to wet soils and ponded surface waters, unusual for a region with such limited precipitation. Changes in climatic conditions significantly affect the thermal regimes of active layer and permafrost (Pavlov 1994, Kane 1997, Frauenfeld et al. 2004, Zhang et al. 2005). Warming of high latitude regions results in an increase of active layer and permafrost temperatures, a deeper active layer and talik development, lateral thawing of permafrost in discontinuous and sporadic permafrost regions, and finally northward movement of the permafrost boundaries (Serreze et al. 2000, Woo 1986, Zhang et al. 2005).

Studies show that near-surface permafrost temperature in northern Russia has increased by 0.6–0.7°C during the period 1970–1990 owing to higher air temperature and deeper snow cover over Siberia (Pavlov 1994). In some regions of Siberia, permafrost temperature has warmed more than 2°C (Zhang et al. 2005, Pavlov 1996), active layer thickness has increased by up to 20 to 30 cm, and talik over permafrost may have developed over the past several decades. It has been predicted that, under a moderate climatic warming scenario, changes in permafrost temperature and active layer thickness will become more significant in the next few decades in the Russian Arctic and Subarctic (Pavlov 1996, Lawrence & Slater 2005, Saito et al. 2007).

Changes in timing, duration, and thickness of seasonal freeze and thaw, talik development, and permafrost conditions have a significant impact on surface runoff and ground hydrology. Changes in active layer thickness directly affect groundwater storage and river discharge through partitioning surface runoff (Kane 1997). A deeper active layer delays the freeze-up dates of the active layer and allows drainage to occur later in the winter. Analysis of soil moisture data in the upper (1 m) layer in the former Soviet Union over recent decades reveals a long-term increasing trend of soil moisture north of 50°N, mainly due to precipitation increases of 10–30 mm every 10 years (Vinikov & Yeserkepova 1991). Observation records show that the absolute amount of water content increases 10–30 mm in the 1 m soil layer, and groundwater level rose by 50–100 cm in Siberia. This increased groundwater storage may result in underground water recharge to the river system, and consequently, a significant increase of runoff in the winter months.

Recent assessments of the large rivers in the Arctic (i.e., the Lena, Ob, and Yenisei—drainage areas between 2,400,000 and 3,000,000 km^2, and contributing more than 45% of the total freshwater inflow to the Arctic Ocean) identify significant changes in streamflow seasonal cycle (Yang et al. 2002, 2004a,b, Ye et al. 2003). For example, since the mid-1930s, the Lena River summer runoff has not changed significantly, but winter runoff has increased 25–80%. In the Yenisei River basin, summer runoff has decreased by 20–30%, and winter discharge has gone up by 35–110%. The Ob River has also experienced a winter runoff increase of 30–40%, and summer runoff has risen in July by 10%. Base (low) flow increases have been reported over Siberian regions and watersheds. This may indicate hydrologic response to climate and permafrost changes. The linkage between streamflow and permafrost changes is not well understood.

This study applies comprehensive statistical methods to examine the linkage between frozen ground and river streamflow changes. Statistical analyses include the combinations of multiple-correlation, stepwise regression, and linear correlation and regression techniques. These methods have been applied to data of river streamflow, temperature, precipitation, soil moisture, and active layer depth. This allows us to establish statistical relationships useful for identifying important climatic and permafrost factors to regional streamflow changes. Further, it helps to quantify lengths of memory of different variables (temperature, precipitation, snow cover, etc.) and their impact on interannual variation of river discharge.

More specifically, this study examines the relation among ground temperature, active layer depth and base flow changes. The focus of the analysis is placed on the regions/basins with significant changes, such as the Aldan tributary in the upper Lena basin, where ground temperatures and winter flows have increased significantly in the last 40–50 years. The results of this work are useful in assessing the impact of permafrost changes on long-term streamflow variations over large watersheds, and they improve our understanding of the processes and interactions among climate, permafrost, and hydrology systems in the arctic regions.

References

Frauenfeld, O., Zhang, T., Barry, R.G. & Gilichinsky, D.G. 2004. Interdecadal changes in seasonal freeze and thaw depths in Russia. *J. Geophys. Res.* 109: D05101, doi:10.1029/2003JD004245.

Kane, D.L. 1997. The impact of Arctic hydrologic perturbations on Arctic ecosystems induced by climate change. In: W.C. Oechel (ed.), *Global Change and Arctic Terrestrial Ecosystems.* Springer-Verlag Ecological Studies 124, 63-81.

Lawrence, D.M. & Slater, A.G. 2005. A projection of severe near-surface permafrost degradation during the 21st century. *Geophys. Res. Lett.* 32: L24401, doi:10.1029/2005GL025080.

Pavlov, A.V. 1994. Current change of climate and permafrost in the Arctic and Subarctic of Russia. *Permafrost and Periglacial Processes* 5: 101-110.

Saito, K., Kimoto, M., Zhang, T., Takata, K. & Emori, S. 2007. Changes in hydro-thermal regimes in frozen ground regions under global warming scenarios simulated by a high-resolution climate model. *J. Geophys. Res.* 112: F02S11, doi:10.1029/2006JF000577.

Serreze, M.C, Walsh, J.E., Chapin, E.C, Osterkamp, T., Dyugerov, M., Romanovsky, V., Oechel, W.C., Morison, J., Zhang, T. & Barry, R.G. 2000. Observation evidence of recent change in the northern high-latitude environment. *Climate Change* 46: 159-207.

Vinnikov, K.Ya. & Yeserkepova, I.B. 1991. Soil moisture: empirical data and model results. *J. Climate* 4: 66-79.

Woo, M.-K. 1986. Permafrost hydrology in North America. *Atmosphere-Ocean* 24(3): 201-234.

Yang, D., Ye, B. & Shiklomanov, A. 2004. Streamflow characteristics and changes over the Ob river watershed in Siberia. *J. of Hydrometeorology* 5(4): 69-84.

Yang, D., Ye, B. & Kane, D. 2004. Streamflow changes over Siberian Yenisei river basin. *J. of Hydrology* 5(4): 69-84.

Yang, D., Kane, D., Hinzman, L., Zhang, X., Zhang, T. & Ye, H. 2002. Siberian Lena river hydrologic regime and recent change. *J. Geophys. Res.* 107(D23): 4694, doi:10.1029/2002JD002542.

Ye, B., Yang, D. & Kane, D. 2003. Changes in Lena river streamflow hydrology: human impacts vs. natural variations. *Water Resources Research* 39(8): 1200, doi: .10.1029/2003WR001991

Zhang, T. 2005. Influence of the seasonal snow cover on the ground thermal regime: An overview. *Reviews of Geophysics* 43: RG4002, doi:10.1029/2004RG000157.

Zhang, T., Frauenfeld, O.W., Serreze, M.D., Etringer, A., Oelke, C., McCreight, J., Barry, R.G., Gilichinsky, D., Yang, D., Ye, H., Ling, F. & Chudinova, S. 2005. Spatial and temporal variability of active layer thickness over the Russian Arctic drainage basin. *J. Geophys. Res.* 110: D16101, doi:10.1029/2004JD005642.

Simulating the Effects of Wildfire on Permafrost and Soil Carbon Dynamics of Black Spruce Over the Yukon River Basin Using a Terrestrial Ecosystem Model

Shuhua Yi
Institute of Arctic Biology, University of Alaska Fairbanks
A. David McGuire
U.S. Geological Survey, Alaska Cooperative Fish and Wildlife Research Unit
Jennifer Harden
U.S. Geological Survey, Menlo Park, California

Introduction

Wildfire is considered an important disturbance agent in boreal forest ecosystems (Kasischke et al. 2006). It can affect high latitude carbon dynamics directly through combustion emissions, and indirectly through vegetation succession and removal of the surface organic layer, which might accelerate the degradation of permafrost and, hence, the release of soil carbon. At the regional scale, the direct effects of fire have received a lot of attention, but the evaluation of the indirect effects has been more limited because the appropriate tools have not yet been developed for application at the regional scale.

Research objectives and questions

In this study, we implemented a dynamic soil layer module in the Terrestrial Ecosystem Model (hereafter DSL-TEM) to answer the following questions: (1) What is the change of permafrost over the Yukon River Basin for periods before and after year 1976, when there was a shift in the Pacific Decadal Oscillation? (2) What is the effect of fire on permafrost? and (3) What is the effect of fire on carbon fluxes between the land surface and the atmosphere?

Model Description

TEM is a process-based ecosystem model that simulates carbon and nitrogen dynamics of plants and soils for terrestrial ecosystems. TEM has been widely used to investigate the effects of climate, carbon dioxide fertilization, and wildfire disturbances on the carbon dynamics of North America. Research has focused on developing TEM for applications in high latitudes, including incorporation of the Goodrich algorithm for calculation of soil temperatures for permafrost and seasonal frost regions; and incorporation of the hydrological module for methane production and transport for high latitude wetlands. In this study, further improvements have been made to account for the indirect effects of wildfire in developing the DSL-TEM. The DSL-TEM consists of four interaction modules: an environmental module, an ecological module, a fire disturbance module, and a dynamic soil layer module (Fig. 1). The environmental module has been evaluated and presented at previous scientific conferences (Yi et al. 2007).

Environmental module

The processes considered in the environmental module are

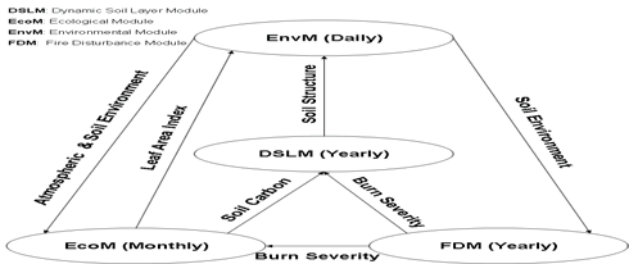

Figure 1. Overall structure of DSL-TEM.

canopy interception of snow and rain; drip and throughfall of snow and rain; canopy transpiration, evaporation, and sublimation; soil evaporation; snow sublimation; melt and accumulation; surface runoff; and subsurface baseflow. A Two-Directional Stefan Algorithm was first applied to simulate the freezing/thawing fronts in soil layers. Temperatures of snow/soil/rock layers were then updated by solving finite difference equations for layers above the first front, layers below the last front, and layers between the first and last fronts. Soil water contents of the unfrozen soil layer were updated by solving Richard's equations.

The above processes are simulated at a daily timestep. The monthly averaged soil temperature and moisture are then passed to the ecological module.

Ecological module

In addition to the carbon and nitrogen dynamics described in previous studies using TEM, a few new features are included in DSL-TEM, including explicit simulation of soil carbon vertical distribution and change of the thicknesses of organic layers based on the soil carbon content.

Soil carbon content of each layer is determined by the litter fall input and carbon decomposition. The above- and below-ground litter fall are assigned to each soil layer according to the fine root distribution. Carbon decomposition is calculated using the soil temperature, moisture, and carbon pool of each soil layer.

The carbon contents of the organic soil layer, including shallow organic and deep organic soil layers, are used to determine the thickness of organic layers, based on the relationship derived from field and laboratory measurements.

The simulated leaf area index is passed to the ecological module; the organic layer thicknesses are passed to the dynamic soil layer module.

Fire disturbance module

The fire disturbance module is run at an annual timestep. When a fire happens, it is used to calculate the fire severity based on the drainage (poorly drained and moderately drained), fire season (early season or late season), and fire size (small, large to ultra-large). The severity is used to calculate the burned organic layer thickness, which is then passed to the dynamic soil layer module.

The above- and below-ground living vegetation is also killed by wildfire. It is assumed that only 1% of above-ground vegetation remains alive, while the fraction of living below-ground vegetation depends on the burned organic layer thickness and the fine root distribution.

Dynamic soil layer module

The dynamic soil layer module is used to manipulate soil layer structures to maintain stability and efficiency of the soil temperature and moisture calculations, when the thickness of the organic layer is changed by wildfire disturbance and ecological processes. There are at most 2 moss layers, 3 shallow organic layers, and 3 deep organic layers. The minimum thickness of a soil layer is set to 2 cm. When an organic layer is too thin, it may be either removed or combined to an adjacent soil layer of the same type. When an organic layer is too thick, it will be divided into two layers.

Datasets

The input datasets include nonspatial datasets (atmospheric CO_2 concentration and fire size), grid-level datasets (0.5° by 0.5°, climate, fire return interval, fire season and soil texture), and pixel-level datasets (1 km by 1 km vegetation type, drainage, and fire history).

Three different cohort-level datasets have been created, based on grid- and pixel-level information. To initialize DSL-TEM, each cohort is run to an equilibrium state using the 1901–1930 mean climate, without disturbances. The equilibrium cohort is a unique combination of drainage, vegetation, and climate. During the next phase of simulation, the spinup stage, each cohort is run using 1901–1930 atmospheric data in a cyclic fashion that considers fire disturbance over the period 1001–1900. Thus the spinup cohort is a unique combination of equilibrium cohort and fire history during period 1001–1900. To save computing time, the fire history has been reclassified into several categories based on the first recorded fire occurrence after 1900. The final phase of the simulation results in a transient cohort that is a unique combination of a spinup cohort and both climate and fire history from 1901–2006.

Overall, for black spruce in the Yukon River Basin, there are 1,167 equilibrium cohorts, 6,858 spinup cohorts, and 40,738 transient cohorts. The total black spruce area in the Yukon River Basin is 213,513 km^2.

Model Experiment

The DSL-TEM was first run to equilibrium state in year 1000 and then through the spinup phase over the period from 1001–1900. A factorial experiment of 8 simulations was then performed over the period from 1901–2006, considering the effects of CO_2 fertilization (constant vs. transient CO_2), climate (constant vs. transient climate), and fire disturbance (with and without fire disturbance).

Results and Discussion

1. The mean annual air temperature increased 0.39 to 1.14°C over the Yukon River Basin (YRB) between 1950–1975 and 1976–2000. Winter precipitation (DJF) increased 4–20 mm at the eastern and western ends of the YRB, and decreased by 7–14 mm in the Tanana River, Eastern Central Yukon, and Koyukuk River sub-basins between the same time periods. The unfrozen column, which is defined as the mean thickness of unfrozen soil layer over a year, increased at both the eastern and westerns ends of the YRB, but decreased in the central YRB. This suggests that winter snowfall plays a more important role than air temperature in affecting permafrost dynamics between the two time periods.

2. For the whole YRB, climate plays a dominant role in determining the thermal state of soil. The effects of fire on soil thermal state are relatively small, in part due to the small fraction of burn area, and in part due to the decrease of winter snowfall in areas with high fire return interval.

3. Fire plays a dominant role in determining the net carbon flux between the land surface and the atmosphere, especially after 1985. The difference between simulations with and without fire can be 140 gC m^{-2}. However, the indirect effect of fire through increasing soil temperature on soil decomposition is relatively small, usually less than 10 gC m^{-2}.

Acknowledgments

We would like to thank other coauthors, including Eric Kasischke, Kristen Manies, Larry Hinzman, Anna Liljedahl, Jim Raderson, Heping Liu, Vladimir Romanovsky, Sergey Marchenko, and Kim Yongwon.

References

Kasischke, E.S. & Turetsky, M.R. 2006. Recent changes in the fire regime across the North American boreal region – Spatial and temporal patterns of burning across Canada and Alaska. *Geophysical Research Letters* 33: doi:10.1029/2006GL025677.

Yi, S., McGuire, A.D., Harden, J., Kasischke, E., Manies, K., Hinzman, L., Liljedahl, A., Randerson, J., Liu, H., Romanovsky, V. & Marchenko, S. 2007. A dynamic soil layer model for assessing the effects of wildfire on high latitude terrestrial ecosystem dynamics. *The 2007 Fall Meeting of American Geophysical Union, December 10–14, 2007, San Francisco, CA*.

Non-Linear Analysis of the Thermal Characteristics of Permafrost Embankment with Crushed-Rock Revetment and Insulation on Qinghai-Tibet Plateau

Mingyi Zhang, Shuangyang Li, Shujuan Zhang, Yuanhong Dong
State Key Laboratory of Frozen Soil Engineering, Cold and Arid Regions Environmental and Engineering Research Institute, Chinese Academy of Sciences, Lanzhou 730000, China

Introduction

The embankment with crushed-rock revetment has been widely used in the construction of the Qinghai-Tibet railway/highway and is an effective measure to ensure the thermal stability of permafrost embankment (Lai et al. 2003, 2004, Sun et al. 2004, Ma et al. 2002); however, because of the influence of global warming, it is difficult to protect the underlying permafrost from warming, even thawing (Wang et al. 1996). Therefore, in order to sufficiently protect the underlying permafrost, a numerical representation of the unsteady two-dimensional continuity, momentum, and energy equations of thermal convection for incompressible fluid in porous media (Nield et al. 1999, Kong et al. 2002) is used to analyze and compare the temperature characteristics of the embankments with crushed-rock revetment, with and without insulation, under the global warming in this study.

Results and Discussions

Based on the temperature and geology conditions on the Qinghai-Tibet Plateau (Cheng et al. 2003, Zhu et al. 1988, Qin, 2002, Lai et al. 2003), the temperature distributions of the three embankment models with crushed-rock revetment, with and without insulation (Fig. 1), constructed on July 15, are simulated and analyzed for 50 years.

Figure 2 is the temperature distribution of the embankment with crushed-rock revetment (1.60 m thick), without insulation on October 15, after 50 years of the construction. It can be seen from this figure that the location of the permafrost table (0°C isotherm) is y = -2.39 m under the natural ground surface, while that is y = -1.79 m in the centerline of the embankment and 0.60 m higher than that under the natural ground surface; furthermore, -0.2°C isotherm is high under the slope foot of the embankment, while low in the middle of embankment.

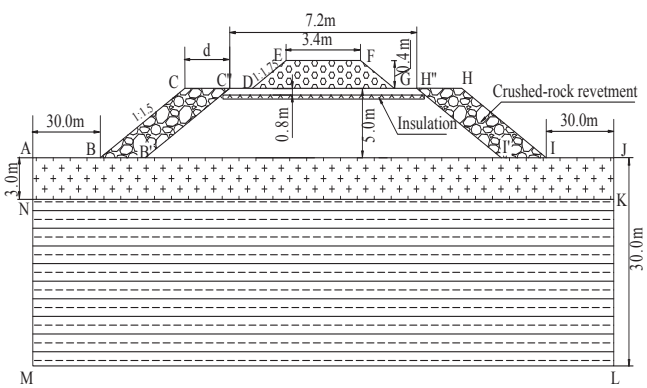

Figure 1. Embankment model with crushed-rock revetment.

Figure 3 shows the temperature distribution of the embankment with crushed-rock revetment (2.0 m thick), without insulation on October 15, after 50 years of the construction. From this figure, we find that the ground temperature distribution is similar to the embankment with crushed-rock revetment (1.60 m thick), without insulation (Fig. 1). In detail, the permafrost table (0°C isotherm) is y = -2.39 m under the ground surface, while that is y = -1.69 m and 0.03 m in the centerline and side slope of the embankment, respectively.

Based on the above the analyses, we can conclude that the embankments with crushed-rock revetment without insulation have an active cooling effect on the underlying permafrost, but cannot effectively reduce the underlying ground temperature. Furthermore, their cooling effects are strongest at the side slope foot, but weak in the middle. We

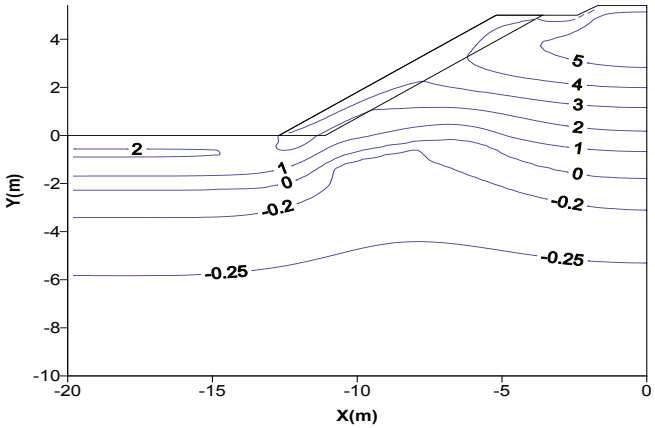

Figure 2. Temperature distribution of the embankment with crushed-rock revetment (1.60 m thick), without insulation on October 15, after 50 years of the construction (Unit: °C)

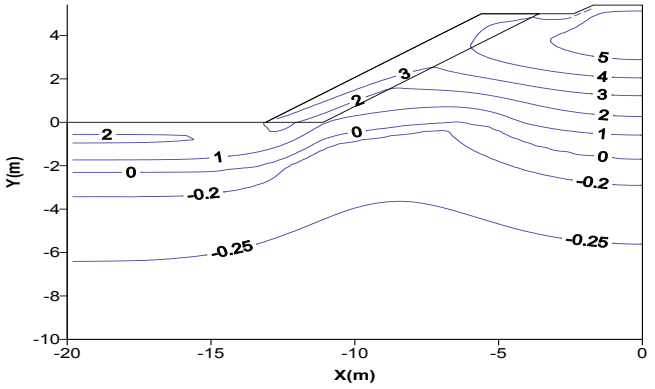

Figure 3. Temperature distribution of the embankment with crushed-rock revetment (2.0 m thick) without insulation on October 15, after 50 years of the construction (Unit: °C).

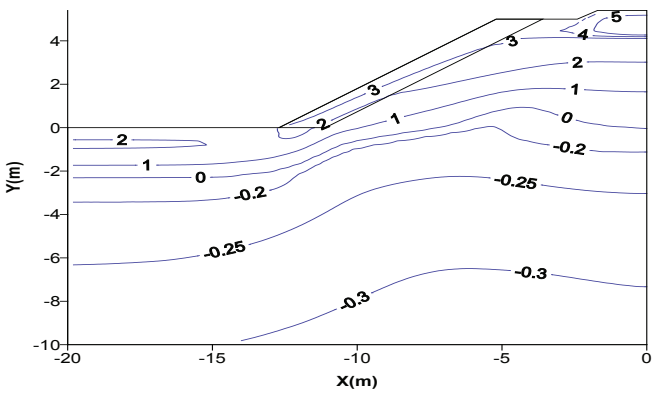

Figure 4. Temperature distribution of the embankment with crushed-rock revetment (1.6 m thick) and insulation on October 15, after 50 years of the construction (Unit: °C).

also find that when the thickness of a crushed-rock revetment reaches a certain value, its cooling effect on the middle part of embankment cannot be effectively increased by adding its thickness only.

Therefore, we propose the embankment with crushed-rock revetment (1.60 m thick) and insulation, namely, add insulation at the upside of the embankment with crushed-rock revetment.

Figure 4 is the temperature distribution of the embankment with crushed-rock revetment (1.6 m thick) and insulation on October 15, after 50 years of the construction. It can be seen from this figure that the permafrost table (0°C isotherm) is y = -2.39 m under the ground surface, while that is y = 0.05 m and 0.92 m in the centerline and side slope of the embankment, respectively. Furthermore, the temperature under the embankment is lower than those under the above two embankments without insulation (Figs. 1, 2), and -0.3°C isotherm still exists under the embankment. This shows that the embankment with crushed-rock revetment and insulation not only can raise the permafrost table, but also reduce the underlying permafrost temperature.

Therefore, it is proposed that, in warm permafrost regions, insulation should be used to increase the cooling effect of embankment with crushed-rock revetment; however, the insulation must be paved in the upper portion of the embankment.

Acknowledgments

This research was supported by the National Natural Science Foundation of China (Grant No. 40601023 and 40730736), the Knowledge Innovation Important Program of the Chinese Academy of Sciences (Grant No. KZCX3-SW-351).

References

Cheng, G.D., Jiang, H., Wang, K.L., et al. 2003. Thawing index and freezing index on the embankment surface in permafrost regions. *Journal of Glaciology and Geocryology* 25(6): 603-607.

Kong, X.Y. & Wu, J.B. 2002. A bifurcation study of non-Darcy free convection in porous media. *Acta Mechanica Sinica* 34(2): 177-185.

Lai, Y.M., Li, J.J., Niu, F.J. et al. 2003. Nonlinear thermal analysis for Qing-Tibet Railway embankments in cold regions. *Journal of Cold Regions Engineering* 17(4): 171-184.

Lai, Y.M., Zhang, S.J., Zhang, L.X. et al. 2004. Adjusting temperature distribution under the south and north slopes of embankment in permafrost regions by the ripped-rock revetment. *Cold Regions Science and Technology* 39(1): 67-79.

Ma, W., Cheng, G.D. & Wu, Q.B. 2002. Preliminary study on technology of cooling foundation in permafrost regions. *Journal of Glaciology and Geocryology* 24(5): 579-587.

Nield, D.A. & Bejan, A. 1999. *Convection in Porous Media,* 2nd ed. New York: Springer-Verlag.

Qin, D.H. 2002. *The Comprehensive Evaluating Report on the Environment Evolvement in West China*. Beijing: Science Press.

Sun, Z.Z., Ma, W. & Li, D.Q. 2004. Experimental study on the cooling effect air convection embankment crushed rock slope protection in permafrost regions. *Journal of Glaciology and Geocryology* 26(4): 435-439.

Wang, S.L., Zhao, X.F., Guo, D.X. et al. 1996. Response of permafrost to climate changes in the Qinghai-Xizang Plateau. *Journal of Glaciology and Geocryology* 18 (suppl): 157-167.

Zhu, L.N. 1988. Study of the adherent layer on different types of ground in permafrost regions on the Qinghai-Xizang Plateau. *Journal of Glaciology and Geocryology* 10(1): 8-14.

Interannual Variability of the Near-Surface Soil Freeze-Thaw Cycle Detected from Passive Microwave Remote Sensing Data in the Northern Hemisphere

Tingjun Zhang
National Snow and Ice Data Center, Cooperative Institute for Research in Environmental Sciences, University of Colorado at Boulder
Richard Armstrong
National Snow and Ice Data Center, Cooperative Institute for Research in Environmental Sciences, University of Colorado at Boulder

Introduction

Better knowledge and understanding of the near-surface freeze-thaw cycle of soils are prerequisite for evaluating the impact of cold season/cold region processes on surface and subsurface hydrology, regional and global climate, carbon exchange between the atmosphere and the land, and the terrestrial ecosystem as a whole. The challenge is to develop new techniques and methodologies to obtain data and information of the near-surface soil freeze-thaw cycle. A combined frozen soil algorithm using passive microwave satellite remote sensing data and numerical modeling was developed and validated to detect the near-surface soil freeze-thaw cycle over snow-free and snow-covered land areas. In this study, we use the NSIDC Frozen Soil Algorithm (Zhang & Armstrong 2001, Zhang et al. 2003) to investigate the interannual variability of the near-surface soil freeze-thaw cycle over the period from 1988 through 2006 in the Northern Hemisphere.

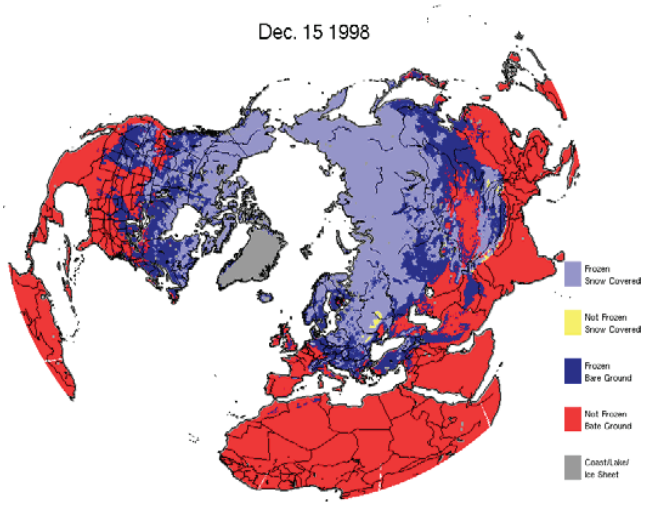

Figure 1. Distribution of the near-surface soil freeze on December 15, 1998, in the Northern Hemisphere.

Data and Methods

The NSIDC Frozen Soil Algorithm consists of two parts: (1) Over snow-free land surface, passive microwave satellite remote sensing algorithm was used to detect the near-surface soil freeze-thaw cycle; (2) Over snow-covered land surface, a one-dimensional heat transfer numerical model with phase change was used to detect soil freeze-thaw status under snow cover (Zhang & Armstrong 2001, Zhang et al. 2003). Using the Defense Meteorological Satellite Program's Special Sensor Microwave Imager (SSM/I) data, the passive microwave algorithm uses a negative spectral gradient between 19 GHz and 37 GHz, vertically polarized brightness temperatures, and a cut-off brightness temperature at 37 GHz with vertical polarization (T_B[37V]). SSM/I data and soil temperature data from 26 stations over the contiguous United States from the two-year period July 1, 1997, through June 30, 1999, were used to calibrate the algorithm (year 1), to validate the algorithm (year 2), and to demonstrate freeze/thaw classification (both years). A cut-off brightness temperature of 258.2 K was obtained based on a linear correlation ($r^2 = 0.84$) between the soil temperature at 5 cm depth and the T_B(37V). The NSIDC Frozen Soil Algorithm provides accuracy for frozen soil detection of about 76% and accuracy for the correct classification of both frozen and unfrozen soils of approximately 83% with a percent error of about 17%. We used the validated NSIDC Frozen Soil Algorithm to investigate the interannual and interdecadal variability of the timing, frequency, duration and number of days, and daily area extent of the near-surface soil freeze-thaw cycle over the period from 1988 through 2006 in the Northern Hemisphere.

Results

In the Northern Hemisphere, the near-surface soil starts to freeze in September, expanding southwards and reaching to maximum extent by January or February, then decreasing in area extent, disappearing in late May or early June. Figure 1 is a snapshot of area extent of snow cover and the near-surface soil freeze on December 15, 1998, detected from the NSIDC Frozen Soil Algorithm. Area extent of the near-surface soil freeze (Fig. 1, dark blue) is larger than that of snow cover (Fig. 1, light blue). Generally speaking, the near-surface soil freeze-thaw or seasonally frozen ground is the largest in extent among all cryospheric components. The timing of snow on ground is very critical for soil freeze/thaw status under snow cover. Snow may not be accumulated when the ground surface temperature is above 0°C, since snow will be melted when it reaches the ground. Soil may be thawed under thick snow cover (Fig. 1, yellow) this is because of the combined impact of geothermal heat flux and snow insulation effect.

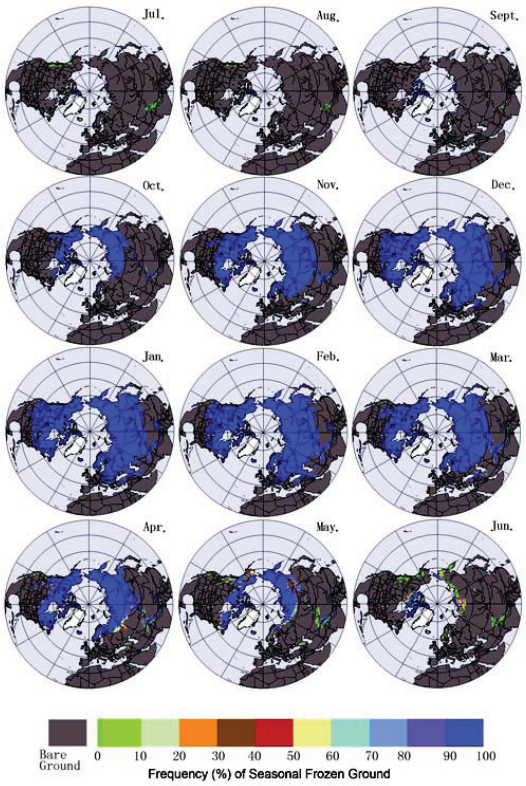

Figure 2. Climatology of monthly area extent of the near-surface soil freeze in the Northern Hemisphere over the period from 1988 through 2006, detected from the NSIDC Frozen Soil Algorithm.

Over the majority of the middle latitude regions and certainly whole high latitude regions, the near-surface soil experiences soil freeze-thaw cycle every year. Near-surface soils occasionally experience freeze in summer months over high elevation mountain areas (Fig. 2). The preliminary results indicate that the long-term average maximum area extent of the near-surface soil freeze-thaw, including permafrost regions, is about 65 x 10^6 km^2 or 68% of the land mass in the Northern Hemisphere (Fig. 2). The absolute maximum area extent can be up to 76 x 10^6 km^2 or 80% of the land mass in the Northern Hemisphere.

The number of days of the near-surface soil freeze varies from a few days in the middle or lower latitude region to several months over high elevation mountain regions and high latitude regions (Fig. 3). For High Arctic regions, such as in Siberia and northern Canada, the near-surface soil experiences up to nine months of freeze per year. As we move southwards, the number of days of soil freeze per year decreases gradually with clear zonal characteristics (Fig. 3).

Another feature is that mean length of a freeze-thaw cycle varies from a few days in middle and low latitude regions, to several months in high elevation mountain and latitude regions. Autumn and spring seasons at high latitude regions are very short, fluctuations of air temperature around 0°C are not as frequent as in the middle latitude regions. When the near-surface soil freezes in autumn at high latitudes, it is expected to be still frozen until next spring thaw.

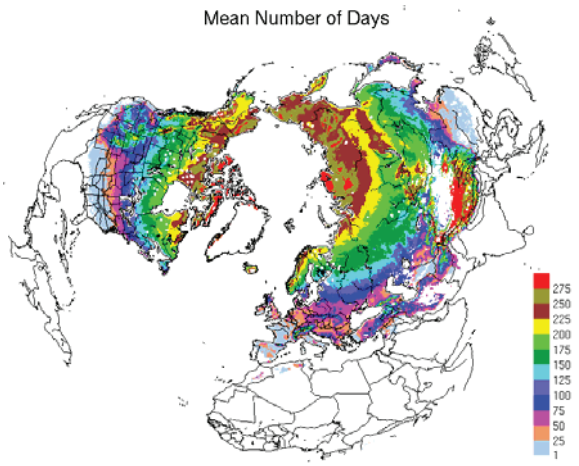

Figure 3. Mean number of days of the near-surface soil freeze in the Northern Hemisphere.

Meanwhile, frequency of the soil freeze-thaw cycle on average varies from more than 20 times in middle and low latitudes to less than 10 times in high mountain and elevation regions.

Based on results from passive microwave satellite remote sensing data, we have not detected any significant trends of changes in timing, duration, and frequency of the near-surface soil freeze-thaw cycle in the Northern Hemisphere from 1988–2006. However, further work is still needed to better validate the NSIDC Frozen Soil Algorithm. The current algorithm is validated using data from the contiguous United States. Data from other parts of the world are needed to further validate the algorithm.

Acknowledgments

We thank Jeff Smith at the National Snow and Ice Data Center (NSIDC), University of Colorado at Boulder, for preparing datasets and graphs. This study was supported by the U.S. National Aeronautics and Space Administration (NASA) grants 13721 and NNX06AE65G.

References

Zhang, T. & Armstrong, R. L. 2001. Soil freeze/thaw cycles over snow-free land detected by passive microwave remote sensing. *Geophysical Research Letters* 28(5): 763-766.

Zhang, T., Armstrong, R.L. & Smith, J. 2003. Investigation of the near-surface soil freeze/thaw cycle in the contiguous United States: Algorithm development and validation. *J. Geophys. Res*. 108(D22): 8860, doi:10.1029/2003JD003530.

Current State and Dynamics of Permafrost in the Siberian Platform

M.N. Zheleznyak
Melnikov Permafrost Institute SB RAS, Yakutsk, Russia
V.T. Balobaev
Melnikov Permafrost Institute SB RAS, Yakutsk, Russia
V.G. Rusakov
Melnikov Permafrost Institute SB RAS, Yakutsk, Russia

The Siberian Platform is a major geological structure in Asia located in the north-central part of the continent. A characteristic feature of the Siberian Platform is the widespread occurrence of permafrost, the thickness and areal distribution of which vary greatly depending on climatic conditions, topography, and the complex interaction of external and internal factors.

The geothermal data collected by the authors during the last 20 years were analyzed to provide a characterization of the geothermal field and permafrost conditions in the region. Heat flow varies across the Siberian Platform from 15 to 65 mW/m^2, and is determined by the structural and tectonic setting of the region. Thermal properties of rocks depend on the age, composition, and moisture content of the material, and vary widely from 1.2 to 7.3 W/m·K. Ground temperatures range from -5.0°C (in the presence of thick permafrost) to 16.0°C (where permafrost is absent) at depths of 500 m and from 0°C to 38.0°C at 1500 m, depending on the heat flow and rock type.

Permafrost occurs in 65% of the Siberian Platform. Its southern boundary is at 63°N latitude over most of the region, rising northwards to the latitude of Igarka in the west. Patches of frozen ground are encountered south of this boundary, where favorable local conditions exist.

The thickness of permafrost in the Siberian Platform varies from a few meters to as much as 1370 m in the Anabar Shield. It is determined by the ground surface temperature, the thermal properties of subsurface materials, and the geothermal heat flow. The latter two factors remain relatively constant over long periods of time, while the ground surface temperatures have changed repeatedly during the permafrost history. The present thermal state of the permafrost is mainly determined by the difference between the present-day temperature and the temperature in the last cold period (the Sartan) (Zheleznyak 2005).

The thermal state of the permafrost is in steady state in some parts of the region and in unsteady state in others.

The steady-state thermal regime is characterized by the constant position of the permafrost base due to the equal heat flows in unfrozen and frozen ground at the phase boundary. Equilibrium permafrost occurs in the areas composed of Early Mesozoic and Paleozoic sedimentary rocks or crystalline and metamorphic rocks. They occupy most of the Siberian Platform, the Verkhoyansk-Chukotka Folded Region, the Aldan-Stanovoy Massif, the Anabar Shield, and some minor uplifted basement blocks. The rocks comprising these structures have low porosity, are poorly fractured, and contain very little water, so their temperatures rise above 0°C rapidly, with minimum heat involved. The high thermal conductivity of these rocks facilitates rapid smoothing of the thermal state and maintains the steady-state regime.

Disequilibrium permafrost is characterized by the difference of heat flows at the lower phase boundary. Since the present epoch is warmer than the previous one, the heat flow in unfrozen ground is greater than in frozen ground, because the internal heat is partially absorbed at the phase boundary during the thawing of ice inclusions. As a result, the lower phase boundary of permafrost rises slowly, and the thickness decreases. In the Siberian Platform, disequilibrium permafrost is confined to the areas of exposed Upper Mesozoic (Jurassic and Cretaceous) and Cenozoic rocks. They occur in the pre-Yenisei zone, the Vilyuisk Basin,

Table 1. Geothermal parameters of permafrost in the Vilyuisk Basin and the Verkhoyansk Trough in Recent Epoch and 200,000 years BP.

Geothermal measurement site	Recent		Sartan		ΔT°C	ΔH, m	Rate of thaw, cm/yr
	H_o, m	T_o, °C	H_s, m	T_s °C			
Bakhynai	650	-5.0	720	-12.4	7.4	-70	-1.7
Balagachi	700	-5.0	760	-13.6	8.6	-60	-1.8
Lindenskaya	400	-2.1	520	-11.6	9.5	-120	-1.9
Srednevilyuisk	485	-1.8	568	-11.8	10.0	-83	-2.2
Vilyuisk	600	-3.0	730	-13.3	10.3	-130	-1.5
Ust-Vilyui	150	-2.8	360	-10.4	7.6	-210	-2.1
Badaran	500	-2.0	610	-11.5	9.5	-110	-1.7
Sobo Khaya	80	-1.7	350	-11.3	9.6	-270	-2.3
Khailakh	600	-5.0	785	-12.5	7.5	-185	-1.4
Namtsy	480	-3.2	580	-10.4	7.2	-100	-1.9
Yakutsk	350	-2.5	578	-10.8	8.3	-228	-1.7

and the Verkhoyansk and Yenisei-Khatanga Troughs. The disequilibrium permafrost is much less in areal extent than the equilibrium permafrost.

The pre-Yenisei zone and the Lena-Vilyui interstream area, located nearly 2000 km apart, have identical temperature fields. In both regions, the heat flow is greater in the unfrozen zone than in the frozen zone, suggesting the thawing of permafrost from below. The only difference is that the present thickness of the permafrost along the lower Yenisei River decreases from north to south under the influence of the maintained relict (Sartan) thickness. In the Vilyuisk Basin, the west–east decreasing trend developed in the Holocene under the influence of the geothermal heat flow increasing in the same direction. This is related to the increasing proximity to the tectonically active Verkhoyansk Range, where the heat flow is greater (60–80 mW/m^2) (Zheleznyak et al. 2007).

Based on the geothermal data and the physical properties of subpermafrost materials, changes in the lower permafrost boundary were estimated for the areas of disequilibrium permafrost. Calculations were made for the Vilyuisk Basin, using the data from key boreholes. The results are given in Table 1. From these values, the average regional rate of bottom thaw during the Holocene and the average difference in heat flow between the unfrozen and frozen zones was calculated, yielding $dH_M/d\tau$ = 1.9 cm/yr and $q_U - q_F$ = 34 mW/m^2. Thus, the permafrost bottom thawed, on average, 140 m during the Holocene in the region.

The geothermal data and information for the region were compiled and synthesized to produce a geothermal database of the Siberian Platform and to construct a series of geothermal sections up to 3000 m in depth and 500 to 2500 km in length.

Acknowledgments

This study was supported by RFBR grant no. 06-05-96126 and INTAS grant no. 06-1000025-9220.

References

Zheleznyak, M.N. 2005. *The Geothermal Field and Permafrost in the South-Eastern Siberian Platform*. Novosibirsk: Nauka, 227 pp.

Zheleznyak, M.N., Gavriliev, R.I., Rusakov, V.G., Shipitsyna, L.I. & Botulu, T.A. 2007. Geothermal field and cryolithozone of Tunguska syneclise and the north-eastern West Siberian Plate. *Proceedings of International Conference on Cryogenic Resources of Polar Regions, Salekhard, June 17–20, 2007*, 2: 143-146.

The Biocomplexity Manipulation Experiment: Effect of Water Table Drop on CH_4 and CO_2 Fluxes in the Alaskan Arctic at the Barrow Environmental Observatory

Donatella Zona
Global Change Research Group, San Diego State University, San Diego, CA
Walter C. Oechel
Global Change Research Group, San Diego State University, San Diego, CA

Introduction

The arctic tundra contains more than 191.8 Pg C as soil organic matter (Post et al. 1982). Increasingly, this carbon is, or is at risk of being, released to the atmosphere as CO_2 (Oechel et al. 1993, Oechel et al. 1994) and/or CH_4 (Vourlitis & Oechel 1993). However, predictions of future rates of release of CO_2 and CH_4 flux, following changes in temperature, moisture, and other variables associated with climate change, are uncertain. To predict with confidence future CO_2 and CH_4 releases to the atmosphere, it is necessary to understand the controls on net CO_2 and CH_4 fluxes. The patterns and controls on net ecosystem CO_2 and CH_4 fluxes are complex and non-linear. Warming and drying of the tundra can result in increased net CO_2 emissions from the Arctic to the atmosphere. However, areas that become warmer and remain wet, or become wetter, may be larger net emitters of CH_4 to the atmosphere.

Results and discussion

According to our study, water table does not have a consistent impact on methane and carbon dioxide flux, and in certain conditions, lower water table is related to higher methane efflux and does not affect carbon dioxide flux. This result is connected to the importance of other factors like thaw depth, soil temperature, and soil moisture more important than water table early in the season. Later in the season, water table depth becomes more important, and we observed higher methane effluxes from the site where the water table was higher. During this period, the CO_2 fluxes appear to be very similar at both sites. This unexpected result is contrary to most of the past studies that showed increased soil respiration and CO_2 release with decrease in water table and increased aeration status of the soil. A possible explanation could be connected to the characteristics of the vegetation in our study site. Even with a water table drop, below surface mosses are able to hold the water and maintain an anaerobic environment. In other words, the two sites with substantially different soil moisture and water table depth are both characterized by largely anaerobic soils. As a consequence, soil respiration is restricted to the shallower soil layers, and it is not influenced by the difference in thaw depth or water table between the two sites. In our study site, mosses are major components of the vegetation representing more than 80% of the biomass.

The differential response of the water table drop on CO_2 and CH_4 fluxes is probably due to the differential importance of shallower aerobic versus deeper anaerobic soil layers on the emission of the two gases. Methanogensis probably occurs in deeper soil layers, so a deeper thaw depth could significantly increase methane production (as we observed in the north site in late season), while shallower soil layers are the ones mainly responsible for the aerobic respiration.

Acknowledgments

We thank Robert Clement, University of Edinburgh for having written the code for the data reduction; Joe Verfaille and Hiroki Ikawa for field and technical assistance; Rob Rhew, Steven Hastings, and Rommel Zulueta for insight and advice; Douglas Deutschman for helpful advice on the statistics analysis; the Barrow Arctic Science Consortium (BASC) and Glenn Sheehan for logistic support. This work was funded by the Biocomplexity Program of the National Science Foundation (award number OPP 0421588).

References

Oechel, W.C., Cowles, S., Grulke, N., Hastings, S.J., Lawrence, B., Prudhomme, T., Riechers, G., Strain, B., Tissue, D. & Vourlitis, G.L. 1994. Transient nature of CO_2 fertilization in Arctic tundra. *Nature* 371: 500-503.

Oechel, W.C., Hastings, S.J., Vourlitis, G.L., Jenkins, M., Riechers, G. & Grulke, N. 1993. Recent Change of Arctic tundra ecosystems from a net carbon dioxide sink to a source. *Nature* 361: 520-523.

Post, W.M., Emanuel, W.R., Zinke, P.J. & Stangenberger, A.G. 1982. Soil carbon pools and world life zones. *Nature* 298: 156-159.

Vourlitis, G.L., Oechel, W.C., Hastings, S.J. & Jenkins, M.A. 1993. The effect of soil moisture and thaw depth on CH_4 flux from wet coastal tundra ecosystem on the north slope of Alaska. *Chemosphere* 26: 329-338.

The Oil Pollution Influence of Frozen Soils on Their Geophysical Characteristics

Yu.D. Zykov
The Moscow State University, Geological Faculty, Geocryology Department
A.V. Koshurnikov
The Moscow State University, Geological Faculty, Geocryology Department
I.V. Anisimova
The Moscow State University, Geological Faculty, Geocryology Department
T.E. Mironova
The Moscow State University, Geological Faculty, Geocryology Department

High rates of oil-extracting development and process industries in the cryolitozone have created a sharp geoenvironmental problem. It is pollution of natural-technical systems by oil and its products. The general losses of oil are estimated within the limits of 2–10% from annual extraction or from 5 to 25 million tons a year (Arens 1994, Masur 1995), in western Siberia approximately 0.7 and 0.4 million tons in the Timano-Pechora region (Permafrost … 2002).

In the Geocryology Department at Moscow State University, a special program on studying moving polluting organic substances (Ershov et al. 1996, Chuvilin et al. 2001) has been carried out. It is found that oil migrates in frozen soil and is present even at negative temperatures (up to -20°C and below). The research is confirmed recently in laboratory (Chuvilin et al. 2001) and field (Biggar et al. 1998).

Hydro carbonic pollution leads to change in the temperature-humid mode of soil thawing due to change in heat conductivity and thermal capacity—properties of frozen disperse soils as the bases of engineering constructions. It can also lead to development of negative geocryological processes and phenomena (Korolev 2001).

Thus, detection of and supervision over the dynamics of the pollution process became one of the serious ecological problems. Geophysical methods can be an important tool if the change in frozen soil properties laws is known. For these purposes laboratory research is executed at some set of values of a pollution degree (Z), from 0 to 10% (to weight of a mineral part) (Zykov et al. 2003).

Specific electric resistance (ρ) and polarizability (η) were measured by peak-phase method on "Spectrum" equipment (Open Company, Moscow State University–Geophysics) with the installation of four-electrodes. Speeds of longitudinal waves (Vp) were measured by ultrasonic equipment UD4-130 (Scientific Industrial Union "LUCH") on frequencies 60 and 100 kHz.

The executed measurements have shown that, in most cases, pollution causes a decrease in ρ (УЭС) [u.e.r.] and V_p. Thus, apparently from the resulting figures, in soils not salted, at negative temperatures, the influence of pollution is shown more strongly (Fig. 1). Except for what is well

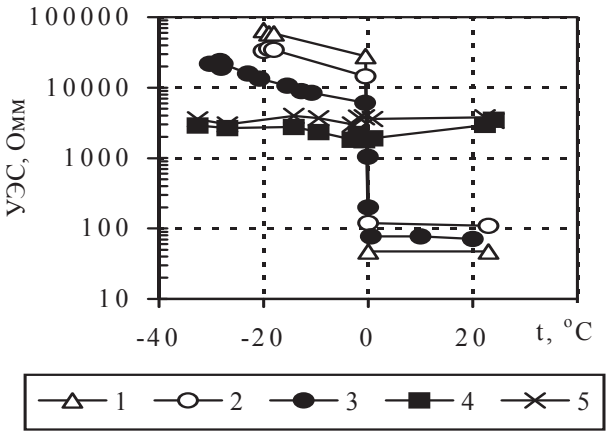

Figure 1. Temperature dependences УЭС [u.e.r.] (ρ) in oil and in not salted polluted sand; a degree of pollution (Z) and humidity (W). 1 – Z = 0, W = 20%; 2 – Z = 0, W = 10%; 3 – Z = 2.5%, W = 10%; 4 – Z = 10%, W = 0; 5 – oil.

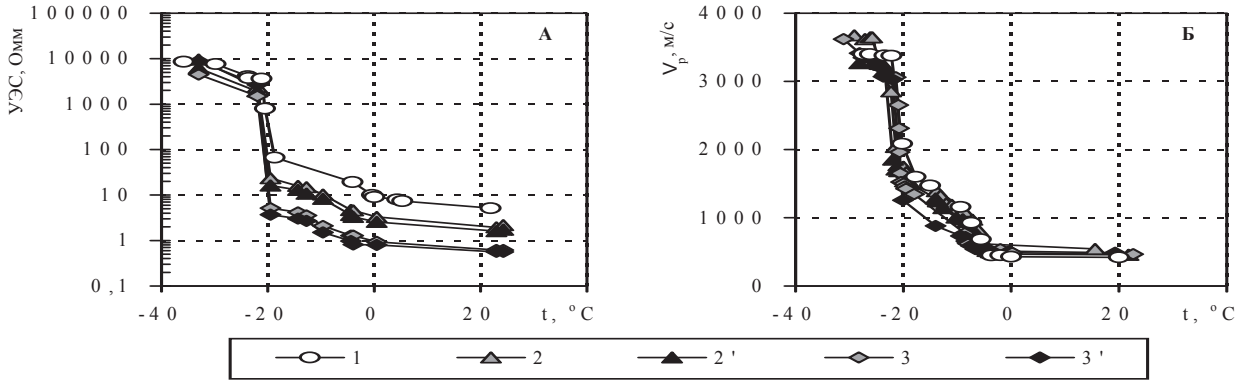

Figure 2. Temperature dependences. A: УЭС [u.e.r.], and B: V_p in the sand salted by solution NaCl of various concentration (C) with various degree of pollution (Z) at the fixed humidity (W = 10%). 1 – C = 0.0476; 2 – Z = 0; 2 – C = 0.0476; Z = 2.5%; 2 ′ – C = 0.0476; Z = 5%; 3 – C = 0.0909; Z = 2.5%; 3 ′ – C = 0.0909; Z = 5%.

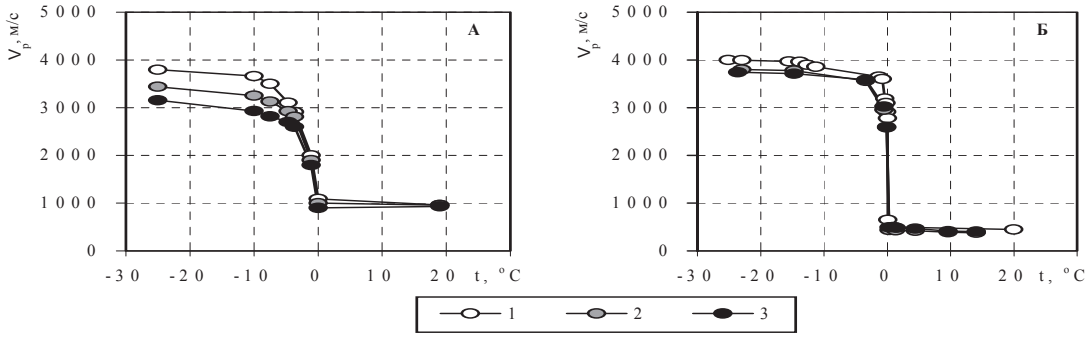

Figure.3. Influence of a degree of oil pollution (Z) for speed of longitudinal waves (V_p). A: in caolin (W = 40%) and sand (W = 20%). 1 – Z = 0; 2 – Z = 2.5%; 3 – Z = 10%.

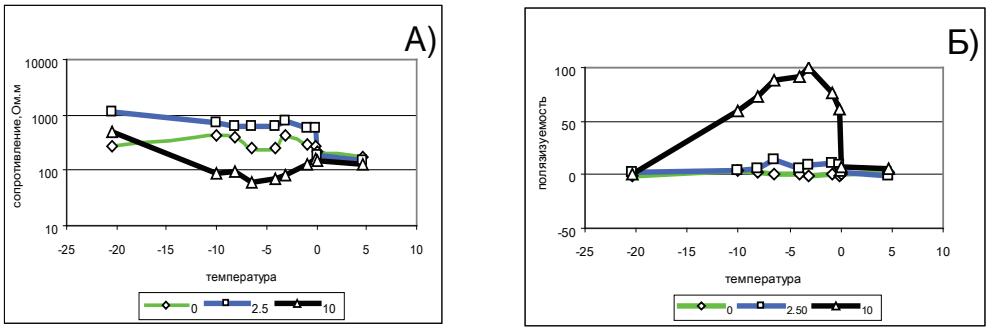

Figure 4. Temperature dependence (ρ) and polarizability (η) on frequency of 4.88 Hz on frequency of 4.88 Hz at various pollution Z (the first cycle).

visible, the initial stages of pollution (from 0 up to 2.5%) affect studied parameters more strongly, than its further increase (from 2.5 up to 10%) (Fig. 2).

Soil research from sand to clay has shown that the influence of pollution increases in the process of increase in dispersiveness (Fig. 3).

The increase in pollution can sometimes result not only in reduction of resistance, but also to its increase (Fig. 4A). In clay, it is connected with various modular conditions at various degrees of pollution. In the first cycle of freezing, data about abnormal high values (to 100%) of the polarizability factor are obtained (Fig. 4B). After thawing and repeated freezing of these polluted soils, an essentially smaller degree of polarizability (to 20%) has been noted. It testifies to the opportunities of using polarizability for studying the degree of pollution.

It is interesting to note the correlation between speed of elastic waves and heat conductivity.

References

Arens, V.Z. et al. 1999. *Clearing of an Environment of Hydrocarbonic Pollution*. Interbook, 371 pp.

Biggar, W., Haider, S., Nahir, M. & Jarrett, P.M. 1998. Site investigations of fuel spill migration into permafrost. *Journal of Cold-Regions Engineering* 12(2): 84-104.

Chuvilin, E.M., Mikljaeva, E.S., Kozlova, E.V. & Instanes, A. 2001. The experimental studying of oil pollution of frozen soils. *Materials of the Second Conference Russia Geocryologist*. I (I): *Physics-Chemistry and Mechanics of Frozen Soils, the Moscow State University,*163-169.

Ershov, E.D., Chuvilin, E., Smirnova, O.G. & Naletova, N.S. 1996. Experimental research of interaction of oil with cryogenic soils. *Materials of the First Conference Russia Geocryologist. Book 2, the Moscow State University,* 153-159.

Geoecological Inspection of the Enterprises Oil Industry. 1999. V.A. Shevnin & I.N. Modin (eds.), RUSSO, 511 pp.

Korolev, V.A. 2001. Clearing soils from pollution. *Interperiodika.* Nauka, 368 pp.

Masur, I.I. 1995. Ekology of objects of the oil and gas industry construction. *NEDRA,* 279 pp.

Permafrost and Development Oil-Gas Areas. 2002. E.S. Melnikov & S.E. Grechishchev (eds.), GEOS, 402 pp.

Zykov, Yu.D., Motenko, R.G., Anisimova, I.V. & Zhuravlyov I.I. 2005. Influence of oil pollution on properties frozen soils. *Earth Cryosphere* IX(3): 28-35.

Author Index